SİNOP ÜNİVERSİTESİ REKTÖRLÜĞÜ
Adres: Korucuk Mahallesi Üniversite Caddesi 15 Temmuz Yerleşkesi No:21B 57010 – SİNOP / TÜRKİYE
Telefon: 0 368 271 57 57 - **Faks:** 0 368 271 57 63 - **Mail:** sufbd@sinop.edu.tr

e-ISSN 2564-7873

Sinop Üniversitesi Fen Bilimleri Dergisi & Sinop University Journal of Natural Sciences

Cilt (9) Sayı (1) 2024

Sinop Üniversitesi Fen Bilimleri Dergisi

&

Sinop University Journal of Natural Sciences

Cilt / Volume 9
Sayı / Number 1
2024

SİNOP ÜNİVERSİTESİ YAYINLARI

SİNOP ÜNİVERSİTESİ
FEN BİLİMLERİ DERGİSİ

SİNOP UNIVERSITY
JOURNAL OF NATURAL SCIENCES

Cilt/Volume 9
Sayı/Number 1
2024

Sinop Üniversitesi'nin 58. Bilimsel Yayınıdır.
It is the 58th Scientific Publication of Sinop University.

***e-ISSN** 2564-7873*

SİNOP ÜNİVERSİTESİ FEN BİLİMLERİ DERGİSİ

Sinop University Journal of Natural Sciences

ADRES/ADDRESS

Sinop Üniversitesi Rektörlüğü, Korucuk Mahallesi Üniversite Caddesi 15 Temmuz Yerleşkesi No:21B 57010–SİNOP/TÜRKİYE

Tel: 0 368 271 57 57 **Faks:** 0 368 271 57 63

https://dergipark.org.tr/sinopfbd

e-Posta: sufbd@sinop.edu.tr

İçindekiler/Contents

e-ISSN 2564-7873

Araştırma Makaleleri/Research Articles

Sayfa/Page

Derlemeler/Reviews

Sinopfbd, 2024; 9(1): 1-13 **https://doi.org/10.33484/sinopfbd.1315640**

Sinop Üniversitesi Fen Bilimleri Dergisi
Sinop Uni J Nat Sci
E-ISSN: 2564-7873

https://dergipark.org.tr/tr/pub/sinopfbd

Parallel Curves Based on Normal Vector

Yasemin SAĞIROĞLU[1] and Gönül KÖSE[2]

How to cite: Sağıroğlu, Y., & Köse, G. (2024). Parallel curves based on normal vector. *Sinop Üniversitesi Fen Bilimleri Dergisi, 9*(1), 1-13. https://doi.org/10.33484/sinopfbd.1315640

Research Article

Corresponding Author
Yasemin SAĞIROĞLU
sagiroglu.yasemin@gmail.com

ORCID of the Authors
Y.S: 0000-0003-0660-211X
G.K: 0009-0007-4855-1353

Received: 16.06.2023
Accepted: 21.01.2024

Abstract
In this paper, the definition of parallel curves based on normal vector is given and the curvature, torsion, Frenet frame of this curve are determined. Furthermore, special cases in curves such as circle and helix are also be exemplified.

Keywords: Curve, Frenet frame, curvature, torsion

Normal Vektöre Dayalı Paralel Eğriler

[1]Karadeniz Technical University, Science Faculty, Mathematics Department,Trabzon, Türkiye

[2]MEB, Trabzon Vocational and Technical Anatolian High School, Trabzon, Türkiye

Öz
Bu çalışmada, normal vektöre dayalı paralel eğrilerin tanımı verilmiş ve bu eğrinin eğriliği, burulması, Frenet çatısı belirlenmiştir. Ayrıca, çember ve helis gibi eğrilerdeki özel durumlar da örneklendirilmiştir.

Anahtar Kelimeler: Eğri, Frenet çatısı, eğrilik, burulma

Introduction

Curves are one of the main tools of differential geometry. Different kinds of curves are determined for giving descriptions and explaining the theory about curves in differential geometry. In the literature, there are many articles on this subject. Arslan and Hacısalihoğlu [1] investigate the harmonic curvatures

of a Frenet curve, Ergin [2] studies generalized Darboux curves, Liu, and Wang [3] examine Mannheim partner curves, İlarslan and Nesovic [4] analyze the rectifying curves, Has and Yılmaz [5] work on quaternionic Bertrand curves. Sağıroğlu [6] studies global differential invariants of affine curves in two dimensional space. These results are carried out in the Euclidean space. Also, curves in different space from Euclidean space are investigated. Divjak [7] investigates special curves on ruled surfaces in Galilean and Pseudo-Galilean spaces, Bükcü and Karacan [8] work on Bishop frame of the spacelike curves in Minkowski 3-Space. Şenyurt et al. [9] define tangent, principal, normal and binormal wise associated curves such that each of these vectors of any given curve lies on the osculating, normal and rectifying plane of its partner, respectively. Güler [10] defines the quasi parallel curve with the help of the quasi frame of a given curve. In addition, curves are the most important examples of their role in Pattern Recognition, Computer Graphics and Computer Vision because of being suitable for modeling real life problems. [11] and [12] are their applications to these subjects. The classical differential geometry of curves is investigated with respect to conformable fractional derivative and fractional integral in Gözütok, Çoban and Sağıroğlu [13]. Curvature and torsion of a conformable curve are defined and the geometric interpretation of these two functions is done. In [14], Aldossary and Gazwani give the similar definition of the unit speed curves using binormal vector. These curves are called parallel curves. The main goal of this paper is to investigate parallel curves using normal vector and to study the associated geometry of these curves. We give a similar definition in [14] using the normal vector. The aim of this study is contribution to the literature on the theory of curves in three-dimensional space. In addition, the studies discussed here will later be expanded to surfaces and their geometric properties will be examined. Also, the instrinsic geometric formulas will be derived from the curvatures. We refer to [15] for the definitions of curvature, torsion and Frenet frame of a curve.

Parallel Curves Based on Normal Vector

Definition1. Let α be a unit speed curve in R^3 and $\boldsymbol{t}(s), \boldsymbol{n}(s), \boldsymbol{b}(s)$ be its Franet frame in a point $\alpha(s)$. Including r to represent a real number constant, parallel curve based on normal vector of the curve α is defined as

$$\boldsymbol{\alpha_n}(s) = \boldsymbol{\alpha}(s) + r\boldsymbol{n}(s).$$

The reason why the curve $\alpha(s)$ taken as unit speed is the convenience in calculations. Fisrtly, the parametrization of the curve according to its arc lenght is obtained and calculations are made for this situation, and then calculations are made when it is arbitrary speed. The reason for this is that when we calculate a parallel curve based on a curve with unit speed, the resulting curve will generally not have unit speed.

Frenet Frame, Curvature and Torsion Functions of the Parallel Curves Based on Normal Vector

Now we consider the parallel curve based on normal vector of α;

$$\boldsymbol{\alpha_n}(s) = \boldsymbol{\alpha}(s) + r\boldsymbol{n}(s)$$

Let the arc length function of this curve be s_2. In this case, the unit tangent vector of the curve $\alpha_n(s)$ is obtained as

$$\boldsymbol{t_n}(s_2) = \frac{d\boldsymbol{\alpha_n}}{ds}.\frac{ds}{ds_2} = (\boldsymbol{t} + r\boldsymbol{n}')\frac{ds}{ds_2} = (\boldsymbol{t} + r(-\kappa\boldsymbol{t} + \tau\boldsymbol{b})\frac{ds}{ds_2} = ((1 - r\kappa)\boldsymbol{t} + r\tau\boldsymbol{b})\frac{ds}{ds_2}$$

Here, $\boldsymbol{t}, \boldsymbol{n}, \boldsymbol{b}$ and κ, τ are Frenet frame vectors and the corresponding curvatures of the curve $\alpha_n(s)$, respectively. If we take the dot product with $\boldsymbol{t}$ of both sides;

$$\langle \boldsymbol{t_n}, \boldsymbol{t} \rangle = (1 - r\kappa)\frac{ds}{ds_2}$$

is obtained. If we also multiply both sides of this equation by the vector $\boldsymbol{b}$, we get

$$\langle \boldsymbol{t_n}, \boldsymbol{b} \rangle = r\tau\frac{ds}{ds_2}.$$

Multiplying both sides by the vector $\boldsymbol{n}$, the equation

$$\langle \boldsymbol{t_n}, \boldsymbol{n} \rangle = 0$$

is obtained, which shows that the vectors $\boldsymbol{t_n}$ and $\boldsymbol{n}$ are orthogonal. If the norm of both sides of the above equation is taken, then we obtain that

$$\|\boldsymbol{t_n}(s_2)\| = \left\|((1 - r\kappa)\boldsymbol{t} + r\tau\boldsymbol{b})\frac{ds}{ds_2}\right\| = \|(1 - r\kappa)\boldsymbol{t} + r\tau\boldsymbol{b}\|\frac{ds}{ds_2}$$

$$= \frac{ds}{ds_2}[((1 - r\kappa)\boldsymbol{t} + r\tau\boldsymbol{b}).((1 - r\kappa)\boldsymbol{t} + r\tau\boldsymbol{b})]^{1/2}$$

$$= \frac{ds}{ds_2}[(1 - r\kappa)^2 + r^2\tau^2]^{1/2}$$

By using $\|\boldsymbol{t_n}(s_2)\| = 1$, it follows that

$$\frac{ds_2}{ds} = \sqrt{(1 - r\kappa)^2 + r^2\tau^2}$$

From here, we get

$$\frac{ds}{ds_2} = \frac{1}{\sqrt{(1 - r\kappa)^2 + r^2\tau^2}}$$

Note that this equation also shows the relationship between the arc lenght parameters of these two curves.

Theorem 1. The expression of the Frenet frame of the parallel curve $\boldsymbol{\alpha_n}(s)$ in terms of the Frenet frame of the curve $\boldsymbol{\alpha}(s)$ is in the form;

$$\boldsymbol{t_n}(s) = \frac{(1-r\kappa)\boldsymbol{t} + r\tau\boldsymbol{b}}{\sqrt{(1-r\kappa)^2 + r^2\tau^2}}$$

$$\boldsymbol{b_n}(s) = \frac{\begin{matrix}(r\tau - r^2\kappa\tau - r^2\tau^3)\boldsymbol{t} + \left(\begin{matrix}-r\tau' + r^2\kappa\tau' \\ -r^2\kappa'\tau\end{matrix}\right)\boldsymbol{n} + \\ (\kappa - 2r\kappa^2 - r\tau^2 + r^2\kappa^3 + r^2\kappa\tau^2)\boldsymbol{b}\end{matrix}}{F(s)}$$

$$\begin{aligned}\boldsymbol{n_n}(s) = \frac{1}{F(s).A(s)}\{&(-r^2\tau\tau' + r^3\kappa\tau\tau' - r^3\kappa'\tau^2)\boldsymbol{t} \\ &+ (-r^2\tau^2 + r^3\kappa\tau^2 + r^3\tau^4 + \kappa - 3r\kappa^2 - r\tau^2 + 3r^2\kappa^3 + 2r^2\kappa\tau^2 - r^3\kappa^4 \\ &- r^3\kappa^2\tau^2)\boldsymbol{n} + (r\tau' - 2r^2\kappa\tau' + r^2\kappa'\tau + r^3\kappa^2\tau' - r^3\kappa\kappa'\tau)\boldsymbol{b}\}\end{aligned}$$

where

$$A(s) = \sqrt{(1-r\kappa)^2 + r^2\tau^2}$$

and

$$F(s) = \sqrt{\begin{matrix}(-r\tau\kappa + r^2\kappa^2\tau + r\tau^3)^2 + (-r\tau' + r^2\kappa\tau' - r^2\kappa'\tau)^2 + \\ (\kappa - 2r\kappa^2 - r\tau^2 + r^2\kappa^3 + r^2\kappa\tau^2)^2\end{matrix}}.$$

Proof. Let us determine the Frenet frame of a curve $\boldsymbol{\alpha_n}(s)$ in terms of the Frenet frame of $\boldsymbol{\alpha}(s)$ in the general case. It is known that

$$\frac{d\boldsymbol{\alpha_n}(s)}{ds} = \frac{d\boldsymbol{\alpha}(s)}{ds} + r\frac{d\boldsymbol{n}(s)}{ds} = \boldsymbol{t} + r(-\kappa\boldsymbol{t} + \tau\boldsymbol{b}) = (1-r\kappa)\boldsymbol{t} + r\tau\boldsymbol{b}.$$

If we take the norm of this expression, then it holds that

$$\left\|\frac{d\boldsymbol{\alpha_n}(s)}{ds}\right\| = \sqrt{(1-r\kappa)^2 + r^2\tau^2} = A(s)$$

Hence, the unit tangent vector $\boldsymbol{t_n}(s)$ is obtained as;

$$\boldsymbol{t_n}(s) = \frac{\frac{d\boldsymbol{\alpha_n}(s)}{ds}}{\left\|\frac{d\boldsymbol{\alpha_n}(s)}{ds}\right\|} = \frac{(1-r\kappa)\boldsymbol{t} + r\tau\boldsymbol{b}}{\sqrt{(1-r\kappa)^2 + r^2\tau^2}}$$

Since

$$\frac{d^2\boldsymbol{\alpha_n}(s)}{ds^2} = -r\kappa'\boldsymbol{t} + (1-r\kappa)\frac{d\boldsymbol{t}}{ds} + r\tau'\boldsymbol{b} + r\tau\frac{d\boldsymbol{b}}{ds}$$

$$= -r\kappa'\boldsymbol{t} + (\kappa - r\kappa^2 - r\tau^2)\boldsymbol{n} + r\tau'\boldsymbol{b}$$

and

$$\frac{d\boldsymbol{\alpha_n}(s)}{ds} \times \frac{d^2\boldsymbol{\alpha_n}(s)}{ds^2} = [(1-r\kappa)\boldsymbol{t} + r\tau\boldsymbol{b}] \times [-r\kappa'\boldsymbol{t} + (\kappa - r\kappa^2 - r\tau^2)\boldsymbol{n} + r\tau'\boldsymbol{b}]$$

$$= (\kappa - r\kappa^2 - r\tau^2 - r\kappa^2 + r^2\kappa^3 + r^2\kappa\tau^2)\boldsymbol{t}\times\boldsymbol{n} + (r\tau' - r^2\kappa\tau')\boldsymbol{t}\times\boldsymbol{b} - r^2\kappa'\tau\boldsymbol{b}\times\boldsymbol{t} + (r\tau\kappa - r^2\kappa^2\tau - r^2\tau^3)\boldsymbol{b}\times\boldsymbol{n}$$

$$= (-r\tau\kappa + r^2\kappa^2\tau + r^2\tau^3)\boldsymbol{t} + (-r\tau' + r^2\kappa\tau' - r^2\kappa'\tau)\boldsymbol{n} + (\kappa - 2r\kappa^2 - r\tau^2 + r^2\kappa^3 + r^2\kappa\tau^2)\boldsymbol{b}$$

and by taking the norm at second term, it is obtained

$$\left\|\frac{d\boldsymbol{\alpha_n}(s)}{ds} \times \frac{d^2\boldsymbol{\alpha_n}(s)}{ds^2}\right\| = \sqrt{\begin{matrix}(-r\tau\kappa + r^2\kappa^2\tau + r^2\tau^3)^2 + (-r\tau' + r^2\kappa\tau' - r^2\kappa'\tau)^2 + \\ (\kappa - 2r\kappa^2 - r\tau^2 + r^2\kappa^3 + r^2\kappa\tau^2)^2\end{matrix}} = F(s)$$

Also the third derivation is obtained as follows;

$$\frac{d^3\boldsymbol{\alpha_n}(s)}{ds^3} = -r\kappa''\,\boldsymbol{t} - r\kappa'\boldsymbol{t}' + (\kappa' - 2r\kappa\kappa' - 2r\tau\tau')\boldsymbol{n} + (\kappa - r\kappa^2 - r\tau^2)\boldsymbol{n}' + r\tau''\boldsymbol{b} + r\tau'\boldsymbol{b}'$$

$$= -r\kappa''\,\boldsymbol{t} - r\kappa\kappa'\boldsymbol{n} + (\kappa' - 2r\kappa\kappa' - 2r\tau\tau')\boldsymbol{n} + (-\kappa^2 + r\kappa^3 + r\kappa\tau^2)\boldsymbol{t} + (\kappa\tau - r\kappa^2\tau - r\tau^3)\boldsymbol{b} + r\tau''\boldsymbol{b} - r\tau\tau'\boldsymbol{n}$$

$$= (-r\kappa''\, - \kappa^2 + r\kappa^3 + r\kappa\tau^2)\boldsymbol{t} + (-3r\kappa\kappa' + \kappa' - 3r\tau\tau')\boldsymbol{n} + (\kappa\tau - r\kappa^2\tau - r\tau^3 + r\tau'')\boldsymbol{b}$$

The product required for the torsion calculation is given by the following;

$$\left\langle\left(\frac{d\boldsymbol{\alpha_n}(s)}{ds} \times \frac{d^2\boldsymbol{\alpha_n}(s)}{ds^2}\right), \frac{d^3\boldsymbol{\alpha_n}(s)}{ds^3}\right\rangle$$

$$= (-r\tau\kappa + r^2\kappa^2\tau + r^2\tau^3)(-r\kappa''\, - \kappa^2 + r\kappa^3 + r\kappa\tau^2)$$
$$+ (-r\tau' + r^2\kappa\tau' - r^2\kappa'\tau)(-3r\kappa\kappa' + \kappa' - 3r\tau\tau')$$
$$+ (\kappa - 2r\kappa^2 - r\tau^2 + r^2\kappa^3 + r^2\kappa\tau^2)(\kappa\tau - r\kappa^2\tau - r\tau^3 + r\tau'') = G(s)$$

We have that;

$$\boldsymbol{t_n}(s) = \frac{\frac{d\boldsymbol{\alpha_n}(s)}{ds}}{\left\|\frac{d\boldsymbol{\alpha_n}(s)}{ds}\right\|} = \frac{(1-r\kappa)\boldsymbol{t} + r\tau\boldsymbol{b}}{\sqrt{(1-r\kappa)^2 + r^2\tau^2}}$$

Now, let us calculate that the vectors $\boldsymbol{b_n}(s)$ and $\boldsymbol{n_n}(s)$.

$$\boldsymbol{b_n}(s) = \frac{\boldsymbol{\alpha_n'}(s) \times \boldsymbol{\alpha_n''}(s)}{\|\boldsymbol{\alpha_n'}(s) \times \boldsymbol{\alpha_n''}(s)\|}$$

$$= \frac{\begin{matrix}(-r\tau\kappa + r^2\kappa^2\tau + r^2\tau^3)\boldsymbol{t} + (-r\tau' + r^2\kappa\tau' - r^2\kappa'\tau)\boldsymbol{n} + \\ (\kappa - 2r\kappa^2 - r\tau^2 + r^2\kappa^3 + r^2\kappa\tau^2)\boldsymbol{b}\end{matrix}}{F(s)}$$

and

$$\boldsymbol{n_n}(s) = \boldsymbol{b_n}(s) \times \boldsymbol{t_n}(s)$$

$$= \frac{1}{F(s)}\begin{bmatrix}(-r\tau\kappa + r^2\kappa^2\tau + r^2\tau^3)\boldsymbol{t} + (-r\tau' + r^2\kappa\tau' - r^2\kappa'\tau)\boldsymbol{n} \\ +(\kappa - 2r\kappa^2 - r\tau^2 + r^2\kappa^3 + r^2\kappa\tau^2)\boldsymbol{b}\end{bmatrix} \times \frac{1}{A(s)}[(1 - r\kappa)\boldsymbol{t} + r\tau\boldsymbol{b}]$$

$$= \frac{1}{F(s).A(s)}\{(-r^2\tau^2\kappa + r^3\kappa^2\tau^2 + r^3\tau^4)\boldsymbol{t} \times \boldsymbol{b}$$
$$+ (-r\tau' + r^2\kappa\tau' - r^2\kappa'\tau + r^2\kappa\tau' - r^3\kappa^2\tau' + r^3\kappa\kappa'\tau)\boldsymbol{n} \times \boldsymbol{t}$$
$$+ (-r^2\tau\tau' + r^3\kappa\tau\tau' - r^3\kappa'\tau^2)\boldsymbol{n} \times \boldsymbol{b}$$
$$+ (\kappa - 2r\kappa^2 - r\tau^2 + r^2\kappa^3 + r^2\kappa\tau^2 - r\kappa^2 + 2r^2\kappa^3 + r^2\kappa\tau^2 - r^3\kappa^4 - r^3\kappa^2\tau^2)\boldsymbol{b}$$
$$\times \boldsymbol{t}\}$$

$$= \frac{1}{F(s).A(s)}\{(-r^2\tau\tau' + r^3\kappa\tau\tau' - r^3\kappa'\tau^2)\boldsymbol{t}$$
$$+ (-r^2\tau^2 + r^3\kappa\tau^2 + r^3\tau^4 + \kappa - 3r\kappa^2 - r\tau^2 + 3r^2\kappa^3 + 2r^2\kappa\tau^2 - r^3\kappa^4$$
$$- r^3\kappa^2\tau^2)\boldsymbol{n} + (r\tau' - 2r^2\kappa\tau' + r^2\kappa'\tau + r^3\kappa^2\tau' - r^3\kappa\kappa'\tau)\boldsymbol{b}\}.$$

Theorem 2. The expression of the curvature and torsion functions of the parallel curve $\boldsymbol{\alpha_n}(s)$ in terms of the curvature and torsion functions of the $\boldsymbol{\alpha}(s)$ are as follows:

$$\kappa_n(s) = \frac{\sqrt{\begin{matrix}(-r\tau\kappa + r^2\kappa^2\tau + r^2\tau^3)^2 + (-r\tau' + r^2\kappa\tau' - r^2\kappa'\tau)^2 + \\ (\kappa - 2r\kappa^2 - r\tau^2 + r^2\kappa^3 + r^2\kappa\tau^2)^2\end{matrix}}}{((1 - r\kappa)^2 + r^2\tau^2)^{3/2}}$$

$$\tau_n(s) = \frac{G(s)}{F^2(s)}$$

where

$$G(s) = (-r\tau\kappa + r^2\kappa^2\tau + r^2\tau^3)(-r\kappa'' - \kappa^2 + r\kappa^3 + r\kappa\tau^2) + (-r\tau' + r^2\kappa\tau' - r^2\kappa'\tau)(-3r\kappa\kappa' + \kappa' - 3r\tau\tau') + (1 - 2r\kappa - r\tau^2 + r^2\kappa^2 + r^2\kappa\tau^2)(\kappa\tau - r\kappa^2\tau - r\tau^3 + r\tau'')$$

and

$$F(s) = \sqrt{\begin{matrix}(-r\tau\kappa + r^2\kappa^2\tau + r^2\tau^3)^2 + (-r\tau' + r^2\kappa\tau' - r^2\kappa'\tau)^2 + \\ (\kappa - 2r\kappa^2 - r\tau^2 + r^2\kappa^3 + r^2\kappa\tau^2)^2\end{matrix}}.$$

Proof. The curvature and torsion functions of the $\boldsymbol{\alpha_n}(s)$ in terms of the curvature and torsion functions of $\boldsymbol{\alpha}(s)$ are as follows:

$$\kappa_n(s) = \frac{\|\boldsymbol{\alpha_n'}(s) \times \boldsymbol{\alpha_n''}(s)\|}{\|\boldsymbol{\alpha_n'}(s)\|^3} = \frac{\sqrt{\begin{matrix}(-r\tau\kappa + r^2\kappa^2\tau + r^2\tau^3)^2 + (-r\tau' + r^2\kappa\tau' - r^2\kappa'\tau)^2 + \\ (\kappa - 2r\kappa^2 - r\tau^2 + r^2\kappa^3 + r^2\kappa\tau^2)^2\end{matrix}}}{((1 - r\kappa)^2 + r^2\tau^2)^{3/2}}$$

$$\tau_n(s) = \frac{\langle(\boldsymbol{\alpha_n'}(s) \times \boldsymbol{\alpha_n''}(s)), \boldsymbol{\alpha_n'''}(s)\rangle}{\|\boldsymbol{\alpha_n'}(s) \times \boldsymbol{\alpha_n''}(s)\|^2} = \frac{G(s)}{F^2(s)}$$

where

$$G(s) = (-r\tau\kappa + r^2\kappa^2\tau + r^2\tau^3)(-r\kappa'' - \kappa^2 + r\kappa^3 + r\kappa\tau^2) + (-r\tau' + r^2\kappa\tau' - r^2\kappa'\tau)(-3r\kappa\kappa' + \kappa' - 3r\tau\tau') + (1 - 2r\kappa - r\tau^2 + r^2\kappa^2 + r^2\kappa\tau^2)(\kappa\tau - r\kappa^2\tau - r\tau^3 + r\tau'')$$

and

$$F(s) = \sqrt{\begin{matrix}(-r\tau\kappa + r^2\kappa^2\tau + r^2\tau^3)^2 + (-r\tau' + r^2\kappa\tau' - r^2\kappa'\tau)^2 + \\ (\kappa - 2r\kappa^2 - r\tau^2 + r^2\kappa^3 + r^2\kappa\tau^2)^2\end{matrix}}$$

as the proof of the first theorem.

Example 1. Consider the curve $\boldsymbol{\alpha}(s) = \left(a\cos\frac{s}{a}, a\sin\frac{s}{a}, 0\right)$, $a > 0$ and calculate the Frenet apparatus of parallel curve.

The definition of the parallel curve based on normal vector of the curve $\boldsymbol{\alpha}(s)$ is $\boldsymbol{\alpha_n}(s) = \boldsymbol{\alpha}(s) + r\boldsymbol{n}(s)$. Let us calculate the normal vector $\boldsymbol{n}(s)$ of the curve $\boldsymbol{\alpha}(s)$. Due the fact that the curve $\boldsymbol{\alpha}(s)$ is a unit speed curve, we obtain that

$$\boldsymbol{t}'(s) = \boldsymbol{\alpha}''(s) = \left(-\frac{1}{a}\cos\frac{s}{a}, -\frac{1}{a}\sin\frac{s}{a}, 0\right)$$

and

$$\|\boldsymbol{t}'(s)\| = \sqrt{\frac{1}{a^2}\cos^2\frac{s}{a} + \frac{1}{a^2}\sin^2\frac{s}{a}} = \frac{1}{a}.$$

So the normal vector is obtained as

$$\boldsymbol{n}(s) = \left(-\cos\frac{s}{a}, -\sin\frac{s}{a}, 0\right).$$

From here, the equation of the curve $\boldsymbol{\alpha_n}(s)$ is,

$$\boldsymbol{\alpha_n}(s) = \left(a\cos\frac{s}{a}, a\sin\frac{s}{a}, 0\right) + r\left(-\cos\frac{s}{a}, -\sin\frac{s}{a}, 0\right) = \left(a\cos\frac{s}{a} - r\cos\frac{s}{a}, a\sin\frac{s}{a} - r\sin\frac{s}{a}, 0\right).$$

Then we get that

$$\boldsymbol{\alpha_n}'(s) = \left(-sin\frac{s}{a} + \frac{r}{a}sin\frac{s}{a}, cos\frac{s}{a} - \frac{r}{a}cos\frac{s}{a}, 0\right)$$

and

$$\|\boldsymbol{\alpha_n}'(s)\| = \left(\left(-sin\frac{s}{a} + \frac{r}{a}sin\frac{s}{a}\right)^2 + \left(cos\frac{s}{a} - \frac{r}{a}cos\frac{s}{a}\right)^2\right)^{1/2}$$

$$= \sqrt{1 - \frac{2r}{a} + \frac{r^2}{a^2}} = \sqrt{\frac{a^2 - 2ar + r^2}{a^2}} = \sqrt{\frac{(a-r)^2}{a^2}} = \frac{|a-r|}{a}$$

So our curve is not unit speed. If we make the necessary calculations on arbitrary speed curves, we get that

$$\boldsymbol{\alpha_n}''(s) = \left(-\frac{1}{a}cos\frac{s}{a} + \frac{r}{a^2}cos\frac{s}{a}, -\frac{1}{a}sin\frac{s}{a} + \frac{r}{a^2}sin\frac{s}{a}, 0\right)$$

$$\boldsymbol{\alpha_n}'''(s) = \left(\frac{1}{a^2}sin\frac{s}{a} - \frac{r}{a^3}sin\frac{s}{a}, -\frac{1}{a^2}cos\frac{s}{a} + \frac{r}{a^3}cos\frac{s}{a}, 0\right)$$

$$\boldsymbol{\alpha_n}'(s) \times \boldsymbol{\alpha_n}''(s) = \begin{vmatrix} U_1 & U_2 & U_3 \\ -sin\frac{s}{a} + \frac{r}{a}sin\frac{s}{a} & cos\frac{s}{a} - \frac{r}{a}cos\frac{s}{a} & 0 \\ -\frac{1}{a}cos\frac{s}{a} + \frac{r}{a^2}cos\frac{s}{a} & -\frac{1}{a}sin\frac{s}{a} + \frac{r}{a^2}sin\frac{s}{a} & 0 \end{vmatrix}$$

$$= \left(0,0,\frac{a^2 - 2ak + r^2}{a^3}\right) = \left(0,0,\frac{(a-r)^2}{a^3}\right)$$

and

$$\|\boldsymbol{\alpha_n}'(s) \times \boldsymbol{\alpha_n}''(s)\| = \sqrt{0^2 + 0^2 + \left(\frac{(a-r)^2}{a^3}\right)^2} = \frac{(a-r)^2}{a^3}$$

$$\langle \boldsymbol{\alpha_n'}(s) \times \boldsymbol{\alpha_n''}(s), \boldsymbol{\alpha_n}'''(s) \rangle = 0$$

So the Frenet apparatus of the curve are;

$$\boldsymbol{t_n}(s) = \frac{\boldsymbol{\alpha_n}'(s)}{\|\boldsymbol{\alpha_n}'(s)\|} = \frac{a}{|a-r|}\left(-sin\frac{s}{a} + \frac{r}{a}sin\frac{s}{a}, cos\frac{s}{a} - \frac{r}{a}cos\frac{s}{a}, 0\right)$$

$$\boldsymbol{b_n}(s) = \frac{\boldsymbol{\alpha_n}'(s) \times \boldsymbol{\alpha_n}''(s)}{\|\boldsymbol{\alpha_n}'(s) \times \boldsymbol{\alpha_n}''(s)\|} = \frac{a^3}{(a-r)^2}\left(0,0,\frac{(a-r)^2}{a^3}\right) = (0,0,1)$$

$$\boldsymbol{n_n}(s) = \boldsymbol{b_n}(s) \times \boldsymbol{t_n}(s) = \frac{a}{|a-r|}\begin{vmatrix} U_1 & U_2 & U_3 \\ 0 & 0 & 1 \\ -sin\frac{s}{a} + \frac{r}{a}sin\frac{s}{a} & cos\frac{s}{a} - \frac{r}{a}cos\frac{s}{a} & 0 \end{vmatrix}$$

$$= \frac{a}{|a-r|}\left(-cos\frac{s}{a} + \frac{r}{a}cos\frac{s}{a}, -sin\frac{s}{a} + \frac{r}{a}sin\frac{s}{a}, 0\right).$$

The curvature and torsion functions of the curve are;

$$\kappa_n(s) = \frac{\|\boldsymbol{\alpha_n}'(s) \times \boldsymbol{\alpha_n}''(s)\|}{\|\boldsymbol{\alpha_n}'(s)\|^3} = \frac{\frac{(a-r)^2}{a^3}}{\left(\frac{|a-r|}{a}\right)^3} = \frac{1}{|a-r|}$$

$$\tau_n(s) = \frac{\langle \boldsymbol{\alpha_n}'(s) \times \boldsymbol{\alpha_n}''(s), \boldsymbol{\alpha_n}'''(s)\rangle}{\|\boldsymbol{\alpha_n}'(s) \times \boldsymbol{\alpha_n}''(s)\|^2} = \frac{0}{\left(\frac{(a-r)^2}{a^3}\right)^2} = 0.$$

This shows that parallel curve is also a circle (Figure 1).

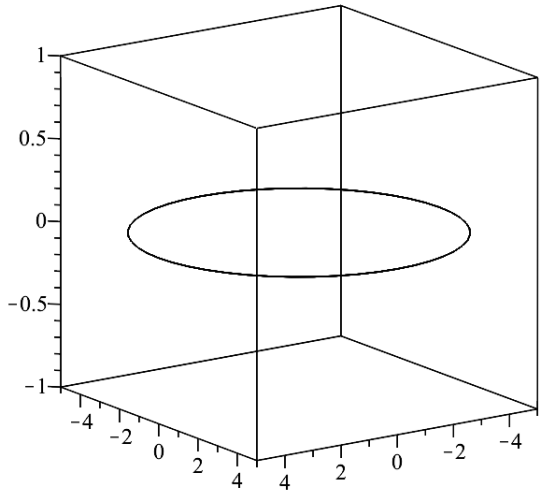

Figure 1. *Parallel curve* $\alpha_n(s)$ *for* $a = 2$ *and* $r = -3$

Remark: It is pointed out that parallel curves give a family of circles centered on the origin for $r \neq a$.

Example 2. Consider the helix $\boldsymbol{\alpha}(s) = \left(cos\frac{s}{\sqrt{2}}, sin\frac{s}{\sqrt{2}}, \frac{s}{\sqrt{2}}\right)$. Then let us calculate the Frenet apparatus of the parallel curve.

The definition of the parallel curve is $\boldsymbol{\alpha_n}(s) = \boldsymbol{\alpha}(s) + r\boldsymbol{n}(s)$. Let us calculate the normal vector $\boldsymbol{n}(s)$ of the curve $\boldsymbol{\alpha}(s)$. Using the fact that the curve $\boldsymbol{\alpha}(s)$ is a unit speed curve, we have that

$$\boldsymbol{t}'(s) = \boldsymbol{\alpha}''(s) = \left(-\frac{1}{2}cos\frac{s}{\sqrt{2}}, -\frac{1}{2}sin\frac{s}{\sqrt{2}}, 0\right)$$

and

$$\|\boldsymbol{t}'(s)\| = \sqrt{\frac{1}{4}cos^2\frac{s}{\sqrt{2}} + \frac{1}{4}sin^2\frac{s}{\sqrt{2}}} = \frac{1}{2}.$$

It holds that

$$\boldsymbol{n}(s) = \left(-cos\frac{s}{\sqrt{2}}, -sin\frac{s}{\sqrt{2}}, 0\right)$$

Then the equation of the curve $\boldsymbol{\alpha_n}(s)$ is,

$$\begin{aligned}\boldsymbol{\alpha_n}(s) &= \left(cos\frac{s}{\sqrt{2}}, sin\frac{s}{\sqrt{2}}, \frac{s}{\sqrt{2}}\right) + r\left(-cos\frac{s}{\sqrt{2}}, -sin\frac{s}{\sqrt{2}}, 0\right)\\ &= \left(cos\frac{s}{\sqrt{2}} - rcos\frac{s}{\sqrt{2}}, sin\frac{s}{\sqrt{2}} - rsin\frac{s}{\sqrt{2}}, \frac{s}{\sqrt{2}}\right)\\ &= \left((1-r)cos\frac{s}{\sqrt{2}}, (1-r)sin\frac{s}{\sqrt{2}}, \frac{s}{\sqrt{2}}\right).\end{aligned}$$

So it can be easily obtained that

$$\boldsymbol{\alpha_n}'(s) = \left(-\frac{(1-r)}{\sqrt{2}}sin\frac{s}{\sqrt{2}}, \frac{(1-r)}{\sqrt{2}}cos\frac{s}{\sqrt{2}}, \frac{1}{\sqrt{2}}\right)$$

and

$$\|\boldsymbol{\alpha_n}'(s)\| = \left(\left(-\frac{(1-r)}{\sqrt{2}}sin\frac{s}{\sqrt{2}}\right)^2 + \left(\frac{(1-r)}{\sqrt{2}}cos\frac{s}{\sqrt{2}}\right)^2 + \left(\frac{1}{\sqrt{2}}\right)^2\right)^{1/2} = \sqrt{\frac{r^2-2r+2}{2}}.$$

Hence our curve is not unit speed curve. If we make the necessary calculations on arbitrary speed curves, then the following equalities hold:

$$\boldsymbol{\alpha_n}''(s) = \left(-\frac{(1-r)}{2}cos\frac{s}{\sqrt{2}}, -\frac{(1-r)}{2}sin\frac{s}{\sqrt{2}}, 0\right)$$

$$\boldsymbol{\alpha_n}'''(s) = \left(\frac{(1-r)}{2\sqrt{2}}sin\frac{s}{\sqrt{2}}, -\frac{(1-r)}{2\sqrt{2}}cos\frac{s}{\sqrt{2}}, 0\right)$$

$$\boldsymbol{\alpha_n}'(s) \times \boldsymbol{\alpha_n}''(s) = \begin{vmatrix} U_1 & U_2 & U_3 \\ -\frac{(1-r)}{\sqrt{2}}sin\frac{s}{\sqrt{2}} & \frac{(1-r)}{\sqrt{2}}cos\frac{s}{\sqrt{2}} & \frac{1}{\sqrt{2}} \\ -\frac{(1-r)}{2}cos\frac{s}{\sqrt{2}} & -\frac{(1-r)}{2}sin\frac{s}{\sqrt{2}} & 0 \end{vmatrix}$$

$$= \left(\frac{(1-r)}{2\sqrt{2}}sin\frac{s}{\sqrt{2}}, -\frac{(1-r)}{2\sqrt{2}}cos\frac{s}{\sqrt{2}}, \frac{(1-r)^2}{2\sqrt{2}}\right)$$

and

$$\|\boldsymbol{\alpha_n}'(s)\times\boldsymbol{\alpha_n}''(s)\| = \sqrt{\left(\frac{1-r}{2\sqrt{2}}\right)^2+\left(\frac{(1-r)^2}{2\sqrt{2}}\right)^2} = \frac{|1-r|\sqrt{2-2r+r^2}}{2\sqrt{2}}$$

$$\langle\boldsymbol{\alpha}_n'(s)\times\boldsymbol{\alpha}_n''(s),\boldsymbol{\alpha}_n'''^{(s)}\rangle = \left(\frac{(1-r)}{2\sqrt{2}}\right)^2 sin^2\frac{s}{\sqrt{2}}+\left(\frac{(1-r)}{2\sqrt{2}}\right)^2 cos^2\frac{s}{\sqrt{2}} = \left(\frac{(1-r)}{2\sqrt{2}}\right)^2$$

Then Frenet frame of the curve is;

$$\boldsymbol{t_n}(s) = \frac{\boldsymbol{\alpha_n}'(s)}{\|\boldsymbol{\alpha_n}'(s)\|} = \frac{\sqrt{2}}{\sqrt{r^2-2r+2}}\left(-\frac{(1-r)}{\sqrt{2}}sin\frac{s}{\sqrt{2}},\frac{(1-r)}{\sqrt{2}}cos\frac{s}{\sqrt{2}},\frac{1}{\sqrt{2}}\right)$$

$$\boldsymbol{b_n}(s) = \frac{\boldsymbol{\alpha}_n'(s)\times\boldsymbol{\alpha}_n''(s)}{\|\boldsymbol{\alpha}_n'(s)\times\boldsymbol{\alpha}_n''(s)\|} = \frac{2\sqrt{2}}{|1-r|\sqrt{2-2r+r^2}}\left(\frac{(1-r)}{2\sqrt{2}}sin\frac{s}{\sqrt{2}},-\frac{(1-r)}{2\sqrt{2}}cos\frac{s}{\sqrt{2}},\frac{(1-r)^2}{2\sqrt{2}}\right)$$

$$= \pm\frac{1}{\sqrt{2-2r+r^2}}\left(sin\frac{s}{\sqrt{2}},-cos\frac{s}{\sqrt{2}},1-r\right)$$

$$\boldsymbol{n_n}(s) = \boldsymbol{b_n}(s)\times\boldsymbol{t_n}(s) = \pm\frac{\sqrt{2}}{2-2r+r^2}\begin{vmatrix} U_1 & U_2 & U_3 \\ sin\frac{s}{\sqrt{2}} & -cos\frac{s}{\sqrt{2}} & 1-r \\ -\frac{(1-r)}{\sqrt{2}}sin\frac{s}{\sqrt{2}} & \frac{(1-r)}{\sqrt{2}}cos\frac{s}{\sqrt{2}} & \frac{1}{\sqrt{2}} \end{vmatrix}$$

$$= \pm\frac{\sqrt{2}}{2-2r+r^2}\left(\left(-\frac{1}{\sqrt{2}}-\frac{(1-r)^2}{\sqrt{2}}\right)cos\frac{s}{\sqrt{2}},\left(-\frac{(1-r)^2}{\sqrt{2}}-\frac{1}{\sqrt{2}}\right)sin\frac{s}{\sqrt{2}},0\right)$$

$$= \pm\left(-cos\frac{s}{\sqrt{2}},-sin\frac{s}{\sqrt{2}},0\right).$$

The curvature and torsion functions of the curve are given as follows:

$$\kappa_n(s) = \frac{\|\boldsymbol{\alpha_n}'(s)\times\boldsymbol{\alpha_n}''(s)\|}{\|\boldsymbol{\alpha_n}'(s)\|^3} = \frac{\frac{|1-r|\sqrt{2-2r+r^2}}{2\sqrt{2}}}{\left(\sqrt{\frac{r^2-2r+2}{2}}\right)^3} = \frac{|1-r|}{2(r^2-2r+2)}$$

$$\tau_n(s) = \frac{\langle\boldsymbol{\alpha}_n'(s)\times\boldsymbol{\alpha}_n''(s),\boldsymbol{\alpha_n}'''(s)\rangle}{\|\boldsymbol{\alpha_n}'(s)\times\boldsymbol{\alpha_n}''(s)\|^2} = \frac{\left(\frac{(1-r)}{2\sqrt{2}}\right)^2}{\left(\frac{|1-r|\sqrt{2-2r+r^2}}{2\sqrt{2}}\right)^2} = \pm\frac{1-r}{\sqrt{2-2r+r^2}}.$$

This shows that parallel curve is also a helix for $r \neq 1$ (Figure 2).

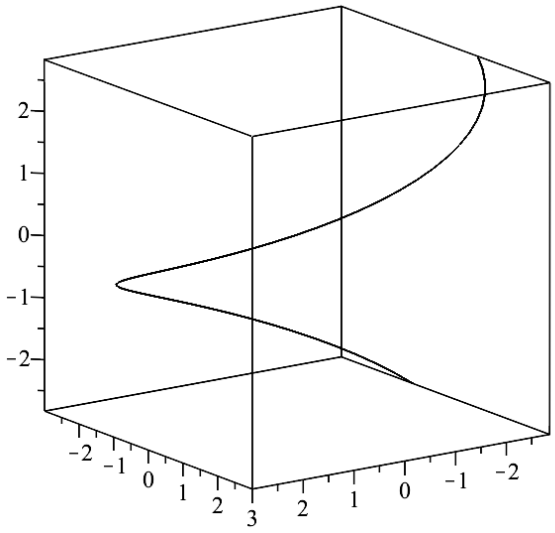

Figure 2. *Parallel curve* $\alpha_n(s)$ *for* $r = -2$

Remark: For $r \neq 1$, parallel curves give a family of helices whose axis is the z axis.

Acknowledgements *-*

Funding/Financial Disclosure The authors have no received any financial support for the research, authorship, or publication of this study.

Ethics Committee Approval and Permissions The work does not require ethics committee approval and any private permission.

Conflict of Interests The authors stated that there are no conflict of interest in this article.

Authors Contribution Authors contributed equally to the study.

References

[1] Arslan, K., & Hacısalihoğlu, H. H. (2000). On harmonic curvatures of a frenet curve. *Communications De La Faculte des Sciences de L'Universite D'Ankara*", *49*, 015-023. https://doi.org/10.1501/Commua1_0000000374

[2] Ergin, A. A. (1992). On the generalized darboux curves, *Communications De La Faculte des Sciences de L'Universite D'Ankara*", *41*, 073-077. https://doi.org/10.1501/Commua1_0000000499

[3] Liu, H., & Wang, F. (2008). Mannheim partner curves in 3-space. *Journal of Geometry*, *88*(1-2), 120-126. https://doi.org/10.1007/s00022-007-1949-0

[4] İlarslan, K., & Nesovic, E. (2008). Some characterization of rectifying curves in the Euclidean Space E^4, *Turkish Journal of Mathematics*, *32*, 21-30.

[5] Has, A., & Yılmaz, B. (2022). On quaternionic bertrand curves in euclidean 3-space. *Turkish Journal of. Mathematics and Computer Science, 14*(2), 355-365. https://doi.org/10.47000/tjmcs.1021801

[6] Sağıroğlu, Y. (2015). Global differential invariants of affine curves in R2. *Far East Journal of Mathematical Sciences*, *96*(4), 497-515.

[7] Divjak, B. (2003). Special curves on ruled surface in galilean and pseudo-galilean space. *Acta Mathematica Hungarica, 98*(3), 203-215. https://doi.org/10.1023/A:1022821824927

[8] Bükcü, B., & Karacan, M. K. (2008). Bishop frame of the spacelike curve with a spacelike principal normal in minkowski 3-space. *Communications De La Faculte des Sciences de L'Universite D'Ankara*", *57*(1), 13-22. https://doi.org/10.1501/Commua1_0000000185

[9] Şenyurt, S., Canlı, D., & Ayvacı, K. H. (2022). Associated curves from a different point of view in E^3. *Communications Faculty of Sciences University of Ankara Series A1 Mathematics and Statistics, 71*(3), 826-845. https://doi.org/10.31801/cfsuasmas.1026359

[10] Güler, F. (2022). The quasi parallel curve of a space curve. *Celal Bayar University Journal of Science, 18*(2), 203-206. https://doi.org/10.18466/cbayarfbe.955974

[11] Srivastava, A., Klassen, E., Shantanu, H. J., & Jermyn, I. H. (2011). Shape analysis of elastic curves in euclidean spaces. *IEEE Transactions on Pattern Analysis and Machine Intelligence, 33*(7), 1415-1428. https://doi.10.1109/TPAMI.2010.184

[12] S´anchez-Reyes, J. (2015). Detecting symmetries in polynomial B´ezier curves. *Journal of Computational and Applied Mathematics, 288*, 274-283. https://doi.org/10.1016/j.cam.2015.04.025

[13] Gözütok, U., Çoban, H. A., & Sağıroğlu, Y. (2019). Frenet frame with respect to conformable derivative. *Filomat, 33*(6), 1541-1550. https://doi.org/10.2298/FIL1906541G

[14] Aldossary, M., T., & Gazwani, M. A. (2020). Motion of parallel curves and surfaces in euclidean 3-space R^3. *Global Journal of Advanced Research on Classical and Modern Geometries, 9*(1), 43-56.

[15] O'Neill, B. (2006). *Elementary Differential Geometry, Revised Second Edition,* Elsevier, USA.

Sinopfbd, 2024; 9(1): 14-25 **https://doi.org/10.33484/sinopfbd.1344047**

Sinop Üniversitesi Fen Bilimleri Dergisi
Sinop Uni J Nat Sci
E-ISSN: 2564-7873

https://dergipark.org.tr/tr/pub/sinopfbd

Böceklerle İlişkili *Micrococcus* sp. Türlerinin Moleküler Karakterizasyonu ve *Galleria mellonella* (Lepidoptera: Pyralidae)'ya Karşı Virülansları

Ali SEVİM

How to cite: Sevim, A. (2024). Böceklerle ilişkili *Micrococcus* sp. türlerinin moleküler karakterizasyonu ve *Galleria mellonella* (Lepidoptera: Pyralidae)'ya karşı virülansları. *Sinop Üniversitesi Fen Bilimleri Dergisi, 9*(1), 14-25. https://doi.org/10.33484/sinopfbd.1344047

Araştırma Makalesi

Sorumlu Yazar
Ali SEVİM
ali.sevim@ahievran.edu.tr

Yazara ait ORCID
A.S: 0000-0003-2472-599X

Received: 15.08.2023
Accepted: 22.01.2024

Öz

Şimdiye kadar 100'den fazla bakteri türünün eklem bacaklılarda hastalık oluşturduğu bilinmektedir. Entomopatojenik bakteriler ucuz olmaları, kitle üretimindeki kolaylık, konak spesifikliği, güvenlik ve çevrede kalıcılık gibi nedenlerden ötürü zararlı böceklerle mikrobiyal mücadelede uzun yıllardan beri kullanılmaktadır. Bu çalışmada çeşitli böcek örneklerinden (*Malacosoma* sp. (Lepidoptera: Lasiocampidae), *Ogcodocera* sp. (Diptera: Bombyliidae) ve *Orgyia* sp. (Lepidoptera: Erebidae)) izole edilen altı (6) adet bakteri suşu ilk etapta morfolojik olarak *Micrococcus* sp. olarak tanımlanmıştır. Daha sonra bu bakteri suşlarının 16S rRNA sekans analizi ile moleküler seviyede tanımlanmaları gerçekleştirilmiştir. Ayrıca bu bakteri suşlarının *Galleria mellonella* (Lepidoptera: Pyralidae) larvalarına karşı öldürücülük etkileri belirlenmiştir. Altı adet bakteri suşu da (MK-5, AS-2, AS-3, AS-4, BB-1 ve BB-5) *Micrococcus* sp. olarak cins düzeyinde tanımlanmıştır. *G. mellonella* larvalarına karşı patojenite testleri sonucunda ise sadece MK-5 suşu %70 ölüm oranına neden olmuş diğer suşlar önemli derecede ölüm oranına neden olmamıştır. Elde edilen sonuçların böceklerle ilişkili simbiyotik bakterilerin tanımlanmasında ve patojenik özelliklerinin belirlenmesinde faydalı olacağı düşünülmektedir.

Anahtar Kelimeler: *Malacosoma* sp., *Ogcodocera* sp., *Orgyia* sp., *Micrococcus*, 16S rRNA, virülans

Molecular Characterization of *Micrococcus* sp. Associated with Insects and Their Virulence Against *Galleria mellonella* (Lepidoptera: Pyralidae)

Kırşehir Ahi Evran Üniversitesi, Ziraat Fakültesi, Bitki Koruma Bölümü, Kırşehir, Türkiye

Abstract

So far, more than 100 species of bacteria are known to cause disease in arthropods. Entomopathogenic bacteria have been used for many years in the microbial control of insect pests due to reasons such as cheapness, ease of mass production, host specificity, safety, and persistence in the environment. In this study, six (6) bacterial strains isolated from various insect samples (*Malacosoma* sp. (Lepidoptera: Lasiocampidae), *Ogcodocera* sp. (Diptera: Bombyliidae) and *Orgyia* sp. (Lepidoptera: Erebidae)) were initially identified as *Micrococcus* sp. at morphological level. These bacterial strains were then identified by 16S rRNA sequence analysis at the molecular level. In addition, the mortality effects of these bacterial strains against *Galleria mellonella* (Lepidoptera: Pyralidae) larvae were determined. Six bacterial strains (MK-5, AS-2, AS-3, AS-4, BB-1, and BB-5) were identified at the genus level as *Micrococcus* sp. As

a result of pathogenicity tests against *G. mellonella* larvae, only the MK-5 strain caused a 70% mortality rate, while the other strains did not cause a significant mortality rate. It is thought that the obtained results could be useful in identifying symbiotic bacteria associated with insects and determining their pathogenic properties.

Keywords: *Malacosoma* sp., *Ogcodocera* sp., *Orgyia* sp., *Micrococcus*, 16S rRNA, virulence

Giriş

Böcekler Dünya üzerinde yaşayan en büyük canlı grubunu oluşturmaktadırlar ve ekosistemde anahtar role sahiptirler. Diğer canlılar gibi böcekler de ekolojilerini ve evrimlerini derin şekilde etkileyen mikroorganizmalarla yakın ilişki içerisinde yaşarlar. Bakteriler, arkealar, funguslar, protozoalar ve virüsler gibi mikroorganizmalar böcek konakları ile kalıcı veya geçici olarak ilişki içerisindedirler [1]. Diğer ökaryotik sistemler gibi farklı böcek ve mikroplar arasındaki simbiyotik ilişkiler mutualistik, kommensalistik, saprofitik ve parazitik (veya patojenik) şeklinde olabilmektedir [2]. Böceklerde yaşayan simbiyotik mikroorganizmalar böceklerin biyolojisi ve fizyolojisindeki pek çok olayı etkilemektedir. Örneğin bu mikroorganizmalar besinlerin sindirilmesi, besin alınımı, üreme, bağışıklığı kuvvetlendirme ve bitki konağı savunma mekanizmasının üstesinden gelme gibi pek çok farklı görevlerde rol alabilmektedir [3, 4]. Böcek grupları içerisinde Lepidoptera takımına ait üyeler Dünya çapında en önemli tarım zararlılarını içermektedir ve bu grup en çeşitli ikinci böcek takımını oluşturmaktadır. Ancak Lepidoptera üyelerinin biyolojisinde temel rol oynayan bakteri türlerine dair net kanıtlar oldukça azdır [5]. Bu yüzden bu takımın üyelerine ait bakteri türlerinin tanımlanması ve rollerinin araştırılması ihtiyaç duyulan bir konu olarak karşımıza çıkmaktadır. Böceklerle ilişikli olan bakterilerin birçoğu mutualistik olmasına rağmen sadece sınırlı sayıda bakteri böceklerde patojenik etkiye sahiptir [6]. Entomopatojenik bakteriler ve ürettikleri toksinler mikrobiyal insektisitler içerisinde ucuz, kitle üretim kolaylığı, konak spesifikliği ve güvenlik gibi nedenlerden ötürü ticari olarak en başarılı olanlardır. Bu organizmalar sindirim sisteminden konağa girmekte, burada toksin üretmekte (veya diğer bazı patojenik faktörleri), bu toksinler orta bağırsak epitelini yıkmakta ve hemosele ulaşarak konak böceği sepsis ile öldürmektedirler [7]. Entomopatojenik bakterilerin çoğunluğu Bacillaceae, Pseudomonadaceae, Enterobacteriaceae, Streptococcaceae ve Micrococcaceae familyası içerisinde yer almaktadır. Bu familyalar arasında en fazla dikkati Bacillaceae familyası çekmiştir [8]. Bacillaceae familyası içerisinde ise en fazla çalışılan tür *Bacillus thuringiensis* (*Bt*) olup toplam insektisit piyasasının yaklaşık %2'sini oluşturmaktadır [9]. *Micrococcus* cinsi spor oluşturmayan, genellikle hareketsiz, Gram pozitif, düzensiz kümeler oluşturan veya tetradlar halinde bulunan küre şeklindeki hücrelerden oluşmaktadır. Cins içerisindeki pek çok tür karotenoid pigment üretmektedir. Cins içerisinde şimdiye kadar toplam dokuz tür tanımlanmıştır (*M. luteus*, *M. lylae*, *M. varians*, *M. roseus*, *M. aqilis*, *M. kristinae*, *M. nishino miyaensis*, *M. sedentarius* ve *M. halobius*) [10]. İnsanları da içeren sıcak kanlı hayvanların derisi genellikle gıdaları kontamine eden *Micrococcus* suşlarının ana rezervuarıdır. Genel

olarak *Micrococcus* cinsi patojenik olarak değerlendirilmez ama bazı türlerin fırsatçı patojen olarak bazı enfeksiyonlara neden olduğu bildirilmiştir [11, 12]. Bu çalışmada çeşitli böcek örneklerinden izole edilen *Micrococcus* sp. suşlarının 16S rRNA dizin analizi ile karakterizasyonu yapılmıştır. Ayrıca elde edilen suşların *Galleria mellonella* (Lepidoptera: Pyralidae) üzerindeki öldürücülük etkileri belirlenmiştir. Elde edilen sonuçların *Micrococcus* türlerinin patojenik özelliklerinin (özellikle böcekler açısından) belirlenmesi açısından faydalı olacağı düşünülmektedir.

Materyal ve Metot

Micrococcus Suşları

Çalışmada kullanılan *Micrococcus* sp. suşları Lepidoptera takımına ait çeşitli böcek örneklerinden (*Malacosoma* sp. (Lepidoptera: Lasiocampidae), *Ogcodocera* sp. (Diptera: Bombyliidae) ve *Orgyia* sp. (Lepidoptera: Erebidae) izole edilmiştir. Larva örnekleri Kırşehir il sınırları içerisinden toplanmıştır. Larvalardan bakteri izolasyonu Demirci ve arkadaşlarının çalışmasında belirtilen yönteme göre gerçekleştirilmiştir [13]. İzole edilen suşlar çizgi ekim ile saflaştırıldıktan sonra 3 ml nütrient broth besiyerinde 30ºC'de gece boyu büyütülmüş ve -20°C'de %20'lik gliserol içerisinde daha sonraki çalışmalarda kullanılmak üzere saklanmıştır. Suşlar sarı pigment üretimi, S-tipi koloni ve küre şeklindeki hücrelere göre seçilmiştir.

16S rRNA Dizin Analizi

Micrococcus sp. suşlarının moleküler karakterizasyonu için 16S rRNA dizin analizi kullanılmıştır. Bunun için stok kültürlerden nütrient agar besiyerine çizgi ekim yapılmış ve 30ºC'de gece boyu inkübasyona bırakılmıştır. Buradan tek koloniler seçilerek genomik DNA izolasyonunda kullanılmıştır. Bakteriyel suşlardan genomik DNA izolasyonu Sambrook ve ark. [14] tarafından belirlenen standart prosedüre göre gerçekleştirilmiştir. *Micrococcus* türleri gram pozitif bakteriler olduğundan standart prosedür uygulamasından önce lizozim enzimi ile hücre duvarının parçalanması sağlanmıştır. İzole edilen DNA'lar 50 µL Tris-EDTA tamponu (10 mmol/L Tris-HCl, 1 mmol/L EDTA, pH 8.0) içerisinde çözülmüş ve kullanılıncaya kadar -20°C'de muhafaza edilmiştir. Her bir bakteriyel suş için 16S rRNA gen bölgesini çoğaltmada ileri primer olarak 27F (5′-AGAGTTTGATCMTGGCTCAG-3′) ve geri primer olarak ise 1492R (5′- GGYTACCTTGTTACGACTT-3′) (Macrogen) kullanılmıştır. PCR reaksiyonları 5 µL 10× *Taq* DNA polimeraz reaksiyon tamponu, 1,5 µL 10 mmol/L dNTP karışımı, 1.5 µL 10 pmol her bir primerden, 1 µL 5 U/ µL *Taq* DNA polimeraz (Fermentas), 3 µL 5 mM $MgCl_2$, 2 µL (100 ng) genomik DNA ve 34.5 µL dH_2O olacak şekilde ayarlanmıştır. PCR koşulları ise 2 dk 94°C'de başlangıç denatürasyonundan sonra 35 döngü (45 s 94°C (denatürasyon), 60 s 55°C (bağlanma) ve 60 s 72°C (uzama) olacak şekilde ayarlanmıştır. Son uzama adımı ise 10 dk 72°C olacak şekilde ayarlanmıştır. PCR reaksiyonlarından sonra her bir PCR ürünü etidyum bromür içeren %1'lik agaroz jelde 90 V'da yürütülmüş ve doğru olarak tespit edilen bantlar saflaştırıldıktan sonra dizin analizi için

Macrogen (Hollanda) firmasına gönderilmiştir. 518F (5′-CCAGCAGCCGCGGTAATACG-3′) ve 800R (5′-TACCAGGGTATCTAATCC -3′) primer çifti dizin analizi için kullanılmıştır [13]. Elde edilen sekanslar NCBI GenBank'ta yer alan BLAST soruşturmasına tabi tutulmuş ve bakteriyel suşların en yakın ilişkili oldukları türler/suşlar belirlenmiştir [15, 16]. Son olarak elde edilen sekanslar filogenetik ağaç oluşturmak için kullanılmıştır.

Patojenite Testleri

G. mellonella'ya karşı patojenite testleri için her bir bakteriyel izolat stok kültürlerden çıkartılmış ve nütrient agar (NA) besiyerine çizgi ekimleri yapılmıştır. Buradan alınan tek koloniler her bir bakteri için ayrı ayrı 3 ml nütrient broth (NB) besiyerine inoküle edilmiş ve 30°C'de çalkalamalı inkübatörde gece boyu inkübasyona bırakılmıştır. İnkübasyon periyodunun sonunda bakteriyel hücre yoğunluğu PBS (fosfat tampon solüsyonu) kullanılarak 600_{nm}'de 1.8×10^9 cfu/ml olacak şekilde ayarlanmıştır [17]. Bioassay deneyleri için, sağlıklı *G. mellonella* larvaları (3 veya 4. evre) laboratuvar kültürlerinden elde edilmiş ve rastgele seçilerek yalnızca sağlıklı larvalar patojenite deneylerinde kullanılmıştır. 20 gr taze hazırlanmış yapay besin (180 gr bal, 180 gr gliserin, 50 gr bal mumu, 260 gr buğday unu, 80 gr kuru maya ve 50 gr buğday kepeği [18] yukarıda anlatıldığı şekilde hazırlanan 1 ml bakteriyel solüsyonla inoküle edilmiştir. Kontrol grubu sadece steril PBS ile inoküle edilmiştir. İnoküle edilmiş yapay besinler ayrı olarak plastik kutular (10 × 10 × 5) içerisine yerleştirilmiştir. Kutuların kapağı hava alması için delinmiştir. Daha sonra 10 adet sağlıklı larva her bir tekrar ve bakteriyel izolat için kontamine besin içeren kuyulara yerleştirilmiş ve larvaların beslenmesi sağlanmıştır. Her bir tekrar için 10 larva kullanılmış ve bütün deneyler 3 kere tekrar edilmiştir. Son olarak plastik kutular 25°C'de inkübasyona bırakılmış ve 10. gün sonunda ölü larvalar sayılmıştır [19].

Veri Analizi

Bakteriyel suşların 16S rRNA genlerine ait sekanslar Bioedit 7.1.3.0 programı ile işlenmiştir [20]. Bakteriyel suşlara ait 16S rRNA sekansları ve GenBank'tan alınan en yakın ilişkili oldukları bakteri suşlarına ait 16S rRNA sekansları Bioedit programında yer alan ClustalW ile hizalanmıştır [20, 21]. Hizalama sonucunda bütün sekansların baş ve son bölgelerinden gerekli kesimler yapılmıştır. Bakteriyel izolatların birbirleri ile olan filogenetik ilişkisi Neighbor-Joining (NJ) metodu kullanarak p-distance analizi ile gerçekleştirilmiştir. Elde edilen ağacın iç dallarının güvenilirliği 1.000 tekrara dayalı bootstrap analizi ile gerçekleştirilmiştir. Analizler MEGA 11.0.13 programı ile gerçekleştirilmiştir [22]. Ölüm değerleri Abbott formülü kullanılarak anlamlandırılmıştır ve yüzde (%) ölüm değerleri hesaplanmıştır [23]. Ölüm değerleri açısından bakteriyel izolatları birbirleri ile karşılaştırmak için tek yönlü varyans analizi (ANOVA) kullanılmıştır. Post hoc testi olarak Tukey testi kullanılmıştır. Bütün veriler Arcsin transformasyonuna tabi tutulmuş ve Levene istatistiği kullanılarak varyans homojenitesi açısından değerlendirilmiştir. Analizler Minitab 17.1.0 programı ile gerçekleştirilmiştir.

Bulgular

Yapılan çalışmada üç farklı böcek örneğinden toplam olarak 6 adet *Micrococcus* sp. suşu elde edilmiştir. *Micrococcus* suşları başlangıçta morfolojik olarak sarı pigment üretmeleri ve düz koloni (S-tipi) oluşturmaları ile seçilmiştir. Daha sonra hücresel düzeyde incelemeler yapılmış ve hepsinin tetradlar veya düzensiz kümeler oluşturan bakteriler oldukları tespit edilmiştir. Bakteriyel suşların moleküler karakterizasyonlarını yapmak için 16S rRNA gen bölgesinin dizin analizi yapılmış ve yüzde (%) benzerlikler ortaya konmuştur. *Micrococcus* izolatlarının 16S rRNA gen bölgesine göre BLAST (GenBank) yüzde (%) benzerlik sonuçları, 16S rRNA gen bölgesi için GenBank numaraları ve izole edildikleri böcek türü Tablo 1'de verilmektedir. Yapılan karakterizasyon çalışmaları sonrasında bütün suşlar (MK-5, AS-2, AS-3, AS-4, BB-1 ve BB-5) *Micrococcus* sp. olarak tanımlanmıştır. Yapılan filogenetik analizler bunu desteklemektedir (Şekil 1).

Tablo 1. *Micrococcus izolatlarının 16S rRNA gen bölgesine göre BLAST (GenBank) yüzde (%) benzerlik sonuçları, 16S rRNA gen bölgesi için GenBank numaraları ve izole edildikleri böcek türü*

İzolat	GenBank numarası	Bakteri türü	En yakın ilişkili olduğu bakteri türleri ve suşları	Örtüşen baz oranı (%)	Yüzde (%) benzerlik	İzole edilen böcek türü
MK-5	OR436472	*Micrococcus* sp.	*Micrococcus* sp. WY3	%99	%99.57	*Malacosoma* sp. (Lepidoptera: Lasiocampidae)
			Micrococcus yunnanensis SJU9	%99	%99.42	
			Micrococcus sp. KA-26	%99	%99.49	
AS-2	OR436473	*Micrococcus* sp.	*Micrococcus* sp. 70025	%98	%99.57	*Ogcodocera* sp. (Diptera: Bombyliidae)
			Micrococcus endophyticus ZGTB14-30	%99	%99.49	
			Micrococcus luteus SC1204	%99	%99.49	
AS-3	OR436474	*Micrococcus* sp.	*Micrococcus endophyticus* S10-46	%99	%99.64	*Ogcodocera* sp. (Diptera: Bombyliidae)
			Micrococcus sp. MG-2010-D12	%99	%99.64	
			Micrococcus sp. MDYND	%99	%99.57	
AS-4	OR436475	*Micrococcus* sp.	*Micrococcus* sp. DSM 105846	%100	%99.58	*Ogcodocera* sp. (Diptera: Bombyliidae)
			Micrococcus sp. CM-CNRG 613	%100	%99.58	
			Micrococcus luteus CGAPGPBBS-084	%100	%99.58	
BB-1	OR436476	*Micrococcus* sp.	*Actinomycetia bacterium* 1032-12.1	%99	%99.93	*Orgyia* sp. (Lepidoptera: Erebidae)
			Micrococcus sp. JNU-H022	%99	%99.93	
			Micrococcus luteus H399	%99	%99.93	
BB-5	OR436477	*Micrococcus* sp.	*Micrococcus* sp. F.1	%99	%99.49	*Orgyia* sp. (Lepidoptera: Erebidae)
			Micrococcus yunnanensis QT410	%100	%99.42	
			Micrococcus sp. XHTSA12	%100	%99.42	

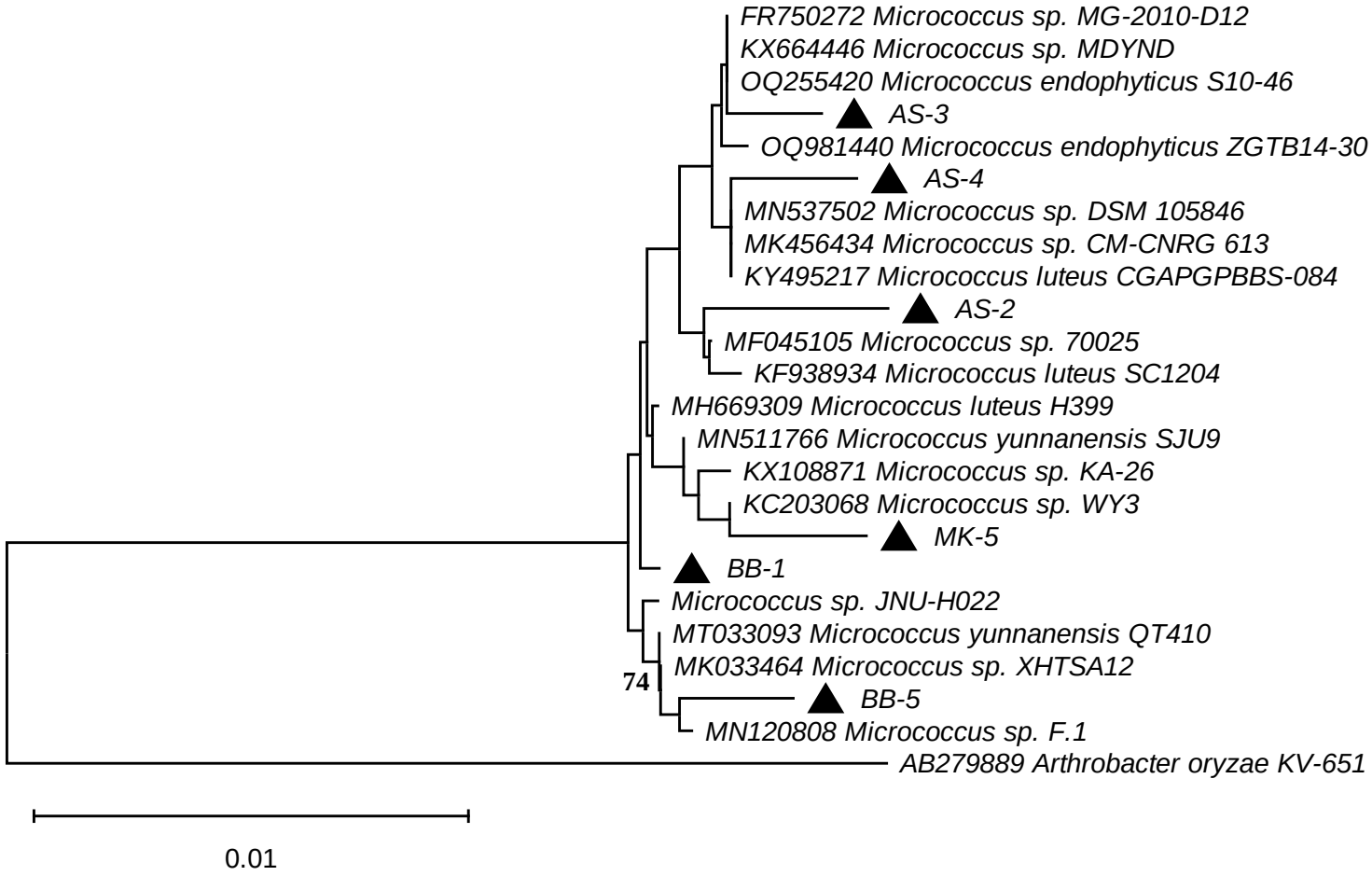

Şekil 1. *Çeşitli böcek örneklerinden izole edilen Micrococcus sp. suşlarının en yakın ilişkili oldukları bakteri türleri ile ilişkisini gösteren dendogram. Filogenetik ağaç 16S rRNA gen bölgesinin kısmi sekansı (yaklaşık 1.500 bp) elde edilerek oluşturulmuştur. Ağaç Neighbor-Joining (N-J) analizi kullanarak p-distance metodu ile oluşturulmuştur. Bootstrap analizi 1000 yalancı tekrara dayalı olarak oluşturulmuş ve %70 ve yukarısında olanlar ağacın dallarında gösterilmiştir. Siyah üçgen Micrococcus sp. suşlarını göstermektedir. Ağacın dibinde yer alan ölçek ise genetik mesafeyi temsil etmektedir. Arthrobacter oryzae KV-651 dış grup olarak kullanılmıştır*

Yapılan patojenite testleri sonucunda sadece bir suş (MK-5) hariç diğerlerinin hepsi kontrol grubu ile aynı ölüm değerine neden olmuştur ($F=12.9$, $df=6$, $p<0.05$). MK-5 suşu ise %70'lik değer ile kontrol grubu ve diğer suşlardan anlamlı derecede farklı ölüm oranına neden olmuştur ($F=12.9$, $df=6$, $p<0.05$) (Şekil 2). En yüksek ölüm değeri MK-5 suşundan elde edilmiştir.

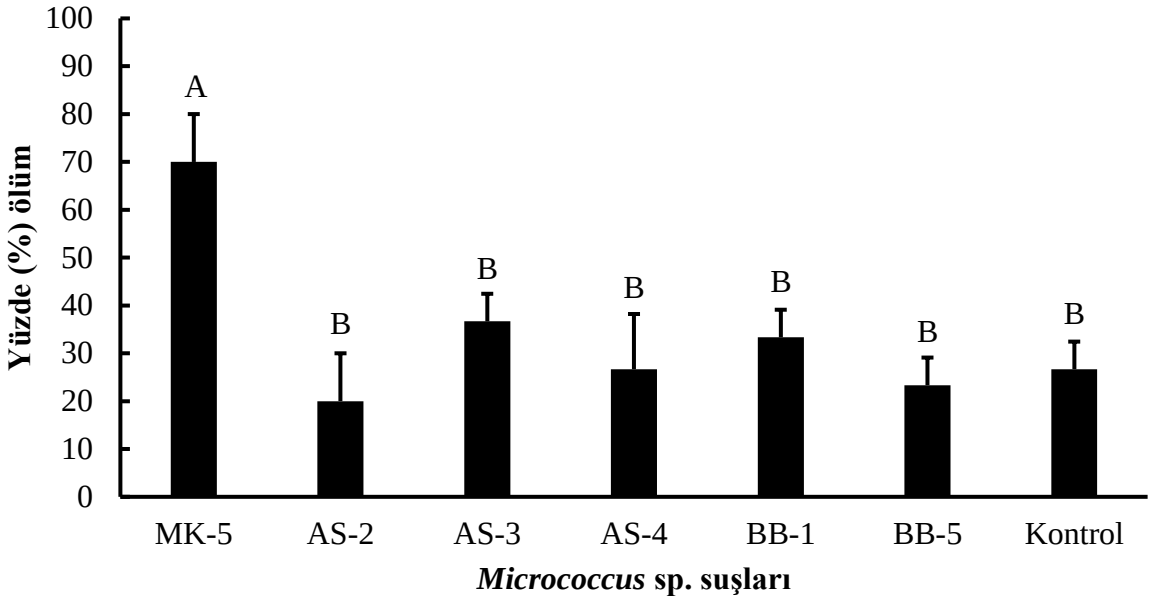

Şekil 2. *Micrococcus sp. izolatlarının 1.8 × 10^9 cfu/ml bakteriyel konsantrasyon kullanarak G. mellonella larvalarına karşı uygulamadan sonra 10. gün sonunda patojenite değerleri. Ölüm değerleri Abbott formülü kullanılarak anlamlandırılmıştır [22]. Barlar standart hatayı göstermektedir. Büyük harfler larva ölüm değerleri arasındaki istatistiksel farklılığı göstermektedir.*

Tartışma ve Sonuç

Mikrobiyal pestisitler bakteri, fungus, virüs, protozoa ve alg gibi mikroorganizmalardan türetilen ve zararlıları kontrol etmek için kullanılan ürünlerdir. Mikroplar genellikle zararlıların büyümesini engellemek veya öldürmek için toksik metabolitleri kullanmaktadırlar [24]. Mikrobiyal pestisitler içerisinde bakteriyal insektisitler ise ticari olarak en fazla önem verilen grubu oluşturmaktadır [25]. Yaklaşık olarak 100 bakteri eklem bacaklılarda patojen olarak tanımlanmasına rağmen sadece birkaç tanesi ticari olarak üretilmektedir. Ticari olarak üretilen türler arasında en fazla önem gösterilen ve popülerlik kazanan türler ise *Bacillus thuringiensis* (*Bt*) ve *Serratia entomophila*'dır [26]. *Micrococcus* suşları toprak, tatlı ve deniz suyu, kum ve bitkisel vejetasyonlar gibi çok geniş bir karasal ve sucul ortamlarda bulunabilmektedir. Aynı zamanda bu bakteriler insan deri florasından yaygın olarak da izole edilmektedirler [11]. Bu cinse ait bakterilerin böceklerden izole edildiğine dair pek çok çalışma bulunmaktadır [13, 27-29]. Lipa ve Wiland [30] *M. luteus*'un *Agrotis segetum* (Lepidoptera: Noctuidae) larvalarına karşı %8 mortaliteye neden olduğunu göstermişlerdir. Sezen ve Demirbağ [31] aynı bakterinin *Balanicus nucum* (Coleoptera: Curculionidae) larvaları üzerinde %30 ölüm değerine neden olduklarını göstermiştir. Yine Sezen ve Demirbağ [28] *M. luteus* As-4 bakterisinin *Agelastica alni* (Coleoptera: Chrysomelidae) larvaları üzerinde %40 öldürücü etki gösterdiğini belirtmişlerdir. Demirci

ve ark. [13] *M. luteus* Pv8 bakterisinin *Plagiodera versicolora* (L.) (Coleoptera: Chrysomelidae)'nın larvaları üzerinde %50 ve erginleri üzerinde ise %40 ölüme neden olduklarını göstermiştir. Buna karşılık böceklerden izole edilen ve konakları üzerinde patojenik etki göstermeyen *M. luteus* veya *Micrococcus* sp. suşları da bulunmaktadır [27, 32]. Bizim çalışmamızda ise MK-5 suşu (%70 ölüm oranı ile) hariç diğer suşlar insektisidal aktivite göstermemiştir. Bütün bu bilgiler *Micrococcus* türlerinin böceklerle yakından ilişkili olduğunu göstermektedir. Fakat böcek patojeni olduklarına dair kesin bir bilgi bulunmamaktadır. Muhtemelen böceklerle simbiyotik ilişki içerisinde yaşayan bu bakterilerin konaklarındaki rollerinin araştırılmasına yönelik çalışmalara ihtiyaç duyulmaktadır. Ayrıca patojenik özelliklerinin ispatlanması ve doğrulanması için daha detaylı (patolojik ve detaylı bioassay deneyleri gibi) çalışmalara ihtiyaç vardır. Bakteriyel taksonomi mikroorganizmaların tanımlanmasını, isimlendirilmesini ve sınıflandırılmasını içermektedir. Modern bakteriyel taksonomide genel olarak filogenetik ilişkilerin kullanılması kabul görmüştür. Bakteriler arasındaki filogenetik ilişkileri belirlemede en yaygın kullanılan metot 16S rRNA gen bölgesine ait sekansların karşılaştırılmalı analizidir [33]. Oysaki 16S rRNA genine ait sekans analizinde yüzde (%) benzerliğin kullanılması doğru tür tanımlaması açısından pek çok sınırlamalara sahiptir. Bundan dolayı günümüzde DNA-DNA hibridizasyonu, genomun % G+C içeriği, pulsed-field jel elektroforezi, çoklu lokus sekans analizi ya da son zamanlarda tüm genom sekansı gibi teknikler doğru tür tanımlaması için tercih edilmektedir [34, 35]. Bunların yanında yeni nesil dizileme ile büyük destek kazanan mikrobiyal genomik taksonomi, hesaplama araçlarıyla birleştirilmiş genomik bilgi elde etmek için hızlı ve uygun maliyetli yaklaşımlar sağlar, böylece yeni taksonomik yaklaşımların güvenilirliğini arttırmaktadır [34]. Bizim çalışmamızda *Micrococcus* suşları 16S rRNA dizin analizi ile cins düzeyinde tanımlanabilmiştir. Bu suşların (özellikle MK-5'in) bakteriyel taksonomide kullanılan polifazik yaklaşım ile ve özellikle yukarıda sayılan ileri moleküler teknikler ile tür düzeyinde tanımlanmaları gerekmektedir. Sonuç olarak farklı böcek örneklerinden izole edilen *Micrococcus* sp. suşları 16S rRNA dizin analizi ile cins düzeyinde tanımlanmıştır. *G. mellonella* larvalarına karşı patojenik özellikleri belirlenmiş ve en yüksek insektisidal aktivite *Micrococcus* sp. MK-5 (%70) suşundan elde edilmiştir. İleride yapılacak çalışmalar ile bu suşların tür düzeyinde tanımlanması ve MK-5 suşu için detaylı virülans testlerinin yapılması gerekmektedir.

Teşekkür -

Fon/Finansman bilgileri -

Etik Kurul Onayı ve İzinler Çalışma etik kurul izni veya herhangi bir özel izin gerektirmemektedir.

Çıkar çatışmaları/Çatışan çıkarlar-

Yazarların Katkısı- Yazar makalenin son halini okumuş ve onaylamıştır.

Kaynaklar

[1] Gurung, K., Wertheim, B., & Salles, J. (2019). The microbiome of pest insects: It is not just bacteria. *Entomologia Experimentalis et Applicata, 167*, 156-170. https://doi.org/10.1111/eea.12768

[2] Boucias, D. G., & Pendland, J. C. (1998). Insect-Pathogen Relationships. In D. G. Boucias, J. C. Pendland, (Eds), *Principles of Insect Pathology*, (pp. 1-30). Springer.

[3] Zhao, M., Lin, X., & Guo, X. (2022). The role of insect symbiotic bacteria in metabolizing phytochemicals and agrochemicals. *Insects*, *13*(7), 583. https://doi.org/10.3390/insects13070583

[4] Salcedo-Porras, N., Umaña-Diaz, C., de Oliveira Barbosa Bitencourt, R., & Lowenberger, C. (2020). The role of bacterial symbionts in triatomines: An evolutionary perspective. *Microorganisms*, *8*(9), 1438. https://doi.org/10.3390/microorganisms8091438

[5] Paniagua Voirol, L. R., Frago, E., Kaltenpoth, M., Hilker, M., & Fatouros, N. E. (2018). Bacterial symbionts in Lepidoptera: Their diversity, transmission, and impact on the host. *Frontiers in Microbiology*, *9*, 556. https://doi.org/10.3389/fmicb.2018.00556

[6] Ruiu, L. (2015) Insect pathogenic bacteria in integrated pest management. *Insects*, *6*(2), 352-367. https://doi.org/10.3390/insects6020352

[7] Glare, T. R., Jurat-Fuentes, J. L., & O'Callaghan, M. (2017). Basic and Applied Research: Entomopathogenic Bacteria. In L. A. Lacey, (Ed), *Microbial Control of Insect and Mite Pests*. (pp. 47-67), Academic Press.

[8] Kalha, C. S., Singh, P. P., Kang, S. S., Hunjan, M. S., Gupta V., & Sharma R. (2014). Entomopathogenic Viruses and Bacteria for Insect-Pest Control. In Abrol D. P., (Ed), *Integrated Pest Management*, (pp. 225-244). Academic Press.

[9] Bravo, A., Likitvivatanavong, S., Gill, S. S., & Soberón, M. (2011). *Bacillus thuringiensis*: A story of a successful bioinsecticide. *Insect Biochemistry and Molecular Biology*, *41*(7), 423-431. https://doi.org/10.1016/j.ibmb.2011.02.006

[10] Kocur, M., Kloos, W. E., & Schleifer, K. H. (2006). The Genus *Micrococcus*. In Dworkin, M., Falkow, S., Rosenberg, E., & Schleifer, K. H., Stackebrandt, E., (Eds), *The Prokaryotes*, (pp. 961-971). Springer.

[11] Nunez, M. (2014). *Micrococcus*. In Batt C. A., Tortorello M. L., (Eds), *Encyclopedia of Food Microbiology*, (pp. 627-633). Academic Press.

[12] Zhu, M., Zhu, Q., Yang, Z., & Liang, Z. (2021). Clinical characteristics of patients with *Micrococcus luteus* bloodstream infection in a Chinese tertiary-care hospital. *Polish Journal of Microbiology*, *70*(3), 321-326. https://doi.org/10.33073/pjm-2021-030

[13] Demirci, M., Sevim, E., Demir, İ., & Sevim, A. (2013). Culturable bacterial microbiota of *Plagiodera versicolora* (L.) (Coleoptera: Chrysomelidae) and virulence of the isolated strains. *Folia Microbiologica*, *58*(3), 201-210. https://doi.org/10.1007/s12223-012-0199-1

[14] Sambrook, J., Fritsch, E. F., & Maniatis, T. (1989). *Molecular Cloning.* Cold Spring Harbor Laboratory Press, p 19.

[15] Altschul, S. F., Gish, W., Miller, W., Myers, E. W., & Lipman, D. J. (1990). Basic local alignment search tool. *Journal of Molecular Biology*, *215*, 403-410. https://doi.org/10.1016/S0022-2836(05)80360-2

[16] Benson, D. A., Karsch-Mizrachi, I., Clark, K., Lipman, D. J., Ostell, J., & Sayers, E. W. (2012). GenBank. *Nucleic Acids Research*, *40* (Database issue), D48-D53. https://doi.org/10.1093/nar/gks1195

[17] Moar, W. J., Pusztzai-Carey, M., & Mack, T. P. (1995). Toxicity of purified proteins and the HD-1 strain from *Bacillus thuringiensis* against lesser cornstalk borer (Lepidoptera: Pyralidae). *Journal of Economic Entomology*, *88*, 606-609. https://doi.org/10.1093/jee/88.3.606

[18] Meyling, N. N. (2007). Methods for isolation of entomopathogenic fungi from the soil environment. Laboratory manual, DARCOF III: Research in Organic Food and Farming (FØJO III).

[19] Sevim, E., Çocar, M., Sezgin, F. M., & Sevim, A. (2018). Aerobic gut bacterial flora of *Cydia pomonella* (L.) (Lepidoptera: Tortricidae) and their virulence to the host. *Egyptian Journal of Biological Pest Control*, *28*, 30. https://doi.org/10.1186/s41938-018-0036-1

[20] Hall, T. A. (1999). BioEdit: A user-friendly biological sequence alignment editor and analysis program for Windows 95/98/NT. *Nucleic Acids Symposium*, *41*, 95-98.

[21] Thomson, J. D., Higgins, D. G., & Gibson T. J. (1994). Clustal W: Improving the sensitivity of progressive multiple sequence alignment through sequence weighting, position-specific gap penalties and weight matrix choice. *Nucleic Acids Research*, *22*, 4673-4680.

[22] Tamura, K., Stecher, G., & Kumar, S. (2021). MEGA11: Molecular Evolutionary Genetics Analysis Version 11. *Molecular Biology and Evolution*, *38*(7), 3022-3027. https://doi.org/10.1093/molbev/msab120

[23] Abbott, W. S. (1925). A method of computing the effectiveness of an insecticide. *Journal of Economic Entomology*, *18*, 265-267.

[24] Ayilara, M. S., Adeleke, B. S., Akinola, S. A., Fayose, C. A., Adeyemi, U. T., Gbadegesin, L. A., Omole, R. K., Johnson, R. M., Uthman, Q. O., & Babalola, O. O. (2023). Biopesticides as a promising alternative to synthetic pesticides: A case for microbial pesticides, phytopesticides, and nanobiopesticides. *Frontiers in Microbiology*, *14*, 1040901. https://doi.org/10.3389/fmicb.2023.1040901

[25] Jouzani, G. S., Valijanian, E., & Sharafi, R. (2017). *Bacillus thuringiensis*: A successful insecticide with new environmental features and tidings. *Applied Microbiology and Biotechnology*, *101*(7), 2691-2711. https://doi.org/10.1007/s00253-017-8175-y

[26] Chattopadhyay, P., Banerjee, G., & Mukherjee, S. (2017). Recent trends of modern bacterial insecticides for pest control practice in integrated crop management system. *3 Biotech*, *7*(1), 60. https://doi.org/ 10.1007/s13205-017-0717-6

[27] Çelebi, Ö., Sevim, E., & Sevim, A. (2014). Investigation of the internal bacterial flora of *Eurygaster integriceps* (Hemiptera: Scutelleridae) and pathogenicity of the flora members. *Biologia*, *69*, 1365-1375. https://doi.org/10.2478/s11756-014-0445-x

[28] Sezen, K., & Demirbag, Z. (2006). Insecticidal effects of some biological agents on *Agelastica alni* (Coleoptera: Chrysomelidae). *Biologia*, *61*, 687-692. https://doi.org/10.2478/s11756-006-0141-6

[29] Indiragandhi, P., Yoon, C., Yang, J. O., Cho, S., Sa, T. M., & Kim, G. H. (2010). Microbial communities in the developmental stages of B and Q biotypes of sweetpotato whitefly, *Bemisia tabaci* (Hemiptera: Aleyrodidae). *Journal of The Korean Society for Applied. Biological Chemistry*, *53*, 605–617. https://doi.org/10.3839/jksabc.2010.093

[30] Lipa, J. J., & Wiland, E. (1972). Bacteria isolated from cutworms and their infectivity to *Agrotis* sp. *Acta Microbiologicas Polonica*, *4*, 127.140.

[31] Sezen, K., & Demirbag, Z. (1999). Isolation and insecticidal activity of some bacteria from the hazelnut beetle (*Balaninus nucum* L.). *Applied Entomology and Zoology*, *34*, 85-89.

[32] Yaman, M., Nalcacioglu, R., & Demirbag, Z. (2002). Studies on bacterial flora in the population of the fall webworm, *Hyphantria cunea* Drury. (Lep., Arctiidae). *Journal of Applied Entomology, 126*, 470–474. https://doi.org/10.1046/j.1439-0418.2002.00681.x

[33] Vaneechoutte, M., & Heyndrickx, M. (2001). Application and Analysis of ARDRA Patterns in Bacterial Identification, Taxonomy and Phylogeny. In Dijkshoorn, L., Towner, K. J., Struelens, M., (Eds), *New Approaches for the Generation and Analysis of Microbial Typing Data*, (pp. 211-247). Elsevier Science B.V.

[34] Raina, V., Nayak, T., Ray, L., Kumari, K., & Suar, M. (2019). A Polyphasic Taxonomic Approach for Designation and Description of Novel Microbial Species. In. Das, S., Dash, H. R., (Eds), *Microbial Diversity in the Genomic Era*, (pp. 137-152). Academic Press

[35] Hugenholtz, P., Chuvochina, M., Oren, A., Parks, D. H., & Soo, R. M. (2021). Prokaryotic taxonomy and nomenclature in the age of big sequence data. *The ISME Journal*, *15*, 1879-1892. https://doi.org/10.1038/s41396-021-00941-x

Sinopfbd, 2024; 9(1): 26-35 **https://doi.org/10.33484/sinopfbd.1343041**

Sinop Üniversitesi Fen Bilimleri Dergisi
Sinop Uni J Nat Sci
E-ISSN: 2564-7873

https://dergipark.org.tr/tr/pub/sinopfbd

Bounds For Spectral Radius and Energy of PIS Graphs

Esra ÖZTÜRK SÖZEN[1] **and Elif ERYAŞAR**[1]

How to cite: Öztürk Sözen, E., & Eryaşar, E. (2024). Bounds for spectral radius and energy of PIS graphs. *Sinop Üniversitesi Fen Bilimleri Dergisi*, *9*(1), 26-35. https://doi.org/10.33484/sinopfbd.1343041

Research Article

Corresponding Author
Elif ERYAŞAR
eeryasar@sinop.edu.tr

ORCID of the Authors
E.Ö.S.: 0000-0002-2632-2193
E.E.: 0000-0002-9852-6662

Received: 14.08.2023
Accepted: 29.01.2024

Abstract
Once the spectral radius and energy of a graph structure have been defined, many properties have been studied. The spectral radius and energy of a graph are related to the eigenvalues of the adjacency matrix of the graph. In this paper, we define an adjacency matrix for a prime ideal sum (PIS) graph and then extend the concepts of spectral radius and energy to PIS graphs. Some bound theorems on the energy and spectral radius of PIS graph structures are given. A SageMath code for plotting these graphs is also provided.

Keywords: Graph energy, prime ideal sum graph, spectral radius

PIS Grafların Spektral Yarıçapı ve Enerjisi İçin Sınırlar

[1]Sinop University,
Department of Mathematics,
57000, Sinop, Türkiye

Öz
Bir graf yapısının spektral yarıçapı ve enerjisi tanımlandıktan sonra birçok özelliği incelenmiştir. Grafların spektral yarıçapı ve enerjisi komşuluk matrisin özdeğerleriyle ilişkilidir. Bu çalışmada bir asal ideal toplam (PIS) graf için bir komşuluk matrisi tanımlanmıştır ve daha sonra spektral yarıçap ve enerji kavramları PIS grafları için genişletilmiştir. PIS graf yapılarının enerjisi ve spektral yarıçapına ilişkin bazı sınır teoremleri verilmiştir. Ayrıca bu grafları çizmek için bir SageMath kodu da sunulmaktadır.

Anahtar Kelimeler: Graf enerjisi, asal ideal toplam graf, spektral yarıçap

Introduction

The graph structure is represented by $G = (V, E)$, where $V = \{v_1, v_2, ..., v_n\}$ is the set of vertices and $E = E(G)$ is the set of edges. Let $i, j \in V$, and we say that two vertices are adjacent if there is at least one edge between i and j. If vertices i and j are adjacent, they are denoted by $i \sim j$. The degree of a point i is the number of edges connected to i and it is denoted by d_i [1]. Spectral graph theory has used spectra of certain matrices associated with a graph, such as the adjacency matrix, the Laplace matrix, or other forms of these, to provide information about a graph. It is possible to characterize certain graph structures with a spectrum (with the help of one of these matrices) [2]. The adjacency matrix is an $n \times n$

matrix, denoted by $A(G)$, and is defined as follows [3]:

$$A(G) = \begin{cases} 1, & \text{i}\sim\text{j} \\ 0, & \text{otherwise} \end{cases}$$

The adjacency matrix is a real and symmetric matrix, and all eigenvalues are real. Given different eigenvalues $\lambda_1, \lambda_2, ..., \lambda_n$ of the adjacency matrix, the inequality $\lambda_1 \geq \lambda_2 \geq ... \geq \lambda_n$ exists for these eigenvalues. The largest eigenvalue λ_1 is called the spectral radius of the graph [4].

Another concept related to the spectrum of a graph is energy. Let $A(G)$ be the adjacency matrix of a graph G, $\lambda_1, \lambda_2, ..., \lambda_n$ be the eigenvalues of this matrix, the energy of a graph is denoted by $E(G)$ and $E(G) = \sum_{i=1}^{n} |\lambda_i|$ [5].

Defining zero divisor graphs over commutative rings is the beginning of graph theory in pure algebra [6, 7]. Nowadays, studies on the zero divisor graph of $\mathbb{Z}_n$ is a trending field in spectral and chemical graph theory [8–10]. Studies on these topics in the literature motivated us to study computing different topological descriptors with respect to the prime ideal sum graphs. The prime ideal sum graph of a ring is described as a graph whose vertices are all non-trivials of the ring and whose edges connect two vertices whenever the sum of these vertices is a prime ideal [11].

In this study, motivated by the works mentioned above, we investigate the spectral radius and energy of some commutative rings according to the prime ideal sum graph structures of them. A SageMath code for drawing PIS graph structures is also provided.

Main Results

Spectral Radius and Energy of PIS Graphs

Definition 1. Let $I, J \in \mathbb{Z}_n$ non-trivial two ideals. Then,

$$AG(\mathbb{Z}_n) = \begin{cases} 1, & I + J \text{ prime} \\ 0, & \text{otherwise} \end{cases}$$

where $AG(\mathbb{Z}_n)$ will represent the adjacency matrix of $PIS(\mathbb{Z}_n)$.

Theorem 1. Let p be a prime number. The sum of the eigenvalues of the adjacency matrix of $\mathbb{Z}_{p^\alpha}$ is zero.

Proof. Let us list all ideals of $\mathbb{Z}_{p^\alpha}$. Then we have $\{0\}, p^{\alpha-1}\mathbb{Z}_{p^\alpha}, p^{\alpha-2}\mathbb{Z}\mathbb{Z}_{p^\alpha}, p^2\mathbb{Z}_{p^\alpha}, p\mathbb{Z}_{p^\alpha}, \mathbb{Z}_{p^\alpha}$. Note that $p\mathbb{Z}_{p^\alpha}$ is a prime ideal of $\mathbb{Z}_{p^\alpha}$.

Taking into account the PIS graph over $\mathbb{Z}_{p^\alpha}$, $p\mathbb{Z}_{p^\alpha}$ is adjacent to $p^{\alpha-1}\mathbb{Z}_{p^\alpha}, p^{\alpha-2}\mathbb{Z}_{p^\alpha}$,...,$p^3\mathbb{Z}_{p^\alpha}, p^2\mathbb{Z}_{p^\alpha}$ as $\mathbb{Z}_{p^\alpha}$ is local and so the sum of these ideals is equal to $\mathbb{Z}_{p^\alpha}$. Considering the following graph representation of $\mathbb{Z}_{p^\alpha}$ Figure 1 the adjacency matrix of $\mathbb{Z}_{p^\alpha}$ is as follows.

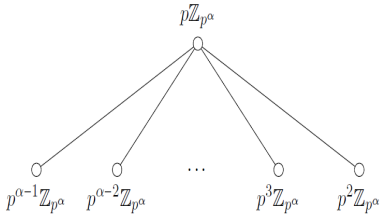

Figure 1. *Prime Ideal Sum Graph of* $\mathbb{Z}_{p^\alpha}$

$$AG(\mathbb{Z}_{p^\alpha}) = \begin{bmatrix} 0 & 1 & 1 & . & . & . & 1 \\ 1 & 0 & 0 & . & . & . & 0 \\ 1 & 0 & 0 & 0 & 0 & 0 & 0 \\ . & . & . & . & . & . & . \\ . & . & . & . & . & . & . \\ . & . & . & . & . & . & . \\ 1 & 0 & 0 & 0 & 0 & 0 & 0 \end{bmatrix}_{nxn}$$

For a matrix of this form, $n-2$ of the n eigenvalues are zero. Since two non-zero eigenvalues have opposite numbers, therefore $\lambda_1 + \lambda_2 + ... + \lambda_n = 0$.

Theorem 2. For two non-zero eigenvalues λ_1, λ_2 of $\mathbb{Z}_{p^\alpha}$ with spectral radius λ_1
$\lambda_1\lambda_2 \leq \lambda_1$.

Proof. It is clear from thm 1.

Theorem 3. Let $E(G)$ denotes the graph energy of $\mathbb{Z}_{p^\alpha}$. Then $E(G) = |\lambda_1| + |\lambda_2|$. Here, since $\lambda_2 = -\lambda_1,\ E(G) = 2\,|\lambda_1|$.

Proof. The adjacency matrix of $\mathbb{Z}_{p^\alpha}$ has two non-zero eigenvalues and since they have opposite numbers, $E(G) = \sum_{i=1}^{n} |\lambda_i| = |\lambda_1| + |\lambda_2| = |\lambda_1| + |-\lambda_1| = 2\,|\lambda_1|$.

Theorem 4. Let p, q be prime numbers. The spectral radius and energy of $\mathbb{Z}_{pq}$ are zero.

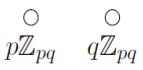

Figure 2. *Prime Ideal Sum Graph of* $\mathbb{Z}_{pq}$

Proof. For the prime ideals $p\mathbb{Z}_{pq}$ and $q\mathbb{Z}_{pq}$, the prime ideal sum graph of $\mathbb{Z}_{pq}$ is as Figure 2. As seen from Figure 2 both $p\mathbb{Z}_{pq}$ and $q\mathbb{Z}_{pq}$ are isolated vertices and so has degree zero. Therefore, its spectral radius and energy are zero.

Theorem 5. Let p, q be prime numbers. For the PIS graph representation of $\mathbb{Z}_{p^2q}$ for the spectral radius λ_1 with $|V(G)| = n = 4$,

$$\sum_{i=1}^{4} \lambda_i \leq \lambda_1 \leq \sum_{u_i \in V(G)} \frac{d(u_i)}{n}.$$

Proof. Let us consider the ideals $u_1 = p\mathbb{Z}_{p^2q}, u_2 = q\mathbb{Z}_{p^2q}, u_3 = pq\mathbb{Z}_{p^2q}, u_4 = p^2\mathbb{Z}_{p^2q}$, where u_1 and u_2 are the prime ones. Then $PIS(\mathbb{Z}_{p^2q})$ is as Figure 3. Thus the adjacency matrix of $\mathbb{Z}_{p^2q}$ is as follows.

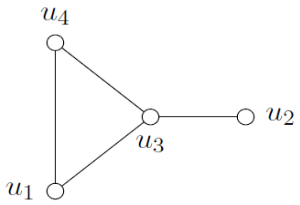

Figure 3. *Prime Ideal Sum Graph of* $\mathbb{Z}_{p^2q}$

$$AG(\mathbb{Z}_{p^2q}) = \begin{bmatrix} 0 & 0 & 1 & 1 \\ 0 & 0 & 0 & 1 \\ 1 & 0 & 0 & 1 \\ 1 & 1 & 1 & 0 \end{bmatrix}_{4x4}$$

Therefore, the eigenvalues are $\lambda_1 = 2.170, \lambda_2 = 0.311, \lambda_3 = -1.481$ and $\lambda_4 = -3$, from which the spectral radius is $\lambda_1 = 2.170$. Also $d(u_1) = 2, d(u_2) = 1, d(u_3) = 3$ and $d(u_4) = 2$, $\sum_{i=1}^{4} \lambda_i \leq \lambda_1 \leq \sum_{u_i \in V(G)} \frac{d(u_i)}{n}$.

Theorem 6. Let $E(G)$ denotes the graph energy of $\mathbb{Z}_{p^2q}$. Then, $E(G) \leq \frac{n \sum_{u_i \in V(G)} d(u_i)}{4}$.

Proof. The graph energy of $\mathbb{Z}_{p^2q}$ is clear from thm 5 that $E(G) = 6.96$. Considering the number of vertices $n = 4$ and the sum of degrees of u_i, we have $E(G) \leq \frac{n \sum_{u_i \in V(G)} d(u_i)}{4}$.

Theorem 7. Let p, q be prime numbers. For the PIS graph representation of $\mathbb{Z}_{p^2q^2}$ for the spectral radius λ_1 with $|V(G)| = n = 7$,

$\sum_{i=1}^{7} \lambda_i \leq \lambda_1 \leq \sum_{u_i \in V(G)} \frac{d(u_i)}{n-1}$.

Proof. Let us consider the ideals $u_1 = p\mathbb{Z}_{p^2q^2}, u_2 = q\mathbb{Z}_{p^2q^2}, u_3 = pq\mathbb{Z}_{p^2q^2}, u_4 = p^2q\mathbb{Z}_{p^2q^2}, u_5 = pq^2\mathbb{Z}_{p^2q^2}, u_6 = p^2\mathbb{Z}_{p^2q^2}, u_7 = q^2\mathbb{Z}_{p^2q^2}$, where u_1 and u_2 are the prime ones. Then $PIS(\mathbb{Z}_{p^2q^2})$ is as Figure 4. Thus the adjacency matrix of $\mathbb{Z}_{p^2q^2}$ is as follows.

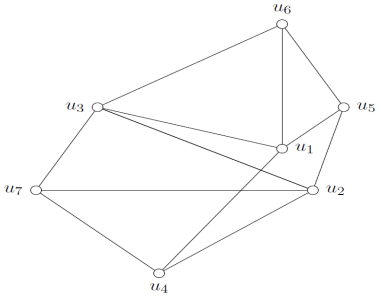

Figure 4. *Prime Ideal Sum Graph of* $\mathbb{Z}_{p^2q^2}$

$$AG(\mathbb{Z}_{p^2q^2}) = \begin{bmatrix} 0 & 0 & 1 & 0 & 1 & 1 & 1 \\ 0 & 0 & 0 & 1 & 1 & 1 & 1 \\ 1 & 0 & 0 & 0 & 1 & 0 & 1 \\ 0 & 1 & 0 & 0 & 1 & 1 & 0 \\ 1 & 1 & 1 & 1 & 0 & 0 & 0 \\ 1 & 1 & 0 & 1 & 0 & 0 & 0 \\ 1 & 1 & 1 & 0 & 0 & 0 & 0 \end{bmatrix}_{7x7}.$$

Therefore, the eigenvalues are $\lambda_1 = 3.48, \lambda_2 = 1.41, \lambda_3 = 0.20, \lambda_4 = 0, \lambda_5 = -1.49, \lambda_6 = -1.41$ and $\lambda_7 = 2.56$ from which the spectral radius is $\lambda_1 = 3.48$. Also $d(u_1) = 4, d(u_2) = 4, d(u_3) = 4, d(u_4) = 3, d(u_5) = 3, d(u_6) = 3$ and $d(u_7) = 3$, $\sum_{i=1}^{7} \lambda_i \leq \lambda_1 \leq \sum_{u_i \in V(G)} \frac{d(u_i)}{n-1}$.

Theorem 8. Let $E(G)$ denotes the graph energy of $\mathbb{Z}_{p^2q^2}$. Then, $E(G) \leq 2 \sum_{u_i \in V(G)} \frac{d(u_i)}{n-3}$.

Proof. The graph energy of $\mathbb{Z}_{p^2q^2}$ is clear from thm 7 that $E(G) = 10.56$. Considering the number of vertices $n = 7$ and the sum of degrees of u_i, we have, $E(G) \leq 2 \sum_{u_i \in V(G)} \frac{d(u_i)}{n-3}$.

Theorem 9. Let p, q and r be prime numbers. From the PIS graph representation of $\mathbb{Z}_{pqr}$ for the spectral radius λ_1 with $|V(G)| = n = 6$,

$\sum_{i=1}^{6} \lambda_i \leq \lambda_1 \leq \frac{\sum_{u_i \in V(G)} d(u_i)}{2(n-4)}$.

Proof. Let us consider the ideals $u_1 = p\mathbb{Z}_{pqr}, u_2 = q\mathbb{Z}_{pqr}, u_3 = r\mathbb{Z}_{pqr}, u_4 = pq\mathbb{Z}_{pqr}, u_5 = pr\mathbb{Z}_{pqr}, u_6 = qr\mathbb{Z}_{pqr}$, where u_1, u_2 and u_3 prime ones. Then $PIS(\mathbb{Z}_{pqr})$ is as Figure 5. Thus the adjacency matrix of $\mathbb{Z}_{pqr}$ is as follows.

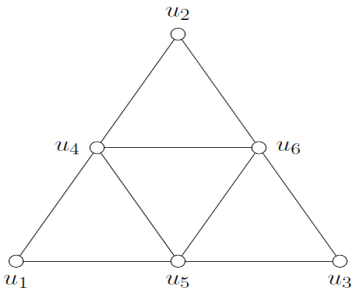

Figure 5. *Prime Ideal Sum Graph of* $\mathbb{Z}_{pqr}$

$$AG(\mathbb{Z}_{pqr}) = \begin{bmatrix} 0 & 0 & 0 & 1 & 1 & 0 \\ 0 & 0 & 0 & 1 & 0 & 1 \\ 0 & 0 & 0 & 0 & 1 & 1 \\ 1 & 1 & 0 & 0 & 1 & 1 \\ 1 & 0 & 1 & 1 & 0 & 1 \\ 0 & 1 & 1 & 1 & 1 & 0 \end{bmatrix}_{6x6}.$$

Therefore, the eigenvalues are $\lambda_1 = 3.24, \lambda_{2,3} = 0.62, \lambda_{4,5} = -1.62$ and $\lambda_6 = -1.23$ from which the spectral radius is $\lambda_1 = 3.24$. Also $d(u_1) = 2, d(u_2) = 2, d(u_3) = 2, d(u_4) = 4, d(u_5) = 4$ and $d(u_6) = 4$,
$\sum_{i=1}^{6} \lambda_i \leq \lambda_1 \leq \frac{\sum_{u_i \in V(G)} d(u_i)}{2(n-4)}$.

Theorem 10. Let $E(G)$ denotes the graph energy of $\mathbb{Z}_{pqr}$. Then, $E(G) \leq \frac{\sum_{u_i \in V(G)} d(u_i)}{2}$.

Proof. The graph energy of $\mathbb{Z}_{pqr}$ is clear from thm 9 that $E(G) = 8.95$. Considering the number of vertices $n = 6$ and the sum of degrees of u_i, we have

$$E(G) \leq \frac{\sum_{u_i \in V(G)} d(u_i)}{2}.$$

Theorem 11. Let p, q be prime numbers. For the PIS graph representation of $\mathbb{Z}_{p^3q}$ for the spectral radius λ_1 with $|V(G)| = n = 6$,
$\sum_{i=1}^{6} \lambda_i \leq \lambda_1 \leq \frac{\sum_{u_i \in V(G)} d(u_i) - 1}{n-1}$

Proof. Let us consider the ideal $u_1 = p\mathbb{Z}_{p^3q}, u_2 = q\mathbb{Z}_{p^3q}, u_3 = p^2\mathbb{Z}_{p^3q}, u_4 = pq\mathbb{Z}_{p^3q}, u_5 = p^3\mathbb{Z}_{p^3q}, u_6 = p^2q\mathbb{Z}_{p^3q}$, where u_1 and u_2 prime ones. Then $PIS(\mathbb{Z}_{p^3q})$ is as Figure 6. Thus the adjacency matrix of $\mathbb{Z}_{p^3q}$ is as follows.

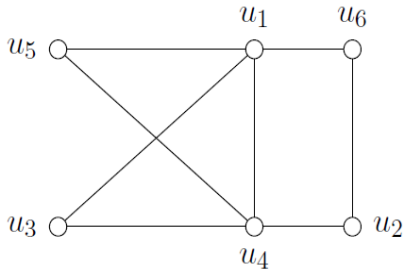

Figure 6. *Prime Ideal Sum Graph of* $\mathbb{Z}_{p^3q}$

$$AG(\mathbb{Z}_{p^3q}) = \begin{bmatrix} 0 & 0 & 1 & 1 & 1 & 1 \\ 0 & 0 & 0 & 0 & 1 & 1 \\ 1 & 0 & 0 & 0 & 1 & 0 \\ 1 & 0 & 0 & 0 & 1 & 0 \\ 1 & 1 & 1 & 1 & 0 & 0 \\ 1 & 1 & 0 & 0 & 0 & 0 \end{bmatrix}_{6x6}.$$

Therefore, the eigenvalues are $\lambda_1 = 2.903, \lambda_2 = 0.806, \lambda_{3,4} = 0, \lambda_5 = -1.709$ and $\lambda_6 = -2$ from which the spectral radius is $\lambda_1 = 2.903$. Also $d(u_1) = 4, d(u_2) = 2, d(u_3) = 2, d(u_4) = 4, d(u_5) = 2$ and $d(u_6) = 2$, $\sum_{i=1}^{6} \lambda_i \leq \lambda_1 \leq \frac{\sum_{u_i \in V(G)} d(u_i) - 1}{n-1}$.

Theorem 12. Let $E(G)$ denotes the graph energy of $\mathbb{Z}_{p^3q}$. Then, $E(G) \leq \frac{\sum_{u_i \in V(G)} d(u_i)}{2}$.

Proof. The graph energy of $\mathbb{Z}_{p^3q}$ is clear from thm 11 that $E(G) = 7.42$. Considering the number of vertices $n = 6$ and the sum of degrees of u_i, we have $E(G) \leq \frac{\sum_{u_i \in V(G)} d(u_i)}{2}$.

Theorem 13. Let p, q and r be prime numbers . From the PIS graph representation of $\mathbb{Z}_{p^2qr}$ for the spectral radius λ_1 with $V(G) = n = 10$, $\sum_{i=1}^{10} \lambda_i \leq \lambda_1 \leq \frac{\sum_{u_i \in V(G)} d(u_i)}{n-2}$.

Proof. Let us consider the ideal $u_1 = p\mathbb{Z}_{p^2qr}, u_2 = q\mathbb{Z}_{p^2qr}, u_3 = r\mathbb{Z}_{p^2qr}, u_4 = p^2\mathbb{Z}_{p^2qr}, u_5 = pq\mathbb{Z}_{p^2qr}, u_6 = pr\mathbb{Z}_{p^2qr}, u_7 = p^2q\mathbb{Z}_{p^2qr}, u_8 = p^2r\mathbb{Z}_{p^2qr}, u_9 = qr\mathbb{Z}_{p^2qr}, u_{10} = pqr\mathbb{Z}_{p^2qr}$, where u_1, u_2 and u_3 prime ones. Then $PIS(\mathbb{Z}_{p^2qr})$ is as Figure 7. Thus the adjacency matrix of $\mathbb{Z}_{p^2qr}$ is as follows.

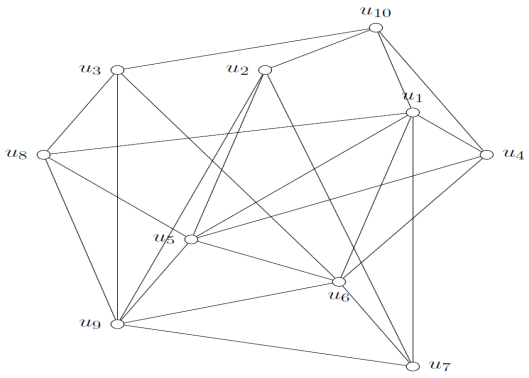

Figure 7. *Prime Ideal Sum Graph of* $\mathbb{Z}_{p^2qr}$

$$AG(\mathbb{Z}_{p^2qr}) = \begin{bmatrix} 0 & 0 & 0 & 1 & 1 & 1 & 1 & 1 & 0 & 1 \\ 0 & 0 & 0 & 0 & 1 & 0 & 1 & 0 & 1 & 1 \\ 0 & 0 & 0 & 0 & 0 & 1 & 0 & 1 & 1 & 1 \\ 1 & 0 & 0 & 0 & 1 & 1 & 0 & 0 & 0 & 1 \\ 1 & 1 & 0 & 1 & 0 & 1 & 0 & 1 & 1 & 0 \\ 1 & 0 & 1 & 1 & 1 & 0 & 1 & 0 & 1 & 0 \\ 1 & 1 & 0 & 0 & 0 & 1 & 0 & 0 & 1 & 0 \\ 1 & 0 & 1 & 0 & 1 & 0 & 0 & 0 & 1 & 0 \\ 0 & 1 & 1 & 0 & 1 & 1 & 1 & 1 & 0 & 0 \\ 1 & 1 & 1 & 1 & 0 & 0 & 0 & 0 & 0 & 0 \end{bmatrix}_{10x10}.$$

Therefore the eigenvalues are $\lambda_1 = 4.98, \lambda_2 = 1.48, \lambda_3 = 1, \lambda_4 = 0.79, \lambda_5 = 0.41, \lambda_6 = -0.09, \lambda_7 = -1.49, \lambda_8 = -2, \lambda_9 = -2.41$ and $\lambda_{10} = -2.67$ from which the spectral radius $\lambda_1 = 4.98$. Also $d(u_1) = 6, d(u_2) = 4, d(u_3) = 4, d(u_4) = 4, d(u_5) = 6, d(u_6) = 6, d(u_7) = 4, d(u_8) = 4, d(u_9) = 6$ and $d(u_{10}) = 4$, $\sum_{i=1}^{10} \lambda_i \leq \lambda_1 \leq \frac{\sum_{u_i \in V(G)} d(u_i)}{n-2}$.

Theorem 14. Let $E(G)$ denotes the graph energy of $\mathbb{Z}_{p^2qr}$. Then, $E(G) \leq \frac{\sum_{u_i \in V(G)} d(u_i)+n}{3}$.

Proof. The graph energy of $\mathbb{Z}_{p^2qr}$ is clear from thm 13 that $E(G) = 17.33$. Considering the number of vertices $n = 10$ and the sum of degrees of u_i, we have $\frac{\sum_{u_i \in V(G)} d(u_i)+n}{3}$.

Theorem 15. Let p, q, r and s be prime numbers . From the PIS graph representation of $\mathbb{Z}_{pqrs}$ for the spectral radius λ_1 with $V(G) = n = 14$, $\sum_{i=1}^{14} \lambda_i \leq \lambda_1 \leq \frac{\sum_{u_i \in V(G)} d(u_i)}{n-2}$.

Proof. Let us consider the ideal $u_1 = p\mathbb{Z}_{pqrs}, u_2 = q\mathbb{Z}_{pqrs}, u_3 = r\mathbb{Z}_{pqrs}, u_4 = pq\mathbb{Z}_{pqrs}, u_5 = s\mathbb{Z}_{pqrs}, u_6 = pr\mathbb{Z}_{pqrs}, u_7 = ps\mathbb{Z}_{pqrs}, u_8 = qr\mathbb{Z}_{pqrs}, u_9 = qs\mathbb{Z}_{pqrs}, u_{10} = pqr\mathbb{Z}_{pqrs}, u_{11} = rs\mathbb{Z}_{pqrs}, u_{12} = pqs\mathbb{Z}_{pqrs}, u_{13} = prs\mathbb{Z}_{pqrs}, u_{14} = qrs\mathbb{Z}_{pqrs}$, where u_1, u_2, u_3 and u_5 prime ones. Then $PIS(\mathbb{Z}_{pqrs})$ is as Figure 8. Thus the adjacency matrix of $\mathbb{Z}_{pqrs}$ is as follows.

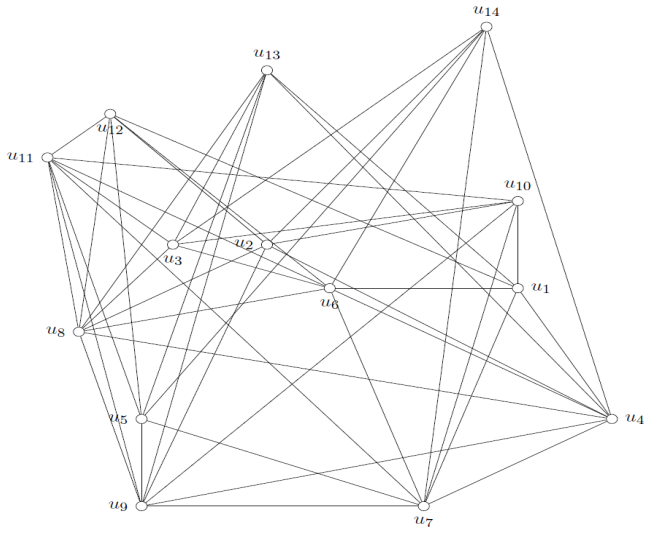

Figure 8. *Prime Ideal Sum Graph of* $\mathbb{Z}_{pqrs}$

$$AG(\mathbb{Z}_{pqrs}) = \begin{bmatrix} 0&0&0&1&0&1&1&0&0&1&0&1&1&0 \\ 0&0&0&1&0&0&0&1&1&1&0&1&0&1 \\ 0&0&0&0&0&1&0&1&0&1&1&0&1&1 \\ 1&1&0&0&0&1&1&1&1&0&0&0&1&1 \\ 0&0&0&0&0&0&1&0&1&0&1&1&1&1 \\ 1&0&1&1&0&0&1&1&0&0&1&1&0&1 \\ 1&0&0&1&1&1&0&0&1&1&1&0&0&1 \\ 0&1&1&1&0&1&0&0&1&0&1&1&1&0 \\ 0&1&0&1&1&0&1&1&0&1&1&0&1&0 \\ 1&1&1&0&0&0&1&0&1&0&1&0&0&0 \\ 0&0&1&0&1&1&1&1&1&1&0&1&0&0 \\ 1&1&0&0&1&1&0&1&0&0&1&0&0&0 \\ 1&0&1&1&1&0&0&1&1&0&0&0&0&0 \\ 0&1&1&1&1&1&1&0&0&0&0&0&0&0 \end{bmatrix}_{14x14}.$$

Therefore the eigenvalues are $\lambda_1 = 7, \lambda_{2,3,4} = 1, \lambda_5 = 0, \lambda_{6,7,8} = -2.56, \lambda_{9,10} = -2, \lambda_{11,12,13} = 1.56$ and $\lambda_{14} = -3$ from which the spectral radius $\lambda_1 = 7$. Also $d(u_1) = 6, d(u_2) = 6, d(u_3) = 6, d(u_4) = 8, d(u_5) = 6, d(u_6) = 8, d(u_7) = 8, d(u_8) = 8, d(u_9) = 8$,$d(u_{10}) = 6, d(u_{11}) = 8$,$d(u_{12}) = 6, d(u_{13}) = 6$ and $d(u_{14}) = 6, \sum_{i=1}^{14} \lambda_i \leq \lambda_1 \leq \frac{\sum_{u_i \in V(G)} d(u_i)}{n-2}$.

Theorem 16. Let $E(G)$ denotes the graph energy of $\mathbb{Z}_{pqrs}$. Then, $E(G) \leq \frac{5 \sum_{u_i \in V(G)} d(u_i)}{n}$.

Proof. The graph energy of $\mathbb{Z}_{pqrs}$ is clear from thm 15 that $E(G) = 29.36$. Considering the number of

vertices $n = 14$ and the sum of degrees of u_i, we have $E(G) \leq \frac{5\sum_{u_i \in V(G)} d(u_i)}{n}$.

Sage code algorithm for drawing $PIS(\mathbb{Z}_n)$

```
n=
V=[ ]
for i in [2..(n-1)]:
if n%i==0:
V.append(i)
E=[ ]
for a in V:
for b in V:
if gcd(a,b).is_prime()==True and a!=b:
E.append((a,b))
G=Graph()
G.add_vertices(V)
G.add_edges(E)
G.plot()
```

Acknowledgments -

Funding/Financial Disclosure The authors have no received any financial support for the research, authorship, or publication of this study.

Ethics Committee Approval and Permissions The work does not require ethics committee approval and any private permission.

Conflict of Interests The authors stated that there are no conflict of interest in this article.

Authors Contribution Authors contributed equally to the study.

References

[1] Bondy, J., & Murty, U. (1982). *Graph theory with applications*. Elsevier Science Publishing.

[2] Hogben, L. (2005). Spectral graph theory and the inverse eigenvalue problem of a graph. *The Electronic Journal of Linear Algebra*, *14*, 12–31. https://doi.org/10.13001/1081-3810.1174

[3] Bapat, R. (2013). On the adjacency matrix of a threshold graph. *Linear Algebra and its Applications*, *439*(10), 3008–3015. https://doi.org/10.1016/j.laa.2013.08.007

[4] Das, K., & Kumar, P. (2004). Some new bounds on the spectral radius of graphs. *Discrete Mathematics*, *281*(1-3), 149–161. https://doi.org/10.1016/j.disc.2003.08.005

[5] Gutman, I. (1978). The energy of a graph. *Ber Math— Statist Sekt Forschungsz Graz*, *103*, 1–22.

[6] Anderson, D., & Livingston, P. (1999). The zero-divisor graph of a commutative ring. *Journal of Algebra*, *217*, 434–447. https://doi.org/10.1006/jabr.1998.7840

[7] Beck, I. (1988). Coloring of commutative rings. *Journal of Algebra*, *116*(1), 208–226. https://doi.org/10.1016/0021-8693(88)90202-5

[8] Banerjee, S. (2022). Laplacian spectrum of comaximal graph of the ring $\mathbb{Z}_n$. *Journal of Algebra*, *10*(1), 285–298. https://doi.org/10.48550/arXiv.2005.02316

[9] Fasfous, W., Rajat, K., & Sharafdini, R. (2020). Various spectra and energies of commuting graphs of finite rings. *Hacettepe Journal of Mathematics and Statistics*, *49*(6), 1915–1925. https://doi.org/10.15672/hujms.540309

[10] Sözen, E., Eryaşar, E., & Abdioğlu, C. (2022). Forgotten topological and wiener indices of prime ideal sum graph of $\mathbb{Z}_n$. *Current Organic Synthesis*. https://doi.org/10.2174/1570179420666230606140448

[11] Saha, M., Çelikel, E., & Abdioğlu, C. (2023). Prime ideal sum graph of a commutative ring. *Hacettepe Journal of Mathematics and Statistics*, *22*(06), 2350121–. https://doi.org/10.1142/S0219498823501219

Sinopfbd, 2024; 9(1): 36-43 **https://doi.org/10.33484/sinopfbd.1381635**

Sinop Üniversitesi Fen Bilimleri Dergisi
Sinop Uni J Nat Sci
E-ISSN: 2564-7873

https://dergipark.org.tr/tr/pub/sinopfbd

Generalization of $\oplus$ −Cofinitely Radical Supplemented Modules

Şeyma HALDIZ[1] and Figen ERYILMAZ[2]

How to cite: Haldız, Ş., & Eryılmaz, F. (2024). Generalization of $\oplus$ −cofinitely radical supplemented modules. *Sinop Üniversitesi Fen Bilimleri Dergisi, 9*(1), 36-43. https://doi.org/10.33484/sinopfbd.1381635

Research Article

Corresponding Author
Figen ERYILMAZ
fyuzbasi@omu.edu.tr

ORCID of the Authors
Ş.H: 0009-0002-2584-8713
F.E: 0000-0002-4178-971X

Received: 26.10.2023
Accepted: 12.02.2024

Abstract
In this study, we clarify $mgs^{\oplus}$ −modules that are the generalization of $\oplus$ −cofinitely radical supplemented modules and look at some of their basic characteristics. Additionally, we determine the prerequisites for the factor module of an arbitrary $mgs^{\oplus}$ −module to be a $mgs^{\oplus}$ −module and characterized semiperfect rings with the aid of this module.

Keywords: Maximal submodule, Rad-supplement, $\oplus$ −cofinitely radical supplemented module

$\oplus$ −Dual (Eş) Sonlu Radikal Tümlenmiş Modüllerin Genelleştirilmesi

[1]Araklı Mehmet Akif Ersoy Anatolian High School, Taraklı, Trabzon, Türkiye

[2]Ondokuz Mayıs University, Faculty of Education, Department of Mathematics Education, 55270, Atakum, Samsun, Türkiye

Öz
Bu makalede $\oplus$ −dual sonlu radikal tümleyen modüllerin genellemesi olarak maksimal alt modülleri $\oplus$ −radikal tümleyene sahip modüller ($mgs^{\oplus}$) tanımlandı ve bu modülün bazı temel özellikleri incelendi. Keyfi bir $mgs^{\oplus}$ −modülünün bölüm modülünün hangi şartlar altında $mgs^{\oplus}$ −modül olduğu gösterildi ve yarı mükemmel halkalar bu modül yardımıyla karakterize edildi.

Anahtar Kelimeler: Maksimal alt modül, radikal tümleyen, $\oplus$ −dual sonlu radikal tümlenmiş modül

Introduction and Preliminaries

All rings would be with identity and associative in this article. Every module is considered a unitary left module. Let W and S be a module and a ring meeting these requirements, respectively. The notation $T \leq W$ will imply that T is a submodule of W and the impression $T \leq_{\oplus} W$ means that T is a direct summand of W. A submodule T of W is referred to as the small module in W, if $W \neq T + T_1$ for any proper submodule T_1 of W and indicated by $T \ll W$. The sum of its small submodules will be shown by $Rad(W)$. A submodule T of W is called as *supplement* of P in W, if it is a minimal element of the

set $\{Y \leq W | W = P + Y\}$ which is equivalent to $W = P + T$ and $P \cap T \ll T$. If each submodule of W has a supplement in W, then W is named *supplemented*, [1]. Let W be a module and $T \leq W$. T is called a *cofinite submodule* of W, if W/T is finitely generated. Cofinite submodules are one of the interesting concept of module theory, and they have various properties and applications in the study of algebraic structures. There are many different studies related with these modules in the literature [2, 3]. If each submodule of W has a supplement that is a direct summand of W, then W is named $\oplus-$*supplemented* [4]. Otherwise, if each cofinite submodule of W has a supplement which is a direct summand of W, then W is called *cofinitely* $\oplus-$*supplemented* [5]. According to [6], a module W is called *radical supplemented* (Rad-supplemented) when each submodule of W has a Rad-supplement in W. In other words, for any submodule T of W, a submodule P of W is named a Rad-supplemented of the submodule T in W if $W = P + T$ and $P \cap T \subseteq Rad(P)$. In reference [7]; radical supplement and radical supplemented modules are called as *generalized supplement* and *generalized supplemented* modules, respectively. By generalizing this definition, cofinite radical supplemented modules are defined. In [8], a module W is called *cofinitely radical supplemented (cofinitely Rad-supplemented)*, if each cofinite submodule of W has a Rad-supplement in W. Besides these, $\oplus-$radical supplemented modules ($\oplus-$Rad-supplemented) are studied and defined in [9, 10]. Meanwhile, $\oplus-$cofinitely radical supplemented modules introduced and examined in [11]. According to this, if each (cofinite) submodule of a module has a Rad-supplement which is a direct summand of itself, then it is called $\oplus-$(cofinitely) radical supplemented. This definition is given as *generalized* $\oplus-$*cofinitely supplemented* in [12]. In [11], $cgs^{\oplus}-$module notation is used briefly instead of $\oplus-$cofinitely radical supplemented modules and basic fundamental aspects of these modules are examined in there. In this article, we studied another version of $cgs^{\oplus}-$module by using the concept of "maximal submodule" instead of "cofinite submodule". A maximal submodule of W is a submodule T where there are no other submodules of W that properly contains T, except for W itself. In other words, if T is maximal, there are no larger submodules contained in W that properly extend T. Equivalently, for T, being a maximal submodule of W implies that for any submodule K of W, either K is equal to T or K is equal to W. Also, it is well known that each maximal submodule is cofinite. A module is called a $mgs^{\oplus}-$*module*, if each maximal submodule of it contains a Rad-supplement that is a direct summand of itself. Since each maximal submodule is a cofinite submodule, this study will be the most general study about this subject in the literature. It will be shown that $mgs^{\oplus}-$modules and $\oplus-$cofinite supplemented modules coincide in coatomic modules. It will be later proved that direct sum of $mgs^{\oplus}-$modules brings out a $mgs^{\oplus}-$module. Nevertheless, we will prove that the factor module created by the fully invariant submodule of $mgs^{\oplus}-$module is also the $mgs^{\oplus}-$module. We will show for a ring that each free $S-$module is a $mgs^{\oplus}-$module if and only if S is semiperfect.

$Mgs^{\oplus}$ −Modules

Definition 1. If each maximal submodule of a module has a Rad-supplement which is a direct summand of it, then it is called a $mgs^{\oplus}-$ module.

Lemma 2. Every $cgs^{\oplus}$ −module is a $mgs^{\oplus}$ −module.

Proof. Let W be a $cgs^{\oplus}$ −module and the submodule X be maximal in W. Since every maximal submodule is cofinite submodule, the rest is easy.

Recall from [8] that, $w-$*local module* is a module which has a unique maximal submodule.

Proposition 3. If a $mgs^{\oplus}$ −module W satisfies the condition $Rad(W) \ll W$, then it is $\oplus$ −cofinitely supplemented.

Proof. Consider the submodule X as a maximal of W. Based on the assumption, there are submodules $T$and T_1 of $W$where$W = X + T, X \cap T \subseteq Rad(T)$ and $W = T \oplus T_1$. Hence, we have $X \cap T \subseteq Rad(T) \subseteq Rad(W) \ll W$ and $T \leq_{\oplus} W$. If we consider [1, 19.3(5)], then we can write $X \cap T \ll T$. Therefore W is $\oplus$ −cofinitely supplemented.

Recall from [1] that, if each proper submodule of W is included in a maximal submodule of W and every coatomic module has a small radical, then $W$is said to be *coatomic*. Thus, the following can be given without its proof.

Corollary 4. Let W be a coatomic module. W is $\oplus$ −cofinitely supplemented if and only if it is a $mgs^{\oplus}-$ module.

Proposition 5. Any w −local module is a $mgs^{\oplus}-$ module.

Proof. It is easily obtained by combining Proposition 2.3 in [11] and Lemma 2.

For any prime p, the $\mathbb{Z}$ −module $\mathbb{Q} \oplus \mathbb{Z}_p$ is w −local because $Rad(\mathbb{Q} \oplus \mathbb{Z}_p) \cong \mathbb{Q}$ is a unique submodule of $\mathbb{Q} \oplus \mathbb{Z}_p$. So, $\mathbb{Q} \oplus \mathbb{Z}_p$ is a $mgs^{\oplus}-$ module.

Theorem 6. Any arbitrary $mgs^{\oplus}$ −module with a maximal submodule includes a w −local direct summand.

Proof. Let W be a $mgs^{\oplus}-$ module and X be a maximal submodule of it. Then, there are submodules Y, Y_1 of W such that $W = X + Y$, $X \cap Y \subseteq Rad(Y)$ and $W = Y \oplus Y_1$. Also, it can be said that $Y$is a Rad-supplement of X in W. If we consider Lemma 3.3 of [8], then we get Y is w −local. Therefore $Y$is a w −local direct summand of W.

We point out the sum of whole w −local direct summands of W by $wLoc^{\oplus}W$ and the sum of whole $mgs^{\oplus}-$ submodules of W by $Mgs^{\oplus}W$.

Lemma 7. $wLoc^{\oplus}W \leq Mgs^{\oplus}W$, for any module W.

Proof. Let L represent a w −local submodule of W where $L \leq_{\oplus} W$. By using Proposition 5, we can say that L is a $mgs^{\oplus}$ −module. Then we get $L < Mgs^{\oplus}W$ and so $wLoc^{\oplus}W \leq Mgs^{\oplus}W$.

Theorem 8. Let any $mgs^{\oplus}-$ submodule of W be a direct summand of W. In that case, ${}^{W}/_{Mgs^{\oplus}W}$ does not include a maximal submodule if and only if W is a $mgs^{\oplus}-$ module.

Proof. ($\Leftarrow$) Suppose that ${}^{L}/_{Mgs^{\oplus}W}$ is a maximal submodule of ${}^{W}/_{Mgs^{\oplus}W}$. Then L is the maximal submodule of W . Based on the hypothesis, there are submodules L_1, K of W such that

$$W = L + L_1, \qquad L \cap L_1 \subseteq Rad(L_1) \text{ and } W = L_1 \oplus K.$$

By Lemma 3.3 in [8], L_1 is a $w-$local module and L_1 is a $mgs^{\oplus}-$ module by Proposition 5.

From here, we can say that $L_1 \subseteq Mgs^{\oplus}W$ and so we can write that

$$\begin{aligned} {}^{W}/_{Mgs^{\oplus}W} &= \left({}^{L}/_{Mgs^{\oplus}W}\right) + \left[{}^{\left(L_1 + Mgs^{\oplus}W\right)}/_{Mgs^{\oplus}W}\right] \\ &= \left({}^{L}/_{Mgs^{\oplus}W}\right) + \left({}^{Mgs^{\oplus}W}/_{Mgs^{\oplus}W}\right). \end{aligned}$$

Consequently, we obtain ${}^{W}/_{Mgs^{\oplus}W} = {}^{L}/_{Mgs^{\oplus}W}$ and so $W = L$ which is a contradiction. Hence ${}^{W}/_{Mgs^{\oplus}W}$ does not include a maximal submodule.

($\Rightarrow$) Let L be a maximal submodule of W. If L includes the $mgs^{\oplus}-$ modules, then $Mgs^{\oplus}W < L$ can be obtained. Thus ${}^{L}/_{Mgs^{\oplus}W}$ would be maximal submodule of ${}^{W}/_{Mgs^{\oplus}W}$, which contradicts the hypothesis. In that case, L does not contain $Mgs^{\oplus}W$ and there is a $mgs^{\oplus}-$submodule X of W where $X \not\subset L$ and $W = X + L$. Remember that ${}^{W}/_{L} \cong {}^{X}/_{X \cap L}$. From here $X \cap L$ is a maximal submodule of X. As X is a $mgs^{\oplus}-$module, there are submodules Y and Y_1 of W where $X = (X \cap L) + Y$, $(X \cap L) \cap Y \subseteq Rad(Y)$ and $X = Y \oplus Y_1$. Therefore, we can obtain that

$W = X + L = (X \cap L) + Y + L = L + Y$, $L \cap Y = L \cap (X \cap Y) = (L \cap X) \cap Y \subseteq Rad(Y)$.

Since $X \leq_{\oplus} W$,there is a submodule X_1 of $W$with $W = X \oplus X_1$. Therefore

$W = X \oplus X_1 = (Y \oplus Y_1) \oplus X_1 = Y \oplus (Y_1 \oplus X_1)$ and so W is a $mgs^{\oplus}-$ module.

Theorem 9. Any direct sum of $mgs^{\oplus}-$ modules is a $mgs^{\oplus}-$ module.

Proof. Assume that $\{W_i\}_{i\in I}$ is a family of $mgs^{\oplus}-$ modules such that $W = \bigoplus_{i\in I} W_i$ and L is maximal submodule of W. Then we can write $W = L + W_{i_0}$ for $W_{i_0} \subset L$, $i_0 \in I$.

Since ${}^{W}/_{L} \cong {}^{W_{i_0}}/_{L \cap W_{i_0}}$ and ${}^{W}/_{L}$ is a simple module, ${}^{W_{i_0}}/_{L \cap W_{i_0}}$ is simple and so $L \cap W_{i_0}$ is a maximal submodule of W_{i_0}.Then, there are submodules X, $X_1$of W_{i_0} where $W_{i_0} = \left(L \cap W_{i_0}\right) + X$, $X \cap \left(L \cap W_{i_0}\right) \subseteq Rad(X)$ and $W_{i_0} = X \oplus X_1$ because W_{i_0} is a $mgs^{\oplus}$-module. From here, we can obtain that $W = L + W_{i_0} = L + \left(L \cap W_{i_0}\right) + X = L + X$ and $L \cap X \subseteq Rad(X)$. Nevertheless, we get $L \leq_{\oplus} W$ since W_{i_0} and X are direct summands of $W$and W_{i_0}, respectively. As a result, $W$is a $mgs^{\oplus}-$ module. Recall from [13] that, a module W has the *summand sum property (SSP)* if the sum of two

direct summands of W is again a direct summand of W. Also, W has the property (D_3), if $X, Y \leq_{\oplus} W$ with $W = X + Y$, then $X \cap Y \leq_{\oplus} W$ [13].

Theorem 10. Let W be a $mgs^{\oplus}-$module which has the property $(D_3)$and (SSP). Then, every maximal direct summand of W is a $mgs^{\oplus}-$ module.

Proof. Let K be a maximal direct summand of W. Then, there is a submodule K_1 of W where $W = K \oplus K_1$ and K_1 is finitely generated. Suppose that T is a maximal submodule of K. Since $W/T = (K/T) \oplus K_1$ is finitely generated, T is a maximal submodule of W. Therefore $W$is a $cgs^{\oplus}-$module by Theorem 2.2 in [11] and there are submodules K_1 and $K_2$of W with $W = T + K_1$, $T \cap K_1 \subseteq Rad(K_1)$ and $W = K_1 \oplus K_2$. Note that $W = T + K_1 = K + K_1$. Since $W = K \oplus K_1, W = K_1 \oplus K_2$, $W = K + K_1$ and W has the property (D_3), it can be written that $K \cap K_1 \leq_{\oplus} W$. Therefore, we can write $W = (K \cap K_1) \oplus X$ for a submodule X of W. Hence one can easily get the equality $K = K \cap W = K \cap (T + K_1) = T + (K \cap K_1)$. Besides these, $T \cap (K \cap K_1) = T \cap K_1 \subseteq Rad(K_1) \subseteq Rad(W)$. If one uses the chapter 19.3 in [1], then $T \cap (K \cap K_1) \subseteq Rad(K \cap K_1)$ can be obtained due to $K \cap K_1 \leq_{\oplus} W$. As a result, by taking the intersection of both sides of the equation $W = (K \cap K_1) \oplus X$ with K, we can obtain that $W = (K \cap K_1) \oplus (K \cap X)$ and so K is a $mgs^{\oplus}-$ module.

Corollary 11. Let W be a $mgs^{\oplus}-$ module and $End_S(W)$ has the (SSP). Then, every maximal direct summand of W is a $mgs^{\oplus}-$ module.

Proof. By Theorem 2.3 in [14], Whas (SIP) and (SSP). It well down that any module having (SIP) satisfies the (D_3) condition. Now the proof follows by Theorem 10.

In [15], a submodule L of $W$is called as *fully invariant* if $f(L)$ is included in L for each endomorphism f of W. It is known that $Rad(W)$ and $\tau(W)$ are fully invariant submodules of W.

Theorem 12. Let W be a $mgs^{\oplus}-$ module and $L \leq W$. If L is a fully invariant submodule of W, then W/L is a $mgs^{\oplus}-$ module.

Proof. Assume that T/L is a maximal submodule of W/L. Then, T is a maximal submodule of W and so we have submodules X, X_1 of $W$where $W = T + X$, $T \cap X \subseteq Rad(X)$ and $W = X \oplus X_1$ by the hypothesis. Since L is a fully invariant submodule of W, we can write $L = (L \cap X) \oplus (L \cap X_1)$ by Lemma 2.1 in [15]. Moreover, $(X + L)/L$ is a Rad-supplement of T/L in W/L according to Proposition 2.6 in [7]. Then $W/L = \left[(X + L)/L\right] \oplus \left[(X_1 + L)/L\right]$. Consequently, $(X + L)/L$ is a Rad-supplement of T/L such that $\left((X + L)/L\right) \leq_{\oplus} W/L$ and W/L is a $mgs^{\oplus}-$ module.

Corollary 13. Let W be a $mgs^{\oplus}-$module. Then $W/Rad(W)$ and $W/\tau(W)$ are $mgs^{\oplus}-$ modules.

Proposition 14. Let W be a $cgs^{\oplus}-$module and L be a fully invariant submodule of W. If L is a maximal direct summand of W, then L is a $mgs^{\oplus}-$module.

Proof. Assume that L is a maximal direct summand of W. Then, there is a submodule L_1 of W satisfying $W = L \oplus L_1$. Let T be a maximal submodule of L. As every maximal submodule is cofinite, evidently L/T is finitely generated. Since $W/L \cong L_1$ is simple and so $W/L \cong L_1$ is finitely generated. Hence T is a cofinite submodule of W. Because

$$W/T = (L \oplus L_1)/T = (L/T) \oplus (L_1 \oplus T)/T \cong (L/T) \oplus L_1$$

is finitely generated. By using the hypothesis, one can write $W = T + K$, $T \cap K \subseteq Rad(K)$ and $W = K \oplus K_1$ where $K, K_1 \leq W$. Since L is a fully invariant submodule of W,we can write $L = (L \cap K) \oplus (L \cap K_1)$ by Lemma 2.1 in [15]. By taking the intersection of both sides of the equation $W = T + K$ with L, we can obtain the following equality $L = L \cap W = L \cap (T + K) = T + (L \cap K)$. In addition to these, it can be written that $T \cap (L \cap K) = T \cap K \subseteq Rad(K) \subseteq Rad(W)$. Since $L \cap K \leq_{\oplus} L$ and $L \leq_{\oplus} W$, we can get $L \cap K \leq_{\oplus} W$. By using chapter 2.2.(6) in [6], $T \cap (L \cap K) = T \cap K \subseteq Rad(L \cap K)$ can be written. This implies that L is a $mgs^{\oplus} -$ module.

Theorem 15. Let Wbe a module and $W_1, W_2 \leq W$ such that $W = W_1 \oplus W_2$. Then W_2 is a $mgs^{\oplus} -$module if and only if there is a submodule T of W_2 such that $T \leq_{\oplus} W$, $W = L + T$ and $L \cap T \subseteq Rad(T)$ for each maximal submodule L/W_1 of W/W_1.

Proof. (⇒)Assume that L/W_1 is a maximal submodule of W/W_1. It is well known that $\left(W/W_1\right)\Big/\left(L/W_1\right) \cong W/L$ is simple. Since the following equality

$$W/L = (W_1 + W_2)/L = \left(W_1 + W_2 + (L \cap W_2)\right)\Big/L = (L + W_2)/L \cong W_2/(L \cap W_2)$$

can be written, we get that $L \cap W_2$ is a maximal submodule of W_2. From the hypothesis, we have submodules, T_1 of W_2 such that $W_2 = (L \cap W_2) + T$, $(L \cap W_2) \cap T \subseteq Rad(T)$ and $W_2 = T \oplus T_1$. From here, $W = L + T$ and $L \cap T \subseteq Rad(T)$ can be obtained. Hence $T \leq_{\oplus} W$ because of $T \leq_{\oplus} W_2$.
(⇐)Let S be a maximal submodule of W_2 . If one consider the following equality

$$\left(W/W_1\right)\Big/\left((S + W_1)/W_1\right) \cong W/(S + W_1) = (W_1 + W_2)\Big/(S + W_1) = (S + W_1 + W_2)\Big/(S + W_1)$$
$$\cong W_2/[W_2 \cap (S + W_1)] = W_2/[S + (W_1 \cap W_2)] = W_2/S.$$

It can be written that $(S + W_1)/W_1$ is a maximal submodule of W/W_1. By the assumption, since there is a submodule T of W_2 where $T \leq_{\oplus} W_2$, $W = T + S + W_1$, $(S + W_1) \cap T \subseteq Rad(T)$, it is easy to

see that $W_2 = T + S$, $W_2 = T \oplus (W_2 \cap T_1)$ and $S \cap T \subseteq (S + W_1) \cap T \subseteq Rad(T)$. Hence, W_2 is a $mgs^{\oplus} -$ module.

Theorem 16. An arbitrary ring S is semiperfect if and only if every free $S-$module is a $mgs^{\oplus} -$module.

Proof. Firstly, assume that W is an arbitrary free $S-$module. By using Theorem 2.4 in [11], ${}_SS$ is a $cgs^{\oplus} -$ module and so ${}_SS$ is a $mgs^{\oplus} -$ module. Conversely, let a free $S-$module be a $mgs^{\oplus} -$ module. Then ${}_SS$ is a $mgs^{\oplus} -$module. ${}_SS$ is (cofinitely) $\oplus$-supplemented, i.e. S is semiperfect, due to Proposition 3.

Acknowledgment The authors would like to thank the referees for their helpful comments and valuable suggestions for improving the manuscript.

Funding/Financial Disclosure The authors have no received any financial support for the research, authorship, or publication of this study.

Ethics Committee Approval and Permissions The work does not require ethics committee approval and any private permission.

Conflicts of Interest The authors stated that there are no conflict of interest in this article.

Authors Contribution Authors contributed equally to the study.

References

[1] Wisbauer, R. (1991). *Foundations of Module and Ring Theory*. Gordon and Breach Science Publishing, Philadelphia.

[2] Eryılmaz, F. & Sözen, E. Ö. (2023). On a generalization of $\oplus -$co-coatomically supplemented modules. *Honam Mathematical Journal*, *45*(1), 146-159. https://doi:10.5831/hmj.2023.45.1.146

[3] Sözen E. Ö. & Eren, Ş. (2018). Modules that have a generalized $\delta -$supplement in every cofinite extension. *JP Journal of Algebra, Number Theory and Applications*, *40*(3), 241-254.

[4] Harmancı, A., Keskin, D. & Smith, P. F. (1999). On $\oplus -$supplemented modules. *Acta Mathematica Hungarica*, *83*(1–2), 161–169.

[5] Çalışıcı, H. & Pancar, A. (2004).$\oplus -$cofinitely supplemented modules. *Czechoslovak Mathematical Journal*, *54*(129), 1083–1088.

[6] Clark, J., Lomp, C., Vajana, N. & Wisbauer, R. (2006). *Lifting Modules*. Birkhauser, Basel.

[7] Wang, Y. & Ding, N. (2006). Generalized supplemented modules. *Taiwanese Journal of Mathematics*, *10*(6), 1589-1601.

[8] Büyükaşık, E. & Lomp,C. (2008). On a recent generalization of semiperfect rings. *Bulletin of Australian Mathematical Society*, *78*, 317-325.

[9] Talebi, Y., Hamzekolaei, A. R. & Tütüncü, D. K. (2009). On Rad-$\oplus$-supplemented modules. *Hadronic Journal*, *32*(5), 505-512.

[10] Talebi, Y. & Mahmoudi, A. R. (2011). On Rad-⊕-supplemented modules. *Thai Journal of Mathematics*, *9*(2), 373–381.

[11] Nişancı, B. & Pancar, A. (2010). On generalization of $\oplus$ −cofinitely supplemented modules. *Ukrainian Mathematical Journal*, *62*(2), 203-209, https://doi.org/10.1007/s11253-010-0344-4

[12] Koşan, M. T. (2009). Generalized cofinitely semiperfect modules. *International Electronic Journal of Algebra*, *5*(5), 58-69.

[13] Mohamed, S. H & Müller, B. J. (1990). *Continuous and Discrete Modules*. Cambridge University Press, Cambridge.

[14] Garcia, J. L. (1989). Properties of direct summands of modules. *Communications in Algebra*, *17*(1), 73-92, https://doi.org/10.1080/00927878908823714

[15] Özcan, A. Ç., Harmancı, A. & Smith, P. F. (2006). Duo modules. *Glasgow Mathematical Journal*, *48*, 533-545, https://doi.org/10.1017/S0017089506003260

Sinopfbd, 2024; 9(1): 44-60 **https://doi.org/10.33484/sinopfbd.1369460**

Sinop Üniversitesi Fen Bilimleri Dergisi
Sinop Uni J Nat Sci
E-ISSN: 2564-7873

https://dergipark.org.tr/tr/pub/sinopfbd

The Effect of Deposition Temperature on Structural, Morphological, and Dielectric Properties of Yttria-Doped Zirconia Thin Films

Şerif RÜZGAR[1] and Veysel ERATİLLA[2]

How to cite: Rüzgar, Ş., & Eratilla, V. (2024). The effect of deposition temperature on structural, morphological, and dielectric properties of yttria-doped zirconia thin films. *Sinop Üniversitesi Fen Bilimleri Dergisi*, *9*(1), 44-60. https://doi.org/10.33484/sinopfbd.1369460

Research Article

Corresponding Author
Şerif RÜZGAR
serif.ruzgar@batman.edu.tr

ORCID of the Authors
Ş.R: 0000-0002-4964-2202
V.E: 0000-0002-3511-5612

Received: 01.10.2023
Accepted: 13.02.2024

Abstract

The aim of this study was to investigate the effect of deposition temperature on the structural, optical, morphological, and dielectric properties of yttria-stabilised zirconia (YSZ) films prepared by sol-gel spin-coating method. X-ray diffraction (XRD) measurements of YSZ films showed that the peaks of the cubic phase were prominent and the peak intensities increased with deposition temperature. The crystallite size, dislocation density, and microstrain of the thin films were identified by XRD. It was observed that the crystal size of the YSZ thin films increased from 16 nm to 22 nm with the deposition temperature. The surface roughness of the thin films was found to have changed as revealed by Atomic Force Microscopy (AFM) measurements. The roughness increased from 7.72 nm to 11.92 nm with increasing temperature. The optical transmittance of the YSZ thin films was investigated in the wavelength range 200-900 nm and was found to increase slightly with increasing deposition temperature. Metal-Oxide-Semiconductor (MOS) devices were fabricated from these YSZ materials for dielectric characterization. The dielectric properties of the Ag/YSZ/n-Si MOS structure were investigated. It was found that the capacitance, conductivity and other dielectric parameters of these structures are strongly frequency dependent.

Keywords: Yttrium stabilized zirconia, MOS, dielectrics, annealing effect, sol gel

Biriktirme Sıcaklığının İtriyum Katkılı Zirkonya İnce Filmlerin Yapısal, Morfolojik ve Dielektrik Özelliklerine Etkisi

[1]Department of Opticianry Program, Vocational School of Health Services, Batman University, Batman, Turkey

[2]Faculty of Dentistry, Prosthetic Dentistry Department, Batman University, Batman, Turkey

Öz

Bu çalışmanın amacı, sol-gel spin-kaplama yöntemiyle hazırlanan itriya ile stabilize edilmiş zirkonya (YSZ) filmlerin yapısal, optik, morfolojik ve dielektrik özelliklerine biriktirme sıcaklığının etkisini araştırmaktır. YSZ filmlerinin X-ışını kırınımı (XRD) ölçümleri, kübik fazın tepe noktalarının belirgin olduğunu ve tepe yoğunluklarının biriktirme sıcaklığıyla birlikte arttığını gösterdi. İnce filmlerin kristalit boyutu, dislokasyon yoğunluğu ve mikro gerilimi XRD ile belirlendi. YSZ ince filmlerinin kristal boyutunun biriktirme sıcaklığıyla birlikte 16 nm'den 22 nm'ye arttığı gözlendi. Atomik Kuvvet Mikroskobu (AFM) ölçümleri sonucunda ince filmlerin yüzey pürüzlülüğünün değiştiği tespit edildi. Artan sıcaklıkla pürüzlülük 7.72 nm'den 11.92 nm'ye yükseldi. YSZ ince filmlerinin optik geçirgenliği 200-900 nm dalga boyu aralığında araştırılmış ve artan biriktirme sıcaklığıyla birlikte hafifçe arttığı

bulunmuştur. Dielektrik karakterizasyonu için bu YSZ malzemelerinden Metal Oksit-Yarı İletken (MOS) cihazlar üretildi. Ag/YSZ/n-Si MOS yapısının dielektrik özellikleri araştırıldı. Bu yapıların kapasitans, iletkenlik ve diğer dielektrik parametrelerinin güçlü bir şekilde frekansa bağlı olduğu bulunmuştur.

Anahtar Kelimeler: İtriyum stabilize zirkonya, MOS, dielektrikler, tavlama etkisi, sol jel

Introduction

Zirconium dioxide, also known as zirconia (ZrO2), was first discovered in 1789 [1]. Zirconia films possess a number of exceptional properties that give them an important role in both theoretical research and real-world applications. Due to its chemical stability, high dielectric constant, high degree of transparency in the ultraviolet and visible spectrum, high forbidden optical band gap, high melting point, high hardness and good thermal insulation properties, this versatile material can be used for a number of practical applications such as thermal and chemical barriers, as buffer layers for growing high-temperature superconducting films and as sensors in microelectronics [2-5]. Traditionally, zirconia has been doped with many metal oxides such as Y2O3, CaO, La2O3, MgO and Ce2O3 [6]. Typically, these oxides are doped to maintain zirconia in its tetragonal or cubic phase at low temperatures [6]. Among these oxides, yttrium oxide, when doped into the zirconia material, also imparts various properties to the host material. Some of these benefits can be listed as follows: Improved mechanical properties: The addition of yttria to zirconia can significantly improve its mechanical properties, including strength, toughness, and fracture resistance. This is due to the formation of a uniform and fine-grained microstructure, which can prevent crack propagation and increase corrosion resistance [7]. A high melting point and high thermal shock resistance make yttrium-stabilized zirconia ideal for high temperature applications such as solid oxide fuel cells, catalysis, and thermal barrier coatings [8]. YSZ is a potential material for use in oxygen sensors due to its high oxygen ion conductivity [9]. Due to its superior biocompatibility, low toxicity, and corrosion resistance, YSZ has been extensively researched for its potential application in dental and orthopedic implants [10, 11]. In addition, it is extensively used in implantology, orthodontics, restorative dentistry and prosthodontics, which are all sub-disciplines of dentistry, to improve the infrastructure of post-core material and crown-bridge restorations [12, 13]. Consequently, YSZ stands out as one of the popular solid electrolytes used in a variety of electrochemical devices such as gas sensors and oxygen membranes [14]. Apart from these devices, MOS structures in which YSZ films can be used as applications also attract attention with their extraordinary features. The MOS structure has been a widely adopted technology for several decades. Due to the interface effect of metal-oxide and oxide-semiconductor, this MOS device is primarily utilized for diodes and MOS capacitors in integrated circuits, particularly photodiodes [15, 16]. Furthermore, MOS structures are suitable for energy storage devices due to the dielectric property of the oxide layer [17]. It is possible to create high-quality YSZ oxides utilizing a range of physical and chemical methods. These techniques include atomic layer deposition [18], laser-assisted plasma coating

[19], power impulse magnetron sputtering [20], chemical vapor deposition [21] and the sol-gel method [22, 23]. Among these methods, sol-gel offers several advantages over other deposition techniques, including: uniformity and control, which allows for precise control over the thickness and composition of the deposited films, low temperature processing, high purity, versatility, cost effectiveness, which is relatively inexpensive compared to other deposition techniques [24-26]. The aim of this study is to investigate the influence of deposition temperature on the properties of YSZ thin films and to explore the underlying mechanisms that control their growth and material properties. The results of this investigation will provide insight into the structure-property relationships of YSZ thin films and facilitate the optimization of their performance for various applications. Ultimately, a better understanding of the effect of deposition temperature on YSZ thin films will enable the production of high quality YSZ thin films with desired properties.

Experimental

In this study, the sol-gel technique was used to deposit thin films. Zirconyl chloride octahydrate (sigma-aldrich) and yttrium (III) nitrate hexahydrate (sigma-aldrich) were employed as starting materials for the synthesis of YSZ thin films. YSZ precursors of 0.1 M were prepared by dissolving zirconium oxychloride octahydrate and yttrium (III) nitrate hexahydrate in 2-methoxyethanol solvent with monoethanolamine stabilizer. The yttrium ratio in the ZrO2 solution was adjusted to 7% of the atomic weight of the zirconium metal. The prepared solution was stirred at 60°C for 2 hours to obtain a transparent liquid. Prior to the formal coating process, the precursor liquid was filtered through a 0.22 μm injection filter. Prior to thin film deposition, Si and quartz substrates were cleaned using RCA (Radio Corporation of America) cleaning techniques. In addition to this cleaning, n-Si substrates were immersed in 1% HF solution and the natural SiO2 on the surface was removed. Finally, the n-Si and quartz substrates were rinsed with deionized water and dried with N_2 gas to obtain a hydrophilic surface. YSZ films were grown on n-Si and quartz substrates at room temperature for 30 s at 3000 rpm. After each deposition, the films were pre-annealed in an oven at 300°C and this process was repeated 10 times. Finally, YSZ films were annealed for 2 hours at 700°C, 900°C, and 1100°C, respectively. These films were designated as YSZ7 (annealed at 700°C), YSZ9 (annealed at 900°C) and YSZ11 (annealed at 1100°C) respectively. The thicknesses of YSZ7, YSZ9, and YSZ11 films were determined by atomic force microscopy to be 220 nm, 120 nm, and 95 nm, respectively. The schematic diagram of the YSZ/n-Si MOS structure, which was fabricated to examine the capacitance properties of the produced thin films, is shown in Figure 1. In order to perform the electrical characterization of the produced MOS structures, silver paste contacts were made on the films. The resistivity of commercially purchased silver paste is 1.59 μΩ-cm. The C-V characterization of the structures was carried out using the Keithley 4200 semiconductor characterization system. Optical, crystallographic and surface properties of thin films

were investigated using Shimadzu UV-19, Rigaku Miniflex II, and Park System XE-100 Atomic Power Microscope, respectively.

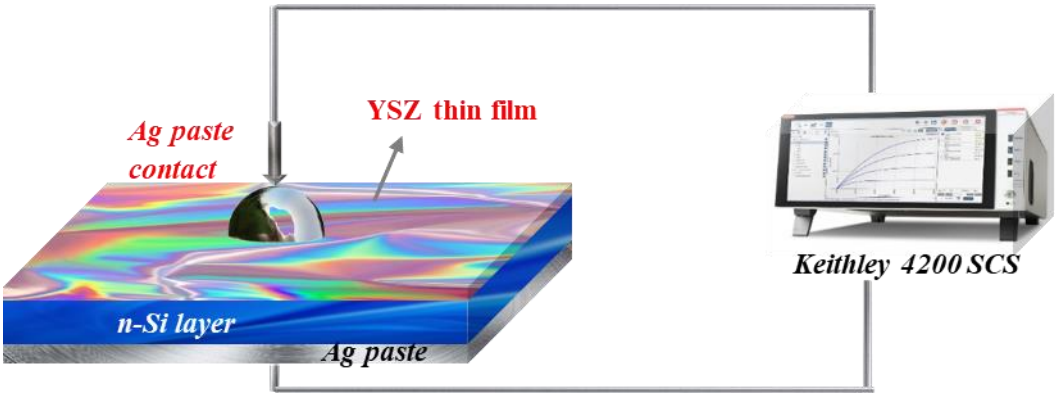

Figure 1. *The schematic diagram of YSZ/n-Si MOS structure*

Result and Discussions

The crystallinity and preferred crystal orientation of the YSZ films were determined through the XRD technique. Figure 2 shows the XRD patterns of YSZ thin films formed on n-Si substrates at 0.1 M with varying deposition temperature and the photograph of the YSZ thin films deposited on n-Si wafers. The cubic crystal structure is confirmed by the four prominent peaks corresponding to (111), (200), (220) and (311) planes in all YSZ thin film samples [27-29]. No impurity peaks are visible either, all of these polycrystalline ZrO2 films are free of impurities. The intensity of the most prominent (111) reflection is observed to increase with increasing deposition temperature, indicating that the improvement in crystal quality of YSZ is caused by the increase in temperature. The (200), (220), and (311) orientations are the other orientations observed with slightly lower intensities. The average crystal size of the nanostructured YSZ films is calculated by the semi-empirical Debye-Scherrer formula [24]:

$$D = \frac{0.9\lambda}{\beta \cos\theta} \quad (1)$$

where D, λ, θ, and β are the mean crystal size, the applied X-ray wavelength, the diffraction angle in degrees and the full width at half maximum (FWHM) of the observed diffraction peak in radians, respectively. The D values for YSZ films were calculated to be 16 nm, 19 nm and 22 nm for YSZ7, YSZ9 and YSZ11 films from AFM micrographs, respectively. The increase in crystallite size with increasing temperature can be explained by the coalescence of smaller crystallites into larger ones. During this process, elevated temperatures can induce grain boundary migration leading to the growth of larger grains [30-32].

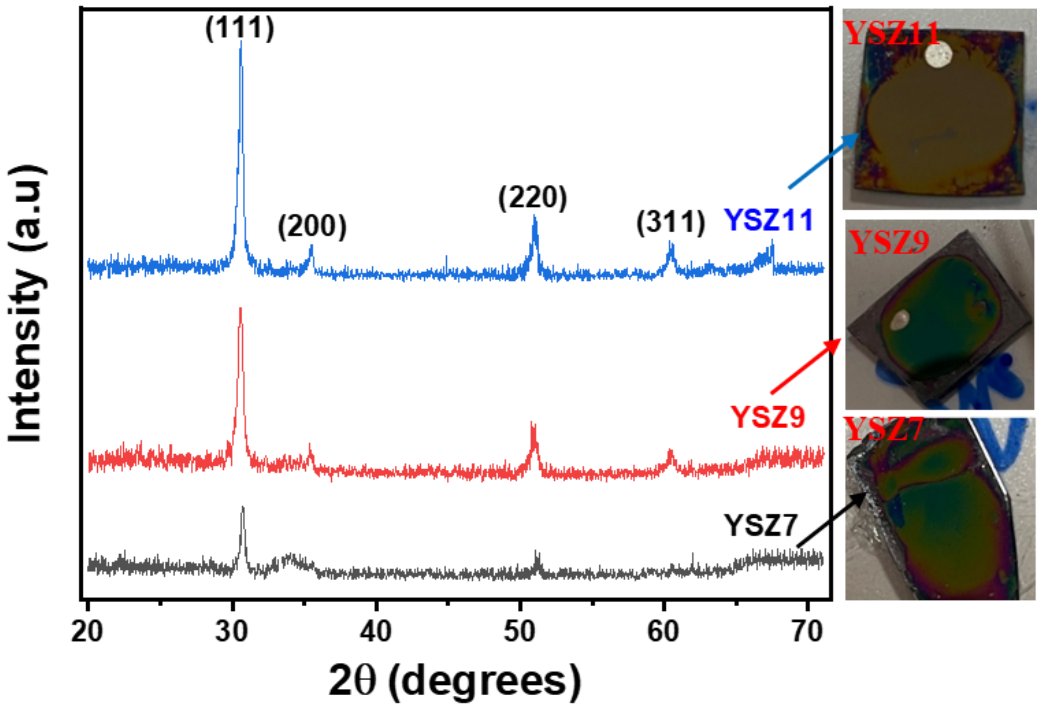

Figure 2. *The XRD patterns of YSZ thin films and the photograph of the YSZ thin films coated on n-Si wafers*

The improved crystallinity is achieved by annealing, which allows the atoms of the film to rearrange into a more ordered structure. In addition, it has been hypothesized that annealing films can reduce residual stress and a defect in the lattice structure, which would increase the growth rate [28, 33]. Other important parameters of crystal structures are dislocation density (δ), which is a measure of the number of dislocations (line defects) present in a crystal structure, and microstrain (ε), which is a measure of the degree of elastic deformation or strain within a crystal structure. These parameters can be defined by the following equations [27];

$$Dislocation\ density\ (\delta) = \frac{1}{D^2} \quad (2)$$

$$Micro\ strain\ (\varepsilon) = \frac{\beta \cos\theta}{4} \quad (3)$$

The D, δ, and ε values of the thin films are given in Table 1. From the observations, it can be concluded that changing the annealing temperature for YSZ thin films causes changes in the recrystallization process and parameters.

Table 1. *Crystallite size, dislocation density and micro strain of YSZ thin films obtained at different deposition temperature*

Sample	Crystallite Size, D (nm)	Dislocation Density, δ (10^{14} m^{-1})	Micro strain, ε (10^{-4})
YSZ7	16	40	22
YSZ9	19	29	18
YSZ11	22	21	16

The effect of annealing temperature on the surface morphology of YSZ films was investigated using AFM. Figure 3 shows the AFM images of the films.

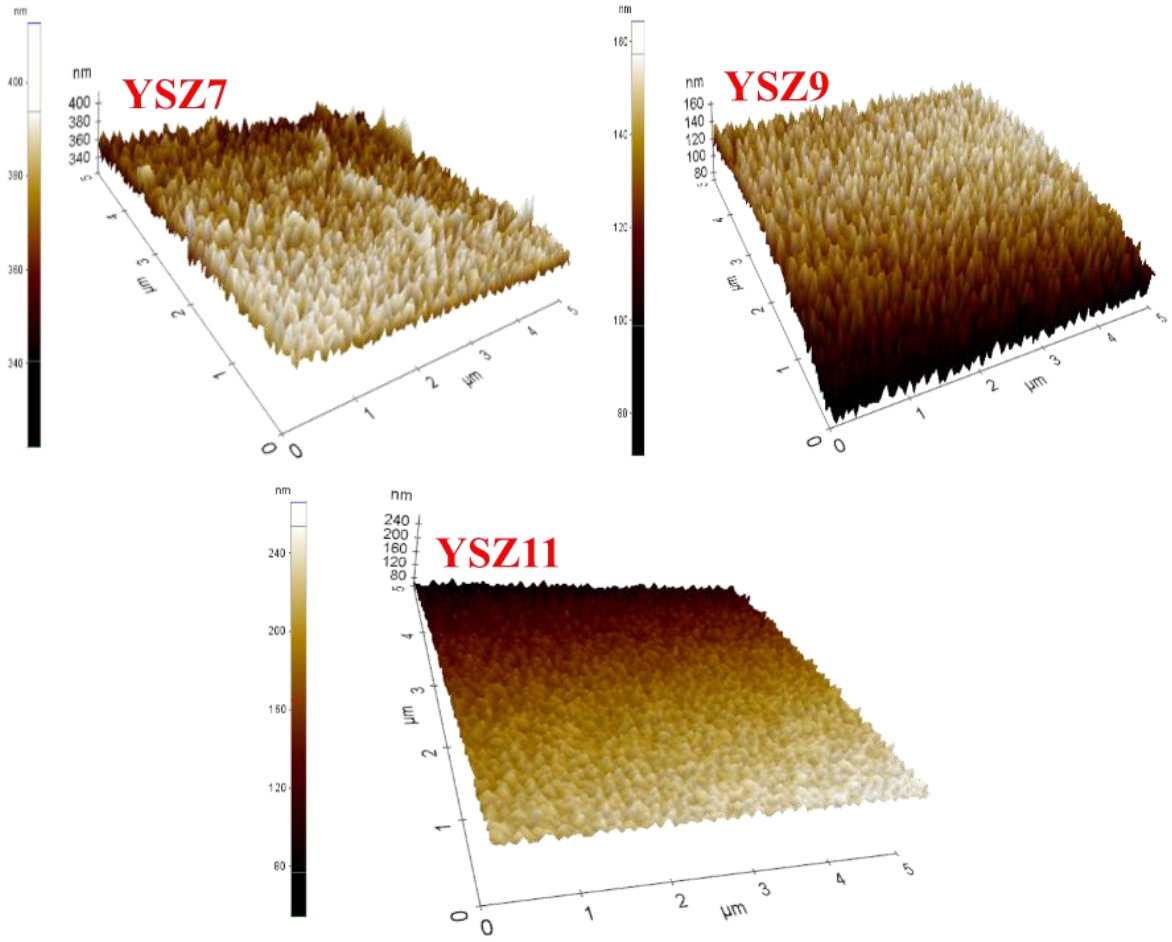

Figure 3. *The AFM images of YSZ thin films*

The surface roughness values for YSZ7, YSZ9 and YSZ11 films are 7.72 nm, 10.25 nm and 11.92 nm respectively. The AFM results showed that rougher films were formed with increasing growth temperature. The increase in roughness of Al doped ZrO2 films with annealing temperature was also reported by Cai et al. [34]. The increased surface roughness associated with annealing at higher temperatures may be due to agglomeration phenomena caused by greater heat absorption or a possible

crystallization factor resulting in large grains [34, 35]. The optical properties of the YSZ thin films were investigated using transmittance analyses. Figure 4 shows the spectra as a function of wavelength obtained by using UV-Vis spectroscopy to define the transmittance spectra in the range 200-900 nm.

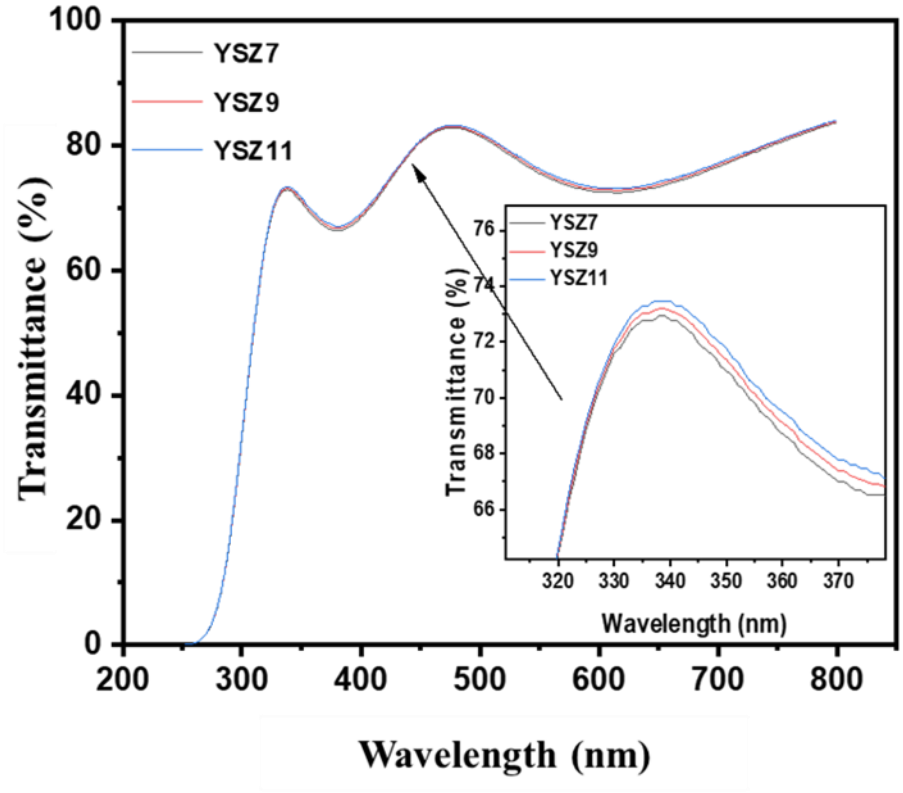

Figure 4. *The transmittance spectra of YSZ thin films. (Inset: Zoom of transmittance spectra)*

When the transmittance measurements of the YSZ films are examined, it can be seen that the thin films have a transmittance in the range of about 66-83%, and it can be seen from the inset graph that the transmittance increases slightly as the growth temperature increases. The transmittance of thin films can be influenced by several factors including the composition, thickness and microstructure of the film [36]. In general, increasing the deposition temperature can improve the crystallinity and reduce the defects in the thin film, leading to higher transmittance [37, 38]. Additionally, the optical transparency analysis of the films revealed slight interference fringes, which could be attributed to the homogeneity and smooth morphology of the thin films [39, 40]. The Tauc model was used to calculate the energy band gap (Eg) of YSZ films. The (ahυ)^2-hυ graphs of thin films are drawn and shown in Figure 5. It was observed from the graph that the optical band gaps of the thin films decreased as the deposition temperature increased. This situation is generally attributed to the quantum size effect [41, 42].

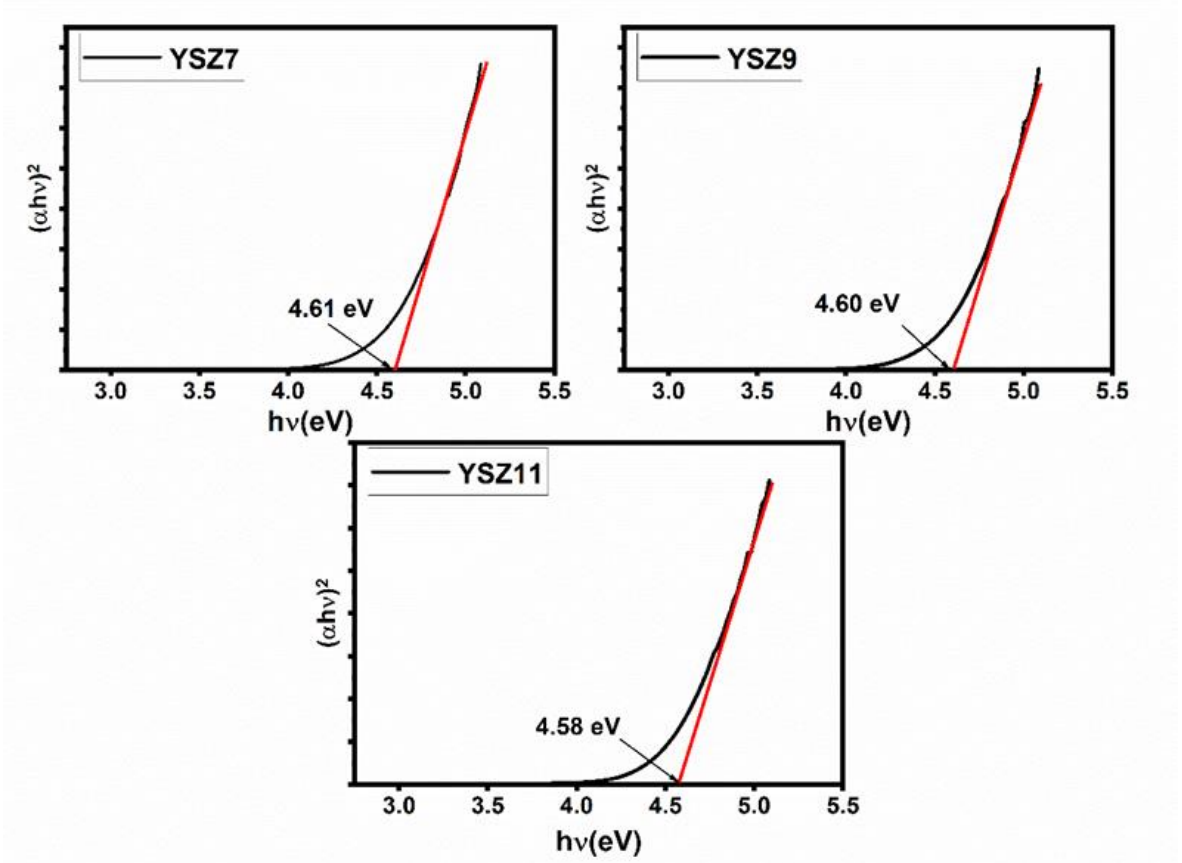

Figure 5. *Band gap prediction of YSZ thin films at various deposition temperatures using the Tauc method*

A dielectric is an insulator that can be polarized under an electric field. When subjected to an external electric field, electric charges within this dielectric material do not generate a current. However, the equilibrium positions of the charges change. As a result, the dielectric material becomes polarized and an electric field is generated within it. The external electric field is partially counteracted by the electric field within the material, which works towards equilibrium. This internal electric field persists, particularly in metals, until the applied external electric field is zeroed. Although the term "insulator" commonly implies low electrical conductivity, the term "dielectric" is typically used to describe materials with a high polarization capability. This is expressed by a quantity called the dielectric constant [43, 44]. In order to investigate some basic physical properties of the fabricated Ag/YSZ/n-Si MOS capacitor, capacitance-frequency (C- log (ω)), and conductance-frequency (G- log (ω)) measurements were investigated in a wide frequency range at room temperature. The C- log (ω) and G- log (ω) plots of the Ag/YSZ/n-Si structure is shown in Figure 6(a) and (b), respectively. The C- log (ω) plot for the fabricated structures is shown in Figure 6(a). According to this graph, the capacitance value decreases with increasing frequency and then reaches a constant value towards higher frequencies. This phenomenon is caused by the ability of the charge carriers to follow the AC signal. The contribution to the capacitance is limited because the charges at the states/traps cannot follow the AC signal at higher frequencies [45]. Upon examining the measurements of the fabricated MOS structures, it was observed

that the conductivity remained relatively unchanged up to 100 kHz, and thereafter, it increased with the rising frequency. The interface states and the ability of the charges to relax with time may be the cause of the change in conductivity with increasing frequency [46, 47]. Figure 6(c) shows the series resistance versus frequency (Rs-log (ω)) curves of MOS's calculated from C-f and G-f values. When the Rs-log (ω) curves of the MOS are examined, it can be seen that the series resistance values decrease with increasing frequency and remain constant at high frequencies. The presence of fixed and mobile oxide charges, as well as trapped charges in the oxide forming the interface states, can be identified as the underlying cause of the observed series resistance behavior [46, 48]. The fact that the series resistance values at high frequencies remain constant with frequency suggests that the interface states may not be able to follow the AC signal at these frequencies [45]. The localized states at the interface and the thickness of the layer are the main contributing elements, and together they have a considerable impact on the interfacial layer's dielectric characteristics and the capacitive performance of the MOS. As the experimental C and G values may change with bias voltage and frequency, a thorough dielectric analysis of the observed capacitive and conductive nature is required to appropriately determine the dielectric characteristic of the MOS [49].

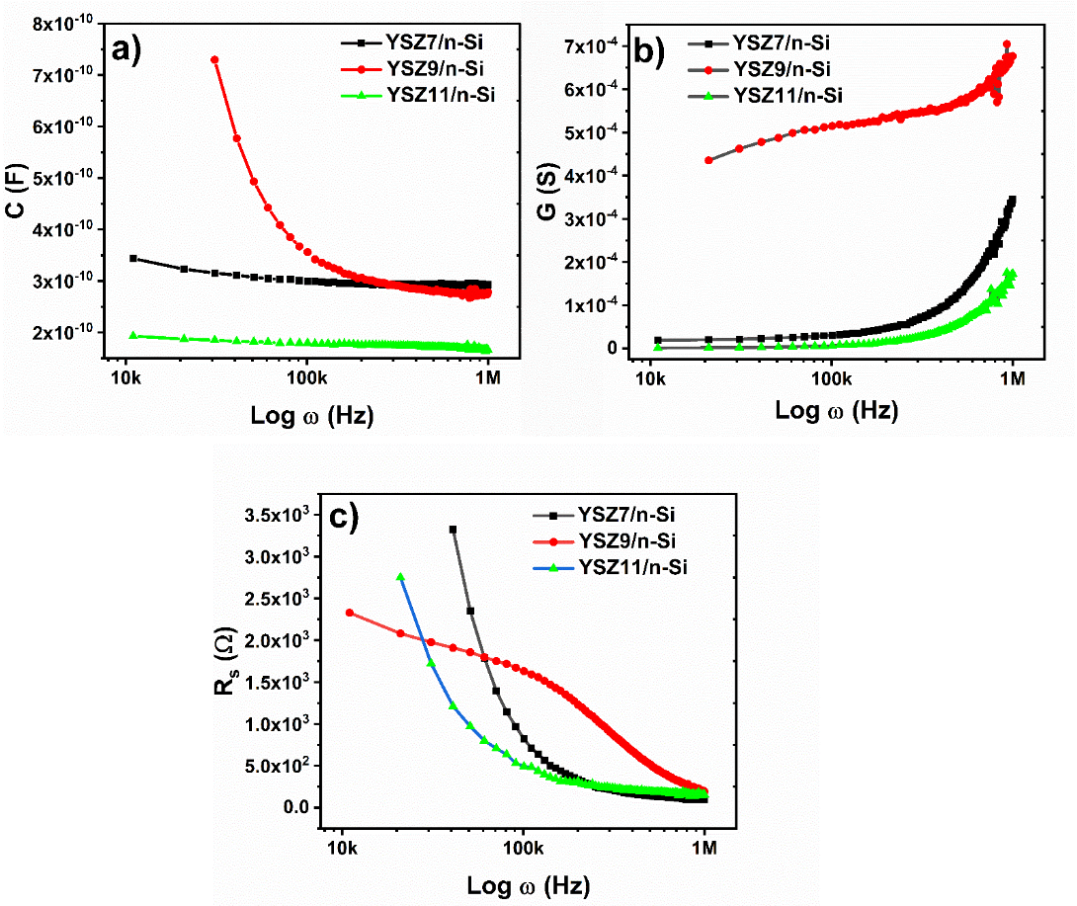

Figure 6. (a) *The plots of C- log (ω)* ***(b)*** *G- log (ω) and* ***(c)*** *Rs- log (ω) for Ag/YSZ/n-Si MOS structures*

In this situation, it is possible to evaluate the dielectric parameters complex dielectric constant (ε∗) and ac electrical conductivity (σ_{ac}). Typically, the ε' and ε" are used to represent the real and imaginary components of the complex dielectric constant (ε∗) for MOS's. The real part, sometimes referred to as the relative permittivity or dielectric constant, is represented by ε'. It is a measure of the ability of the material to store electric charge in an electric field. ε" represents the imaginary part, which is also known as the dielectric loss factor. It is a measure of the energy that is lost as heat when the material is subjected to an electric field. The values of ε' and ε" for MOS's depend on factors such as the materials used in the MOS and the frequency of the applied electric field. The complex dielectric constant can be defined as follows equation;

$$\varepsilon^* = \varepsilon' - i\varepsilon'' \tag{4}$$

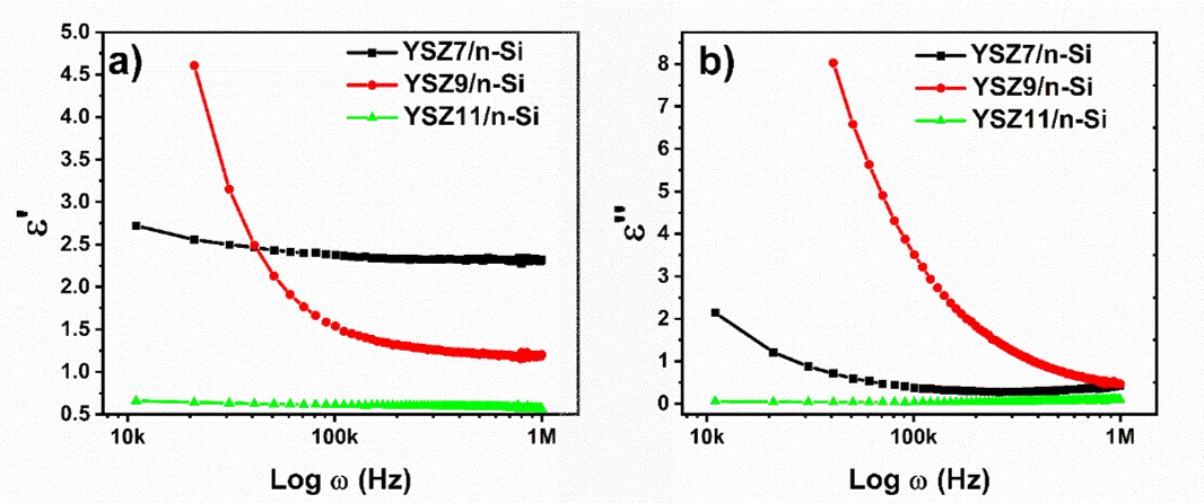

Figure 7. *(a) The plots of ε^'- log (ω) and (b) ε^''- log (ω) for Ag/YSZ/n-Si MOS structures*

This formulation can be stated as follows: given the admittance measurements,

$$\varepsilon^* = \frac{Y^*}{i\omega C_0} = \frac{C}{C_0} - i\frac{G}{\omega C_0} \tag{5}$$

where ω is the angular frequency of the applied electric field, and Y*, C, G, and C0 represent the measured admittance, capacitance, conductance, and capacitance of empty space of the dielectric material, respectively. Consequently, ε' and ε" can be expressed by the following equations:

$$\varepsilon' = \frac{C}{C_0} \qquad \varepsilon'' = \frac{G}{\omega C_0} \tag{6}$$

The frequency dependent ε^' and ε^" versus log (ω) are indicated in Figure 7 (a)-(b). When the graph is examined, it shows that ε and ε″ values are a strong function of frequency and that these values decrease with rising frequency. The decline in these values with frequency is usually attributed to the density of surface states, dipole, and interfacial polarization [50]. The loss tangent (tan δ) is a measure of the dielectric losses in a material, and it is commonly used to describe the electrical behavior of dielectric

materials. The ratio of the imaginary to real components of the dielectric constant is known as the loss tangent:

$$tan\ \delta\ = \frac{\varepsilon''}{\varepsilon'} \quad (7)$$

The term "loss tangent" refers to the process by which electrical energy dissipates within a dielectric material as a result of internal mechanisms that transform electrical energy into heat or other types of energy. Other examples of these mechanisms include electronic polarization, dipole relaxation, and molecular rotations. Furthermore, because the loss tangent is a frequency-dependent metric, it changes depending on the frequency of the electrical field that is being applied. Molecular and dipole rotations are frequently the dominant phenomena in the loss tangent at high frequencies, whereas electronic polarization predominates at low frequencies. Figure 8 (a) demonstrates the tan δ versus log (ω) for fabricated MOS structures. The loss tangent is an important parameter for dielectric materials because it affects the performance of various electrical devices, such as capacitors, transmission lines, and antennas [51]. High loss tangent materials are typically used in applications where energy dissipation is desired, such as in damping materials, while low loss tangent materials are preferred for applications where energy conservation is important, such as in high-Q resonators or microwave components [51]. There are not many studies in the literature examining the effect of deposition temperature on the dielectric properties of thin films on Si substrates. One of these few researches is the study conducted by Mehraj et al. [52], which examined the effect of annealing temperature on SnO_2. They reported that the peak in the tan δ graph occurs at high frequencies and that the jumping speed of charged particles (e−) increases as the annealing temperature increases. The Rezlescu model [53] provides a well-explained reasoning for the increased intensity of relaxation peak with annealing temperature. Based on this model, the relaxation peaks are a result of the combined contribution of n-type and p-type charge carriers [54]. Another important parameter for MOS structures is the AC electrical conductivity (σ_AC). The σ_AC is a complex quantity that describes the ability of a dielectric material to conduct AC current under the influence of an electric field. The expression for the AC electrical conductivity is:

$$\sigma_{AC}\ = \varepsilon''\omega\varepsilon_0 \quad (8)$$

Here ε_0 is the permittivity of free space. The variation in AC conductivity with frequency for Ag/YSZ/n-Si MOS at room temperature is presented in Figure 8 (b). The figure shows that the AC conductivity of the structures exhibits frequency-dependent behavior, and an increase in AC conductivity is observed with the increase in frequency. The observed increase in AC conductivity may be due to an improvement in the conduction process at a specific temperature within the high frequency range [55].

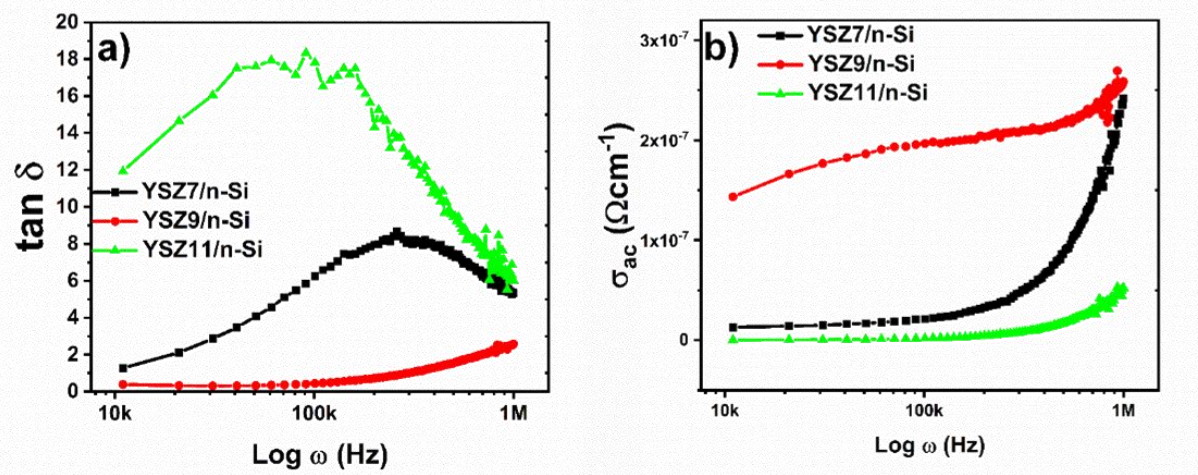

Figure 8. (a) *The plots of tan δ- log (ω) and* ***(b)*** σ_{AC}*- log (ω) for Ag/YSZ/n-Si MOS structures*

Conclusion

The yttrium-stabilized zirconia thin films were successfully grown at different deposition temperatures by sol-gel spin-coating technique. XRD analysis of YSZ films with thicknesses ranging from 95 to 220 nm showed that the cubic phase peaks were prominent and their intensities increased with higher deposition temperature. The XRD analysis also identified the crystallite sizes, dislocation density and microstrain of the thin films. It was observed that the crystal size of the YSZ thin films increased from 16 nm to 22 nm with increasing deposition temperature. AFM measurements showed that the surface roughness of the thin films changed with the deposition temperature, increasing from 7.72 nm to 11.92 nm. The optical transmittance of the YSZ thin films was investigated over a wavelength range of 200-900 nm, including both visible and near infrared spectra. The results showed a slight increase in optical transmittance with higher deposition temperature. Finally, MOS devices were fabricated using the YSZ films to evaluate their dielectric properties. The dielectric parameters of the Ag/YSZ/n-Si MOS structures were strongly dependent on frequency, including capacitance, conductivity and other related properties.

Acknowledgement We would like to thank Dr. Canan Aytug Ava for her contribution to the acquisition of AFM images. Batman University Commission of Scientific Research Project under Grant No. BTUBAP-2024-SHMYO-01 provided support for this study.

Funding/Financial Disclosure Not applicable.

Ethics Committee Approval and Permissions The study does not require ethics committee approval or any special permission.

Conflicts of Interest The authors declare that they have no known competing financial interests or personal relationships that could have appeared to influence the work reported in this paper.

Authors Contribution The author contributions to this article are as follows: Veysel Eratilla, Discussion, Editing and interpretation, Serif Ruzgar, Thin film deposition and MOS fabrication, Electrical and Optical measurements, Data analyses and graphs, Discussion, interpretation, Writing and editing.

References

[1] Piconi, C., & Maccauro, G. (1999). Zirconia as a ceramic biomaterial. *Biomaterials, 20*(1), 1-25. https://doi.org/10.1016/S0142-9612(98)00010-6

[2] Sprio, S., Guicciardi, S., Bellosi, A., & Pezzotti, G. (2006). Yttria-stabilized zirconia films grown by radiofrequency magnetron sputtering: Structure, properties and residual stresses. *Surface and Coatings Technology, 200*(14), 4579-4585. https://doi.org/10.1016/j.surfcoat.2005.04.003

[3] Kumar, D., Singh, A., Saini, B. S., Choudhary, B. C., Shinde, V., & Kaur, R. (2021). Effect of Ni doping on the structural and optical properties of ZrO_2 thin films. *Journal of Electronic Materials, 50*(1), 65-74. https://doi.org/10.1007/s11664-020-08558-0

[4] Kandpal, K., Gupta, N., Singh, J., & Shekhar, C. (2020). On the threshold voltage and performance of ZnO-based thin-film transistors with a ZrO_2 gate dielectric. *Journal of Electronic Materials, 49*(5), 3156-3164. https://doi.org/10.1007/s11664-020-08055-4

[5] Van, H. N., Van Huan, P., Nguyen, D.-H., Vu, N. H., & Pham, V.-H. (2019). Up/down-conversion luminescence of Er_3+ doped $ZrO_2 \cdot Al_2O_3$ powder. *Journal of Electronic Materials, 48*(12), 8054-8060. https://doi.org/10.1007/s11664-019-07644-2

[6] Kumar, D., Singh, A., Kaur, N., Thakur, A., & Kaur, R. (2020). Tailoring structural and optical properties of ZrO_2 with nickel doping. *SN Applied Sciences, 2*(4), 644. https://doi.org/10.1007/s42452-020-2491-z

[7] Chevalier, J. (2006). What future for zirconia as a biomaterial? *Biomaterials, 27*(4), 535-543. https://doi.org/10.1016/j.biomaterials.2005.07.034

[8] Chen, L. B. (2006). Yttria-stabilized zirconia thermal barrier coatings-A review. *Surface Review and Letters, 13*(05), 535-544. https://doi.org/10.1142/S0218625X06008670

[9] Guo, X., Vasco, E., Mi, S., Szot, K., Wachsman, E., & Waser, R. (2005). Ionic conduction in zirconia films of nanometer thickness. *Acta Materialia, 53*(19), 5161-5166. https://doi.org/10.1016/j.actamat.2005.07.033

[10] Flinn, B. D., deGroot, D. A., Mancl, L. A., & Raigrodski, A. J. (2012). Accelerated aging characteristics of three yttria-stabilized tetragonal zirconia polycrystalline dental materials. *The Journal of Prosthetic Dentistry, 108*(4), 223-230. https://doi.org/10.1016/S0022-3913(12)60166-8

[11] Cano, F. J., Castilleja-Escobedo, O., Espinoza-Pérez, L. J., Reynosa-Martínez, C., & Lopez-Honorato, E. (2021). Effect of deposition conditions on phase content and mechanical properties of yttria-stabilized zirconia thin films deposited by sol-gel/dip-coating. *Journal of Nanomaterials*, e4449890. https://doi.org/10.1155/2021/4449890

[12] Guven, S., Beydemir, K., Dundar, S., & Eratilla, V. (2015). Evaluation of stress distributions in peri-implant and periodontal bone tissues in 3- and 5-unit tooth and implant-supported fixed zirconia restorations by finite elements analysis. *European Journal of Dentistry, 9*(3), 329-339. https://doi.org/10.4103/1305-7456.163223

[13] Eratilla, V., Yildiz, A. D., Guven, S., Eratilla, E. A., Karaman, T., Aguloglu, S., & Sumer, E. (2016). Measuring the resistance of different substructure materials by sticking them to dentine with two different resin cements in vitro. *Nigerian Journal of Clinical Practice, 19*(6). https://doi.org/10.4314/njcp.v19i6

[14] Zscherp, M. F., Glaser, J., Becker, C., Beyer, A., Cop, P., Schörmann, J., Volz, K., & Elm, M. T. (2020). Epitaxial growth and structural characterization of ceria deposited by atomic layer deposition on high-surface porous yttria-stabilized zirconia thin films. *Crystal Growth & Design, 20*(4), 2194-2201. https://doi.org/10.1021/acs.cgd.9b01112

[15] Liu, C.-F., Tang, X.-G., Guo, X.-B., Liu, Q.-X., Jiang, Y.-P., Tang, Z.-H., & Li, W.-H. (2020). Photodiode characteristics of HfO_2 thin films prepared by magnetron sputtering. *Materials & Design, 188,* 108465. https://doi.org/10.1016/j.matdes.2019.108465

[16] Liu, C. W., Liu, W. T., Lee, M. H., Kuo, W. S., & Hsu, B. C. (2000). A novel photodetector using MOS tunneling structures. *IEEE Electron Device Letters, 21*(6), 307-309. https://doi.org/10.1109/55.843159

[17] Çokduygulular, E., Çetinkaya, Ç., Yalçın, Y., & Kınacı, B. (2020). A comprehensive study on Cu-doped ZnO (CZO) interlayered MOS structure. *Journal of Materials Science: Materials in Electronics, 31*(16), 13646-13656. https://doi.org/10.1007/s10854-020-03922-6

[18] Jang, D. Y., Kim, H. K., Kim, J. W., Bae, K., Schlupp, M. V. F., Park, S. W., Prestat, M., & Shim, J. H. (2015). Low-temperature performance of yttria-stabilized zirconia prepared by atomic layer deposition. *Journal of Power Sources, 274,* 611-618. https://doi.org/10.1016/j.jpowsour.2014.10.022

[19] Ouyang, Z., Meng, L., Raman, P., Cho, T. S., & Ruzic, D. N. (2011). Laser-assisted plasma coating at atmospheric pressure: Production of yttria-stabilized zirconia thermal barriers. *Journal of Physics D: Applied Physics, 44*(26), 265202. https://doi.org/10.1088/0022-3727/44/26/265202

[20] Sønderby, S., Aijaz, A., Helmersson, U., Sarakinos, K., & Eklund, P. (2014). Deposition of yttria-stabilized zirconia thin films by high power impulse magnetron sputtering and pulsed magnetron sputtering. *Surface and Coatings Technology, 240,* 1-6. https://doi.org/10.1016/j.surfcoat.2013.12.001

[21] Schlupp, M. V. F., Prestat, M., Martynczuk, J., Rupp, J. L. M., Bieberle-Hütter, A., & Gauckler, L. J. (2012). Thin film growth of yttria stabilized zirconia by aerosol assisted chemical vapor deposition. *Journal of Power Sources, 202,* 47-55. https://doi.org/10.1016/j.jpowsour.2011.11.016

[22] Díaz-Parralejo, A., Macías-García, A., Sánchez-González, J., Díaz-Díez, M. Á., & Cuerda-Correa, E. M. (2011). A novel strategy for the preparation of yttria-stabilized zirconia powders: Deposition and scratching of thin films obtained by the sol–gel method. *Journal of Non-Crystalline Solids, 357*(3), 1090-1095. https://doi.org/10.1016/j.jnoncrysol.2010.10.025

[23] Courtin, E., Boy, P., Rouhet, C., Bianchi, L., Bruneton, E., Poirot, N., Laberty-Robert, C., & Sanchez, C. (2012). Optimized sol–gel routes to synthesize yttria-stabilized zirconia thin films as solid electrolytes for solid oxide fuel cells. *Chemistry of Materials, 24*(23), 4540-4548. https://doi.org/10.1021/cm302177s

[24] Pakma, O., Özdemir, C., Kariper, İ. A., Özaydın, C., & Güllü, Ö. (2016). Wet chemical methods for producing mixing crystalline phase ZrO_2 thin film. *Applied Surface Science, 377,* 159-166. https://doi.org/10.1016/j.apsusc.2016.03.107

[25] Mathew Simon, S., George, G., M s, S., V p, P., Anna Jose, T., Vasudevan, P., Saritha, A. C., Biju, P. R., Joseph, C., & Unnikrishnan, N. V. (2021). Recent advancements in multifunctional applications of sol-gel derived polymer incorporated TiO_2-ZrO_2 composite coatings: A comprehensive review. *Applied Surface Science Advances, 6,* 100173. https://doi.org/10.1016/j.apsadv.2021.100173

[26] Shao, Z., Zhou, W., & Zhu, Z. (2012). Advanced synthesis of materials for intermediate-temperature solid oxide fuel cells. *Progress in Materials Science, 57*(4), 804-874. https://doi.org/10.1016/j.pmatsci.2011.08.002

[27] Waghmare, M., Sonone, P., Patil, P., Kadam, V., Pathan, H., & Ubale, A. (2018). Spray pyrolytic deposition of zirconium oxide thin films: influence of concentration on structural and optical properties. *Engineered Science, 5*(2), 79-87.

[28] Rusli, N. A., Muhammad, R., Ghoshal, S. K., Nur, H., & Nayan, N. (2020). Annealing temperature induced improved crystallinity of YSZ thin film. *Materials Research Express, 7*(5), 056406. https://doi.org/10.1088/2053-1591/ab9039

[29] Ramos-Guerra, A. I., Guzmán-Mendoza, J., García-Hipólito, M., Alvarez-Fregoso, O., & Falcony, C. (2015). Multicolored photoluminescence and structural properties of zirconium oxide films co-doped with Tb3+ and Eu3+ ions. *Ceramics International, 41*(9, Part A), 11279-11286. https://doi.org/10.1016/j.ceramint.2015.05.084

[30] Malek, M. F., Mamat, M. H., Musa, M. Z., Khusaimi, Z., Sahdan, M. Z., Suriani, A. B., Ishak, A., Saurdi, I., Rahman, S. A., & Rusop, M. (2014). Thermal annealing-induced formation of ZnO nanoparticles: Minimum strain and stress ameliorate preferred c-axis orientation and crystal-growth properties. *Journal of Alloys and Compounds, 610,* 575-588. https://doi.org/10.1016/j.jallcom.2014.05.036

[31] Aksoy, S., & Caglar, Y. (2014). Structural transformations of TiO_2 films with deposition temperature and electrical properties of nanostructure n-TiO_2/p-Si heterojunction diode. *Journal of Alloys and Compounds, 613,* 330-337. https://doi.org/10.1016/j.jallcom.2014.05.192

[32] Hu, S. Y., Lee, Y. C., Lee, J. W., Huang, J. C., Shen, J. L., & Water, W. (2008). The structural and optical properties of ZnO/Si thin films by RTA treatments. *Applied Surface Science, 254*(6), 1578-1582. https://doi.org/10.1016/j.apsusc.2007.07.134

[33] Heiroth, S., Frison, R., Rupp, J. L. M., Lippert, T., Barthazy Meier, E. J., Müller Gubler, E., Döbeli, M., Conder, K., Wokaun, A., & Gauckler, L. J. (2011). Crystallization and grain growth characteristics of yttria-stabilized zirconia thin films grown by pulsed laser deposition. *Solid State Ionics, 191*(1), 12-23. https://doi.org/10.1016/j.ssi.2011.04.002

[34] Cai, H., Tuokedaerhan, K., Lu, Z., Zhang, R., & Du, H. (2022). Effect of annealing temperature on the structural, optical, and electrical properties of al-doped ZrO_2 gate dielectric films treated by the sol–gel method. *Coatings, 12*(12). https://doi.org/10.3390/coatings12121837

[35] Fan, C., Liu, A., Meng, Y., Guo, Z., Liu, G., & Shan, F. (2017). Solution-processed SrOx-gated oxide thin-film transistors and inverters. *IEEE Transactions on Electron Devices, 64*(10), 4137-4143. https://doi.org/10.1109/TED.2017.2742060

[36] Tilli, M., Paulasto-Krockel, M., Motooka, T., Lindroos, V., Airaksinen, V.-M., Franssila, S., & Lehto, A. (2009). Handbook of Silicon Based MEMS Materials and Technologies. Elsevier.

[37] Wang, C. (2021). Effect of annealing temperature on the structure and optical properties of Mn doped ZnS thin films. *Journal of Modern Optics, 68*(14), 771-775. https://doi.org/10.1080/09500340.2021.1946183

[38] Li, J., Yang, W., Su, J., & Yang, C. (2018). Effects of deposition temperature on structural, optical properties and laser damage of laTiO$_3$ thin films. *Advances in Condensed Matter Physics,* e7328429. https://doi.org/10.1155/2018/7328429

[39] Hojabri, A. (2016). Structural and optical characterization of ZrO_2 thin films grown on silicon and quartz substrates. *Journal of Theoretical and Applied Physics, 10*(3), 219-224. https://doi.org/10.1007/s40094-016-0218-8

[40] Bakacak, P. K., Gur, E., Bayram, O., Tuzemen, S., & Simsek, O. (2021). Photoluminescence and structural properties of zirconium dioxide thin films produced by RF sputtering technique. *Journal of Materials Science: Materials in Electronics, 32*(6), 7541-7549. https://doi.org/10.1007/s10854-021-05468-7

[41] Satoh, N., Nakashima, T., Kamikura, K., & Yamamoto, K. (2008). Quantum size effect in TiO_2 nanoparticles prepared by finely controlled metal assembly on dendrimer templates. *Nature Nanotechnology, 3*(2). https://doi.org/10.1038/nnano.2008.2

[42] Gu, P., Zhu, X., & Yang, D. (2019). Effect of annealing temperature on the performance of photoconductive ultraviolet detectors based on ZnO thin films. *Applied Physics A, 125*(1), 50. https://doi.org/10.1007/s00339-018-2361-3

[43] Murarka, S. P., Eizenberg, M., & Sinha, A. K. (2003). Interlayer Dielectrics for Semiconductor Technologies. Elsevier.

[44] Özdemir, M. C., Sevgili, Ö., Orak, İ., & Türüt, A. (2020). Arayüzey doğal oksit tabakalı Al/p-Si/Al yapıların dielektrik karakteristiklerine ölçüm frekansının etkileri. *Journal of the Institute of Science and Technology, 10*(1). https://doi.org/10.21597/jist.612518

[45] Yıldız, D. E., & Dökme, İ. (2011). Frequency and gate voltage effects on the dielectric properties and electrical conductivity of Al/SiO_2/p-Si metal-insulator-semiconductor Schottky diodes. *Journal of Applied Physics, 110*(1), 014507-014507-5. https://doi.org/10.1063/1.3602090

[46] Cavdar, S., Demirolmez, Y., Turan, N., Koralay, H., & Tuğluoğlu, N. (2022). Analysis of voltage and frequency-dependent series resistance and interface states of Al/$ZnCo_2O_4$: Gelatin/n-Si diode. *Journal of Materials Science: Materials in Electronics, 33*(29), 22932-22940. https://doi.org/10.1007/s10854-022-09063-2

[47] Lok, R., Budak, E., & Yilmaz, E. (2020). Structural characterization and electrical properties of Nd_2O_3 by sol–gel method. *Journal of Materials Science: Materials in Electronics, 31*(4), 3111-3118. https://doi.org/10.1007/s10854-020-02857-2

[48] Elgazzar, E., Tataroğlu, A., Al-Ghamdi, A. A., Al-Turki, Y., Farooq, W. A., El-Tantawy, F., & Yakuphanoglu, F. (2016). Thermal sensors based on delafossite film/p-silicon diode for low-temperature measurements. *Applied Physics A, 122*(6), 617. https://doi.org/10.1007/s00339-016-0148-y

[49] Gullu, H. H., Yildiz, D. E., Surucu, O., & Parlak, M. (2020). Frequency effect on electrical and dielectric characteristics of HfO_2-interlayered Si-based Schottky barrier diode. *Journal of Materials Science: Materials in Electronics, 31*(12), 9394-9407. https://doi.org/10.1007/s10854-020-03479-4

[50] Pirgholi-Givi, G., Altındal, Ş., Shahedi Asl, M., Sabahi Namini, A., Farazin, J., & Azizian-Kalandaragh, Y. (2021). The effect of cadmium impurities in the (PVP–TeO_2) interlayer in Al/p-Si (MS) Schottky barrier diodes (SBDs): Exploring its electrophysical parameters. *Physica B: Condensed Matter, 604,* 412617. https://doi.org/10.1016/j.physb.2020.412617

[51] Sebastian, M. T. (2010). Dielectric Materials for Wireless Communication. Elsevier.

[52] Mehraj, S., Ansari, M. S., & Alimuddin. (2015). Annealed SnO_2 thin films: Structural, electrical and their magnetic properties. *Thin Solid Films, 589,* 57-65. https://doi.org/10.1016/j.tsf.2015.04.065

[53] Rezlescu, N., & Rezlescu, E. (1974). Dielectric properties of copper containing ferrites. *Physica Status Solidi (a), 23*(2), 575-582. https://doi.org/10.1002/pssa.2210230229

[54] Jonscher, A. K. (1999). Dielectric relaxation in solids. *Journal of Physics D: Applied Physics, 32*(14), R57. https://doi.org/10.1088/0022-3727/32/14/201

[55] Shukla, N., & Dwivedi, D. K. (2016). Dielectric relaxation and AC conductivity studies of Se90Cd10−xInx glassy alloys. *Journal of Asian Ceramic Societies*, *4*(2), 178-184. https://doi.org/10.1016/j.jascer.2016.02.003

Sinopfbd, 2024; 9(1): 61-71 **https://doi.org/10.33484/sinopfbd.1391287**

Sinop Üniversitesi Fen Bilimleri Dergisi
Sinop Uni J Nat Sci
E-ISSN: 2564-7873

https://dergipark.org.tr/tr/pub/sinopfbd

Topraktan Uygulanan Yarasa Gübresinin Mercimek Gelişimi ile Rizosfer Toprağının Bazı Biyolojik Özelliklerine Etkisi

Çiğdem KÜÇÜK[1] ve Ayşegül ARSLAN[2]

How to cite: Küçük, Ç., & Arslan, A. (2024). Topraktan uygulanan yarasa gübresinin mercimek gelişimi ile rizosfer toprağının bazı biyolojik özelliklerine etkisi. *Sinop Üniversitesi Fen Bilimleri Dergisi, 9*(1), 61-71. https://doi.org/10.33484/sinopfbd.1391287

Araştırma Makalesi

Sorumlu Yazar
Çiğdem KÜÇÜK
ckucuk@harran.edu.tr

Yazarlara ait ORCID
Ç.K: 0000-0001-5688-5440
A.A: 0000-0001-7425-3674

Received: 15.11.2023
Accepted: 14.02.2024

Öz

İnorganik gübrelerin sürekli kullanımı toprağın yapısını bozmakta, çevreye ve insan sağlığında olumsuz etkilere neden olmaktadır. Organik gübre uygulaması, bitki büyümesi için gerekli besin maddelerinin sağlanması açısından da güvenli alternatiflerden biridir. Bu çalışmada, organik gübre olarak kullanılan yarasa gübresinin mercimek gelişimi ve rizosferin bazı toprak mikrobiyolojik özellikleri üzerine etkisi araştırılmıştır. Toprağa farklı dozlarda uygulanan yarasa gübresinin mercimeğin bitki boyu, yeşil aksam ve kök kuru ağırlığı, kök uzunluğu, klorofil içeriği olumlu yönde etkilediği tespit edilmiştir. Uygulanan yarasa gübresinin rizosfer bölgesinin CO_2 içeriği, β-glukosidaz aktivitesi, maya+küf ve toplam bakteri düzeyini kontrole göre önemli oranda arttığı belirlenmiştir.

Anahtar Kelimeler: Yarasa gübresi, mercimek, rizosferin bazı biyolojik özellikleri

The Effect of Bat Guano Applied from Soil on Lentil Growth and Some Biological Properties of Rhizosphere Soil

[1]Harran Üniversitesi, Fen Edebiyat Fakültesi, Biyoloji Bölümü, Şanlıurfa, Türkiye

[2]Harran Üniversitesi, Fen Bilimleri Enstitüsü, Şanlıurfa, Türkiye

Abstract

Continuous use of inorganic fertilizers destroys the structure of the soil and causes negative effects on the environment and human health. Application of organic fertilizer is one of the safe alternatives in terms of providing the nutrients necessary for plant growth. In this study, the effect of bat fertilizer used as organic fertilizer on lentil growth and some soil microbiological properties of the rhizosphere was investigated. It has been determined that bat fertilizer applied to the soil at different doses positively affects plant height, green parts and root dry weight, root length and chlorophyll content of lentils. It was determined that the CO_2 content, β-glucosidase activity, yeast + mold and total bacteria levels of the rhizosphere region of the applied bat fertilizer increased significantly compared to the control.

Keywords: Bat fertilizer, lentils, some biological properties of the rhizosphere

Giriş

Son yıllarda oluşan iklim değişikliği nedeniyle dünyadaki tüm ülkelerin en önemli amacı; çevresel bozulmanın önlenerek yeterli, güvenli ve sağlıklı gıdanın sağlanmasıdır [1]. Organik tarım; çevre koşullarının tarım üzerindeki etkisini azaltarak sürdürülebilir gıda üretimi için alternatif bir tarım biçimi olarak düşünülmüştür [2-4]. Düşük oranlarda mineral gübrelerin bitki verimliliği ile toprağın kimyasal ve mikrobiyolojik özellikleri üzerinde olumlu etkisi olduğu yapılan çalışmalarda belirlenmiştir. İnorganik gübrelerin, amonifikasyon ve nitrifikasyon mikroorganizmalarının büyümesinin yanı sıra spor oluşturan bakterilerin çoğalmasını teşvik ettiği ve ürün atıklarının mineralizasyonunu uyardığı açıklanmıştır. Ancak verimliliği artırmak için inorganik gübrelerin kullanılmasının toprağın tamamen bozulmasına neden olduğu bildirilmiştir [5]. Yapılan araştırmalar, organik gübrelemenin inorganik gübrelemeye göre avantajını göstermiştir. Organik gübre uygulamasının ekolojiye ve çevreye minimum zarar veren bir bitkisel üretim sistemi olduğuna inanılmaktadır [4, 5]. Tarımsal alanlarda organik gübrelerin uzun süreli kullanımı toprak yapısını iyileştirmiş, toprağın agregat yapısını arttırabilmiş, bitki büyümesi ve üretimi için olumlu sonuç vermiştir [4, 5]. Ayrıca organik gübre; toprağın organik karbon havuzunu artırabildiğinden, bu da sonuçta karbon tutulmasının artmasına neden olmaktadır [5]. Günümüzde, büyükbaş hayvan gübresi ve idrarı, koyun gübresi, kümes hayvanı gübresi, yarasa gübresi, ipekböceği atıkları, solucan humusu gibi hayvan kökenli çeşitli organik gübrelerin kullanımı mevcuttur [6].

Yarasa gübresi N, P, K ve Ca açısından zengin olduğundan dünyanın birçok yerinde tamamlayıcı gübre olarak kullanılmaktadır [7]. Yarasa gübresinin, bitkinin ihtiyaç duyduğu tüm makro ve mikro besin maddelerini doğal formda içerdiğinden; gübre, toprak yapıcı, toprak temizleyici, nematosit, fungisit ve kompost aktivatörü olarak kullanıldığı açıklanmıştır [8]. Toprağa uygulanan yarasa gübresinin marul [9], karnabahar [10], mısır [11], biber [12] gelişimini olumlu yönde etkilediği tespit edilmiştir. Yapılan bir çalışmada da mısır ve buğday veriminin toprağın organik karbon, azot içeriğinin organik gübre uygulamaları ile arttığı, sakkaraz, üreaz ve glukosidaz enzim aktivitelerinin, toprak fauna popülasyonunun organik gübre uygulamaları sonucu arttığı rapor edilmiştir [13]. Fitriani ve ark. [14] farklı dozlarda uygulanan yarasa guanosunun biber gelişimi ve verimi üzerine etkilerini araştırdıkları çalışmalarında uygulama dozunun artışına bağlı olarak verimin arttığını saptamışlardır. Ayrıca araştırıcılar çalışmalarında; gübrenin uygulama dozunun toprak özellikleri, bitki gereksinimine bağlı olarak değiştiğini belirtmişlerdir [14]. Toprak mikroorganizmaları ile ilgili çalışmalar, küçük bir toprak hacminde yüksek miktarda bulunmaları nedeniyle oldukça zordur ancak ekosistem stabilitesi, toprak metabolizması ve verimlilik açısından çok önemlidir [15, 16]. Toprakta en aktif olan mikroorganizmaların en önemlileri olduğu, toprağa uygulanan gübrelerin de bu mikroorganizmalar üzerindeki etkisinin olduğu ortaya konmuştur [16]. Toprak mikroorganizmaları toprak verimliliği açısından büyük öneme sahiptir ve bunların biyokütlesindeki azot ve fosfor, bitki besinlerinin önemli

kaynaklarıdır [17]. Toprak ortamının kalitesi, mikrobiyal topluluğun bileşimini doğrudan etkileyebilmekte ve dolayısıyla bitki büyümesini ve sağlığını etkileyebilmiştir [18]. Tarımsal ekosistemlerdeki uygun bir mikrobiyal topluluk yapısı bitki gelişimini destekleyebilir ve toprağın mikrobiyal topluluk yapısındaki değişiklik, toprak sağlığı ve ürün veriminin önemli bir göstergesi olarak kullanılmaktadır [19]. FAO verileri dikkate alınarak incelendiğinde; mercimek verimi 2021 yılı itibarıyla 1.6 milyon tonluk üretimle Kanada dünya mercimek üretiminin yaklaşık %29'unu karşılayarak ilk sırada, Türkiye ise 263 bin ton üretim ile dördüncü sırada yer almıştır [20]. 2022 yılında ekim alanına göre Türkiye'de kırmızı mercimek ekim alanının %91.9'unun Güneydoğu Anadolu (2.7 milyon) Bölgesi'nde yapıldığı ve mercimek ekim alanının en fazla yapıldığı ilin 1.3 milyon dekar ekim alanı ile Şanlıurfa olduğu açıklanmıştır [20]. Yukarıdaki bilgiler ışığında, bu çalışmanın amacı yarasa gübresinin farklı dozlarının toprağa uygulanması ile mercimek bitkisinin büyüme özelliklerini ve rizosfer toprağın bazı mikrobiyolojik özellikleri üzerindeki etkisini değerlendirmektir.

Materyal ve Yöntem

Denemede bitki materyali olarak mercimek kullanılmıştır. Yarasa gübresi (organik madde içeriği %30, organik azot %3, fosfor %5, humik asit + fulvik asit %8, pH 6) ticari olarak satın alınmıştır. Topraklar 3 ardışık gün 121ºC'de 15 dakika otoklavlanarak kullanılmıştır. Kullanılan toprak killi bünyeye sahip olup; organik madde içeriği %1.65, fosfor içeriği 4.81 kg/da, tuz içeriği ise 0.82 dS/m, pH 7.68'dir. Deneme tesadüf parselleri deneme desenine göre 3 tekerrürlü olarak doğal ışık alan serada kurulmuştur. Yarasa gübresi %0 (kontrol), %0.5, %1 ve %1.5 (sırasıyla 0, 15 g, 30 g, 45 g olarak verilmiştir) olarak ekimle birlikte 3kg'lık saksılara uygulanmıştır. Tohumlar saksılara ekilmiş, gerektiğinde çeşme suyu (EC 310 µS/m, pH 7.45) ile sulanmış, ekimden 9 hafta sonra hasat edilmiştir. Hasat öncesi bir kısım yaprak örnekleri klorofil tayini için kullanılmıştır. Aşağıda açıklanan ölçümler yapılmıştır.

Bitki Boyu ve Kök uzunluğu

Hasat sırasında bitkinin toprakla temas ettiği kısımdan bitki uç kısmının uzunluğu cetvel ile ölçülerek bitki boyu belirlenmiştir. Kök boğazından kesilen kökler, topraktan arındırılmış, kurutma kağıdı üzerinde nemi alındıktan sonra cetvelle ölçülmüş, kök uzunluğu kaydedilmiştir.

Bitki Yeşil Aksam ve Kök Kuru Ağırlıkları

Hasat sonunda uygulamalardaki yeşil aksam ve kökler, kök boğazından kesilmiş, ayrı ayrı terazide tartılarak yaş ağırlıkları belirlenmiştir. Yaş ağırlıkları alınan örnekler 70ºC'de sabit ağırlığa gelinceye kadar kurutulmuş ve tartılarak kuru ağırlıkları belirlenmiştir.

Klorofil Tayini

Hasat sırasında her bir uygulamaya ait yaprak örnekleri (2 g) alınmış, yaprak örnekleri üzerine aseton: su karışımı eklenerek homojenize edilmiştir. Homojenize edilen örnekler Whatman no 2 filtre

kağıdından süzüldükten sonra, içerik spektrofotometrede 663 nm ve 645 nm'de okunmuş, toplam klorofil içeriği Arnon [21]'a göre hesaplanmıştır.

Rizosfer Bölgesinin Bazı Mikrobiyolojik Özellikleri

Hasat sırasında rizosfer bölgesinden alınan toprak örnekleri, 2 mm'lik eIekten elenerek, steril kapaklı torbalara konulmuş ve buz çantası ile laboratuvara getirilmiştir. Enzim aktivite testleri hemen yapılmış, mikroorganizma sayımı için toprak örnekleri -80°C'de saklanmıştır. Hasat sonrası her bir uygulamanın rizosferinden (bitki kök bölgesinden) alınan toprak örneklerinde mikrobiyolojik aktiviteyi belirlemek amacıyla Mikrobiyal toprak solunumu (CO_2 oluşumu) Anderson [22]'e göre; β-glukosidaz aktivite Küçük ve Cevheri [23]'e göre yapılmıştır. Uygulamalardan ayrı ayrı alınan toprak örneklerinden dilüsyonlar hazırlanmış, rizosferdeki toplam bakteri sayısı Nutrient agar, maya ve küf sayısı ise Sabouraud agar kullanılarak belirlenmiştir [24].

İstatistik Analiz

Deneme sonunda uygulamalara ait veriler JMP 11 istatistik programı kullanılarak analiz edilmiştir. Her bir analiz 3 tekerrürlü olarak yapılmıştır. Sonuçlar LSD testine göre gruplandırılmış, ortalamaların yanında harfle gösterilmiştir.

Bulgular ve Tartışma

Gereksiz ve aşırı inorganik gübre uygulaması çevreye zarar vermekte, su kaynaklarını kirletmekte ve faydalı canlı organizmaların azalmasına neden olmaktadır [25]. Bununla birlikte, organik tarım sistemleri inorganik gübre uygulamasından kaçınmakta ve bunun yerine verimi en üst düzeye çıkarmak için ürün rotasyonuna, organik gübrelere ve besin maddelerinin biyolojik mobilizasyon sistemlerine güvenmektedir [13]. Bu nedenle, inorganik gübrelere bağımlılığı azaltmak, ürün verimini artırmak, gıda arzını güvence altına almak ve organik maddenin geri dönüşümü ile çevreyi korumak için organik gübrelerin tek başına veya diğer gübrelerle birlikte büyüme performansı, verim potansiyeli ve ürün kalitesi üzerindeki etkinliğini araştırmak önemlidir. Bu çalışmada, farklı dozlarda uygulanan yarasa gübresinin, mercimek bitki boyu ve kök uzunluğu üzerinde etkileri Tablo 1'de görülmektedir.

Tablo 1. *Yarasa gübresinin farklı dozlarının mercimek bitki boyu ve kök uzunluğu, kuru ağırlık ve toplam klorofil içeriğine etkisi*

Doz (%)	Bitki Boyu (cm)	Kök Uzunluğu (cm)	Yeşil Aksam Kuru Ağırlığı (g/bitki)	Kök Kuru Ağırlığı (g/ bitki)	Toplam klorofil içeriği (µg/g yaprak)
Kontrol	26.3^{b}	11.0^{b}	0.391^{b}	0.081^{c}	1.74^{c}
0.5	31.0^{a}	16.7^{a}	0.587^{a}	0.118^{a}	2.42^{b}
1.0	31.0^{a}	16.0^{a}	0.580^{a}	0.119^{a}	2.55^{a}
1.5	30.3^{a}	12.0^{b}	0.509^{a}	0.111^{b}	2.52^{a}

Farklı harfler birbirinden farklı olan değerleri göstermektedir ($P < 0.05$).

Çalışmada farklı dozların mercimek bitki boyu ve kök uzunluğu incelendiğinde; hiçbir uygulamanın yapılmadığı kontrolle kıyaslandığında farklı artışlar sağlamıştır. Yarasa gübresinin %1.5 uygulama dozu bitki boyunu kontrole göre %13.2 oranında arttırmış, %0.5 ve %1'lik dozlar ise kontrolle karşılaştırıldığında %15.1 oranında bitki boyunda artışa neden olmuşlardır. Kök uzunlukları ise kontrolle karşılaştırıldığında; en yüksek artış %0.5 doz uygulamasında (%34.1) alınmış, bunu %1 (%31.25) ve %1.5 (%9 oranında artış) uygulama dozları izlemiştir. Farklı miktarlarda yarasa gübresinin toprağa ilave edilmesinin marulun kalite ve verim özellikleri üzerinde farklı artışlar olduğu, yarasa gübresi uygulaması ile marul boyunda artış olduğu yapılan bir çalışmada tespit edilmiştir [9]. Farklı organik gübrelerin karnabahar üzerindeki etkilerinin incelendiği araştırmada ise; sıvı formdaki yarasa gübresinin uygulanan diğer organik gübreler ile karşılaştırıldığında karnabaharın kök uzunluğu üzerinde daha etkili olduğu tespit edilmiştir [10]. Yarasa gübresinin farklı dozlarının mercimek yeşil aksam ve kök kuru ağırlıklarında artış sağladığı Tablo 1'de görülmektedir. Yarasa gübresinin %0.5, %1 ve %1.5 uygulama dozları kontrolle karşılaştırıldığında yeşil aksam ağırlığını sırası ile; %33.3, %32.5 ve %23.2 oranında arttırmıştır. Tablo 1'de görüldüğü gibi, yarasa gübresi uygulanmayan mercimek kök kuru ağırlığı 0.081 g/bitki olarak kaydedilmiş; % 0.5, % 1, % 1.5 dozlarının uygulanması ile sırasıyla 0.118 g/bitki, 0.119 g/bitki ve 0.111 g/bitki olarak belirlenmiştir. Uygulama dozlarının kuru ağırlık üzerine etkileri de yeşil aksam ağırlıklarında olduğu gibidir. Kontrolle karşılaştırıldığında; %0.5 uygulama dozunda kök kuru ağırlık %31.3, %1 uygulama dozunda kök kuru ağırlık %31.9 ve %1.5 uygulama dozunda kök kuru ağırlık ise %27 oranında artmıştır. Bitki büyümesini destekleyen mikro elementler ve bitki büyüme düzenleyicileri içeren yarasa gübresinin gübre olarak uygulanmasının bitki gelişimini artırdığı saptanmıştır [26, 27]. Yarasa gübresinin topraklara uygulanmasının bitkiler üzerindeki olumlu etkisinin yarasa gübresi içinde mevcut olan besin elementlerinden kaynaklandığı, gübrenin topraklara ilavesinin bitki yetiştirme bakımından da toprağın özelliklerinin de iyileştirildiği yapılan çalışmada da bildirilmiştir [4]. Çiçek [28] tarafından yapılan bir çalışmada; yarasa gübresi ve vermikompost uygulamalarının kadife çiçeği üzerindeki etkileri araştırılmıştır. Araştırıcı, her iki organik gübrenin uygulama dozlarının kadife çiçeğinin çiçek ağırlığı, bitki boyu, bitki ve kök yaş ve kuru ağırlıkları, kök uzunluğu, klorofil içeriği üzerinde etkili olduğunu tespit etmiştir. Bitkinin gelişimi ve besin alımı açısından kök gelişiminin ve kök bölgesinin aktivitesinin etkisi rapor edilmiştir [29]. Tarla ve sera koşullarında vermikompost ve yarasa gübresinin uygulanması ile bitkinin kök ağırlığının kimyasal gübre uygulaması yapılan bitkilerle karşılaştırıldığında daha fazla olduğu saptanmıştır [28]. Çalışmamızda da farklı dozlarda uygulanan yarasa gübresi; bitki yeşil aksam ve kök kuru ağırlığını farklı düzeyde etkilemiştir. Yarasa gübresinin uygulama dozlarının kontrole göre bitki ağırlığını artırması Misra ve ark. [29], Ulukapı ve Şener [10] tarafından da saptanmıştır. Fotosentez, bitkisel üretimi belirleyen ana metabolik süreçtir. Yaprak fotosentezi çeşitli iç ve çevresel parametreler tarafından düzenlenir [1]. Topraklara uygulanan farklı dozlardaki yarasa gübresinin yapraklardaki toplam klorofil içeriğine etkisi Tablo 1'de verilmiştir. Uygulanan yarasa gübresinin farklı dozları

mercimek yapraklarında klorofil içeriğini, kontrole göre arttırmıştır. En yüksek klorofil içeriği sırasıyla yarasa gübresinin %1 ve %1.5 uygulama dozlarında belirlenmiş, kontrole göre sırası ile %31.7 ve %30.95 ortamında artmıştır. Bu artış; bitkinin farklı dozlardaki yarasa gübresi uygulaması ile daha iyi besin durumu kazanması nedeniyle bitki kloroplastını daha verimli bir şekilde muhafaza etme yeteneğinden kaynaklanabilir [1]. Yapılan çalışmalarda; taze ve biriktirilmiş yarasa guanosunun; mısır ve darının büyüme biyokütlesi ve fotosentez üzerinde teşvik edici bir etkiye sahip olduğu belirlenmiş, bitki büyümesi ve ürün verimliliği için organik gübrenin yerine kullanılabileceğini öne sürülmüştür [1, 11]. Bay [12] yaptığı araştırmada; kapya biberi filkulağı ve postal çeşitlerinin yetiştirme ortamına leonardit ve yarasa gübresi uygulamış, en yüksek klorofil içeriğinin leonardit gübre uygulanmış filkulağı çeşidinde ve yarasa gübre uygulanmış bitki yapraklarında olduğunu saptamıştır. Çalışmamızda da kontrole göre klorofil içeriğindeki artış araştırıcıların bulguları ile de uyumludur. Farklı dozlarda uygulanan yarasa gübresi mercimek kök bölgesindeki CO_2 içeriğini arttırmıştır (Tablo 2). Toprak solunumu, bir sistemin mikrobiyal aktivitesini değerlendirmek için bir parametre olarak yaygın şekilde kullanılmaktadır [30]. Farklı dozlarda uygulanan yarasa gübresinin mercimek rizosfer toprağındaki CO_2 içeriği incelendiğinde; uygulanan %0.5, %1.0, %1.5 dozlar ile rizosferdeki CO_2 içeriği sırasıyla 55 mg CO_2-C/kg, 70.7 mg CO_2-C/kg ve 116.7 mg CO_2-C/kg olarak bulunmuştur, rizosfer toprağındaki CO_2 içeriğinin kontrole göre artış göstermesi; toprağa uygulanan organik maddenin aerobik mikroorganizmaların solunumu için enerji kaynağı sağladığı ve bu yüzden CO_2 içeriğinin yarasa gübresi uygulanan toprakta yüksek olduğu şeklinde düşünülmektedir.

Tablo 2. *Topraktan uygulanan yarasa gübresinin mercimek kök bölgesi bazı mikrobiyolojik özellikler üzerine etkisi*

Doz (%)	CO_2 içeriği (mg CO_2-C/kg toprak)	β-glukosidaz (µmol/PNP/g toprak)	Toplam Maya+Küf (x10^6 cfu/g)	Toplam Bakteri (x10^6 cfu/g)
Kontrol	39.7^{d}	1.63^{d}	0.34^{d}	1.60^{d}
0.5	55.0^{c}	4.62^{c}	2.26^{c}	8.81^{c}
1.0	70.7^{b}	5.18^{b}	8.13^{a}	9.14^{b}
1.5	116.7^{a}	5.41^{a}	6.93^{b}	16.33^{a}

Farklı harfler birbirinden farklı olan değerleri göstermektedir ***(P < 0.05).***

Çalışmada mercimek rizosfer toprağında CO_2 içeriği kontrolle karşılaştırıldığında; %0.5 uygulama dozunda %27.8, %1 uygulama dozunda %43.8 ve %1.5 uygulama dozunda %65.9 oranında artmıştır. Uygulama dozunun artması ile toprakta CO_2 içeriğinin artmasının nedeni; yarasa gübresinin rizosferde mikrobiyal popülasyonunu uyardığından kaynaklanabilir. Toprak solunumu sıklıkla toprak mikroorganizmalarının toplam aktivitesini ölçmek ve toprak verimliliğini değerlendirmek için kullanılır, gübreleme ve ekim düzeninden etkilenir [31]. Gübre uygulanmayan topraklarla karşılaştırıldığında farklı dozlardaki yarasa gübresi uygulaması, toprağın solunumunu önemli ölçüde iyileştirebilmiştir (Tablo 2). Bunun nedeni, gübrenin topraktaki azotun kullanılabilirliğini arttırması, bitki köklerinin ve kök salgılarının bitki büyümesini teşvik etmesi ve mikrobiyal solunumu arttırması

olabilir [13, 32]. Topraktaki enzimatik aktivite büyük ölçüde mikroorganizmalar [33], mevcut besinler [34] ve kök eksüdaları [35] ile ilişkilidir. Martens ve ark. [36] organik madde katkılı topraklarda enzim aktivitelerinin katkısız topraklara kıyasla ortalama iki kat ile dört kat arasında arttığını bildirmişlerdir. Bu sonuçlar, yarasa gübresinin %0.5, %1 ve %1.5 uygulamalarının yapıldığı topraklardaki β-glukosidaz aktivitelerinin kontroldeki aktiviteye göre daha yüksek olduğunu belirlememizle benzerlik göstermektedir. Topraktaki hücre dışı enzimlerden, toprağın organik maddesinin parçalanmasında rol oynayan β-glukosidaz, bitki polisakkaritlerinin ana bileşeni olan selülozun parçalanması sürecinde yer alan enzimdir. β-glukosidaz mikroorganizmalar için önemli bir enerji kaynağını sağlayan enzimdir [37]. Tablo 2'de farklı dozlarda topraklara uygulanan yarasa gübresi rizosferdeki mikroorganizma sayısını arttırmıştır. Bunun ana nedeni, organik gübrelerin toprağın organik madde içeriğine katkı sağlaması ve dolayısıyla topraktaki mikroorganizmaların sayısını arttırması, mikrobiyal solunumdan kaynaklanan CO_2 emisyonlarının artması olabilir [38]. Gübreleme ve ekim düzenindeki değişikliklerin mikroorganizmaların sayısını ve dağılımını etkileyerek dolaylı olarak toprak solunumu üzerinde de etkili olduğu rapor edilmiştir [30]. Yarasa gübresi içeriğinin besin maddelerince zengin olmasından dolayı, topraktaki mikroorganizma popülasyonunu arttırdığı yapılan çalışmalarda da açıklanmıştır [37, 38]. Kontrolle karşılaştırıldığında maya + küf sayısında en fazla artış; %95.8 oranı ile yarasa gübresinin topraklara %1 oranında uygulama dozunda tespit edilmiştir. Bakteri sayısı ise kontrole oranla yarasa gübresinin %1.5 uygulama dozunda %90.2 oranında artış göstermiştir. Doğadaki sağlıklı bitkilerin, çeşitli mikroorganizmalar tarafından kolonize edildiği, bitki ile ilişkili mikrobiyal topluluğun, bitki büyümesi ve üretkenliği üzerindeki etkisinden dolayı bitkinin ikinci genomu olarak anıldığı açıklanmıştır [37, 39]. Bu çalışmada, organik gübre olarak yarasa gübresinin kullanımının topraktaki mikroorganizma popülasyonunu önemli ölçüde artırdığı tespit edilmiştir. Verilerimiz Lazcano ve ark. [39]'nın bulgularıyla uyumludur. Ayrıca çeşitli araştırmacılar, organik katkıların topraktaki mikrobiyal aktiviteyi, mikrobiyal çeşitliliği ve bakteri yoğunluğunu artırdığını yaptıkları araştırmalarında göstermiştir [37, 39, 40]. Topraktaki mikroorganizma sayısının artmasındaki bir diğer neden ise; gübrenin biyolojik ve mikrobiyal faaliyetleri teşvik etmesi ve bunun da eklenen gübredeki organik maddelerin parçalanmasını hızlandırmasından kaynaklanabilir. Gübre uygulanmış topraktaki biyolojik aktiviteler, nispeten yüksek karbon içeriği ve enzim aktiviteleriyle artabilir. Wang ve ark. [41] tarafından bildirildiği gibi, mikrobiyal biyokütle topraktaki organik madde ve besin maddelerinin döngüsünü de yönlendirir. Topraklara uygulanan organik gübrelerin miktar ve cinsinin topraktaki farklı gruptaki mikroorganizmaları ve aktivitelerini etkilediği rapor edilmiştir [41].

Sonuç

Yarasa gübresinin toprağın dokusunu ve yapısını iyileştirdiği, toprağı makro ve mikro besin elementleri ile zenginleştirdiği, yapraklara uygulandığında fungisit görevi gördüğü yapılan çeşitli çalışmalarda da açıklanmıştır [1, 10, 26, 27]. Uygulama oranlarının diğer gübrelere göre daha az olduğu, ayrıca diğer

gübreler ile karşılaştırıldığında oldukça az veya hiç kokunun olmaması ve ayrışma sürecinde hızlı etkisinin olmasının da kullanımının avantajları arasında olduğu açıklanmıştır [13]. Çalışmamızda farklı dozlardaki yarasa gübresinin toprağa uygulanması ile mercimek rizosferindeki bazı mikrobiyolojik özellikleri olumlu etkilediği, mercimek gelişimine katkı sağladığı tespit edilmiştir. Yarasa gübresinin içerdiği besin maddelerinin bitki gelişimini ve toprağın mikrobiyolojik aktivitesini teşvik edebileceği düşünülmektedir. Yarasa gübresinin çalışmamızda topraktaki mikrobiyal aktiviteyi de uyardığı belirlendiğinden, antibiyotiklere karşı çoklu direnç gösteren bakterilerin yanı sıra salgın potansiyeli olan patojenik mikroorganizmaların da varlığı gübre içeriğinde olabileceği göz önünde bulundurulduğunda, yarasa gübresindeki bitki gelişimini teşvik eden mikroorganizmaların varlığını ve bunların tarımdaki uygulamalarını araştırmak için daha ileri çalışmalara ihtiyaç vardır.

Teşekkür Bu çalışma Ayşegül Arslan'ın yüksek lisans tezinin bir kısmıdır.

Fon/Finansman bilgileri Herhangi bir kurum veya kuruluş tarafından desteklenmemiştir.

Etik Kurul Onayı ve İzinler Çalışma, etik kurul izni veya herhangi bir özel izin gerektirmemektedir.

Çıkar çatışmaları/Çatışan çıkarlar- Herhangi bir çıkar çatışması yoktur.

Yazarların Katkısı- 1. yazar %60 oranında, 2. yazar %40 oranında katkı sağlamıştır. Yazarlar makalenin son halini okumuş ve onaylamıştır.

Kaynaklar

[1] Palita, K. S., Panigrahi, R. & Panda, D. (2021). Potentiality of bat guano as organic manure for improvement of growth and photosynthetic response in crop plants. *Proceedings* of the *National Academy* of *Sciences, India Section B*: *Biological Sciences, 91*, 185-193. https://doi.org/10.1007/s40011-020-01205-y

[2] Badgley, C., Moghtader, J., Quintero, E., Zakern, E., Chappell, J., Aviles-Vazquez, K., Samulon, A & Perfecto, I. (2007). Organic agriculture and the global food supply. *Renewable Agriculture and Food Systems, 22*, 86–108. http://dx.doi.org/10.1017/S1742170507001640

[3] Seufert, V., Ramankutty, N. & Foley, A. E. (2012). Comparing the yields of organic and conventional agriculture. *Nature, 485*, 229–232. https://doi.org/10.1038/nature11069

[4] Padbhushan, R., Das, A., Rakshit, R., Sharma, R. P., Kohli, A. & Kumar, R. (2016). Long-term organic amendment application improves influence on soil aggregation, aggregate associated carbon and carbon pools under scented rice-potato-onion cropping system after the 9th crop cycle. *Communications in Soil Science and Plant Analysis, 47,* 2445–2457. https://doi.org/10.1080/00103624.2016.1254785

[5] He, Z., Pagiliari, P. H. & Waldrip, H. M. (2016). Applied and environmental chemistry of animal manure: A Review. *Pedobiologia, 26*, 779–816.https://doi.org/10.1016/S1002-0160(15)60087-X

[6] Fenton, M. B., Cumming, H. M., Rautenbach, I. L., Cumming, G. S., Cumming, M. S., Ford, G., Tylor, R. D., Dunlop, J., Havorka, M. D., Johnston, D. S., Portfors, C. V., Kalcounis, M. C. & Mahlanga, Z. (1998). Bats and the loss tree canopy in African woodlands. *Conservation Biology, 12*, 399–407.

[7] Keleher, H., & Sara, A. (1996). Guano: bats' gift to gardeners. *Bats, 14*, 15–17.

[8] Shetty, S., Sreepada, K. S. & Bhat, R. (2013). Effect of bat guano on the growth of *Vigna radiata* L. *International Journal of Scientific and Research Publication, 3*, 1–8.

[9] Aydın Can, B., Ünal, M. & Can, O. (2019). Farklı yarasa gübresi uygulamalarının marul yetiştiriciliğin de verim ve kalite üzerine etkileri. *Uluslararası Tarım ve Yaban Hayatı Bilimleri Dergisi, 5*, 18-24. https://doi.org/10.24180/ijaws.481660

[10] Ulukapı, K. & Şener, S. (2018). Farklı organik gübrelerin tarla ve örtüaltı koşullarında yetiştirilen karnabaharın bitki gelişimi ve verim parametreleri üzerine etkisi. *Selçuk Journal of Agriculture and Food Sciences, 32*, 510-515. https://doi.org/10.15316/SJAFS.2018.130

[11] Ojobor, S. A.; Omovie-Stephen, O. F. (2022). Influence of formulated palm mill effluent and bat guano mixture on maize performance and soil chemical properties in Delta State, Nigeria. *Indian Journal of Agricultural Research,56,* 28–32. https://doi.org/10.18805/IJARe.A-620

[12] Bay, S. B. (2019). *Kapya Tipi Biber (Capsicum annuum L. cv. Kapya) Yetiştiriciliğinde Kullanılan Organik Gübrelerin Bitki Gelişimi ve Meyve Kalitesi Üzerine Etkileri.* (Tez no.555776) [Yüksek Lisans Tezi, Bursa Uludağ Üniversitesi].

[13] Zhou, Z., Zhang, S., Jiang, N., Xiu, W., Zhao, J. & Yang, D. (2022). Effects of organic fertilizer incorporation practices on crops yield, soil quality, and soil fauna feeding activity in the wheat-maize rotation system. *Frontiers in Environmental Sciences, 10,* 1-13. https://doi.org/10.3389/fenvs.2022.1058071

[14] Fitriani, A., Rizali, A., Saputra, R. A., Sari, N. (2022). The responses of some doses fertilizer bat guano on the crop yield of Hiyung Chili pepper in the ultisols. *Savana Cendana, 7,* 27-28. https://doi.org/10.32938/sc.v7i02.1020

[15] Jacoby, R., Peukert, M., Succurro, A., Koprivova, A. & Kopriva, S. (2017). The role of soil microorganisms in plant mineral nutrition current knowledge and future directions. *Frontiers in Plant Science, 8*, 1617. https://doi.org/10.3389/fpls.2017.01617

[16] Jannson, J. K. & Hofmockel, K. S. (2018). The soil microbiome—From metagenomics to metaphenomics. *Current Opinion in Microbiology, 43,* 162–168. https://doi.org/10.1016/j.mib.2018.01.013

[17] Chen, J., Zheng, M. J., Pang, D. W., Yin, Y. P., Han, M. M. & Li, Y. X. (2017). Straw return and appropriate tillage method improve grain yield and nitrogen efficiency of winter wheat. *Journal of Integrative Agriculture*, *16*, 1708–1719. https://doi.org/10.1016/S2095-3119(16)61589-7

[18] Li, L. R., Feng, J. L., Liu, M. M., Mei, H., Kang, Z. Y. & Cai, Q. N. (2021). Effect of crop planting patterns on soil microorganisms and crop pests in farmland. *Chinese Agricultural Science Bulletin, 37*, 99–106. https://doi.org/10.3389/fenvs.2023.1232527

[19] Liu, J. A., Shu, A. P., Song, W. F., Shi, W. C., Li, M. C. & Zhang, W. X. (2021). Long-term organic fertilizer substitution increases rice yield by improving soil properties and regulating soil bacteria. *Geoderma, 404*, 115287. https://10.1016/j.geoderma.2021.115287

[20] Burucu, D. (2023). Ürün raporu: Kuru baklagil. Tarım ve Orman Bakanlığı, Tarımsal Ekonomi ve Politika Geliştirme Enstitüsü, 68 sayfa (https://arastirma.tarimorman.gov.tr/tepge/Belgeler)

[21] Arnon, D. T. (1949). Copper enzymes in isolated chloroplast polyphenol oxidase in *Beta vulgaris*. *Plant Physiology, 24*, 1- 15. http:// doi:10.1104/pp.24.1.1

[22] Anderson, J. P. E. (1982). *Soil Respiration*. In: methods of soil analysis, part 2, chemical and microbiological properties (Ed. A. L. Page). ASA-SSSA, Madison, Winsconsin. pp. 831-871.

[23] Küçük, Ç., & Cevheri, C. (2018). Some microbiological properties in soil samples taken from maize grown fields in Sanliurfa. *Aksaray University Journal* of *Science* and *Engineering*, *2*, 28-40. http://doi: 10.29002/asujse.316782.

[24] Pepper, I. L. & Gerba, C. P. & Brendecke, J. W. (1995). *Brendecke: Environmental Microbiology, A Laboratory Manual.* Academic Press, New York.

[25] Krasilnikov, P., Taboada, M. A. & Amanullah, A. (2022). Fertilizer Use, Soil Health and Agricultural Sustainability. *Agriculture, 12*, 462. https://doi.org/10.3390/agriculture12040462

[26] Ünal, M., Can, O., Aydın Can, A., & Poyraz, K. (2018). The effect of bat guano applied to the soil in different forms and doses on some plant nutrient contents. *Communications in Soil Science and Plant Analysis, 49*, 708-716. https://doi.org/10.1080/00103624.2018.1434540

[27] Nagar, N. K., Goud, V. V. & Kumar, R. (2016). Effect of organic manures and crop residue managament on physical, chemical and biological properties of soil under pigeon pea based intercropping system. *International Journal of Farm Sciences, 6*, 101-103.

[28] Çiçek, N. (2021). Kadife (*Tagetes erecta*) çiçeğinin bazı kalite ve gelişim parametrelerine yarasa gübresi ve vermikompostun etkileri. *Journal of Biotechnology, 2*, 24-31.

[29] Misra, P. K., Gautam, N. K., & Elangovan, V. (2019). Bat guano: a rich source of macro and microelements essential for plant growth. *Annals of Plant and Soil Research, 21*, 82-86.

[30] Han, G. X., Zhou, G. S. & Xu, Z. Z. (2008). Research and prospects for soil respiration of farmland ecosys tems in China. *Chinese Journal of Plant Ecology*, *32*, 719–733. https://doi.org/10.3773/j.issn.1005-264x.2008.03.022

[31] Raich, J. W. & Tufekciogul, A. (2000). Vegetation and soil respiration: Correlations and controls. *Biogeochemistry, 48*, 71–90. https://doi.org/10.1023/A:1006112000616

[32] Dimande, P., Arrobas, M. & Rodrigues, M. A. (2023). Under a tropical climate and in sandy soils, bat guano mineralises very quickly, behaving more like a mineral fertiliser than a conventional farmyard manure. *Agronomy, 13*(5), 1367. https://doi.org/10.3390/agronomy13051367

[33] Moreno-Espindola, I. P., Ferrara-Guerrero, M. J., Luna-Guido, M. L., Ramírez-Villanueva, D. A., de Leon-Lorenzana, A. S., Gomez-Acata, S., González-Terreros, E., Ramírez-Barajas, B., Navarro-Noya, Y. E. & Sanchez-Rodriguez, L. M. (2018). The bacterial community structure and microbial activity in a traditional organic milpamarming system under different soil moisture conditions. *Frontiers in Microbiology, 9*, 1–19. https://doi.org/10.3389/fmicb.2018.02737

[34] Caldwell, B. A. (2005). Enzyme activities as a component of soil biodiversity: A review. *Pedobiologia*, *49*, 637–644. https://doi.org/10.1016/j.pedobi.2005.06.003

[35] Shi, J., Yuan, X., Lin, H., Yang, Y. & Li, Z. (2011). Differences in soil properties and bacterial communities between the rhizosphere and bulk soil and among different production areas of the medicinal plant *Fritillaria thunbergii*. *International Journal of Molecular Sciences, 12*, 3770–3785. https://doi.org/10.3390/ijms12063770

[36] Martens, D. A., Johanson, J. B. & Frankenberger, J. W. T. (1992). Production and persistence of soil enzymes with repeatedaddition of organic residues. *Soil Sciences, 153*, 53–61. https://doi.org/10.1097/00010694-199201000-00008

[37] Majumdar, B., Saha, A. R., Ghoai, A. K., Sarkar, S. K., Chowdhury, H., Kundu, D. K. & Mahapatra, B. S. (2014). Effect of fertilizer treatments on jüte (*Chorchorus olitorius*), microbial dynamics in its rhizosphere and residual fertility status of soil. *Indian Journal of Agricultural Sciences, 84*, 503-508. https://doi.org/10.56093/ijas.v84i4.39467

[38] Latha, H. S. & Sharanappa, A. (2014). Effect of organic amendments on the productivity and quality of produce and soil in groundnut (*Arachis hypoqaea*), onion (*Allium cepa*) cropping system. *Indian Journal of Agricultural Sciences, 84*, 999-1003. http://doi.org 10.56093/ijas.v84i8.43138

[39] Lazcano, C., Gomez-Brandon, M., Revilla, P. & Dominguez, J. (2013). Short-term effects of organic and inorganic fertilizers on soil microbial community structure and function. *Biology and Fertility of Soils, 49*, 723-733. http://doi.org 10.1007/s00374-012-0761-7

[40] Wang, Y., Li, Q., Li, C. (2023). Organic fertilizer has a greater effect on soil microbial community structure and carbon and nitrogen mineralization than planting pattern in rainfed farmland of the Loess Plateau. *Frontiers in Environmental Sciences, 11*, 1-13. https://doi.org/10.3389/fenvs.2023.1232527

[41] Wang, J. W., Zhang, G. Y. & Yu, C. Q. (2020). A Meta-analysis of the effects of organic and inorganic fertilizers on the soil microbial community. *Journal of Resources and Ecology, 11*, 298–303. http://10.5814/j.issn.1674-764X.2020.03.007

Sinopfbd, 2024; 9(1): 72-95 **https://doi.org/10.33484/sinopfbd.1370598**

Sinop Üniversitesi Fen Bilimleri Dergisi
Sinop Uni J Nat Sci
E-ISSN: 2564-7873

https://dergipark.org.tr/tr/pub/sinopfbd

Crystal Structure and Hirshfeld Surface Analysis of a Heterometallic Hofmann-Type-Like Compound

Zeki KARTAL[1] and Zarife Sibel ŞAHİN[2]

How to cite: Kartal, Z., & Şahin, Z. S. (2024). Crystal structure and Hirshfeld surface analysis of a heterometallic Hofmann-type-like compound. *Sinop Üniversitesi Fen Bilimleri Dergisi, 9*(1), 72-95. https://doi.org/10.33484/sinopfbd.1370598

Research Article

Corresponding Author
Zarife Sibel ŞAHİN
zarifesibel@sinop.edu.tr

ORCID of the Authors
Z.K: 0000-0001-9739-0858
Z.S.Ş: 0000-0003-2745-7871

Received: 04.10.2023
Accepted: 22.02.2024

Abstract

In this study; a new heterometallic compound defined by the open formula $[Cd(H_2O)_2Ni(CN)_4]_4[Cd(H_2O)_4Ni(CN)_4]_5$ was synthesized in crystal form. Consisting of components such as water molecules, $[Ni(CN)_4]^{2-}$ anions, and cadmium transition metal atoms, this new crystal structure has no analogues which might have been previously obtained, even with other transition metal atoms. It is a new compound and a unique example of a crystal. The structural properties of this heterometallic compound have been characterized by single crystal X-ray diffraction spectroscopy (SC-XRD), FT-IR spectroscopy, thermal analysis and elemental analysis methods. According to the data obtained from the SC-XRD technique, this heterometallic compound has a monoclinic crystal system and a *C2/c* space group. The asymmetric unit of this compound consists of five Cd(II) ions, five Ni(II) ions, eighteen cyanide ligands, and fourteen coordinated water ligand molecules. In addition, theoretical calculations have been made with the Gaussian 03 program in order to obtain more information about this heterometallic Hofmann-type-like compound. The chemical properties of this new compound have been calculated using its HOMO and LUMO values and the natural bond orbital (NBO) analyses. In addition, Hirshfeld surface analysis of the asymmetric unit of this compound has been performed with the CrystalExplorer program. As a result of the Hirshfeld surface analysis, extensive information has been obtained about the weak intramolecular and intermolecular forces that form this new crystalline compound.

Keywords: Hofmann-type-like compound, SC-XRD analysis, FT-IR spectroscopy, Theoretical calculations, Hirshfeld surface analysis

Heterometalik Hofmann Tipi Benzeri Bir Bileşiğin Kristal Yapısı ve Hirshfeld Yüzey Analizi

[1]Retired Professor, Kütahya, 43000, Türkiye

[2]Sinop University, Faculty of Engineering and Architecture, Department of Energy Systems Engineering, Sinop, 57000, Türkiye

Öz

Bu çalışmada; açık formül $[Cd(H_2O)_2Ni(CN)_4]_4[Cd(H_2O)_4Ni(CN)_4]_5$ ile tanımlanan yeni bir heterometalik bileşik, kristal formda sentezlendi. Su molekülleri, $[Ni(CN)_4]^{2-}$ anyonları ve kadmiyum geçiş metali atomları gibi bileşenlerden oluşan bu yeni kristal yapının, diğer geçiş metali atomlarıyla bile daha önce elde edilmiş olabilecek hiçbir analogu yoktur. Yeni bir bileşik ve kristalin eşsiz bir örneğidir. Bu heterometalik bileşiğin yapısal özellikleri, tek kristal X-ışını kırınım spektroskopisi (SC-XRD), FT-IR spektroskopisi, termal analiz ve elementel analiz yöntemleriyle karakterize edilmiştir. SC-XRD tekniğinden elde edilen

verilere göre bu heterometalik bileşik, monoklinik kristal sistemine ve *C2/c* uzay grubuna sahiptir. Bu bileşiğin asimetrik birimi beş Cd(II) iyonu, beş Ni(II) iyonu, on sekiz siyanür ligandı ve on dört koordineli su ligandı molekülünden oluşur. Ayrıca bu heterometalik Hofmann tipi bileşik hakkında daha fazla bilgi edinmek amacıyla Gaussian 03 programı ile teorik hesaplamalar yapılmıştır. Bu yeni bileşiğin kimyasal özellikleri, HOMO ve LUMO değerleri ve doğal bağ yörünge (NBO) analizleri kullanılarak hesaplandı. Ayrıca bu bileşiğin asimetrik biriminin Hirshfeld yüzey analizi CrystalExplorer programı ile yapılmıştır. Hirshfeld yüzey analizi sonucunda bu yeni kristal bileşiği oluşturan zayıf molekül içi ve moleküller arası kuvvetler hakkında kapsamlı bilgiler elde edildi.

Anahtar Kelimeler: Hofmann tipi bileşik, Tek-kristal XRD analizi, FT-IR spektroskopisi, Teorik hesaplamalar, Hirshfeld yüzey analizi

Introduction

In organic and inorganic chemistry, compounds obtained by reacting some metal atoms, especially transition metal atoms with some ligand molecules ionic groups, are called "coordination compounds" [1]. The coordination compounds are very interesting compounds in terms of their physical and chemical properties. The interest in them in the field of science is increasing along with the number of researchers working on coordination compounds and consequently the scientific research results published about them. As a result of the chemical interactions of carbon and nitrogen atoms, either uncharged groups or charged ionic groups can be formed, depending on the number of atoms involved and the type of bonds formed between them. One of these ionic groups is the cyanide group $(C\equiv N)^-$, which has a negative charge. In the formation of Hofmann-type and Hofmann-type-like compounds, compounds are obtained, $K_2Ni\ (CN)_4$ compound, which is formed chemically by the cyanide group with potassium atom and nickel atom, is the most widely used basis compound. [2]. By using the $K_2Ni\ (CN)_4$ compound, various ligand molecules and transition metal atoms, many different compounds from 1D to 3D can be obtained in powder form or crystal form. The general formulae of Hofmann type compounds and Hofmann-type-like compounds are given as $M(II)LNi(CN)_4$ and $M(II)LL'Ni(CN)_4$, respectively. In these formulae, the symbols L and L′ indicate different ligand molecules in the compounds. In Hofmann type compounds, the number of this ligand molecule can be 1 or at most 2 depending on the nature of the L ligand molecule [3-5]. Moreover, by replacing the Ni atom in the $Ni\ (CN)_4$ ion group with palladium (Pd) and platinum (Pt) atoms, new types of Hofmann compounds were formed, and by replacing Ni atom with zinc (Zn), cadmium (Cd) and mercury (Hg) atoms, Hofmann-T_d-type compounds were formed [3-5]. In Hofmann-type-like compounds, the number of these ligand molecules can be 1, 2, or more, depending on the nature of the L and L′ ligand molecules. In Hofmann-type-like compounds, the number of a single ligand molecule must be either one or more than two (never n equals two). The compounds formed in all these cases are the Hofmann-type-like compounds. Extensive information can be found on Hofmann-type compounds and Hofmann-type-like compounds in previous works by us and other researchers [6-19]. The results of adding another ligand molecule to the structure of Hofmann-type and Hofmann-type-like compounds formed by a kind of ligand with a transition metal atom can be examined by comparing their

spectroscopic and crystalline data. If the effect of the additional ligand or ligands increases the stability of the formed crystal structure, the storage volume and some other properties, this is a positive situation for newly obtained compounds. In a previous study, some new Hofmann-type compounds and Hofmann-type-like clathrates were obtained in powder and crystal form by using water molecules (H_2O), $K_2Ni(CN)_4$ compound and zinc (Zn) transition metal atoms [16, 18, 19]. The aim of this study is to synthesize Hofmann-type and Hofmann-type-like compounds in crystal form by using potassium tetracyanonickelate (II) monohydrate [$K_2Ni(CN)_4 \cdot H_2O$] compound, cadmium (II) chloride monohydrate ($CdCl_2 \cdot H_2O$) compound and water (H_2O) molecules. In these chemical processes, the water molecule acts as both a solvent and a ligand molecule. As a result of this study, it is expected to obtain a Hofmann-type compound or a Hofmann type water clathrate in crystal form. The chemical formula of this compound is either [$Cd(H_2O)_mNi(CN)_4$] ($m > 2$) or [$Cd(H_2O)_2Ni(CN)_4] \cdot n(H_2O)$ ($n = 1, 2, 3, \dots$) is expected. The "m" and "n" coefficients in the formulae show the number of ligand molecules in the compound and the number of guest molecules in the clathrate, respectively. No data matching or similar to all data were found for this Hofmann-type-like compound obtained in crystalline form. Therefore, this compound is currently a first in its field.

Experimental

Materials

In this study, all chemical compounds such as potassium tetracyanonickelate(II) monohydrate $K_2[Ni(CN)_4] \cdot H_2O$, (Fluka, 96%), cadmium(II) chloride monohydrate ($CdCl_2 \cdot H_2O$), (Sigma Aldrich, 99+ %), and ammonia solution (NH_3, Merck, 25%) were used to obtain the targeted compound.

Synthesis of Compounds with Formulae [$Cd(H_2O)_MNi(CN)_4$] or [$Cd(H_2O)_2Ni(CN)_4$]•$N(H_2O)$

The compound in question was obtained as a result of the following processes. 1 mmol of $K_2[Ni(CN)_4] \cdot H_2O$ (0.259 g) was dissolved in 10 mL of twice distilled hot water. The compound $CdCl_2 \cdot H_2O$ (0.202 g) was added to this solution. In this study, the distilled water was used both as a solvent and a ligand molecule. As a result of all these chemical reactions, Hofmann-type-like compound or Hofmann type water clathrate, whose open formula is thought to be [$Cd(H_2O)_mNi(CN)_4$] ($m > 2$) or [$Cd(H_2O)_2Ni(CN)_4] \cdot n(H_2O)$ ($n = 1, 2, 3, \dots$), was formed. It was a colorless suspension. By adding diluted ammonia solution to this medium, the medium was made more transparent and purified from all impurities in the medium. This clear mixture was stirred at 65°C for two hours, then filtered through the most tightly meshed filter paper and allowed to crystallize at room temperature. As a result of this study, after about two and a half months, a transparent, thin and long rod-like compound in crystalline form was obtained. The compounds formed by transition metal atoms in a chemical interaction environment with cyanide compounds, even with other ligand molecules and solvent molecules in the environment,

can occur in very different numbers and in structural conditions, depending on the number of cyanide ligands that bond [20, 21]. According to the data obtained from various techniques for this compound obtained in crystal form, it was understood that it is an example of a Hofmann-type-like compound. The full formula of this compound was determined as $[Cd\ (H_2O)_2Ni\ (CN)_4]_4[Cd(H_2O)_4Ni(CN)_4]_5$ as a result of various experimental studies. This compound will be denoted as **1** for short hereafter. The new crystalline compound obtained is a very specific example of Hofmann-type-like compounds, as it contains both a Hofmann-type compound with the formula $ML_2Ni\ (CN)_4$ and a Hofmann-type-like compound with the formula $ML_4Ni(CN)_4$ (see Figure 1).

Instrumentation

A suitable crystal of **1** was selected for data collection which was performed on a D8-QUEST diffractometer equipped with a graphite-monochromatic Mo-K_α radiation at 296 K. The structure was solved by direct methods using SHELXS-2013 [22] and refined by full-matrix least-squares methods on F^2 using SHELXL-2013 [23]. The H atoms were located in a difference map refined freely. The high residual electron densities (maxima and minima) and metal center separations are 0.964 and 0.849 Å. Therefore, these high residual electron densities could not be defined from the refinement of the structure. The following procedures were implemented in our analysis: data collection: Bruker APEX2 [24]; program used for molecular graphics were as follows: MERCURY programs [25]; software used to prepare material for publication: WinGX [26]. The FT-IR spectrum of compound **1** was gained immediately as soon as the crystal was obtained under normal laboratory conditions using the Bruker Optics Vertex 70 FT-IR Spectrometer (3650 – 400) cm^{-1} wavenumber range, 2 cm^{-1} resolution, using the KBr technique. The metal amounts in the structure of compound **1** were analyzed with the Perkin-Elmer optima 4300 DV ICP-OES device, and the carbon, nitrogen and hydrogen amounts were analyzed with the CHNS-932 (LECO) elemental measuring device. TG and DTG analysis curves of the thermal behavior of compound **1** were recorded with an SII EXSTAR 6000 TG/DTA 6300 thermal analyzer in a temperature range (20–800) °C at a heating rate of 5 °C/min in the nitrogen atmosphere. Since there is an FT-IR device in our laboratory, FT-IR spectra of all compounds in powder or crystal form can be obtained by us as soon as possible. However, since the analysis of the elements in the structure of any compound or the SC-XRD structure analysis is carried out with devices in other departments or even in other cities of our institution, these processes can take place after a very long time after the synthesis of the compound. Some changes in the structure of some compounds (such as loss of water and guest molecules) may occur during this long period of time. For this reason, some differences may occur between the FT-IR results of some compounds and the elemental analysis and SC-XRD results. A similar situation for compound **1** is described in section 3.3.1.

Results and Discussion

Crystallographic Analysis of Compound 1.

The experimentally measured and theoretically calculated amounts of C, H, N, Cd and Ni atoms in the structure of compound **1** are listed in Table 1.

Table 1 *Elemental analysis of compound* ***1***.

Open formula of compound 1 and its molecular mass M_r (g)	Elemental analysis, found (%) / (calculated) (%)				
	C	**H**	**N**	**Cd**	**Ni**
$[Cd(H_2O)_2Ni(CN)_4]_4[Cd(H_2O)_4Ni(CN)_4]_5$	14.19	1.95	17.06	34.03	17.35
M_r = 2980.99	(14.50)	(1.89)	(16.93)	(33.94)	(17.72)

The asymmetric unit of the heterometallic compound **1** consists of five Cd (II) ions, five Ni (II) ions, eighteen cyanide ligands and fourteen coordinated water molecules (see Figure 1). The Cd (II) ions in this heterometallic compound have two different types of coordination geometry. In the first of these coordination geometries, the Cd1, Cd3 and Cd5 ions are coordinated by two nitrogen atoms from cyanide ligands and four oxygen atoms from water molecules, thus showing distorted octahedral coordination geometry.

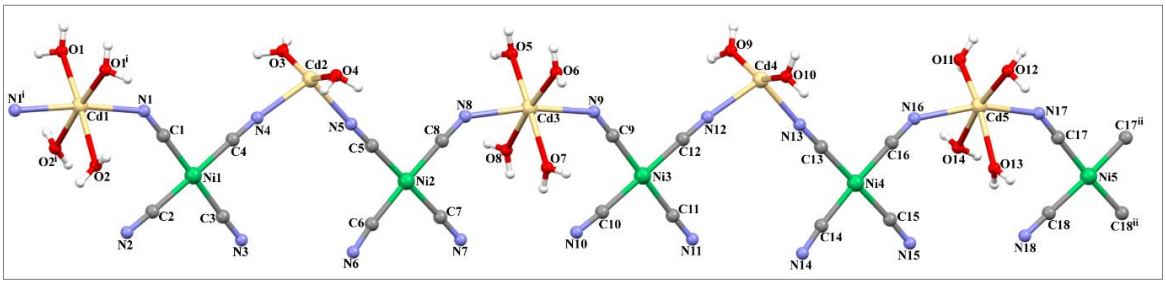

Figure 1. *The molecular structure of* ***1*** *showing the atom numbering scheme.*

In the second coordination geometry, the Cd2 and Cd4 ions are coordinated by two nitrogen atoms from cyanide ligands and two oxygen atoms from water molecules, thus showing distorted tetrahedral coordination geometry. Details of data collection and crystal structure determinations are given in Table 2. The Cd–N bond distances range between 2.209(10) and 2.442(8) Å [26-28], while the Cd–O bond distances range between 2.178(9) and 2.586(12) Å. As it can be seen in Figure 1 and Table 3, the Cd atoms and water molecules in the structure of compound **1** are sequentially bonded to each other, either double or quadruple. The bond formed when two water molecules are attached to the Cd atoms is shorter than the bond formed when four water molecules are attached to the Cd atoms. That is, the Cd atom attracts two water molecules more strongly than four water molecules. The distance between the C and N atoms in the C≡N groups in compound **1** varies between 1.12 and 1.17 Å. Depending on this situation, the bond constants of the triple bonds in the C≡N groups will also take different values. As a result of this situation, multiple splits are observed in the stretching vibrations of the C≡N group. Similar

situations are also seen between Ni-N atoms. The implications of these results will reveal the different aspects in the spectroscopic and thermal behavior of compound **1**.

Table 2 *Crystal data and structure refinement parameters for compound 1.*

Empirical formula	$C_{36}H_{56}Cd_9N_{36}Ni_9O_{28}$
Formula weight	2981.15
Crystal system	Monoclinic
Space group	*C2/c*
a (Å)	31.761 (4)
b (Å)	15.954 (2)
c (Å)	18.546 (2)
β (º)	98.379 (4)
V (Å^3)	9297.3 (19)
Z	4
D_c (g cm^{-3})	2.130
μ (mm^{-1})	3.86
θ range (º)	3.0-28.3
Measured refls.	89261
Independent refls.	8972
R_{int}	0.057
S	1.18
R1/wR2	0.077/0.163
T_{max}/T_{min}	5.92/-2.67
CCDC	1851097

Each Ni (II) ion is surrounded by four cyanide ligands, the Ni–C bond distances range between 1.842(10) and 1.883(11) Å, respectively. The coordination around Ni(II) ions are square-planar. The Cd (II) and Ni (II) ions are bridged by cyanide ligands, generating 1D coordination polymer running parallel to the [111] direction, with Cd···Ni distances ranging between 5.049 and 5.313 Å [29, 30]. The various bond types in compound **1** and the necessary information about them are given in Tables 3 and 4. Adjacent these 1D coordination polymers are further joined by O-H···N hydrogen bonds. The combination of these interactions produces 2D network (see Figure 2).

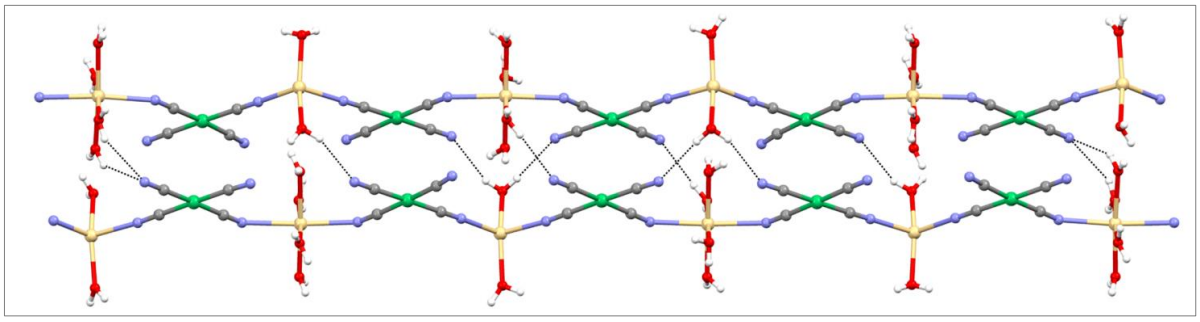

Figure 2. *An infinite 2D network in compound **1**.*

Table 3 *Selected bond distances for compound* ***1*** *(Å)*

C1-Ni1	1.853(11)	C2-Ni1	1.883(11)	C3-Ni1	1.877(11)
C4-Ni1	1.856(11)	C5-Ni2	1.863(10)	C6-Ni2	1.872(11)
C7-Ni2	1.863(11)	C8-Ni2	1.849(11)	C9-Ni3	1.863(10)
C10-Ni3	1.877(10)	C11-Ni3	1.868(11)	C12-Ni3	1.881(11)
C13-Ni4	1.867(12)	C14-Ni4	1.859(12)	C15-Ni4	1.873(11)
C16-Ni4	1.857(11)	C17-Ni5	1.842(10)	C18-Ni5	1.872(11)
Cd1-O1	2.318(9)	Cd1-O2	2.360(10)	Cd1-N1	2.420(8)
Cd2-O3	2.178(9)	Cd2-O4	2.191(9)	Cd2-N5	2.258(9)
Cd2-N4	2.291(8)	Cd3-O6	2.313(10)	Cd3-O5	2.308(9)
Cd3-O7	2.373(9)	Cd3-N8	2.375(9)	Cd3-O8	2.397(10)
Cd3-N9	2.442(8)	Cd4-O10	2.185(10)	Cd4-O9	2.185(9)
Cd4-N13	2.209(10)	Cd4-N12	2.291(9)	Cd5-O11	2.257(10)
Cd5-O12	2.282(11)	Cd5-O13	2.329(11)	Cd5-N16	2.337(9)
Cd5-O14	2.586(12)	Cd5-N17	2.375(9)		
C1-N1	1.154(13)	C2-N2	1.140(14)	C3-N3	1.124(14)
C4-N4	1.142(13)	C5-N5	1.134(13)	C6-N6	1.141(14)
C7-N7	1.146(15)	C8-N8	1.151(14)	C9-N9	1.138(13)

Table 4. *Hydrogen-bond parameters for compound* ***1*** *(Å, º)*

D-H· · ·A	D-H	H···A	D···A	D-H···A
O1—H1A···N3^{iv}	0.85	2.45	3.254 (14)	158
O1—H1B···N6^{iv}	0.84	2.45	3.274 (13)	171
O2—H2A···N3^{v}	0.88	2.59	3.461 (16)	172
O3—H3A···N7^{iv}	0.84	2.43	3.189 (14)	151
O3—H3B···N9^{vi}	0.84	2.59	3.289 (13)	142
O4—H4A···N2^{vii}	0.84	2.43	3.238 (14)	161
O4—H4B···N2^{v}	0.84	2.37	3.205 (13)	174
O5—H5A···N14^{iv}	0.84	2.61	3.305 (15)	142
O5—H5B···N11^{iv}	0.84	2.49	3.260 (14)	154
O6—H6B···N6^{vii}	0.84	2.49	3.288 (13)	160
O6—H6A···N3^{vii}	0.84	2.50	3.233 (14)	147
O7—H7A···N3^{vii}	0.97	2.58	3.495 (16)	158
O8—H8B···N11^{iv}	0.85	2.62	3.454 (15)	165
O9—H9B···N1^{vi}	0.83	2.53	3.245 (13)	146
O9—H9A···N15^{iv}	0.83	2.36	3.132 (14)	154
O10—H10B···N7^{vii}	0.84	2.50	3.178 (14)	139
O10—H10A···N10^{vii}	0.83	2.43	3.245 (14)	169
O11—H11A···N15^{iii}	0.89	2.55	3.426 (15)	174
O11—H11B···N18^{iii}	0.85	2.51	3.287 (15)	154
O12—H12B···N11^{vii}	0.81	2.49	3.193 (15)	145
O12—H12A···N14^{vii}	0.83	2.51	3.204 (16)	143
O14—H14B···N17	0.90	2.42	3.165 (18)	141
O14—H14A···O11	0.89	2.46	3.150 (18)	134

Symmetry codes: (iii) −x+2, −y+1, −z+3; (iv) x, −y+1, z−1/2; (v) −x+1, −y+1, −z; (vi) −x+3/2, −y+3/2, −z+1; (vii) x, −y+1, z+1/2.

A closer look at the smaller particles that make up compound **1** shows that these particles have two different structures. The first of these different structures is the example of a Hofmann-type-like compound formed by the Cd1 and its attached Ni $(CN)_4$ group with four water ligand molecules. The other is an example of a Hofmann-type compound formed by the Cd2 and its attached Ni $(CN)_4$ group with two water ligand molecules (see Figure 3).

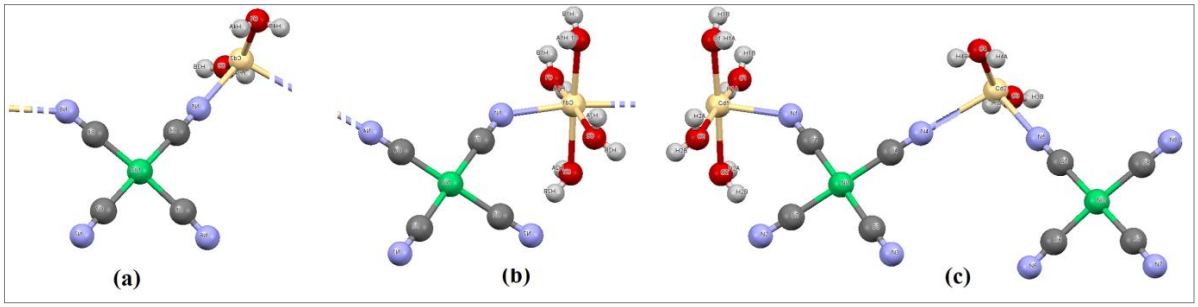

Figure 3. *Types of compounds formed by $Ni(CN)_4$ groups attached to Cd1 and Cd2 Hofmann type compound (a), Hofmann-type-like compound (b) and (c).*

As it can be clearly seen from Figure 1, the structure of compound **1** is not only in the same type. That is, it is not only in the form of a Hofmann type compound or just in the form of a Hofmann-type-like compound. The crystal structure of compound **1** consists of the sequential and regular bonding of parts (a) and (b) is shown in Figure 3. As such, the structure of compound **1** can be said to belong to the group of Hofmann-type-like compounds (Figure 3 (c)). This kind of structure is a situation that has emerged for the first time in our experimental studies. A similar structure has not been encountered in the studies of other researchers. In addition, the approximate dimensions of compound **1**'s asymmetric unit have a length of 39.30 Å and a width of 6.53 Å [in the (0bc) plane]. The approximate dimensions of a complete unit molecule in the same plane are 78.59 Å in length and 6.53 Å in width. The dimensions of the asymmetric unit of no compound we have obtained so far have not had such large values. In terms of its size values, compound **1** almost approaches the group of "supramolecules". In order to understand the structural size of compound **1**, the packed state of its crystal structure is given in Figure 4.

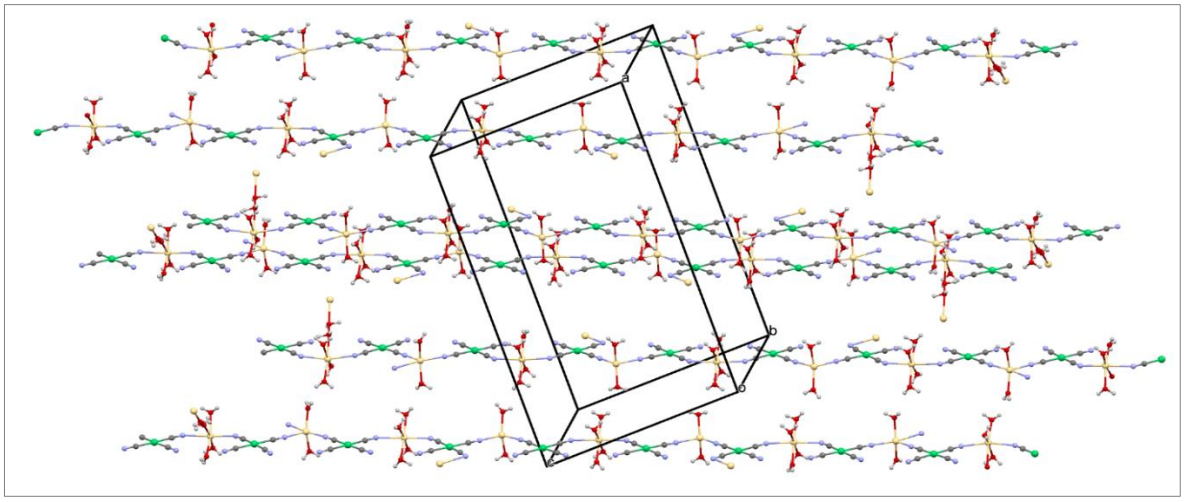

Figure 4. *The packed state of the crystal structure of compound **1**.*

Computational Studies on Compound 1

Gaussian 03 program, DFT/B3LYP method and LanL2MB basis set [31] were used in all theoretical calculations of compound **1** [32]. All the calculated values of compound **1** were made visible with the help of GaussView 4.1 program [33]. To calculate molecular geometry, atomic coordinates obtained from X-ray geometry were used. DFT calculations with a hybrid functional B3LYP (Becke's three parameters hybrid functional using the Lee-Young-Parr (LYP) correlation functional [34, 35]) using the Berny method [36, 37] were performed.

HOMO-LUMO Energy Levels of Compound 1

The HOMO and LUMO concepts of a chemical compound are defined as the "boundary orbital" of that compound. The energy difference between these boundaries orbital indicates the physical and chemical properties of that compound. In order to better understand the structure of compound **1** with some of its chemical and electronic properties, a simple model of it was made. This simple model was created from the smallest units that make up the structure of compound **1** (Figures 3 (a) and Figures 3 (b)) and their combination (Figure 3 (c)). The first part of this simple model (Figure 3 (a)) will hereinafter be referred to briefly as (**1-a**) and the second part (Figure 3 (b)) hereinafter briefly referred to as (**1-b**). Similarly, the third part (Figure 3 (c)); which is the simple model of compound **1**, hereinafter briefly referred to as (**1-c**). Some theoretical calculations have been made about each of these simple models with the Gaussian 03 program DFT/B3LYP method LanL2MB basic set [32]. In addition to these calculations, some theoretical calculations were made with the same basis set for the asymmetric part of compound **1** and for the whole. These new calculation results are hereinafter referred to as (**1-asy**) and (**1**), respectively. Theoretical calculations of all the obtained parts are listed in Table 5. These calculations were made separately for the structures in Figure 3 (a) and Figure 3 (b) and for the combined structure in Figure 3 (c). The Figure 3 (c) here is a combined form of these two simple structures, taking into account the structural symmetry of compound **1**, as an example of the main compound. Thus, it was investigated how the chemical and electronic properties of Hofmann-type compounds and Hofmann-type-like compounds change as a result of the combination of these compounds. The boundary orbitals of simple models assumed to contribute to the formation of compound **1** and compound **1** are given in Figure 5 and Figure 6, respectively.

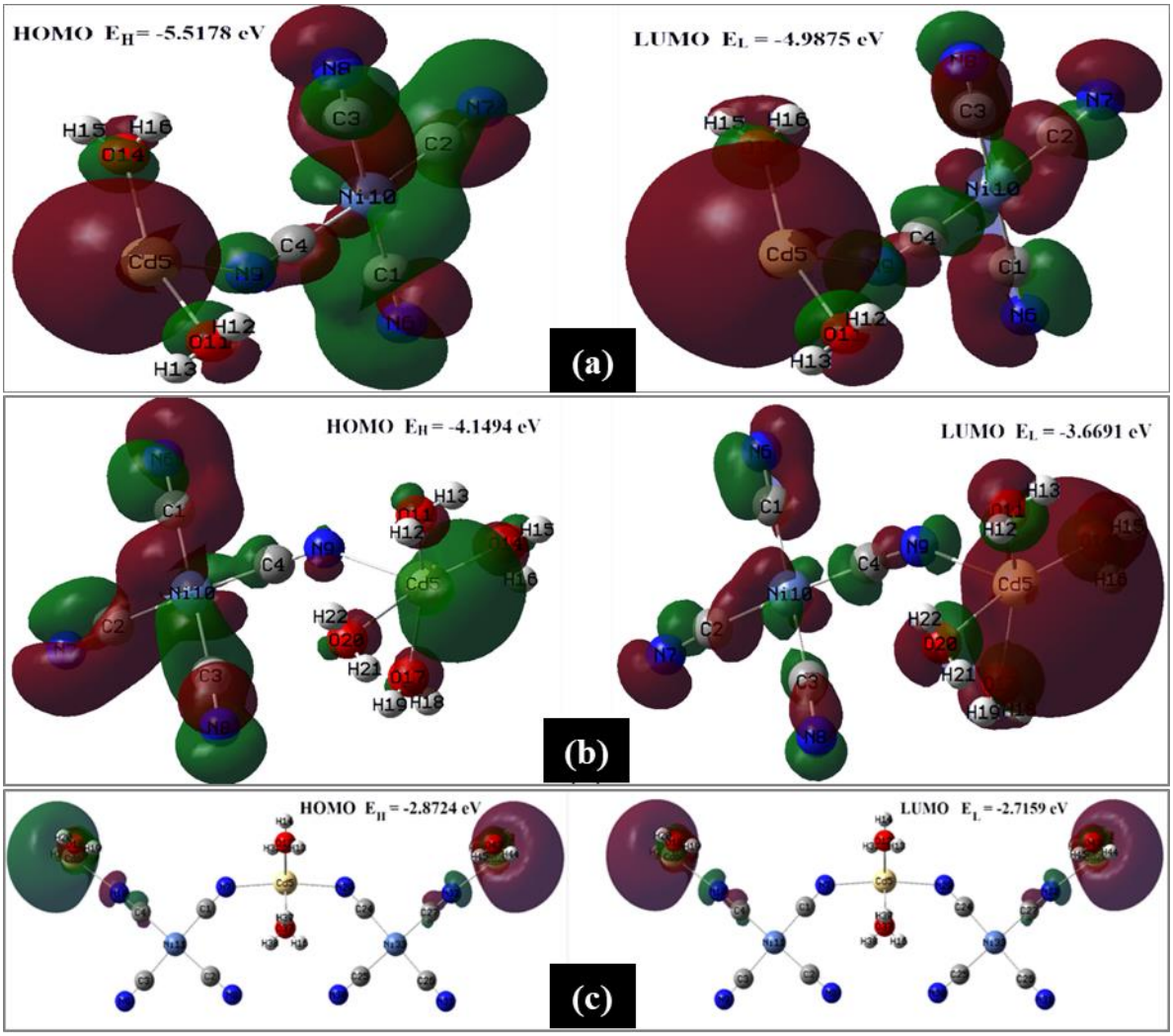

Figure 5. *According to the DFT/B3LYP method and the LanL2MB basis set, the graphics of boundary orbitals of the theoretical units of compound 1 (a) and (b) and of their combinations (c).*

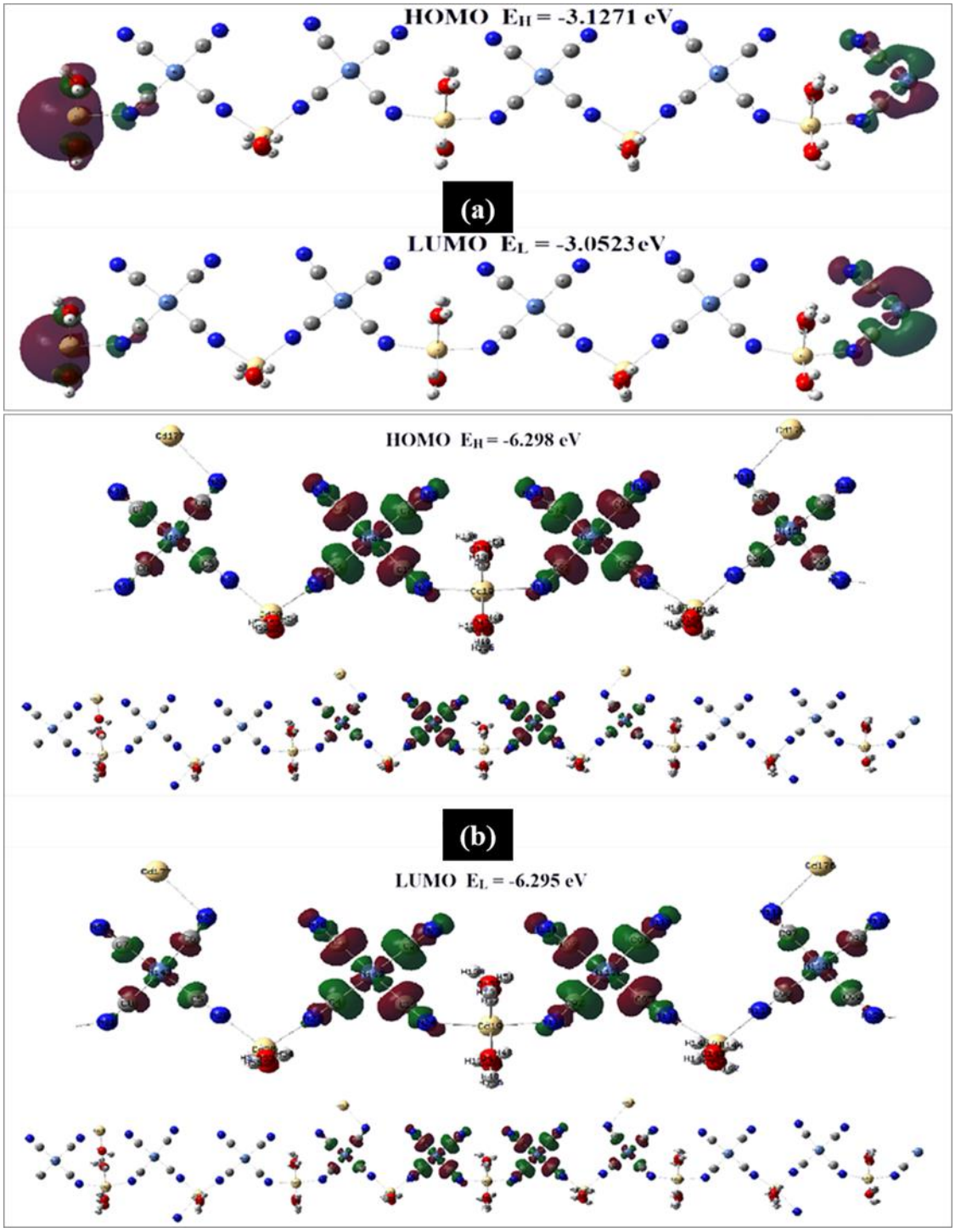

Figure 6. *Also, the graphics of boundary orbitals of the asymmetric unit of experimental compound* ***1*** *(a) and of all experimental compound* ***1*** *(b).*

On closer inspection of Figure 5, it can be seen that in simple models of compound **1** with few atoms, the boundary orbitals are distributed over almost all atoms (see Figure 5 (a) and Figure 5 (b)). In Figure 5 (c) and Figure 6 (a), it is seen that the boundary orbitals prefer to be located at the ends of the structure in structures with more atoms. It is seen that the boundary orbitals of compound **1** are located on the $[Ni(CN)_4]^2$ ion groups located in the middle of the structure (see Figure 6 (b)). They have been re-inserted into this figure at greater magnification to give a better view of the boundary orbitals. The following

conclusion can be drawn from this: the shape and arrangement of the boundary orbitals in a compound are closely related to the number of atoms and ion groups in that compound and to their arrangement with respect to each other. The occupied orbital, vacant orbital, total orbital numbers and HOMO, LUMO values of the compounds and some chemical efficiency values are given in Table 5.

The electronic properties of a compound obtained by chemical methods are calculated with the help of its ionization potential (I = -HOMO) and Electron affinity (A = -LUMO) values. The formulae for some parameters that can be calculated with the help of the ionization potential (I) and electron affinity (A) values of a compound are listed below [38-41].

$\Delta E = A - I$ (Energy gap value) (1)

$\chi = (I + A) / 2 = -\mu$ (Electronegativity, Negative chemical potential) (2)

$\eta = (I - A) / 2$ (Chemical hardness) (3)

$S = 1 / 2\eta$ (Chemical softness) (4)

$\omega = \mu^2 / 2\eta$ (Electrophilicity index) (5)

The energy gap value (ΔE), electronegativity (χ), negative chemical potential (-μ), chemical hardness (η), chemical softness (S) and electrophilicity index values (ω) calculated for all compounds according to these formulae are given in Table 5 in term (eV) unit.

Table 5 *Calculated frontier molecular orbitals energies and chemical reactivity descriptors (in "eV" units)*

Chemical efficiency values	**Compounds**				
	1-a	**1-b**	**1-c**	**1-asy**	**1**
Occupied orbital	51	61	128	262	550
Vacant orbital	25	29	61	126	264
Total orbital	76	90	189	388	814
HOMO (-I)	-5.5178	-4.1494	-2.8724	-3.1271	-6.298
LUMO (-A)	-4.9875	-3.6691	-2.7159	-3.0523	-6.295
ΔE = (A – I)	0.5303	0.4803	0,1565	0.0748	0.00272
χ	5.2527	3.9093	2.7942	3.0897	6.2966
μ	-5.2527	-3.9093	-2.7942	-3.0897	-6.2966
η	0.2652	0.2402	0.0783	0.0374	0.00136
S $(eV)^{-1}$	1.8854	2.0816	6.3898	13.3690	367.647
ω	34.0983	31.8123	49.8885	127.6238	14570.376

After examining the theoretical values in Table 5, the following conclusions can be reached:

- The number of occupied, vacant and total orbital in a compound increases in direct proportion to the number of atoms in that compound.
- The difference between HOMO and LUMO energy levels in a compound is inversely proportional to the number of atoms in that compound.
- The values of HOMO and LUMO energy levels in a compound depend more on the type of atoms and the arrangement of those atoms than on the number of atoms in that compound.

- While the η value of a compound is inversely proportional to the number of atoms in that compound, the S and ω values are generally directly proportional to the number of atoms in that compound.

Calculations of Some Other Chemical Properties of Compound 1 and Its Theoretical Representatives

The electric dipole moment of a compound composed of different atoms and molecules is due to the molecular charge distribution of that compound. The electric dipole moment of a compound has a 3D vector character in 3D space. Therefore, the electric dipole moment can be used to show the motion of electric charges in a compound. The orientation of the dipole moment vector in a compound in 3D space depends on the location of the centers of the positive and negative charges in that compound. The dipole moment of a compound in electrostatic equilibrium is constant and its positioning is precisely determined. If an external electric field is applied to the electron cloud of any compound in electrostatic equilibrium, its electric charges will move and its charge balance will be disturbed. This degree of distribution is called "polarizability" for that compound. Often, the term "polarizability" is used instead of the term "mean polarizability". The electric dipole moments (μ), average polarizability (α_0), polarizability anisotropies (Δα) and first-order hyperpolarizability (β_0) values of the asymmetric part of compound **1** and its theoretical representatives were calculated by the finite field method using the LanL2MB basis set in DFT/B3LYP [31, 32]. When trying to calculate the μ, α_0, Δα and β_0 values of all of compound **1** with the same method, a negative result was always encountered. This negative result is thought to be due to the fact that the structure of compound **1** is too large to be resolved by the calculation method used. The formulae used to obtain the amounts of (μ), (α_0), (Δα) and (β_0) specific values of these compounds are given below, respectively. These formulae have been used by many researchers and us before [42-44].

$$\mu = \sqrt{\mu_x^2 + \mu_y^2 + \mu_z^2} \quad \text{(Dipole moment)} \tag{6}$$

$$\alpha_0 = \frac{\alpha_{xx}+\alpha_{yy}+\alpha_{zz}}{3} \quad \text{(Mean polarizability)} \tag{7}$$

$$\Delta\alpha = \sqrt{\frac{(\alpha_{xx}-\alpha_{yy})^2+(\alpha_{yy}-\alpha_{zz})^2+(\alpha_{zz}-\alpha_{xx})^2+6(\alpha_{xy}^2+\alpha_{xz}^2+\alpha_{zy}^2)}{2}} \quad \text{(Anisotropies of polarizability)} \tag{8}$$

$$\beta_0 = \sqrt{\beta_x^2 + \beta_y^2 + \beta_z^2} \quad \text{(First-order hyperpolarizability)} \tag{9}$$

$$\beta_x = \beta_{xxx} + \beta_{xyy} + \beta_{xzz} \quad \text{(x component of } \beta_0\text{)} \tag{10}$$

$$\beta_y = \beta_{yyy} + \beta_{xxy} + \beta_{yzz} \quad \text{(y component of } \beta_0\text{)} \tag{11}$$

$$\beta_z = \beta_{zzz} + \beta_{xxz} + \beta_{yyz} \quad \text{(z component of } \beta_0\text{)} \tag{12}$$

The calculated (μ), (α_0), (Δα) and (β_0) values of the compounds using these formulae are given in Table 6. In this study, the theoretically calculated $\Delta\alpha$, α_0 and β_0 values for the compounds were converted

from atomic units (au) to electrostatic units (esu) with the factors of 0.1482×10^{-24} and 8.6393×10^{-33}, respectively. [42, 43].

***Table 6**. The μ, α_0, Δα and β_0 values of the asymmetric part of compound **1** and its theoretical representatives*

Parameters	Compounds			
	1-a	**1-b**	**1-c**	**1-asy**
μ_x (D)	-24.6654	35.6274	0.0643	73.8146
μ_y (D)	2.2919	-4.6636	38.7170	-78.5181
μ_z (D)	1.2564	1.8401	0.8494	0.8494
μ (D)	24.8035	35.9785	38.7264	107.7668
α_{xx} (au)	-89.1973	-107.8012	-169.8287	-22.7458
α_{xy} (au)	2.6674	-0.5592	-0.1760	6.4194
α_{yy} (au)	-92.7932	-111.7138	-274.7731	-479.5327
α_{xz} (au)	-11.1955	3.7203	-14.1062	12.7070
α_{yz} (au)	-14.4335	1.2258	0.3310	27.5447
α_{zz} (au)	-78.0362	-69.5888	-129.9467	-301.9711
Δα (esu)	5.1337×10^{-24}	6.0582×10^{-24}	1.9203×10^{-23}	5.9642×10^{-23}
α_0 (esu)	-3.8536×10^{-23}	-4.2845×10^{-23}	-2.8383×10^{-23}	-3.973×10^{-23}
β_{xxx} (au)	-526.5466	734.0383	4.3061	22328.6763
β_{xxy} (au)	-33.5952	27.0237	1207.2505	-8235.3116
β_{xyy} (au)	-153.5749	179.2955	-0.7505	383.2087
β_{yyy} (a.u.)	43.5007	-51.1417	701.2097	-1473.0625
β_{xxz} (au)	49.8452	15.6047	40.8439	-85.3687
β_{xyz} (au)	10.3340	0.4362	-94.1506	-262.8113
β_{yyz} (au)	-14.7025	-3.5084	3.5014	-32.2804
β_{xzz} (au)	-96.4647	149.0481	-0.1803	-47.8405
β_{yzz} (au)	1.7828	-24.1799	202.3563	-374.1381
β_{zzz} (au)	3.5123	15.8444	4.1633	4.6113
β_0 (esu)	6.7182×10^{-30}	7.9053×10^{-30}	1.0438×10^{-29}	2.0946×10^{-28}

According to the analysis made on the values in Table 6, the following results were obtained.

- The dipole moment values of the studied theoretical and experimental compounds are directly proportional to their atomic number, that is, to their electric charge.
- Since α_0 and Δα values of the studied theoretical and experimental compounds depend on the distribution of their atoms and electric charges in 3D space, there is no certain proportionality between these values.
- The β_0 values of the studied theoretical and experimental compounds are equal to the square root of the sum of the squares of their β_x, β_y and β_z components. In other words, these values are increasing in direct proportion to the number of atoms in the compounds and their electrical charges.

Hirshfeld Surface Analysis of Compound 1

Types of bonds that ensure the stability of a crystalline structure; They are in the form of metallic bonds, various types of bonds between other atoms in the structure, hydrogen-hydrogen and van der Walls interactions of smaller intensity. A program called CrystalExplorer was created by Spackman et al to calculate weak interactions in crystal structures [45]. This program can calculate the surface types of a

crystal such as Hirshfeld, Promolecule, Crystal Voids, Electron Density, Deformation Density, Electrostatic Potentials, Molecular Orbitals and Spin Density [45]. A 2D map of the Hirshfeld surface calculated for a molecular structure is very important in understanding the intramolecular interactions of that molecular structure. Hirshfeld surface analysis, which is used to identify various interactions in a crystal structure, identifies these interactions with the help of red, blue and white colors. Red areas on a Hirshfeld surface indicate hydrogen bond interactions, blue areas indicate long-reach interactions, and white areas indicate van der Waals interactions. The intensity of each color on the Hirshfeld surface of a crystal structure is directly proportional to the magnitude of the interactions [45]. The Hirshfeld surface analysis approach of compound **1** is a graph-based tool that facilitates understanding interactions in that molecular structure [45]. The different views of the Hirshfeld surface created by the CrystalExplorer program for compound **1** and the 2D fingerprint graphs produced from them and the percentages of various interactions are shown in Figure 7.

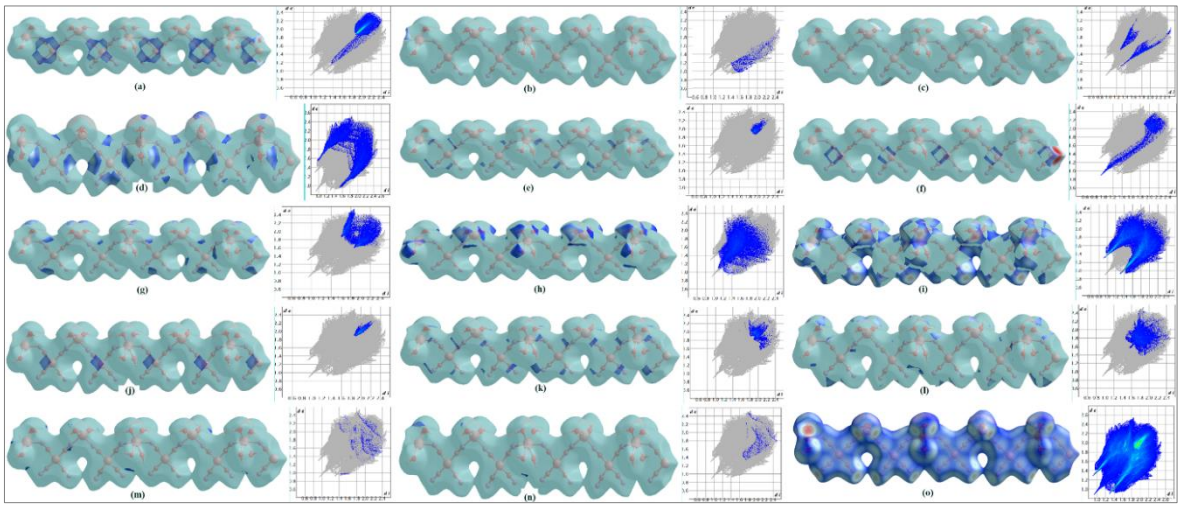

Figure 7. *Percentages of contribution of some intramolecular and extramolecular interactions in the asymmetric part of compound* ***1*** *to crystal formation; C…C (a), Cd…H/H…Cd (b), Cd…N/N…Cd (c), C…H/H…C (d), C…N/N…C (e), C…Ni/Ni…C (f), C…O/O…C (g), H…H (h), N…H/H…N (I), Ni…Ni (j), N…N (k), N…O/O…N (l), O…H/H…O (m), O…O (n), and 2D fingerprint plot of all interactions in the asymmetric part of compound* ***1*** *(o)*

A 2D fingerprint graph of a crystal structure makes it possible to quantitatively examine all the molecular interactions in that crystal structure together. The 2D fingerprint graph provides the advantage of highlighting and distinguishing short-range contacts in the crystalline structure [45]. From all the 2D fingerprint views of compound **1**, the interactions that hold the molecules together in its crystal structure are N-H, C-H, C-C, H-H, C-C, C-O, N-O, C-Ni, N-N, Cd-N, N-N, Ni-Ni … and others. The contributions of these interactions to the formation of the crystal structure of compound **1** are shown in Table 7.

Tablo 7. *The contribution percentages of each of the intramolecular and intermolecular interactions that form the crystal structure in the asymmetric part of compound **1** to the Hirshfeld surfaces, ordered from largest to smallest.*

Interactions	Contribution (%)
N--H/H--N	40.8
H--H	12.4
C--H/H--C	10.3
C--C	8.3
C--O/O--C	6.5
N--O/O--N	6.4
C--Ni/Ni--C	3.2
N--N	2.7
Cd--N/N--Cd	2.6
Ni--Ni	2.2
C--N/N--C	1.3
Cd--O/O--Cd	0.9
O--H/H--O	0.7
O--O	0.6
Cd--H/H--Cd	0.5

Interpretation of The FT-IR Spectrum of Compound 1

Experimental FT-IR spectrum of compound **1** is given in Figure 8. In this spectrum, firstly, the vibration modes of the water molecule, which is the ligand, and then the $[Ni(CN)_4]^{2-}$ ion group were investigated separately.

Vibrations of the H_2O in Compound 1

Since there are two hydrogen and one oxygen atoms in the structure of the water molecule, it has three vibration modes defined as νas(OH), νs(OH) and δ(OH) in its FT-IR spectrum [46 - 48]. A new vibration band is formed as a result of the overlapping of νas(OH) and νs(OH) modes in the FT-IR spectrum of the compound formed by bonding a water molecule to a metal atom. This new vibration band belongs to the water molecule and is a very broad band in the range of wavenumbers of about 3500 and 3200 cm-1. If a compound has unbounded water molecules in its structure, then in its FT-IR spectrum, a single very sharp and intense stretching vibration peak appears around the wavenumber of 3600 cm-1. However, in some cases, in the FT-IR spectra of aqueous compounds with bound water molecules, the vibration modes νas(OH) and νs(OH) can be seen separately at lower wavenumbers than in the free water molecule. The vibration modes of liquid water were experimentally obtained in our laboratory at wavenumbers ν_{as}(OH) 3470 cm^{-1}, ν_s(OH) 3257 cm^{-1} and δ(OH) 1641 cm^{-1}. As can be easily seen from all the figures of the crystal structure of compound **1**, the water molecules are attached to the Cd atoms as two different groups. The physical conditions are different for the bound water molecule in each different group. Therefore, at least two different vibration groups should be expected for the bound water molecules. In fact, in the same region, peaks belonging to the combination and overtones of some of the vibration modes formed at lower wavenumbers of the H_2O molecule and the $[Ni(CN)_4]^{2-}$ ion group can

be found.

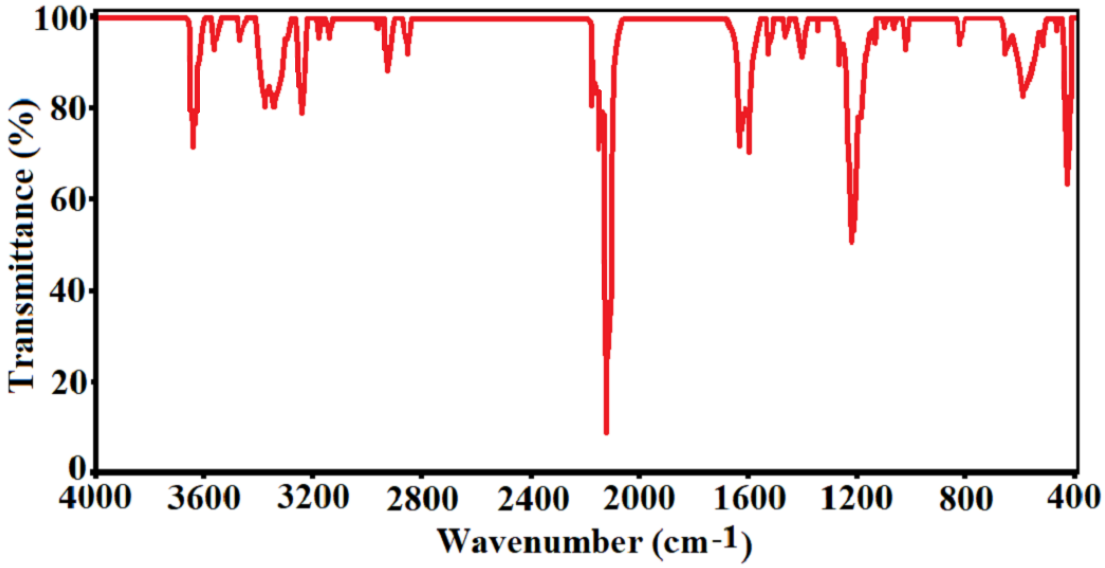

Figure 8*. The experimental FT-IR spectra of compound* ***1****.*

It is a fact that water molecules bonded to Cd atoms as binary groups will be under the influence of a stronger attraction force by the Cd atom than water molecules bonded as quaternary groups. As a result of this situation, the vibrations found in the higher wavenumber will belong to the water molecules that are bonded in binary. From the FT-IR spectrum of compound **1**, values of 3567 and 3373 cm^{-1} with 3548 and 3346 cm^{-1} can be assigned for ν_{as}(OH) and ν_{s}(OH) vibrations for binary and quaternary H_2O groups, respectively. From these results, it was seen that the ν_{as}(OH) and ν_{s}(OH) vibration modes of the binary and quaternary H_2O groups in compound **1** shifted to higher wavenumbers compared to the values of the vibrations in the liquid water molecule. The shift values to this high wavenumber are (97 - 78) cm^{-1} and (116 - 89) cm^{-1}, respectively. The vibration peak seen at wave number 3643 cm^{-1} in the FT-IR spectrum of compound **1** indicates that some water molecules are guests in the cavities of the crystal structure, without binding to any atoms. However, there is no water molecule as a guest in the crystal structure of compound **1**, which was resolved by the SC-XRD method. The explanation for this is when compound **1** first formed; its immediate FT-IR spectrum was taken. At that moment, there are some guest water molecules in compound **1**. However, about six months after obtaining compound **1**, its crystal structure was resolved and its elemental analysis was carried out. During this long period of time, the guest water molecules were separated from the crystal structure of compound **1**. The two peaks observed at wavenumbers 1625 and 1602 cm^{-1} in the FT-IR spectrum of compound **1** in Figure 4 correspond to the bending vibrations of the two different water groups in compound **1**. These bending vibrations shifted to the wavenumber region as low as 16 and 39 cm^{-1} value relative to the values in the free water molecule.

Vibrations of the $[Ni(CN)_4]^{2-}$ Ion Group in Compound 1

Various theoretical and experimental information about the $[Ni(CN)_4]^{2-}$ ion group can be seen in

previous articles of ours and other researchers [6, 7, 9-19, 45, 46]. The vibration modes of the [Ni $(CN)_4]^{2-}$ ion in the $K_2[Ni(CN)_4]\cdot H_2O$ compound and the vibration modes of the $[Ni(CN)_4]^{2-}$ ion in the compound **1**'s structure were compared with each other. In this way, the effect of compound formation on these modes was investigated. In the FT-IR spectrum of a compound with a cyanide group, sharp peaks with varying intensity in the wavenumber range of 2200-2000 cm^{-1} correspond to cyanide groups [20, 46]. The study of McCullough et al on this subject was used to determine the vibration modes of the [Ni $(CN)_4]^{2-}$ ion in compound **1** [50]. Let us examine the most important vibration modes of $K_2[Ni(CN)_4]\cdot H_2O$ in order from largest wavenumber to smallest. In the FT-IR spectrum of $K_2[Ni(CN)_4]\cdot H_2O$, the ν_8(Ni–CN), E_u mode is at 2122 cm^{-1}. This vibration mode was observed in compound **1** at wavenumbers 2168, 2145, and 2123 cm^{-1} as splitting into three. The reason for this triple splitting can be understood by examining the crystal structure of compound **1**. The nitrogen atoms of the four cyan groups in the structure of compound 1 form three different bonding patterns with other atoms around it. These bonding forms are the bond between N and two different H atoms, the bond between N and Cd atoms, and the bond between N and Cd and H atoms, respectively. It can be said that the bond constants of these bonds are in the same order of magnitude but at different values close to each other. These three types of bonds with different bond constants cause the vibration mode of the cyan group to be split into three. It can be said that ν_9(Ni–CN), E_u; π(Ni–CN), A_{2u} and δ(Ni–CN), E_u vibration modes appear in the FT-IR spectrum of compound **1** at wavenumbers of 584, 462 and 420 cm^{-1}. However, in the FT-IR spectrum of compound **1**, it is very difficult to accurately interpret the peak values in this region. Because, in this region, stretching and bending vibrations of CN groups with three different properties and various modes of some other groups coexist.

Thermal Behavior of the Compound 1

TGA and DTG graphs of compound **1** are given in Figure 9. According to his TGA graph, compound **1** preserved its crystalline structure while heating from 20 °C to 90 °C. However, after this temperature, water molecules, which are ligands, started to separate from the crystal structure of compound **1**. In this first step of the thermal analysis, 4 water molecules attached to the Cd atom left the crystal structure of compound **1**. These 4 water molecules were first separated from the crystal structure of compound **1** because they have weaker bonds than the 2 water molecules attached to the other Cd atom. This first step of the thermal analysis occurred in the low temperature range of 90 - 116 °C, with a peak of about 105 °C. [found/(calc.)% = 11.85/(12.09)%].

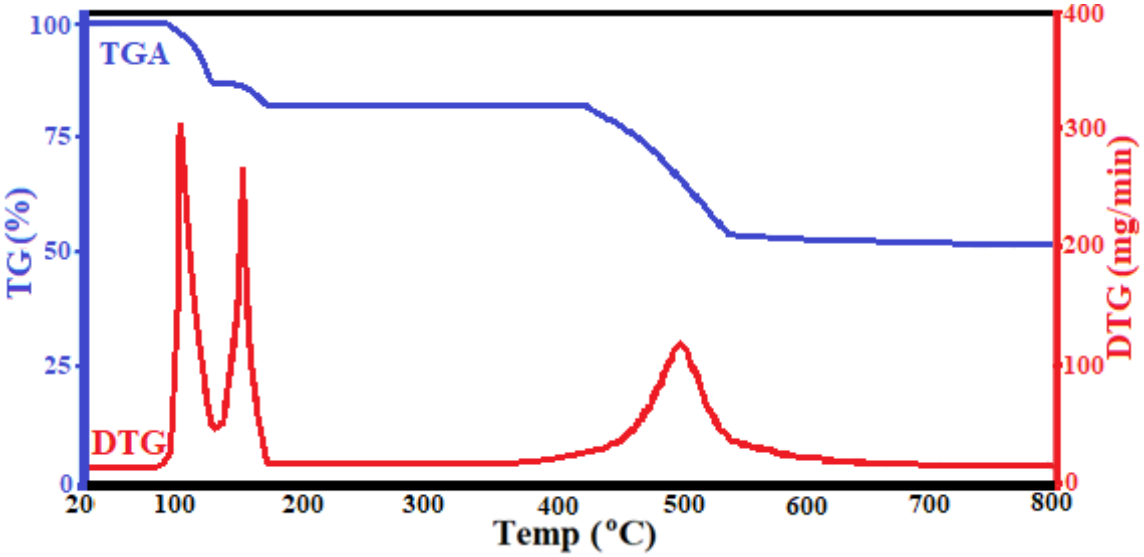

Figure 9*. Thermal graphic of compound **1**.*

In the second step of the thermal analysis of compound **1**, 2 water molecules, which were more tightly bound as ligands to the other Cd atom in the crystal structure, were separated from the crystal structure of compound **1**. This second step of the thermal analysis took place in the temperature range 125–180 °C, which is a slightly higher temperature range than the first temperature range, with a peak at 158 °C. [found/(calc.)% = 4.48/(4.84) %]. In the third step of the thermal analysis, it is thought that the square planar $Ni(CN)_4$ bridges in the structure of compound **1** deteriorate with the effect of increasing temperature. In this step, the triple bonds in the CN groups were broken, and then the C and N atoms were burned out by the effect of high temperature. It can be seen from Figure 9 that the third step of the thermal analysis occurs in the temperature range of about 442–544 °C and has a peak at 497 °C. [found/(calc.) % = 30.87/(31.43) %]. Finally, it is understood that only Cd and Ni atoms remained in the thermal analysis of compound **1**. [found/(calculated)% = 51.18/(51.66)%].

Conclusion

In this study, a new heterometallic Hofmann-type-like compound defined by the open formula $[Cd(H_2O)_2Ni(CN)_4]_4[Cd(H_2O)_4Ni(CN)_4]_5$ was synthesized in crystal form by chemical reaction. In the reaction medium, water was used both as a ligand molecule and as a solvent. In this heterometallic new Hofmann-type-like compound, the H_2O ligand molecule behaved like a monodentate ligand molecule by binding from the O atom to the Cd transition metal atoms. These Cd-O bonds played a very important role in the formation and stability of the crystal structure of the obtained new heterometallic compound **1**. In obtaining the crystal structure of compound **1**, the bonds made by the oxygen atom of the ligand water molecule with the Cd transition metal atom, as well as the various bonds made by its hydrogen atoms with different atoms in the environment played very important roles. The various bonds that the hydrogen atoms of the ligand water molecule make with different atoms in the environment show a distribution ranging from the strongest to the weakest bonds forming the crystal structure of compound

1 (see Table 7). In addition, due to the weak interaction forces between the ligand water molecules forming the structure of compound **1**, it was thought that its volume could easily change depending on the guest molecules that would enter this structure. Therefore, the volumes of the host structures formed by the ligand water molecule will be able to stretch at a certain rate. Therefore, it can be thought that these new structures are more suitable for the storage of certain gases and other guest molecules than the host structures formed by larger ligand molecules. Furthermore, all Ni (II) ions in the structure of the crystal of compound 1 are surrounded by four cyanide groups, forming a square planar arrangement. In contrast, Cd (II) ions possess two distinct environmental arrangements within the structure. In one of these coordination geometries, some Cd (II) ions have a distorted octahedral coordination geometry formed by the two nitrogen atoms of the cyanide groups and the four oxygen atoms of the ligand water molecules. In the other coordination geometry, the other Cd (II) ions have a distorted tetrahedral coordination geometry formed by the two nitrogen atoms of the cyanide groups and the two oxygen atoms of the ligand water molecules. The probabilities of various guest molecules of suitable size entering the gaps in the structure of compound **1**, which is a Hofmann-type-like compound obtained in crystalline form, can be investigated experimentally. Consequently, clathrate forms of compound **1** can be obtained in future studies.

Acknowledgement -

Funding/Financial Disclosure The authors wish to thank in particular Kütahya Dumlupınar University, Türkiye, for the technical [Department of Physics and Chemistry; Advanced Technologies Center (İLTEM)] and financial support with the project number 2017/25.

Ethics Committee Approval and Permissions The study does not require ethics committee approval or any special permission.

Conflicts of Interest The authors declare that they have no known competing financial interests or personal relationships that could have appeared to influence the work reported in this paper.

Authors Contribution Authors contributed equally to the work.

References

[1] OpenStax, Chemistry. OpenStax CNX. Jun 20, 2016 http://cnx.org/contents/85abf193-2bd2-4908-8563-90b8a7ac8df6@9.311.

[2] The Materials Project (2020). Materials Data on $K_2Ni(CN)_4$ by Materials Project. United States. https://doi.org/10.17188/1307699

[3] Hofmann, K. A. & Küspert, F. (1897). Verbindungen von kohlenwasserstoffen mit metallsalzen. *Zeitschrift Für Anorganische Chemie, 15(1),* 204-207. http:/doi.org/10.1002/zaac.18970150118

[4] Hagan, M. (1962). *Clathrate Inclusion Compounds.* Reinhold Publishing Corporation, Chapman & Hall Ltd., New York. p. 5.

[5] Iwamoto, T. (1984). Inclusion Compounds, Vol. 1, Chapter 2 (Eds. J. L. Atwood, J. E. D. Davies, and D. D. MacNicol). Academic Press, London, p. 29.

[6] Türköz, D., Kartal, Z., & Bahçeli, S. (2004). Ft-Ir Spectroscopic Study Of Co(1-Propanethiol)$_2$Ni(CN)$_4$·Benzene Clathrate. *Zeitschrift Für Naturforschung A*, *59*, 7-8. http:/doi.org/10.1515/zna-2004-7-819

[7] Kartal, Z. (2005). IR spectroscopic study of M (benzoic acid)$_2$Ni(CN)$_4$.(1,4-dioxane) clathrate (M = Ni, Cd and Co). *Zeitschrift für Naturforschung A*, *60*(A), 469-472. http:/doi.org/10.1515/zna-2005-0613

[8] Kartal, Z., Parlak, C., Şentürk, Ş., Aytekin, M. T. & Şenyel, M. (2007). FT-IR Spectroscopic Study of the Hofmann-Td-type Clathrates: Ni(1,9- diaminononane)M′(CN)$_4$·2G (M′ = Cd or Hg, G = Benzene, 1,2-Dichlorobenzene or 1,4-Dichlorobenzene). *Croatica Chemica Acta*, *80*(1), 9-15. https://hrcak.srce.hr/12805

[9] Kartal, Z. (2009). FT-IR spectroscopic study on some Hofmann-type clathrates: M(p-Benzoquinone)Ni(CN)$_4$·2G (M = Mn, Co, Ni or Hg; G = Aniline). *Journal of Molecular Structure*, *938*(1-3), 70–75. http:/doi.org/10.1016/j.molstruc.2009.09.005

[10] Kartal, Z. & Sayın, E. (2011). FTIR spectroscopic and thermal study of M(Cyclohexanethiol)$_2$Ni(CN)$_4$.(1,4-dioxane) clathrate (M = Mn, Co, Ni and Cd). *Journal of Molecular Structure*, *994*, 170-178. http:/doi.org/10.1016/j.molstruc.2011.03.014

[11] Kartal, Z. (2012). Vibrational spectroscopic investigation on some M(Benzonitrile)$_2$Ni(CN)$_4$ complexes (M = Ni, Zn, Cd and Hg). *Brazilian Journal of Physics*, *42*, 6-13. http:/doi.org/10.1007/s13538-011-0054-x

[12] Kartal, Z. & Türk, T. (2021). FT-IR spectroscopic and thermal study of M(1,6-hexanedithiol) Ni(CN)$_4$.2(1,4-dioxane) clathrate(M = Mn, Co, Ni and Cd). *Journal of Molecular Structure, 1014*, 74-80. http:/doi.org/10.1016/j.molstruc.2012.01.031

[13] Kartal, Z. (2016). Synthesis, spectroscopic, thermal and structural properties of [M(3-aminopyridine)$_2$Ni(μ-CN)$_2$(CN)$_2$]$_n$ [M(II) = Co and Cu] heteropolynuclear cyano-bridged complexes. *Spectrochimica Acta Part A: Molecular and Biomolecular Spectroscopy*, *152*, 577–583. http:/doi.org/10.1016/j.saa.2014.12.117

[14] Kartal, Z. & Yavuz, A. (2018). The synthesis and the spectroscopic, thermal, and structural properties of the M$_2$[(fumarate)Ni(CN)$_4$].2(1,4-dioxane) clathrate (M = Co, Ni, Cd and Hg). *Journal of Molecular Structure*, *1155*, 171-183. http:/doi.org/ 10.1016/j.molstruc.2017.10.107

[15] Kartal, Z., Şahin, O. & Yavuz, A. (2018). The synthesis of two new Hofmann-type M(3-aminopyridine)$_2$Ni(CN)$_4$ [M = Zn(II)and Cd(II)] complexes and the characterization of their crystal structure by various spectroscopic methods. *Journal of Molecular Structure, 1171*, 578-586. http:/doi.org/10.1016/j.molstruc.2018.06.042

[16] Kartal, Z. & Şahin, O. (2021). Synthesis, spectroscopic, thermal, crystal structure prop- erties and characterization of new Hofmann-type-like clathrates with 4-aminopyridine and water. *Turkish Journal of Chemistry, 45*, 616–633. http:/doi.org/10.3906/ kim- 2011- 29

[17] Kartal, Z. & Şahin, O. (2021). Synthesis, spectroscopic, thermal, crystal structure prop- erties, and characterization of new Hofmann-T$_d$-type complexes with 3- aminopyridine, *Turkish. Journal of Chemistry, 45*, 942–955. http:/doi.org/10.3906/kim-2101-32

[18] Kartal, Z., Şahin, O. & Yavuz, A. (2019). Synthesis of Hofmann-type $Zn(H_2O)_2Ni(CN)_4.nG$ (G = water and 1,4-dioxane) clathrates and the determination of their structural properties by various spectroscopic methods, *Turkish Journal of Chemistry*, *43(6)*, 1608–1621. http:/doi.org/10.3906/kim-1906-26

[19] Kartal, Z. & Şahin, O. (2022). Synthesis of two Hofmann type and Hofmann-type-like compounds in crystal form from 4-aminopyridine and their characterizations by various methods. *Journal of Molecular Structure*, *1252*, 132088. https://doi.org/10.1016/j.molstruc.2021.132088.

[20] Nakamoto, K. (2009). *Infrared and Raman Spectra of Inorganic and Coordination Compounds, Part B, Applications in coordination, organometallic, and bioinorganic chemistry,* John Wiley and Sons, Hoboken, New Jersey.

[21] Smékal, Z., Císařová, I. & Mroziński, J. (2001). Cyano-bridged bimetallic complexes of copper(II) with tetracyanonickelate(II). Crystal structure of $[Cu(dpt)Ni(CN)_4]$. *Polyhedron*, *20*, 3301–3306.http:/ doi.org/10.1016/S0277-5387(01)00942-1

[22] Sheldrick, G. M. (2008). A short history of SHELX. *Acta Crystallographica*, *A64*,112-122. https://doi.org/10.1107/S0108767307043930.

[23] Sheldrick, G. M. (2015). Crystal structure refinement with SHELXL. *Acta Crystallographica*, *C71*, 3-8. http://dx.doi.org/10.1107/S2053229614024218

[24] APEX2, Bruker AXS Inc. Madison Wisconsin USA (2013).

[25] Macrae, C. F., Sovago, I., Cottrell, S. J., Galek, P. T. A., McCabe, P., Pidcock, E., Platings, M., Shields, G. P., Stevens, J. S., Towler, M. & Wood, P. A. (2020). Mercury 4.0: from visualization to analysis, design and prediction. *Journal of Applied. Crystalography*, *53*, 226-235. https://doi.org/10.1107/S1600576719014092

[26] Şenocak, A., Karadağ, A., Soylu, M. S. & Andac, O. (2015). Two novel cyanido-bridged polymeric complexes with suspension bridge type connections and a series of related complex salts: crystallographic and thermal characterizations. *New Journal of Chemistry*, *39(5)*, 3675-3686. https://doi.org/10.1039/C5NJ00071H

[27] Kurkcuoglu, G. S., Hokelek, T., Aksel, M., Yesilel, O. Z. & Dal, H. (2011). Cyano-Bridged Heteropolynuclear Ni(II), Cu(II) and Cd(II) Complexes, [M(deten) Ni(μ-CN) (CN)]. *Journal of Inorganic and Organometallic Polymers and Materials*, *21(3)*, 602-610. http:/doi.org/10.1007/s10904-011-9494-6

[28] Kürkçüoğlu, G. S., Sayin, E. & Şahin, O. (2015). Cyanide bridged hetero-metallic polymeric complexes: Syntheses, vibrational spectra, thermal analyses and crystal structures of complexes $[M(1,2\text{-dmi})_2\ Ni(\mu\text{-}CN)_4]_n$ (M = Zn (II) and Cd (II)). *Journal of Molecular Structure*, *1101*, 82-90. https://doi.org/10.1016/j.molstruc.2015.08.013

[29] Kürkçüoğlu, G. S., Hökelek, T., Yesilel, O. Z. & Aksay, S. (2008). Synthesis, IR spectrum, thermal property and crystal structure of cyano-bridged heteronuclear polymeric complex, [Cd(teta)Ni(mu-CN)(2)(CN)(2)] center dot 2H(2)O. *Structural Chemistry*, *19(3)*, 493-499. http:/doi.org/ 10.1007/s11224-008-9309-8

[30] Paharova, J., Cernak, J., Zak, Z. & Marek, J. (2007). Use of multi-N-donor ligands for preparation of organic–inorganic hybrid materials: Crystal structures of ionic $[M(aepn)_2][Ni(CN)_4]\cdot H_2O$ and polymeric $M(aepn)Ni(CN)_4$ (M=Zn(II), Cd(II); aepn=N-(2-aminoethyl)-1,3-propanediamine). *Journal of Molecular Structure*, *842*, 117-124. http:/doi.org/10.1016/j.molstruc.2006.12.022

[31] Collins, J. B., Schleyer, P. v. R., Binkley, J. S. & Pople, J. A. (1976) Self-Consistent molecular orbital methods. 17. Geometries and binding energies of second-row molecules. A comparison of three basis sets. *Journal of Chemical Physics*, *64*, 5142-5151. http:/doi.org/10.1063/1.432189

[32] Frisch, M. J., Trucks, G. W., Schlegel, H. B., Scuseria, G. E., Robb, M. A., Cheeseman, J. R., Montgomery, Jr. J. A., Vreven, T., Kudin, K. N., Burant, J. C., Millam, J. M., Iyengar, S. S., Tomasi, J., Barone, V., Mennucci, B., Cossi, M., Scalmani, G., Rega, N., Petersson, G. A., Nakatsuji, H., Hada, M., Ehara, M., Toyota, K., Fukuda, R., Hasegawa, J., Ishida, M., Nakajima, T., Honda, Y., Kitao, O., Nakai, H., Klene, M., Li, X., Knox, J. E., Hratchian, H. P., Cross, J. B., Bakken, V., Adamo, C., Jaramillo, J., Gomperts, R., Stratmann, R. E., Yazyev, O., Austin, A. J., Cammi, R., Pomelli, C., Ochterski, J. W., Ayala, P. Y., Morokuma, K., Voth, G. A., Salvador, P., Dannenberg, J. J., Zakrzewski, V. G., Dapprich, S., Daniels, A. D., Strain, M. C., Farkas, O., Malick, D. K., Rabuck, A. D., Raghavachari, K., Foresman, J. B., Ortiz, J. V., Cui, Q., Baboul, A. G., Clifford, S., Cioslowski, J., Stefanov, B. B., Liu, G., Liashenko, A., Piskorz, P., Komaromi, I., Martin, R. L., Fox, D. J., Keith, T., Al-Laham, M. A., Peng, C. Y., Nanayakkara, A., Challacombe, M., Gill, P. M. W., Johnson, B., Chen, W., Wong, M. W., Gonzalez, C. & Pople, J. A. (2004). Gaussian 03 Revision D.01. Gaussian, Inc., Wallingford CT.

[33] Dennington, R., Keith, T. & Millam, J. (2007). Gauss View, Version 4.1.2. Semichem Inc., Shawnee Mission.

[34] Becke, A. D. (1993). Density-functional thermochemistry. III. The role of exact exchange. *Journal of Chemical Physics*, *98*, 5648–5652. http:/doi.org/10.1063/1.464913

[35] Lee, C., Yang, W. & Parr, R. G. (1988). Development of the Colle-Salvetti correlation-energy formula into a functional of the electron density. *Physical Review B*, *37*, 785–789. http:/doi.org/ 10.1103/PhysRevB.37.785

[36] Peng, C., Ayala, P. Y., Schlegel, H. B. & Frisch, M. J. (1996). Using redundant internal coordinates to optimize equilibrium geometries and transition states. *Journal of Computaional Chemistry*, *17*, 49–56.

[37] Stephens, P. J., Devlin, F. J., Chablowski, C. F. & Frisch, M. J. (1994). Ab Initio calculation of vibrational absorption and circular dichroism spectra using density functional force fields. *Journal of Physical Chemistry*, *98*, 11623–11627. https://doi.org/10.1021/j100096a001

[38] Pearson, P. G. (2005). Chemical hardness and density functional theory. *Journal of Chemical Sciences*, *117*, 5, 369-377. https://doi.org/10.1007/BF02708340

[39] Parr, R. G. & Pearson, R. G. (1983). Absolute hardness: companion parameter to absolute electronegativity. *Journal of American Chemical Society*, *105*, 26, 7512-7516. https://doi.org/10.1021/ja00364a005

[40] Mebi, C. A. (2011). DFT study on structure, electronic properties, and reactivity of cis-isomers of $[(NC_5H_4\text{-}S)_2Fe(CO)_2]$. *Journal of Chemical Sciences*, *123*, 727–731.https://doi.org/10.1007/s12039-011-0131-2

[41] Kumar, C. P. & Buddhadev, M. (2003). HSAB principle applied to the time evolution of chemical reactions. *Journal of American Chemical Society*, *125*, 9, 2705-2710. https://doi.org/10.1021/ja0276063

[42] Nataraj, A., Balachandran, V. & Karthick, T. (2013). Molecular orbital studies (hardness, chemical potential, electrophilicity, and first electron excitation), vibrational investigation and theoretical

NBO analysis of 2-hydroxy-5-bromobenzaldehyde by density functional method. *Journal of Molecular Structure, 1031*, 221–233. http:/doi.org/10.1016/j.molstruc.2012.09.047

[43] Elusta, M. I., Başaran, M. A. & Kandemirli, F. (2019). Theoretical studies on mild steel corrosion inhibition by 5-substituted 1h-tetrazoles in acidic media. *International Journal of Electrochemical Science, 14*, 2743 – 2756. http:/doi.org/10.20964/2019.03.46

[44] Kartal, Z. & Şahin, O. (2022). Synthesis of two Hofmann type and Hofmann-type-like compounds in crystal form from 4-aminopyridine and their characterizations by various methods. *Journal of Molecular Structure, 1252*, 132088. https://doi.org/10.1016/j.molstruc.2021.132088

[45] Spackman, P. R., Turner, M. J., McKinnon, J. J., Wolff, S. K., Grimwood, D. J., Jayatilaka, D. & Spackman, M. A. (2021). CrystalExplorer: a program for Hirshfeld surface analysis, visualization and quantitative analysis of molecular crystals. *Journal of Applied Crystalography, 54(3)*, 1006–1011. http:/doi.org/10.1107/S1600576721002910

[46] Praprotnik, M., Janežič, D. & Mavri, J. (2004). Temperature dependence of water vibrational spectrum: a molecular Dynamics simulation study. *Journal of Physical Chemistry A, 108*, 11056-11062. http://doi.org/10.1021/jp046158d

[47] Carey, D. M. & Korenowski, G. M. (1998). Measurement of the Raman spectrum of liquid water. *Journal of Chemical Physics, 108(7)*, 2669-2675. http://doi.org/10.1063/1.475659

[48] Zhang, C., Khaliullin, R. Z, Bovi, D., Guidoni, L. & Kühne, T. D. (2013). Vibrational signature of water molecules in asymmetric hydrogen bonding environments. *Journal of Physical Chemistry Letters, 4(19)*, 3245-3250. http://doi.org/10.1021/jz401321x

[49] Sharpe, A. G. (1976). *The Chemistry of Cyano Complexes of the Transition Metals*, Academic Press, London.

[50] McCullough, R. L., Jones, L. H. & Crosby, G. A. (1960). An analysis of the vibrational spectrum of the tetracyanonickelate(II) ion in a crystal lattice, *Spectrochimica Acta, 16(8)*, 929–944. https://doi.org/10.1016/0371-1951(60)80057-4

Sinopfbd, 2024; 9(1): 96-113 **https://doi.org/10.33484/sinopfbd.1379682**

Sinop Üniversitesi Fen Bilimleri Dergisi
Sinop Uni J Nat Sci
E-ISSN: 2564-7873

https://dergipark.org.tr/tr/pub/sinopfbd

Characterization of Acid Mine Drainage in Tailings and Ore Stock Areas of Coal Mine Areas: Kinetic Test Moisture Cell Method

Tugay AKTAŞ[1] and Ömer Faruk ÖZTÜRK[2]

How to cite: Aktaş, T., & Öztürk, Ö. F. (2024). Characterization of acid mine drainage in tailings and ore stock areas of coal mine areas: kinetic test moisture cell method. *Sinop Üniversitesi Fen Bilimleri Dergisi, 9*(1), 96-113. https://doi.org/10.33484/sinopfbd.1379682

Research Article

Corresponding Author
Ömer Faruk ÖZTÜRK
ofozturk@comu.edu.tr

ORCID of the Authors
T.A: 0000-0002-2732-7383
Ö.F.Ö: 0000-0002-9244-6805

Received: 24.10.2023
Accepted: 04.03.2024

Abstract

In addition to evaluating the economic inputs of mining, it is important to examine the symptoms and concerns of the results of these activities. Appropriate legal regulations in the operation of mining facilities are implemented in an integrated manner with mining activities and growth effects in order to prevent negative growth effects on future generations. The most important environmental problems specific to mining are the inability to adequately examine the characterization of wastes and the failure to accurately determine whether these wastes can be obtained over the years. Especially during the opening, operation and separation of coal mines, which are rich in sulfur minerals, the reactions of these minerals are exposed to temperature interruptions and the formation of Acid Mine Drainage (AMD) poses a danger to natural life. In order to estimate the AMD formation potential of ore and waste, static and kinetic tests are applied to determine the mineralogical and chemical composition of the field. Among these tests, the most appropriate test in terms of representing natural conditions is the kinetic test method. Within the scope of the study, field conditions were simulated in columns prepared according to ASTM D5744-18 standard, physical and chemical analyzes of the resulting leachate were performed and the results were evaluated. According to the data obtained, no acid formation was observed during the 20-week test period, and metal emissions were characterized at a low rate. It has been determined that the clay structures in the geology of the sampled area are effective on the leakage rate.

Keywords: Coal mine site, acid mine drainage, kinetic test, ore, pasha, mine waste

Kömür Maden Sahalarının Atık ve Maden Stok Alanlarında Asit Maden Drenajının Karakterizasyonu: Kinetik Test Nem Hücresi Yöntemi

[1]GEMAR Çevre Ölçüm ve Analiz Laboratuvarı
Çanakkale/Turkiye

[2]Çanakkale Onsekiz Mart University, Faculty of Science
Chemistry Department
Çanakkale/Turkiye

Öz

Madencilik faaliyetlerinin ekonomik girdilerinin değerlendirilmesinin yanı sıra bu faaliyetler sonucunda ortaya çıkabilecek çevresel kaygıların da incelenmesi önemlidir. Gelecek nesiller üzerinde olumsuz çevresel etkilerin önlenmesi için madencilik tesislerinin işletilmesine ilişkin yasal düzenlemelerin madencilik faaliyetleri ve çevresel etkilerle bütünleşik bir şekilde uygulanması gerekmektedir. Madenciliğe özgü en önemli çevre sorunları, maden atıklarının karakterizasyonunun yeterince incelenmemesi ve bu atıkların yıllar içinde çevreye verebileceği kirliliğin tam olarak tespit edilememesidir. Özellikle kükürt mineralleri açısından zengin olan kömür madenlerinin açılması, işletilmesi ve kapatılması

sırasında atmosferik işlemlere maruz kalan bu minerallerin reaksiyonları sonucu ortaya çıkan Asit Maden Drenajı (AMD) oluşumu doğal yaşamı tehdit etmektedir. Cevher ve atığın AMD oluşum potansiyelini tahmin etmek amacıyla sahanın mineralojik ve kimyasal bileşimini belirlemek amacıyla statik ve kinetik testler uygulanmaktadır. Bu testler arasında doğa koşullarını temsil etmesi açısından en uygun test kinetik test yöntemidir. Çalışma kapsamında ASTM D5744-18 standardına göre hazırlanan kolonlarda saha koşulları simüle edilmiş, ortaya çıkan sızıntı suyunun fiziksel ve kimyasal analizleri yapılarak sonuçlar değerlendirilmiştir. Elde edilen verilere göre 20 Haftalık test süresinde asit oluşumu gözlemlenmemiş, metal salınımları ise düşük oranda karakterize edilmiştir. Örnekleme yapılan bölgenin jeolojisinde bulunan kil yapılarının sızıntı oranında etkili olduğu tespit edilmiştir.

Anahtar Kelimeler: Kömür madeni sahası, asit madeni drenajı, kinetik test, cevher, atık, maden atığı

Introduction

In addition to evaluating the economic inputs of mining activities (grade, price, mine life, etc.), it is also very important to examine the environmental concerns that may arise as a result of these activities from an environmental perspective. In order to prevent negative environmental impacts on future generations, legal regulations regarding the operation of mining facilities must be implemented in an integrated manner with mining activities and environmental impacts. For this, businesses need to create appropriate environmental policies. The mining sector is one of the leading sectors of our country and one of the most basic sectors that constitutes an important input to the economy. Since mines must be operated at their location or in existing suitable facilities located nearby, it is necessary to keep mining activities separate from other industrial activities. While it is possible to establish any industrial facility in an organized industrial zone or in places close to raw materials, there is no such possibility when it comes to opening mines. Mines are operated in the location where the ore is located, with open or closed mining (gallery) methods [1]. The most important environmental problems specific to mining are the insufficient examination of the physical and chemical properties of mine wastes and the inability to accurately detect the pollution that these wastes may cause to the environment over the years. Acid Mine Drainage threatens natural life as a result of the degradation of these minerals, which are exposed to atmospheric processes during the opening, operation and closure of coal mines, which are especially rich in sulfur minerals. From AMD, which is defined as one of the biggest environmental problems of the mining industry; This situation shows that in developed countries such as the USA and Canada, the financial costs of the world's leading mining companies to eliminate the problems caused by AMD vary between 2-5 billion dollars for a total of 12500 hectares of acidic fine-grained residue and 750 million tons of acidic bedrock [2]. It provides a very good example in terms of perceiving the dimensions of the problem. The formation of acidic drainage by sulphide minerals may occur under geogenic (hydrolysis and oxidation of sulphide ores in the natural environment) conditions, or it may occur when the ore or sulfurous wastes come into contact with the air and moisture (water) environment as a result of intensive mining activities (especially open pit mines). Terminologically, acid production under natural conditions

is Acid Rock Drainage (ACD); Acidic drainages caused by anthropogenic factors are called Acid Mine Drainage (AMD). As expected, the AMD formation process occurs faster than the AKD formation process. The major mechanisms of both ACD and AMD formation include hydrolysis and oxidation of the mineral pyrite (FeS_2), which is a very common mineral in nature [1]. Acid Mine Drainage greatly affects the receiving environment by changing the ambient pH and dissolved concentration of different chemical species [3]. Minerals contained in AMD can also precipitate at the bottom of receiving water bodies such as streams and rivers and affect benthic organisms [4]. In AMD, hazardous substances such as arsenic (As), chromium (Cr), iron (Fe), aluminum (Al), copper (Cu), zinc (Zn), lead (Pb), molybdenum (Mo) and nickel (Ni) are present. The presence of toxic chemical species is of primary concern [5]. Exposure to these pollutants can cause ecotoxicological, carcinogenic, mutagenic and teratogenic effects [6]. In addition to negatively impacting aquatic ecosystems, AMD also affects the quality of natural water bodies for human consumption or irrigation [7]. Therefore, preventing or effectively improving acid formation can protect human health and the environment. Remediation of acid typically relies on active (frequently driven by the input of chemicals, energy, and equipment) or passive (based on oxidation or reduction) technologies. However, these technologies have variable effectiveness in removing contaminants and also produce sludge and/or brine that can cause secondary pollution if not properly managed [8]. AMD usually contains high concentrations of Fe and sulfate (SO_4^{2-}) as well as rare earth elements and yttrium [9]. Determining the acid-producing or acid-neutralizing status of rock layers before failure [10] helps develop overburden handling and placement plans. Kinetic tests such as moisture cell sand leaching columns are important because they examine the rate of acid-producing and neutralization reactions [11]. This information from kinetic testing can complement the information provided by Acid-Base Accounting and assist regulators in permitting decisions. For example, the rate of sulfide oxidation and release of contaminants can occur rapidly before neutralizing materials have time to react. Therefore, early pulses of contaminants can be released for a short period of time when the reactions stabilize. [12] Detection of AMD formation potential plays a major role in planning mining activities and preventing their environmental impacts. According to the 14th paragraph of the 11th article of the Mining Wastes Regulation dated 15.07.2015 and numbered 29417 of the Ministry of Environment and Urbanization, "Although the provisions of this article are not applied for waste storage areas, stability measures are taken in the storage areas. In addition, sulfur-containing and acid rock drainage Potential wastes are stored in a way that prevents contact with air and water, by buffering them with wastes with neutralization capacity or by using the necessary collection techniques. With appropriate slope and shoulder systems, the leachate is treated and rehabilitated after storage. "Effects of these areas on surface/surface and groundwater are monitored with water samples taken from observation points and observation wells." Detecting AMD formation in the field and determining the measures to be taken to minimize its impact on the receiving environment. In order to estimate the AMD formation potential of ore and waste, static and kinetic tests are applied to determine the mineralogical

and chemical composition of the field. Among these tests, the most appropriate test in terms of representing natural conditions is the kinetic test method. In this context, field conditions will be simulated in columns prepared according to the ASTM D5744-18 "Standard Test Method for the Separation of Solids in the Laboratory Using a Humidity Cell" standard and physical and chemical analyzes of the resulting leachate will be performed. In addition, XRD analyzes were performed before moisture cell tests to determine the mineralogical structure of the field. This study aims to determine the potential for AMD formation in the ore and waste areas of the high-sulfur coal mine operating in Çan District of Çanakkale Province. Previous studies were examined in selecting the region where the research would be conducted. The fact that the geology of the region is suitable for AMD formation and that kinetic test studies have not been conducted before reveals the importance of this study. The kinetic tests subject to the study are used to simulate field conditions and evaluate the physical and chemical properties of the leachates they create, determine their potential to form acid mine drainage (AMD) and determine the precautions that can be taken. Thanks to this work, pollution that may arise from mining companies operating or will continue to operate in the region will be prevented. To achieve this goal;

- Appropriate samples were taken from the waste areas of the Open Pit Mine operated in Çan District of Çanakkale Province.
- That were formed as a result of excavations for coal production and were exposed to decomposition processes under natural conditions, were fragmented and especially open to atmospheric processes, were determined.
- Mechanisms were prepared to be used in kinetic tests, taking into account the field of mineralogy.
- During kinetic column experiments, pH and electrical conductivity (Ec) measurements taken over time and changes in elements and compounds determined by chemical analyzes were examined, and the relationship between AMD formation and these changes was investigated in kinetic column experiments.

Examining AMD formation potentials in ore and waste areas is very important in terms of protecting the environment from negative effects. For this reason, similar studies are carried out in sulfur-containing mining areas in our country and around the world, and it is aimed to minimize these effects by detecting the negative effects in advance. The data obtained as a result of the work to be carried out in the field within the scope of the project is of great importance in terms of preventing environmental pollution that may occur in the region. This will contribute to the preservation of the ecological balance of the region, especially by protecting the water resources from which the surrounding settlements provide drinking water and preventing the pollution of soil, air, surface and groundwater.

Materials and Methods

Acid mine drainage; It is defined as the phenomenon in which iron minerals such as pyrite, pyrrhotite and marcasite are exposed to oxidation in a humid environment in a mining area, giving protons (H+

ions) to the aqueous environment as a result of the reactions and the solution turning into solution. Acidic mineral waters with corrosive and solvent character generally contain up to 50 mg/l Cu, up to 1000 mg/l Fe, and up to 12 mg Pb, as well as high sulphate (800 - 1800 mg/l) content. /l. and may contain up to 1700 mg/l of Zn metals. In addition, AMDs formed as a result of the leaching process contain cyanide, thiosulfate, etc. It is also known to contain [13]. Although pyrite (FeS_2) and arsenopyrite (FeAsS) are mainly responsible for AMD formation, iron sulfides (Fe_xS_x), pentlandite ($(Fe, Ni)_9S_8$ chalcopyrite ($CuFeS_2$), villamaninite ($Cu2_S$), covellite (CuS), molybdenite Weathering of other sulfide-rich or sulfide-containing minerals such as (MoS_2), sphalerite ((Fe, Zn)S), millerite (NiS) and Galena (PbS) contributes to the formation of AMD [14]. These minerals are typically organic-rich (reducing) and are found in sediments (e.g. coal beds) [9]. These minerals are typically encountered in organic-rich (reductive) sediments (e.g., coal deposits) or in rocks altered by sulfur-rich hydrothermal fluids, such as volcanogenic sulfide ore, which produce metals such as copper, gold, and zinc. When exposed to the atmosphere, typically through mining activities (e.g., surface or deep mines, tailings piles, and tailings), they oxidize and form AMD; Iron sulfide minerals (typically pyrite) are the main minerals behind the formation of AMD and others. Sulfur minerals contribute only to a limited extent [15].

Table 1. *Chemical decomposition processes effective in the formation of acid mine drainage*

Chemical Degradation Process Stages	**Explanation**
$FeS_2 + 7/2O_2 + H_2O \rightarrow Fe^{2+} + SO_4^{2-} + 2H^+$	Oxidation of Pyrite
$Silicates + H^+ \rightarrow SiO_2 + Al^{3+} + Mg^{2+} + Ca^{2+} + Mn^{2+}$	Dissolution of Clays with Acid
$CaCO_3 + H^+ \rightarrow Ca^{2+} + H_2O + CO_2$	Neutralizing Acid with Calcite
$Fe^{2+} + 1/4O_2 + H^+ \rightarrow Fe^{3+} + 1/2H_2O$	Ferro Iron Oxidation
$Fe^{3+} + 3OH^- \rightarrow Fe(OH)_3$	Ferric Iron Hydrolysis "Yellow Layer Formation"
$Al^{3+} + 3OH^- \rightarrow Al(OH)_3$	Aluminum Hydrolysis
$Fe^{2+} + 1/4O_2 + 5/2H_2O \rightarrow Fe(OH)_3 + 2\ hours + H^+$	Iron Oxidation and Hydrolysis Reactions
$H^+ + HCO^{3-} \rightarrow H_2O + CO_2$	Acid Neutralization of Bicarbonate Ion
$H^+ + OH^- \rightarrow H_2O$	Acid Neutralization with Hydroxyl Ion

Figure 1. *Abandoned coal mine site in çanakkale çan region with amd formation observed. turning to red color after oxidation with atmospheric weather conditions.*

The type of sulfur minerals found in mine wastes, humidity, oxygen concentration, presence of bacteria, properties and amounts of alkaline minerals are the main factors affecting the formation of AMD. On the other hand, the distribution of sulfide and alkaline ores in the waste pile, the surface area of the sulfide ores and therefore the grain size and oxidation rate are important parameters affecting the formation of AMD. The potential of mine tailings to produce acids and release pollutants depends on several factors [16]. The main factors affecting the formation of AMD include sulfur minerals (Table 2), water, oxygen, the presence of bacteria that catalyze oxidation, and the heat generated as a result of the reaction. Secondary factors are; While it refers to tertiary factors such as neutralization of the acid produced, it consists of dissolved metal ions and their effects that change the character of the waste through acid production. Tertiary factors; Physical properties of materials, storage of acid-producing and neutralizing materials, and hydrological regime near the waste. The view of the AMD pond in the abandoned coal mine area, which turned red after oxidation due to atmospheric weather conditions, is given in Figure 1. Forms Fe^{2+} and SO_4 and H^+ as shown in the reaction in Table 1. This process is key to AMD formation. Mineral composition, environmental microbial activity, and external conditions such as oxygen and water influence pyrite oxidation and H^+ release, determines the speed. In an environment where there is sufficient oxygen and necessary microorganisms (pH>3.5), Fe^{2+} released in the reaction, depending on the reaction, it can be oxidized to Fe^{3+}. Since the pH is 2.3–3.5 , Fe^{3+} will precipitate $Fe(OH)_3$ and release H^+ as shown in the reaction. As the H^+ released increases, the pH will gradually decrease. When pH<2, $Fe(OH)_3$ will hydrolyze again, allowing Fe^{3+} to return to solution and

promoting the oxidation of FeS_2 (When pH<3, the oxidation rate of FeS_2 by Fe^{3+} is about 10– In the reaction [17] from O_2) as shown It is 100 times faster (Figure 2).

Table 2. *Some important metal sulfides, of which pyrite and marcasite are the dominant acid producers [18].*

Metal Sulphide	Chemical Formula
Pyrite	FeS_2 _
Marcasite	FeS_2 _
Pyrrhotite	$Fe_{1-x}S$
Chalcocite	Cu_2S _ _
Chalcocite	Whoa
Chalcopyrite	$CuFeS_2$ _ _
Molybdenite	MoS_2 _
Millerite	NiS
Galena	PbS
Sphalerite	ZnS
Arsenopyrite	FeAsS

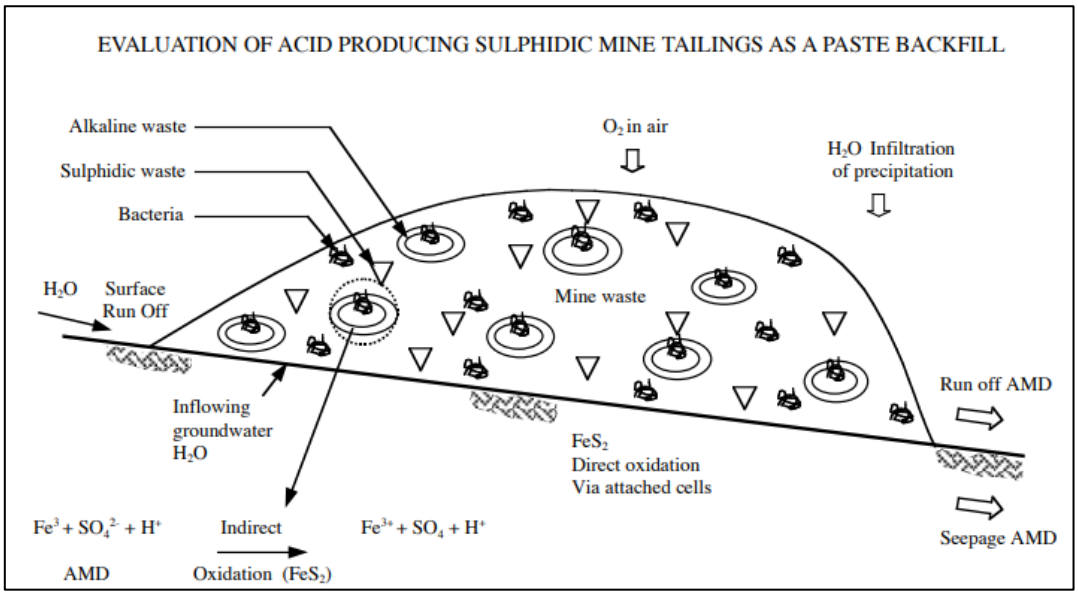

Figure 2. *Bacterial oxidation of pyrite and acid formation via direct and ındirect paths* [19]

Geology and Stratigraphy of the Study Area

The basement rock unit observed in the study area and its surroundings is the Cretaceous -Paleocene aged complex, according to Okay et al. [20] it is named as Çetmi ophiolite mélange. Çetmi ophiolite mélange, which crops out in the west of Karabiga, consists mostly of spilite, various types of limestone blocks and less of shale, sandstone, serpentinite and radiolarite. Spilites are dark green, blackish green colored spilites generally do not show foliation and consist of albite, pinkish Ti-Augite and chlorite. Only eclogites located around tectonic eclogite blocks show a distinct foliation and a greenschist facies mineral assemblage characterized by actinolite and epidote [20]. This unit is unconformably covered by

the Early-Middle Miocene aged Doyran Volcanics and the continental Çan Formation, which was deposited at the same time as this volcanism [21]. The youngest geological unit in the region is Quaternary alluviums. In the study area where TKİ Çan Lignites Enterprise is located, there are Çan volcanics [22], which have reached the surface by cutting older units on the Biga Peninsula, and Çan formation [23] and Kulfa formation [24], which consist of clastic and visual sediments containing lignite. The average coal thickness in the Çan Formation, where coal production takes place, is approximately 17 meters.

Findings and Conclusions

Previous Studies Performed in the Field

Turkish Coal Enterprises (TKİ), Çan Lignite Enterprise Directorate (ÇLİ) Çanakkale province, Çan district, with the aim of determining the acid production potential of the waste areas of the open pit enterprise with license number IR: 3378, by Kütahya Dumlupınar University Faculty of Engineering, Mining Engineering Department in 2020. A study was conducted and as a result of the sulfur analysis and static tests of the samples taken, the acid production potential (APP) of the field was found to be 19.99 kg $CaCO_3$ t^{-1} on average and the neutralization potential (NP) was 80.55 kg $CaCO_3$ t^{-1} on average. In addition to minerals with neutralizing properties such as clay, montmorillonite, kaolinite, andesite, muscovite and calcite, the presence of minerals with acid-producing properties such as pyrite has also been determined. The following findings were determined as a result of static tests carried out by Dumlupınar University for the purpose of determining AUP in the mining area under investigation.

- In the pH measurements made for a short time (3 days) in the samples taken from the field, it was determined that the pH values varied between 6.67 - 9.79, therefore there was no acid production in the short term.
- The average sulphide-sulfur value of 95 different samples taken from different coordinates of the waste area was determined as 0.64%
- The acid production potentials of the samples were determined with a theoretical approach (ABA standard method) according to sulfur values, and the average acid production potential of the waste area was calculated as 19.99% kg $CaCO_3$/t.
- The average neutralization potentials of the samples taken from the license areas were determined as 80.55 kg $CaCO_3$/t.

In this study, the acid production potential and neutralization potential of the tailings area were determined by static tests that can be answered in a short time based on prediction. In the final evaluation of such fields; it is recommended to use leaching-based kinetic tests in which the field is simulated by monitoring the oxidation and degradation of samples subjected to water and oxygen over a longer period of time.

Sampling

Sampling procedures: 2 waste samples containing high sulfur were taken on 03.08.2021, taking into account the Static Test results. Approximately 50 kg samples were collected from the Research Pit dug at a depth of 8 meters with a diameter of 9 inches using the Rok -Bit Blow Hole Drilling Machine (9 inch diameter, 8 meter rod length), CEN_TR 15310-3_2006 Characterization. Bulk Sample Reduction from Waste Subsampling Standard was reduced according to Method 2 and taken as 20 kg. Sampling procedures and sample reduction processes carried out in the field are given in Figure 3. The samples were transferred to a 40 micron thick, 35x70 sized plastic nylon bag, a legibly written note describing the sample was placed inside the bag, and the mouth of the bag was closed with waterproof, strong adhesive tape. Explanatory information was noted on both sides of the bag with an indelible pen and the prepared sample bags were transported to the Laboratory. The physical properties of the samples are given in Table 3.

Table 3. *Information about the samples*

Simple Code	Sample Quantity	Colour	Homogeneity	Particle Type	Gas Output	Heat Production	Reaction Occurrence
CN-7	20 kg	Dark brown	Homogeneous	various type	NO	NO	NO
CN-25	20 kg	Dark brown	Homogeneous	Monotype	NO	NO	NO

Figure 3 *Sampling processes view*

Preparation of Field Samples for Laboratory Experiments

The samples collected as a result of field studies were made ready for analysis using appropriate techniques (Homogenization, Drying, Particle Size Reduction, Preparation of Subsamples) according to the TS EN 15002 "Waste Characterization - Preparation of test sample pieces from laboratory samples" standard. "standard. The samples were dried under atmospheric conditions (at room temperature) for 3

days to remove moisture. After the drying process, all samples were passed through a 6.3 mm (0.25 inch) sieve, and samples with a grain size larger than 15.2 cm were passed through crushers and gradually refined. For this purpose, it was first passed through the crusher set at 1.92 cm, then through the crusher set at 0.95 cm, and finally through the crusher set at 0.64 cm. After each crushing process, the samples were passed through a 6.3 mm sieve and the next stage was started. Since crushing processes cause the release of acid-producing and acid-consuming minerals, they may cause the characteristic features of the samples to deteriorate. This effect was taken into account in the analysis processes. Then the samples;

- Using a Sample Divider with a 2.54 cm slit, the sample was split into 8 1 kg test samples and stored in a ziplock bag. One of the test samples was loaded into the moisture cell for kinetic testing.
- One of the separated test samples was taken and crushed through a 1.7 mm (10 mesh) sieve to pass 95%, and then the sample was divided into 2 with a 6.35 mm slotted sample separator.
- These samples were ground to pass through a 150 μm (100 mesh) sieve and 250 grams of sample was taken for XRD analysis.

Minerological Tests of Samples

In order to determine the mineralogical characteristics of the geological units that create waste in the wastewater field and to detect the minerals that will create acidity through neutralization, PANalytical was conducted in Çanakkale. Analyzes were made with Empyrean brand XRD (X-Ray Diffraction) device. Onsekiz Mart University ÇOBİLTÜM - Science and Technology Application and Research Center. The mineralogy test results of the samples are given in Table 4, and the distribution according to mineral groups is given in Figure 4.

Table 4. *Minerological analysis results*

Mineral	**Formula**	**Group**	**CN-7**	**CN-25**
Pyrite	$Fe2_{S\_}$	Oxide Group	3.9%	3.5%
Cristobalite	$SiO2_{\_}$	Silicate Group	24.4%	27.8%
Montmorite	$2Al_2O_3.8SiO_2.2H_2OnH_2O$	Silicate Group	28.1%	29.7%
Quartz Low	$SiO2_{\_}$	Silicate Group	-	9.6%
İlitis	$K_{0.65}Al_{2.0}(Al_{0.65}Si_{3.35}O_{10})(OH)$	Silicate Group	-	19.0%
Zeolite	$(M^{+}, M^{+2})O.Al_2O_3.9SiO_2.nH_2O$	Silicate Group	1.0%	0.8%
Albite High	$NaAlSi_3O_8$	Silicate Group	42.5%	-
Plaster	$CaS04\ 2H_2O_{\_}$	Sulfate Group	-	1.6%
Aragonite	$(Ca, Sr, Pb, Zn)CO_3$	Carbonate Group	-	8.0%

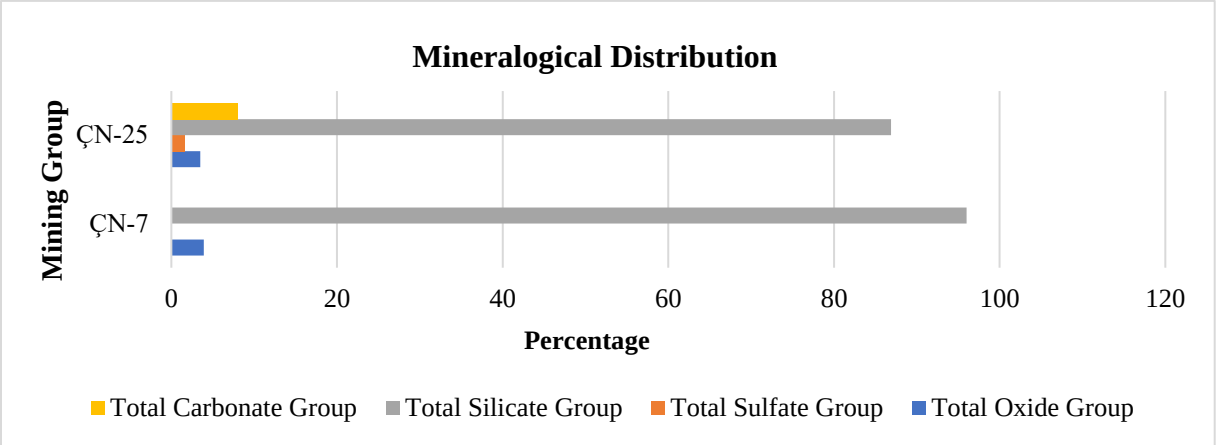

Figure 4. *Mineralogical distribution graph*

Kinetic Tests (Moisture Cell Test)

Kinetic tests are the next step up from static tests and are essentially simulation tests. They are performed to reduce uncertainties in static tests, verify the data obtained, identify decisive reactions, detect acid production rate and determine drainage water quality. In this technique, the field is simulated by monitoring the oxidation and degradation of samples over time as they are exposed to water and oxygen. Kinetic tests known in the literatüre are the “Moisture Cell” test, the “Column” test, the “Soxhclet” test. “Lkstıahnon” Test, “British Colombia These are tests such as the "Research " test. Considering that acid production in waste areas will develop over time, kinetic tests should be used when evaluating new and old mine areas and waste areas. Method for 2 samples with Acid Producing Potential to test AMD formation in the waste area. for Laboratory Kinetic Humidity Cell Test procedures were carried out in accordance with the " Weathering of Solid Materials Using a Humidity Cell" standard . pH, Acidity, Conductivity, Alkalinity, Acidity, Anion-Cation and Metal were determined by planning the moisture cell method in the wastewater collected weekly, every fifteen days or monthly. Parameters were analyzed. The samples to be loaded into the cells were 100% sieved or broken, and since their dimensions were 6.3 mm, cells with an inner diameter of 10.2 cm and a height of 20.3 cm were used. ASTM D5788-18 Standard Option A method was used for weekly cycles. According to this method, after the first leakage sample was taken from the cells, three days of dry air (relative humidity less than 10%) and three days of water-saturated air (relative humidity around 95%) were applied to the cells weekly. humidity). Approximately 2 L/min of dry air and moist air were supplied to the cells during all weekly cycles (Figure 5).

Figure 5. *Kinetic test setup view*

Grain Size Distributions in the Moisture Cell

The particle size distribution of the samples loaded into the moisture cell is given in Figure 6.

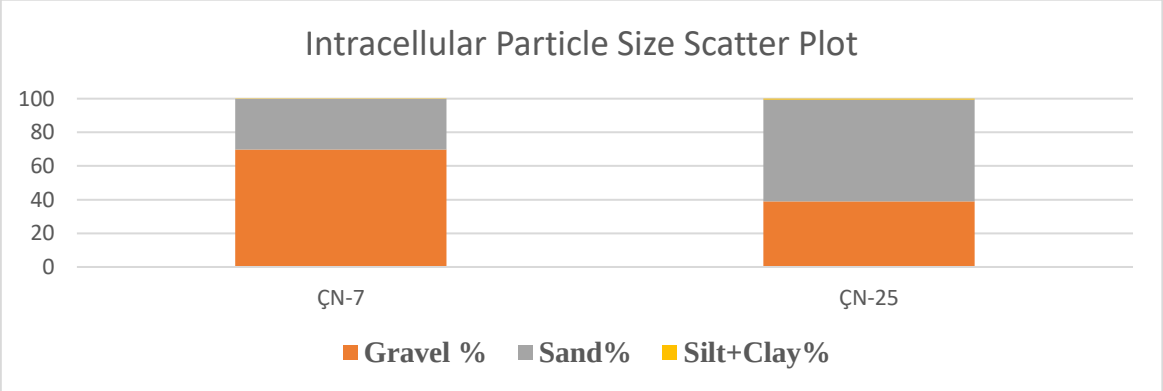

Figure 6. *Intra-cellular particle distribution plot*

Fixing the First Leak

The first water leaching is flood leaching. Week 0 leaching started with the first addition of water. This determines the initial characteristics of the leak. Moisture cell testing consists of a 7-day cycle. The sample was always filtered on the same day of the week (Monday). 1 L of water was added using a measuring tape and this amount could be 500 ml depending on the type of sample. During the water addition process, air inlets and water inlets were closed and water was added from the sides of the cell walls. After the filtration process was completed, the upper lids were closed and the filtration process was left overnight. When the filtration process was completed, the weights of each cell and collection containers were weighed and recorded. The pH and conductivity values of the collected leachate were measured, the collected sample volume was recorded and analyzed as Week 0 Sample. Then, to complete the weekly cycle, the air inlets of the cells were opened again and the operations were started.

Next Weekly Leachate

On the 7th day of the first weekly cycle, the second water was added and filtered and called the 1st week sample. The same procedures were carried out in subsequent weekly cycles.

Leachate Analysis

Priority pH, Dissolved Oxygen and Conductivity parameters of the leachate collected from moisture cells were measured and recorded. Then, filtration was performed using a filter with a pore diameter of 0.45 μm, and the solids remaining in the filter were taken back into the moisture cell. Leachate pH, alkalinity, acidity and conductivity analyzes is 20 weeks. These analyzes should be performed at weeks 0, 1, 2, 4, 6, 8, 10, 12, 14, 16, 18 and 20 of the test. There is no need to analyze weekly samples for chemical characterization; Instead, analysis at minimum 0, 1, 2, 4, 6, 8, 12, 16 and 20 weeks is sufficient. Analyzes were carried out for 20 weeks and the results were interpreted.

Discussion and Conclusion

The obtained measurement and analysis results were interpreted with reference to the PD CEN TR 16363-2012 "Characterization of wastes, kinetic testing for evaluation of acid production potential of sulfuric wastes originating from mining industries" standard.

Evaluation of Minerological Analyzes

While Oxide and Sulphate Group minerals, which may have acidic properties, were found in small amounts in the samples, Silicate and Carbonate Group minerals with Neutralization Potential were predominantly detected. When minerals with neutralization potential were examined, it was determined that silicates, which have lower neutralization capacity than carbonates, were predominantly present. In the mineralogical description of the samples, gypsum and pyrite minerals were determined as the main sulfur sources. Gypsum sulphate sulfur; Pyrite disulfide contains sulfur. Gypsum is known to have moderate solubility in water (4). Pyrite represents the presence of sulfur that has not yet undergone oxidation. Plaster does not have an increasing or decreasing effect on acidity (6). When pyrite undergoes hydrolysis and oxidation, it releases protons into water and increases the acidity of the environment.

Leachate Analysis

The results of the leachate analyzes performed to determine the quality of the drainage water of the waste samples loaded into the moisture cells are given in Table 5 and Table 6, and the following findings were obtained according to the analysis results.

Table 5. *Physical analysis results*

pH												
Example	**0.**	**one.**	**2.**	**4.**	**6.**	**8.**	**10.**	**12.**	**14.**	**16.**	**18.**	**20.**
CN-7	7.14	7.31	7.60	7.23	7.50	7.75	7.47	7.33	7.17	7.50	7,10	6.92
CN-25	7.11	7.51	7.54	7.34	7.45	7.78	7.50	7.40	7.45	7.70	7.27	7.27
CONDUCTIVITY µS/cm												
CN-7	3460	1260	956	709	516	1662	665	636	542	662	713	747
CN-25	7730	2770	2044	1610	1475	1159	933	783	539	538	556	584
ALKALINITY mg ($CaCO_3$)/L												
CN-7	48.2	46.8	52.6	38.0	41.6	64.0	29.6	26.6	36.0	37.4	54.8	58.2
CN-25	109.4	112.2	103.2	93.6	92.8	89.6	83.6	98.8	81.0	66.0	65.0	91.2

Table 6. *Chemical analysis results*

SULFATE mg									
Example	**0.**	**one.**	**2.**	**4.**	**6.**	**8.**	**12.**	**16.**	**20.**
CN-7	1197.0	394.2	304.6	87.5	176.8	661.1	226.5	283.0	285.5
CN-25	1596.0	906.3	716.6	639.3	640.8	467.7	297.4	200.2	194.7
CADMINIUM (Cd) mg									
CN-7	<LOQ	<LOQ	<LOQ	<LOQ	<LOQ	<LOQ	<LOQ	<LOQ	<LOQ
CN-25	<LOQ	<LOQ	<LOQ	<LOQ	<LOQ	<LOQ	<LOQ	<LOQ	<LOQ
ZINC (Zn) mg									
CN-7	0.016	<LOQ	<LOQ	0.017	<LOQ	<LOQ	<LOQ	0.014	0.006
CN-25	0.015	<LOQ	<LOQ	0.015	<LOQ	<LOQ	<LOQ	0.014	<LOQ
IRON (Fe) mg									
CN-7	0.246	<LOQ	<LOQ	0.016	0.076	<LOQ	<LOQ	0.081	0.188
CN-25	<LOQ	<LOQ	<LOQ	<LOQ	<LOQ	<LOQ	<LOQ	<LOQ	<LOQ
MAGNESIUM (Mg) mg									
CN-7	12.66	4.62	3.85	3.97	2.48	6.30	2.04	4.57	4.54
CN-25	39.37	10,18	9.55	9.62	10.87	9.40	6.87	5.90	5.26
SODIUM (Na) mg									
CN-7	417.56	142.25	124.96	70.63	56.37	165.43	90.79	88.90	85.82
CN-25	823.39	317.18	224.70	107.63	98.37	67.31	41.19	27.66	22.11
Potassium (K) mg									
CN-7	14.08	4.02	3.02	2.77	2.17	4.41	2.05	2.25	2.51
CN-25	28.62	11.06	8.86	6.22	6.86	3.01	2.46	1.36	1.09
CALCIUM (Ca) mg									
CN-7	93.33	32.66	29.74	13.78	54.78	71.69	14.49	32.11	30.95
CN-25	182.86	65.76	81.36	57.88	134.01	109.58	77.28	70.04	61.97
FLUORIDE (F) mg									
CN-7	0.41	<LOQ	0.39	0.71	0.13	0.59	0.60	0.39	0.47
CN-25	0.81	0.48	0.79	0.42	0.62	0.62	0.32	0.55	0.37
CHLORIDE (Cl) mg									
CN-7	3.81	5.85	16.96	10.29	6.87	12.96	9.54	10.44	8.29
CN-25	25.10	5.11	13.82	10.47	8.71	11.21	5.34	9.97	7.29

*LOQ = Measurement Detection Limits

pH

pH values vary between 6.92 and 7.78. pH values increased until the 8th week and started to decrease between the 8th and 20th weeks. The pH value in the MP-7 code sample, which does not contain carbonate minerals with high neutralization potential in its structure, is lower than the MP-25 code sample, which contains carbonate minerals.

Alkalinity

When the alkalinity results are examined, it is seen that the results of the sample coded CN-25, which contains carbonate minerals in its structure, are higher than the results of the CN-7 sample, which consists mostly of silicates.

Sulfate

Considering the sulfate concentrations, the sample coded CN-25, which contains the sulfate group gypsum mineral in its structure, decreased from 1.596.0 mg to 194.7 mg after 20 weeks. It was observed that the CN-7 sample, which does not contain sulfate group minerals, released a maximum of 1.197.0 mg sulfate.

Conductivity

It was observed that the conductivity results of the CN-25 coded sample containing carbonate minerals were higher than the CN-7 coded sample containing predominantly silicate groups and gradually decreased in weekly analyses.

Ficklin Metal Values

Ficklin metal value was calculated in two samples by considering the sum of Cd, Co, Cu, Zn, Pb and Ni elements mobilized under low pH conditions of filtered waters. According to the relationship between Ficklin metal and pH, the waste samples were characterized by low metal release, as the Ficklin metal value was below 1000 µg/L under neutral conditions.

Leakage Rate and Hydraulic Structure of the Material

The amount of element leached per unit mass and time is called leaching rate. Hydraulic Structure describes the general character of a rock as shown in terms of grain size and shape, degree of crystallinity and arrangement of the particles that compose it. This structure has an impact not only on the "hydraulic conditions" (including air intake), but also on the weathering and sensitivity to weather conditions and the formation/release conditions of the components. The texture and hydraulic properties of the material are important factors that determine contact with water and air in the kinetic test cell. At the site scale, the (physical) heterogeneity of the waste area will lead to nonuniform flow fields (preferential flow paths) that have an impact on the contact between water, air and waste and the transport of

decomposition products. While calculating the leakage rates of the samples, it was calculated that the leakage rate of the sample coded CN-25 was higher than that of CN-7.

Evaluating Whether the Material Is Acidic

When the pH values of the samples are examined, no acid formation is observed in either sample during the 20-week period. In addition to sulfate emissions, there are also easily soluble neutralizing minerals that create alkalinity and cause the consumption of hydrogen ions produced.

Defining the Acid Consuming Reaction Rate

Identification of acid-consuming reactions can be done using Humidity cell tests in response to the rate of acid production in a system where sulfur oxidation is stopped by water saturation and the flow through a batch reactor or reactor. Since minerals that rapidly consume acid will be calcium carbonate minerals, calcium and magnesium values in the leachate will give indicators of acid-consuming minerals. Silicate minerals (especially calcium-rich plagioclase and mafic minerals) also have the potential to consume acid. When the 20-week leachate results are examined, it is seen that the rapidly acid-consuming Ca+Mg values of the CN-7 coded sample are 418.6 mg, and the CN-25 coded sample is 947.8 mg. These results support the results obtained in mineralogical tests.

Predicting When Material Will Become Acidic

Calculating the Neutralization Potential exhaustion time and Acid Potential exhaustion time can be used when assessing when the material will become acidic. It can be said that the materials will not produce acid if the neutralization potential consumption is longer than the acid potential. For this calculation, the sulfate production rates of the samples, that is, the total acidity produced, are important. Accordingly, in the example coded CN-7, it is estimated that the NP consumption period will be 5.03 years later and the AP consumption period will be 2.61 years later. In the example coded CN25, the NP consumption period will be 17.27 years and the AP consumption period will be 11.71 years later. Since AP will be consumed before NP, it is predicted that the two waste samples will not produce acid in the long term.

Acknowledgement-

Funding/Financial Disclosure This study was supported by Çanakkale Onsekiz Mart University Scientific Research Projects Coordination Unit (Project number: FYL-2021-3778).

Ethics Committee Approval and Permissions The study does not require ethics committee approval or any special permission.

Conflicts of Interest The authors declare no conflict of interest.

Authors Contribution All authors read and approved the final manuscript.

References

[1] Saglam, E. S., & Akçay, M. (2016). Chemical and mineralogical changes of waste and tailings from the Murgul Cu deposit (Artvin, NE Turkey): implications for occurrence of acid mine drainage. *Environmental Science and Pollution Research, 23,* 6584–6607. https://doi.org/10.1007/s11356-015-5835-2

[2] Paktunc, A. D., & Davé, N. K. (2002). Formation of secondary pyrite and carbonate minerals in the Lower Williams Lake tailings basin, Elliot Lake, Ontario, Canada. *American Mineralogist, 87*(5-6), 593-602. https://doi.org/10.2138/am-2002-5-601

[3] Masindi, V., & Muedi, K. L. (2018). Environmental contamination by heavy metals In El-Din, H., Saleh, M., Aglan, R. F. (Eds), *Heavy Metals*, IntechOpen. https://books.google.com.tr/books?hl=tr&lr=&id=dnuQDwAAQBAJ&oi=fnd&pg=PA115&dq=Masindi,+Vhahangwele,+and+Khathutshelo+L.+Muedi+.+%22+Environmental+contamination+by+heavy+heavy+metals%E2%80%9D+(2018):+115-132.&ots=UYnqVocWjR&sig=VL9B56igQ7jObrbB2sYDAzXlKS8&redir_esc=y#v=onepage&q&f=false

[4] Hogsden, K. L., & Harding, J. S. (2012). Consequences of acid mine drainage for the structure and function of benthic stream communities: a review. *Freshwater Science*, *31*(1), 108-120.

[5] Masindi, V., & Tekere, M. (2020). Innovative routes for acid mine drainage (AMD) valorization: advocating for a circular economy. In Fosso-Kankeu, E., Wolkerdorfer, C., Burgess, J. (Eds), *Recovery of Byproducts from Acid Mine Drainage Treatment*, Wiley. (pp. 189-218). https://onlinelibrary.wiley.com/doi/abs/10.1002/9781119620204.ch7

[6] Graham, S., Liu, X., Bartlett, B., Ng, C., Harris, K. R., Aitken, A., Barkel, A., Kavanaugh, C., & Talukdar, J. (2018). Reading for writing: A meta-analysis of the impact of reading interventions on writing. *Review of Educational Research*, *88*(2), 243-284. https://doi.org/10.3102/0034654317746927

[7] Zhao, M. M., Chen, Y. P., Xue, L. G., & Fan, T. T. (2020). Three kinds of ammonia oxidizing microorganisms play an important role in ammonia nitrogen self-purification in the Yellow River. *Chemosphere, 243,* 125405. https://doi.org/10.1016/j.chemosphere.2019.125405

[8] Kefeni, K. K., Msagati, T. A., & Mamba, B. B. (2017). Acid mine drainage: Prevention, treatment options, and resource recovery: A review. *Journal of Cleaner Production, 151,* 475-493. https://doi.org/10.1016/j.jclepro.2017.03.082

[9] Akinwekomi, V., Maree, J. P., Masindi, V., Zvinowanda, C., Osman, M. S., Foteinis, S., Mpenyana-Monyatsi L., & Chatzisymeon, E. (2020). Beneficiation of acid mine drainage (AMD): A viable option for the synthesis of goethite, hematite, magnetite, and gypsum–Gearing towards a circular economy concept. *Minerals Engineering*, *148*, 106204. https://doi.org/10.1016/j.mineng.2020.106204

[10] Modis, K., & Komnitsas, K. (2007). Optimum sampling density for the prediction of acid mine drainage in an underground sulphide mine. *Mine Water and the Environment, 26*, 237-242. https://doi.org/10.1007/s10230-007-0014-4

[11] Geidel, G., Caruccio, F. T., Hornberger, R., & Brady, K. (2000). Guidelines and recommendations for use of kinetic tests for coal mining (AMD) prediction in the eastern US Chapter 5. *Prediction of Water Quality at Surface Coal Mines. National Mine Land Reclamation Center, West Virginia*

University, Morgantown, WV. https://wvwri.wvu.edu/files/d/f0ffc22a-db9b-417f-a895-c3e3dee97477/00-prediction-amd-handbook-kleinmann-2000.pdf

[12] Li, J., Wang, W., He, X., Shao, F., &, Bai, Y. (2023). Release characteristics of harmful trace elements during dynamic leaching and static ımmersion of coal gangue in Xinjiang, *ACS Omega, 9*(1), 393-400. https://doi.org/10.1021/acsomega.3c05736

[13] Nicholson, R. V. (1994). Iron-sulfide oxidation mechanisms: laboratory studies. *Environmental Geochemistry of Sulphide Mine-Wastes, 22*, 163-183.

[14] Simate, G. S., & Ndlovu, S. (2014). Acid mine drainage: challenges and opportunities. *Journal of Environmental Chemical Engineering, 2*(3), 1785-1803.

[15] Nordstrom, D. K., Blowes, D. W., & Ptacek, C. J. (2015). Hydrogeochemistry and microbiology of mine drainage: An update. *Applied Geochemistry*, *57*, 3-16. https://doi.org/10.1016/j.apgeochem.2015.02.008

[16] White, W. W., Lapakko, K. A., & Cox, R. L. (1997). Static-test methods most commonly used to predict acid-mine drainage: Practical guidelines for use and interpretation. In G.S. Plumlee, M.J. Logsdon, & L.F. Filipek (Eds.), *The Environmental Geochemistry of Mineral Deposits: Part A: Processes, Techniques, and Health Issues Part B: Case Studies and Research Topics*. Society of Economic Geologists, Inc. https://doi.org/10.5382/Rev.06.15

[17] Nleya, Y., Simate, G. S., & Ndlovu, S. (2016). Sustainability assessment of the recovery and utilisation of acid from acid mine drainage. *Journal of Cleaner Production*, *113*, 17-27. https://doi.org/10.1016/j.jclepro.2015.11.005

[18] Skousen, J., Rose, A., Geidel, G., Foreman, J., Evans, R., & Hellier, W. (1998). Handbook of technologies for avoidance and remediation of acid mine drainage. *National Mine Land Reclamation Center, Morgantown, 131*. https://wvwri.wvu.edu/files/d/c2e42b2b-e40d-4ada-8bad-3c264d867e76/99-handbook-avoidance-remediation.pdf

[19] Kuyucak, N. (2002). Acid mine drainage prevention and control options. *CIM Bulletin*, 96-102.

[20] Okay, A. I., Siyako, M., & Bürkan, K. A. (1991). Geology and tectonic evolution of the Biga Peninsula, northwest Turkey. *Bulletin of the Technical University of Istanbul, 44*(1-2), 191-256.

[21] Siyako, M., Bürkan, K. A., & Okay, A. I. (1989). Tertiary geology and hydrocarbon potential of the Biga and Gelibolu peninsulas. *Turkish Association of Petroleum Geologists Bulletin, 1*(3), 183-99.

[22] Ercan, T., Satır, M., Steınıtz, G., Dora, A., Sarıfakıoğlu, E., Adls, C., Walter, H. J., Yıldırım, T. (1995). Features of the tertiary volcanizm observed at Biga Peninsula and Gökçeada, Tavşan Islands. *Bulletin of the Mineral Research and Exploration, 117*(117), 40-41.

[23] Karaca, Ö., & Bozcu, M. (2019). Determination of tectonic and volcanic structures with the aid of lineaments: example from Çan-Etili (Canakkale) lignite basin. *Türkiye Jeoloji Bülteni, 62*(3), 247-262. https://doi.org/10.25288/tjb.570362

[24] Bozcu, M., Akgün, F., Gürdal, G., Bozcu, A., Yeşilyurt, S. K., Karaca, Ö., & Akkiraz, M. S. (2015). Evolution of Çan-Etili (Çanakkale-NW Turkey) lignite basin: Sedimentology, petrology, palynology and lignite characterization. *International Journal of Sediment Research, 30*(3), 190-207. https://doi.org/10.1016/j.ijsrc.2015.03.009

Sinopfbd, 2024; 9(1): 114-127 **https://doi.org/10.33484/sinopfbd.1411952**

Sinop Üniversitesi Fen Bilimleri Dergisi
Sinop Uni J Nat Sci
E-ISSN: 2564-7873

https://dergipark.org.tr/tr/pub/sinopfbd

A Study On A New Generalization of δ-Supplemented Modules

Emine ÖNAL KIR

How to cite: Önal Kır, E. (2024). A study on a new generalization of δ-supplemented modules. *Sinop Üniversitesi Fen Bilimleri Dergisi*, *9*(1), 114-127. https://doi.org/10.33484/sinopfbd.1411952

Research Article

Corresponding Author
Emine ÖNAL KIR
emine.onal@ahievran.edu.tr

ORCID of the Author
E.Ö.K: 0000-0002-3025-3290

Received: 29.12.2023
Accepted: 03.04.2024

Abstract

For any ring S and an S-module W, a submodule G of W is termed *co$_\delta$-coatomic* if the quotient module W/G is δ-coatomic. In this study, we introduce the term ($\oplus$-)*co$_\delta$-coatomically δ-supplemented module*, or shortly ($\oplus$-)*co$_\delta$-δ-supplemented module* to describe a module W where each co$_\delta$-coatomic submodule has a δ-supplement (that is a direct summand) in W. Furthermore, a module W is identified as *co$_\delta$-coatomically δ-semiperfect*, or shortly *co$_\delta$-δ-semiperfect*, provided each δ-coatomic quotient module of W has a projective δ-cover. It has been proved that over a δ-semiperfect ring S, the module ${}_SS$ is $\oplus_\delta$-co-coatomically supplemented if and only if ${}_SS$ is co$_\delta$-δ-semiperfect if and only if ${}_SS$ is $\oplus$-co$_\delta$-δ-supplemented.

Keywords: co$_\delta$-coatomic submodule, co$_\delta$-coatomically δ-supplemented module, $\oplus$-co$_\delta$-coatomically δ-supplemented module, co$_\delta$-coatomically δ-semiperfect module

δ-Tümlenmiş Modüllerin Yeni Bir Genelleştirilişi Üzerine Bir Çalışma

Ahi Evran University, Department of Mathematics, Kırşehir, Türkiye

Öz

Herhangi bir S halkası ve bir W S-modülü için, W modülünün bir G alt modülü, eğer W/G bölüm modülü δ-eşatom ise *eş$_\delta$-eşatom* olarak adlandırılır. Bu çalışmada, ($\oplus$-)*eş$_\delta$-eşatom δ-tümlenmiş modül*, veya kısaca ($\oplus$-)*eş$_\delta$-δ-tümlenmiş modül* terimini her eş$_\delta$-eşatom alt modülü (direkt toplam terimi olan) bir δ-tümleyene sahip olan bir W modülünü belirtmek için tanıtıyoruz. Ayrıca, W modülü, eğer her bir δ-eşatom bölüm modülü, projektif bir δ-örtüye sahipse *eş$_\delta$-eşatom δ-yarı mükemmel* veya kısaca *eş$_\delta$-δ-yarı mükemmel* olarak tanımlanır. Bir δ-yarı mükemmel S halkası üzerinde, ${}_SS$ modülünün $\oplus_\delta$-eş-eşatom tümlenmiş olmasının ${}_SS$ modülünün eş$_\delta$-δ-yarı mükemmel olmasına ve ${}_SS$ modülünün $\oplus$-eş$_\delta$-δ-tümlenmiş olmasına denk olduğu kanıtlanmıştır.

Anahtar Kelimeler: eş$_\delta$-eşatom alt modül, eş$_\delta$-eşatom δ-tümlenmiş modül, $\oplus$-eş$_\delta$-eşatom δ-tümlenmiş modül, eş$_\delta$-eşatom δ-yarı mükemmel modül

Introduction

All along the current manuscript, we regard that whole rings are associative having identity element and whole modules are unital left S-modules. Let S be a ring of such nature and W be a module falling into this category. The impressions $G \leq W$ and $G \leq_{\oplus} W$ signify that G functions as a submodule of W and G functions as a direct summand of W, respectively. Referring to a submodule G of W as *small* in W, denoted as $G \ll W$, implies that $W \neq G + L$ for each proper submodule L of W. The symbol $Rad(W)$ represents the intersection of whole maximal submodules of W or, equivalently, the sum of whole small submodules of W. Dually, a submodule G of W is classified as *essential* in W, denoted by $G \trianglelefteq W$, provided $G \cap H \neq 0$ where $0 \neq H \leq W$. A module W is termed *singular* if $W \cong W'/G$ for some module W' and $G \trianglelefteq W'$. The notion of a *projective cover* for a module W refers to a pair comprising a module P and a homomorphism $h : P \to W$, where P is projective, and h is an epimorphism with $Ker(h) \ll P$ (refer to [1]). A module W is termed *coatomic* if each proper submodule is included in a maximal submodule of W (see [2]). Examples of coatomic modules encompass finitely generated, semisimple, and local modules. Initially introduced by Alizade and Güngör in [3] the concept of co-coatomic submodules is articulated as follows. A submodule G of W is denoted as *co-coatomic* when the quotient module W/G is coatomic.

As a particular instance derived from the concept of coatomic modules, the notion of δ-coatomic modules is described in [4]. A module W is characterized as *δ-coatomic* provided, each submodule which is different from W of W is encompassed within a maximal submodule H of W where W/H is singular (refer to [4, Lemma 2.1]). In the context of [4], a ring S is denoted as *left (right) δ-coatomic* if the left (right) S-module ${}_SS$ (S_S) is δ-coatomic.

The subsequent proposition is a consequence of [4, Proposition 2.5], and we will invoke it consistently in the course of this paper.

Proposition 1. Suppose that $0 \to G \to W \to L \to 0$ is an exact sequence consisting of modules.

1. When W is δ-coatomic, L is δ-coatomic.
2. When G and L are δ-coatomic, W is δ-coatomic.

In particular, for any δ-coatomic module W, $G \leq_{\oplus} W$ is δ-coatomic.

Consider submodules G and H of a module W. The term *supplement* is attributed to H in relation to G within W if H is minimal while satisfying $W = G + H$. It is a well-established fact that H serves as a supplement of G in W if and only if $W = G + H$ and $G \cap H \ll H$. A module W is said to be a *supplemented module* provided each submodule of W possesses a supplement in W. Examples of supplemented modules include semisimple modules and hollow modules (refer to [1, Section 41]). In [3], W is termed *co-coatomically supplemented module* when each co-coatomic submodule of W possesses a supplement in W.

In [5], the authors put forth the concept that W is denoted as *$\oplus$-co-coatomically supplemented module* provided any co-coatomic submodule possesses a supplement G with $G \leq_{\oplus} W$. Furthermore, in the same paper, W is characterized as *co-coatomically semiperfect module* provided any coatomic quotient module of W admits a projective cover.

Zhou described the concept of δ-small submodules, a generalization of small submodules that play a pivotal role in the framework of supplemented modules, as presented in [6]. For a submodule $G \leq W$, G is designated as δ-small in W and is denoted by $G \ll_\delta W$ if $W \neq G + H$ holds for each proper submodule H of W where W/H is singular. In accordance with the notation in [6, Lemma 1.5], $\delta(W)$ signifies the sum of whole δ-small submodules of W.

We compile the fundamental features of submodules which are δ-small in the subsequent lemma, sourced from [6, Lemma 1.2 and 1.3].

Lemma 1. Suppose that W is a module.

1. For any submodule G of W, $G \ll_\delta W$ if and only if whenever $W = X + G$ there is a semisimple projective submodule G' of G with $X \oplus G' = W$.
2. When $G \ll_\delta W$ and $h : W \to L$ is a homomorphism, then $h(G) \ll_\delta L$. In particular, $G \ll_\delta W \leq L$, then $G \ll_\delta L$.
3. When $G_1 \ll_\delta H_1 \leq W$ and $G_2 \ll_\delta H_2 \leq W$, $G_1 + G_2 \ll_\delta H_1 + H_2$.
4. When $W = \bigoplus_{\lambda\in\Lambda} W_\lambda$, $\delta(W) = \bigoplus_{\lambda\in\Lambda} \delta(W_\lambda)$.
5. When $G \leq H \leq W$, $G \ll_\delta W$ and $H \leq_\oplus W$, $G \ll_\delta H$.

In [7], a module W is defined as δ-*supplemented* provided any submodule G of W possesses a δ-supplement H in W, characterized by $W = G + H$ and $G \cap H \ll_\delta H$. For more comprehensive details and characterizations of δ-supplemented modules, additional information can be found in [8] and [7].

In [9], a module W is referred to as *co-coatomically δ-supplemented* ($\oplus_\delta$*-co-coatomically supplemented*) provided any co-coatomic submodule of W possesses a δ-supplement G with $G \leq_\oplus W$. In the same paper, a module W is identified as *co-coatomically δ-semiperfect* provided any co-coatomic quotient module of W possesses a projective δ-cover. The authors thoroughly examined the structure of these modules in the same paper and provided new characterizations of rings based on these modules.

In this note, we introduce a special case of co-coatomic submodules. Let G be a submodule of a module W. We designate G as a *co$_\delta$-coatomic submodule* of W if the quotient module W/G is δ-coatomic. It is evident that δ-coatomic modules are coatomic. Consequently, each submodule which is co$_\delta$-coatomic of a module is also co-coatomic. According to [4, Corollary 2.9], since each semisimple singular module is δ-coatomic, it follows that each submodule of semisimple singular modules is co$_\delta$-coatomic.

In the other part of this paper, we delve into the introduction and examination of the concept of co$_\delta$-coatomically δ-supplemented modules, shortly co$_\delta$-δ-supplemented modules, and $\oplus$-co$_\delta$-coatomically δ-supplemented modules, shortly $\oplus$-co$_\delta$-δ-supplemented modules, as notions stronger than the previously defined co-coatomically δ-supplemented modules and $\oplus_\delta$-co-coatomically supplemented modules. We commence by presenting an example of a module that is co$_\delta$-δ-supplemented but not δ-supplemented. It is demonstrated that the class of co$_\delta$-δ-supplemented modules is closed under quotient modules and finite sums. We establish that a ring S is left δ-coatomic if and only if each simple S-module is singular, and this equivalence extends to the statement that each coatomic S-module is δ-coatomic. Consequently, it is deduced that over left δ-coatomic rings, co-coatomically δ-supplemented modules and co$_\delta$-δ-supplemented modules coincide. Additionally, an example is provided of a ring S over which

each co$_\delta$-δ-supplemented S-module is co-coatomically δ-supplemented. It is established that the quotient module of a $\oplus$-co$_\delta$-δ-supplemented module by a fully invariant submodule is also $\oplus$-co$_\delta$-δ-supplemented. Consequently, it is proven that for a $\oplus$-co$_\delta$-δ-supplemented module W, the quotient module $W/\delta(W)$ is $\oplus$-co$_\delta$-δ-supplemented. Moreover, it is shown that the class of $\oplus$-co$_\delta$-δ-supplemented modules is closed under finite direct sums.

In the last part of this article, we introduce the definitions of co$_\delta$-coatomically δ-semiperfect modules, shortly co$_\delta$-δ-semiperfect modules, as a generalization of co-coatomically δ-semiperfect modules. It is demonstrated that for a projective module W, W is co$_\delta$-δ-semiperfect if and only if W is $\oplus$-co$_\delta$-δ-supplemented. It is established that the class of co$_\delta$-δ-semiperfect modules is closed under quotient modules and δ-covers. Furthermore, it is shown that the finite direct sum of projective co$_\delta$-δ-semiperfect modules is co$_\delta$-δ-semiperfect if and only if each direct summand is co$_\delta$-δ-semiperfect. Additionally, it is proven that for a δ-semiperfect ring S, ${}_SS$ is $\oplus_\delta$-co-coatomically supplemented if and only if ${}_SS$ is co$_\delta$-δ-semiperfect if and only if ${}_SS$ is $\oplus$-co$_\delta$-δ-supplemented.

Co$_\delta$-Coatomically δ-Supplemented Modules

Definition 1. We term a module W *co$_\delta$-coatomically δ-supplemented, shortly co$_\delta$-δ-supplemented* provided each co$_\delta$-coatomic submodule of W possesses a δ-supplement in W.W is named *$\oplus$-co$_\delta$-coatomically δ-supplemented, shortly $\oplus$-co$_\delta$-δ-supplemented* provided each co$_\delta$-coatomic submodule of W has a δ-supplement G with $G \leq_\oplus W$.

It is evident that co-coatomically δ-supplemented modules are co$_\delta$-δ-supplemented, as co$_\delta$-coatomic submodules are co-coatomic. In the subsequent discussion, we will provide an example of a ring for which co$_\delta$-δ-supplemented modules are co-coatomically δ-supplemented. It is apparent that modules which are δ-supplemented are also co$_\delta$-δ-supplemented. However, the example which will be given next illustrates that a co$_\delta$-δ-supplemented module does not necessarily need to be δ-supplemented.

Example 1. Let's consider the $\mathbb{Z}$-module $\mathbb{Q}$. Given that $\mathbb{Q}$ has only $\mathbb{Q}$ as a co$_\delta$-coatomic submodule, $\mathbb{Q}$ qualifies as a co$_\delta$-δ-supplemented module. However, it's important to note that $\mathbb{Q}$ is not a δ-supplemented module.

Proposition 2. Suppose that W is a δ-coatomic module. In that case, W is co$_\delta$-δ-supplemented if and only if W is δ-supplemented.

Proof. The sufficiency is evident. To prove the necessity, let G be any submodule of W. Since W is δ-coatomic, then W/G is δ-coatomic by Proposition 1. Thus G has a δ-supplement in W, by the assumption. Hence W is δ-supplemented.

Corollary 1. Suppose that W is a semisimple singular module. Then W is co$_\delta$-δ-supplemented if and only if W is δ-supplemented.

Proof. Note that by [4, Corollary 2.9], W is δ-coatomic. Thus the result is derived from Proposition 2.

Corollary 2. For a module W, assume that $\delta(W) \ll_\delta W$ and W satisfies either

1. $W/\delta(W)$ is semisimple, or

2. For each submodule G of W, there exists a submodule H of W such that $W = G + H$ and $G \cap H \ll_\delta W$.

Then W being co$_\delta$-δ-supplemented is equivalent to being δ-supplemented.

Proof. W is δ-coatomic module by [4, Theorem 2.2]. Thus the result is supported by Proposition 2.

Proposition 3. Co$_\delta$-δ-supplemented modules exhibit transfer properties through their quotient modules.

Proof. Suppose that W is a co$_\delta$-δ-supplemented module and $G \leq W$. Then any co$_\delta$-coatomic submodule of W/G is a submodule of the form L/G where L is co$_\delta$-coatomic submodule of W. By the hypothesis, L has a δ-supplement in W, say X. According to [8, Proposition 2.3], we achieve that
$(X + G)/G$ is a δ-supplement of L/G in W/G.

Corollary 3. The property of being co$_\delta$-δ-supplemented module is transferred by direct summands.

Proposition 4. Suppose that W is a co$_\delta$-δ-supplemented module. In that case, each co$_\delta$-coatomic submodule of the module $W/\delta(W)$ is a direct summand.

Proof. Suppose that $G/\delta(W)$ is a co$_\delta$-coatomic submodule of $W/\delta(W)$. Then G is co$_\delta$-coatomic submodule of W. By the hypothesis, there exists a submodule H of W such that $W = G + H$ and $G \cap H \ll_\delta H$. Note that $G \cap H \leq \delta(W)$. Thus
$W/\delta(W) = G/\delta(W) + (H + \delta(W))/\delta(W)$,
$(G/\delta(W)) \cap ((H + \delta(W))/\delta(W)) = ((G \cap H) + \delta(W))/\delta(W) = 0$.
Hence $W/\delta(W) = (G/\delta(W)) \oplus (H + \delta(W))/\delta(W)$.

Corollary 4. Suppose that W is a co$_\delta$-δ-supplemented module. In that case, $W/\delta(W)$ is $\oplus$-co$_\delta$-δ-supplemented.

Next, we aim demonstrating that the sum of a finite number of co$_\delta$-δ-supplemented modules becomes a co$_\delta$-δ-supplemented module. To begin with, we establish the following lemma as a preliminary step.

Lemma 2. Suppose that W is a module and $G, H \leq W$. Assume that G is co$_\delta$-coatomic, H is co$_\delta$-δ-supplemented and $G + H$ possesses a δ-supplement in W. Then G possesses a δ-supplement in W.

Proof. Let X be a δ-supplement of $G + H$ in W. Note that
$H/(H \cap (G + X)) \cong (G + H + X)/(G + X) = W/(G + X)$
is δ-coatomic as a quotient module of the δ-coatomic module W/G. Thus there exists a submodule H' of H such that
$H = H' + (H \cap (G + X))$ and $H' \cap (H \cap (G + X)) = H' \cap (G + X) \ll_\delta H'$. Therefore we have $W = G + H + X = G + (H' + H \cap (G + X)) + X = G + H' + X$ and $G \cap (H' + X) \leq H' \cap (G + X) + X \cap (G + H') \leq H' \cap (G + X) + X \cap (G + H) \ll_\delta H' + X$. Hence $H' + X$ is a δ-supplement of G in W.

Theorem 1. A finite sum of co$_\delta$-δ-supplemented modules remains co$_\delta$-δ-supplemented.

Proof. It is sufficient to prove that the sum, say W, of co$_\delta$-δ-supplemented modules W_1 and W_2 is co$_\delta$-δ-supplemented. For this, assume that G is a co$_\delta$-coatomic submodule of W. Then $W = W_1 + W_2 + G$. Note that $(W/G)/((W_2 + G)/G) \cong W/(W_2 + G)$ is δ-coatomic. Since $W_2 + G$ is co$_\delta$-coatomic submodule of W and W_1 is co$_\delta$-δ-supplemented, then $W_2 + G$ has a δ-supplement in W by Lemma 2. By using Lemma 2 once more again, we conclude that G has a δ-supplement in W because W_2 is co$_\delta$-δ-supplemented module and G is a co$_\delta$-coatomic submodule of W. Hence W is co$_\delta$-δ-supplemented.
Consider modules W and L. L is designated as *finitely W-generated* in case there exists an epimorphism $f : W^{(\Lambda)} \to L$ where Λ is a finite set.
The subsequent corollary naturally follows from Proposition 3 and Theorem 1.

Corollary 5. In case W is co$_\delta$-δ-supplemented module, then any finitely W-generated module is a co$_\delta$-δ-supplemented module.

Theorem 2. Let G be a co$_\delta$-δ-supplemented submodule of a module W such that W/G has no maximal submodule. Then W is a co$_\delta$-δ-supplemented module.

Proof. Let L be a co$_\delta$-coatomic submodule of W. Then $W/(G + L)$ is δ-coatomic as a quotient module of the δ-coatomic module W/L . Thus $W/(G+L)$ is coatomic. Since W/G has no maximal submodule, $W/(G + L)$ also has no maximal submodule. Thus $W = G + L$. By Lemma 2, L has a δ-supplement in W. Hence W is co$_\delta$-δ-supplemented module.

Corollary 6. Suppose that W is a module and $W/Soc(W)$ has no maximal submodule. Then W is co$_\delta$-δ-supplemented module.

As a reminder from [10], a module W is termed *δ-local* in case $\delta(W) \ll_\delta W$ and the submodule $\delta(W)$ is maximal in W.

Proposition 5. Let W be a co$_\delta$-δ-supplemented module. If W contains a maximal submodule H with singular W/H, then W contains a δ-local or projective semisimple submodule.

Proof. Assume that W is a co$_\delta$-δ-supplemented module and H is a maximal submodule of W such that W/H is singular. Then H is co$_\delta$-coatomic submodule of W. By the assumption, there exists a submodule X of W such that $W = H + X$ and $H \cap X \ll_\delta X$. Therefore, X is δ-local or semisimple projective by [11, Lemma 2.22].

Lemma 3. Suppose that W is a module and H is a maximal submodule that contains whole semisimple singular submodules of W. If W/H is singular and X is a δ-supplement of H in W, then X is δ-local.

Proof. By the hypothesis, $W = H + X$ and $H \cap X \ll_\delta X$. Assume that $H \cap X$ is not an essential submodule of X. Then there exists a submodule X' of X such that $(H \cap X) \cap X' = 0$, and so $X = (H \cap X) \oplus X'$. Thus $X' \cong X/(H \cap X) \cong W/H$ is simple singular, by the assumption. Also we get $W = H + X = H + (H \cap X) \oplus X' = H + X'$. It leads to the conclusion that H does not contain X'. This contradicts with the hypothesis. Hence $H \cap X$ is an essential submodule of X, and so $\delta(X) \leq H \cap X$. Hence $\delta(X) = H \cap X$.

Proposition 6. The expressions below are equivalent for a δ-coatomic module W:

1. W is co$_\delta$-δ-supplemented.

2. Each maximal submodule H of W with singular W/H has a δ-supplement in W.

3. $W = W_1 + W_2 + ... + W_n$ where each W_λ is either simple or δ-local.

Proof. When W is semisimple singular, then these stated equivalences above are evidently valid. So, we posit that W is not semisimple singular.
$(1) \Longrightarrow (2)$ It is evident.
$(2) \Longrightarrow (3)$ Let X be the sum of whole submodules which are δ-supplement of maximal submodules H of W with singular W/H and $Soc(W) \leq H$. Then by Lemma 3, X is a sum of δ-local submodules of W. Now assume that $W \neq Soc(W) + X$. Since W is δ-coatomic module, then there is a maximal submodule G of W such that $Soc(W) + X \leq G$ and W/G is singular. By the hypothesis, G possesses a δ-supplement Y in W. Therefore, $Y \leq X \leq G$ and $G = W$, but this is a contradiction. Hence, $W = Soc(W) + X$ and the result holds.
$(3) \Longrightarrow (1)$ It is supported by [10, Lemma 3.3] that δ-local modules are δ-supplemented, and so co$_\delta$-δ-supplemented. Moreover, it is evident that simple modules are co$_\delta$-δ-supplemented. Hence W is co$_\delta$-δ-supplemented as a finite sum of co$_\delta$-δ-supplemented modules by Theorem 1.

Corollary 7. Suppose that W is a δ-coatomic module. In case W is δ-supplemented, $W = W_1 + W_2 + ... + W_n$ where each W_λ is either simple or δ-local.

Proposition 7. Suppose that S is a ring. The expressions below are equivalent:

1. S is a left δ-coatomic ring.

2. Each simple S-module is singular.

3. Each coatomic S-module is δ-coatomic.

Proof. $(1) \Longrightarrow (2)$ It is supported by [4, Theorem 2.18].
$(2) \Longrightarrow (3)$ Let W be a coatomic module. Then each submodule which is proper of W is included in a maximal submodule G. By the assumption, W/G is singular. Thus we conclude that each submodule which is proper of W is included in a maximal submodule G where W/G is singular. This means that W is δ-coatomic.
$(3) \Longrightarrow (1)$ By (3), the module ${}_SS$ is δ-coatomic. Hence S is a left δ-coatomic ring.

Corollary 8. Suppose that S is a δ-coatomic ring and W is an S-module. In that case, the expressions below are equivalent:

1. W is co-coatomically δ-supplemented.

2. W is co$_\delta$-δ-supplemented.

Proof. $(1) \Longrightarrow (2)$ It is evident.
$(2) \Longrightarrow (1)$ Suppose that G is a co-coatomic submodule of W, that is, W/G is coatomic. Then W/G is δ-coatomic by Proposition 7, as S is a left δ-coatomic ring, by the assumption. Thus $G \leq W$ is co$_\delta$-coatomic. As W is co$_\delta$-δ-supplemented, G possesses a δ-supplement in W, as desired.

Heed the information derived from [6] that, concerning the modules P and W, an epimorphism $h : P \to W$ is denominated a δ-*cover* of W under the condition that $Ker(h) \ll_\delta P$. A δ-cover $h : P \to W$ is labeled as a *projective* δ-*cover* provided that P is a projective module. A ring S is characterized as δ-*semiperfect* in case each simple S-module possesses a projective δ-cover (refer to [6]).

Corollary 9. Suppose that S is a δ-semiperfect ring and W is an S-module. In that case, the expressions below are equivalent:

1. W is co-coatomically δ-supplemented.
2. W is co$_\delta$-δ-supplemented.

Proof. Since δ-semiperfect rings are left δ-coatomic by [4, Proposition 2.15], then the result is supported by Corollary 8.

Corollary 10. The expressions below are equivalent for a δ-semiperfect ring S:

1. ${}_SS$ is ($\oplus_\delta$-co-coatomically supplemented) co-coatomically δ-supplemented.
2. ${}_SS$ is ($\oplus$-co$_\delta$-δ-supplemented) co$_\delta$-δ-supplemented.

Presently, we provide an instance of a ring where each co$_\delta$-δ-supplemented S-module is simultaneously co-coatomically δ-supplemented.

Example 2. Suppose that S is an incomplete discrete valuation ring and Q denotes its field of fractions. Let p be the maximal ideal of S. Then p is essential in S. Hence the simple S-module S/p is singular. Hence each simple S-module is singular. So S has no simple projective S-modules. Also as stated in the [11, Example 2.2], δ-small submodules are small over the ring S. Therefore over this ring, modules which are co-coatomically δ-supplemented are co-coatomically supplemented, and also co$_\delta$-δ-supplemented modules are co-coatomically δ-supplemented by Proposition 7. Moreover, $Q \oplus Q$ is co$_\delta$-δ-supplemented as it is supplemented by [12, Theorem 2.2].

Consider a module W. A submodule G within W is denoted as *fully invariant* if $\gamma(G) \leq G$ for any endomorphism γ of W. In case each submodule of W is fully invariant, W is termed *duo* (refer to [13]).

Proposition 8. Suppose that W is a $\oplus$-co$_\delta$-δ-supplemented module and G is a fully invariant submodule of W. In that case, the quotient module W/G is $\oplus$-co$_\delta$-δ-supplemented.

Proof. Assume that L/G is a co$_\delta$-coatomic submodule of W/G. Then $(W/G)/(L/G) \cong (W/L)$ is δ-coatomic, and hence L is a co$_\delta$-coatomic submodule of W. By the assumption, there exists a decomposition $W = X \oplus X'$ of W such that $W = L + X$ and $L \cap X \ll_\delta X$. This leads to the conclusion that $(G + X)/G$ is a δ-supplement of L/G in W/G by [8, Proposition 2.3]. Therefore, we conclude that $G = (G \cap X) \oplus (G \cap X')$, since G is fully invariant by [13, Lemma 2.1]. This decomposition implies that $W/G = ((G + X)/G) \oplus ((G + X')/G)$. Hence W/G is $\oplus$-co$_\delta$-δ-supplemented.

Retrieve from [6, Lemma 1.5(2)] the fact that the submodule $\delta(W)$ of a module W is fully invariant.

Corollary 11. Suppose that W is a $\oplus$-co$_\delta$-δ-supplemented module. In that case, $W/\delta(W)$ is $\oplus$-co$_\delta$-δ-supplemented.

Corollary 12. Suppose that W is a $\oplus$-co$_\delta$-δ-supplemented duo module. In that case each quotient module of W is $\oplus$-co$_\delta$-δ-supplemented.

Proposition 9. Each co$_\delta$-coatomic fully invariant direct summand of a $\oplus$-co$_\delta$-δ-supplemented module is $\oplus$-co$_\delta$-δ-supplemented.

Proof. Suppose that W is a $\oplus$-co$_\delta$-δ-supplemented module and $G \leq_\oplus W$ is co$_\delta$-coatomic fully invariant. Let X be a co$_\delta$-coatomic submodule of G. By the assumption, there exists a δ-coatomic submodule G' of W such that $W = G \oplus G'$. Thus we have that $W/X = ((G \oplus G')/X) \oplus G' \cong G/X \oplus G'$ is δ-coatomic since it is a direct sum of two δ-coatomic modules by [4, Proposition 2.6]. Therefore, by the assumption there is a submodule T which is δ-supplement of X in W such that $W = T \oplus T'$. By the modular law, we get that $G = G \cap (X + T) = X + (G \cap T)$. Note here that $G = (G \cap T) \oplus (G \cap T')$ by [13, Lemma 2.1], since G is a fully invariant submodule of W. So, $G \cap T \leq_\oplus G$. Since $X \cap (G \cap T) = X \cap T \ll_\delta T$, then $X \cap (G \cap T) \ll_\delta G \cap T$ by Lemma 1-(5). Hence G is $\oplus$-co$_\delta$-δ-supplemented.

Proposition 10. Suppose that W is a $\oplus$-co$_\delta$-δ-supplemented module and G is a submodule of W. Assume that for each $X \leq_\oplus W$, $(G + X)/G \leq_\oplus W/G$. Then W/G is a $\oplus$-co$_\delta$-δ-supplemented.

Proof. Assume that L/G is a co$_\delta$-coatomic submodule of W/G. Then L is a δ-coatomic submodule of W. By the assumption, there exists a decomposition $W = X \oplus X'$ of W such that $W = L + X$ and $L \cap X \ll_\delta X$. Thus we get that $W/G = (L/G) + ((G + X)/G)$. By the hypothesis, $(G + X)/G \leq_\oplus W/G$. On the other hand, since $L \cap X \ll_\delta X$, $(L \cap (G + X))/G = (G + (L \cap X))/G = \pi(L \cap X) \ll_\delta \pi(X) = (G + X)/G$ where $\pi : W \to W/G$ is a canonical projection by Lemma 1-(2). This completes the proof.

As per the definition in [14], a module W is designated to possess the *Summand Sum Property (SSP)* in case the sum $W_1 + W_2 \leq_\oplus W$ where $W_1, W_2 \leq_\oplus W$.

Proposition 11. Suppose that W is a $\oplus$-co$_\delta$-δ-supplemented module. In case W possesses (SSP), each $G \leq_\oplus W$ is $\oplus$-co$_\delta$-δ-supplemented.

Proof. Assume that $W_1 \leq_\oplus W$ such that $W = W_1 \oplus W_2$. Regarding any $X \leq_\oplus W$, we achieve that $W = (X + W_1) \oplus K$ for some submodule K of W, as W has (SSP) by the assumption. Note that $W/W_2 = ((X + W_1)/W_2) \oplus ((K + W_2)/W_2)$. Here according to Proposition 10, W/W_2 is $\oplus$-co$_\delta$-δ-supplemented module.

Referencing [15], it can be recalled that a module W is termed *distributive* if, for submodules G, H, L of W, the equality $G \cap (H + L) = (G \cap H) + (G \cap L)$ or $G + (H \cap L) = (G + H) \cap (G + L)$ is satisfied.

Proposition 12. Suppose that W is a $\oplus$-co$_\delta$-δ-supplemented module and G is a submodule of W. In case W is distributive, W/G is $\oplus$-co$_\delta$-δ-supplemented.

Proof. The claim can be proved by using Proposition 10. For this, take $K \leq_\oplus W$. Then we have the decomposition $W = K \oplus K'$ for some $K' \leq W$. Thus $W/G = ((G + K)/G) + ((G + K')/G)$. By the assumption, since W is distributive, then $G = G + (K \cap K') = (G + K) \cap (G + K')$. We infer from here that $W/G = ((G + K)/G) \oplus ((G + K')/G)$. Thus W/G is $\oplus$-co$_\delta$-δ-supplemented module by Proposition 10.

Refer to [16] for the reminder that a module W is termed an (D_3)-*module* in case the intersection of direct summands, the sum of which yields W, is also a direct summand of W.

Proposition 13. Suppose that W is a $\oplus$-co$_\delta$-δ-supplemented (D_3)-module. In that case, each co$_\delta$-coatomic $K \leq_\oplus W$ is $\oplus$-co$_\delta$-δ-supplemented.

Proof. Assume that $K \leq_\oplus W$ is co$_\delta$-coatomic and X is a co$_\delta$-coatomic submodule of K. Then there exists a δ-coatomic submodule K' of M such that $W = K \oplus K'$. Therefore, we deduce that $W/X \cong (K/X) \oplus K'$ is δ-coatomic as a direct sum of two δ-coatomic modules by [4, Proposition 2.6]. Since W is $\oplus$-co$_\delta$-δ-supplemented, then there exists a δ-supplement T of X in W with $T \leq_\oplus W$. It gives the result that $K = K \cap (T + X) = (K \cap T) + X$. Since W is a (D_3)-module, $K \cap T \leq_\oplus W$, and thus $K \cap T \leq_\oplus K$. Also, $X \cap (K \cap T) = X \cap T \ll_\delta K \cap T$ by Lemma 1-(5). Hence K is $\oplus$-co$_\delta$-δ-supplemented.

In the sequel, we provide a helpful lemma to establish that any finite direct sum of modules that are $\oplus$-co$_\delta$-δ-supplemented remains $\oplus$-co$_\delta$-δ-supplemented.

Lemma 4. Let W be a module and G, H be submodules of W such that G is co$_\delta$-δ-supplemented, H is co$_\delta$-coatomic and $G+H$ possesses a δ-supplement T in W. Then $G\cap(H+T)$ possesses a δ-supplement T' in G and $T + T'$ is a δ-supplement of H in W.

Proof. Since T is a δ-supplement of $G+H$ in W, we have that $W = (G+H)+T$ and $(G+H)\cap T \ll_\delta T$. Moreover,
$G/(G\cap(H+T)) \cong (G+H+T)/(H+T) = W/(H+T) \cong (W/H)/((H+T)/H)$ is δ-coatomic as it is quotient module of the δ-coatomic module W/H. Thus there exists a δ-supplement X of $G\cap(H+T)$ in G, by the hypothesis. So, $G = (G\cap(H+T)) + X$ and $(G\cap(H+T))\cap X = (H+T)\cap X \ll_\delta X$. Therefore, we have $W = (G+H)+T = (G\cap(H+T)+X)+H)+T = H+T+X$ and
$H\cap(T+X) \leq T\cap(H+X)+X\cap(T+H) \leq T\cap(H+G)+X\cap(T+H) \ll_\delta T+X$ by Lemma 1-(3). Hence $T + X$ is a δ-supplement of H in W where X is a δ-supplement of $G \cap (H + T)$ in G.

Theorem 3. Any finite direct sum of $\oplus$-co$_\delta$-δ-supplemented modules is $\oplus$-co$_\delta$-δ-supplemented.

Proof. Assume that $W_1, W_2, ..., W_n$ is a finite collection of $\oplus$-co$_\delta$-δ-supplemented modules and $W = \bigoplus_{\lambda=1}^{n} W_\lambda$. To show that W is $\oplus$-co$_\delta$-δ-supplemented, we will prove the claim in case $n = 2$ and the proof is completed by induction. Let W be the direct sum of $\oplus$-co$_\delta$-δ-supplemented modules W_1, W_2 and G be a co$_\delta$-coatomic submodule of W. Then note that $W = W_1 + W_2 + G$ and 0 is a δ-supplement of $W_1 + W_2 + G$ in W. Since
$W_2/(W_2 \cap (W_1 + G)) \cong (W_1 + W_2 + G)/(W_1 + G) \cong (W/G)/((W_1 + G)/G)$
is δ-coatomic as it is quotient module of the δ-coatomic module W/G, then $W_2 \cap (W_1 + G) \leq W_2$ is co$_\delta$-coatomic. Thus by the hypothesis, W_2 possesses a $K \leq_\oplus W_2$ that is a δ-supplement of $W_2 \cap (W_1 + G)$ in W_2. Then K is a δ-supplement of W_1+G by Lemma 4. Now it is easy to see that $W_1/W_1\cap(G+K)$ is δ-coatomic, and thus $W_1 \cap (G + K)$ possesses a δ-supplement T in W with $T \leq_\oplus W_1$. By using Lemma 4 once again, $K + T$ is a δ-supplement of G in W_1 such that $K \oplus T \leq_\oplus W$. Hence W is $\oplus$-co$_\delta$-δ-supplemented module.

Co$_\delta$-Coatomically δ-Semiperfect Modules

Definition 2. We term a module W *co$_\delta$-coatomically δ-semiperfect, shortly co$_\delta$-δ-semiperfect*, provided each quotient module of W by a co$_\delta$-coatomic submodule, or equivalently each δ-coatomic quotient module of W possesses a projective δ-cover.

Proposition 14. Suppose that W is a projective module. In that case, W is co$_\delta$-δ-semiperfect if and only if W is $\oplus$-co$_\delta$-δ-supplemented.

Proof. ($\Longrightarrow$) Assume that G is a co$_\delta$-coatomic submodule of W. There is a projective δ-cover $h : P \to W/G$, by the assumption. Then according to [6, Lemma 2.4] there are submodules W_1, W_2 of W such that $W = W_1 \oplus W_2$ with $W_1 \leq G$ and $W_2 \cap G \ll_\delta W$. Applying Lemma 1-(5), we conclude that $W_2 \cap G \ll_\delta W_2$. It leads to the conclusion that W_2 is a δ-supplement of G.
($\Longleftarrow$) Assume that G is a co$_\delta$-coatomic submodule of W. As W is $\oplus$-co$_\delta$-δ-supplemented, then W has a decomposition $W = W_1 \oplus W_2$ such that $W = W_1 + G$ and $W_1 \cap G \ll_\delta W_1$. Note that W_1 is projective. Consider the canonical injection $\iota : W_1 \to W$ and the canonical projection $\pi : W \to W/G$. By this way, there exists an epimorphism $\pi\iota : W_1 \to W/G$ with $Ker(\pi\iota) = W_1 \cap G \ll_\delta W_1$.

Theorem 4. Suppose that W is a co$_\delta$-δ-semiperfect module. In that case, each homomorphic image of W is co$_\delta$-δ-semiperfect.

Proof. Assume that $h : W \to L$ is a homomorphism and G is co$_\delta$-coatomic submodule of $h(W)$. Consider the epimorphism $\psi : W \to h(W)/G$ defined by $\psi(w) = h(w)+G$ for whole $w \in W$. As W is co$_\delta$-δ-semiperfect, $h(W)/G \cong W/h^{-1}(G)$ has a projective δ-cover. Hence $h(W)$ is co$_\delta$-δ-semiperfect module.

Corollary 13. Each quotient module of a co$_\delta$-δ-semiperfect module is co$_\delta$-δ-semiperfect.

Corollary 14. Each projective quotient module of a co$_\delta$-δ-semiperfect module is $\oplus$-co$_\delta$-δ-supplemented module.

Proof. The proof can be easily seen by Corollary 13 and Proposition 14.

Theorem 5. Each δ-cover of a co$_\delta$-δ-semiperfect module is co$_\delta$-δ-semiperfect.

Proof. Assume that W is co$_\delta$-δ-semiperfect module and $f : L \to W$ is a δ-cover of W. For the δ-coatomic quotient module L/G of L, the homomorphism $\psi : L/G \to W/f(G)$ defined by $\psi(l+G) = f(l) + f(G)$ for all $l \in L$ is an epimorphism. Also, we claim that $Ker(\psi) \ll_\delta L/G$. To prove this, assume that $Ker(\psi) + X/G = L/G$ where $(L/G)/(X/G)$ is singular. Note that $Ker(\psi) = (G + Ker(f))/G$. Thus we have that $L = X + Ker(f)$ and $(L/G)/(X/G) \cong L/X$ is singular. As $Ker(f) \ll_\delta L$, then $X = L$. This leads to the conclusion that $Ker(\psi) \ll_\delta L/G$. Since $W/f(G) = \psi(L/G) \cong (L/G)/(G+Ker(f))/G$ is δ-coatomic, then by assumption $W/f(G)$ possesses a projective δ-cover $\mu : P \to W/f(G)$. As P is projective, there is a homomorphism $\alpha : P \to L/G$ such that the

following diagram

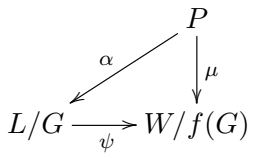

is commutative, that is, $\mu = \psi\alpha$. Then $L/G = \alpha(P) + Ker(\psi)$. Since $Ker(\psi) \ll_\delta L/G$, there exists a semisimple projective submodule S of $Ker(\psi)$ such that $L/G = \alpha(P) + S$ by Lemma 1-(1). Now we can define the homomorphism $\beta : P \oplus S \to L/G$ via $\beta(p, s) = \alpha(p) + G$. β is an epimorphism and $Ker(\beta) = Ker(\alpha) \oplus 0$. Since $Ker(\alpha) \leq Ker(\mu) \ll_\delta P$, then $Ker(\alpha) \oplus 0 \ll_\delta P \oplus S$. Consequently, $P \oplus S$ is a δ-cover of L/G.

Corollary 15. Suppose that G is a δ-small submodule of a module W and W/G is co$_\delta$-δ-semiperfect. In that case, W is a co$_\delta$-δ-semiperfect module.

Corollary 16. Suppose that W is and that $f : P \to W$ is a projective δ-cover of W. In that case, the expressions below are equivalent:

1. W is co$_\delta$-δ-semiperfect.
2. P is co$_\delta$-δ-semiperfect.
3. P is $\oplus$-co$_\delta$-δ-supplemented.

Proof. $(1) \Longrightarrow (2)$ It is derived from Theorem 5.
$(2) \Longrightarrow (1)$ It is supported by Corollary 13.
$(2) \Longleftrightarrow (3)$ It is Proposition 14.

Theorem 6. Suppose that W_λ is a collection of projective modules where $\lambda \in \Lambda$ and Λ is a finite index set. In that case, $W = \bigoplus_{\lambda\in\Lambda} W_\lambda$ is co$_\delta$-δ-semiperfect module if and only if W_λ is co$_\delta$-δ-semiperfect for each $\lambda \in \Lambda$.

Proof. $(\Longrightarrow)$ Let $W = \bigoplus_{\lambda\in\Lambda} W_\lambda$ is co$_\delta$-δ-semiperfect module. Then by Corollary 13,
$W_\lambda \cong W/(\bigoplus_{\eta\in\Lambda\setminus\{\lambda\}} W_\eta)$ is co$_\delta$-δ-semiperfect for each $\lambda \in \Lambda$.
$(\Longleftarrow)$ Let W_λ be a projective co$_\delta$-δ-semiperfect module for each $\lambda \in \Lambda$. Thus W_λ is $\oplus$-co$_\delta$-δ-supplemented by Proposition 14, for each $\lambda \in \Lambda$. Therefore, W is $\oplus$-co$_\delta$-δ-supplemented by Theorem 3. Applying Proposition 14 once again, we deduce that W is co$_\delta$-δ-semiperfect.

Now the next result is obviously seen by Corollary 13 and Theorem 6.

Corollary 17. Suppose that W is a projective module. In case W is co$_\delta$-δ-semiperfect module, any finitely W-generated module is co$_\delta$-δ-semiperfect.

Finally, we determine over which rings the R-module ${}_RR$ is equivalent to being $\oplus_\delta$-co-coatomically supplemented, being co$_\delta$-δ-semiperfect and being $\oplus$-co$_\delta$-δ-supplemented.

Theorem 7. The expressions below are equivalent for a δ-semiperfect ring S:

1. ${}_SS$ is $\oplus_\delta$-co-coatomically supplemented.

2. ${}_SS$ is co$_\delta$-δ-semiperfect.

3. ${}_SS$ is $\oplus$-co$_\delta$-δ-supplemented.

Proof. $(1) \Longleftrightarrow (3)$ It is Corollary 10.
$(2) \Longleftrightarrow (3)$ It is Proposition 14.

Acknowledgments -

Funding/Financial Disclosure The author has no received any financial support for the research, or publication of this study.

Ethics Committee Approval and Permissions The work does not require ethics committee approval and any private permission.

Conflict of Interests The author stated that there are no conflict of interest in this article.

Authors Contribution The author read and approved the final manuscript.

References

[1] Wisbauer R. (1991). *Foundations of Modules and Rings*. Gordon and Breach Science Publishers, Philadelphia.

[2] Zöschinger H., & Rosenberg F. A. (1980). Koatomare moduln. *Mathematische Zeitschrift*, *170*, 221–232. https://doi.org/10.1007/BF01214862

[3] Alizade R., & Güngör S. (2017). Co-coatomically supplemented modules. *Ukrainian Mathematical Journal*, *69*(7), 1007–1018. https://doi.org/10.1007/s11253-017-1411-x

[4] Koşan M. T., & Harmancı A. (2005). Generalizations of coatomic modules. *Open Mathematics*, *3*(2), 273–281. https://doi.org/10.2478/BF02479203

[5] Alizade R., & Güngör S. (2018). $\oplus$-co-coatomically supplemented and co-coatomically semiperfect modules. *Hacettepe Journal of Mathematics and Statistics*, *47*(6), 1417–1426. https://dergipark.org.tr/en/pub/hujms

[6] Zhou Y. (2000). Generalizations of perfect, semiperfect and semiregular rings. *Algebra colloquium*, *7*(3), 305–318.

[7] Koşan M. T. (2007). δ-Lifting and δ-supplemented modules. *Algebra colloquium*, *14*(1), 53–60. https://doi.org/10.1142/S1005386707000065

[8] Abdioğlu C., & Şahinkaya S. (2015). Some results on δ-semiperfect rings and δ-supplemented modules. *Kyungpook Mathematical Journal*, *55*, 289–300. https://dx.doi.org/10.5666/KMJ.2015.55.2.289

[9] Eryılmaz F, & Öztürk Sözen E. (2023). On a generalization of $\oplus$-co-coatomically supplemented modules. *Honam Mathmatical Journal*, *45*(1), 146–159. https://doi.org/10.5831/HMJ.2023.45.1.146

[10] Büyükaşık E., & Lomp C. (2010). When δ-semiperfect rings are semiperfect. *Turkish Journal of Mathematics*, *34*(3), 317–324. https://doi.org/10.3906/mat-0810-15

[11] Tribak R. (2012). Finitely generated δ-supplemented modules are amply δ-supplemented. *Bulletin of the Australian Mathematical Society*, *86*, 430–439. https://doi.org/10.1017/S0004972711003406

[12] Zöschinger H. (1974). Komplemente als direkte summanden. *Archiv der Mathematik*, *25*, 241–253. https://doi.org/10.1007/BF01238671

[13] Özcan A. Ç., & Alkan M. (2006). Duo modules. *Glasgow Mathematical Journal*, *48*, 533–545. https://doi.org/10.1017/S0017089506003260

[14] Garcia J. L. (1989). Properties of direct summands of modules. *Communications in Algebra*, *17*, 73–92. https://doi.org/10.1080/00927878908823714

[15] Tuganbaev A. (1999). *Distributive Modules and Related Topics*. Gordon and Breach Science Publishers.

[16] Mohamed S. H., & Müller B. J. (1990). *Continuous and Discrete Modules*. Cambridge University Press.

Sinopfbd, 2024; 9(1): 128-144 **https://doi.org/10.33484/sinopfbd.1434171**

Sinop Üniversitesi Fen Bilimleri Dergisi
Sinop Uni J Nat Sci
E-ISSN: 2564-7873

https://dergipark.org.tr/tr/pub/sinopfbd

Türkiye'deki Akademisyenlerin Yapay Zekâ (YZ) Uygulama ve Araçlarını Kullanımları Hakkında Bir Araştırma

Cihan ÜNAL[1] ve Hakan YILDIRIM[2]

How to cite: Ünal, C., & Yıldırım, H. (2024). Türkiye'deki akademisyenlerin Yapay Zekâ (YZ) uygulama ve araçlarını kullanımları hakkında bir araştırma. *Sinop Üniversitesi Fen Bilimleri Dergisi, 9*(1), 128-144. https://doi.org/10.33484/sinopfbd.1434171

Araştırma Makalesi

Sorumlu Yazar
Cihan ÜNAL
cihan.unal@hacettepe.edu.tr

Yazarlara ait ORCID
C.Ü: 0000-0002-5255-4078
H.Y: 0000-0002-5959-2691

Received: 08.02.2024
Accepted: 16.04.2024

Öz

Bu makale, Türkiye'deki akademisyenlerin Yapay Zekâ (YZ) ürünlerini (uygulama ve araçlarını) kullanma alışkanlıklarını ve kullanım nedenlerini inceleyen bir araştırmanın sonuçlarını sunmaktadır. Veriler, geniş bir akademik topluluğun katılımıyla gerçekleştirilen bir anket aracılığıyla toplanmıştır. Bulgular, YZ konusunda yeterli farkındalık olduğunu, YZ ürünlerinin kullanıldığını ancak YZ ürünlerinin yeterince yaygın ve çok yönlü bir şekilde kullanılmadığını göstermektedir. Araştırmayla YZ kullanımının yaygınlığı, etkisi ve gelecekteki araştırmalar için potansiyel yönleri, beraberinde getirdiği telif, patent ve mahremiyet ihlali gibi yeni sorunları matematiksel bulgularla ortaya konmuş ve sonuçları tartışılmıştır. Bu çalışma, YZ teknolojilerinin akademik çalışmalar ve öğretimdeki rolünün anlaşılması ve daha yaygın kullanımı için katkıda bulunmayı amaçlamaktadır.

Anahtar Kelimeler: Yapay zekâ, sohbet botları, öğretim elemanı

A Survey on the Use of Artificial Intelligence (AI) Applications and Tools by Academics in Turkey

[1]Hacettepe Üniversitesi, Başkent OSB Teknik Bilimler MYO, Bilgisayar Programcılığı Bölümü, Ankara, Türkiye

[2]Beykent Üniversitesi, Mimarlık Mühendislik Fakültesi, Bilgisayar Mühendisliği Bölümü, İstanbul, Türkiye

Abstract

This article presents the results of a study investigating the habits and reasons for use of Artificial Intelligence (AI) products (applications and tools) among academics in Turkey. Data were collected through a survey conducted with the participation of a broad academic community. The findings indicate that there is adequate awareness about AI and its usage, but AI products are not being used extensively and diversely enough. The study has demonstrated the prevalence, impact, and potential directions for future studies of AI utilization, along with new issues it raises such as copyright, patent infringement, and privacy violations, all underpinned by mathematical findings and the results have been discussed.This study aims to contribute to the understanding and wider use of AI technologies in academic research and teaching.

Keywords: Artificial intelligence, chatbots, academic staff

Giriş

Yapay Zekâ (YZ), akademik alan dâhil olmak üzere çeşitli sektörlerde dönüştürücü bir güç olarak ortaya çıkmıştır. Uygulamalar ve araçlar gibi YZ ürünlerinin akademik uygulamalara entegrasyonu, araştırma, öğretim ve genel eğitim deneyimini geliştirme potansiyeline sahiptir. Bu çalışma, Türkiye'deki akademisyenlerin YZ ürünlerini kullanma alışkanlıklarını ve bu alışkanlıkların altındaki motivasyonları araştırmayı amaçlamaktadır. Böylece mevcut durumun anlaşılması sağlanacak ve bunu temel alan hedefleri belirlemek mümkün olacaktır. Son yıllarda YZ teknolojileri hızla evrim geçirmiş ve sesli asistanlar, dil çevirileri, navigasyon, sosyal güvenlik, sağlık hizmetleri, e-ticaret, yardımcı robot uygulamaları, siber güvenlik, doğal dil işleme ile makine öğrenme algoritmaları gibi sayısız güçlü yetenekler sunmaktadır. Bu teknolojiler, akademik araştırma ve öğretimde verimliliği, doğruluğu ve inovasyon artırma fırsatlarını sunmaktadır [1]. Ancak Türkiye'deki akademisyenlerin YZ araçları ve uygulamalarını ne ölçüde benimsediği konusu açıkça belli değildir. Çalışmanın bu alandaki önemli bir boşluğu doldurması hedeflenmiştir. Tüm dünyada olduğu gibi ülkemizde de YZ konusundaki ilerlemelerin ve gelişimin en önemli odağı akademidir. Akademik camianın en temel ve en birinci unsuru ise öğretim elemanları yani (akademisyenlerdir). Bu araştırmanın önemi, Türkiye'deki akademik toplum içinde YZ'nın benimsenme durumunu aydınlatma potansiyeline dayanmaktadır. Bu çalışma, akademisyenlerin kullanım alışkanlıklarını, farkındalık düzeylerini ve karşılaştıkları engelleri anlayarak, akademik alandaki YZ entegrasyonunu teşvik etmek için geliştirilecek stratejilere katkıda bulunabilir. Ayrıca, akademik ortamlarda YZ kullanımı ile ilişkilendirilen etik ve pratik endişeler de ele alınmaktadır. Makalenin ilerleyen bölümlerinde sorunlar ve metodolojik yaklaşım, anket sonuçları ve bulguları, YZ benimseme üzerine yapılan tartışmalar ve gelecekteki araştırmalar için öneriler bulunmaktadır. Bu araştırma ile Türkiye'deki akademik araştırma ve eğitimde YZ teknolojilerinin daha geniş bir şekilde benimsenmesi, teşvik edilmesi ve bunların etkisinin daha iyi anlaşılması amaçlanmaktadır. Araştırmamız anket yöntemi ile yapılmıştır. Ankette sorulan sorular hazırlanırken bu alanda yapılmış öncül ve olabildiğince yakın tarihli çalışmalardan oluşan bir literatür taraması yapılmıştır. YZ ürün ve uygulamalarının yaygınlaşması son birkaç on yılla sınırlı olduğu için araştırdığımız akademik kaynakların yayın tarihlerinin YZ ürün ve araçlarının bir anda yaygınlaşmaya başladığı bu dönem ve daha sonraki yıllara ait olmasına özen gösterilmiştir. Benzer çalışmaların yer aldığı literatür çalışmalarından eldeki bu çalışmaya ışık tutacağını düşündüğümüz alanları ve buna dayalı soruları oluştururken öncelikle "DOĞRU VE TAM" olma (Soundness and Completeness) unsurlarına dikkat edilmiştir [2]. İlgili kaynakların taranması ve yapılan ön araştırmalar sonucu olarak özellikle akademik camiada kullanıma sunulan en son YZ uygulama ve araçlarının kullanımını araştırmaya yönelik sorular oluşturulmuştur. Araştırmamıza Türkiye'deki her düzeydeki akademisyen katılmıştır. Sorularımızın ilk bölümünde anketi dolduran katılımcıların demografik özellikleri (çalıştığı üniversitenin özelliği, yaş, unvan, eğitim, bilim alanı vb.) ve diğer ilgili bilgileri araştırılmıştır. Ardından kullanılan ürün ve araçlar ve bunların kullanım alanlarını araştırmaya yönelik sorular sorulmuştur. Son

kısımda ise YZ ürünlerinin kökten değiştirmeye başladığı, intihal, patent hakları, mahremiyet ve kişisel veri güvenliği ihlalleri konusundaki algı düzeyinin anlaşılmasına yönelik sorular sorulmuştur. Soruların sonunda ise katılımcıların her türlü görüş ve önerisini serbestçe yazabilecekleri bir alan eklenmiştir. Anket, özel bir form doldurma yazılımının linki ile katılımcılara elektronik iletişim araçları vasıtasıyla iletilmiştir. Anket sonuçlarının analizinden dağılımın dengeli olduğu da anlaşılmıştır. Buna göre bölüm-unvan-yaş ve üniversite özellikleri gibi konularda Türkiye ortalaması ile uyumlu bir sonuç gözlenmiştir. Toplanan veriler öncelikle veri toplama aracının sunduğu analiz araçları kullanılarak değerlendirilmiş ancak bunun yetmediği yerlerde daha ileri istatistiksel veri analiz yöntemleri de kullanılmıştır. Bunlar, Gözden Geçirme ve Temizleme, Güvenilirlik, Geçerlik, Eksik Veri, Anomali Tespiti, Mantıksal Tutarsızlık, Çapraz Kontrol, Faktör Analizi gibi yöntemlerdir. Ortaya çıkan sonuçların güvenilir olduğu hem elle yapılan denetimlerimizle hem de ileri analiz olanağı veren istatistiksel ölçüm araçları aracılığıyla doğrulanmıştır. Ardından veriler analize tabi tutulmuştur. Çalışmamızda; Araştırma Konuları ve Yöntemi bölümünde literatür taraması yapılmıştır. Materyal ve Metot bölümünde anket tasarımı ve veri toplama yöntemleri anlatılmıştır. Bulgular ve Tartışma bölümünde anket çalışmasının bulguları anlatılmış ve tartışılmıştır. Sonuçlar bölümünde ise elde edilen bulguların özeti verilmiş ve bulgular doğrultusunda akademik camiada söz sahibi olan taraflara öneriler sunulmuştur.

Araştırma Konuları ve Yöntemi

Araştırmanın Konuları (Sorunlar)

YZ ürünlerinin kullanılması beraberinde yeni olgu-konu ve sorunları da getirmiştir. Bu sorunların neler olduğuna genel bir bakıştan sonra akademisyenlerin bu ürünleri akademik ve özel hayatlarında kullanımına dair yapılan araştırmanın sonuçları tartışılmıştır. Sorunlar; kullanım, hukuk, fikri mülkiyet, içerik üretimi, intihal, mahremiyet ve diğer sorunlar başlıkları altında incelenmiştir. Sorunlar aynı zamanda araştıracağımız konulara ve belirlenen anket sorularına ışık tutmaktadır.

Kullanım Sorunları

Önyargı ve Adaletsizlik

YZ algoritmaları, eğitim sürecinde kendilerine kaynak olarak gösterilen veri setlerinin içerdiği önyargıları da öğrenebilir ve bu önyargıları çalışma sistematiklerine ve elde ettikleri sonuçlara yansıtabilir. Eğitim verilerinde var olan önyargılar, YZ'nın karar verme mekanizmalarında adaletsizliklere (haksızlıklara) sebep olabilecek şekilde sonuçlar üretmesine yol açabilir. Ön yargıların varlığı, sıklıkla henüz normlar ve kuralların tam olarak yerleşmediği, gelişmekte olan alanlarda daha fazla hissedilebilir [3].

Güvenilirlik Sorunları

YZ sistemlerinin ürettiği sonuçlar her zaman güvenilir olmayabilir. Özellikle, YZ modelleri beklenmedik yeni durumlarla karşılaştıklarında adaptasyon ve doğru sonuçlar üretme konusunda sınırlamalara sahip olabilirler. Teknolojinin hızla ilerlediği ve sürekli değişim gösterdiği alanlarda, YZ sistemlerinin güncelliğini koruma ve doğru bilgiyi işleme konusunda zorluklar yaşanması muhtemeldir [4].

Etiğe Uygunluk Sorunları

YZ'nın etik kurallara ne derece uygun olduğu, teknoloji alanında sürekli olarak tartışılan bir konudur. Kişisel mahremiyet, güvenlik ve toplumsal etkiler gibi konularda, etik düzenlemelere ve standartlara duyulan ihtiyaç giderek artmaktadır. YZ'nın etik yönleri, özellikle yeni ve gelişmekte olan etik kurallar ve standartlar oluşturulurken daha belirgin hale gelmektedir [5]. Etik kuralları ileride yasal düzenlemeler takip edecek olsa bile etik kurallar önemini yitirmeyecek ve bu alandaki boşluğu dolduracaktır.

Hukuki Sorunlar

Sorumluluk ve Hukuki Çerçeve

YZ sistemlerinin kararları sonucu meydana gelen zararlar, sorumluluğun tespiti konusunda hukuki belirsizlikler yaratmaktadır. Özellikle, otomatik karar verme süreçlerinde hata nedeniyle oluşan zararların kim ya da ne tarafından telafi edileceği hukuki çevrelerde tartışma konusudur [6]. YZ sistemlerinin giderek daha karmaşık ve otomatik hale gelmesiyle, bu sistemlerin yanlış kararlar alması veya hatalı sonuçlar üretmesi durumunda oluşabilecek zararlar ve bu zararların kim tarafından telafi edileceği konusu önemli bir hukuki tartışma konusu haline gelmiştir. YZ sistemlerinin kararlarının neden olduğu zararlar, birçok durumda geleneksel hukuk kurallarına ve sorumluluk ilkelerine uygun olarak ele alınamayabilir. Bu nedenle, YZ sistemlerinin hukuki sorumluluğuyla ilgili yeni düzenlemeler, standartlar ve hukuki çerçeveler oluşturulması gerekmektedir. Asaro'nun [6] bahsettiği gibi, özellikle otomatik karar verme süreçlerindeki hataların sonuçlarına karşı hukuki sorumluluk konusunda belirsizlikler vardır. Bu tür durumlar, YZ sistemlerinin etik, hukuki ve sosyal sonuçlarını değerlendirmek için daha fazla araştırma ve düzenleme gerektirir. YZ kararlarının hukuki sorumluluğuyla ilgili genel bir anlayışı yansıtmaktadır ve YZ teknolojilerinin hukuki çerçevesi ve sorumlulukları konusundaki tartışmalar ve eldeki gibi araştırmalar sorumluluk ve hukuki çerçeveyi daha da belirginleştirecektir.

Kararlar ve Doğurduğu Zararların Hukuki Boyutu

YZ sistemleri tarafından oluşturulan hatalı kararlardan doğması muhtemel zararların kim tarafından üstlenileceğini belirlemek açısından zorluklar vardır. Bu durum, otomatik kararların sonuçlarına yönelik hukuki mücadelede netlik sağlama ihtiyacını ortaya koymaktadır [7].

İnsan Faktörü ve YZ Sorumluluğu

YZ sistemlerinin geliştirilmesi ve denetimi insanlar tarafından yapıldığından, hata durumunda insan müdahalesinin sorumluluk derecesi belirsizdir. Bu, geliştiricilerin, operatörlerin ve denetçilerin sorumluluğunun ne ölçüde olacağına dair hukuki çerçeveyi zorunlu kılar [6].

Mevcut Hukuki Çerçevenin Yetersizlikleri

YZ için henüz net ve kapsamlı bir hukuki çerçeve mevcut değildir. Mevcut yasaların YZ uygulamalarına uygulanabilirliği ve cezai, sivil veya idari sorumlulukları nasıl şekillendirdiği ve gelecekte nasıl roller oynayacağı konularında önemli belirsizlikler bulunmaktadır [8].

Fikri Mülkiyet ve İntihal Sorunları

YZ Üretimi ve Fikri Mülkiyet Hakları

YZ tarafından üretilen içeriklerde fikri mülkiyet haklarının belirsizliği, içerik üreticileri ve tüketicileri için hukuki ve etik sorunlar doğurur. İntihal, bu tür ürünlerin kullanımıyla ortaya çıkan en önemli hukuki meselelerden biridir [9].

İçerik Üretimi

YZ ve sohbet botları, eğitildikleri büyük veri setleri sayesinde geniş bir metin bilgisine sahiptirler, ancak bu veriler arasında telif haklarına tabi metinler de bulunabilir. Bu durum, telif hakları ihlali riskini beraberinde getirir [10].

İzinsiz Kullanılan İçerikler

YZ sohbet botları, geniş veri tabanlarına erişim sağlarlar ve bu süreçte telif haklarına tabi içerikleri izinsiz kullanılabilir ki bu da içerik sahiplerinin haklarının ihlal edilmesine sebep olma potansiyelini taşımaktadır [11].

Türetilmiş ve Otomatik İçerikler

YZ tarafından üretilen içerikler genellikle eğitim verilerinden türetilmiştir ve bu benzerlik, telif hakları ihlallerini gündeme getirebilir. YZ ürünleri arasında türetilmiş içeriklerin orijinal içerikten farklılığını sağlayacak ürünler olduğu da gözlemlenmektedir, ancak bunun günümüzdeki ve gelecekteki etik ve yasal koşulları ne kadar karşıladığı konusu şimdilik belirsizdir [12].

Bilgi Hırsızlığı Sorunları

Riskler

YZ, büyük veri kümelerinden öğrenir ve bu süreçte diğer kaynaklardan alıntı yapma veya benzer içerikler oluşturma riski taşır, bu da intihal sorunlarına yol açabilir [5].

Bilinçsiz Kopyalama

YZ modelleri, eğitildikleri veri setindeki ifadeleri doğrudan kullanabilir, bu da intihal riskini artırır ve yaratıcı içerik üretiminin haklarını tehdit eder [13].

Eğitim Veri Setlerinin Telif Hukuku

YZ sistemleri, eğitildikleri veri setlerini kullanırken, bu verilerin telif haklarına saygı göstermeyen uygulamaları ortaya çıkarabilir [14].

YZ İnovasyonları ve Patent

YZ alanında geliştirilen yeni teknolojiler, patent hakları konusunda belirsizliklere yol açtığı için; inovasyonun teşvik edilmesi ile hukuki karmaşa arasında dengenin sağlanması gerekir [15].

Mahremiyet ve Veri Koruma Sorunları

Mahremiyet

YZ uygulamalarının yaygınlaşması, mahremiyet ve kişisel veri güvenliği ihlallerinde çok önemli artışa yol açmıştır. Mahremiyet ihlalleri, veri toplama ve işleme süreçlerindeki açıklardan kaynaklanabilir [16].

Kişisel Verilerin Korunması

YZ ve sohbet botları, kişisel verilerin korunması konusunda yeni zorluklar yaratır. Bu teknolojiler, veri güvenliğini ve korumasını sağlamak için yeni düzenlemeleri zorunlu kılar [17]. YZ ürünleri, genellikle kullanıcı davranışlarını ve tercihlerini analiz etmek için büyük miktarda veri toplar. Bu durum, bireylerin kişisel yaşamlarıyla ilgili detayların, izinleri olmaksızın toplanmasına yol açabilir. Bu veri kullanımının kontrolsüz olması, kişisel veri güvenliği ihlallerine neden olabilir [18].

Veri İhlalleri ve Güvenlik

YZ algoritmalarının kullanımıyla ilgili güvenlik açıkları ve veri ihlalleri, gelişen teknolojilerle birlikte ele alınması gereken öncelikli konulardandır [19].

Diğer Sorunlar

Sesli Asistanlar

Sesli asistanlar, kullanıcıların sesli komutlarını algılayarak yanıtlar üretir. Ancak, bu süreç sırasında cihazın sürekli olarak sesi kaydetmesi, kullanıcıların mahremiyetini tehlikeye atabilir. Sesli asistanların bu kayıtları ne kadar süreyle sakladığı ve nasıl koruduğu konusundaki belirsizlikler, güvenlik endişelerini artırabilir [20].

Algılayıcı Teknolojiler ve Yüz Tanıma Sistemler

YZ ürünleri, yüz tanıma ve diğer algılayıcı teknolojileri kullanarak kullanıcıları tanıyabilir. Bunun neticesinde ise bu teknolojilerin yanlış kullanımı veya kötü niyetli amaçlar için kullanılması, bireylerin gizliliğini tehlikeye atabilir. Özellikle kamusal alanlarda kullanılan yüz tanıma sistemleri, mahremiyet ihlallerine ve kişisel veri güvenliği risklerine yol açabilir [21].

Veri Saklama ve Paylaşım Politikalarının Belirsizliği

YZ ürünleri genellikle büyük veri setleri üzerinde çalışır ve bu veriler genellikle bulut tabanlı hizmetlerde saklanır. Veri saklama ve paylaşım politikalarının belirsiz veya yetersiz olması, kullanıcı verilerinin izinsiz erişime veya kötü niyetli kullanıma açık hale gelmesine neden olabilir [22].

Regülasyon ve Hukuki Çerçeve

YZ ve mahremiyetle ilgili mevcut yasal düzenlemeler ve YZ kullanımının daha iyi düzenlenmesi ve mahremiyetin korunması için etkili ve teknolojinin bugününe uygun olarak araştırılması öncelikli konulardır [23].

Etik Kurallar

YZ kullanımının etik boyutları ile YZ geliştiricilerinin ve kullanıcılarının dikkate alması gereken etik standartların YZ konusundaki yenilikleri içerecek şekilde yeniden kodlanması ve bilinmesi gerekmektedir [24].

Politikasızlık

Yeni ortaya çıkan konularda genel olarak politikaların belirlenmesi ve istikrarlı bir hal alması zaman almaktadır. Üniversitelerin YZ ürünlerini akademik faaliyetlerde kullanması ve akademisyenlerin ve öğrencilerin bu alanda teşviki konusunda belirli bir politikaya sahip olmadıkları halde bu konuda politika sahibi hale gelmelerinin zaman alması doğaldır [25].

Ekonomik Sorunlar

Ülkemizdeki akademisyenlerin YZ ürün ve araçlarını kullanımı bakımından önemli bir engel de bu ürün ve araçların ülkemizdeki gelir seviyesi düşünüldüğünde pahalı olmasıdır. Bu alanda teşvikler ve bunun için de politikalar gerekmektedir [26].

Materyal ve Metot

Genel Bakış

Türkiye'deki akademisyenlerin Yapay Zekâ (YZ) ürünlerini kullanımı üzerine yapılan bu çalışma kapsamlı ve çok yönlü olup, bulguların geçerliliğini ve güvenilirliğini sağlamak için çeşitli yöntemler kullanmıştır.

Anket Tasarımı

Anket sorularını bilgilendirmek için YZ'nın son gelişmelerine odaklanarak detaylı bir literatür taraması yapılmıştır. Literatür tarandıktan sonra elde edilen bulgular kullanılarak anket tasarlanmıştır. Anket, demografik sorular ve YZ ürünlerinin kullanımı, farkındalığı ve bu ürünlere karşı tutumlar hakkında soruları içermiştir. Türkiye'deki geniş bir akademik personel yelpazesine anket dağıtımını kolaylaştırmak için çevrimiçi bir form kullanılmıştır. Anketin dağıtımından önce Hacettepe Üniversitesinden "Etik Komite Onayı" alınmıştır. Anket soruları oluşturulurken olabildiğince kullanılan plug-in ürünlerinin adları kullanılarak ve katılımcılardan spesifik ürün adı istenerek kullanım çeşitliliği ve ürünlerin pazar durumları ve kullanıcı alışkanlıklarını yöneten motifler anlaşılmaya çalışılmıştır. Ayrıca anketimizde teknolojik özellikler derinlemesine araştırılırken bir yandan da mahremiyet, güvenlik, intihal ve telif hakları gibi konular aynı anket içinde irdelenerek konunun hem teknik hem de hukuki boyutu aynı anda ve derinlemesine irdelenmiş ve bu konuda bilinç yaratılmaya çalışılmıştır.

Katılımcı Demografisi ve Diğer Özellikleri

Çeşitli ve temsili bir örneklem elde etmek için Türkiye'deki tüm akademik seviyelerden katılımcılar çalışmaya dâhil edilmiştir. Bölüm-unvan-yaş ve üniversite özellikleri gibi demografik veriler toplanmıştır. Ankette sorulan sorularla akademisyenlerin bölüm-unvan-yaş ve üniversite özellikleri; YZ ürünlerinin kullanımı bakımından mevcut durum ve beklentiler, YZ ürünlerinin kullanımı ile ilgili avantajların farkındalığı, telif, patent ve mahremiyet hassasiyetleri olarak grupladığımız konularında ortaya çıkan yeni durumun farkındalığı ve YZ ürünlerinin oluşturduğu tehlikelerle ilgili farkındalık düzeylerinin ölçülmesini sağlayan toplam 24 adet özgün soru sorulmuştur. Soruların tamamına ilgili linkten (https://www.jotform.com/form/232742934735058) erişilebilir.

Veri Toplama ve Analizi

Dengeli bir temsil sağlamak için, anket özel bir form takdim ve istek yazısı eşliğinde çevrimiçi forma erişim linki kullanılarak dağıtılmıştır. Toplanan verilere İnceleme ve Gözden Geçirme ve Temizleme, Güvenilirlik, Geçerlik, Eksik Veri, Anomali Tespiti, Mantıksal Tutarsızlık, Çapraz Kontrol, Faktör Analizi dâhil olmak üzere ileri istatistiksel yöntemler uygulanmıştır. En son analiz ise hem manuel kontroller hem de istatistiksel araçlar yoluyla sonuçların güvenilirliğini teyit etmiştir. Dengeli bir temsil için anketten topladığımız eldeki veriler ve Yükseköğretim Kurulu (YÖK) istatistiklerinin sunulduğu resmi internet sayfası (https://istatistik.yok.gov.tr/) üzerindeki veriler ki-kare testi (Chi-square test) kullanılarak gruplar arasındaki tutarlılık izlenmiştir [27]. Söz konusu veriler arasındaki tutarlılık veya tutarsızlık ise ANOVA ve t-test kullanılarak ölçülmüştür. Elde edilen sonuçlar ise iki grup arasında tutarlılık olduğunu göstermiş olup anketimizin bu bakımdan yani ana evren ve test edilen gruplar arasında dengeli dağılım olduğunu ve anketimizden elde edilen sonuçların güvenilir olduğu ortaya koymuştur.

Sınırlamalar ve Etik Değerlendirmeler

Araştırma, e-posta yoluyla ulaşılabilecek akademisyenlerle sınırlı kalmıştır, daha yüksek bir yanıt oranının daha ince ayrıntılı içgörüler sağlayabileceği kabul edilmiştir. Anket sorularının oluşturulmasında ve verilerin işlenmesinde etik kaygılar ele alınmıştır. Bu çalışmada benimsenen metodoloji, Türkiye'deki akademisyenler arasında YZ kullanımının genel durumunu başarıyla haritalamış ve son teknolojik değişikliklerin verdiği olanaklardan yararlanarak detaylı sonuçları anlaşılmıştır. Çok katmanlı yaklaşım, elde edilen verilerin sağlam ve akademik sektördeki mevcut eğilim ve tutumları yansıtacak şekilde olmasını sağlamıştır.

Bulgular ve Tartışma

Pek çok konuda olduğu gibi bilimsel, teknik ve inovatif konularda da toplumdaki değişim ve dönüşümün motor ve lokomotif gücü akademisyenlerdir. Araştırmada katılımcıların bölüm-unvan-yaş ve üniversite özellikleri gibi ayırt edici özelliklerinin YZ ürünlerini kullanım durumları ve YZ ürünlerinin yaygınlaşmasıyla birlikte yeni bir boyut ve hukuki statüye bürünen telif, patent ve mahremiyet konularına olan yaklaşımlarının ölçmek ve kıyaslamak amaçlanmıştır. Bunun için Likert ölçeği kullanılmıştır. Likert ölçekleme tekniği Rensis Likert tarafından geliştirilmiştir. Likert ölçekleme tekniği ile ilgili ilk düşünce araştırmacının 1932'de "Archive of Psychology" isimli bir dergide yayınladığı "A Technique for the Measurement of Attitudes" isimli makalesinde yer alır. Likert ölçekleme tekniğinde "beşli cevaplama" şöyledir; "Kesinlikle Onaylıyorum", "Onaylıyorum", "Kararsızım", "Onaylamıyorum" ve "Kesinlikle Onaylamıyorum" [28]. Üniversite türüne göre telif, patent ve mahremiyet hassasiyetleri Likert ölçeği verilerine göre Tablo-1'de verilmiştir.

Tablo 1. *Türkiye'de akademisyenlerin telif, patent ve mahremiyet konularındaki algılarının üniversite özelliklerine bağlı olarak nasıl değiştiğini gösteren likert dağılımı*

Üniversite	Telif	Patent	Mahremiyet
Devlet	3.99	3.15	3.68
Vakıf	3.81	2.67	3.67

Ayrıca Üniversite türüne göre telif, patent ve mahremiyet hassasiyetleri Likert ölçeği verilerine göre grafik olarak Şekil 1'de sunulmuştur. Bölüme, unvana, yaşa ve üniversiteye göre toplu olarak likert ölçeği verileri Şekil 2'de toplu olarak verilmiştir.

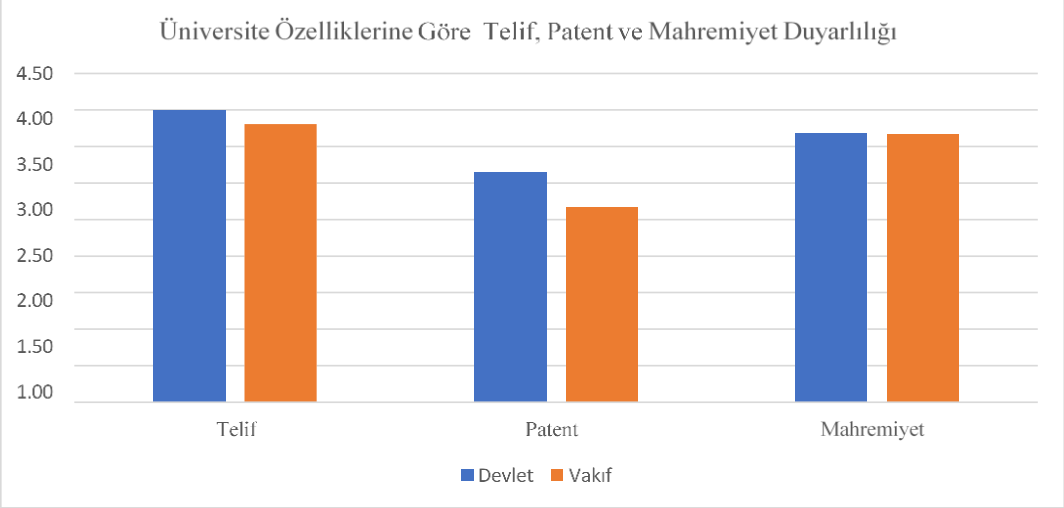

Şekil 1. *Türkiye'de akademisyenlerin telif, patent ve mahremiyet konularındaki algılarının üniversite özelliklerine bağlı olarak nasıl değiştiğini gösteren likert dağılımı*

Bir yandan da bu ürünlerin akademik faaliyetlerde kullanım ağırlığı ve bu ürünlerin getirdiği olanak ve kabiliyetlerden ne ölçüde haberdar oldukları, ayrıca bu ürünlerin kullanımı için üniversitelerin belirlediği politikalar ve ekonomik kaygıların boyutları da araştırılmıştır. YZ'nın kullanımının yaygınlığı, hangi akademik faaliyetlerde daha çok kullanıldığı, üniversitelerin akademisyenleri; akademisyenlerin ise öğrencilerini teşvik edip etmediği, YZ ürünlerinin ücretli olmasının kullanım yaygınlığı konusunda bir engel teşkil edip etmediği, akademisyenlerin bu ürünleri özel yaşantılarında da kullanıp kullanmadığı ve ayrıca intihal, telif, patent ve mahremiyet alanlarında yeni ortaya çıkan konu ve sorunlara bakışları ve algıları konusunda Şekil 1 ve Şekil 2 önemli oranda konuyu özetlemektedir.

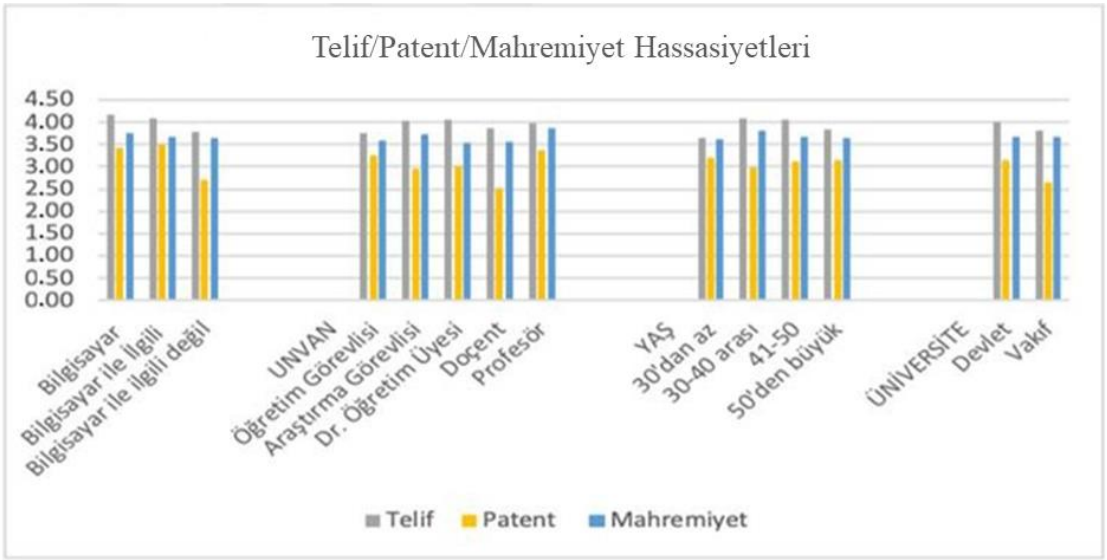

Şekil 2. *Türkiye'de akademisyenlerin telif, patent ve mahremiyet konularındaki algılarının bölüm-unvan-yaş ve üniversite özellikleri bağlı olarak nasıl değiştiğini gösteren likert dağılımı*

Çalışmanın kolay anlaşılması ve değerlendirilmesi için ise YZ ürünlerinin kullanımı konusunda bölüm-unvan-yaş ve üniversite özelliklerinin belirgin ve anlamlı farklar yaratmadığı anlaşılmaktadır. Bu alanda önemi vurgulanması gereken konu; telif, patent ve mahremiyet alanlarındaki algı düzeyinde temel olarak katılımcılar arasında belirgin ve anlamlı bir fark olmamakla birlikte üç alanda da profesör olan katılımcıların diğerlerinden belirgin şekilde daha duyarlı olduğu gözlemlenmiş olduğudur. Öte yandan Şekil 2'deki çalışma yine tüm gruplara (bölüm-unvan-yaş ve üniversite özellikleri) birlikte bakıldığında en yüksek hassasiyetin telif ve intihal alanında olduğu bunu mahremiyet kaygılarının takip ettiği ve en az duyarlılığın ise patent konularında olduğu görülmektedir. YZ ürün ve araçlarının akademik camiada kullanımının araştırıldığı çalışmada, ankete verilen cevaplar ileri matematik tabanlı araçlar ile grafik ve görsel olarak analiz edilmiştir. Buna göre genel olarak (telif, patent ve mahremiyet) konularında duyarlı olduğu ancak bunun içinde en yüksek duyarlılığın ise telif hakları ve intihal konuları olduğu ifade edilebilir. Likert ölçeğine göre elde edilen sonuçların 5 üzerinden 5'e yakın olduğu anlaşılmaktadır. Bununla birlikte 'profesör' grubunun tüm alanlarda olduğu gibi intihal konusunda da diğer tüm gruplardan daha duyarlı olduğu gözlenmiştir. Çalışmaya başlarken, akademisyenin görev yaptığı alanın bilgisayar ve bununla yakın ilişkili bir bölüm olması halinde bunun YZ kullanımı konusunda önemli bir ayraç olabileceği beklenmiştir. Elde edilen sonuçlar ise bu hipotezin doğru olduğunu ve YZ ürünlerini kullanım yaygınlığı ve çeşitliliği bakımından önemli ve anlamlı fark ortaya koyduğunu göstermiştir. Buna göre bilgisayar ve ilgili bölümlerde görev yapan akademisyenler YZ konuları ve ürünleri ile ilgili daha bilgili ve potansiyel risk ve sonuçlarından da daha çok haberdardır. Benzer şekilde, bilim alanı bilgisayar ve bununla doğrudan ilgili alanlarda görev yapan akademisyenlerin kendi güvenliklerini almış oldukları düşüncesiyle mahremiyet ihlali konusunda duydukları endişe bakımından daha farklı sonuçlar elde edilme ihtimali yüksek görülmüştü. Ancak bu konuda duyulan endişe bakımından bilgisayar bilim alanında çalışanlar ile diğerleri arasında anlamlı bir fark olmadığı görülmüştür. Anlaşılan odur ki, YZ ürünlerinin kişilerin özellikle ses ve görüntülerini açık kaynaklardan elde edilen verilerle yapılan taklitlerinin insan göz ve kulağıyla gerçeğinden ayrılamayacak düzeye geldiği ve mevzuattaki boşluk ile birlikte düşünüldüğünde alınacak önlemlerin yetersiz ve sınırlı olduğu bilinci sadece bilgisayar bilim alanında değil tüm diğer alanlarda görev yapan akademisyenlerde de yeterince oluşmuştur. Çalışmaya başlarken veri dağılımının üniversite özelliği (devlet-vakıf) bakımından değişmemesi beklenmiştir. Bunun sebebi ise ülkemizin içinde bulunduğu ekonomik koşullar ve buna bağlı olarak çalışanların haklarının geri gittiğine ilişkin gözlemlerimizdir. Üniversitelerin vakıf veya devlet üniversitesi olmasının vizyon ve misyonları bakımından çok önemli bir değişime sebep olabilecek olanaklar ya da kurumsal kültür farklılığı getirmeyeceği düşünülmüş araştırma sonuçlarının ise bu hipotezi doğrulamıştır. Buna göre YZ kullanımı ve YZ ile ortaya çıkan yenilikler ve yeni bakış açıları konusunda üniversitenin türünün belirgin bir ayraç olmadığı sonucuna varılmıştır. Araştırmadan elde edilen sonuçlara göre genel olarak ülkemizdeki üniversitelerde görev yapan akademisyenlerin bu alanda likert

ölçeği baz alınarak 5 üzerinden 3 yani orta seviyede yer aldıkları gözlemlenmiştir. Yani ne bu konuları önemsiz ve ilgisiz gören ne de bu konularda bilgi veren durumda oldukları ortaya çıkmıştır.

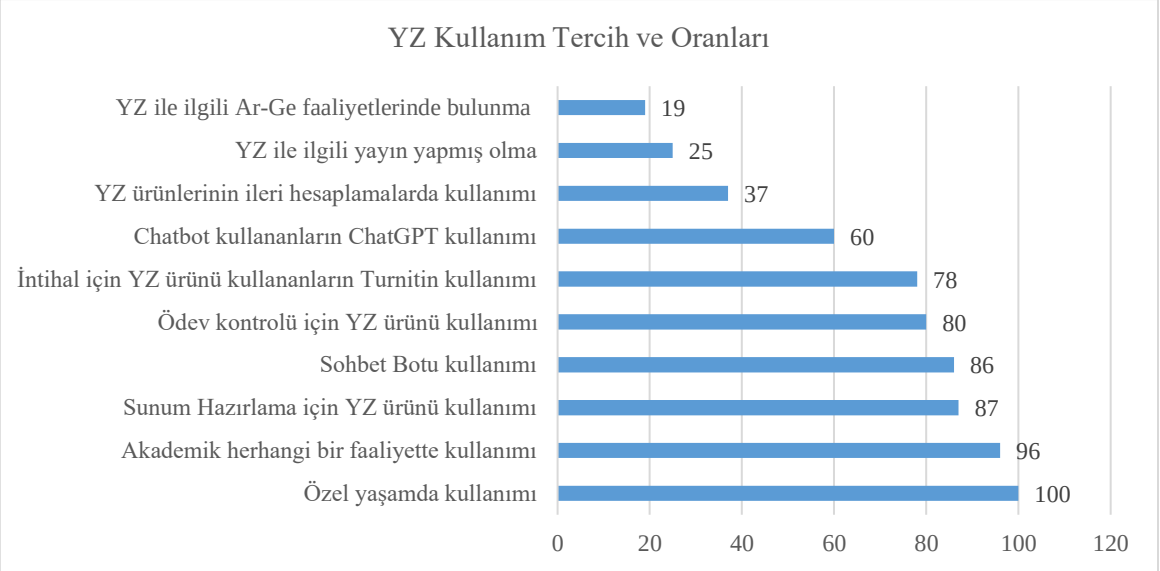

Şekil 3. *Türkiye'de akademisyenlerin YZ ürünlerini kullanımı konusundaki tercihleri ve oranları*

YZ Ürünlerinin Kullanımı Konusunda Öne Çıkan Konular

Şekil 3'de genel olarak akademisyenlerin özel yaşantısında mutlaka ve en az bir YZ ürünü kullandığı anlaşılmaktadır. Bununla birlikte, akademik herhangi bir faaliyette YZ ürünü kullanımının da hemen hemen bütün akademisyenlerde yaygın olduğu anlaşılmaktadır. Bunların içinde ise sunum hazırlama faaliyeti öne çıkmaktadır. Göze çarpan bir diğer husus ise çok bilinen bir YZ sohbet botunun ve intihal için kullanılan ve yine çok bilinen bir aracın kullanımının da açık ara önde olduğu anlaşılmaktadır. Söz konusu YZ araçları (ileri hesaplamalar, kod üretimi), YZ konusunda yayın ve Ar-Ge faaliyetlerine katılmak olunca bu oranlar düşmekle birlikte yine de umut verici düzeyde faaliyetler olduğu anlaşılmıştır.

YZ ürünlerinin kullanımı konusunda üniversitelerin tutumu

Bu konuda öncelikle vakıf ve devlet üniversiteleri arasında anlamlı ve belirgin bir fark olmadığı görülmüştür. Genel ortalamaya bakıldığında ise üniversitelerin bu konuda ne teşvik eden ne de yasaklamaya çalışan bir durumda olduğu anlaşılmaktadır. Daha açık bir ifadeyle bu alanda akademik yönetimlerin belirgin bir politika ve stratejiye sahip olmadıkları anlaşılmaktadır. Akademisyenlerin ücretli veya ücretsiz YZ ürünlerini kullanımı konusundaki tutumu, büyük bir oranda ücretsiz YZ ürünlerini kullanmaya yöneliktir. Ücretli YZ ürünlerinin dolar ve avro gibi para birimleri üzerinden satışının yapılması karşısında, ülkemizdeki genel alım gücü, kur paritesi ve akademisyenlerin maaş dilimine birlikte bakıldığında bu alandaki ödemelerin akademisyenler açısından zor olduğu ve bu yüzden ücretsiz ürünlere yöneldikleri çıkarımını yapmak doğal bir sonuçtur.

Akademisyenlerin hangi YZ ürünlerini tercih ettiği konusundaki bulgular

Araştırma sonuçlarında akademisyenlerin yukarıda da belirtildiği gibi öncelikle ücretsiz ürünleri kullanmaya yöneldikleri anlaşılmıştır. Ancak intihal konusunda ise akademisyenlerin ücret ödemedikleri bununla birlikte aboneliği üniversiteler/enstitüler tarafından sağlanan ücretli programların kullanıldığı görülmüştür. Akademisyenlerin değişik alanlarda çok çeşitli YZ ürünlerini kullanmaları konusuna ücret politikasının engel olduğu çıkarımını yapmak yerinde olacaktır.

Akademisyenlerin meslek ve özel yaşantılarında tercih ettiği YZ ürünleri

Öncelikle sohbet botları konusunda ücretsiz kullanımı mümkün olan, çok bilinen sohbet botunun kullanımının diğer tüm ürünlere göre açık ara önde olduğu görülmüştür. Bununla birlikte bilinme oranı bakımından hemen ardından gelen ve yine ücretsiz versiyonları olan iki diğer sohbet botu ürününün de kullanım bakımından ön sıralarda olduğu anlaşılmaktadır. Ayrıca GitHub, Turnitin gibi ürünlerin de yaygın kullanıldığı anlaşılmıştır. Özel ve belli alanlarda kullanılan YZ ürünlerinin ise özellikle bilgisayar ve bununla ilgili bilim alanlarına mensup akademisyenler tarafından kullanıldığı ancak yine ekonomik sebeplerle olduğunu düşündüren şekilde istenilen yaygınlık seviyesinde olmadığı görülmüştür. YZ ile birlikte öne çıkan konulardan birisi de "telif hakları" ve buna dair ihlallerin kolaylaşması olmuştur. YZ ürünleri bir yandan intihali kolaylaştırmıştır. Ancak öte yandan bu konudaki başka ürünlerle bu ihlallerin tespitini de daha kolay bir hale getirmiştir. Bu çerçevede kelimesi kelimesine yapılan intihaller, yerini YZ ürünleri aracılığıyla yeniden yazım tekniklerine bırakacak gibi durmaktadır. Ancak bu defa bunun adı "intihal" değil olsa olsa "fikir hırsızlığı" olabilir. YZ ürünleri kullanılarak yapılacak muhtemel fikir hırsızlıkları ise fikri mülkiyet hakları kapsamında ele alınması mümkün olmayan konulardır. İntihal, başkasının çalışmasını izinsiz olarak kullanmak ve kendi çalışmasıymış gibi sunmak olarak tanımlanmaktadır. Oysa Fikir Hırsızlığı ise özgün fikirlerin veya konseptlerin izinsiz kullanımıdır [9]. Kuşkusuz ki önümüzdeki günlerde hem bu fikirler mülkiyet kapsamından çıkacak hem de tespit edebilecek yeni ürünler ortaya çıkacak ve buna dayalı olarak da yeni etik ve yasal kodlar gelişecektir. Araştırmadan elde edilen verilere dayanarak, akademisyenlerin YZ ürünlerini akademik faaliyetlerin en az bir alanında olacak şekilde kullanımı akademisyenlerin neredeyse tamamında kullandıkları görülmektedir. YZ kullanımının artan bir trend içinde olduğu, intihal ve sunum hazırlamanın yanı sıra akademisyenlerin özel hayatlarında da bu ürünlerin kullanımının çok yaygın olduğu ve tercih edildiği görülmüştür. Ancak daha ileri uygulamalar için özellikle paralı ürünlerin kullanılması gerektiği anlaşılmakta ve bu konuda akademisyenlerin kurumsal olarak desteklenmesi gerektiği açık şekilde görülmektedir.

Sonuçlar

Bu çalışma, Türkiye'deki akademisyenlerin Yapay Zekâ (YZ) teknolojilerini kullanım alışkanlıklarını, tercihlerini ve bu teknolojilerin karşılaştığı hukuki, etik ve mahremiyetle ilgili sorunları incelemiştir. Akademisyenlerin büyük çoğunluğunun YZ ürünlerine olumlu yaklaştığı ancak kullanımın yetersiz

kaldığı tespit edilmiştir. Bu durum, üniversitelerin ve akademik kurumların YZ politikalarını netleştirmesi ve geliştirmesi gerekliliğini ortaya koymaktadır. Araştırma sonuçları ülkemizde YZ konusunda yeterli bir bilinç düzeyinin olduğunu ancak kullanımı konusunda başta ekonomik olmak üzere çeşitli engellerin olduğunu ortaya koymuştur. Diğer engeller ise öncelikle mevzuata dayalı engeller, politika yetersizliği ve bazı güvenlik kaygılarıdır. Araştırmamız, katılımcıların ücretsiz ürünlere yöneldiğini açıkça ortaya koymuştur. Her yenilikte olduğu gibi bu alanda da mevzuat fiili durumun arkasından gelecektir. Ancak geçiş aşamasında boşluklar ve eksiklikler olması son derece normaldir. Bu durum üniversitelerin bağımsız ya da merkezi yönlendirmeye dayalı politika geliştirmesine engel teşkil etmektedir. Ayrıca her geçen gün bir yenisi görülen ve gerçeğinden ayırt edilemeyen ses ve görüntü teknolojileri, kullanıcılar üzerinde açıkça kaygı oluşturmuştur. İster bu alandaki ürünleri kullansın isterse kullanmasın neredeyse tüm akademik personelin bu açıdan kaygılı olması bu bulgumuzun temelini teşkil etmektedir. Akademik camiada, intihal ve telif haklarına ilişkin bilinç yüksek olmakla birlikte, YZ ürünlerinin bu sorunları hem kolaylaştırdığı hem de tespitini sağladığı çelişkisi gözlemlenmiştir. Ayrıca, akademisyenlerin mahremiyet konusunda endişeleri bulunmakta, ancak bu endişelerin bölüm-unvan-yaş ve üniversite özellikleri gibi demografik faktörlere bağlı olarak anlamlı ve belirgin farklılık göstermediği belirlenmiştir. Başka bir ifadeyle mahremiyet konusunda tüm kesimler ve gruplar belirgin şekilde kaygı taşımaktadır. Sadece profesör unvanlı grubun, diğer tüm alanlardaki kaygı ve hassasiyetlerinde olduğu gibi bu konudaki kaygı ve hassasiyeti de diğerlerine oranla daha yüksektir. Bu bağlamda, üniversitelerin ve diğer akademik kurumların YZ kullanımını teşvik etmek amacıyla şu öneriler sunulmaktadır:

Eğitim Programları ve Seminerler

Akademisyenlerin YZ ürünlerini daha bilinçli ve etik bir şekilde kullanmalarını teşvik etmek için eğitim programları ve seminerler düzenlenmelidir.

Ekonomik Destekler ve Sair Teşvikler

Ülkemizdeki ekonomik sorunlar akademik camiayı da derinden etkilemektedir. Akademisyenler ücretsiz ürünleri kullanma konusunda istekli iken ücretli sohbet botlarından uzak durmaktadırlar. Akademisyenler bu alanda desteklenirse başarılı sonuçlar alınacağı düşünülmektedir. Akademisyenlerin bu konulardaki kullanımlarına ve akademik çalışmalarına çeşitli ödül, puan vs. teşvikler de sunulmalıdır.

İntihalle Mücadele

Üniversiteler, intihalle mücadelede YZ ürünlerinin etkin kullanımını destekleyecek kaynakları sağlamalıdır. Ayrıca yeni nesil bir intihal ve özgünlük anlayışı geliştirilmeli ve hukuki boyutlarıyla ele alınmalıdır. Zira eski intihal anlayışı giderek kendisini yeni nesil bir anlayışa bırakacak gibidir.

Patent Bilinci

Esasen bu alanda patent ve faydalı model başvuruları bakımında genel bir zaaf görülmüştür. Akademik çalışmalarla birlikte bu alanda da teşvikler sunulması gereklidir. Patent konusundaki zaafın konunun önemsizliğinden daha çok akademisyenlerin gündeminde yer almaması ile ilgili olduğu düşüncesi ağır basmaktadır. Konunun bu boyutuyla yani yeni icat ve keşifler yapacak akademisyenler yetiştirme bakımından da ele alınmasında fayda görülmektedir.

Mahremiyet Bilinci

Mahremiyet konusunda bilinçlendirici seminerler ve atölye çalışmaları düzenlenmeli, akademik yükselme kriterleri arasına mahremiyetle ilgili çalışmalar dâhil edilmelidir.

Hukuki ve Etik Düzenlemeler

YZ kullanımını düzenleyen hukuki çerçeveler oluşturulmalı ve güncellenmeli, etik kurallar netleştirilmelidir. Bu düzenlemeler öncelikle yukarıda sayılan intihal, patent ve mahremiyet konularında yoğunlaşmalıdır. Ancak bu konular giderek ceza gibi yaptırım gücü yüksek alanlara da girmek zorunda kalacaktır. Şimdilik ve en azından akademik alanda yapılacak düzenlemeler akademik yayınlara farklı bir değerlendirme ve boyut katacak düzeyde olmalıdır.

Şeffaflık ve Hesap Verebilirlik

Geliştirici firmalar, YZ algoritmalarının çalışma prensiplerini açık ve anlaşılır bir şekilde sunmalı, kullanıcı verilerinin korunması için şeffaf politikalar geliştirmelidir. Bu sayede özellikle telif, patent ve mahremiyet konularında alınacak önlemler için geliştiricilerin işi kolaylaştırılmalıdır.

Kurumsal Politikalar

Tüm bu konuları içeren Hükümet, YÖK, Türkiye Bilimsel ve Teknik Araştırma Kurumu (TÜBİTAK) ve üniversitelerin kurumsal destekleyici politikaları olmalıdır. Akademisyenler bu konudaki çalışmalarında kendilerini yalnız hissetmelerinin önüne geçilmelidir. Akademisyenler akademik ve Ar-Ge faaliyetlerinde, başta görev yaptıkları kurumlar olmak üzere Hükümet, YÖK, TÜBİTAK ve tüm akademik camianın desteğini arkalarında hissetmelidir. Bu bağlamda, akademisyenlerin ve araştırmacıların YZ ürünlerini kullanırken mahremiyet ve kişisel veri güvenliği konusunda bilinçli ve dikkatli olmaları gerekmektedir. Üreticilerden güvenli ve şeffaf ürünler talep etmek ve hükümetlerin bu konuda düzenleyici önlemler alması bu süreçte kritik rol oynayacaktır. Bu çalışma, gelecekteki araştırmalar için bir temel oluşturmak ve YZ teknolojilerinin eğitim ve araştırma alanlarındaki potansiyelini daha iyi anlamak ve kullanmak için yürütülmüştür. Elde edilen bulgular, YZ teknolojisinin ve ürünlerinin akademik camiada daha etkili bir şekilde entegrasyonuna yardımcı olacak stratejilerin geliştirilmesine katkı sağlayacaktır.

Teşekkür Necmettin Erbakan Üniversitesi Ahmet Keleşoğlu Eğitim Fakültesi Ölçme ve Değerlendirme Anabilim Dalı Başkanı Prof. Dr. Ercan YILMAZ'a ve Hacettepe Üniversitesi Eğitim Fakültesi Ölçme ve Değerlendirme Ana Bilim Dalı Başkanı Prof. Dr. Selahattin GELBAL'a katkılarından dolayı çok teşekkür ederiz.

Fon/Finansman bilgileri Herhangi bir kurum veya kuruluş tarafından desteklenmemiştir.

Etik Kurul Onayı ve İzinler "Türkiye'deki Akademisyenlerin Yapay Zeka (YZ) Ürünlerini (Uygulama ve Araçlarını) Kullanımları Hakkında Bir Araştırma" başlıklı araştırma Hacettepe Üniversitesi Sosyal ve Beşerî Bilimler Araştırma Etik Kurulunun 12.10.2023 tarih E-66777842-900-00003135694 sayılı onayı ile etik açıdan uygun bulunmuştur.

Çıkar çatışmaları/Çatışan çıkarlar- Herhangi bir çıkar çatışması yoktur.

Yazarların Katkısı- Yazarlar çalışmaya eşit oranda katkı sağlamışlardır. Yazarlar makalenin son halini okumuş ve onaylamıştır.

Kaynaklar

[1] Seaman, W. (2014). A multi-perspective approach to knowledge production. *Kybernetes*, *43*(9/10), 1412-1424.

[2] Russell, S. J., & Norvig, P. (2010). *Artificial Intelligence A Modern Approach*. London.

[3] Lee, S. (2023). Book Review: Algorithms of Oppression: How Search Engines Reinforce Racism. *InterActions: UCLA Journal of Education and Information Studies*, *18*(1). https://doi.org/10.5070/D418160873

[4] Amodei, D., Olah, C., Steinhardt, J., Christiano, P., Schulman, J., & Mané, D. (2016). Concrete problems in AI safety. *arXiv preprint arXiv:1606.06565*. https://doi.org/10.48550/arXiv.1606.06565

[5] Bostrom, N., & Yudkowsky, E. (2018). The ethics of artificial intelligence. In *Artificial intelligence safety and security* (pp. 57-69). Chapman and Hall/CRC.

[6] Asaro, P. (2012). On banning autonomous weapon systems: human rights, automation, and the dehumanization of lethal decision-making. *International review of the Red Cross*, *94*(886), 687-709. https://doi.org/10.1017/S1816383112000768

[7] Pagallo, U. (2013). *The laws of robots: Crimes, contracts, and torts* (Vol. 10). Springer Science & Business Media.

[8] Turner, J. (2018). *Robot rules: Regulating artificial intelligence*. Springer.

[9] Senders, S. (2008). Academic plagiarism and the limits of theft. *Originality, imitation, and plagiarism: Teaching writing in the digital age*, 195-207.

[10] Burk, D. L., & Lemley, M. A. (2003). Policy levers in patent law. *Virginia Law Review*, 1575-1696. https://doi.org/10.2307/3202360

[11] Samuelson, P. (2010). Legislative Alternatives to the Google Book Settlement. *The Columbia Journal of Law & the Arts*, *34*, 697.

[12] Menell, P. S., Lemley, M. A., Merges, R. P., & Balganesh, S. (2023). *Intellectual Property in the New Technological Age, Vol. I: Perspectives, Trade Secrets and Patents*. Faculty Books. 374.

[13] Chen, X., Xie, H., & Hwang, G. J. (2020). A multi-perspective study on artificial intelligence in education: Grants, conferences, journals, software tools, institutions, and researchers. *Computers and Education: Artificial Intelligence, 1*, 100005. https://doi.org/10.1016/j.caeai.2020.100005

[14] Dean, J. (2014). *Big data, data mining, and machine learning: value creation for business leaders and practitioners*. John Wiley & Sons.

[15] Abbott, R. (2016). I think, therefore I invent: creative computers and the future of patent law. *Boston College Law Review*, *57*, 1079.

[16] Calo, R. (2011). The boundaries of privacy harm. *Indiana Law Journal*, *86*, 1131.

[17] Schwartz, P. M., & Solove, D. J. (2014). Reconciling personal information in the United States and European Union. *California Law Review*, *102*, 877.

[18] Taylor, L., Floridi, L., & Van der Sloot, B. (Eds.). (2016). *Group privacy: New challenges of data Technologies (Vol. 126)*. Springer.

[19] Tene, O., & Polonetsky, J. (2012). Big data for all: Privacy and user control in the age of analytics. *Nortwestern Journal of Technology and Intellectual Property, 11*, 239.

[20] McReynolds, E., Hubbard, S., Lau, T., Saraf, A., Cakmak, M., & Roesner, F. (2017, May). Toys that listen: A study of parents, children, and internet-connected toys. In *Proceedings of the 2017 CHI conference on human factors in computing systems* (pp. 5197-5207). https://doi.org/10.1145/3025453.3025735

[21] Garvie, C. (2016). *The perpetual line-up: Unregulated police face recognition in America*. Georgetown Law, Center on Privacy & Technology.

[22] Hon, W. K., Millard, C., & Walden, I. (2012). Negotiating cloud contracts: Looking at clouds from both sides now. *Stanford Technology Law Review, 16*, 79.

[23] Koops, B. J. (2014). The trouble with European data protection law. *International data privacy law*, *4*(4), 250-261. https://doi.org/10.1093/idpl/ipu023

[24] Mittelstadt, B. D., Allo, P., Taddeo, M., Wachter, S., & Floridi, L. (2016). The ethics of algorithms: Mapping the debate. *Big Data & Society*, *3*(2), 2053951716679679. https://doi.org/10.1177/2053951716679679

[25] Olejniczak, K., Borkowska-Waszak, S., Domaradzka-Widła, A., & Park, Y. (2020). Policy labs: the next frontier of policy design and evaluation?. *Policy & Politics*, *48*(1), 89-110. https://doi.org/10.1332/030557319X15579230420108

[26] Lahti, R. J. (2020). Making Accessibility Services Accessible Through Implementation of Information and Communication Technology. *The Organizational Improvement Plan at Western University, 134.*

[27] Yükseköğretim Bilgi Yönetim Sistemi (2023, Ağustos 30). *Öğrenci İstatistikleri*.

[28] Bayat, B. (2014). Uygulamalı sosyal bilim araştırmalarında ölçme, ölçekler ve "likert" ölçek kurma tekniği. *Gazi Üniversitesi İktisadi ve İdari Bilimler Fakültesi Dergisi, 16*(3), 1-24.

Sinopfbd, 2024; 9(1): 145-153 **https://doi.org/10.33484/sinopfbd.1377778**

Sinop Üniversitesi Fen Bilimleri Dergisi
Sinop Uni J Nat Sci
E-ISSN: 2564-7873

https://dergipark.org.tr/tr/pub/sinopfbd

Farklı İndüktif Etkilere Sahip Yan Gruplar İçeren Naftalimit Türevlerinin DNA Bağlanma Aktivitelerinin Belirlenmesi

Ufuk YILDIZ[1], Fatma ÖZLEMİŞ[1], Melek ÜNAL[1] ve Güldan AYDIN[1]

How to cite: Yıldız, U., Özlemiş, F., Ünal, M., & Aydın, G. (2024). Farklı indüktif etkilere sahip yan gruplar içeren naftalimit türevlerinin DNA bağlanma aktivitelerinin belirlenmesi. *Sinop Üniversitesi Fen Bilimleri Dergisi*, *9*(1), 145-153. https://doi.org/10.33484/sinopfbd.1377778

Araştırma Makalesi

Sorumlu Yazar
Ufuk YILDIZ
ufukyildiz@beun.edu.tr

Yazarlara ait ORCID
U.Y: 0000-0002-0419-0011
F.Ö: 0009-0008-4017-5063
M.Ü: 0009-0003-1200-5765
G.A: 0009-0009-8962-869X

Received: 19.10.2023
Accepted: 04.05.2024

Öz

Naftalimit türevleri, son yıllarda yapılan çalışmalarda yüksek biyolojik aktiviteye sahip bileşikler olarak karşımıza çıkmaktadır. Bu doğrultuda yeni türevlerin DNA etkileşim yollarının belirlenmesi ve literatüre kazandırılması büyük önem taşımaktadır. Bu çalışmada farklı yan gruplar içeren naftalimit türevlerinin DNA etkileşimleri incelenmiştir. UV titrasyonu ile bağlanma türünün interkalasyon olduğu anlaşılmıştır. Etidyumbromür ile yarışmalı floresans deneyleri gerçekleştirilerek bağlanma türü hakkında daha kesin bilgiler elde edilmiştir. Bileşiklerin plazmid DNA üzerinde gerçekleştirdikleri form değişiklikleri agaroz jel elektroforez yöntemiyle incelenmiş ve aktif konsantrasyona karar verilmiştir.

Anahtar Kelimeler: DNA, interkalasyon, naftalimit

Determination of DNA Binding Activities of Naphthalimide Derivatives Containing Side Groups with Different Inductive Effects

[1]Zonguldak Bülent Ecevit Üniversitesi, Fen Fakültesi, Kimya Bölümü, Zonguldak, Türkiye

Abstract

Naphthalimide derivatives appear as compounds with high biological activity in recent studies. In this regard, it is of great importance to determine the DNA interaction pathways of new derivatives and introduce them to literature. In this study, DNA interactions of naphthalimide derivatives containing different side groups were examined. It was understood by UV titration that the binding mode was intercalation. More precise information about the binding mode was obtained by performing competitive fluorescence experiments with ethidium bromide. The form changes of the compounds on plasmid DNA were examined by agarose gel electrophoresis method and the active concentration was decided.

Keywords: DNA, intercalation, naphthalimide

Giriş

Heterosiklik bileşikler medisinal kimya alanında birçok uygulama alanına sahip önemli bir ligant grubudur. Bu türevler gösterdikleri antifungal, antikanser, antibakteriyel ve antiviral gibi birçok aktiviteleri sayesinde çok ilgi çekmektedir [1-4]. Günümüzde kullanılan heterosiklik kemoterapik

ajanların büyük kısmı DNA'ya bağlanan ilaçlardan oluşmaktadır [5, 6]. Küçük heterosiklik bileşiklerin DNA bağlanma aktivitelerinin incelenmesi yeni antikanser ajanların geliştirilmesinde önemli bilgiler sağlayacaktır. Naftalimit temelli bileşikler, aynı anda hem florofor hem de π-elektronları yoksunu bir aromatik sistem içerdiklerinden dolayı yeni antikanser ajanların geliştirilmesi için iyi aday moleküllerdir [7-10]. Naftalimitler iyi birer DNA interkalatörtürler ve topo II enzimini inhibe edebilmektedirler [11]. Bu tür bileşiklerin biyolojik çalışmaları incelendiğinde, bileşiklerin DNA hasarı yapmadan DNA'yı hedefleyebildikleri görülmüştür. Bu durum potansiyel antikanser ajanların yan etkilerini azaltmaktadır [12]. Naftalimitlerin farklı pozisyonlar üzerinden modifiye edilmesi yan etkilerin düşürülmesi için etkili bir yoldur [13, 14]. Hatta naftalen halkası üzerindeki 4-pozisyonundan yapılan sübstitüent değişimlerinin antitümör aktivite üzerinde anahtar konumda olduğu anlaşılmıştır [9, 15]. Bunun yanında anhidrit grubu üzerinden eklemlenecek yeni halkalar, naftalimit bileşiğinin yüzey alanını genişleterek interkalasyon yapma yeteneğini artıracaktır. Bu çalışma kapsamında daha önce sentezlenerek literatüre kazandırılmış [16], geniş π-elektron dağılımına sahip ve 4-pozisyonu üzerinden farklı indüktif etki gösterebilecek fonksiyonel grup içeren 3 naftalimit türevinin (Şekil 1) DNA bağlanma aktivitelerinin belirlenerek düşük yan etkiye sahip olabilecek yeni antikanser ajanlar olarak önerilmesi amaçlanmıştır.

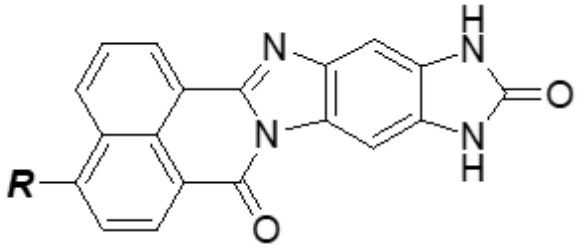

R = -H (**1**), -NO_2 (**2**) -NH_2 (**3**)

Şekil 1. *Çalışma kapsamında DNA bağlanma aktiviteleri incelenen bileşikler*

Materyal ve Metot

Materyaller ve Cihazlar

Tüm reaktifler ve çözücüler ticari olarak alınmıştır ve aksi belirtilmedikçe daha fazla saflaştırılmadan kullanılmıştır. Dana timus DNA'sı (CT-DNA, Sigma'dan satın alınmıştır) çözeltileri 100 mM KCl, 10 mM Tris (pH 7,5) tampon içerisinde hazırlanmıştır. DNA çözeltilerinin konsantrosyonu 260 nm dalga boyunda spektroskopik olarak belirlenmiştir (ϵ=6600 $M^{-1}cm^{-1}$). UV-Vis absorbsiyon ölçümleri Varian Cary 100 spektrofotometre cihazı kullanılarak gerçekleştirilmiştir. Yatay elektroforez çalışmasında Thermo Electron Corporation EC-330 Midicell Primo sistemi kullanılmıştır. Emisyon spektrumları PerkinElmer LS55 spektroflorometre kullanılarak kaydedilmiştir.

DNA Bağlanma Aktivite Çalışmaları

UV-Vis Absorspsiyon Titrasyonları

Bileşiklerin çözeltileri, minimum miktarda DMSO içerisinde çözüldükten sonra Tris-HCl (pH 7.5) kullanılarak 20 µM konsantrosyona seyreltilerek hazırlanmıştır. Daha sonra bileşiklerin UV-Vis spektrumu kaydedilmiş ve 1.25 mM ct-DNA çözeltisinden 2 µl'lik porsiyonlar halinde bileşik çözeltisi üzerine eklenerek spektrum tekrar kaydedilmiştir. Titrasyona spektrumda değişiklik görülmeyinceye kadar devam edilmiştir.

Emisyon Titrasyonları

Bileşiklerin etidyumbromür (EB) ile yarışmalı olarak DNA'ya bağlanma kapasiteleri floresans spektroskopisi ile incelenmiştir. DNA-EB kompleks çözeltisi DNA:EB oranı 50:1 olacak şekilde hazırlanmış ve etkileşimin tamamlanması için 27 °C sıcaklıkta 30 dakika bekletilmiştir. Daha sonra 427 nm dalgaboyunda uyarılarak emisyon spektrumu kaydedilmiştir. Bileşiğin DNA baz çiftleri arasından EB moleküllerini çıkarma gücünü ölçmek için 1 µl'lik porsiyonlar halinde 1 mM stok bileşik çözeltisinden eklenerek spektrum tekrar kaydedilmiştir.

Agaroz Jel ile DNA Kırılma Çalışmaları

Jel elektroforez çalışmaları TBE tamponu içerisinde süper sarmal plazmit DNA olan pBR322 kullanılarak %1'lik agaroz jel üzerinde gerçekleştirilmiştir. 10 µl hacme sahip reaksiyon karışımları 0.1 µg pBR322 ve farklı konsantrasyonlarda (0, 20, 40, 60, 100 ve 200 µM) 1, 2 ve 3 numaralı bileşikleri içerecek şekilde hazırlanmıştır. Hazırlanan karışımlar 1 saat boyunca 36 °C sıcaklıkta inkübe edilmiştir. Hazırlanan karışımlara 2.5 µl %0.25 bromofenol eklendikten sonra jele yüklenmiştir ve 35 V ile 4 saat boyunca elektrik akımı uygulanmıştır. Son olarak jel EB çözeltisi içerisinde boyanmış ve UV ışığı altında fotoğraflanmıştır.

Sonuçlar

UV-Vis Absorspsiyon Titrasyonları

UV-Vis spektroskopisi, DNA ve küçük moleküller arasındaki etkileşimleri incelemek için sıklıkla kullanılan önemli bir yöntemdir. Elektrostatik etkileşimler, oluk bağlama ve interkalasyon gibi etkileşim türlerinin belirlenmesinde çok faydalıdır. Küçük moleküller DNA ile oluk bağlanma modu ile etkileşirken, hidrojen bağı veya van der Waals etkileşimleri oluşur ve bir nükleik asit bazı ile bir bileşik arasındaki etkileşim sonucu maksimum absorbans pikinde hiperkromizm gözlemlenir. İnterkalasyon yoluyla DNA'ya bağlanan durumlarda, genellikle hipokromizm ile birlikte batokromizm gözlenir [17]. Sabit porsiyonlar halinde ct-DNA ilavesi sonrası bileşiklere ait UV-Vis spektrumlarında 300 nm civarında interkalasyon ile uyumlu olan hipokromizm gözlenmiştir (Şekil 2).

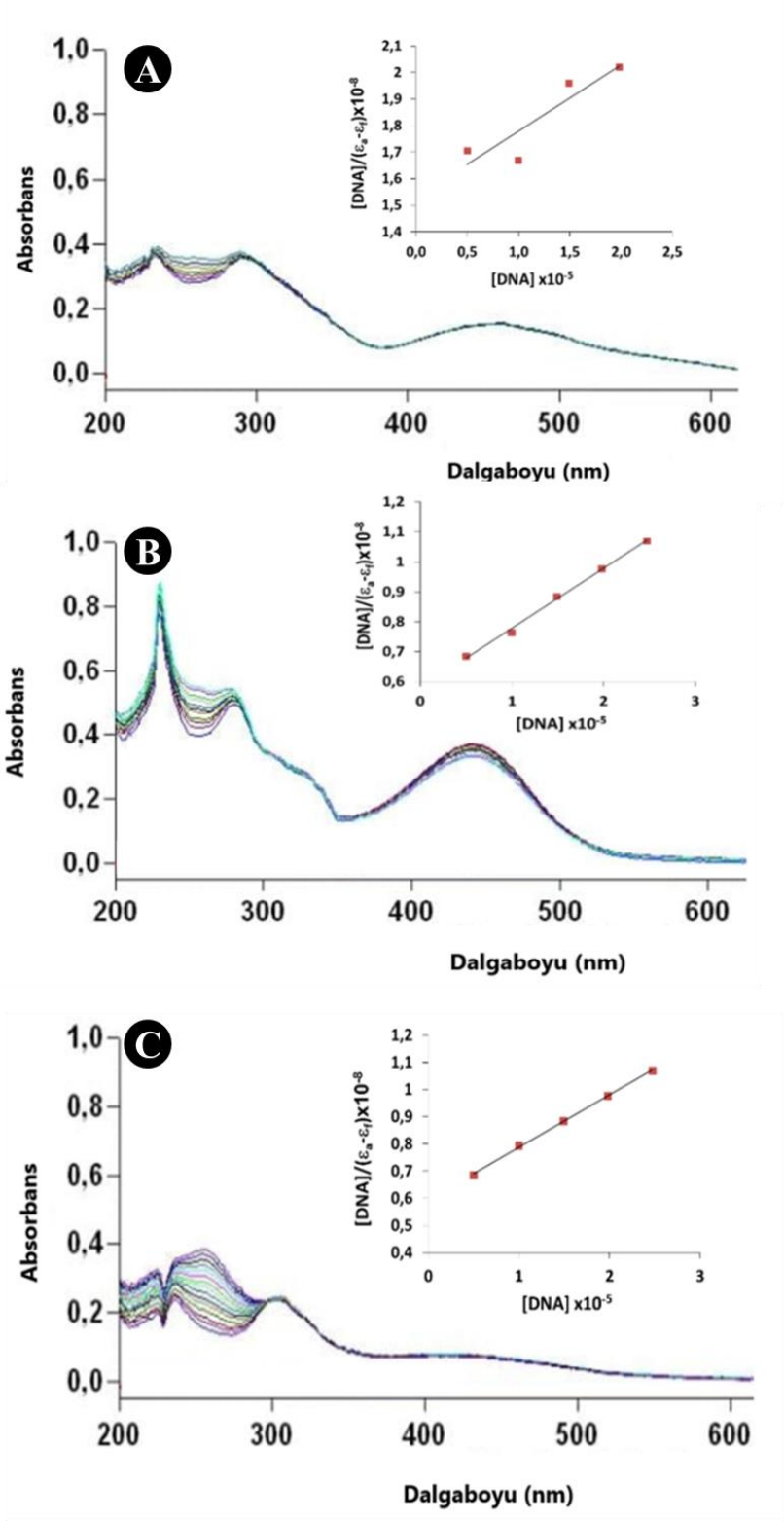

Şekil 2. *1 (A), 2 (B) ve 3 (C) numaralı bileşikler için UV-Vis titrasyon spektrumları*

Titrasyon sonucu elde edilen değerler sayesinde bileşiklerin DNA'ya hangi kuvvetle bağlandığını gösteren bağlanma sabiti (K_b) değerleri hesaplanmıştır.

$$[DNA] / (\varepsilon_A - \varepsilon_f) = [DNA] / (\varepsilon_B - \varepsilon_f) + 1 / K_b (\varepsilon_B - \varepsilon_f) \quad (1)$$

Formülde ε_A; ölçülen konsantrosyandaki sönüm katsayısı, ε_B; DNA'ya tüm bileşiğin bağlanması sonrasındaki sönüm katsayısı ve ε_f; serbest haldeki bileşiğin sönüm katsayısı olarak açıklanabilir. Hesaplama sonucu elde edilen bağlanma sabitleri sırasıyla 1,75 x 10^4, 3,05 x 10^4 ve 3,32 x 10^4 M^{-1} olarak bulunmuştur.

EB ile Yarışmalı Emisyon Titrasyonu Sonuçları

Yarışmalı emisyon titrasyonu DNA'ya interkalasyon yoluyla bağlanmış EB moleküllerinin çalışılan bileşik tarafından yerinden çıkarılmasının incelendiği bir yöntemdir. Sulu çözeltilerde EB molekülü çok düşük emisyon vermektedir. Ancak ortama DNA eklendiğinde EB molekülleri hidrofobik oldukları bilinen DNA baz çiftleri arasına yerleşerek yüksek emisyon verebilmektedir [18]. DNA'ya interkalasyon yoluyla kuvvetli bir şekilde bağlanabilen bir bileşik EB molekülünü DNA baz çiftleri arasından çıkararak emisyonda düşüşe sebep olacaktır. Şekil 3'te görüldüğü gibi EB-DNA karışımı üzerine sabit porsiyonlar halinde (1 mM'lık çözeltiden 2 µl) bileşik 1 (A), bileşik 2 (B) ve bileşik 3 (C) eklenmesiyle DNA'ya bağlı EB emisyonunda belirgin düşüşler olmuştur.

Bileşiklerin DNA bağlanma kuvvetleri aşağıdaki Stern-Volmer eşitliği kullanılarak hesaplanmıştır.

$$F_0/F = 1 + K_{SV}[Q] \quad (2)$$

Eşitlikte F_0 yarışmacı bileşik yokluğunda, F yarışmacı bileşik varlığında EB-DNA emisyonu ve [Q] ise eklenen yarışmacı bileşik konsantrasyonunu ifade etmektedir. Bileşikler için K_{SV} sabitleri 1, 2 ve 3 için sırasıyla 8,04 x 10^4, 7,86 x 10^4 ve 2,19 x 10^4 M^{-1} olarak hesaplanmıştır. Ayrıca EB-DNA emisyonunu yarıya düşürmek için gerekli olan bileşik konsantrasyonları (DC_{50}); eklenen bileşik konsantrasyonu ([L]) değerlerinin I_0/I değerlerine karşı grafiğe geçirilmesiyle elde edilen doğrusal grafiğin denkleminde "y" yerine (I_0/I) 2 yazılarak sırasıyla 14 µM, 12 µM ve 45 µM olarak bulunmuştur. Bu sonuç elektron çekici grupların DNA bağlanma aktivitesine uyumludur [19].

Agaroz Jel ile DNA Kırılma Sonuçları

Bileşiklerin DNA kırma potansiyelleri pBR322 DNA ile agaroz jel elektroforez kullanılarak gerçekleştirilmiştir. Dairesel plazmit DNA jel elektroforez ile çalışıldığında en hızlı göç eden form süpersarmal form (form I) olacaktır. Eğer kırılma sadece bir zincirde olursa süper sarmal biraz rahatlayarak form II oluşacak ve göç yavaşlayacaktır. Her iki zincir kırıldığında ise lineer form (form III) oluşacak ve form I ve form II arasında bir göç mesafesi olacaktır [20]. Sabit miktarda (20 ng) pBR322 plazmit DNA ve artan miktarlarda (sırasıyla hat 1-6; 0, 10, 20, 50, 100, 200 µM bileşik) içeren farklı karışımların 38°C'de 1 saat bekletilmesi sonucu elde edilen elektroforez sonuçları Şekil 4'te görülmektedir.

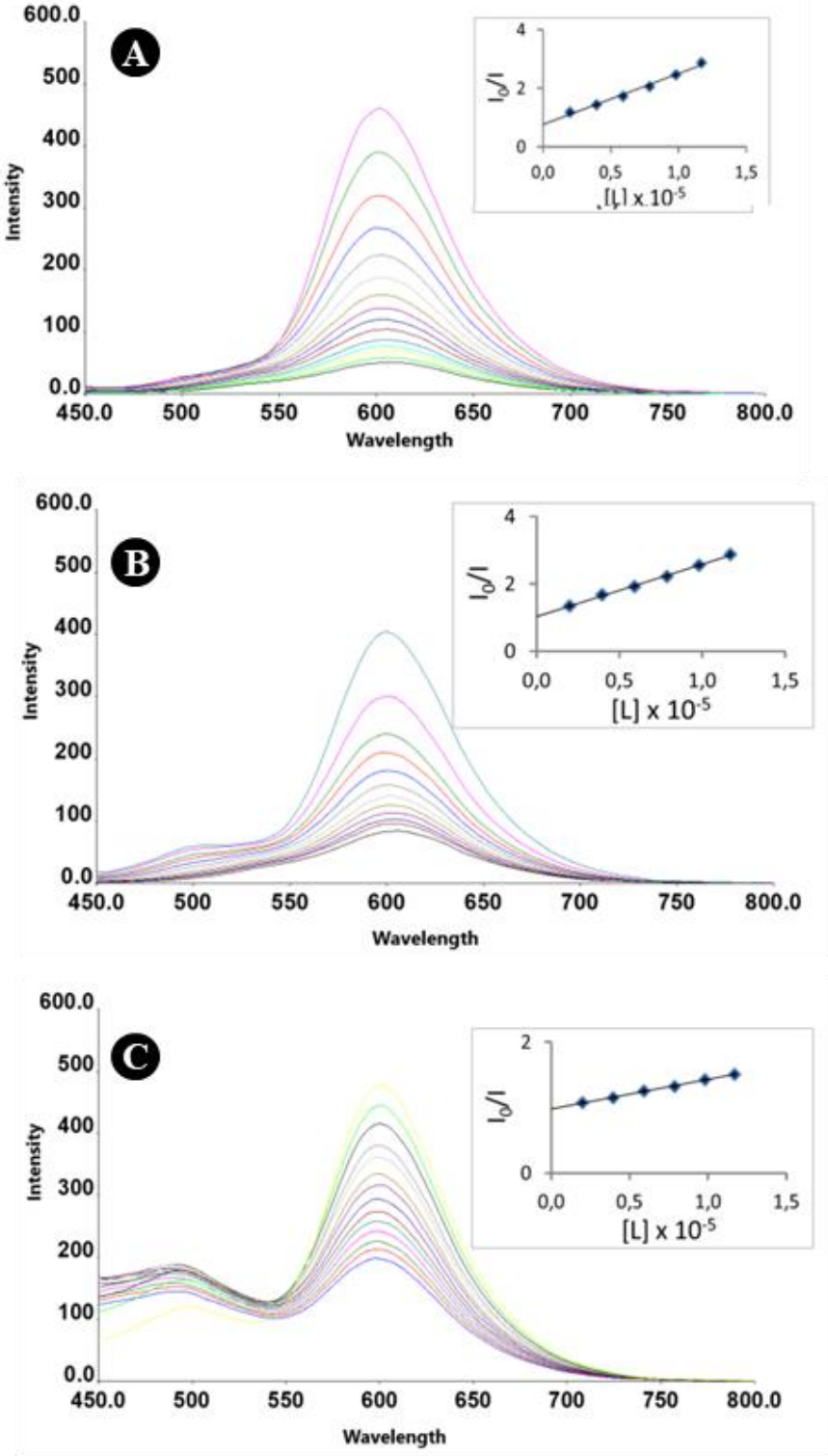

Şekil 3. *1 (A), 2 (B) ve 3 (C) numaralı bileşikler için EB ile yarışmalı emisyon titrasyonu spektrumları*

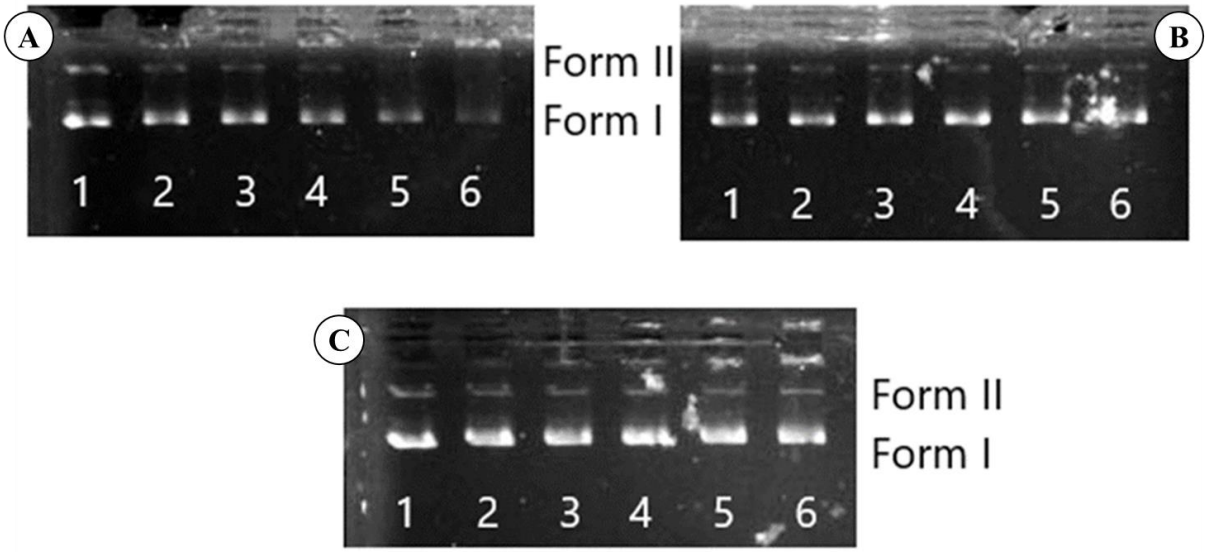

Şekil 4. *Artan oranlarda 1 (A), 2 (B) ve 3 (C) bileşikleri içeren karışımlara ait elektroforez görüntüleri*

Elektroforez sonuçları incelendiğinde şekil 4A'da 4 numaralı hatta kullanılan 50 µM bileşik 1'in form II oluşumuna sebep olduğu görülmektedir. Derişim arttıkça form I'in azalarak kaybolduğu anlaşılmaktadır. Bileşik 2 ve bileşik 3 çalışılan derişim aralıklarında plazmit DNA üzerinde herhangi bir form değişikliği oluşturmamaktadır.

Tartışma

Çalışma kapsamında farklı indüktif etkiler gösteren fonksiyonel gruplar içeren 3 naftalimit türevinin çift sarmal DNA bağlanma afiniteleri incelenmiştir. UV titrasyonu sonuçları bileşiklerin DNA'ya interkalasyon yoluyla bağlandığını göstermiştir. EB ile gerçekleştirilen yarışmalı çalışmalar bu bilgiyi doğrulamıştır ve DC_{50} değeri en düşük olan bileşik 2'nin interkalasyon kuvvetinin yüksek olduğu anlaşılmıştır. Elektroforez sonuçları bileşiklerin plazmit DNA üzerinde form değişikliği yapabildiğini göstermiştir. Literatür incelendiğinde elektron çekici grupların DNA kırma aktivitesini azalttığı görülmektedir [21]. Bununla uyumlu olarak elektron çekici nitro grubu içeren 2 numaralı bileşik ve çalışılan pH'ta protonlanabilen amino grubu üzerinden elektron çekici olabilecek 3 numaralı bileşik DNA formunu değiştirmezken 1 numaralı bileşikte form değişikliği görülmektedir. Hem UV titrasyon hem yarışmalı emisyon hemde elektroforez çalışması sonuçları yapılacak ileri in vitro bağlanma ve sitotoksitite çalışmaları için bileşik 1'in en iyi aday olduğunu göstermektedir.

Teşekkür Bu makaledeki veriler ve sonuçlar 1919B012111464 numaralı TÜBİTAK 2209-A projesi kapsamında elde edilmiştir. TÜBİTAK ve Zonguldak Bülent Ecevit Üniversitesi'ne teşekkürlerimizi sunarız.

Fon/Finansman Bilgileri Bu çalışma 1919B012111464 numaralı TÜBİTAK 2209-A projesi kapsamında desteklenmiştir.

Etik Kurul Onayı ve İzinler Çalışma, etik kurul izni veya herhangi bir özel izin gerektirmemektedir.

Çıkar Çatışmaları/Çatışan Çıkarlar Herhangi bir çıkar çatışması yoktur.

Yazarların Katkısı Yazarlar çalışmaya eşit oranda katkı sağlamıştır. Yazarlar makalenin son halini okumuş ve onaylamıştır.

Kaynaklar

[1] Zhao, S., Zhang, X., Wei, P., Su, X., Zhao, L., Wu, M., Hao, C., Liu, C., Zhao, D., & Cheng, M. (2017). Design, synthesis and evaluation of aromatic heterocyclic derivatives as potent antifungal agents. *European Journal of Medicinal Chemistry, 137,* 96-107. https://doi.org/10.1016/j.ejmech.2017.05.043

[2] Mi, Y., Zhang, J., Chen, Y., Sun, X., Tan, W., Li, Q., & Guo, Z. (2020). New synthetic chitosan derivatives bearing benzenoid/heterocyclic moieties with enhanced antioxidant and antifungal activities. *Carbohydrate Polymers, 249,* 116847. https://doi.org/10.1016/j.carbpol.2020.116847

[3] Alblewi, F. F., Okasha, R. M., Hritani, Z. M., Mohamed, H. M., El-Nassag, M. A. A., Halawa, A. H., Mora, A., Fouda, A. M., Assiri, M. A., Al-Dies, A. A. M., Afifi, T. H., & El-Agrody, A. M. (2019). Antiproliferative effect, cell cycle arrest and apoptosis generation of novel synthesized anticancer heterocyclic derivatives based 4H-benzo[h]chromene. *Bioorganic Chemistry, 87,* 560-571. https://doi.org/10.1016/j.bioorg.2019.03.059

[4] Ravula, S., Bobbala, R. R., & Kolli, B. (2020). Synthesis of novel isoxazole functionalized pyrazolo[3,4-b]pyridine derivatives; their anticancer activity. *Journal of Heterocyclic Chemistry, 57*(6), 2535-2538. https://doi.org/10.1002/jhet.3968

[5] Luo, Y., Zhou, Y., Fu, J., & Zhu, H. L. (2014). 4,5-Dihydropyrazole derivatives containing oxygen-bearing heterocycles as potential telomerase inhibitors with anticancer activity. *RSC Advances, 4*(45), 23904-23913. https://doi.org/10.1039/C4RA02200A

[6] Liang, G. B., Wei, J. H., Jiang, H., Huang, R. Z., Qin, J. T., Wang, H. L., Wang, H. S., & Zhang, Y. (2021). Design, synthesis and antitumor evaluation of new 1,8-naphthalimide derivatives targeting nuclear DNA. *European Journal of Medicinal Chemistry, 210,* 112951. https://doi.org/10.1016/j.ejmech.2020.112951

[7] Dhar, S., Singha Roy, S., Rana, D. K., Bhattacharya, S., Bhattacharya, S., & Bhattacharya, S. C. (2011). Tunable solvatochromic response of newly synthesized antioxidative naphthalimide derivatives: intramolecular charge transfer associated with hydrogen bonding effect. *The Journal of Physical Chemistry A, 115*(11), 2216-2224. https://doi.org/10.1021/jp1117773

[8] Sk, U. H., Prakasha Gowda, A. S., Crampsie, M. A., Yun, J. K., Spratt, T. E., Amin, S., & Sharma, A. K. (2011). Development of novel naphthalimide derivatives and their evaluation as potential melanoma therapeutics. *European Journal of Medicinal Chemistry, 46*(8), 3331-3338. https://doi.org/10.1016/j.ejmech.2011.04.058

[9] Braña, M. F., Cacho, M., Gradillas, A., De Pascual-Teresa, B., & Ramos, A. (2001). Intercalators as anticancer drugs. *Current Pharmaceutical Design, 7*(17), 1745-1780. http://doi.org/10.2174/1381612013397113

[10] Van Quaquebeke, E., Mahieu, T., Dumont, P., Dewelle, J., Ribaucour, F., Simon, G., Sauvage, S., Gaussin, J. F., Tuti, J., El Yazidi, M., Van Vynckt, F., Mijatovic, T., Lefranc, F., Darro, F., & Kiss,

R. (2007). 2,2,2-Trichloro-N-({2-[2-(dimethylamino)ethyl]-1,3-dioxo-2,3-dihydro-1H-benzo[de]isoquinolin- 5-yl}carbamoyl)acetamide (UNBS3157), a novel nonhematotoxic naphthalimide derivative with potent antitumor activity. *Journal of Medicinal Chemistry, 50*(17), 4122-4134. https://doi.org/10.1021/jm070315q

[11] Chen, Z., Liang, X., Zhang, H., Xie, H., Liu, J., Xu, Y., Zhu, W., Wang, Y., Wang, X., Tan, S., Kuang, D., & Qian, X. (2010). A new class of naphthalimide-based antitumor agents that inhibit topoisomerase II and induce lysosomal membrane permeabilization and apoptosis. *Journal of Medicinal Chemistry, 53*(6), 2589-2600. https://doi.org/10.1021/jm100025u

[12] Gurova, K. (2009). New hopes from old drugs: revisiting DNA-binding small molecules as anticancer agents. *Future Oncology, 5*(10), 1685-1704. https://doi.org/10.2217%2Ffon.09.127

[13] Lv, J. S., Peng, X. M., Kishore, B., & Zhou, C. H. (2014). 1,2,3-Triazole-derived naphthalimides as a novel type of potential antimicrobial agents: Synthesis, antimicrobial activity, interaction with calf thymus DNA and human serum albumin. *Bioorganic & Medicinal Chemistry Letters, 24*(1), 308-313. https://doi.org/10.1016/j.bmcl.2013.11.013

[14] Mijatovic, T., Mahieu, T., Bruyère, C., Nève, N. D., Dewelle, J., Simon, G., Dehoux, M. J. M., Aar, E. V. D., Haibe-Kains, B., Bontempi, G., Decaestecker, C., Quaquebeke, E. V., Darro, F., & Kiss, R. (2008). UNBS5162, a novel naphthalimide that decreases CXCL chemokine expression in experimental prostate cancers. *Neoplasia, 10*(6), 573-586. https://doi.org/10.1593/neo.08290

[15] Ott, I., Xu, Y., Liu, J., Kokoschka, M., Harlos, M., Sheldrick, W. S., & Qian, X. (2008). Sulfur-substituted naphthalimides as photoactivatable anticancer agents: DNA interaction, fluorescence imaging, and phototoxic effects in cultured tumor cells. *Bioorganic & Medicinal Chemistry, 16*(15), 7107-7116. https://doi.org/10.1016/j.bmc.2008.06.052

[16] Yıldız, U. (2021). Synthesis and antioxidant activities of novel naphthalimide derivatives. *Kocaeli Journal of Science and Engineering, 4*(1), 51-58. https://doi.org/10.34088/kojose.816212

[17] Lerman, L. S. (1961). Structural considerations in the interaction of DNA and acridines. *Journal of Molecular Biology, 3*(1), 18-IN14. https://doi.org/10.1016/S0022-2836(61)80004-1

[18] Baguley, B. C., & Le Bret, M. (1984). Quenching of DNA-ethidium fluorescence by amsacrine and other antitumor agents: a possible electron-transfer effect. *Biochemistry, 23*(5), 937-943. https://doi.org/10.1021/bi00300a022

[19] Cusumano, M., Di Pietro, M. L., & Giannetto, A. (1999). Stacking surface effect in the DNA intercalation of some polypyridine platinum(II) complexes. *Inorganic Chemistry, 38*(8), 1754-1758. https://doi.org/10.1021/ic9809759

[20] Barton, J. K., Danishefsky, A., & Goldberg, J. (1984). Tris (phenanthroline) ruthenium (II): stereoselectivity in binding to DNA. *Journal of the American Chemical Society, 106*(7), 2172-2176. https://doi.org/10.1021/ja00319a043

[21] Wang, W., Young, A., Kim, G., & Kim, S. K., (2015). Oxidative DNA cleavage by Cu(II) complexes: Effect of periphery substituent groups. *Journal of Inorganic Biochemistry, 153*, 143-149. https://doi.org/10.1016/j.jinorgbio.2015.07.015

Sinopfbd, 2024; 9(1): 154-166 **https://doi.org/10.33484/sinopfbd.1434260**

Sinop Üniversitesi Fen Bilimleri Dergisi
Sinop Uni J Nat Sci
E-ISSN: 2564-7873

https://dergipark.org.tr/tr/pub/sinopfbd

Çoklu Doğrusal Bağlantılı Nadir Olayların Modellenmesinde Lasso ve Ridge Regresyon ile Boosting Algoritmalarının Performans Karşılaştırması

Olcay ALPAY

How to cite: Alpay, O. (2024). Çoklu doğrusal bağlantılı nadir olayların modellenmesinde Lasso ve Ridge regresyon ile Boosting algoritmalarının performans karşılaştırması. *Sinop Üniversitesi Fen Bilimleri Dergisi, 9*(1), 154-166. https://doi.org/10.33484/sinopfbd.1434260

Araştırma Makalesi

Sorumlu Yazar
Olcay ALPAY
olcayb@sinop.edu.tr

Yazara ait ORCID
O.A: 0000-0003-1446-0801

Received: 09.02.2024
Accepted: 21.05.2024

Öz

Bu çalışma, iki durumlu olayları modellemek için kullanılan makine öğrenmesi tekniklerinde karşılaşılan nadirlik ve "çoklu doğrusal bağlantı" ya da sadece "çoklu bağlantı" olarak tanımlanan sorunu ele alınmaktadır. Çoklu doğrusal bağlantı (ÇDB), bağımsız değişkenler arasında bir ya da birden fazla kuvvetli doğrusal bağımlılık olma durumudur ve bir sorun olarak ortaya çıkar. Üzerinde çalışılan veri içerisinde çoklu doğrusal bağlantı probleminin var olması regresyon katsayılarının varyanslarının büyümesi gibi olumsuz bir sonuca sebebiyet verir. Bu çalışmada, Lasso ve Ridge Regresyon ile GradientBoost, XGBoost, LightGBM ve AdaBoost gibi artırma algoritmaları içeren düzenleme ve ölçeklendirme tekniklerinin, çoklu doğrusal bağlantılı nadir olayların modellenmesinde, algoritmaların performanslarını karşılaştırmak için detaylı bir simülasyon çalışması sunulmaktadır. Simülasyon çalışmasında, verideki dengesizliği ortadan kaldırmak amacıyla yeniden örnekleme yöntemleri kullanılarak sonuçlara etkisi Hata Kareler Ortalaması (*HKO*), R^2, Hassasiyet (Precision-Prec), Duyarlılık (Recall-Rec) ve Eğri Altında Kalan Alan (Area Under the Curve-AUC) gibi performans metrikleri ve İşlem Karakteristik Eğrisi (Receiver Operating Characteristic- ROC) grafikleri ile araştırılmaktadır. Sonuçlar Lasso, Ridge ve Boosting algoritmalarının ÇDB'ya sahip nadir olayların modellenmesinde hangi yöntemin uygun olduğunu belirlemek açısından katkı sunmaktadır.

Anahtar Kelimeler: Lasso regresyon, Ridge regresyon, Boosting algoritmaları, performans metrikleri, yeniden örnekleme teknikleri

Performance Comparison of Lasso and Ridge Regression and Boosting Algorithms for Modeling Rare Events with Multicollinearity

Sinop Üniversitesi, Fen Edebiyat Fakültesi, İstatistik Bölümü, Sinop, Türkiye

Abstract

This study examines the issues of rarity and multicollinearity in machine learning techniques used to model binary events. Multicollinearity (MC) is the presence of strong linear dependencies among independent variables, which poses a problem. In the context of the data being studied, the existence of multicollinearity leads to undesired consequences such as an enlargement of the variances of the regression coefficients. This study presents a simulation comparing the performance of algorithms in modelling multicollinear and rare events. Regularization and scaling techniques such as Lasso and Ridge Regression, as well as Boosting algorithms like GradientBoost, XGBoost, LightGBM, and AdaBoost are

utilized. The impact of resampling methods to reduce data imbalance is also investigated using performance metrics such as Mean Squared Error (MSE), R^2, Precision (Prec), Recall (Rec) and AUC values, along with ROC curves. The results help to determine the appropriate method for modelling rare events with multicollinearity and provide insight into the performance of Lasso, Ridge and Boosting algorithms.

Keywords: Lasso regression, Ridge regression, Boosting algorithms, performance metrics, resampling techniques

Giriş

Çoklu doğrusal bağlantı (ÇDB), çoklu regresyon modellinin temel varsayımlardan birinin ihlalidir ve regresyon modellerindeki bağımsız değişkenler arasında yüksek bir ilişki olduğunda ortaya çıkan bir sorundur. Veri içerisinde çoklu doğrusal bağlantı problemi olması, regresyon katsayılarının varyanslarının büyümesine sebep olur, dolaysıyla tahmin edilen parametrelerin güvenilirliği azalır [1]. İki durumlu olayların modellenmesinde kullanılan birçok farklı makine öğrenmesi algoritması bulunmaktadır. Bunlardan en yaygın olanı ise lojistik regresyondur. Özellikle, nadir olayların modellenmesinde lojistik regresyon, parametrelerinin değerlerini olması gerekenden daha düşük tahmin etme eğilimindedir [2]. Nadir görülen olaylara örnek olarak savaşlar, çok şiddetli depremler, büyük çaplı salgınlar verilebilir [3]. Lojistik regresyonda da çoklu doğrusal bağlantı sorunlarıyla karşılaşılabilir. Dolayısıyla, çoklu doğrusal bağlantı, lojistik regresyon modelinde bağımsız değişkenler arasındaki ilişkiyi etkileyebilir ve nadirlik yüzünden olması gerekenden daha düşük değerli tahmin edilen model parametrelerinin güvenilirliğini daha da azaltabilir. Bu nedenle, lojistik regresyon modelleri oluştururken çoklu doğrusal bağlantı sorununa dikkat etmek ve etkilerini azaltmak önemlidir. Ridge veya Lasso regresyon gibi düzenleme teknikleri, modeldeki katsayıları sıfıra yaklaştırarak veya sıfıra eşitleyerek çoklu doğrusal bağlantı sorununu azaltabilir. Bu şekilde, lojistik regresyon modelinin performansı ve güvenilirliği artırılabilir. Shrivastava ve ark. [4] finansal sistemde önemli bir role sahip bankalar üzerine bir çalışma yürütmüşlerdir. Hindistan'da batan bankalara ait veri setindeki dengesizliği dikkate alarak ve SMOTE yeniden örnekleme tekniğini kullanarak Lasso regresyon, AdaBoost ve başka makine öğrenmesi algoritmaları ile bankaların başarısızlığını tahmin etmek için uygun makine öğrenme tekniğinin seçilmesi üzerine bir yaklaşım sunmayı amaçlamışlardır. 2020 yılında Rochayani ve ark. [5] yüksek boyutlu ve dengesiz sınıflı gen veri setlerinde kanser sınıflandırması için az örnekleme (undersampling) ve gen seçimi üzerine bir çalışma gerçekleştirmişlerdir. Veri setini dengelemek için rastgele az örnekleme yöntemini kullanmışlar ve gen seçimi için Lasso regresyonu tercih etmişlerdir. Ridge regresyon ile ilgili yapılan literatür taramasında, Ridge regresyonun dengeli veri setlerindeki uygulamalarına sıkça rastlanmış, ancak nadir olaylar üzerinde Sıradan Ridge Regresyonu (Ordinary Ridge Regression) kullanan bir çalışma ile karşılaşılmamıştır. Değişkenler arasında çoklu doğrusal bağlantı olduğunda kullanılabilecek diğer bir yaklaşım, makine öğrenmesi çerçevesinde incelenen Boosting algoritmalarıdır. Bu konu ile ilgili literatürde yapılan çalışmalardan bazıları şöyledir: Cahyana ve ark. [6] yaptıkları çalışmada göğüs kanseri verisinde başta SMOTE olmak üzere çeşitli yeniden

örnekleme yöntemlerini GradientBoost algoritmasında kullanmış ve performanslarını değerlendirmişlerdir. Zaten yüksek başarı gösteren GradientBoost algoritmasının performansının aşırı örnekleme (oversampling) ile daha da arttığı yaptıkları çalışmada gösterilmiştir. Tanha ve ark. [7] yaptıkları çalışmada ise içlerinde GradientBoost, XGBoost, LightGBM ve AdaBoost'un da olduğu Boosting algoritmalarının dengesiz veri kümeleri üzerindeki performansını analiz etmek için kapsamlı bir deneysel karşılaştırma yapmışlardır. Ashraf ve ark. [8] yaptıkları çalışmada, XGBoost algoritmasında SMOTE, Tomek bağlantısı ve başka yeniden örnekleme yöntemlerini kullanarak yanlış yönden araç kullanımına bağlı kazalar için yüksek riskli yol kesimlerinin belirlenmesi üzerine bir çalışma yürütmüşlerdir. Prec, Rec, AUC ve ROC sonuçlarını kullanarak performans değerlendirmesini sunmuşlardır. Bu çalışma ile literatürde daha önce nadir olaylarda kullanılmamış Ridge regresyonu ilk kez incelemek amaçlanmıştır. Aynı zamanda, Boosting algoritmalarının Lasso ve Ridge regresyon ile farklı yeniden örnekleme teknikleri ve örneklem büyüklüklerinde performanslarını karşılaştırılarak literatüre katkı sağlamak hedeflenmiştir. Çalışmanın takip eden bölümünde nadir olayları modellemek için kullanılacak Lasso ve Ridge Regresyon ile Boosting algoritmaları, SMOTE, Tomek Bağlantısı ve SMOTETomek yeniden örnekleme teknikleri, son olarak da sınıflandırma performansını değerlendirmek için kullanılan ölçümler açıklanacaktır. Bir sonraki bölümde simülasyon çalışması verilecek ve son bölümde ise elde edilen sonuçlar değerlendirilecektir.

Metodoloji

Lasso Regresyon

Lasso regresyon, katsayıların mutlak değerlerinin toplamının bir sabitten küçük olması koşuluyla artık kareler toplamını en aza indirir. Bu yöntem, bazı regresyon katsayılarının büyüklüğünü tam sıfır olarak üreterek sınırlar ve modelin karmaşıklığını azaltır.

$$\hat{\beta}_{lasso} = argmin \left\{ \sum_{i=1}^{N} \left(y_i - \beta_0 - \sum_j \beta_j x_{ij} \right)^2 + \lambda \sum_j |\beta_j| \right\}$$

Buradaki $\lambda \geq 0$ büzülme miktarını kontrol eden ayarlama parametresidir [9]. $\sum_j |\beta_j|$'nin kullanılması parametre tahminlerini sıfırlamaya zorladığı için modelin değişken sayısını azaltıp, daha az değişkene sahip bir model seçmeyi ve tahmin yapmayı sağlar [10].

Ridge Regresyon

Hoerl ve Kennard tarafından 1970 yılında tanıtılan Ridge tahmin edicisi, açıklayıcı değişkenlerin arasındaki ÇDB sorununu çözmek ve böylece tahmin edicilerin varyanslarını azaltmak için önerilmiştir [11]. Bu yöntem büyük katsayıları küçültür, ancak sıfıra indirmez.

$$\hat{\beta}_{ridge} = argmin\left\{\sum_{i=1}^{N}\left(y_i - \beta_0 - \sum_j \beta_j x_{ij}\right)^2 + \lambda \sum_j \beta_j^2\right\}$$

Burada λ ayarlama parametresidir.

Boosting Algoritmaları

"Boosting", yanlılığı ve varyansı azaltmak amacıyla zayıf öğrenicileri güçlü öğrenicilere dönüştüren bir topluluk öğrenme tekniğidir [12]. Çalışmada kullanılan bu ailenin en yaygın tekniklerinden aşağıda bahsedilmiştir.

GradientBoost (Gradient Boosting)

GradientBoost, kendinden önceki zayıf modellerdeki (zayıf öğrenenler) yanlışlıkları hesaba katarak modeli kapsamlı bir şekilde ayarlayan ve daha güçlü tahmin modeli oluşturan bir makine öğrenme algoritmasıdır [13]. Algoritmanın en önemli dezavantajı, önceki ağaçların hatasını azaltabilmek amacıyla sürekli yeni ağaçlar oluşturması ve küçük veri setlerinin bile eğitiminin çok zaman almasıdır [14].

GradientBoost Algoritması [15]:
Adım 1: Başlangıç tahmini yap
Adım 2: Kayıp fonksiyonunu kullanarak negatif gradiyenti hesapla
Adım 3: Hatayı düzeltmek için yeni öğrenici oluştur
Adım 4: Öğrenme oranı ile ağırlıklandır ve hatayı düzelt
Adım 5: Sonuç tahmini yap

XGBoost (eXtreme Gradient Boosting)

XGBoost, Chen tarafından 2016 yılında tanıtılan GradientBoost'un optimize edilmiş bir versiyonudur. XGBoost, geleneksel GradientBoost algoritmasının eğitim aşamasındaki aşırı uyumunu, ayrık ve eksik değerlerini kontrol etmek için verimli bazı özelliklerin eklenmiş versiyonudur. XGBoost, uygulama düzeyinde mükemmel iyileştirmeler yapmış, çok büyük veri kümeleri için uygulanabilir bir algoritmadır [7]. XGBoost'un GradientBoost'a göre en büyük avantajı, ağaçların ayrı ayrı birden fazla çekirdek kullanılarak oluşturulmasıdır. Bu sayede veriler, arama süreleri kısalacak şekilde düzenlenir [14]. Ayrıca, güçlü genelleme yeteneği ve yüksek genişletilebilirlik avantajlarına sahiptir [16].

LightGBM (Light Gradient Boosting Machine)

LightGBM, Ke ve ark. tarafından 2017'de yüksek boyutlu özellik uzayı veya büyük boyutlu verilerde GradientBoost'un verimlilik ve ölçeklenebilirlik sorununu çözmek için önerilmiştir [7]. Algoritma,

hesaplama gücünü ve tahmin doğruluğunu iyileştirmek için temel olarak histogram algoritmasını ve diğer algoritmaları kullanır [17].

LightGBM Algoritması [18]:

Adım 1: Veri hazırlığı yap
Adım 2: Modeli başlat
Adım 3: Özelliklerin boyutunu azalt
Adım 4: Örneklerin gradiyentlerini hesapla
Adım 5: Büyük gradiyentli örnekleri tut
Adım 6: Histogram oluştur
Adım 7: Optimal segmentasyonu bulmak için histogramı çaprazla
Adım 8: Tahmin yap

AdaBoost (Adaptive Boosting)

AdaBoost algoritması Boosting algoritmaları içinde en iyi olanlardan biridir [19]. AdaBoost'ta ilk olarak, eğitim veri kümesine eşit ağırlık atanır. Daha sonra, AdaBoost minimum ağırlığa sahip en iyi özelliği dikkate alan çok kısa bir ağaç oluşturarak başlatılır. Ağırlıklar tüm özellikler için aynı olduğundan, ilk ağaç ilk özelliği dikkate alır, daha sonra tüm ağaçlar diğer özelliklere göre oluşturulur. Tüm ağaçlar için Gini endeksi hesaplanır ve tüm düğümlerin tüm ağaçlar üzerindeki ağırlığı değerlendirilir. Ardından, yeni ağırlık eski ağırlığın yerini alır. Sonraki aşamada, AdaBoost yapılan yanlışlara odaklanarak yeni ağaçları bir önceki ağacın yaptığı hataya göre oluşturur. Yani, bu ağaç önceki ağaçlardan biraz daha iyi ve biraz daha büyüktür. AdaBoost bu prosedürde uygun olana kadar sürekli olarak yeni ağaçlar oluşturur [6].

AdaBoost Algoritması [15]:

Adım 1: Başlangıç ağırlıklarını ata
Adım 2: Veri setindeki örneklerin ağırlıklarına göre bir öğrenici oluştur
Adım 3: Öğrenciyi eğit
Adım 4: Hatayı hesapla
Adım 5: Ağırlıkları belirle
Adım 6: Sonuç tahminini yap

Yeniden Örnekleme Teknikleri

Yeniden örnekleme, sınıf dengesizliği sorununu çözmek için yaygın olarak kullanılan bir yöntemdir. Örneklemenin amacı, geleneksel sınıflandırıcıların daha dengeli bir sınıf dağılımına sahip bir veri seti oluşturarak çoğunluk ve nadir sınıflar arasındaki karar sınırını daha doğru bir şekilde yakalamasına olanak sağlamaktır [20].

SMOTE

SMOTE (sentetik azınlık aşırı örnekleme tekniği), nadir sınıfı aşırı örnekleyerek verileri dengeleyen önemli bir yaklaşımdır [21]. Aşırı örnekleme teknikleri, veri kümesindeki nadir olayların temsilini iyileştirebilse de aşırı uyumla ilgili sorunlara yol açabilir [20].

Tomek Bağlantısı

Dengeli veri seti elde etmek amacıyla çoğunluk sınıfının bazı gözlemlerini hariç tutarak veri setini rastgele örneklemeyi ifade eder. Bu şekilde nadir olaylar veri setinde daha iyi temsil edilir [22]. Ancak veri setinin nadirlik seviyesine bağlı olarak çok sayıda verinin silinmesine sebep olabilir.

SMOTETomek

SMOTETomek, SMOTE ile Tomek bağlantısını birleştiren hibrit bir yaklaşımdır. SMOTE, nadir olayların sayısını baskın sınıfın sayısına eşit olana kadar çoğaltan ve Tomek bağlantısı ile araştırmada veri işleme sonrasında temizleme adımını gerçekleştirilen bir alt örnekleme yöntemidir [23]. Bu hibrit yaklaşım, ana sınıfın azaltılmasının önemli bir bilgi kaybına yol açmamasını sağlarken aynı zamanda aşırı örneklemeden kaynaklanabilecek aşırı uyum sorununu da önler [20]. Genel olarak yeniden örnekleme yöntemlerinin çalışma prensipleri özetlenecek olursa, SMOTE tekniğinde sınıfların dengelenmesi, nadir sınıf için üretilen sentetik verilerle çoğunluk sınıfının yoğunluğuna ulaşarak sağlanırken, Tomek bağlantısında çoğunluk sınıfın veri sayısının azaltılarak nadir sınıfa yaklaştırılmasıyla gerçekleştirilir. Hibrit yaklaşımda ise SMOTE ile veri çoğaltma ve Tomek bağlantısı ile veri azaltma durumu söz konusudur [24].

Performans Metrikleri

Sınıflandırıcılar aracılığıyla ikili sınıflandırma yapılırken, doğru sınıflandırma oranının ölçülerek performans değerlendirilmesi yapılmasına ihtiyaç vardır. Bu amaçla nadir olan sınıfın tahmin performansını belirlemek için HKO, $R^2, Prec, Rec$ ve AUC gibi performans metrikleri bu çalışmada kullanılmıştır.

$\hat{y}_i$, i. örneklemin tahmini, y_i karşılık gelen gerçek değeri ve n test veri setinin boyutunu göstermek üzere HKO ve R^2 aşağıdaki gibi hesaplanmaktadır.

$$HKO(y, \hat{y}) = \frac{1}{n}\sum_{i=0}^{n-1}(y_i - \hat{y}_i)^2$$

ve

$$R^2(y, \hat{y}) = 1 - \frac{\sum_{i=1}^{n}(y_i - \hat{y}_i)^2}{\sum_{i=1}^{n}(y_i - \bar{y})^2}$$

Diğer metrikleri hesaplamak için kullanılan karışıklık matrisi ise şu şekilde tanımlanır:

		Tahmin edilen	
		1	0
Gözlenen	1(nadir sınıf)	DP	YN
	0	YP	DN

Prec ve Rec metrikleri aşağıdaki gibidir.

$$Prec = \frac{DP}{DP + YP}$$

$$Rec = \frac{DP}{DP + YN}$$

DP: Doğru Pozitif, **YP**: Yanlış Pozitif, **DN**: Doğru Negatif ve **YN**: Yanlış Negatifi ifade etmektedir. ROC eğrisi, duyarlılık ile 1-özgüllük arasındaki ilişkiyi gösteren bir haritadır [25]. Çeşitli kesme değerlerine göre elde edilen yanlış pozitif oranlara karşı hassasiyetlerin grafiğini çizerek bir sınıflandırıcının tanısal yeteneğini değerlendirmek için kullanılır [26]. ROC güçlü bir performans ölçütü olmasına rağmen eğri altındaki alanın (AUC) nadir olay sınıflandırması için daha uygun olduğu öne sürülmüştür [27]. AUC, tüm ROC eğrilerinin iyi bir özetini sunar [28].

Simülasyon Çalışması

İkili olayların modellenmesi için kullanılacak olan algoritmaların deneysel performanslarının değerlendirilmesinde, kesişme katsayısı olan β_0, ilgilenilen olayın veri seti içindeki oranını belirlediğinden bu değeri en iyi şekilde temsil edebilmek adına örneklem ölçümü en az $n = 1000$ ve en çok $n = 5000$ olarak seçilmiştir. İlgilenilen nadir olay "1" ile gösterilmekte olup örneklem içindeki oranı %15'tir. Nadir olayın oluşması ve %15'lik nadirlik seviyesine ulaşılabilmesi için, 1000 birimlik örneklem büyüklüğünde $\beta_0 = -21.4$ ve 5000 birimlik örneklem büyüklüğünde ise $\beta_0 = -26.1$ olarak belirlenmiştir. Standartlaştırılmış $\beta_i = 1$ ve $X_i \sim N(0,1)\ i = 1,2,\dots,10$ normal dağılıma sahip 10 açıklayıcı değişkenden oluşan simülasyon tasarımında, değişkenler arasında ilişki oluşturabilmek amacıyla bazı değişkenler arasında doğrusal ilişki kurulmuş ve Tablo 1'de verilen ilişki değerleri elde edilmiştir. Daha sonra yukarıdaki ayarlara sahip ikili olay şu şekilde oluşturulmuştur:

$$y(\pi(x)) = \begin{cases} 0, & eğer\ \pi < u \\ 1, & d.d. \end{cases}$$

burada *u* yapay değişkendir.

Python Spyder 5.4.3'te yazılan ve 100 tekrar ile gerçekleştirilen simülasyonda veri setleri rasgele olarak eğitim ve test setlerine 2/3:1/3 oranında ayrılmıştır. İlk olarak dengesiz dağılıma sahip, sonrasında ise imblearn [29] kütüphanesinden yararlanarak yeniden örnekleme teknikleriyle dengeli hale getirilmiş

verilerin, eğitim setinde model öğrenimi gerçekleştirildikten sonra test setinden tahmin değerleri elde edilmiş ve gerekli metrikler hesaplanmıştır. Simülasyon sayısı kadar tekrarlanan çalışma sonunda elde edilen ortalama değerler Tablo 2-4'te sunulmuştur.

Tablo 1 *İlişki matrisi*

	X_1	X_2	X_3	X_4	X_5	X_6	X_7	X_8	X_9	X_{10}
X_1	1	0.60	0.15	0.20	0.41	0.25	0.14	0.72	0.12	0.09
X_2	0.60	1	0.18	0.23	0.07	0.27	0.31	0.14	0.07	0.01
X_3	0.15	0.18	1	0.05	0.11	0.28	0.15	0.02	0.40	0.31
X_4	0.20	0.23	0.05	1	0.08	0.16	0.07	0.30	0.19	0.01
X_5	0.41	0.07	0.11	0.08	1	0.04	0.19	0.12	0.10	0
X_6	0.25	0.27	0.28	0.16	0.04	1	0	0.01	0.72	0.08
X_7	0.14	0.31	0.15	0.07	0.19	0	1	0.11	0.08	0.17
X_8	0.72	0.14	0.02	0.30	0.12	0.01	0.11	1	0	0
X_9	0.12	0.07	0.40	0.19	0.10	0.72	0.08	0	1	0
X_{10}	0.09	0.01	0.31	0.01	0	0	0.17	0	0	1

Tablo 2'de algoritmaların oluşturdukları modellere ait Hata Kareler Ortalaması (*HKO*) ve Tablo 3'te model açıklayıcılıkları (R^2) sunulmaktadır. Tablolar detaylı olarak incelendiğinde örneklem ölçümü büyüdüğünde, Lasso regresyonun *HKO* değerinin yükseldiği ve buna bağlı olarak model açıklayıcılığının bir miktar düştüğü görülmektedir. Ridge regresyon açısından değerlendirme yapıldığında ise örneklem ölçümünün artması *HKO* ve R^2 açısından çok büyük farklılıklara sebep olmamıştır. Boosting algoritmalarına bakılacak olursa yeniden örnekleme yapılmadan veya yeniden örnekleme tekniklerinin tümü için en düşük *HKO* ve en yüksek R^2 değerine sahip algoritmanın LightGBM olduğu görülmektedir. GradientBoost en iyi performansını veri dağılımındaki dengenin çoğunluk sınıfın sayısını nadir olay sayısına yaklaştırmayı hedefleyen Tomek bağlantısı kullanıldığında elde etmiştir. Bu durum XGBoost ve AdaBoost için de benzer şekildedir.

Tablo 2 *Algoritmaların örneklem ölçümlerine bağlı HKO değerleri*

HKO	**Yeniden Örnekleme Yok**		**SMOTE**		**Tomek Bağlantısı**		**SMOTETomek**	
Model	**n=1000**	**n=5000**	**n=1000**	**n=5000**	**n=1000**	**n=5000**	**n=1000**	**n=5000**
Lasso	0.088	0.089	0.108	0.110	0.086	0.088	0.107	0.111
Ridge	0.074	0.074	0.105	0.104	0.073	0.073	0.104	0.105
GradientBoost	0.030	0.027	0.035	0.038	0.028	0.027	0.034	0.037
XGBoost	0.033	0.028	0.036	0.033	0.032	0.028	0.033	0.032
LightGBM	**0.026**	**0.024**	**0.027**	**0.028**	**0.025**	**0.025**	**0.025**	**0.027**
AdaBoost	**0.026**	0.041	0.029	0.047	0.025	0.041	0.028	0.048

Tablo 3 *Algoritmaların örneklem ölçümlerine bağlı R^2 değerleri*

R^2	Yeniden Örnekleme Yok		SMOTE		Tomek Bağlantısı		SMOTETomek	
Model	**n=1000**	**n=5000**	**n=1000**	**n=5000**	**n=1000**	**n=5000**	**n=1000**	**n=5000**
Lasso	0.312	0.303	0.150	0.133	0.322	0.308	0.137	0.134
Ridge	0.418	0.424	0.175	0.180	0.424	0.421	0.166	0.181
GradientBoost	0.763	0.790	0.722	0.706	0.776	0.789	0.731	0.707
XGBoost	0.735	0.784	0.716	0.742	0.750	0.779	0.733	0.748
LightGBM	**0.796**	**0.809**	**0.785**	**0.784**	**0.806**	**0.806**	**0.797**	**0.787**
AdaBoost	0.795	0.678	0.775	0.628	0.805	0.674	0.775	0.625

Tablo 4'te ise algoritmaların doğru sınıflandırma performanslarını belirlemek amacıyla hesaplanan metrikler verilmiştir. Lasso regresyon metrikler açısından en yüksek skorlarını örneklem ölçümünden bağımsız olarak SMOTE yeniden örneklemesinde elde etmiştir. Ridge regresyon, Prec metriği açısından SMOTETomek, Rec açısından Tomek bağlantısı ve AUC açısından ise tüm örneklem ölçümleri ve tüm yeniden örnekleme tekniklerinde en iyi performansı göstermiştir. GradientBoost' un tüm performans metrikleri için örneklem ölçümü ve yeniden örnekleme tekniği fark etmeksizin birbirine yakın değerler verdiği görülmektedir. Bu durum XGBoost ve LightGBM içinde benzerdir. Prec ve Rec metriklerine göre AdaBoost yöntemi neredeyse tüm örneklem ölçümü ve örnekleme tekniklerinde iyi performans değerlerine sahiptir.

Tablo 4 *Algoritmaların örneklem ölçümlerine bağlı performans metrik değerleri*

		Yeniden Örnekleme Yok		SMOTE		Tomek Bağlantısı		SMOTETomek	
Model		**n=1000**	**n=5000**	**n=1000**	**n=5000**	**n=1000**	**n=5000**	**n=1000**	**n=5000**
Lasso	**Prec**	0.842	0.869	0.934	0.934	0.858	0.872	0.938	0.933
	Rec	0.855	0.851	0.888	0.882	0.856	0.853	0.895	0.881
	AUC	0.975	0.990	0.990	0.991	0.976	0.990	0.991	0.991
Ridge	**Prec**	0.925	0.926	0.940	0.935	0.929	0.931	0.942	0.935
	Rec	0.911	0.917	0.886	0.867	0.917	0.923	0.890	0.867
	AUC	**0.996**	**0.998**	**0.997**	**0.998**	**0.997**	**0.998**	**0.997**	**0.998**
GradientBoost	**Prec**	0.959	0.965	0.956	0.957	0.962	0.965	0.958	0.957
	Rec	0.960	0.966	0.951	0.946	0.962	0.965	0.954	0.947
	AUC	0.987	0.993	0.987	0.992	0.987	0.993	0.988	0.992
XGBoost	**Prec**	0.957	0.962	0.956	0.958	0.960	0.962	0.959	**0.969**
	Rec	0.957	0.962	0.953	0.955	0.959	0.961	0.956	0.956
	AUC	0.978	0.987	0.979	0.985	0.981	0.987	0.981	0.986
LightGBM	**Prec**	0.969	0.966	0.965	0.963	0.971	0.966	0.968	0.965
	Rec	0.969	0.966	0.964	0.961	0.971	0.966	0.967	**0.962**
	AUC	0.989	0.993	0.989	0.991	0.988	0.993	0.989	0.992
AdaBoost	**Prec**	**0.972**	**0.968**	**0.972**	**0.965**	**0.973**	**0.968**	**0.974**	0.965
	Rec	**0.972**	**0.967**	**0.971**	**0.959**	**0.973**	**0.967**	**0.973**	0.959
	AUC	0.992	0.993	0.993	0.993	0.992	0.993	0.994	0.994

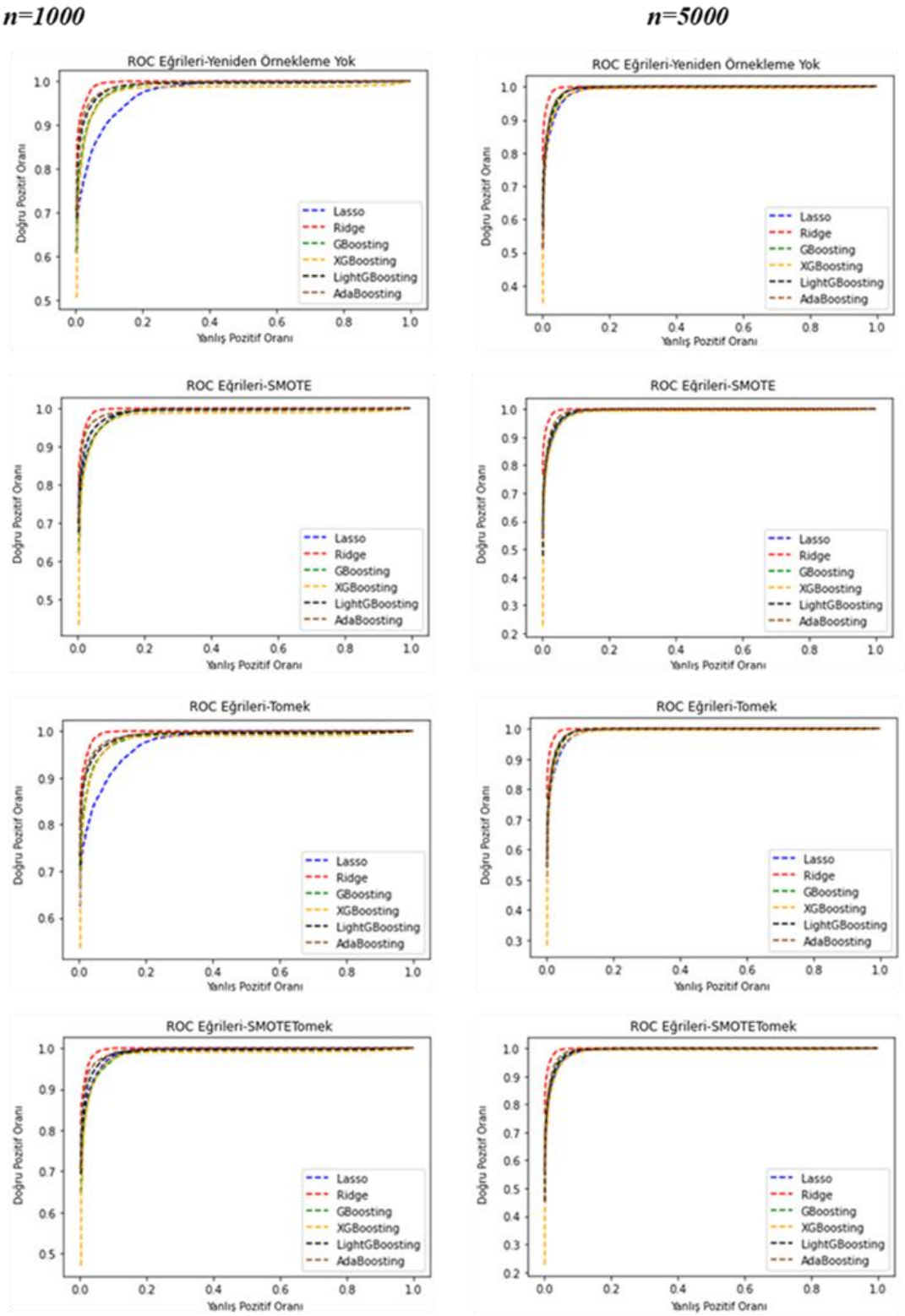

Şekil 1 *Örneklem ölçümlerine bağlı ROC eğrileri*

Şekil 1'de verilen ROC eğrileri incelendiğinde Ridge regresyonun hem gerçek pozitifleri hem de gerçek negatifleri en doğru şekilde sınıflandırdığı görülmektedir. Bu durum Tablo 4'teki AUC sonuçlarını desteklemektedir.

Sonuçlar

Farklı regresyon ve Boosting algoritmalarının performansları incelendiğinde, örneklem ölçümü arttıkça bazı algoritmaların performansının değiştiği gözlenmiştir. Bu değişim Lasso regresyonunda, örneklemin büyümesiyle birlikte *HKO*'da artış ve model açıklayıcılığında düşüş olarak ortaya çıkmıştır. Ridge regresyonunda, örneklem ölçümündeki artış, *HKO* ve R^2 üzerinde belirgin bir etki yaratmamıştır. Boosting algoritmaları açısından bakıldığında, LightGBM'in yeniden örnekleme tekniği kullanılıp kullanılmamasından bağımsız olarak en düşük *HKO* ve en yüksek R^2 değerlerine sahip algoritma olduğu gözlenmiştir. GradientBoost, çoğunluk sınıfın sayısının nadir sınıfın sayısına yaklaştırılması ile dağılımı dengeleyen Tomek bağlantısını kullandığında en iyi performansını elde etmiştir. Benzer şekilde, XGBoost ve AdaBoost için de bu durum geçerlidir. Doğru sınıflandırma performansını değerlendirmek için hesaplanan metriklerde ise farklı sonuçlar elde edilmiştir. Lasso regresyon, metrikler açısından en yüksek skorlarını örneklem ölçümünden bağımsız olarak SMOTE yeniden örneklemesinde elde etmiştir. Ridge regresyon, Prec ve Rec metrikleri açısından farklı örneklem ölçümleri ve yeniden örnekleme tekniklerinde iyi performans gösterirken, AUC açısından örneklem ölçümü ve yeniden örnekleme tekniğinden bağımsız en yüksek değerleri elde etmiştir. Boosting algoritmaları içinde Prec ve Rec açısından en iyi sonuçlar AdaBoost tarafından üretilmiştir. Tüm bu bulgular, algoritmaların farklı veri dengeleme tekniklerinde farklı performanslar sergilediğini göstermektedir. Kolay uygulanabilirliği sebebiyle dengesiz veri setlerinde Lasso veya Ridge regresyondan biri kullanılmak istenirse, Lasso regresyonunun tercih edilmesi durumunda performansın istikrarsız olabileceği, Ridge regresyonun ise daha stabil bir performans sergileyeceği göz önünde tutularak Ridge regresyon tercih edilebilir. Ancak sonuçlar genel olarak değerlendirildiğinde düşük hata ve yüksek açıklayıcılık oranları ile Boosting algoritmalarının Lasso ve Ridge regresyondan daha iyi performans sergilediği ve tercih edilebilirliklerinin daha fazla olduğu sonucu çıkarılabilir.

Teşekkür Yazar, değerli yorumları için Editörlere ve anonim hakemlere teşekkür eder.

Fon/Finansman Bilgileri Çalışma için herhangi bir mali sorumluluk yoktur.

Etik Kurul Onayı ve İzinler Çalışma etik kurul izni veya herhangi bir özel izin gerektirmemektedir.

Çıkar Çatışmaları/Çatışan Çıkarlar- Makale için herhangi bir çıkar çatışması yoktur.

Yazarların Katkısı Yazar makalenin son halini okumuş ve onaylamıştır.

Kaynaklar

[1] Bayman, O. E., & Dexter, F. (2021). Multicollinearity in logistic regression models. *Anesthesia & Analgesia*, *133*(2), 362-365. https://doi: 10.1213/ane.0000000000005593

[2] King, G., & Zeng, L. (2001). Logistic regression in rare events data. *Political Analysis, 9*(2), 137-163. https://doi:10.1093/oxfordjournals.pan.a004868

[3] Maalouf, M., & Trafalis, T. B. (2011). Robust weighted kernel logistic regression in imbalanced and rare events data. *Computational Statistics & Data Analysis*, *55*(1), 168-183. https://doi:10.1016/j.csda.2010.06.014

[4] Shrivastava, S., Jeyanthi, P. M., & Singh, S. (2020). Failure prediction of Indian Banks using SMOTE, Lasso regression, bagging and Boosting. *Cogent Economics & Finance*, *8*(1), 1729569. https://doi.org/10.1080/23322039.2020.1729569

[5] Rochayani, M. Y., Sa'adah, U., & Astuti, A. B. (2020). Finding biomarkers from a high-dimensional imbalanced dataset using the hybrid method of random undersampling and lasso. *Comtech: Computer, Mathematics and Engineering Applications*, *11*(2), 75-81. https://doi:10.21512/comtech.v11i2.6452

[6] Cahyana, N., Khomsah, S., & Aribowo, A. S. (2019). *Improving imbalanced dataset classification using oversampling and gradient Boosting* [Bildiri sunumu]. 5th international conference on science in information technology (ICSITech), China.

[7] Tanha, J., Abdi, Y., Samadi, N., Razzaghi, N., & Asadpour, M. (2020). Boosting methods for multi-class imbalanced data classification: an experimental review. *Journal of Big Data*, *7*, 1-47. https://doi.org/10.1186/s40537-020-00349-y

[8] Ashraf, M. T., Dey, K., & Mishra, S. (2023). Identification of high-risk roadway segments for wrong-way driving crash using rare event modeling and data augmentation techniques. *Accident Analysis & Prevention*, *181*, 106933. https://doi.org/10.1016/j.aap.2022.106933

[9] Tibshirani, R. (1996). Regression shrinkage and selection via the lasso. *Journal of the Royal Statistical Society Series B: Statistical Methodology*, *58*(1), 267-288.

[10] Göv, A., & Kapkara Kaya, S. (2023). Türkiye örneğinde çevresel kalitenin belirleyicileri: lasso yaklaşımı. *Pamukkale Üniversitesi Sosyal Bilimler Enstitüsü Dergisi*, (54), 25-37. https://doi:10.30794/pausbed.1097352

[11] Yüzbaşı, B., & Pala, M. (2022). Ridge regresyon parametre seçimi: Türkiye'nin doğrudan yabancı yatırım örneği. *İstatistikçiler Dergisi: İstatistik ve Aktüerya*, *15*(1), 1-18.

[12] Mahesh, B. (2020). Machine learning algorithms - a review. *International Journal of Science and Research (IJSR)*, *9*(1), 381-386. https://doi: 10.21275/ART20203995

[13] Friedman, J. H. (2002). Stochastic gradient Boosting. *Computational Statistics & Data Analysis*, *38*(4), 367-378.

[14] Ali, Z. A., Abduljabbar, Z. H., Taher, H. A., Sallow, A. B., & Almufti, S. M. (2023). Exploring the power of extreme gradient Boosting algorithm in machine learning: A review. *Academic Journal of Nawroz University*, *12*(2), 320-334.

[15] Tyralis, H., & Papacharalampous, G. (2021). Boosting algorithms in energy research: A systematic review. *Neural Computing and Applications*, *33*(21), 14101-14117. https://doi.org/10.1007/s00521-021-05995-8

[16] Li, S., & Zhang, X. (2020). Research on orthopedic auxiliary classification and prediction model based on XGBoost algorithm. *Neural Computing and Applications*, *32*(7), 1971-1979. https://doi.org/10.1007/s00521-019-04378-4

[17] Wang, D. N., Li, L., & Zhao, D. (2022). Corporate finance risk prediction based on LightGBM. *Information Sciences*, *602*, 259-268. https://doi.org/10.1016/j.ins.2022.04.058

[18] Gu, Q., Sun, W., Li, X., Jiang, S., & Tian, J. (2023). A new ensemble classification approach based on Rotation Forest and LightGBM. *Neural Computing and Applications*, *35*(15), 11287-11308. https://doi.org/10.1007/s00521-023-08297-3

[19] Ying, C., Qi-Guang, M., Jia-Chen, L., ve Lin, G. (2013). Advance and prospects of AdaBoost algorithm. *Acta Automatica Sinica*, *39*(6), 745-758. https://doi.org/10.1016/S1874-1029(13)60052-X

[20] Hoens, T. R., & Chawla, N. V. (2013). Imbalanced datasets: from sampling to classifiers. H. He & Y. Ma (Ed.), *Imbalanced learning: Foundations, algorithms, and applications*, (s.43-59). Wiley Online Library.

[21] Wang, J., Xu, M., Wang, H., & Zhang, J. (2006). *Classification of imbalanced data by using the SMOTE algorithm and locally linear embedding* [Bildiri sunumu]. In 8th international conference on signal processing (IEEE), China.

[22] Birla, S., Kohli, K., & Dutta, A. (2016). *Machine learning on imbalanced data in credit risk* [Bildiri sunumu]. In 2016 IEEE 7th annual information technology, electronics and mobile communication conference (IEMCON), Canada.

[23] Wang, Z. H. E., Wu, C., Zheng, K., Niu, X., & Wang, X. (2019). SMOTETomek-based resampling for personality recognition. *IEEE access*, *7*, 129678-129689. https://doi:10.1109/ACCESS.2019.2940061

[24] Werner de Vargas, V., Schneider Aranda, J. A., dos Santos Costa, R., da Silva Pereira, P. R., & Victória Barbosa, J. L. (2023). Imbalanced data preprocessing techniques for machine learning: a systematic mapping study. *Knowledge and Information Systems*, *65*(1), 31-57. https://doi.org/10.1007/s10115-022-01772-8

[25] Mandrekar, J. N. (2010). Receiver operating characteristic curve in diagnostic test assessment. *Journal of Thoracic Oncology*, *5*(9), 1315-1316. https://doi.org/10.1097/JTO.0b013e3181ec173d

[26] Keçeoğlu, Ç. R., Gelbal, S., & Doğan, N. (2016). Roc eğrisi yöntemi ile kesme puaninin belirlenmesi. *The Journal of Academic Social Science Studies, 50*(2), 553-562. http://dx.doi.org/10.9761/JASSS3564

[27] Oommen, T., Baise, L. G., & Vogel, R. M. (2011). Sampling bias and class imbalance in maximum-likelihood logistic regression. *Mathematical Geosciences*, *43*, 99-120. https://doi10.1007/s11004-010-9311-8

[28] Huang, J., & Ling, C. X. (2005). Using AUC and accuracy in evaluating learning algorithms. *IEEE Transactions on knowledge and Data Engineering*, *17*(3), 299-310.

[29] LemaÃŽtre, G., Nogueira, F., & Aridas, C. K. (2017). Imbalanced-learn: A python toolbox to tackle the curse of imbalanced datasets in machine learning. *Journal of Machine Learning Research*, *18*(17), 1-5.

Sinopfbd, 2024; 9(1): 167-183 **https://doi.org/10.33484/sinopfbd.1401042**

Sinop Üniversitesi Fen Bilimleri Dergisi
Sinop Uni J Nat Sci
E-ISSN: 2564-7873

https://dergipark.org.tr/tr/pub/sinopfbd

Pell Collocation Approach For The Nonlinear Pantograph Differential Equations

Pınar ALBAYRAK

How to cite: Albayrak, P. (2024). Pell collocation approach for the nonlinear pantograph differential equations. *Sinop Üniversitesi Fen Bilimleri Dergisi*, *9*(1), 167-183. https://doi.org/10.33484/sinopfbd.1401042

Research Article

Corresponding Author
Pınar ALBAYRAK
pkanar@yildiz.edu.tr

ORCID of the Author
P.A: 0000-0002-7973-3500

Received: 07.12.2023
Accepted: 27.05.2024

Abstract

Pantograph equations, which we encounter in the branches of pure and applied mathematics such as electrodynamics, control systems and quantum mechanics, are essentially a particular form of the functional differential equations characterized with proportional delays. This study focuses on exploring the approximate solution to the Pantograph differential equation. Since there is no analytic solutions for this equation class, only the approximate solutions can be obtain. For this purpose, Pell Collocation Method which is one of the numerical solution methods is chosen. As the result of applying the method to the equation, an algebraic equation system has been gained and then the approximate solution has been found by using MATHEMATICA via the given initial conditions. The method is applied to the some test examples and then the results are presented by both graphically and by table. The error estimations show that the method works accurately and efficiently.

Keywords: Approximate solution, pantograph differential equation, collocation method

Lineer Olmayan Pantograf Diferansiyel Denklemleri İçin Pell Sıralama Yaklaşımı

Yıldız Technical University,
Department of Mathematics,
Istanbul, Türkiye

Öz

Elektrodinamik, kontrol sistemleri ve kuantum mekaniği gibi teorik ve uygulamalı matematiğin dallarında karşılaştığımız Pantograf denklemleri, orantısal gecikmeli fonksiyonel diferansiyel denklemlerin özel bir türüdür. Bu çalışmada, Pantograf diferansiyel denklemin yaklaşık çözümleri üzerine çalışılmıştır. Bu denklem sınıfı için analitik çözüm olmadığından sadece yaklaşık çözümleri bulunabilir. Bu amaçla sayısal çözüm yöntemlerinden biri olan Pell sıralama yöntemi seçilmiştir. Yöntemin denkleme uygulanması sonucunda bir cebirsel denklem sistemi elde edilmiş ve MATHEMATICA programı kullanılarak verilen başlangıç koşulları ile yaklaşık çözüm bulunmuştur. Bu yöntem bazı test örneklerine uygulanmış ve sonuçlar hem grafiksel olarak hem de tablo olarak ifade edilmiştir. Hata analizleri bu yöntemin doğru ve etkili çalıştığını göstermiştir.

Anahtar Kelimeler: Yaklaşık çözüm, pantograf diferansiyel denklemi, sıralama yöntemi

Introduction

Many problems that we encounter in every aspect of our lives are modeled via mathematics and solutions of the models are one of the main topic for the researchers. Differential equations take an important place in these modeling. One of these differential equations is the Pantograph differential equation. The Pantograph differential equation (PDE) is a special class of the functional differential equations. Actually, Pantograph is a device that collects electric current from electric poles in vehicles such as trains and trams. For the modelling of the problem, PDE was firstly mentioned in the study [1] by J.R. Ockendon and A.B.Tayler in 1971. In this study, the Pantograph of the electric locomotive was modeled. Later, many studies were conducted on this subject. Since the PDE equation does not have an exact solution, only approximate solution can be found. To obtain the approximate solution, various numerical methods such as homotopy methods, Haar wavelets, Legendre approximations, Sinc collocation method can be considered. To get more information about these numerical methods, readers can be look into [2-11]. In recent years different numerical approaches are applied to the PDE. For instance, Sedaghat et. al. applied a numerical approach to find the approximate solution of the PDE with the help of Chebyshev polynomials in [12]. In the work [13] Jafari et. al. provide an efficient transferred Legendre pseudospectral method for solving PDE. M. M. Bahşi and M. Çevik resorted to the Perturbation approach for Pantograph delay differential equation (PDDE) in [14]. R. Alrebdi and H. K. Al-jeaid in [15] examined the PDDE with the help of the Laplace transformation, which is one of the integral transformations. For more work related to PDE see [16-20].

In recent years, some collocation methods to solve the linear and nonlinear differential, integral and pantograph equations have been presented in many articles. Such as Legendre-Gauss collocation method [21], Chebyshev collocation method [22], Fibonacci wavelet collocation method [23], Hermite collocation approach [24], Legendre spectral collocation method [25] and Lagrange-collocation method [26]. In addition to these methods, there are also Pell collocation method and Pell-Lucas collocation methods. These two collocation methods based on Pell and Pell-Lucas polynomials respectively. These polynomials belong to families of orthogonal polynomials and are characterized by recursive expressions and satisfy the following properties [27]: Pell polynomials, $P_n(x)$, are defined as follows

$$P_{n+2}(x) = 2xP_{n+1}(x) + P_n(x) \ , \ n \geqslant 0$$

where $P_0(x) = 0,\ P_1(x) = 1$. Pell-Lucas polynomials, $Q_n(x)$, are defined by

$$Q_{n+2}(x) = 2xQ_{n+1}(x) + Q_n(x) \ , \ n \geqslant 0$$

where $Q_0(x) = 2,\ Q_1(x) = 2x$. There are many studies using methods based on Pell and Pell-Lucas polynomials [28-32]. In our paper, we tried to obtain the approximate solution by applying the Pell collocation method (PCM) to a class of nonlinear PDE (NPDE).

Let us consider a class of NPDE defined as

$$\begin{aligned}&\sum_{s=0}^{n}\sum_{p=0}^{m} R_{sp}(x)v^{p}\left(\alpha_{sp}x+\beta_{sp}\left(x\right)\right)v^{(s)}(\lambda_{sp}x+\gamma_{sp}\left(x\right))\\&+\sum_{s=1}^{n}\sum_{p=1}^{m} Q_{sp}(x)v^{(p)}\left(\alpha_{sp}x+\beta_{sp}\left(x\right)\right)v^{(s)}(\lambda_{sp}x+\gamma_{sp}\left(x\right))=g(x),\ \text{for } a\leq x\leq b\end{aligned} \tag{1}$$

with the initial conditions

$$\sum_{s=0}^{n}\left[a_{js}v^{(s)}(0)+b_{js}v^{(s)}(0)\right]=\delta_{j},\qquad j=0,1. \tag{2}$$

Here, $v^{(0)}(x)=v(x),\ v^{0}(x)=1$. Also, $v(x)$ is an unknown function; the functions $R_{sp}(x)$, $Q_{sp}(x)$ and $g(x)$ are continuous on $[0,1]$; $a_{js},\ b_{js},\alpha_{sp},\ \lambda_{sp}$ and δ_{j} are constants. Additionally, $\beta_{sp}\left(x\right)$ and $\gamma_{sp}\left(x\right)$ are either appropriate constants or random variables. In our approach, we will consider the approximate solution to be the truncated Pell series, represented as:

$$v\left(x\right)=\sum_{m=1}^{M+1}c_{m}P_{m}(x). \tag{3}$$

In this series, $P_{m}(x)\ (1\leq m\leq M+1)$ are the Pell polynomials; c_{m} are the coefficients to be found and $M\in\mathbb{Z}^{+}(M\geq n)$. The first few Pell polynomials are as follows:

$$\begin{aligned}P_{0}(x)=&0,\\P_{1}(x)=&\mathbf{1},\\P_{2}(x)=&2x,\\P_{3}(x)=&\mathbf{4}x^{2}+\mathbf{1},\\P_{4}(x)=&8x^{3}+4x,\\P_{5}(x)=&16x^{4}+12x^{2}+1,\\&\vdots\end{aligned} \tag{4}$$

Fundamental Relations

Let Eq. (3) be our approximate solution of Eq. (1). In order to obtain the approximate solution, we will try to write Eq. (1) in matrix form according to the solution of Eq. (3).
i) If $\alpha_{sp}=\ \lambda_{sp}=1,\beta_{sp}\left(x\right)\ =\gamma_{sp}\left(x\right)=0,$ Pell polynomials in Eq. (4) can be represented in matrix format as

$$\mathbf{P}\left(x\right)=\mathbf{\Gamma}\left(x\right)\mathbf{N}. \tag{5}$$

Here, $P(x) = [P_1(x)\ P_2(x) \cdots P_{M+1}(x)]$, $\mathbf{\Gamma}(x) = \left(1\ x\ x^2\ x^3 ... x^M\right)$, $\mathbf{C} = (c_1\ c_2\ \cdots c_{M+1})^T$ and

$$\mathbf{N} = \begin{bmatrix} \mathbf{1} & 0 & \mathbf{1} & 0 & \mathbf{1} & 0 & \mathbf{1} & 0 & \mathbf{1} & \cdots \\ 0 & 2 & 0 & 4 & 0 & 6 & 0 & 8 & 0 & \cdots \\ 0 & 0 & \mathbf{4} & 0 & \mathbf{12} & 0 & \mathbf{24} & 0 & \mathbf{40} & \cdots \\ 0 & 0 & 0 & 8 & 0 & 32 & 0 & 80 & 0 & \cdots \\ 0 & 0 & 0 & 0 & \mathbf{16} & 0 & \mathbf{80} & 0 & \mathbf{240} & \cdots \\ 0 & 0 & 0 & 0 & 0 & 32 & 0 & 192 & 0 & \cdots \\ 0 & 0 & 0 & 0 & 0 & 0 & \mathbf{64} & 0 & \mathbf{448} & \cdots \\ 0 & 0 & 0 & 0 & 0 & 0 & 0 & 128 & 0 & \cdots \\ 0 & 0 & 0 & 0 & 0 & 0 & 0 & 0 & \mathbf{256} & \cdots \\ \vdots & \vdots & \vdots & \vdots & \vdots & \vdots & \vdots & \vdots & \vdots & \ddots \end{bmatrix}.$$

So, we can express Eq. (3) as

$$v(x) = \mathbf{P}(x)\,\mathbf{C}. \tag{6}$$

If we put Eq. (5) in Eq. (6), then $v(x)$ will be

$$\begin{aligned} v(x) &\cong v_M(x) = \mathbf{\Gamma}(x)\,\mathbf{NC}, \\ v'(x) &\cong v'_M(x) = \mathbf{\Gamma}(x)\,\mathbf{BNC}, \\ v''(x) &\cong v''_M(x) = \mathbf{\Gamma}(x)\,\mathbf{B}^2\mathbf{NC}, \\ &\vdots \\ v^{(s)}(x) &\cong v_M^{(s)}(x) = \mathbf{\Gamma}(x)\,\mathbf{B}^s\mathbf{NC}. \end{aligned} \tag{7}$$

Also,

$$\begin{aligned} \mathbf{\Gamma}'(x) &= \mathbf{\Gamma}(x)\,\mathbf{B}, \\ \mathbf{\Gamma}''(x) &= \mathbf{\Gamma}(x)\,\mathbf{B}^2, \\ \mathbf{\Gamma}'''(x) &= \mathbf{\Gamma}(x)\,\mathbf{B}^3, \\ &\vdots \\ \mathbf{\Gamma}^{(s)}(x) &= \mathbf{\Gamma}(x)\,\mathbf{B}^s. \end{aligned} \tag{8}$$

In Eq. (8)

$$\mathbf{B}=\begin{bmatrix} 0 & 1 & 0 & 0 & 0 & 0 & \cdots & 0 \\ 0 & 0 & 2 & 0 & 0 & 0 & \cdots & 0 \\ 0 & 0 & 0 & 3 & 0 & 0 & \cdots & 0 \\ 0 & 0 & 0 & 0 & 4 & 0 & \cdots & 0 \\ 0 & 0 & 0 & 0 & 0 & 5 & \cdots & 0 \\ 0 & 0 & 0 & 0 & 0 & 0 & \cdots & 0 \\ \vdots & \vdots & \vdots & \vdots & \vdots & \ddots & \ddots & M \\ 0 & 0 & 0 & 0 & 0 & 0 & \cdots & 0 \end{bmatrix}, \mathbf{B}^0=\begin{bmatrix} 1 & 0 & 0 & 0 & 0 & 0 & \cdots & 0 \\ 0 & 1 & 0 & 0 & 0 & 0 & \cdots & 0 \\ 0 & 0 & 1 & 0 & 0 & 0 & \cdots & 0 \\ 0 & 0 & 0 & 1 & 0 & 0 & \cdots & 0 \\ 0 & 0 & 0 & 0 & 1 & 0 & \cdots & 0 \\ 0 & 0 & 0 & 0 & 0 & 1 & \cdots & 0 \\ \vdots & \vdots & \vdots & \vdots & \vdots & \ddots & \ddots & 0 \\ 0 & 0 & 0 & 0 & 0 & 0 & \cdots & 1 \end{bmatrix},$$

$$\mathbf{\Gamma}_{1,0}=\begin{bmatrix} 1 & x_0 & ... & x_0^M \\ 1 & x_1 & ... & x_1^M \\ 1 & \vdots & ... & \vdots \\ 1 & x_M & ... & x_M^M \end{bmatrix}.$$

ii) If α_{sp} , λ_{sp} , $\beta_{sp}(x)$ and $\gamma_{sp}(x)$ are either random constants or variables, then the approximate solution using the Pell polynomials in Eq. (3) can be represented in the matrix format

$$v(\lambda_{sp}x+\gamma_{sp}(x)) \cong v_M(\lambda_{sp}x+\gamma_{sp}(x)) = \mathbf{P}(\lambda_{sp}x+\gamma_{sp}(x))\,\mathbf{C}. \tag{9}$$

By considering Eq. (5) and Eq. (6) in Eq. (9), we get the matrix forms

$$\begin{aligned} v(\lambda_{sp}x+\gamma_{sp}(x)) \cong & v_M(\lambda_{sp}x+\gamma_{sp}(x)) = \mathbf{P}(\lambda_{sp}x+\gamma_{sp}(x))\,\mathbf{C} = \mathbf{\Gamma}(\lambda_{sp}x+\gamma_{sp}(x))\,\mathbf{NC}, \\ v'(\lambda_{sp}x+\gamma_{sp}(x)) \cong & v'_M(\lambda_{sp}x+\gamma_{sp}(x)) = \mathbf{\Gamma}_{(\lambda,\,\gamma)}(x)\,\mathbf{BNC}, \\ v''(\lambda_{sp}x+\gamma_{sp}(x)) \cong & v''_M(\lambda_{sp}x+\gamma_{sp}(x)) = \mathbf{\Gamma}_{(\lambda,\,\gamma)}(x)\,\mathbf{B}^2\mathbf{NC}, \\ & \vdots \\ v^{(s)}(\lambda_{sp}x+\gamma_{sp}(x)) \cong & v_M^{(s)}(\lambda_{sp}x+\gamma_{sp}(x)) = \mathbf{\Gamma}_{(\lambda,\,\gamma)}(x)\,\mathbf{B}^s\mathbf{NC}. \end{aligned} \tag{10}$$

Furthermore, the relationships between $\mathbf{\Gamma}(\lambda_{sp}x+\gamma_{sp}(x))$ and its derivatives
$\mathbf{\Gamma}'(\lambda_{sp}x+\gamma_{sp}(x))$, $\mathbf{\Gamma}''(\lambda_{sp}x+\gamma_{sp}(x))$,..., $\mathbf{\Gamma}^{(s)}(\lambda_{sp}x+\gamma_{sp}(x))$ are described as

$$\begin{aligned} \mathbf{\Gamma}'(\lambda_{sp}x+\gamma_{sp}(x)) = & \mathbf{\Gamma}(\lambda_{sp}x+\gamma_{sp}(x))\,\mathbf{B}, \\ \mathbf{\Gamma}''(\lambda_{sp}x+\gamma_{sp}(x)) = & \mathbf{\Gamma}(\lambda_{sp}x+\gamma_{sp}(x))\,\mathbf{B}^2, \\ \mathbf{\Gamma}'''(\lambda_{sp}x+\gamma_{sp}(x)) = & \mathbf{\Gamma}(\lambda_{sp}x+\gamma_{sp}(x))\,\mathbf{B}^3, \\ & \vdots \\ \mathbf{\Gamma}^{(s)}(\lambda_{sp}x+\gamma_{sp}(x)) = & \mathbf{\Gamma}(\lambda_{sp}x+\gamma_{sp}(x))\,\mathbf{B}^s, \end{aligned} \tag{11}$$

where

$$\mathbf{\Gamma}_{\lambda,\,\gamma}=\begin{bmatrix}\mathbf{\Gamma}\left(\lambda_{sp}x_0+\gamma_{sp}\left(x_0\right)\right)\\ \mathbf{\Gamma}\left(\lambda_{sp}x_1+\gamma_{sp}\left(x_1\right)\right)\\ \vdots\\ \mathbf{\Gamma}\left(\lambda_{sp}x_M+\gamma_{sp}\left(x_M\right)\right)\end{bmatrix}=\begin{bmatrix}1 & \lambda_{sp}x_0+\gamma_{sp}\left(x_0\right) & ... & \left(\lambda_{sp}x_0+\gamma_{sp}\left(x_0\right)\right)^M\\ 1 & \lambda_{sp}x_1+\gamma_{sp}\left(x_1\right) & ... & \left(\lambda_{sp}x_1+\gamma_{sp}\left(x_1\right)\right)^M\\ 1 & \vdots & ... & \vdots\\ 1 & \lambda_{sp}x_M+\gamma_{sp}\left(x_M\right) & ... & \left(\lambda_{sp}x_M+\gamma_{sp}\left(x_M\right)\right)^M\end{bmatrix}.$$

With the help of Eq. (10) and Eq. (11), we find

$$v^{(s)}\left(\lambda_{sp}x+\gamma_{sp}\left(x\right)\right)=\mathbf{\Gamma}\left(\lambda_{sp}x+\gamma_{sp}\left(x\right)\right)\mathbf{B}^s\mathbf{NC}. \tag{12}$$

The Pell collocation points are defined by

$$x_i=a+\frac{\left(b-a\right)i}{M},\,i=0,1,...,M. \tag{13}$$

If we substitute these grid points into Eq. (12), we get

$$v^{(s)}\left(\lambda_{sp}x_i+\gamma_{sp}\left(x_i\right)\right)=\mathbf{\Gamma}_{\lambda,\,\gamma}\left(x_i\right)\mathbf{B}^s\mathbf{NC},\;s=0,1,...,n \tag{14}$$

and the closed form of the Eq. (14) can be stated as:

$$\mathbf{V}^{(s)}=\mathbf{\Gamma}_{\lambda,\,\gamma}\mathbf{B}^s\mathbf{NC},\;s=0,1,...,n. \tag{15}$$

Here

$$\mathbf{V}^{(s)}=\begin{bmatrix}v^{(s)}\left(\lambda_{sp}x_0+\gamma_{sp}\left(x_0\right)\right)\\ v^{(s)}\left(\lambda_{sp}x_1+\gamma_{sp}\left(x_1\right)\right)\\ \vdots\\ v^{(s)}\left(\lambda_{sp}x_M+\gamma_{sp}\left(x_M\right)\right)\end{bmatrix}.$$

In addition, the matrix forms of $\left(\hat{\mathbf{V}}\right)^{p}\ \mathbf{V}^{(s)}$ and $\left(\hat{\mathbf{V}}\right)^{(p)}\ \mathbf{V}^{(s)}$ which emerges in Eq. (1) are

$$\left(\hat{\mathbf{V}}\right)^{p}\ \mathbf{V}^{(s)} = \begin{bmatrix} v^{p}\left(\alpha_{sp}x_0+\beta_{sp}\left(x_0\right)\right)v^{(s)}\left(\lambda_{sp}x_0+\gamma_{sp}\left(x_0\right)\right) \\ v^{p}\left(\alpha_{sp}x_1+\beta_{sp}\left(x_1\right)\right)v^{(s)}\left(\lambda_{sp}x_1+\gamma_{sp}\left(x_1\right)\right) \\ \vdots \\ v^{p}\left(\alpha_{sp}x_M+\beta_{sp}\left(x_M\right)\right)v^{(s)}\left(\lambda_{sp}x_M+\gamma_{sp}\left(x_M\right)\right) \end{bmatrix}$$

$$= \begin{bmatrix} v^{p}\left(\alpha_{sp}x_0+\beta_{sp}\left(x_0\right)\right) & 0 & \dots & 0 \\ 0 & v^{p}\left(\alpha_{sp}x_1+\beta_{sp}\left(x_1\right)\right) & \dots & 0 \\ \vdots & \vdots & \ddots & \vdots \\ 0 & 0 & \dots & v^{p}\left(\alpha_{sp}x_M+\beta_{sp}\left(x_M\right)\right) \end{bmatrix}$$

$$\times \begin{bmatrix} v^{(s)}\left(\lambda_{sp}x_0+\gamma_{sp}\left(x_0\right)\right) \\ v^{(s)}\left(\lambda_{sp}x_1+\gamma_{sp}\left(x_1\right)\right) \\ \vdots \\ v^{(s)}\left(\lambda_{sp}x_M+\gamma_{sp}\left(x_M\right)\right) \end{bmatrix}$$

$$\left(\hat{\mathbf{V}}\right)^{(p)}\ \mathbf{V}^{(s)} = \begin{bmatrix} v^{(p)}\left(\alpha_{sp}x_0+\beta_{sp}\left(x_0\right)\right)v^{(s)}\left(\lambda_{sp}x_0+\gamma_{sp}\left(x_0\right)\right) \\ v^{(p)}\left(\alpha_{sp}x_1+\beta_{sp}\left(x_1\right)\right)v^{(s)}\left(\lambda_{sp}x_1+\gamma_{sp}\left(x_1\right)\right) \\ \vdots \\ v^{(p)}\left(\alpha_{sp}x_M+\beta_{sp}\left(x_M\right)\right)v^{(s)}\left(\lambda_{sp}x_M+\gamma_{sp}\left(x_M\right)\right) \end{bmatrix} \tag{16}$$

$$= \begin{bmatrix} v^{(p)}\left(\alpha_{sp}x_0+\beta_{sp}\left(x_0\right)\right) & 0 & \dots & 0 \\ 0 & v^{(p)}\left(\alpha_{sp}x_1+\beta_{sp}\left(x_1\right)\right) & \dots & 0 \\ \vdots & \vdots & \ddots & \vdots \\ 0 & 0 & \dots & v^{(p)}\left(\alpha_{sp}x_M+\beta_{sp}\left(x_M\right)\right) \end{bmatrix}$$

$$\times \begin{bmatrix} v^{(s)}\left(\lambda_{sp}x_0+\gamma_{sp}\left(x_0\right)\right) \\ v^{(s)}\left(\lambda_{sp}x_1+\gamma_{sp}\left(x_1\right)\right) \\ \vdots \\ v^{(s)}\left(\lambda_{sp}x_M+\gamma_{sp}\left(x_M\right)\right) \end{bmatrix}$$

where

$$\hat{\mathbf{V}} = \hat{\mathbf{\Gamma}}\ \hat{\mathbf{N}}\ \hat{\mathbf{C}} \text{ and } \left(\hat{\mathbf{V}}\right)^{(p)} = \hat{\mathbf{\Gamma}}\left(\hat{\mathbf{B}}\right)^{p}\ \hat{\mathbf{N}}\ \hat{\mathbf{C}}, \tag{17}$$

$$\hat{\mathbf{\Gamma}}_{\lambda,\gamma} = \begin{bmatrix} \mathbf{\Gamma}\left(\lambda_{sp}x_0+\gamma_{sp}\left(x_0\right)\right) & 0 & \dots & 0 \\ 0 & \mathbf{\Gamma}\left(\lambda_{sp}x_1+\gamma_{sp}\left(x_1\right)\right) & \dots & 0 \\ \vdots & \vdots & \ddots & \vdots \\ 0 & 0 & \dots & \mathbf{\Gamma}\left(\lambda_{sp}x_M+\gamma_{sp}\left(x_M\right)\right) \end{bmatrix},$$

$$\hat{\mathbf{B}} = \begin{bmatrix} \mathbf{B} & 0 & ... & 0 \\ 0 & \mathbf{B} & ... & 0 \\ \vdots & \vdots & \ddots & \vdots \\ 0 & 0 & ... & \mathbf{B} \end{bmatrix}, \ \hat{\mathbf{N}} = \begin{bmatrix} \mathbf{N} & 0 & ... & 0 \\ 0 & \mathbf{N} & ... & 0 \\ \vdots & \vdots & \ddots & \vdots \\ 0 & 0 & ... & \mathbf{N} \end{bmatrix}, \ \hat{\mathbf{C}} = \begin{bmatrix} \mathbf{C} & 0 & ... & 0 \\ 0 & \mathbf{C} & ... & 0 \\ \vdots & \vdots & \ddots & \vdots \\ 0 & 0 & ... & \mathbf{C} \end{bmatrix}.$$

By alternating the grid points given in Eq. (13) into Eq. (16), the following equation system is obtained

$$\begin{aligned} &\sum_{s=0}^{n}\sum_{p=0}^{m} R_{sp}(x_i) v^{p}\left(\alpha_{sp}x_i+\beta_{sp}\left(x_i\right)\right) v^{(s)}(\lambda_{sp}x_i+\gamma_{sp}\left(x_i\right)) \\ &+\sum_{s=1}^{n}\sum_{p=1}^{m} Q_{sp}(x_i) v^{(p)}\left(\alpha_{sp}x_i+\beta_{sp}\left(x_i\right)\right) v^{(s)}(\lambda_{sp}x_i+\gamma_{sp}\left(x_i\right)) \\ &=g(x_i), \end{aligned} \tag{18}$$

which can be represented using Eqs. (14) and (16) as

$$\sum_{s=0}^{n}\sum_{p=0}^{m} \mathbf{R}_{sp}\left(\hat{\mathbf{V}}\right)^{p}\ \mathbf{V}^{(s)}+\sum_{s=1}^{n}\sum_{p=1}^{m} \mathbf{Q}_{sp}\left(\hat{\mathbf{V}}\right)^{(p)}\ \mathbf{V}^{(s)}=\mathbf{G}, \tag{19}$$

where

$$\begin{aligned} \mathbf{R}_{sp} &= diag\left[R_{sp}(x_0)\ \ R_{sp}(x_1)\ \ ...\ \ R_{sp}(x_M)\right], \\ \mathbf{Q}_{sp} &= diag\left[Q_{sp}(x_0)\ \ Q_{sp}(x_1)\ \ ...\ \ Q_{sp}(x_M)\right], \\ \mathbf{G} &= \left[\ g(x_0)\quad g(x_1)\quad ...\quad g(x_M)\ \right]^{T}. \end{aligned}$$

By substituting the relations (15) and (17) into Eq. (19), the fundamental matrix equation is achieved as

$$\left\{\sum_{s=0}^{n}\sum_{p=0}^{m} \mathbf{R}_{sp}\left(\hat{\mathbf{\Gamma}}_{\alpha,\beta}\,\hat{\mathbf{N}}\,\hat{\mathbf{C}}\ \right)^{p}\ \mathbf{\Gamma}_{\lambda,\gamma}\mathbf{B}^{s}\mathbf{N}+\sum_{s=1}^{n}\sum_{p=1}^{m} \mathbf{Q}_{sp}\hat{\mathbf{\Gamma}}_{\alpha,\beta}\ \left(\hat{\mathbf{B}}\right)^{p}\ \hat{\mathbf{N}}\,\hat{\mathbf{C}}\ \mathbf{\Gamma}_{\lambda,\gamma}\mathbf{B}^{s}\mathbf{N}\right\}\mathbf{C}=\mathbf{G}. \tag{20}$$

Briefly, Eq. (20) can also be shown as,

$$\mathbf{WC}=\mathbf{G}\ \ \text{or}\ \left[\mathbf{W};\mathbf{G}\right], \tag{21}$$

where

$$\mathbf{W}=\sum_{s=0}^{n}\sum_{p=0}^{m} \mathbf{R}_{sp}\left(\hat{\mathbf{\Gamma}}_{\alpha,\beta}\,\hat{\mathbf{N}}\,\hat{\mathbf{C}}\ \right)^{p}\ \mathbf{\Gamma}_{\lambda,\gamma}\mathbf{B}^{s}\mathbf{N}+\sum_{s=1}^{n}\sum_{p=1}^{m} \mathbf{Q}_{sp}\hat{\mathbf{\Gamma}}_{\alpha,\beta}\ \left(\hat{\mathbf{B}}\right)^{p}\ \hat{\mathbf{N}}\,\hat{\mathbf{C}}\ \mathbf{\Gamma}_{\lambda,\gamma}\mathbf{B}^{s}\mathbf{N}.$$

Here, Eq. (21) represents a system comprising $(M+1)$ nonlinear algebraic equations involving $(M+1)$ unknown Pell coefficients. Utilizing Eq. (15) for the values a and b, we formulate the matrix representation of the conditions stated in Eq. (2) as

$$\left\{\sum_{s=0}^{n-1}\left[a_{js}\mathbf{\Gamma}\left(0\right)+b_{js}\mathbf{\Gamma}\left(0\right)\right]\left(\mathbf{B}\right)^{(s)}\mathbf{N}\right\}\mathbf{C}=\delta_j,\ j=0,1,2,...,n-1$$

alternatively, this can be expressed as

$$\mathbf{U}_j\ \mathbf{C}=[\delta_j]\qquad\text{or}\quad[\mathbf{U}_j;\delta_j];\quad j=0,1,2,...,n-1 \tag{22}$$

Here

$$\mathbf{U}_j=\sum_{s=0}^{n-1}\left[a_{js}\mathbf{\Gamma}\left(0\right)+b_{js}\mathbf{\Gamma}\left(0\right)\right]\left(\mathbf{B}\right)^{(s)}\mathbf{N}=\left[u_{j0}\ \ u_{j1}\ \ u_{j2}\ ...\ u_{jM}\right].$$

Hence, through the substitution of the condition matrices in (22) with the n rows of the augmented matrix in (21), the new augmented matrix is achieved as

$$\left[\hat{\mathbf{W}};\hat{\mathbf{G}}\right]=\left[\begin{array}{ccccccc}
w_{00} & w_{01} & w_{02} & \cdots & w_{0M} & ; & g(x_0)\\
w_{10} & w_{11} & w_{12} & \cdots & w_{1M} & ; & g(x_1)\\
w_{20} & w_{21} & w_{22} & \cdots & w_{2M} & ; & g(x_2)\\
\vdots & \vdots & \vdots & \ddots & \vdots & ; & \vdots\\
w_{(M-n)0} & w_{(M-n)1} & w_{(M-n)2} & \cdots & w_{(M-n)M} & ; & g(x_{M-n})\\
u_{00} & u_{01} & u_{02} & \cdots & u_{0M} & ; & \delta_0\\
u_{10} & u_{11} & u_{12} & \cdots & u_{1M} & ; & \delta_1\\
u_{20} & u_{21} & u_{22} & \cdots & u_{2M} & ; & \delta_2\\
\vdots & \vdots & \vdots & \ddots & \vdots & ; & \vdots\\
u_{(n-1)0} & u_{(n-1)1} & u_{(n-1)2} & \cdots & u_{(n-1)M} & ; & \delta_{n-1}
\end{array}\right] \tag{23}$$

Thus, the determination of the unknown Pell coefficients $c_m,\ m=1,2,...,M+1$ is achieved through the solution of the system outlined in Eq. (23). Next, the coefficients are inserted into Eq. (3) to derive the approximate solution.

Error Estimation

To determine the accuracy of the proposed method, we define the error function $E_M(x)$ as following

$$E_M(x)=|v_M(x)-v(x)|. \tag{24}$$

Here, $v_M(x)$ is the approximate solution and $v(x)$ is the exact solution of Eq.(1).

Illustrative Example

This section provides four numerical examples to showcase the effectiveness of the proposed method. By using the error function $E_M(x)$, the method has been tested on these problems. The numerical results obtained have been displayed through tables and graphics.

Example 1. Let us examine the differential equation:

$$v''(x)+v'(\frac{x}{4})v\left(\frac{x}{5}\right)-v^2\left(\frac{x}{2}\right)=-\frac{x^4}{16}+\frac{x^3}{50}-\frac{x^2}{2}+\frac{x}{2}+1, \tag{25}$$

with the initial conditions

$v(0)=1,\ \ v'(0)=0.$

Eq. (25) is the second-order nonlinear pantograph differential equation and the function $v(x)=x^2+1$ is the exact solution of this equation. The solution $v(x)$ approximated by the Pell polynomials is obtained as

$$v\left(x\right)=\sum_{m=1}^{M+1}c_m P_m(x)$$

where $M=2,\ R_{20}\left(x\right)=1,\ \alpha_{20}=1,\ \beta_{20}=0,\ R_{11}\left(x\right)=1,\ \alpha_{11}=\frac{1}{4},\ \beta_{11}=0,\ \lambda_{11}=\frac{1}{5},\ \gamma_{11}=0,\ R_{01}\left(x\right)=-1,\ \alpha_{01}=\frac{1}{2},\ \beta_{01}=0,\ \lambda_{01}=\frac{1}{2},\ \gamma_{01}=0$, and $g\left(x\right)=-\frac{x^4}{16}+\frac{x^3}{50}-\frac{x^2}{2}+\frac{x}{2}+1$. Thus, for $M=2$ the set of obtained collocation points by Eq. (13) are computed as

$$x_0=0,\ \ x_1=\frac{1}{2},\ x_2=1$$

From Eq. (20), we obtain

$$\left\{\mathbf{R}_{20}\mathbf{\Gamma}_{1,0}\mathbf{B}^2\mathbf{N}+\mathbf{R}_{11}\hat{\mathbf{\Gamma}}_{\frac{1}{5},0}\hat{\mathbf{N}}\hat{\mathbf{C}}\mathbf{\Gamma}_{\frac{1}{4},0}\mathbf{B}\mathbf{N}+\mathbf{R}_{01}\hat{\mathbf{\Gamma}}_{\frac{1}{2},0}\,\hat{\mathbf{N}}\,\hat{\mathbf{C}}\,\mathbf{\Gamma}_{\frac{1}{2},0}\mathbf{N}\right\}\mathbf{C}=\mathbf{G}$$

where

$$\mathbf{W}=\mathbf{R}_{20}\mathbf{\Gamma}_{1,0}\mathbf{B}^2\mathbf{N}+\mathbf{R}_{11}\hat{\mathbf{\Gamma}}_{\frac{1}{5},0}\hat{\mathbf{N}}\hat{\mathbf{C}}\mathbf{\Gamma}_{\frac{1}{4},0}\mathbf{B}\mathbf{N}+\mathbf{R}_{01}\hat{\mathbf{\Gamma}}_{\frac{1}{2},0}\,\hat{\mathbf{N}}\,\hat{\mathbf{C}}\,\mathbf{\Gamma}_{\frac{1}{2},0}\mathbf{N}$$

$$\begin{aligned}
\mathbf{R}_{20} &= \mathbf{R}_{11}=\begin{bmatrix}1&0&0\\0&1&0\\0&0&1\end{bmatrix},\ \mathbf{R}_{01}=\begin{bmatrix}-1&0&0\\0&-1&0\\0&0&-1\end{bmatrix},\\
\mathbf{\Gamma}_{1,0} &= \mathbf{\Gamma}=\begin{bmatrix}\mathbf{\Gamma}\left(0\right)\\ \mathbf{\Gamma}\left(\frac{1}{2}\right)\\ \mathbf{\Gamma}\left(1\right)\end{bmatrix}=\begin{bmatrix}1&0&0\\1&\frac{1}{2}&\frac{1}{4}\\1&1&1\end{bmatrix},\ \hat{\mathbf{\Gamma}}_{1,0}=\begin{bmatrix}\mathbf{\Gamma}\left(0\right)&0&0\\0&\mathbf{\Gamma}\left(\frac{1}{2}\right)&0\\0&0&\mathbf{\Gamma}\left(1\right)\end{bmatrix},\\
\mathbf{\Gamma}_{\frac{1}{2},0} &= \begin{bmatrix}1&0&0\\1&\frac{1}{4}&\frac{1}{16}\\1&\frac{1}{2}&\frac{1}{4}\end{bmatrix},\ \hat{\mathbf{\Gamma}}_{\frac{1}{2},0}=\begin{bmatrix}\mathbf{\Gamma}_{\frac{1}{2},0}\left(0\right)&0&0\\0&\mathbf{\Gamma}_{\frac{1}{2},0}\left(\frac{1}{2}\right)&0\\0&0&\mathbf{\Gamma}_{\frac{1}{2},0}\left(1\right)\end{bmatrix}
\end{aligned}$$

$$\mathbf{\Gamma}_{\frac{1}{4},0} = \begin{bmatrix} 1 & 0 & 0 \\ 1 & \frac{1}{8} & \frac{1}{64} \\ 1 & \frac{1}{4} & \frac{1}{16} \end{bmatrix}, \ \hat{\mathbf{\Gamma}}_{\frac{1}{4},0} = \begin{bmatrix} \mathbf{\Gamma}_{\frac{1}{4},0}(0) & 0 & 0 \\ 0 & \mathbf{\Gamma}_{\frac{1}{4},0}\left(\frac{1}{2}\right) & 0 \\ 0 & 0 & \mathbf{\Gamma}_{\frac{1}{4},0}(1) \end{bmatrix}$$

$$\mathbf{\Gamma}_{\frac{1}{5},0} = \begin{bmatrix} 1 & 0 & 0 \\ 1 & \frac{1}{10} & \frac{1}{100} \\ 1 & \frac{1}{5} & \frac{1}{25} \end{bmatrix}, \ \hat{\mathbf{\Gamma}}_{\frac{1}{5},0} = \begin{bmatrix} \mathbf{\Gamma}_{\frac{1}{5},0}(0) & 0 & 0 \\ 0 & \mathbf{\Gamma}_{\frac{1}{5},0}\left(\frac{1}{2}\right) & 0 \\ 0 & 0 & \mathbf{\Gamma}_{\frac{1}{5},0}(1) \end{bmatrix}$$

$$\mathbf{N} = \begin{bmatrix} 1 & 0 & 1 \\ 0 & 2 & 0 \\ 0 & 0 & 4 \end{bmatrix}, \ \hat{\mathbf{N}} = \begin{bmatrix} N & 0 & 0 \\ 0 & N & 0 \\ 0 & 0 & N \end{bmatrix},$$

$$\mathbf{B} = \begin{bmatrix} 0 & 1 & 0 \\ 0 & 0 & 2 \\ 0 & 0 & 0 \end{bmatrix}, \ \hat{\mathbf{B}} = \begin{bmatrix} \mathbf{B} & 0 & 0 \\ 0 & \mathbf{B} & 0 \\ 0 & 0 & \mathbf{B} \end{bmatrix} \ \hat{\mathbf{C}} = \begin{bmatrix} \mathbf{C} & 0 & 0 \\ 0 & \mathbf{C} & 0 \\ 0 & 0 & \mathbf{C} \end{bmatrix}, \ \mathbf{G} = \begin{bmatrix} 1 \\ \frac{7191}{6400} \\ \frac{383}{400} \end{bmatrix}.$$

From Eq. (22), the matrix representation of the initial condition is

$$[\mathbf{U}_0;\ \delta_0] = [1\ \ 0\ \ 1\ \ ;\ \mathbf{1}],\ [\mathbf{U}_1;\ \delta_1] = [0\ \ 2\ \ 0\ \ ;\ \mathbf{0}].$$

Hence, the resulting augmented matrix $[\hat{\mathbf{W}};\hat{\mathbf{G}}]$ is obtained as following

$$[\hat{\mathbf{W}};\hat{\mathbf{G}}] = \begin{bmatrix} -a-c & 2a+2c & 8-c-a & ; & 1 \\ \mathbf{1} & \mathbf{0} & \mathbf{1} & ; & \mathbf{1} \\ \mathbf{0} & \mathbf{2} & \mathbf{0} & ; & \mathbf{0} \end{bmatrix}.$$

The matrix of Pell coefficients C is established by solving this system:

$$\mathbf{C} = \begin{bmatrix} \frac{3}{4} & 0 & \frac{1}{4} \end{bmatrix}^T$$

Then, for $M = 2$, the solution approximated using the Pell polynomials is

$$v_2(x) = x^2 + 1.$$

Example 2. Consider the following differential equation

$$v''(x) - v(x) + \frac{8}{x^2}v^2\left(\frac{x}{2}\right) = 0; \quad v(0) = 0, v'(0) = 1. \tag{26}$$

We know that the exact solution of Eq. (26) is found by $v(x) = xe^{-x}$. Table 1 provides the error function values and offers a numerical comparison between the proposed method and the modified differential transform method (MDTM) [33] for $M = 8$ and $M = 11$. Figure 1 depicts a visual comparison between the approximate and exact solutions derived using the proposed method for $M = 3, 4, 5$.

Table 1. *The numerical results of the error function E_M are provided for different values of M for Example 2*

x	$E_8(MDTM)$	$E_{11}(MDTM)$	E_8	E_{11}
0.1	3.56812×10^{-12}	3.59265×10^{-12}	2.21233×10^{-9}	3.60961×10^{-13}
0.3	4.67857×10^{-10}	4.52835×10^{-12}	6.10001×10^{-9}	9.75359×10^{-13}
0.5	4.58254×10^{-8}	5.85598×10^{-11}	7.06047×10^{-9}	1.14569×10^{-12}
0.7	9.28161×10^{-7}	2.78563×10^{-10}	5.60762×10^{-9}	1.11228×10^{-12}
0.9	8.72761×10^{-6}	6.64594×10^{-9}	8.19878×10^{-10}	1.40254×10^{-12}

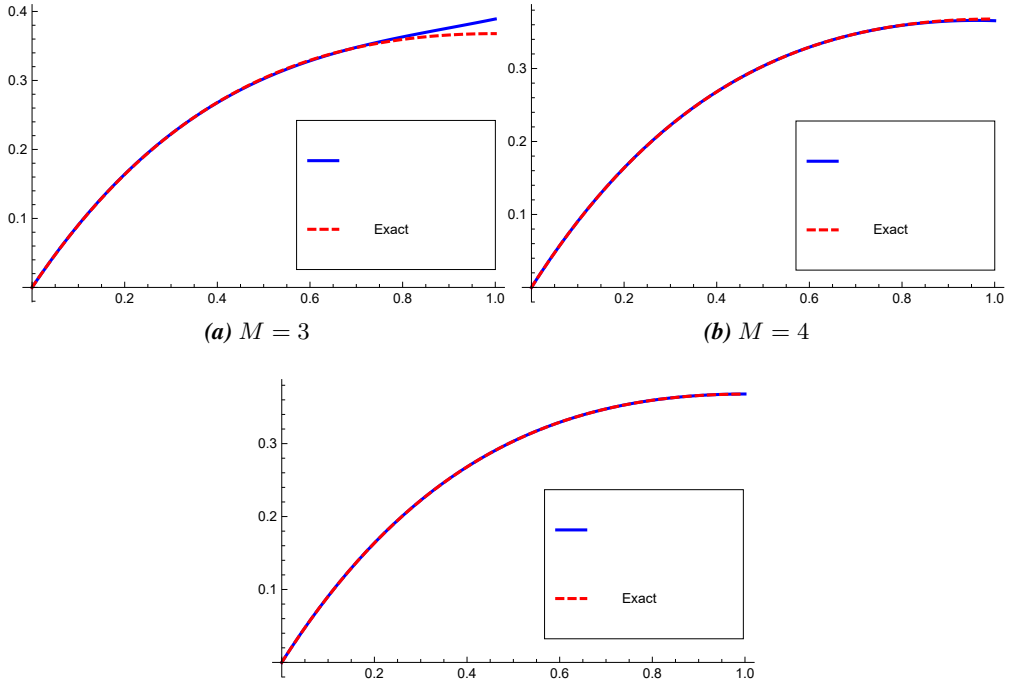

(a) $M = 3$ ***(b)*** $M = 4$

(c) $M = 5$

Figure 1. *Graphical comparison illustrating exact and approximate solutions for Example 2 at* $M = 3, 4, 5$

Example 3. Let us consider following differential equation [34]

$$v''(x) + 2v(x) - v^2(x) + v\left(\frac{x^3}{8}\right) = g(x); \quad v(0) = 0, v'(0) = 1 \tag{27}$$

where

$$g(x) = \sin x - \sin^2 x + \sin\left(\frac{x^3}{8}\right)$$

$v(x) = \sin x$ is the exact solution of Eq.(27). Values of the error function specified in Eq.(24) for Eq.(27) are displayed in Table 2, for $M = 9, 10, 11$. Figure 2 depicts the graphical representation of the estimated error function for $M = 2, 3$ and 4.

Table 2. *The numerical results of the error function E_M are provided for $M = 9, 10, 11$ for Example 3*

x	E_9	E_{10}	E_{11}
0.1	4.49765×10^{-13}	4.39510×10^{-14}	5.55112×10^{-16}
0.3	1.83259×10^{-12}	1.69309×10^{-13}	2.05391×10^{-15}
0.5	3.08087×10^{-12}	2.83495×10^{-13}	3.38618×10^{-15}
0.7	4.14413×10^{-12}	3.87912×10^{-13}	4.55191×10^{-15}
0.9	6.41098×10^{-12}	9.74887×10^{-13}	8.88178×10^{-16}

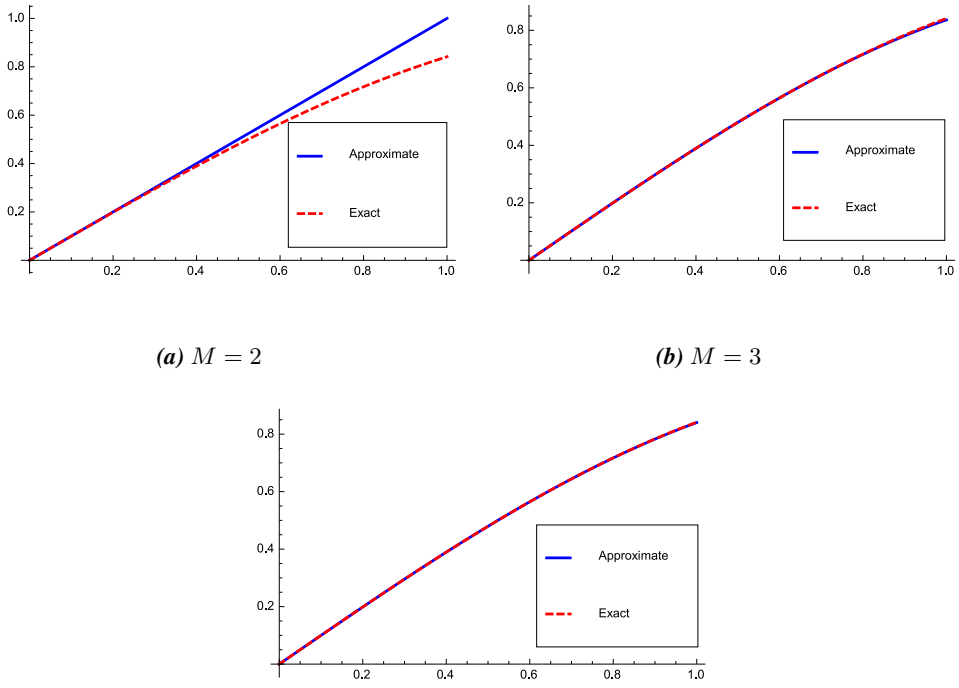

(a) $M = 2$ ***(b)*** $M = 3$

(c) $M = 4$

Figure 2. *The graphical comparison illustrating exact and approximate solutions for Example 3 at M = 2, 3, 4*

Example 4. Let us consider the following differential equation

$$xv'(\frac{x}{2})v^2(x) + v''(\frac{x}{4}) + v\left(\frac{x}{2}\right) + v'(x - 0.5) = g(x); \quad 0 \le x \le 1; \quad v(0) = 1,\ v'(0) = 0 \tag{28}$$

where

$$g(x) = -\sin(x - 0.5) + \cos(x/2) - \cos(x/4) - x\sin(x/2)\cos^2(x).$$

$v(x) = \cos(x)$ is the exact solution of Eq.28. For $M = 5, 7, 9$; values of the error function specified in Eq.(24) for Eq.(28) are showed in Table 3. The graphical representation of the estimated error function for $M = 3, 4, 5$ is depicted in Figure 3.

Table 3. *The numerical results of the error function E_M are provided for different values of M for Example 4*

x	E_5	E_7	E_9
0.1	3.91136×10^{-7}	3.34594×10^{-9}	1.23668×10^{-11}
0.3	2.81310×10^{-6}	2.21417×10^{-8}	6.88932×10^{-11}
0.5	3.83995×10^{-5}	2.74960×10^{-7}	6.02225×10^{-10}
0.7	2.73856×10^{-4}	1.41557×10^{-6}	2.76425×10^{-9}
0.9	1.17411×10^{-3}	2.09302×10^{-6}	2.20612×10^{-8}

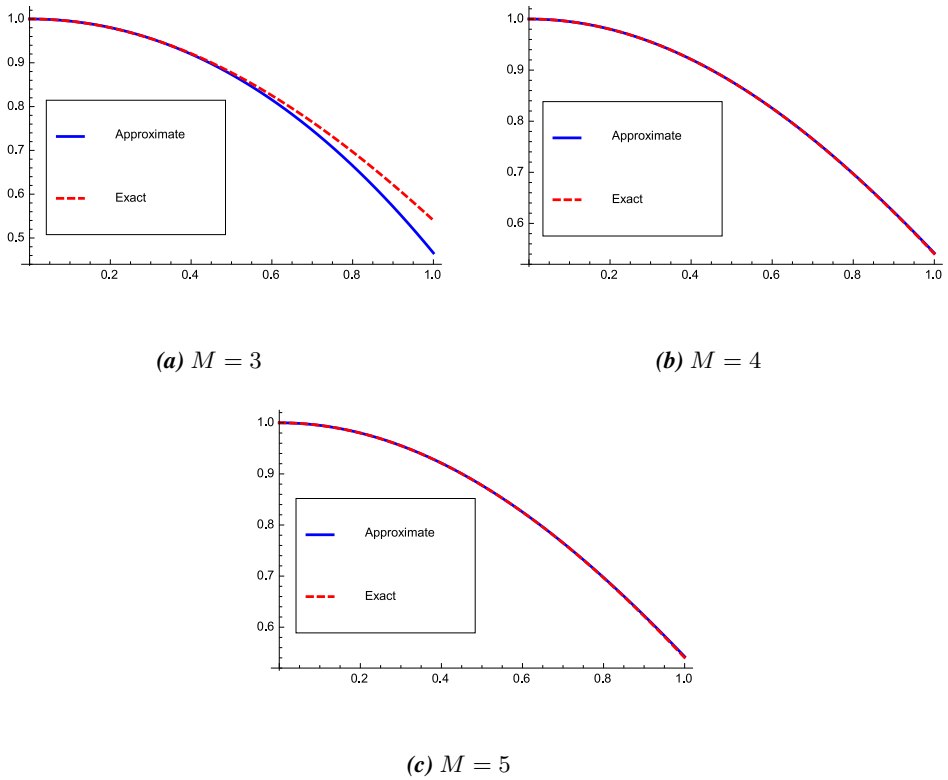

(a) $M = 3$ ***(b)*** $M = 4$

(c) $M = 5$

Figure 3. *Graphical comparison illustrating exact and approximate solutions for Example 4 at M = 3, 4, 5*

Conclusion

This study utilized the Pell collocation method to solve a class of nonlinear Pantograph differential equations. The method's efficiency and accuracy are demonstrated through four distinct examples. The approximate and error results obtained are compared with those obtained using the modified differential transform method. From these comparisons, it can be inferred that the method is notably effective in acquiring approximate solutions for nonlinear Pantograph differential equations.

Acknowledgments -

Funding/Financial Disclosure The author has no received any financial support for the research, or publication of this study.

Ethics Committee Approval and Permissions The work does not require ethics committee approval and any private permission.

Conflict of Interests The author stated that there are no conflict of interest in this article.

Authors Contribution The author read and approved the final manuscript.

References

[1] Ockendon, J. R., & Tayler, A. B. (1971). The dynamics of a current collection system for an electric locomotive. *Proceedings of the Royal Society of London, Series A, Mathematical and Physical Sciences*, 322 (1551), 447-468.

[2] Alkan, S., Aydin, M. N., & Coban, R. (2019). A numerical approach to solve the model of an electromechanical system. *Mathematical Methods in the Applied Sciences, 42*(16), 5266-5273.

[3] Alkan, S., & Secer, A. (2018). A collocation method for solving boundary value problems of fractional order. *Sakarya University Journal of Science, 22*(6), 1601-1608.

[4] Hesameddini, E., & Asadollahifard, E. (2015). Numerical solution of multi-order fractional differential equations via the sinc-collocation method. *Iranian Journal of Numerical Analysis and Optimization, 5*(1), 37-48.

[5] Nagy, A. M. (2017). Numerical solution of time fractional nonlinear Klein–Gordon equation using Sinc–Chebyshev collocation method. *Applied Mathematics and Computation*, 310, 139-148.

[6] Zhi, M., Aiguo, X., Zuguo, Y., & Long, S. (2014). Finite difference and Sinc-collocation approximations to a class of fractional diffusion-wave equations. *Journal of Applied Mathematics*, 536030.

[7] Moshtaghi, N., & Saadatmandi, A. (2021). Numerical solution of time fractional cable equation via the Sinc-Bernoulli collocation method. *Journal of Applied and Computational Mechanics, 7*(4), 1916-1924.

[8] Jalili, P., Jalili, B., Ahmad, I., Hendy, A., Ali, M., & Ganji, D. D. (2024). Python approach for Using homotopy perturbation method to investigate heat transfer problems, *Case Studies in Thermal Engineering, 54,* 104049.

[9] Hatipoglu, V. F. (2021). A novel model for the contamination of a system of three artificial lakes. *Discrete and Continuous Dynamical Systems-S, 14*(7), 2261-2272.

[10] Hatipoglu, V. F. (2019). A numerical algorithm for the solution of nonlinear fractional differential equations via beta-derivatives. *Mathematical Methods in the Applied Sciences, 42*(16), 5258-5265.

[11] Bayram, M., Hatipoglu, V. F., Alkan, S., & Das, S. E. (2018). A solution method for integro-differential equations of conformable fractional derivative. *Thermal Science, 22*(1), S7-S14.

[12] Sedaghat, S., Ordokhani, Y., & Dehghan, M. (2012). Numerical solution of the delay differential equations of pantograph type via Chebyshev polynomials. *Communications in Nonlinear Science and Numerical Simulation, 17*(12), 4815-4830.

[13] Jafari, H., Mahmoudi, M., & Skandari, M. H. N. (2021). A new numerical method to solve pantograph delay differential equations with convergence analysis. *Advances in Difference Equations, 2021*(1), 129.

[14] Bahşi, M. M., & Çevik, M. (2015). Numerical solution of pantograph-type delay differential equations using perturbation-iteration algorithms. *Journal of Applied Mathematics*, 139821.

[15] Alrebdi, R., & Al-Jeaid, H. K. (2023). Accurate solution for the pantograph delay differential equation via Laplace transform. *Mathematics, 11*(9), 2031.

[16] Izadi, M., & Srivastava, H. M. (2021). A novel matrix technique for multi-order pantograph differential equations of fractional order. *Proceedings of the Royal Society A: Mathematical, Physical and Engineering Sciences, 477*(2253), 20210321.

[17] Abdo, M. S., Abdeljawad, T., Kucche, K. D., Ali, S. M., & Jeelani, M.B. (2021). On nonlinear pantograph fractional differential equations with Atangana–Baleanu–Caputo derivative. *Advances in Difference Equations, 2021*(1), 65.

[18] Rahimkhani, P., Ordokhani, Y., & Babolian, E. (2017). Numerical solution of fractional pantograph differential equations by using generalized fractional-order Bernoulli wavelet. *Journal of Computational and Applied Mathematics*, 309, 493–510.

[19] Ali, I., Brunner, H., & Tang, T. (2009). Spectral methods for pantograph-type differential and integral equations with multiple delays. *Frontiers of Mathematics in China, 4*(1), 49–61.

[20] Rabiei, K., & Ordokhani, Y. (2019). Solving fractional pantograph delay differential equations via fractional-order Boubaker polynomials. *Engineering with Computers, 35*(4), 1431–1441.

[21] Xu, Y., Zhang, Y., & Zhao, J. (2019). Error analysis of the Legendre-Gauss collocation methods for the nonlinear distributed-order fractional differential equation. *Applied Numerical Mathematics*, 142, 122-138.

[22] Gebril, E., El-Azab, M. S., & Sameeh, M. (2024). Chebyshev collocation method for fractional Newell-Whitehead-Segel equation. *Alexandria Engineering Journal*, 87, 39-46.

[23] Manohara, G., & Kumbinarasaiah, S. (2024). An innovative Fibonacci wavelet collocation method for the numerical approximation of Emden-Fowler equations. *Applied Numerical Mathematics*, 201, 347-369.

[24] Kumari, A., & Kukreja, V. K. (2023). Study of 4th order Kuramoto-Sivashinsky equation by septic Hermite collocation method. *Applied Numerical Mathematics*, 188, 88-105.

[25] Saad, K. M. (2020). New fractional derivative with non-singular kernel for deriving Legendre spectral collocation method. *Alexandria Engineering Journal, 59*(4), 1909-1917.

[26] Wang, K., & Wang, Q. (2013). Lagrange collocation method for solving Volterra–Fredholm integral equations. *Applied Mathematics and Computation, 219*(21), 10434-10440.

[27] Horadam, A. F., & Mahon, J. M. (1985). Pell and pell-lucas polynomials. *Fibonacci Quart, 23*(1), 7-20.

[28] Taghipour, M., & Aminikhah, H. (2022). A fast collocation method for solving the weakly singular fractional integro-differential equation. *Computational and Applied Mathematics, 41*(4), 142.

[29] Sabermahani, S., Ordokhani, Y., & Razzaghi, M. (2023). Ritz-generalized Pell wavelet method: Application for two classes of fractional pantograph problems.*Communications in Nonlinear Science and Numerical Simulation* , 119, 107138.

[30] Sahin, M., & Sezer, M. (2018). Pell-Lucas collocation method for solving high-order functional differential equations with hybrid delays. *Celal Bayar University Journal of Science, 14*(2), 141-149.

[31] Cayan, S., & Sezer, M. (2019). Pell polynomial approach for Dirichlet problem related to partial differential equations, *Journal of Science and Arts, 19*(3), 613-628.

[32] Yüzbasi, Ş., &Yildirim, G. (2020). Pell-Lucas collocation method to solve high-order linear Fredholm-Volterra integro-differential equations and residual correction, *Turkish Journal of Mathematics, 44*(4), 1065-1091.

[33] Noori, S. R. M., & Taghizadeh, N. (2020). Modified differential transform method for solving linear and nonlinear pantograph type of differential and Volterra integro-differential equations with proportional delays. *Advances in Difference Equations, 2020*(1), 1-25.

[34] Gümgüm, S., Savaşaneril, N. B., Kürkçü, Ö. K.,& Sezer, M. (2020). Lucas polynomial solution of nonlinear differential equations with variable delays. *Hacettepe Journal of Mathematics and Statistics, 49*(2), 553-564.

Sinopfbd, 2024; 9(1): 184-193 **https://doi.org/10.33484/sinopfbd.1404628**

Sinop Üniversitesi Fen Bilimleri Dergisi
Sinop Uni J Nat Sci

E-ISSN: 2564-7873

https://dergipark.org.tr/tr/pub/sinopfbd

Antibacterial and Antifungal Activity of *Abies nordmanniana* subsp. *equi-trojani* (Aschers. & Sint. ex Boiss) Extracts

Gülçin ÖZCAN ATEŞ[1] and Tülay BİCAN SÜERDEM[2]

How to cite: Özcan Ateş, G., & Bican Süerdem, T. (2024). Antibacterial and antifungal activity of *Abies nordmanniana* subsp. *equi-trojani* (*Aschers. & Sint. ex Boiss*) extracts. *Sinop Üniversitesi Fen Bilimleri Dergisi, 9*(1), 184-193. https://doi.org/10.33484/sinopfbd.1404628

Research Article

Corresponding Author
Gülçin ÖZCAN ATEŞ
gulcinozcan@comu.edu.tr

ORCID of the Authors
G.Ö.A.: 0000-0002-8467-2378
T.B.S: 0000-0003-0521-9338

Received: 13.12.2023
Accepted: 28.05.2024

Abstract

In this study, the antibacterial and antifungal activity of *Abies nordmanniana* subsp. *equi-trojani* cone spangles, which are endemic and endangered and grow in Çanakkale Ida Mountains, was investigated by agar well diffusion and microplate methods. The antibacterial and antifungal activity of distilled water, ethanol, methanol and dimethylsulfoxide (DMSO) extracts of cone spangles was evaluated against gram-positive and gram-negative bacteria and yeasts. As a result, it was determined that the DMSO extract had antibacterial and antifungal activity against the tested microorganisms, while the extract prepared with distilled water had no activity. The antimicrobial activity of the methanol and ethanol extracts varied depending on the microorganism type. When the results of this study were compared with the positive control (penicillin G and fluconazole), it was determined that the extracts were not as effective as the antibiotic and antifungal disc. As a result, it is important to use alternative products that are abundant in nature instead of products derived from endangered species.

Keywords: *A. equi-trojani*, Fir, Ida Mountains, antimicrobial activity

Abies nordmanniana subsp. *equi-trojani* (Aschers. & Sint. ex Boiss) Ekstraktlarının Antibakteriyel ve Antifungal Aktivitesi

[1]Çanakkale Onsekiz Mart University, Vocational School of Health Services, Department of Medical Services and Techniques, Çanakkale, Türkiye

[2]Çanakkale Onsekiz Mart University, Faculty of Science, Department of Biology, Çanakkale, Türkiye

Öz

Bu çalışmada Çanakkale Kazdağlarında yetişen endemik ve yok olma tehlikesiyle karşı karşıya olan *Abies nordmanniana* subsp. *equi-trojani* kozalak pullarının antibakteriyel ve antifungal aktivitesi agar kuyu ve mikroplak yöntemiyle araştırılmıştır. Kozalak pullarının distile su, etanol, metanol ve dimetilsülfoksit (DMSO) ekstraktlarının antimikrobiyal aktivitesi gram pozitif ve gram negatif bakteriler ile mayalara karşı değerlendirilmiştir. Sonuç olarak özellikle DMSO ekstraktının test edilen mikroorganizmalara karşı antibakteriyel ve antifungal aktiviteye sahip olduğu tespit edilmiştir. Distile su ile hazırlanan ekstraktının ise herhangi bir aktiviteye sahip olmadığı belirlendi. Metanol ve etanol ekstraktlarının ise mikroorganizma türüne göre aktivite gösterdiği belirlendi. Bu çalışmanın sonuçları pozitif kontrol (penisilin G ve flukonazol) ile karşılaştırıldığında, ekstraktların antibiyotik ve antifungal disk kadar etkili olmadığı belirlendi. Sonuç olarak nesli yok olma tehlikesiyle karşı karşıya kalan bu türün ürünleri yerine doğada bol bulunan alternatif ürünlerin kullanılması önem arz etmektedir.

Anahtar Kelimeler: *A. equi-trojani*, Köknar, Kazdağı, antimikrobiyal aktivite

Introduction

The genus *Abies* includes more than 50 species worldwide and is widespread in Europe, North Africa, Asia and North America. *Abies* species grow at high altitudes, especially in mountainous areas [1]. Based on morphological and anatomical features such as hairy or hairless shoots, resinous or slightly resinous bud structures, seed structures, shape and size of cones and spangles, the classification of firs growing in Anatolia is well-known to botanists [2]. Four species are common throughout Turkey: *Abies bornmuelleriana* Mattf., *Abies cilicica* Carr., *Abies nordmanniana* Link. and *Abies nordmanniana* subsp. *equi-trojani* Aschers. & Sint. ex Boiss. The homeland of the Turkish Fir *A. bornmuelleriana* species is Central-Northern Anatolia. There are two subspecies of the *A. cilicica*. *A. cilicica* subsp. *cilicica* and *A. cilicica* subsp. *isaurica* are specific to the central-eastern Toros Mountains and are endemic. *A. nordmanniana*, Caucasian fir or Nordmann fir, which has a wide distribution area in the Caucasus extending to Georgia and Russia, is found in northeastern Turkey. *A. nordmanniana* subsp. *equi-trojani* species naturally grows only in the limited area from Southern Çanakkale to the ancient city of Troy and is endemic to that region [1, 2]. Different species of *Abies* are used for therapeutic purposes in folk medicine. *Abies numidica* has been used in folk medicine against lung, cold, stomachache, indigestion, vascular, and venereal diseases [3]. The species *A. nordmanniana* subsp. *equi-trojani* is used as an ointment for wounds and boils due to its microbiocidal effect, and the syrup created by boiling its leaves and fresh green cones is used for respiratory diseases. Additionally, it is also used in furniture production [4]. However, this species is classified as an endangered (in danger of extinction in the near future) tree species by the International Union for Conservation of Nature and has been included in the Red List due to its small population sizes, extinction risks and habitat degradation [1, 5]. It has been determined that extracts and essential oils from different parts of the *Abies* species contain compounds such as phenols, flavonoids, lignans, steroids, triterpenoids and fatty acids [3]. For this reason, there are different studies on the essential oils and extracts of *Abies* species growing in various geographical and ecological conditions [2, 3, 6, 7]. Additionally, studies have found that *Abies* species have different biological activities such as antibacterial, antifungal, antihypertensive, anti-inflammatory, anti-ulcerogenic, antitussive, antitumor, and activity on the central nervous system [3]. Therefore, in this study, the antibacterial and antifungal activity of *A. nordmanniana* subsp. *equi-trojani* cone spangle extracts were investigated.

Materials and Method

Plant Material

Dried cones of *Abies nordmanniana* subsp. *equi-trojani* were obtained from a commercial phytotherapy shop (Malatya Kuruyemiş) in Çanakkale Küçükkuyu, Türkiye, in May 2021.

Preparation of Extracts

The extraction process of the Ida Mountain *A. nordmanniana* subsp. *equi-trojani* cone was carried out using four different solvents: distilled water (DW), methanol (M) (Merck, Germany), ethanol (E) (Isolab, Türkiye), and dimethyl sulfoxide (DMSO) (Merck, Germany). For the extraction of the cone, a 40 g spangle and a 10 g high-speed ground spangle (Figure 1) were mixed, and a 1:10 (w:v) solvent was added. The mixture was then extracted with Soxhlet for 24 hours. After extraction, the extracts were filtered using sterile filter papers, placed in sterile dark-colored bottles, and stored at +4°C.

Figure 1. *Supplied Abies nordmanniana subsp equi-trojani cone spangles and ground powder*

Cultures

In the study, standard cultures and clinical isolates from the collections of Dr. Gülçin ÖZCAN ATEŞ and Dr. Nükhet ZORBA in Çanakkale Onsekiz Mart University Food Engineering Microbiology Laboratory were used.

The Inoculum Suspension Preparation

The stock cultures were inoculated on Tryptic Soy Agar (TSA) (Merck, Germany) and revived overnight at 37°C. After the incubation period, colonies selected from the petri dish were suspended in a physiological saline solution (0.85% NaCl w/v) until the turbidity matched the 0.5 McFarland standard.

Agar Well Diffusion Method

The extracts were tested for their antibacterial and antifungal properties by creating wells on the surface of the Mueller-Hinton Agar (MHA) (Merck, Germany) plates using a cork borer set, instead of using the disk specified in EUCAST [8]. The inoculum suspension was prepared and inoculated onto the dried surface of the MHA plate using a sterile swab, after which 20 µL of the extracted sample was added to the 6mm diameter wells. The Petri dishes were incubated at 37°C for 24 hours, and the zone diameters were measured using a digital calliper. Penicillin G (10 µg, Bioanalyse, Turkey) antibiotic and

fluconazole (25 mcg, Himedia, India) antifungal disc were used as positive controls, while solvents were used as negative control. The study was conducted in triplicate, and the results were presented as mean (M) ± standard deviation (sd).

Determination of Minimum Inhibitory Concentration (MIC)

The MIC value of the DMSO extract, which was found to possess antibacterial and antifungal properties through agar well diffusion tests, was further determined using the microplate method with 96-well U-bottom microplates by CLSI guidelines [9]. First, the extract concentrations were prepared in Muller Hinton Broth (MHB) (Merck, Germany), containing double layers of medium. 100 µL of the prepared concentrations was added to the wells of rows B-G of the microplates, followed by the addition of 100 µL of cell suspension. The final extract concentrations were 40, 20, 10, 5, 2.5 and 1 µL/mL. Row A of the microplates was used as a negative (MHB containing 40 µL/mL extract) control, and row H was used as a positive (MHB+culture) control. After the microplates were incubated for 18-48 hours at 36±1°C, 10 µL of 1% (w/v) 2,3,5 tetrazolium chloride (Merck, Germany) solution was dropped into each well to observe the colour change. The first well with no colour change was determined as the MIC value. The study was carried out in three parallels.

Results

The current study includes the antibacterial and antifungal activity results of distilled water, ethanol, methanol and DMSO extracts of *A. nordmanniana* subsp. *equi-trojani* cone spangles against eight clinical isolates, 14 standard bacteria and six standard yeast cultures. As seen in Tables 1, 2 and 3 it was determined that DMSO extract exhibited antibacterial activity against the tested bacterial cultures. Although it was found that extracts did not have any antifungal activity against the five *Candida* cultures tested, it was recorded that ethanol, methanol, and DMSO extracts showed antifungal activity against the *C. neofermans* ATCC 90112 yeast (Table 3).

Table 1. *Agar well diffusion results of Abies nordmanniana subsp. equi-trojani cone spangles extract against Gram-negative bacteria (in mm)*

Microorganisms	**DW**	**M**	**E**	**DMSO**	**Penicillin G**
Acinetobacter baumannii (clinical isolate 1048)	6.00±0.01	6.00±0.01	9.77±0.63	11.17±0.86	15.48±0.17
Acinetobacter baumannii (clinical isolate 1132)	6.00±0.01	6.00±0.01	10.06±0.73	11.56±0.97	6.43±1.48
Acinetobacter baumannii (clinical isolate 2685)	6.00±0.01	6.00±0.01	9.68±0.92	15.27±1.80	6.00±0.01
Escherichia coli ATCC 8739	6.00±0.01	6.00±0.01	6.00±0.01	11.04±2.47	21.45±1.77
Escherichia coli ATCC 25922	6.00±0.01	6.00±0.01	6.00±0.01	8.55±0.21	20.63±1.07
Escherichia coli NRRL B-3704	6.00±0.01	6.00±0.01	6.00±0.01	10.28±0.38	10.11±1.11
Klebsiella quasipneumoniae ATCC 700603	6.00±0.01	7.89±0.69	7.71±2.57	9.91±1.57	6.55±1.90
Klebsiella pneumoniae (clinical isolate 1042)	6.00±0.01	6.00±0.01	6.00±0.01	6.00±0.01	7.26±0.21
Salmonella enterica subsp. *enterica* ATCC 13076	6.00±0.01	8.75±1.47	6.00±0.01	8.40±1.25	22.16±0.35
Pseudomonas aeruginosa ATCC 10145	6.00±0.01	6.00±0.01	6.00±0.01	8.61±0.16	11.43±0.28
Pseudomonas aeruginosa ATCC 27853	6.00±0.01	6.00±0.01	6.00±0.01	10.42±1.03	6.00±0.01
Proteus vulgaris ATCC 13315	6.00±0.01	6.00±0.01	6.00±0.01	7.00±0.01	19.47±0.88

Table 2. *Agar well diffusion results of Abies nordmanniana subsp. equi-trojani cone spangles extract against Gram-positive bacteria (in mm)*

Microorganisms	DW	M	E	DMSO	Penicillin G
Basillus subtilis	6.00±0.01	6.00±0.01	6.00±0.01	10.62±0.55	21.47±0.77
Basillus subtilis subsp. *spizizenii* ATCC 6633	6.00±0.01	9.72±2.51	10.44±1.89	15.79±4.30	6.00±0.01
Enterococcus faecalis ATCC 29212	6.00±0.01	6.00±0.01	6.00±0.01	10.37±1.23	6.00±0.01
Enterococcus faecalis (clinical isolate 1075)	6.00±0.01	6.00±0.01	6.00±0.01	9.71±0.52	8.98±0.40
Staphylococcus aureus ATCC 29213	6.00±0.01	8.52±1.24	6.00±0.01	11.00±1.14	23.42±2.20
Staphylococcus aureus ATCC 25923	6.00±0.01	6.00±0.01	6.00±0.01	10.06±1.59	11.52±0.59
Staphylococcus aureus ATCC 6538	6.00±0.01	6.00±0.01	6.00±0.01	9.31±0.31	22.55±0.36
Staphylococcus epidermidis (clinical isolate 2657)	6.00±0.01	12.03±1.20	6.00±0.01	13.12±1.83	6.00±0.01
Staphylococcus epidermidis (clinical isolate 2671)	6.00±0.01	6.00±0.01	12.55±1.35	11.88±2.46	6.00±0.01
Staphylococcus gallinarum (clinical isolate 1093)	6.00±0.01	12.88±3.16	11.99±1.45	13.69±1.34	28.63±1.91

Table 3. *Agar well diffusion results of Abies nordmanniana subsp. equi-trojani cone spangles extract against yeast (in mm)*

Microorganisms	DW	M	E	DMSO	Fluconazol
Candida albicans ATCC 10231	6.00±0.01	6.00±0.01	6.00±0.01	6.00±0.01	39.33±1.13
Candida albicans ATCC 24433	6.00±0.01	6.00±0.01	6.00±0.01	6.00±0.01	37.57±0.56
Candida albicans ATCC 90028	6.00±0.01	6.00±0.01	6.00±0.01	6.00±0.01	37.97±1.02
Candida tropicalis ATCC 1021	6.00±0.01	6.00±0.01	6.00±0.01	6.00±0.01	27.77±0.46
Candida parapsilosis ATCC 22019	6.00±0.01	6.00±0.01	6.00±0.01	6.00±0.01	36.25±0.94
Cryptococcus neofermans ATCC 90112	6.00±0.01	11.69±1.66	12.80±1.87	11.10±1.49	37.77±0.04

Agar well diffusion results of DMSO extract showed that the inhibition zone diameter ranged from 7.00±0.01 to 15.27±1.80 mm. It was determined that the lowest inhibition zone diameter was against *P. vulgaris* ATCC 13315, and the highest inhibition zone diameter was against the clinical isolate *A. baumannii* (2685). The antifungal activity of DMSO extract against yeasts was detected only against *C. neofermans* ATCC 90112, and the inhibition zone diameter was found to be 11.10±1.49 mm. The ethanol extract has been detected, giving an inhibition zone between 7.71±2.57 and 12.80±1.87 mm against three *A. baumanni* clinical isolates, *K. quasipneumoniae* ATCC 700603, *B. subtilis* subsp. *spizizenii* ATCC 6633 *S. epidermidis* (clinical isolate 2671), *S. gallinarum* (clinical isolate 1093), and *C. neofermans* ATCC 90112. It was determined that the methanol extract showed antimicrobial activity against *K. quasipneumoniae* ATCC 700603, *S. enterica* subsp. *enterica* ATCC 13076, *B. subtilis* subsp. *spizizenii* ATCC 6633, *S. aureus* ATCC 29213, *S. epidermidis* (clinical isolate 2657), *S. gallinarum* (clinical isolate 1093), and *C. neofermans* ATCC 90112 and gave an inhibition zone between 7.89±0.69 and 12.88±3.16 mm. It was found that the extract prepared with distilled water did not exhibit both antibacterial and antifungal activity. Additionally, it was found that DMSO extracts had a smaller inhibition zone against 12 bacteria (-178.14% to -14.51%) and a larger inhibition zone against 13 bacteria (1.65% to 62%). The MIC value of DMSO extract, which was found to have antibacterial and antifungal activity, was determined. Figure 1 shows that the MIC value for most of the microorganisms tested was 40 µL/mL. The lowest MIC value of the DMSO extract was determined to be 2.5 µL/mL against the *S. epidermidis* (clinical isolate 2657) isolate, and the second lowest MIC value was 5 µL/mL against the *A. baumannii* (clinical isolate 1048) isolates. However, the MIC value against the cultures of *E. coli* NRRL B-3704, *P. aeruginosa* ATCC 10145 and ATCC 27853, *E. faecalis* (clinical isolate 1075), *S. aureus* ATCC 25923 and 6538 was outside the tested concentrations, and the MIC value was >40 µL/mL.

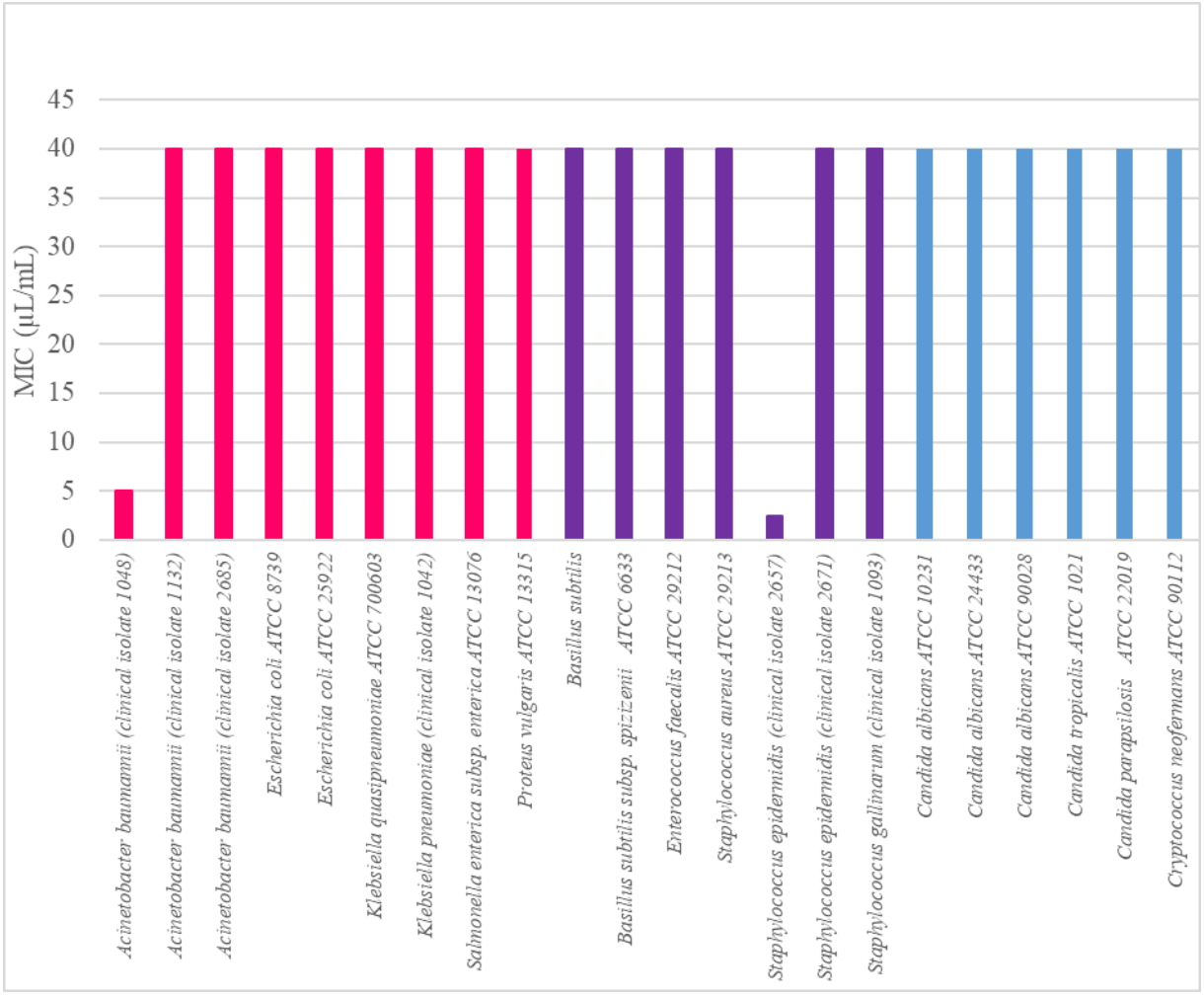

Figure 1. *MIC values of Abies nordmanniana subsp. equi-trojani cone spangles DMSO extract*

Discussion

It was determined that the *A. nordmanniana* subsp. *equi-trojani* cone spangle extracts used in this study were not as effective as the positive control antibiotic and antifungal disks. Bağcı and Dığrak [10] determined that the essential oil they extracted from the needle branches of *A. equi-trojani* by hydrodistillation for three hours did not have antimicrobial activity against *E. coli, S. aureus* and *S. cerevisiae*. Sakar et al. [11] reported that methanol, ethanol and chloroform extracts of *A. nordmanniana subsp. equi-trojani* cones collected from Ida Mountain Balıkesir in 1991 gave a 9 mm inhibition zone against *B. subtilis* ATCC 6633 at a 4000 µg/disc concentration. They found that chloroform and methanol extract gave 7- and 10-mm inhibition zones against *S. aureus*. They found that it did not give an inhibition zone against *S.* Typhimurium CMC 583, *E. coli* ATCC 11230 and *Candida utilis*. Eryılmaz et al. [12] reported that the ether extract of Balıkesir *A. nordmanniana subsp. equi-trojani* cones gave a 7 mm inhibition zone against *B. subtilis* ATCC 6633 and *P. aeruginosa* ATCC 27853. They noted that it did not show any inhibition against *S. aureus* ATCC 43300 (methicillin-resistant S. aureus), *E. coli* ATCC 25922, *K. pneumoniae* RSKK 574, and *C. albicans* ATCC 10231. Öztürk Pulatoğlu et al. [7] collected *A. nordmanniana subsp. equi-trojani* from Kastamonu in 2017. They determined that the

essential oil obtained from *A. nordmanniana subsp. equi-trojani* cones by Clevenger hydrodistillation had MIC values between 0.195 and 25 µg/ml against the gram-negative and gram-positive bacteria they tested. It has been determined that *A. nordmanniana subsp. equi-trojani* species collected at different times and places in our country have different effects on bacteria and yeasts, and the results of this study are parallel to the results in literature.

Conclusions

Over the last fifty years, the population of Fir trees has decreased significantly due to several factors, including environmental conditions and wildfires, like the 2023 Çanakkale forest fires. However, in Çanakkale districts, people still believe that the cones of the Kazdağı fir are good for respiratory diseases, so they consume the cones by brewing them as tea. These cones are also sold commercially. However, different studies found that Ida Mountain fir extracts were less effective than antibiotic substances. Therefore, it is recommended to use herbal products with higher antimicrobial activity that are abundant in our environment instead of this endemic species that is in danger of extinction. Additionally, it is essential to raise public awareness about this issue to ensure the continuity of the species.

Acknowledgement We would like to thank Sevgi KARAKAYA, who mediated for the supply of Kazdağı fir cone spangles, and Malatya Kuruyemiş Reis Daşdemir (Küçükkuyu, Çanakkale), who provided the cone spangles. We also thank Dr. Nükhet ZORBA for providing us with some standard bacterial cultures.

Funding/Financial Disclosure This study was not supported by any institution or organisation.

Ethics Committee Approval and Permissions The study does not require ethics committee approval or any special permission.

Conflicts of Interest The authors declared no conflict of interest.

Authors Contribution Gülçin ÖZCAN ATEŞ's contribution to the article is 50%; she planned the project, analysed and wrote the article. Tülay BİCAN SÜERDEM's contribution to the article was 50%; she analysed and wrote the article.

References

[1] Özden Keleş, S., Ünal, S., & Karadeniz, M. (2021). The effect of *Melampsorella caryophyllacearum* (fir broom rust) on the morphological and anatomical traits of *Abies nordmanniana* subsp. *equi-trojani*. *Forest Pathology*, *51*(6), e12721. https://doi: 10.1111/efp.12721

[2] Uçar, G., Uçar, M. B., Özdemir, H., & Atıcı, E. (2010). Chemical Characterization of Volatile Needle Oils from Anatolian Fir Species: *Abies nordmanniana* (Stev.) Mattf., *A. bornmülleriana* Mattf., *A. equi-trojani* Aschers et Sint. and *A. cilicica* Carr. *Journal of Essential Oil Research*, *22*(6), 548-554. https://doi: 10.1080/10412905.2010.9700397

[3] Belhadj Mostefa, M., Abedini, A., Voutquenne-Nazabadioko, L., Gangloff, S. C., Kabouche, A., & Kabouche, Z. (2017). Abietane diterpenes from the cones of *Abies numidica* de Lannoy ex Carrière (Pinaceae) and in vitro evaluation of their antimicrobial properties. *Natural Product Research*, *31*(5), 568-571. https://doi: 10.1080/14786419.2016.1190723

[4] Anonim, (2023). https://onedio.com/haber/endemik-diyari-kazdaglari-nda-yetisen-her-derde-deva-10-bitki-turu-712686 Erişim tarihi: 13/12/2023

[5] Usta N., & Tavşanoğlu, Ç. (2023). Anadolu endemiği Kazdağı göknarı (*Abies nordmanniana* (Stev.) subsp. *equi-trojani* (Aschers. & Sint. ex Boiss) Coode et Cullen): Bildiklerimiz ve araştırma gereksinimleri. *Turkish Journal of Forestry*, *24*(3), 329-345. https://doi: 10.18182/tjf.1293159

[6] Benouchenne, D., Bellil, I., Akkal, S., & Khelifi, D. (2021). Investigation of phytochemical and evaluation of antioxidant and antibacterial activities from *Abies* extract. *The Scientific Journal of King Faisal University*, *22*, 26-32. https://doi: 10.37575/b/sci/210009

[7] Öztürk Pulatoğlu, A. Ö., Güney, K., Çeter, T., & Yılmaz, E. S. (2023). Chemical Composition of Essential Oils Obtained from *Abies* taxa in Türkiye and Investigation of Antimicrobial Activities. *Kastamonu University Journal of Forestry Faculty*, *23*(1), 31-46. https://doi: 10.17475/kastorman.1269485

[8] EUCAST (2021). Disk Diffusion Method for Antimicrobial Susceptibility Testing, Version 9.0 (January 2021). https://www.eucast.org/fileadmin/src/media/PDFs/EUCAST_files/Disk_test_documents/2021_manuals/Manual_v_9.0_EUCAST_Disk_Test_2021.pdf

[9] CLSI (2012) Clinical and Laboratory Standards Institute Methods for Dilution Antimicrobial Susceptibility Tests for Bacteria That Grow Aerobically; Approved Standard—Ninth Edition. CLSI Document M07-A9. Vol. 32 No. 2. Clinical and Laboratory Standards Institute, Wayne.

[10] Bağcı, E., & Dığrak, M. (1997). In Vitro Antimicrobial Activities of some Fir Essential Oils. *Turkish Journal of Biology, 21*(3), 273-281.

[11] Sakar, M. K., Ercil, D., Tamer, A. U., & Sahin, N. (1998). Antimicrobial activity and cytotoxicity of *Abies nordmanniana* subsp. *equi-trojani extracts*. *Fitoterapia*, *69*(5), 457-459.

[12] Eryilmaz, M., Tosun, A., & Tümen, İ. (2016). Antimicrobial activity of some species from Pinaceae and Cupressaceae. *Turkish Journal of Pharmaceutical Sciences*, *13*(1), 35-40.

Sinopfbd, 2024; 9(1): 194-206 **https://doi.org/10.33484/sinopfbd.1464962**

Sinop Üniversitesi Fen Bilimleri Dergisi
Sinop Uni J Nat Sci

E-ISSN: 2564-7873

https://dergipark.org.tr/tr/pub/sinopfbd

Two New Records of Polychaetes (Annelida) from Makran Coast of Balochistan, Pakistan (Northern Arabian Sea)

Qadeer Mohammad ALI[1], Quratulan AHMED[1], Ateeqa BALOCH[1], Shumaila MUBARAK[1], Hafsa QAZI[1], Iqra SHAIKH[1], Güley KURT[2] and Levent BAT[3]

How to cite: Ali, Q. M., Ahmed, Q., Baloch, A., Mubarak, S., Qazi, H., Shaikh, I., Kurt, G., & Bat, L. (2024). Two new records of Polychaetes (Annelida) from Makran coast of Balochistan, Pakistan (Northern Arabian Sea). *Sinop Üniversitesi Fen Bilimleri Dergisi, 9*(1), 194-206. https://doi.org/10.33484/sinopfbd.1464962

Research Article

Corresponding Author
Quratulan Ahmed
quratulanahmed_ku@yahoo.com

ORCID of the Authors
Q.M.A: 0000-0002-0499-0801
Q.A: 0000-0002-7597-2483
A.B: 0009-0008-8036-3237
S.M: 0000-0003-1208-1728
H.Q: 0009-0004-1952-8654
I.S: 0000-0003-2482-1631
G.K: 0000-0002-9996-4365
L.B: 0000-0002-2289-6691

Received: 05.04.2024
Accepted: 05.06.2024

Abstract

The Makran coast of Balochistan (Pakistan) is rich in terms of biodiversity particularly marine invertebrates. The study based on comprehensive assessment of the morphological and taxonomical description of two polychaete species (*Eunice petersi* Fauchald, 1992 and Hesione intertexta Grube, 1878). The newly recorded polychaete species for the coast of Pakistan belong to the Eunicidae and Hesionidae families and were identified in benthic samples collected from the intertidal zone on Garyan and Bandari beaches at Jiwani of the Makran coast (Northern Arabian Sea). The descriptions, photographs, and drawings of the taxonomic characters of species and their distribution are provided. The specimens are deposited in the repository of the Marine Reference Collection and Resource Centre, University of Karachi.

Keywords: Polychaeta, new records, invertebrate, description, taxonomy

Balochistan'ın Makran Kıyısından Pakistan (Kuzey Arap Denizi) İki Yeni Poliket (Annelida) Kaydı

[1]The Marine Reference Collection and Resource Centre, 75270, University of Karachi, Pakistan

[2]Sinop University, Faculty of Arts and Sciences, Department of Biology, 57000 Sinop, Türkiye

[3]Sinop University, Fisheries Faculty, Department of Hydrobiology, 57000, Sinop, Türkiye

Öz

Balochistan 'ın (Pakistan) Makran kıyıları biyoçeşitlilik, özellikle de deniz omurgasızları açısından oldukça zengindir. Bu çalışma, iki poliket türünün (*Eunice petersi* Fauchald, 1992 ve *Hesione intertexta* Grube, 1878) morfolojik ve taksonomik tanımlarının kapsamlı bir değerlendirmesine dayanmaktadır. Pakistan kıyıları için yeni kaydedilen poliket türleri Eunicidae ve Hesionidae familyalarına aittir ve Makran kıyısındaki (Kuzey Arap Denizi) Jiwanio'daki Garyan ve Bandari plajlarındaki gelgit bölgesinden toplanan bentik örneklerde tanımlanmıştır. Türlerin tanımları, fotoğrafları, taksonomik karakterlerinin çizimleri ve dağılımları verilmiştir. Örnekler, Karachi Üniversitesi Deniz Referans Koleksiyonu ve Kaynak Merkezi deposunda saklanmaktadır.

Anahtar Kelimeler: Polychaeta, yeni kayıtlar, omurgasız, tanımlama, taksonomi

Introduction

The coast of Balochistan with a coastline of 645 km, stretches from the east of the Hub River to the mid of the Gwatar Bay to the west. The coast is primarily deserted, with unusual landforms such as sandy beaches, mudflats, rocky cliffs, headlands, bays, and deltas. The Balochistan coast is known for its rocky shores and cliffs at Jiwani, Pishukan, Gwadar, Pasni and Ormara with magnificent headlands. The coast of Makran is one of just a few coastlines in the world that experiences high rates of tectonic uplift and manifests interesting interactions between active sedimentation, erosion and tectonics. Jiwani is situated at Makran coast of Balochistan, in the extreme southwest, close to the border between Pakistan and Iran. The region is a genuine delegate of a dry environment. It has freshwater, desert, marine, tropical thorn forests, mangroves, and a scrub zone, among other habitats.

Over 12,000 species of polychaetes have been identified to far [1]. The family Hesionidae presently contains about 175 species in 28 genera [2], whereas the family Eunicidae currently includes 460 species and 33 genera that have been described 11 of which have been taxonomically recognised [3]. In the previous studies, the family Hesionidae only had two genera and four species, while just 12 species belonging to five genera of the Eunicidae were known to reside in Pakistan [4]. Information on the polychaete fauna of the Makran coast was lacking until when Ali *et al*. [5, 6] reported the distribution of polychaete worms from several rocky areas at the Makran coast. Polychaetes due to their extra ordinary resilience are referred as predominant metazoans in the marine benthic environment and are important representatives of the benthic macrofauna. These versatile creatures can be found in nearly all marine and estuarine sediment types [7]. They frequently dominate the macrobenthos community in terms of both species diversity and population numbers [8, 9]. Due to their diverse presence and abundance, polychaetes have frequently been employed in environmental monitoring programs to assess potential disturbances in the environment [10]. Eunicidae family stands out as one of the larger groups within Polychaeta, and its members are known to inhabit various types of substrates, including hard structures like reefs and rocks, as well as softer materials like sand [2]. Within marine benthic environments, these species primarily exhibit carnivorous or omnivorous tendencies and are equipped with well-developed jaws [11]. Their feeding habits encompass predation on different invertebrates, scavenging, and herbivorous behaviour [2]. Eunicids, in their ecological role, serve as significant contributors to coral block destruction and are instrumental in bioerosion processes. They are renowned for their ability to bore into the calcareous skeletons of hard corals using their implicated and exceptionally durable apparatus of jaws [12]. Some species within this family have been observed in association with other non-stalked invertebrates, particularly soft corals, and sponges [13], while others have specialized in the excavation of seagrass fronds [14]. Hesionids are benthic polychaetes known for

their distinctive cephalization and typically possess several anterior segments bearing long tentacular and dorsal cirri. They can vary greatly in size, with some species having small bodies, while larger ones can reach up to 55 mm in length and possess up to 80 segments. However, due to their delicate nature and diminutive size, many species of hesionids lack comprehensive descriptions [15]. Hesionidae species are commonly found in a wide range of habitats, including rocky or sandy bottoms, spanning from subtidal areas, which encompass both solid substrates and pliable sediments, to the depths of the deep sea. They are less frequently encountered in intertidal zones, except in the form of interstitial individuals [16]. They are predominantly free-living and are generally considered carnivorous or microphagous, particularly in the case of a few symbiotic formations. However, most species have limited data available [11]. *Hesione* species feature striking patterns of colour that may be sufficient to distinguish between species; however, since the pigments in these species rapidly become paler when kept in ethanol as early indicated by Grube [17], pigmentation is not a characteristic utilized for diagnosis. The present study reports two new records of Polychaeta species for the coast of Pakistan belonging to the families Eunicidae and Hesionidae collected from Garyan and Bandari beaches at Jiwani, along the Makran coast.

Materials and Methods

Polychaetes were randomly and qualitatively collected at low tide from the intertidal zones at two stations of Jiwani, along the Makran coast [Garyan (25º00’57’’N, 61º46’40’’E) and Bandari beach (25°03’09’’N 61°44’36’’E)] (Figure 1) on 30.01.2022. Samples were obtained from study areas under rocks using forceps. After sorting benthic material, the samples were preserved with 5% formaldehyde in the field. In the laboratory, the samples were rinsed with water, and transferred into the tubes containing 70% ethanol for taxonomic studies. Measurements were recorded and photographs were taken. The samples were dissected and examined at a magnification of 10x50 using a stereo-zoom microscope (Wild 181300, Switzerland). Temporary mounts of parapodia were prepared and examined using an upright microscope (Nikon LABOPHOT-2) at 10x4and 10x10 magnifications. The specimens were identified up to the species level with the help of available literatures [18, 19, 20]. The specimens were catalogued (MRC&RC-UOK-ANNE-27; MRC&RC-UOK-ANNE-28) and deposited in the University of Karachi's Marine Reference Collection and Resource Centre repository.

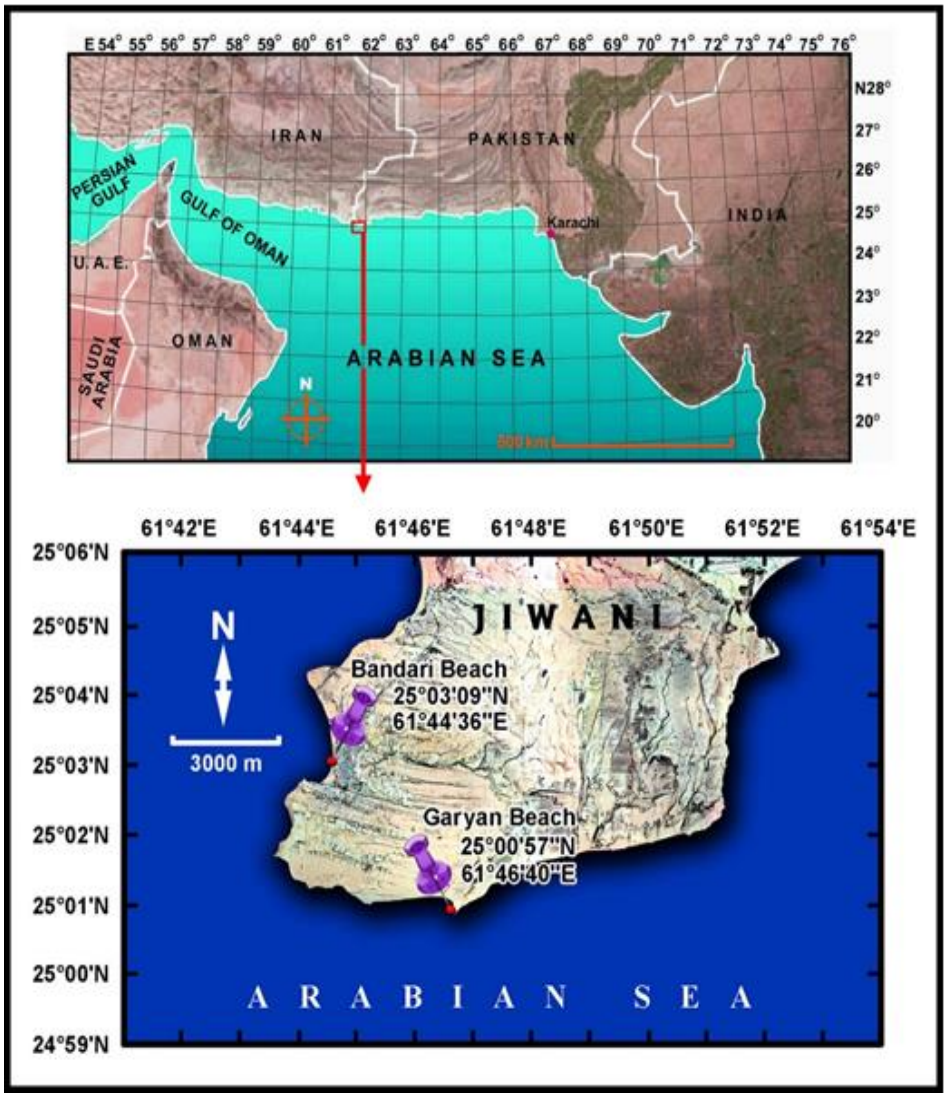

Figure 1. *Map showing study areas: [Garyan (25º00'57''N, 61°46'40''E) and Bandari Beach (25°03'09''N 61°44'36''E).*

Results

Taxonomic Account

Class: Polychaeta (Grube, 1850)

Subclass: Errantia (Audouin & H Milne-Edwards, 1832)

Order: Eunicida

Family: Eunicidae (Berthold, 1827)

Genus: *Eunice* (Cuvier, 1817)

Species: ***Eunice petersi* Fauchald, 1992** (Figures 2 & 3)

Material Examined: 2 specimens, Garyan, (25º01'57''N, 61º46'38''E), intertidal rocky shores, 30.01.2022, Catalogue no: (MRC&RC-UOK-ANNE-27)

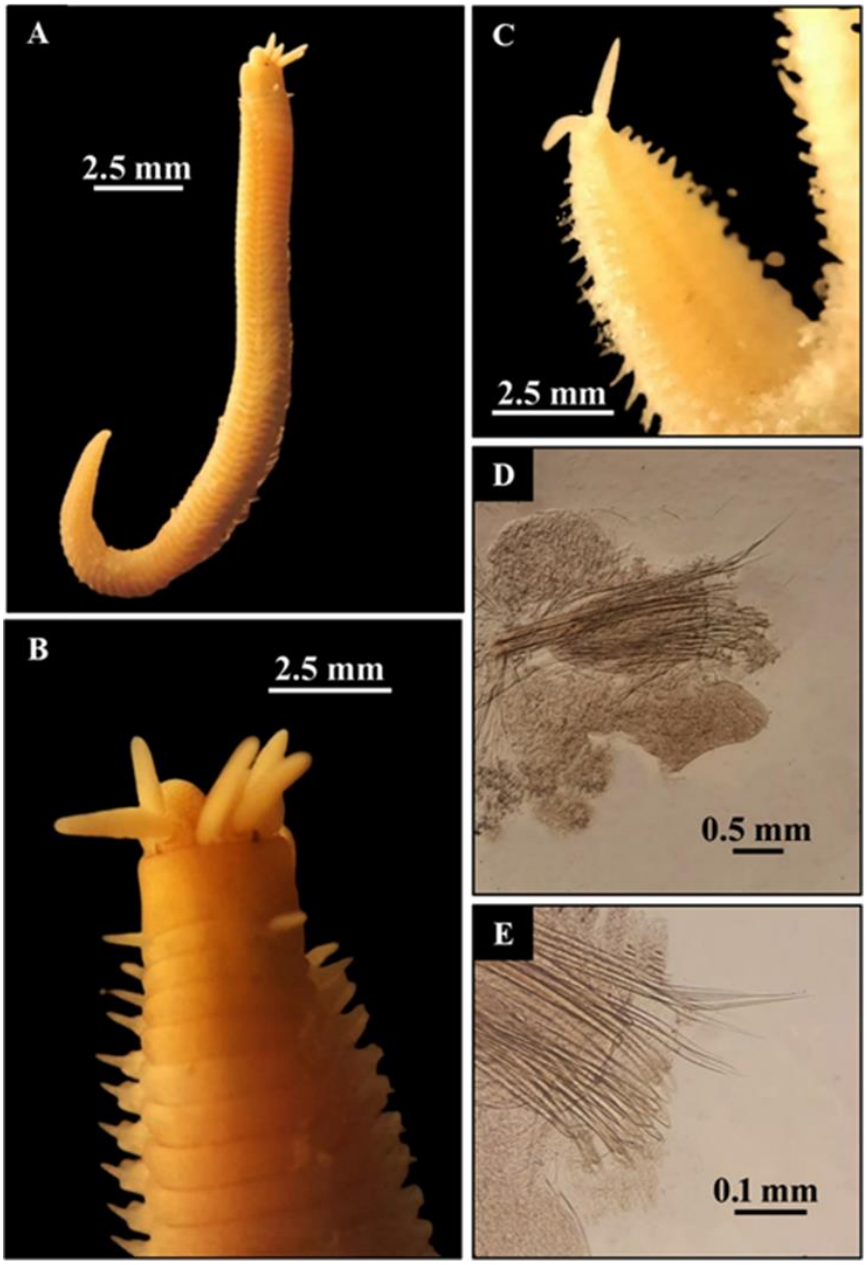

Figure 2. A. *Eunice petersi;* ***B.*** *Anterior end, dorsal view,* ***C.*** *Posterior end, dorsal view,* ***D.*** *Parapodium (chaetiger 17),* ***E.*** *Compound falciger and limbate chaetae.*

Description: Body small and cylindrical, measuring 1.5-2 cm in total length with 72-85 segments (Figures 2A, 2C) and colour creamish yellow in ethanol. Prostomium (Figures 2B, 3A) is notably shorter than peristomium and approximately as wide. Prostomial lobes frontally rounded, dorsally overstated, middle sulcus profound. Antennae in a straight line, alike in width and consistently spaced. Branchiae pectinate, clearly longer than notopodial cirri, and preliminary from chaetiger15 to chaetiger 65. Parapodium 17 (Figures 2D, 3B) with digitate chaetal lobes in anterior chaetiger, narrowing in the middle segments. Cirro style bases cylindrical, connected completely; dorsal cirri with tips mislaid, smaller than body breadth. Ventral cirri flat at the base and often ridged, medially, and distally frequently, extending further than chaetal lobes. Limbate chaeta slender, faintly flattened. Pectinate

chaeta narrowing flatly (Figure 3E). One marginal tooth longer than other teeth (Figures 2E, 3C) clearly inflates, slightly ragged or flat. Pseudo-composite falcigers and compound spinigers not present. Aciculae single, with brown cores and clear sheaths, slender, straight, and tapering with a round cross-section. Subacicular hooks (Figure 3D) with brown cores and noticeable sheaths, bidentate hooks slender, narrow, with diminutive heads. Proximal teeth bigger than distal teeth, narrowing, across directed. Distal teeth slender, distally intended obliquely.

Type locality: Indian Ocean, Mozambique.

Habitat: Rocky shores, found in crevices and areas under the rocks.

Distribution: Indo-West Pacific: Mozambique and New Caledonia; Red Sea.

Remarks: *Eunice petersi* is a new addition to the polychaete fauna of Pakistan. The present species was synonymized as *E. afra punctata* Peters, 1854 and was particularly found in the Indian Ocean. The descriptions of the species agreed with Fauchald [19].

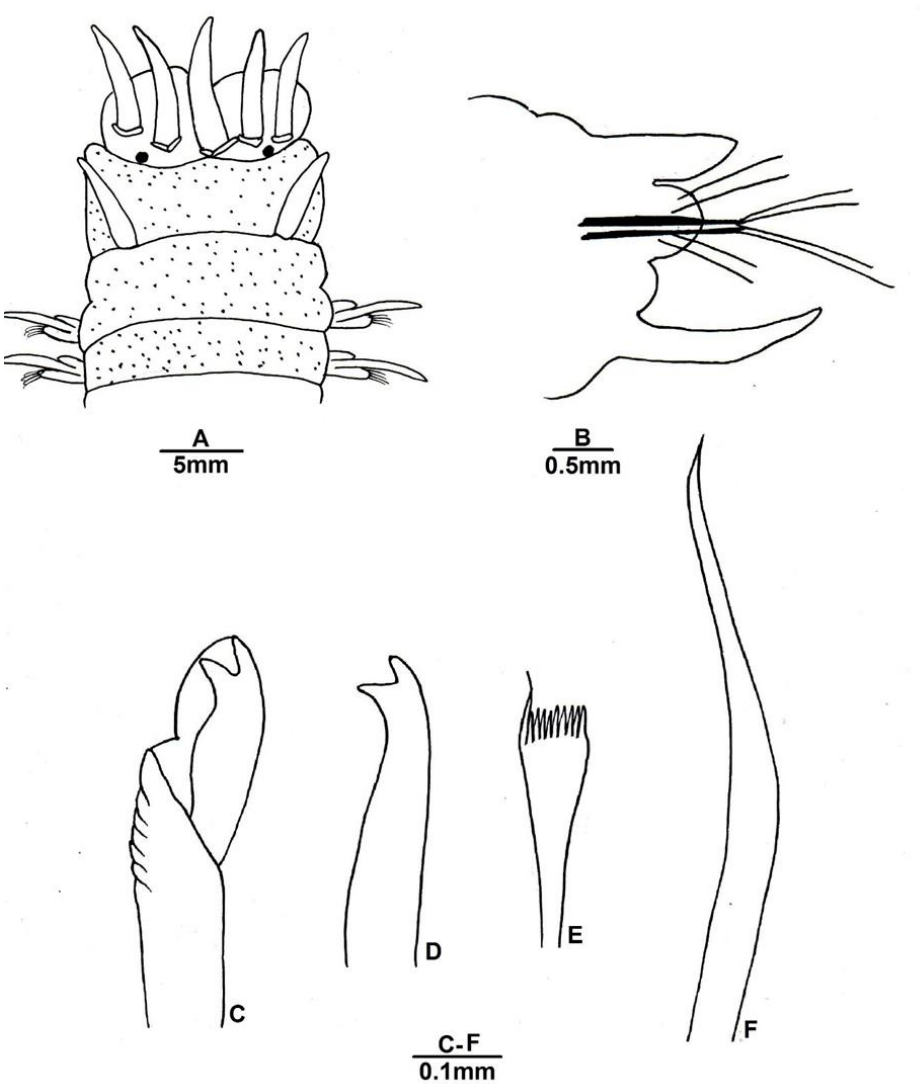

Figure 3. *Eunice petersi* ***A.*** *Anterior end, dorsal view,* ***B.*** *Parapodium (chaetiger 17),* ***C.*** *Compound falciger,* ***D.*** *Subacicular hooks,* ***E.*** *Pectinate chaeta,* ***F.*** *Limbate chaeta.*

Order: Phyllodocida

Family: Hesionidae Grube, 1850

Genus: *Hesione* Lamarck, 1818

Species: ***Hesione intertexta* Grube, 1878** (Figures 4, 5).

Material Examined: 2 specimens, Bandari (25°03’09’’N 61°44’36’’E) collected from intertidal rocky shore on 30-1-2022, Catalogue no: (MRC&RC-UOK-ANNE-28)

Description: Body slightly bent ventrally, subcylindrical, slightly tapered posteriorly measuring 5.5 and 6.0 cm in total body length, with 16 chaetigers (Figures 4A, 4D). Living specimens brownish to reddish-brown; creamish in ethanol. Pigmentation pattern with sub-continuous elongated lateral bands, along with smaller, lightly darker mid-dorsal bands intermittent by erratically oval, pale areas of equal length and width. Prostomium (Figures 4B-C, 5A) wide, with anterior margin projecting forward, rounded lateral margins, and exposed posterior margin. Antennae digitate, measuring 3-4 times their width. Frontal eyes black and brownish posteriorly; frontal eyes faintly bigger than posterior ones. Tentacular cirri entire, varying in contraction, with the longest one reaching chaetiger 5. Parapodium 8 (Figures 4E, 5B) with digitate chaetal lobes in anterior chaetiger, tapering in median segments. Cirro style bases cylindrical, expressed completely, dorsal cirri with lost tips, smaller than body width. Ventral cirriusually ridged, have a flat base, reach more distally and medially than chaetal lobes. Two neuraciculae per neuropodium; whitish in anterior chaetigers and blackish in median and posterior ones. Single, digitate to tapering acicular lobe. Neurochaetal blades bidentate (Figures 4F-H, 5C-F), with longer chaetal blades in anterior parapodia, 5-6 times their width, and shorter blades in median chaetigers, 3-4 times their width. While some anterior chaetigers' upper neurochaetae with lateral teeth and a slighter subdistal denticle that guards the distal tooth, others with lateral teeth and a lesser subdistal denticle. The posterior region tapered, narrowed into a blunt tube, with a distended pygidium, terminal anus and 12 slight anal papillae (Figure 4D).

Type locality: Western Pacific, Philippines.

Habitat: Rocky shores, found under rocks.

Distribution: New Caledonia; Philippine Islands; Australia; Arabian Sea, Indian Ocean [18].

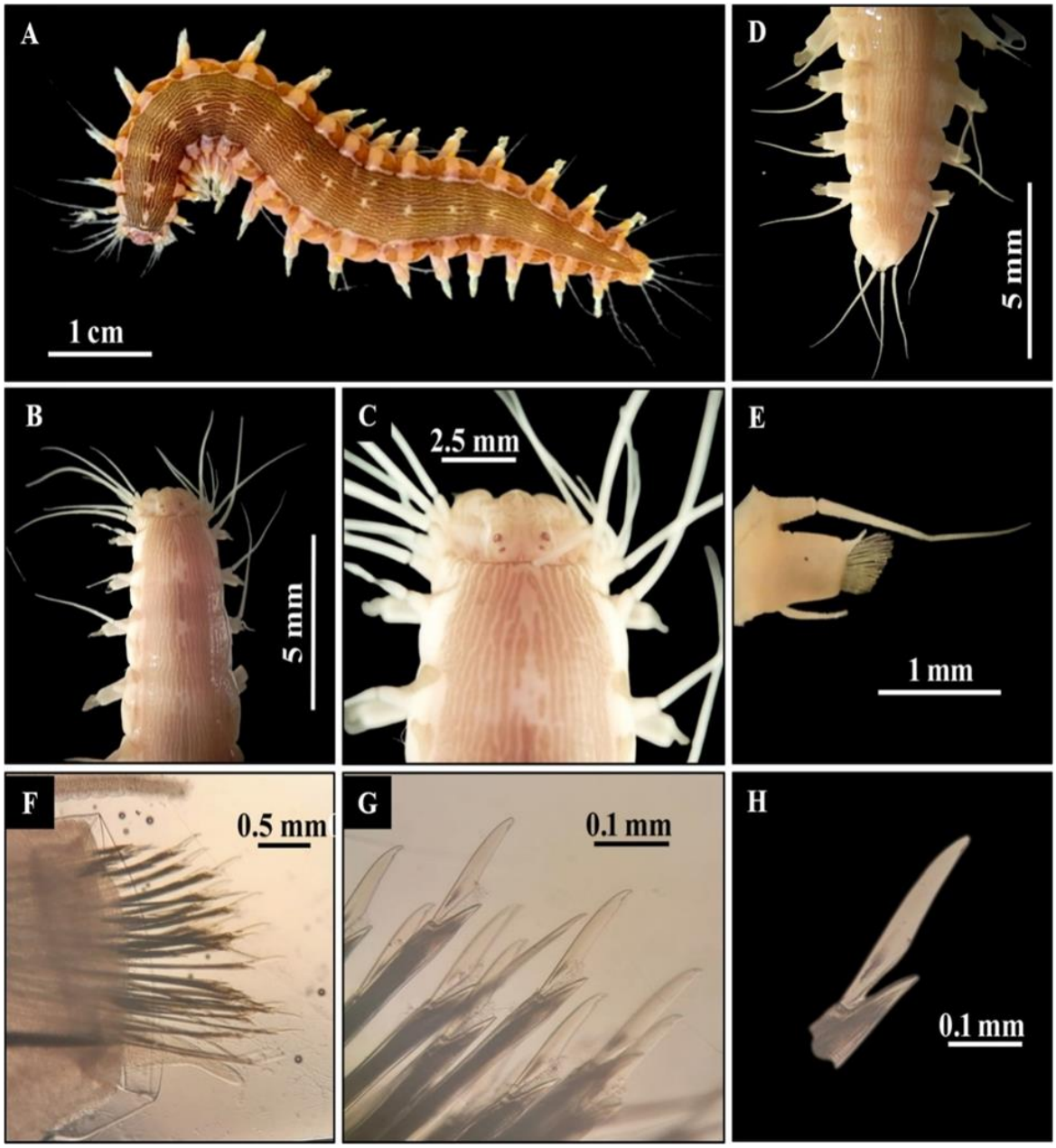

Figure 4. A. *Hesione intertexta, Live specimen,* ***B-C.*** *Anterior end, dorsal view,* ***D.*** *Posterior end, dorsal view,* ***E.*** *Parapodium (chaetiger 8),* ***F-G.*** *Neurochaetal bundle,* ***H.****Tip of neurochaetal blade.*

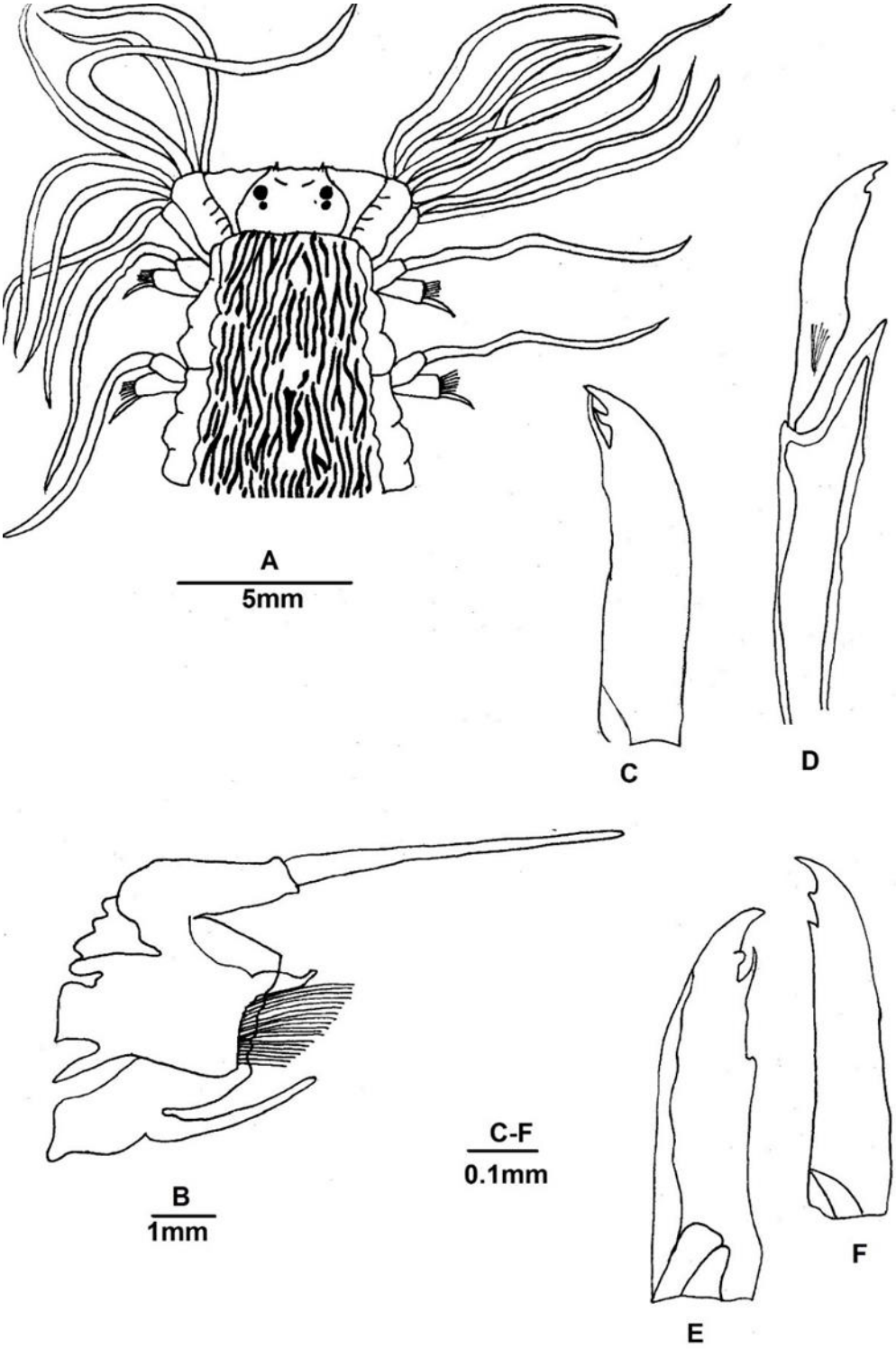

Figure 5. A. *Hesione intertexta; Anterior end, dorsal view,* ***B.*** *Parapodium (chaetiger 8),* ***C, E, F.*** *Tip of neurochaetal blades,* ***D.*** *Neurochaeta.*

Discussion

The research paper presents a detailed study based on inclusive assessment of the morphological and taxonomical descriptions of *Eunice petersi* and *Hesione intertexta* belonging to the families Eunicidae and Hesionidae, respectively, collected for the first time from Garyan and Bandari beach of Jiwani,

along Makran coast, Balochistan (Northern Arabian Sea). There have been several reports of the genus *Eunice* worldwide. Only two species of genus *Eunice* (*Eunice manorae* Aziz, 1938 and *Eunice indica* Kinberg, 1865) have been reported from Pakistan [21]. According to the World Register of Marine Species (WoRMS) [22] *E. petersi* is now valid name for the *E. afra punctata*. In 1957, Day [23] categorized *E. punctata* as a subspecies of *E. afra* (Peters, 1854). However, Fauchald, [19] renamed *E. punctata* to *E. petersi* due to its status as a junior secondary homonym to *E. punctata* (Risso, 1826) and recognized it as a valid species. *Eunice petersi* pays tribute to the scientist who described a highly valuable and early collection from its type locality Mozambique. *Eunice afra punctata* was also comparatively examined by many scientists [21-24]. Based on Fauchald's holotype, the specimens of Arabian Sea agree well with the descriptions of *E. petersi* [19]. The specimen's branchial distribution reported by Day, [23] from South Africa started from the 15th-17th chaetigers, Miura [25, 26] from Ishigaki Island and Veeramuthu *et al.* [27] from Great Nicobar Islands discussed that the first branchia occurs on chaetiger 16 whereas Fauchald [19] reported branchia from chaetiger 13 to chaetiger 200. The present studied specimens correspond to Day, [23] in terms of branchial distribution starting from chaetiger 15. According to Fauchald [19] and Veeramuthu *et al.* [27] the specimens had distally rounded guards on the bidentate compound falcigers which are similar the present observations. The genus *Hesione* has several nominal species found all over the world, the first of which is *Hesione splendid* Lamarck, 1818 from the Red Sea [28]. Only two species of the genus *Hesione* have been documented from Pakistan, including *H. splendida* and *H. pantherina* Risso, 1826 [21]. The type locality of *H. intertexta* is Philippines, Western Pacific and it was also recorded from Gulf of Mannar, Arabian Sea [18]. *Hesione intertexta* was comparatively examined by [17, 18, 20, 29, 30]. Species from similar forms, including *H. splendida*, *H. pantherina*, *H. intertexta* and *H. ceylonica* Grube, 1874 involve the colour pattern on the dorsal surface. *Hesione pantherina* and *H. intertexta* have longitudinal lines, whereas bright greyish in *H. splendida*, transverse bands, as in *Hesione genetta* Grube, 1866 long and wide pale patches, as in *H. ceylonica*, and middorsal oval to foliose. *Hesione pantherina* and *H. intertexta* differ in the size of the neurochaetal guards in relation to the teeth of blades, which gets close to *H. intertexta* apical tooth and *H. pantherina* subapical tooth. The examined specimen matches the descriptions of *H. intertexta* based on the holotype by [17, 18, 20]. Grube [17] highlighted how the original description and images combined longitudinal pigment lines with transverse annulations or striae. Usually connected to dorsal surfaces, these characteristics do not extend to lateral cushions; yet, in the original description of *H. intertexta*, even the lateral cushions appear to be granular in texture as opposed to smooth texture. Recent illustrations by Lee and Ong [30] established to each of these characteristics.

Documenting new records of Eunicidae and Hesionidae polychaete inhabiting unexplored locations along the Makran coast was the main goal of this research endeavour. This comprehensive investigation has produced an invaluable compilation of information about the distribution and character of the

polychaete fauna on the Makran coastal areas, which is a noteworthy accomplishment. These results emphasize the necessity of more research and the possibility of identifying new species in the area.

Acknowledgement The authors gratefully acknowledge to The Marine Reference collecting and Resource Centre at the University of Karachi provided laboratory and field research facilities. We appreciate the assistance of Mr. Kashif Jameel, and Mr. Umer as field assistant, who helped in sample collection. Mr. Abrar Ali provided valuable support with scientific illustrations and photography.

Funding/Financial Disclosure The authors have no received any financial support for the research, authorship, or publication of this study.

Ethics Committee Approval and Permissions The study does not require ethics committee approval or any special permission.

Conflicts of Interest The authors state that there is no conflict of interest related to this article.

Authors Contribution All authors read and approved the final manuscript.

References

[1] Read, G., & Fauchald, K. (2021, 20 February). World Polychaeta Database. http://www.marinespecies.org/polychaeta

[2] Rouse, G. W., Carvajal, J. I., & Pleijel, F. (2018). Phylogeny of Hesionidae (Aciculata, Annelida), with four new species from deep-sea eastern Pacific methane seeps, and resolution of the affinity of *Hesiolyra*. *Invertebrate Systematics*, *32*(5), 1050-1068.

[3] Zanol, J., Carrera-Parra, L. F., Steiner, T. M., Amaral, A. C. Z., Wiklund, H., Ravara, A. & Budaeva, N. (2021). The current state of Eunicida (Annelida) systematics and biodiversity. *Diversity*, *13,* 74. https://doi.org/10.3390/d13020074

[4] Kazmi, Q. B. (2022). *Marine faunal diversity of Pakistan inventory and taxonomic resources* (AR Shakoori Ed.). Zoological Society of Pakistan.

[5] Ali, Q. M., Ahmed, Q., Kurt, G., Bat, L., Mubarak, S., Qazi, H., Baloch A., Shaikh I., Baloch A., Aziz, N., Ahmed, S., Ali, A., Ahmed, I., & Ghalib, A. (2023). First report on distribution of polychaetes (Annelida: Polychaeta) along the Makran coast of Pakistan, northern Arabian Sea. *Journal of Materials and Environmental Science*, *14* (3), 277, 292.

[6] Ali, Q., Ahmed, Q., Mubarak, S., Baloch, A., Bat, L., Qazi, H., & Shaikh, I. (2023). Two new records of Eunicidae (Annelida, Errantia) along the Makran coast of Pakistan, northern Arabian Sea. *Natural and Engineering Sciences*, *8*(3), 168-182. https://doi.org/10.28978/nesciences.1405169

[7] Fauchald, K. (1977). The polychaete worms. Definitions and keys to the orders, families and genera. *Natural History Museum of Los Angeles County, Science Series*, *28,* 1-190.

[8] Grassle, J. F., & Maciolek, N. J. (1992). Deep-sea species richness: regional and local diversity estimates from quantitative bottom samples. *The American Naturalist, 139*(2), 313-341.

[9] Ward, T. J., & Hutchings, P. A. (1996). Effects of trace metals on infaunal species composition in polluted intertidal and subtidal marine sediments near a lead smelter, Spencer Gulf, South Australia. *Marine Ecology Progress Series., 135,* 123-135.

[10] Bat, L., & Kurt, G. (2020). Use of Polychaeta species as bioindicator for heavy metal pollution in marine environments. (In): Bayram T, Zayachuk Y, Gupta DK. (Eds.) Environmental radioactivity in Turkish environment. *Sivas Cumhuriyet Üniversitesi Matbaası*, 259-281.

[11] Jumars, P. A., Dorgan, K. M., & Lindsay, S. M. (2015). Diet of worms emended: an update of polychaete feeding guilds. *Annual Review of Marine Science, 7*, 497-520.

[12] Hutchings, P.A. (1986). Biological destruction of coral reefs: a review. *Coral Reefs, 4*, 239-252.

[13] Hartmann-Schröder, G., & Zibrowius, H. (1998). Polychaeta associated with Antipatharia (Cnidaria: Anthozoa): description of Polynoidae and Eunicidae. *Mitteilungen aus dem Hamburgischen Zoologischen Museum und Institute, 95*, 29-44.

[14] Gambi, M. C., Van, B. I., & Brearley, A. (2003). Mesofaunal borers in seagrasses: world-wide occurrence and a new record of boring polychaetes in the Mexican Caribbean. *Aquatic Botany, 76*(1), 65-77.

[15] Blake, J. A. (1985). Polychaeta from the vicinity of deep-sea geothermal vents in the eastern Pacific. I: Euphrosinidae, Phyllodocidae, Hesionidae, Nereididae, Glyceridae, Dorvilleidae, Orbiniidae and Maldanidae. *Bulletin of the Biological Society of Washington*, *6*, 67-101.

[16] Beesley, P. L., Glasby, C. J., & Ross, G. J. (Eds.). (2000). *Fauna of Australia 4 A, Polychaetes &Allies: The southern synthesis*. CSIRO publishing.

[17] Grube A. E. (1880). Mittheilungenüber die Famile der Phyllodoceen und Hesioneen. *Jahresbericht der Schlesischen Gesellschaft fürvaterländische Cultur*, *57*, 204-228.

[18] Fauvel, P. (1953). *The fauna of India including Pakistan, Ceylon, Burma and Malaysia-Annelida Polychaeta*. India: The Indian Press, Ltd..

[19] Fauchald, K. (1992). *A review of the genus Eunice (Polychaeta: Eunicidae) based upon type material*. Smithsonian Institution Press Washington D.C..

[20] Salazar-Vallejo, S. I. (2018). Revision of *Hesione* Savigny in Lamarck, 1818 (Annelida, Errantia, Hesionidae). *Zoosystema*, *40*(3), 227-325.

[21] Aziz, N. D. (1938). Fauna of Karachi, 2 Polychaetes. *Memoirs of Department of Zoology, Punjab University*, Lahore, 1: 19-52.

[22] World Register of Marine Species (WoRMS) (2024, 05, January). https://www.marinespecies.org

[23] Day, J. H. (1957). The polychaete fauna of South Africa. Part 4. New species and records from Natal and Mozambique. *Bulletin of the British Museum (Natural History), 14*, 59-129.

[24] Sekar, V., Rajasekaran, R., Balakrishnan, S., & Raguraman, R. (2019). Taxonomical Keys for Morphological Identification of Coral-Associated Polychaetes from Great Nicobar Islands. *Natural Resources Management and Biological Sciences*, 1-33.

[25] Miura, T. (1979). Eunicid polychaetous annelids from Japan-III. *Ibid.*, *17*, 33-42.

[26] Miura, T. (1986). Japanese polychaetes of the genera *Eunice* and *Euniphysa*: Taxonomy and branchial distribution patterns. *Publications of the Seto Marine Biological Laboratory*, *31*(3-6), 269-325.

[27] Veeramuthu, S., Ramadoss, R., Subramaniyan, B., Jeyaram, S., & Fernando, O. J. (2012). Abundance of the Boring Polychaetes of Eunicidae (Annelida) in Great Nicobar Islands. *Our Nature*, *10*, 76-88.

[28] Costa, D. D. A., & Christoffersen, M. L. (2016). Revision and global distribution of *Hesiones plendida* (Annelida, Polychaeta, Hesionidae) (Annelida, Polychaeta, Hesionidae). *Gaia Scientia*, *10* (4), 1-30.

[29] Wu, B., Shen, S., & Chen, M. (1975). Preliminary report of polychaetous annelids from Xisha Islands, Guangdong Province, China. Studia. *Marina Sinica*, *10*, 65-104.

[30] Lee, Y., & Ong, R. (2015). New records of two hesionid polychaetes from the Singapore Strait. *Singapore Biodiversity Records*, 201-204.

Sinopfbd, 2024; 9(1): 207-216 **https://doi.org/10.33484/sinopfbd.1437668**

Sinop Üniversitesi Fen Bilimleri Dergisi
Sinop Uni J Nat Sci
E-ISSN: 2564-7873

https://dergipark.org.tr/tr/pub/sinopfbd

A new Alien Fish from the Southern Black Sea (Sinop, Türkiye): *Sebastes schlegelii* Hilgendorf, 1880 (Scorpaeniformes, Sebastidae)

Orçin UYGUN[1], Hasan Can ÖZTEKİN[2], Ayşah ÖZTEKİN[1] and Levent BAT[1]

How to cite: Uygun, O., Öztekin, H.C., Öztekin, A., & Bat, L. (2024). A new alien fish from the southern black sea (Sinop, Türkiye): *Sebastes schlegelii* Hilgendorf, 1880 (Scorpaeniformes, Sebastidae). *Sinop Üniversitesi Fen Bilimleri Dergisi, 9*(1), 207-216. https://doi.org/10.33484/sinopfbd.1437668

Research Article

Corresponding Author
Orçin UYGUN
orcin.uygun@ege.edu.tr

ORCID of the Authors
O.U: 0000-0001-7778-5211
H.C.Ö: 0000-0001-8213-1490
A.Ö: 0000-0002-3726-7134
L.B: 0000-0002-2289-6691

Received: 16.02.2024
Accepted: 24.06.2024

Abstract

Sebastes schlegelii Hilgendorf, 1880 is an Indo-Pacific species with a widespread distribution in the coastal waters of the Far Eastern region. This study represents the first documentation of *S. schlegelii* off Sinop coast from the Southern Black Sea. The four specimens collected on 28 May 2023 and 18 June 2023 from rocky habitat at a depth of about 6 meters off Sinop coast had a total length range of 226 to 237 mm and weights ranging from 197.57 to 254.98 g. The spread of this species to the southern Black Sea coast is attributed to the transportation of early life stage individuals from the northern coast of the Black Sea to the southern coast via the cyclonic Rim Current.

Keywords: Black rockfish, exotic species, new record, Black Sea

Güney Karadeniz'de (Sinop, Türkiye) Yeni Bir Yabancı Balık Türü: *Sebastes schlegelii* Hilgendorf, 1880 (Scorpaeniformes, Sebastidae)

[1]Department of Hydrobiology, Faculty of Fisheries, Sinop University, 57000, Sinop Türkiye

[2] Sinop Municipality, 57000, Sinop Türkiye

Öz

Sebastes schlegelii Hilgendorf, 1880, Uzak Doğu bölgesinin kıyı sularında yaygın bir dağılıma sahip İndo-Pasifik bir balık türüdür. Bu çalışma, *S. schlegelii*'nin Sinop'un Karadeniz kıyılarından ilk kaydını temsil etmektedir. Sinop açıklarında yaklaşık 6 metre derinlikteki kayalık habitattan 28 Mayıs 2023 ve 18 Haziran 2023 tarihlerinde toplanan dört örneğin total boyları 226 ila 237 mm, ağırlıkları ise 197.57 ile 254.98 g arasında değişmektedir. Bu türün Güney Karadeniz kıyılarına yayılmasının, erken yaşam evresindeki bireylerin Karadeniz'in kuzey kıyılarından güney kıyılarına siklonik Rim Akıntısı aracılığıyla taşınmasına dayandığı düşünülmektedir.

Anahtar Kelimeler: Kara kaya iskorpiti, egzotik tür, yeni kayıt, Karadeniz

Introduction

Introduction of alien, or non-indigenous species into different habitats has been recognised as one of the major problems [1]. A non-indigenous species is considered to be any species whose historical

translocation into an environment outside of its native geographic habitat has been either intentionally or accidentally man-mediated or an action of active dispersal via natural pathways [2, 3]. Several major categories make up the global vectors for alien marine species and include canals, aquaculture fisheries, and commercial shipping operations [1, 3]. The Black Sea is one of the unique seas in the world, with a 423,000 km^2 area, 547,000 km^3 volume, a maximum depth of 2212 m representing a semi-closed sea, connected with the Kerch Strait to the Sea of Azov, and with the Bosphorus and Dardanelles Straits to the Marmara and Mediterranean Seas and covered with a oxygen-poor water layer [4-7]. The Black Sea with its low species diversity creates a favourable environment for introduction of alien species. This leads to less competition, diverse habitats, and numerous available niches, and some of these species can become invasive, disrupting ecosystem stability, and functionality, and threatening native species [8, 9]. The Mediterranization of the Black Sea is one of the factors that affect the introduction and distribution of alien species in the Black Sea. The ecosystem and fish populations in the Black Sea are significantly impacted by climate change, pollution, overfishing, and illegal fishing, as well as by invasive species [10]. The black rockfish, *Sebastes schlegelii*, falls under the order Scorpaeniformes, and the family Sebastidae [11]. It is an economically significant species in aquaculture in various Asian countries, including South Korea, Japan, and China due to its rich nutritional composition, high market demand, rapid growth rate, and ability to withstand low water temperatures [12, 13]. This study presents the initial record of the black rockfish along the Sinop coast of the Black Sea. The primary aim of this investigation is to perform a comprehensive examination and documentation of the morphological characteristics of black rockfish specimens, while concurrently evaluating the present status of this species within the Black Sea ecosystem.

Materials and Methods

Four specimens were collected on 28/05/2023 and 18/06/2023 from rocky habitat at a depth of approximately 6 meters off the Sinop coast (41.927ºN, 35.090ºW) (Figure 1).

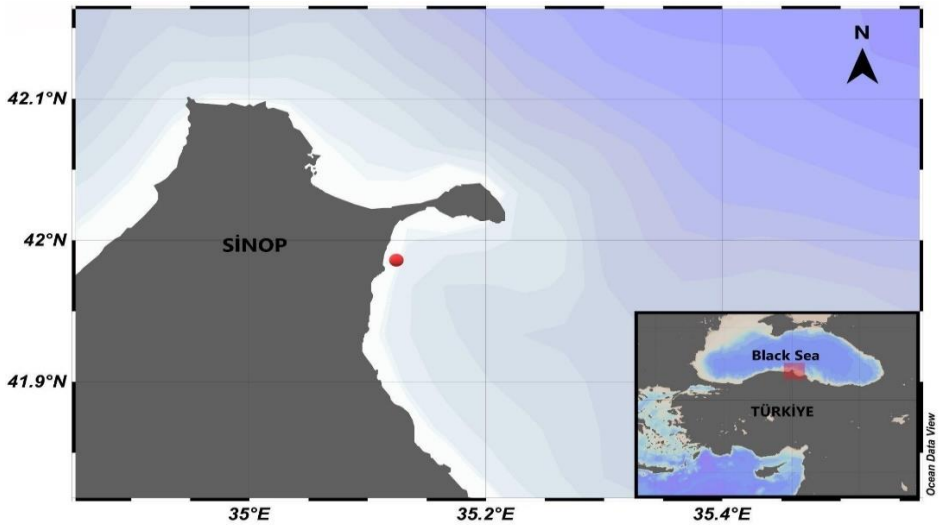

Figure 1. *Map of the region where the black rockfish species was recorded*

Fish samples were collected using a fishing line by H. C. Öztekin and K. A. Usta and identified by O. Uygun. The four samples exhibited total lengths ranging from 226 to 237 mm, standard lengths ranging from 198 to 201 mm, and weights ranging from 197.57 to 254.98 g (Figure 2). Precise morphometric measurements, including length (±0.1 mm), weight (±0.01 g), and meristic counts, were meticulously recorded. Subsequently, the fish were photographed and preserved in a 4% buffered formaldehyde-borax solution. The preserved specimen was then deposited at the Biology Laboratory of the Fisheries Faculty, Sinop University (Sinop, Türkiye) serving as a reference sample. Although it is currently unnumbered, it will be an essential resource for future reference and research purposes. Morphometric measurements and meristic counts of all captured specimens were conducted using the traditional method as described by Takács et al. [14]. The map was created using Ocean Data View v5.6 software [15].

Figure 2. *Sebastes schlegelii caught at Sinop, Southern Black Sea, Türkiye. The standard length is 199 mm.*

Results

Descriptions

The morphological characteristics of *S. schlegelii* include dorsal fin rays XIII+13, anal fin rays III+8, pectoral fin rays 18, ventral fin rays I+5, caudal fin rays 15-16, and the lateral line containing 45-47 pores. The anterior portion of the body is moderately narrow and gradually tapers towards the posterior region. The head of individuals in this species exhibit notable anatomical features, including the presence of three lacrimal spines, five preopercular spines (the second preopercular spine is the longest, while the lengths of the lower spines progressively decrease), and two opercular spines. The occipital region exhibits two flat bony projections, with the upper extremity resembling a spine in shape. Mouth large, protractile, and slightly oblique. The snout is devoid of scales. The mandible is positioned slightly anterior to the maxilla. The maxilla and mandible exhibit a continuous series of villiform teeth, while the presence of teeth on the vomer bone is evident, and no palatines are present. The tips of both the upper and lower lips display a distinct black colouration. Additionally, two oblique dark bands on the preoperculum serve as characteristic features of this species. The lateral line follows a parallel course to the dorsal profile of the body, extending from the posterior edge of the opercule to the base of the caudal fin. The pectoral fin base is positioned slightly anterior to the pelvic fin base, while the caudal

fin has a round shape. Notably, there is a prominent papilla protrusion in the urogenital opening. The colouration of this species is characterised by a dark grey and brown hue, adorned with a marbled pattern consisting of small, indistinct dark spots scattered across the body. Detailed morphometric measurements and body proportions as percentages are given in Table 1.

Table 1. *The morphometric characteristics of the Sinop specimens of Sebastes schlegelii in the Black Sea (± Standard Error)*

	Present study	**[20]**	**[21]**	**[22]**	**[23]**	**[43]**	**[42]**
Number of specimen(s)	4	5	1	1	6	1	1
TL (mm)	226-237	325-391	349.6	245	230	275	311
SL (mm)	191-201	277	299.3	206	200	240	264
W (g)	197.6-255.0	710.0-1151.2		282.1	227	459.2	
Meristic counts							
Dorsal-fin rays	XIII- 13	XIII- 13	XIII-13	XIII-11	XIII-13	XIII-13	XIII-13
Pectoral-fin rays	18	18	18	18	18	18	18
Pelvic-fin rays	I-5	I-5	I-5	I-5	I-5	I-5	I-5
Anal-fin rays	III-8	III-8	III-8	III-8	III-8	III-6	III-8
Caudal-fin rays	15-16		16	15-16	15-16	15	
Pored lateral line scales	45-47	47-49	47	44	47		46
Morphometric measurements % of SL							
Predorsal length	28.7 ±0.54	34.4	31.7	27.1	27.5	33.3	29.4
Prepectoral length	32.2 ±0.45	34.6		29.8	34	37.1	33.5
Preanal length	62.3 ±0.28	68.5		66.7	64	68.8	67.8
Prepelvic length	36.9 ±0,21	38.2	34.7	39	38	22.5	39.3
Length of dorsal fin	14.0 ±0,12		16.1		11.5		
Length of pectoral fin	23.1 ±0.24	22.1	20.6	25.2	22.5	24.2	22.5
Length of pelvic fin	18.8 ±0.26	20.5	34.7	22.7	19.5		18.7
Length of anal fin	14.8 ±0.39	16	18.1	15.9			16.6
Length of caudal fin	17.2 ±0.21	21.2	17.3	13.4			20.8
Length of caudal peduncle	14.5 ±0.30	10.4	10.4	9.7	9	9.2	9.8
Dorsal fin base length	59.4 ±0.52	62.6		60.8	56	63.8	58.8
Anal fin base length	19.4 ±0.31	15.9		15.9	16.5	20.4	16.6
Maximum body depth	36.3 ±0.64			36.5	32	38.3	34.2
Minimum body depth	10.8 ±0.33						
Head length (HL)	35.0 ±0.46	37.8	31.1	34	36.5	36.7	34.3
Morphometric measurements % of HL							
Preorbital length	21.9 ±0.42	30.9	30.6	19.8			
Postorbital length	54.8 ±0.53	52.5		61.5			62.6
Eye diameter	20.6 ±0.32	19.7	18.9	18.7			17.1
Interorbital distance	24.0 ±0.68	27.1	30.9				
Maxilla length	45.3 ±0.62	45.1		45.5			35.7
Mandible length	46.7 ±0.59	46.6					

[20]Karpova et al., (2021), **[21]**Yağlıoglu et al., (2023), **[22]**Bilecenoğlu et al., (2023), **[23]**Ivanova et al., (2024), **[43]**Karadurmuş et al., (2024), **[42]**Uzer et al., (2024)

Discussion and Conclusions

This article presents an additional record of *S. schlegelii* in the Black Sea and a new record for the Sinop coastline. The Black rockfish, commonly known as the black rockfish, is a widely recognised sedentary species that inhabits nearshore rocky bottoms within a depth range of 10 to 100 meters [16]. The black rockfish is a species with a widespread distribution in the Pacific Northwest waters, including regions such as South Korea, Japan, and China [17]. The initial documented occurrence of the species outside its native habitat was observed along the Dutch coast in the North Sea [18]. Black rockfish in the Black Sea was first described as *Ephinephelus caninus* Valenciennes, 1834 off the coast of Crimea in May 2013 [19]. However, Karpova et al. [20] stated in their study that the description made by Boltachev & Karpova [19] was incorrect and revealed that this species was *S. schlegelii* by morphometric measurements and descriptions. Karpova et al. [20] reported this species from the west coast of Crimea in April 2019 and gave morphometric characteristics of the species. The study by Yağlıoğlu et al. [21], which includes the morphological and genetic record of the species detected in May 2022, is the first record from the Turkish coast in the southern Black Sea. Ivanova et al. [23] provided the first morphological and genetic record of the species from the Varna and Burgas coast in the western Black Sea, detected in May 2022 and August 2023. Bilecenoğlu et al. [22] provided morphological and genetic record of the species from the Ordu/Ünye coasts in the southern Black Sea, detected in August 2023. Uzer et al. [42] reported the species from the Şile/Istanbul coast at the south of Black Sea in December 2023, along with its morphometric characteristics. Karadurmuş et al. [43] gave its first record from the Sea of Marmara, the Gulf of İzmit in January 2024, and stated that the geographical spread of the species is rapidly expanding. This study represents the last record of the species in the Black Sea (Sinop coast of the southern Black Sea) found in May and June 2023 (Figure 3). The morphometric measurements and meristic counts in our study seem to match with literature [17, 20-23, 42, 43]. It has been emphasised that the Pacific oyster *Crassostrea gigas* which can come from farms or ships via ballast waters is the reason for the presence of this species in areas different from its natural habitat [18, 20]. Karpova et al. stated that the black rockfish juveniles may have entered the Black Sea ecosystem along with the shipments of the giant Pacific oyster *Crassostrea gigas*, which are regularly imported live to the southern coast of Crimea [20]. However, there are no *C. gigas* farms around Sinop. For this reason, the presence of this species on the coasts of Sinop may be due to several reasons. It is possible that the early life stages of this species arrived through the ballast water of ships. Therefore, it is known that this species has a resident population in the Crimea region [20]. Sinop is situated approximately 150 nautical miles south of Crimea. However, *Sebastes* spp. are demersal and sedentary species, typically distributed at a maximum depth of 100 meters [16, 17]. As the depth along this path is greater, it is thought that the population is unlikely to migrate from this area.

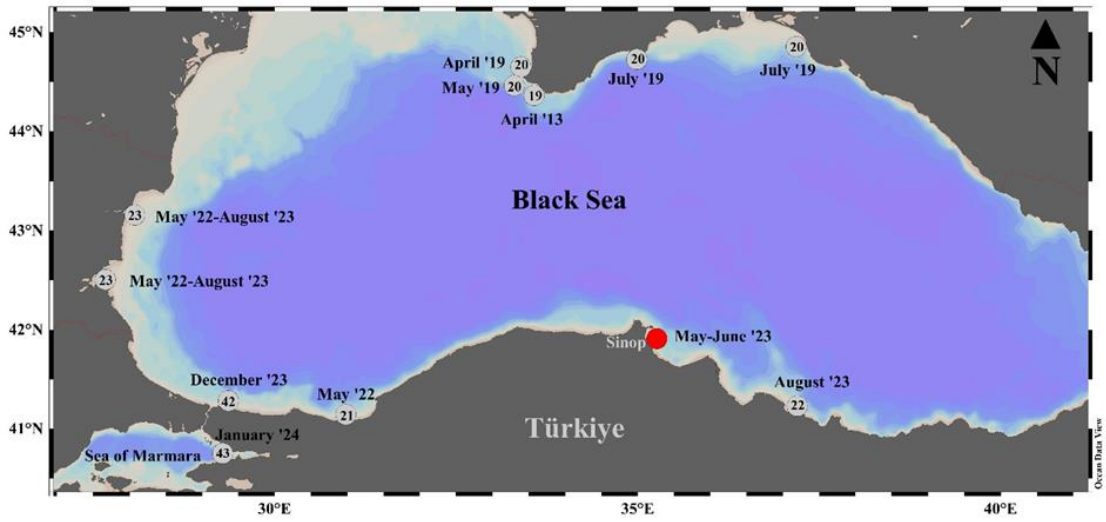

Figure 3. *Chronological distribution of Sebastes schlegelii in the Black Sea and the Sea of Marmara (Red dot indicates the current study. Gray dots denote other studies, with reference numbers of studies provided within gray dots.)*

The black rockfish is a viviparous fish with a pelagic larval stage. Following spawning, the larvae inhabit the upper water layer. The larvae and juveniles exhibit a propensity for seeking shelter amidst floating algae, proximity to logs, buoys, and various objects, or forming dense assemblages [20, 24-27]. The existing circulation pattern of the Black Sea is defined by a cyclonic rim current [28, 29]. In this context, the hypothesis posits that early life stage individuals of the black rockfish were transported from the western coast of the Black Sea to the coast of Sinop via the cyclonic current, leading to the establishment of a population. This proposition gains support from the fact that records of the black rockfish in the western Black Sea were identified in May 2022, reinforcing this assumption [21, 23]. The black rockfish, being a piscivorous predator, primarily prey on fish and shrimp species [30]. Its diet predominantly consists of small fish, including anchovies [31]. In the Turkish waters of the Black Sea, known for its abundant fish populations, particularly small pelagic species like anchovy, sprat, and horse mackerel [32], the black rockfish may find favourable feeding conditions. Furthermore, the presence of shrimp species such as *Crangon crangon*, *Palaemon adspersus*, and *Palaemon elegans* in the waters of Sinop [33] suggests that this area may serve as a favourable feeding habitat for black rockfish. It has been determined that the most effective environmental condition for the distribution of *S. schlegelii* is the bottom temperature, and it has been stated that the most suitable temperature for the species is between 3-20 °C [34]. It was determined that the optimum temperature for this species is between 5-28 °C in the experimental investigations made under aquaculture conditions [35, 36]. Despite the customary salinity protocol of approximately 30 psu for black rockfish in aquaculture settings [16, 37], a comparative study investigating the growth of juvenile black rockfish under diverse environmental conditions unveiled that optimal growth and survival outcomes were attained in brackish water environments [38]. Sinop waters, exhibit characteristics of brackish water, with an average salinity of 18 psu and annual temperature fluctuations ranging from 8 to 26°C [39, 40]. Consequently, considering the available literature, it is

believed to serve as a favourable environment for the feeding and growth of black rockfish. The alien species pose a threat to the biodiversity of native species in the ecosystem and lead to significant changes in native ecosystems on a global scale [41]. Therefore, competition between *S. schlegelii* and local species sharing the same habitat and having similar trophic levels is inevitable. However, *S. schlegelii* holds significant economic value in Asian countries, primarily due to its desirable attributes that make it well-suited for aquaculture. The commercial importance of the species may create the potential for aquaculture and local fisheries in the Black Sea. The Black Sea coasts are postulated to provide a conducive ecological environment for the black rockfish, considering its ecological requirements and habitat preferences. Therefore, we posit that monitoring the present status of this species in the Black Sea and tracking the population dynamics of indigenous species occupying the same trophic level is imperative for a comprehensive understanding of the ecological implications.

Acknowledgement The authors thank the amateur fisherman K.A. Usta and the Hamsilos Fishing Market for the dark rockfish specimens provided by them.

Funding/Financial Disclosure No funding was received for conducting this study.

Ethics Committee Approval and Permissions The study does not require ethics committee approval or any special permission. All applicable international, national and/or institutional guidelines for the care and use of animals have been followed.

Conflicts of Interest The authors declare no conflicts of interest.

Authors Contribution 1. Author: %40, 2. Author: %20, 3. Author: %20, 4. Author: %20.

References

[1] Bax, N., Carlton, J. T, Mathews-Amos, A., Haedrich, R. L., Hogwarth, F. G., Purcell, J. E., Raiser, A. & Gray, A. (2001). The control of biological invasions in the world's oceans. *Conservation Biology, 15*, 1234-1246. https://doi.org/10.1111/j.1523-1739.2001.99487.x

[2] Olenin, S., & Leppakoski, E. (2002). Baltic Sea Alien Species Data Base. Online. Available: http://www.ku.lt/nemo/

[3] Yankova, M. (2016). Alien invasive fish species in Bulgarian waters: An overview. *International Journal of Fisheries and Aquatic Studies, 4*(2), 282-290.

[4] Zaitsev, Y., & Mamaev, V. (1997). Marine biological diversity in the Black Sea. A study of change and decline. *GEF Black Sea Environmental Series, 3*, 208.

[5] Borysova, O., Kondakov, A., Paleari, S., Rautalahti-Miettinen, E., Stolberg, F., & Daler, D. (2005). *Eutrophication in the Black Sea Region; Impact Assessment and Causal Chain Analysis.* Sunds Tryck Öland AB, University of Kalmar.

[6] Lyratzopouoou, D., & Zarotiadis, G. (2014). Black Sea: old trade routes and current perspectives of socioeconomic co-operation. *Procedia Economics and Finance, 9*, 74–82. https://doi.org/10.1016/S2212-5671(14)00009-4

[7] Bat, L., Öztekin, A., Şahin, F., Arıcı, E., & Özsandıkçı, U. (2018). An overview of the Black Sea pollution in Turkey. *Mediterranean Fisheries and Aquaculture Research, 1*(2), 66-86.

[8] CIESM. (2010). Climate forcing and its impacts on the Black Sea marine biota. N 39 in Ciesm Workshop Mongraphs [F. Briand, Ed.], Monaco, pp. 152.

[9] Bat, L., Sezgin, M., Satilmis, H. H., Sahin, F., Üstün, F., Özdemir, Z. B., Baki, O. G. (2011). Biological diversity of the Turkish Black Sea coast. *Turkish Journal of Fisheries and Aquatic Sciences, 11*(4), 683-692. https://doi.org/10.4194/1303-2712-v11_4_04

[10] Radulescu, V. (2023). Environmental Conditions and the Fish Stocks Situation in the Black Sea, between Climate Change, War, and Pollution. *Water, 15*(6), 1012. https://doi.org/10.3390/w15061012

[11] Nelson, J. S., Grande, T. C., & Wilson, M. V. (2016). *Fishes of the World.* John Wiley & Sons.

[12] Lee, S. M., Jeon, I. G., & Lee, J. Y. (2002). Effects of digestible protein and lipid levels in practical diets on growth, protein utilization and body composition of juvenile rockfish (*Sebastes schlegeli*). *Aquaculture, 211*(1-4), 227-239. https://doi.org/10.1016/S0044-8486(01)00880-8

[13] Cao, M., Zhang, M., Yang, N., Fu, Q., Su, B., Zhang, X., Li, Q., Yan, X., Thongda, W., & Li, C. (2020). Full length transcriptome profiling reveals novel immune-related genes in black rockfish (*Sebastes schlegelii*). *Fish & Shellfish Immunology, 106*, 1078-1086. https://doi.org/10.1016/j.fsi.2020.09.015

[14] Takács, P., Vitál, Z., Ferincz, Á., & Staszny, Á. (2016). Repeatability, reproducibility, separative power and subjectivity of different fish morphometric analysis methods. *PLoS One, 11*(6): e0157890. https://doi.org/10.1371/journal.pone.0157890

[15] Schlitzer, R. (2023). Ocean Data View, https://odv.awi.de

[16] Hwang, H. K., Son, M. H., Myeong, J. I., Kim, C. W., & Min, B. H. (2014). Effects of stocking density on the cage culture of Korean rockfish (*Sebastes schlegeli*). *Aquaculture, 434*, 303-306. https://doi.org/10.1016/j.aquaculture.2014.08.016

[17] Froese, R., & D. Pauly. (2023). Editors. FishBase. World Wide Web electronic publication. www.fishbase.org, (01/06/2023)

[18] Kai, Y. & Soes, D. M. (2009). A record of *Sebastes schlegelii* Hilgendorf, 1880 from Dutch coastal waters. *Aquatic Invasions, 4*(2), 417-419. https://doi.org/10.3391/ai.2009.4.2.23

[19] Boltachev, A., & Karpova, E. (2013). First record of dogtooth grouper *Epinephelus caninus* (Valenciennes, 1834), Perciformes, Serranidae, in the Black Sea. *BioInvasions Records, 2*(3), 257. http://dx.doi.org/10.3391/bir.2013.2.3.14

[20] Karpova, E. P., Tamoykin, I. Y., & Kuleshov, V. S. (2021). Findings of the Korean Rockfish *Sebastes schlegelii* Hilgendorf, 1880 in the Black Sea. *Russian Journal of Marine Biology, 47*, 29-34. https://doi.org/10.1134/S106307402101003X

[21] Yağlıoğlu, D., Doğdu, S. A., & Turan, C. (2023). First Morphological and Genetic Record and Confirmation of Korean Rockfish *Sebastes schlegelii* Hilgendorf, 1880 in the Black Sea Coast of Türkiye. *Natural and Engineering Sciences, 8*(3), 140-150. https://doi.org/10.28978/nesciences.1363941

[22] Bilecenoğlu, M., Yokeş, M. B., & Aydin, M. (2023). First record of *Sebastes schlegelii* Hilgendorf, 1880, along the Turkish Black Sea coast–new addition to the alien species inventory. *Turkish Journal of Maritime and Marine Sciences*, 1-9. https://doi.org/10.52998/trjmms.1358814

[23] Ivanova, P. P., Dzhembekova, N. S., Raykov, V. S., & Raev, Y. (2024). A first record of non-native Korean (black) rockfish *Sebastes schlegelii* Hilgendorf, 1880 from the Bulgarian Black Sea coast. *BioInvasions Records*, *13.*

[24] Safran, P. (1990). Drifting seaweed and associated ichthyofauna: Floating nursery in Tohoku waters. *La Mer*, *28*, (4), 225–239.

[25] Moser, H. G., & Boehlert, G. W. (1991). Ecology of pelagic larvae and juveniles of the genus *Sebastes*. *Environmental Biology of Fishes, 30*, 203-224. https://doi.org/10.1007/BF02296890

[26] Hyde, J. R., & Vetter, R. D. (2007). The origin, evolution, and diversification of rockfishes of the genus Sebastes (Cuvier), *Molecular Phylogenetics and Evolution, 44*(2), 790–811. https://doi.org/10.1016/j.ympev.2006.12.026

[27] Tengfei, D., Yongshuang, X., Haixia, Z., Li, Z., Qinghua, L., Xueying, W., Jun, L., Shihong, X., Yanfeng, W., Jiachen, Y., Lele, W., Yunong, W. & Guang, G. (2021). Multiple fetal nutritional patterns before parturition in viviparous fish *Sebastes schlegelii* (Hilgendorf, 1880). *Frontiers in Marine Science, 7*, 571946. https://doi.org/10.3389/fmars.2020.571946

[28] Oğuz, T., Latun, V. S., Latif, M. A., Vladimirov, V. V., Sur, H. I., Markov, A. A., Özsoy, E., Kotovshchikov, B. B., Eremeev, V. V., & Ünlüata, Ü. (1993). Circulation in the surface and intermediate layers of the Black Sea. *Deep Sea Research Part I: Oceanographic Research Paper, 40*(8), 1597-1612. https://doi.org/10.1016/0967-0637(93)90018-X

[29] Kubryakov, A. A., & Stanichny, S. V. (2015). Seasonal and interannual variability of the Black Sea eddies and its dependence on characteristics of the large-scale circulation. Deep Sea Research Part I: *Oceanographic Research Papers, 97*, 80-91. https://doi.org/10.1016/j.dsr.2014.12.002

[30] Zhang, B., Li, Z., & Jin, X. (2014). Food composition and prey selectivity of *Sebastes schlegeli*. *Journal of Fishery Sciences of China, 21*(1), 134-141.

[31] Zhang, Y., Xu, Q., Xu, Q., Alós, J., Zhang, H., & Yang, H. (2018). Dietary Composition and Trophic Niche Partitioning of Spotty-bellied Greenlings *Hexagrammos agrammus*, Fat Greenlings *H. otakii*, Korean Rockfish *Sebastes schlegelii*, and Japanese Seaperc*h Lateolabrax japonicus* in the Yellow Sea Revealed by Stomach Content Analysis and Stable Isotope Analysis. *Marine and Coastal Fisheries*, *10*(2), 255-268. https://doi.org/10.1002/mcf2.10019

[32] TUIK, (2023). Turkish Statistical Institute Databases Medas. https://biruni.tuik.gov.tr/medas/?locale=tr Accessed June 06, 2023.

[33] Bilgin, S. & Samsun, O. (2006). Fecundity and Egg Size of Three Shrimp Species, *Crangon crangon*, *Palaemon adspersus*, and *Palaemon elegans* (Crustacea: Decapoda: Caridea), off Sinop Peninsula (Turkey) in the Black Sea. *Turkish Journal of Zoology, 30*(4), 11. Available at: https://journals.tubitak.gov.tr/zoology/vol30/iss4/11

[34] Chen, Y., Shan, X., Ovando, D., Yang, T., Dai, F., & Jin, X. (2021). Predicting current and future global distribution of black rockfish (*Sebastes schlegelii*) under changing climate. *Ecological Indicators*, *128*, 107799. https://doi.org/10.1016/j.ecolind.2021.107799

[35] Hong Kim, K., Jung Hwang, Y., & Ryun Kwon, S. (2001). Influence of daily water temperature changes on the chemiluminescent response and mortality of cultured rockfish (*Sebastes schlegeli*). *Aquaculture, 192*, 93–99. https://doi.org/10.1016/S0044-8486(00)00460-9

[36] Lyu, L., Wen, H., Li, Y., Li, J., Zhao, J., Zhang, S., Song, M., & Wang, X. (2018). Deep transcriptomic analysis of black rockfish (*Sebastes schlegelii*) provides new insights on responses to acute temperature stress. *Scientific Reports, 8*(1), 9113. https://doi.org/10.1038/s41598-018-27013-z

[37] Zhang, Z., Fu, Y., Guo, H., & Zhang, X. (2021). Effect of environmental enrichment on the stress response of juvenile black rockfish *Sebastes schlegelii*. *Aquaculture, 533*, 736088. https://doi.org/10.1016/j.aquaculture.2020.736088

[38] Chin, B. S., Nakagawa, M., Noda, T., Wada, T., & Yamashita, Y. (2013). Determining optimal release habitat for black rockfish, *Sebastes schlegelii*: examining growth rate, feeding condition, and return rate. *Reviews in Fisheries Science, 21*(3-4), 286-298. https://doi.org/10.1080/10641262.2013.837364

[39] Uygun, O. (2015). *Balık larvalarının Sinop-Akliman kıyılarındaki kompozisyonu.* (Tez no.409921) [Yüksek Lisans Tezi, Sinop Üniversitesi].

[40] Üstün, F. (2019). Seasonal cycle of zooplankton abundance and biomass in Hamsilos Bay, Sinop, Southern Black Sea, Turkey. *Journal of Natural History*, *53*(7-8), 365-389.

[41] Gavioli, A., Milardi, M., Castaldelli, G., Fano, E. A., & Soininen, J. (2019). Diversity patterns of native and exotic fish species suggest homogenization processes, but partly fail to highlight extinction threats. *Diversity and Distributions, 25(*6), 983-994. https://doi.org/10.1111/ddi.12904

[42] Uzer, U., Karakulak, F. S., & Kabasakal, H. (2024). Prebosphoric occurrence of Korean rockfish, *Sebastes schlegelii* Hilgendorf, 1880 in southwestern Black Sea with notes on its morphometry and dispersal potential. *Ege Journal of Fisheries & Aquatic Sciences, 41*(1), 63-68. https://doi.org/10.12714/egejfas.41.1.09

[43] Karadurmuş, U., Güner, A., & Aydın, M. (2024). First Record and Geographic Expansion of the *Sebastes schlegelii* in the Sea of Marmara. *Journal of Anatolian Environmental and Animal Sciences*, *9*(1), 82-86. https://doi.org/10.35229/jaes.1431890

Sinopfbd, 2024; 9(1): 217-239 **https://doi.org/10.33484/sinopfbd.1445215**

Sinop Üniversitesi Fen Bilimleri Dergisi
Sinop Uni J Nat Sci
E-ISSN: 2564-7873

https://dergipark.org.tr/tr/pub/sinopfbd

Using Artificial Intelligence Techniques for the Analysis of Obesity Status According to the Individuals' Social and Physical Activities

Niğmet KÖKLÜ[1] and Süleyman Alpaslan SULAK[2]

How to cite: Koklu, N., & Sulak, S.A. (2024). Using artificial intelligence techniques for the analysis of obesity status according to the individuals' social and physical activities. *Sinop Üniversitesi Fen Bilimleri Dergisi, 9*(1), 217-239. https://doi.org/10.33484/sinopfbd.1445215

Research Article

Corresponding Author
Niğmet KÖKLÜ
nkoklu@ktun.edu.tr

ORCID of the Authors
N.K: 0000-0001-9563-3473
S.A.S: 0000-0001-9716-9336

Received: 29.02.2024
Accepted: 10.06.2024

Abstract

Obesity is a serious and chronic disease with genetic and environmental interactions. It is defined as an excessive amount of fat tissue in the body that is harmful to health. The main risk factors for obesity include social, psychological, and eating habits. Obesity is a significant health problem for all age groups in the world. Currently, more than 2 billion people worldwide are obese or overweight. Research has shown that obesity can be prevented. In this study, artificial intelligence methods were used to identify individuals at risk of obesity. An online survey was conducted on 1610 individuals to create the obesity dataset. To analyze the survey data, four commonly used artificial intelligence methods in literature, namely Artificial Neural Network, K Nearest Neighbors, Random Forest and Support Vector Machine, were employed after pre-processing. As a result of this analysis, obesity classes were predicted correctly with success rates of 74.96%, 74.03%, 74.03% and 87.82%, respectively. Random Forest was the most successful artificial intelligence method for this dataset and accurately classified obesity with a success rate of 87.82%.

Keywords: Obesity dataset, artificial intelligence methods, artificial neural network, support vector machine, k nearest neighbors, random forest

Kişilerin Sosyal ve Fiziksel Aktivitelerine Göre Obezite Durumunun Analizi için Yapay Zeka Tekniklerinin Kullanımı

[1] Technical Science Vocational High School, Konya Technical University, Konya, Türkiye

[2] Ahmet Keleşoğlu Educational Faculty, Necmettin Erbakan University, Konya, Türkiye

Öz

Obezite, genetik ve çevresel etkileşimlere sahip ciddi ve kronik bir hastalıktır. Sağlığa zararlı olan vücuttaki aşırı miktardaki yağ dokusu olarak tanımlanır. Obezitenin başlıca risk faktörleri, sosyal, psikolojik ve beslenme alışkanlıklarını içerir. Obezite, dünya genelinde tüm yaş grupları için önemli bir sağlık sorunudur. Şu anda dünya genelinde 2 milyardan fazla insan obez veya aşırı kilolu durumdadır. Araştırmalar, obezitenin önlenebileceğini göstermektedir. Bu çalışmada, obezite riski taşıyan bireyleri tanımlamak için yapay zeka yöntemleri kullanıldı. Obezite veri setini oluşturmak için 1610 birey üzerinde çevrimiçi bir anket yapıldı. Anket verilerini analiz etmek için literatürde yaygın olarak kullanılan dört yapay zeka yöntemi olan Yapay Sinir Ağı, K En Yakın Komşu, Rastgele Orman ve Destek Vektör Makinesi, kullanıldı. Bu analizin sonucunda, obezite sınıfları sırasıyla %74.96, %74.03, %74.03 ve %87.82 başarı oranlarıyla doğru bir şekilde tahmin edildi. Rastgele Orman, bu veri seti

için en başarılı yapay zeka yöntemi oldu ve obeziteyi %87.82 başarı oranıyla doğru bir şekilde sınıflandırdı.

Anahtar Kelimeler: Obezite veri seti, yapay zeka yöntemleri, yapay sinir ağı, destek vektör makinesi, k- en yakın komşu, rastgele orman

Introduction

Nutrition is a behavior that should be done consciously to protect human health and increase the quality of life to take the nutrients needed by the body in sufficient quantities and at appropriate times. Adequate and balanced nutrition is one of the basic conditions for an individual to live healthily, develop economically and socially, and increase the level of welfare [1]. While scientific, technological, and economic developments cause a decrease in health problems related to malnutrition, they also cause problems related to overnutrition and excess energy intake [2]. Obesity refers to the accumulation of an excessive amount of adipose tissue in specific areas of the body, which may pose health risks [3]. This rise presents a risk to the typical health development in individuals of all ages. Many adults complain weight gain caused by factors associated with high-calorie food, sedentary lifestyles, and modes of transportation [4]. Obesity is caused by the fact that the energy taken by the body with food is more than the energy spent. It is crucial not only to manage the intake of energy but also ensure a balance in energy expenditure to prevent obesity [5]. Obesity is a significant health issue affecting individuals of all ages worldwide [6, 7]. Defined by the World Health Organization (WHO) as a significant determinant of death and disability, obesity stands out as the fourth most common risk factor in terms of non-communicable diseases, following high blood pressure, dietary risks, and tobacco [8, 9]. The issue of obesity has transformed into a global health challenge and is progressively escalating in numerous nations, starting from childhood and adolescence [10, 11]. It is prevalent among individuals with middle and low incomes in developed countries, while in developing nations, it is more prevalent among individuals with middle to high incomes [12]. Over the years, the prevalence of obesity has multiplied several times. As of 2016, 39% of adults were overweight and 13% were obese. Moreover, over 340 million children aged between 5-18 years were either overweight or obese [13]. Today, more than two billion people worldwide are overweight or obese [14]. Many studies have stated that obesity can be prevented [15]. Studies on the spread of diseases have recognized a high body mass index as a risk element for an increasing number of long-term illnesses [16]. Obesity can occur due to hereditary reasons. It can be leptin, monogenic, syndromic, and polygenic [17]. Additional contributing factors to obesity include social, psychological, and eating habits. The risk of obesity is affected by the environmental factor in early life [18]. Obesity can be caused by a combination of environmental, biological, and cultural factors [19, 20]. The incorporation of physical activity into daily life is considered the first step towards a healthy lifestyle and is also recognized as a crucial factor in preventing obesity [21]. Around 25-50% of the energy expended by humans is due to physical activity. As body mass increases, so does the energy used because moving a heavier object requires more energy

expenditure [22]. According to a study, the number of overweight adults exceeds one billion, and body mass increases across all regions of the world when considering the entire population distribution [23]. In addition, obesity has adverse effects not only on physical health but also on psychosocial and emotional health [24]. The prejudice and negative social perspective of society against obesity can lead to psychosocial problems such as decreased self-esteem, low body image, difficulty in finding a job, and working with lower wages in individuals who have this problem [25]. Factors such as age, gender, dietary habits, sociocultural factors, and physical inactivity have a significant role in the development of obesity [26]. Research shows that children with low physical activity are more likely to be obese as observed in adults [27]. School interventions involving physical activity have been found to have a greater impact on body weight compared to interventions that do not include physical activity [28, 29]. Therefore, emphasis should be placed on physical activity during school age [30, 31]. Determining the factors affecting the prevalence of obesity is important for solving possible health problems and taking necessary precautions [32]. The primary factors responsible for the development of obesity are: a high-fat diet (HF diet), positive energy imbalances determined as genetic factors, and environmental factors [33]. Deep learning is a machine learning class. Deep learning methods have been used in many problems that are being solved with artificial intelligence and many deep learning approaches have been revealed [34]. In recent years, deep learning techniques have been used in many studies in the field of obesity. In particular, deep learning models have been developed to predict obesity and their performance has been evaluated with various metrics. For example, in the study conducted by [35], the relationships between obesity and the environment and physical activities were investigated using deep learning techniques. Similarly, in another study conducted by Alkhalaf and colleagues, a model was developed for determining and classifying the risk of obesity using deep learning methods [36]. These studies demonstrate the potential of deep learning techniques in predicting and classifying obesity.

As the prevalence of overweight and obesity continues to rise, there is an increasing need to develop new methods to predict who will benefit from dietary interventions. AI has the potential to solve problems using computer systems integrated with large data sources. In the field of nutrition, AI applications can offer benefits such as effective nutrition planning, interpretation, diet analysis, quality nutrition counseling, and providing in-depth knowledge about the effects of nutrition on health [37, 38]. Apart from the success metric, the data collection method should also be taken into account. Data mining is a field of computer science that investigates algorithms designed to learn from data, and it has been applied to various problems, including examining the efficacy of interventions [4]. With current advancements in technology, there are potentially alternative methods to provide better forecasting. Researchers and experts in this field have employed diverse data mining techniques [39, 40]. Nowadays, data mining is utilized in numerous industries, including the field of medicine, where it is used to enhance decision-making in medical affairs [41]. The surge of data in the medical field has resulted in greater levels of uncertainty, highlighting the growing significance of data mining in managing such

uncertainties [42, 43]. The vast number of datasets present in biomedicine leads to a multitude of potential patterns that cannot be easily predicted, but data mining techniques offer a valuable tool for uncovering such patterns [44]. Utilizing data mining techniques can assist medical professionals in shifting their focus from population-based to individual-based approaches [45]. Considering the studies in literature, 4 different artificial intelligence methods were used in this study to determine 4 different obesity states based on 14 features. Concerning literature, this study provides the following contributions.

- Researchers working in this field will have access to a numerical dataset obtained from 1610 individuals.
- Fourteen (14) different variables were examined to determine whether individuals had obesity or not.
- Instead of statistical prediction methods, four different artificial intelligence methods were used: Artificial Neural Network (ANN), K Nearest Neighbor (KNN) Support Vector Machine (SVM), and Random Forest (RF).
- Detailed performance analyses of ANN, SVM, KNN, and RF methods were conducted.

The rest of the article is organized in the following manner: Part two presents an overview of the dataset, methods employed, and the metrics used to assess performance. Part three presents the experimental results. Finally, in part four, the study's findings and recommendations are presented.

Methods and Techniques

This section offers a comprehensive overview of the dataset employed in the study, the artificial intelligence techniques utilized, and the performance criteria used to evaluate these models. The application was developed by applying the programming language Python and its accompanying libraries. The study's general structure and operation are illustrated in Figure 1 through a flowchart.

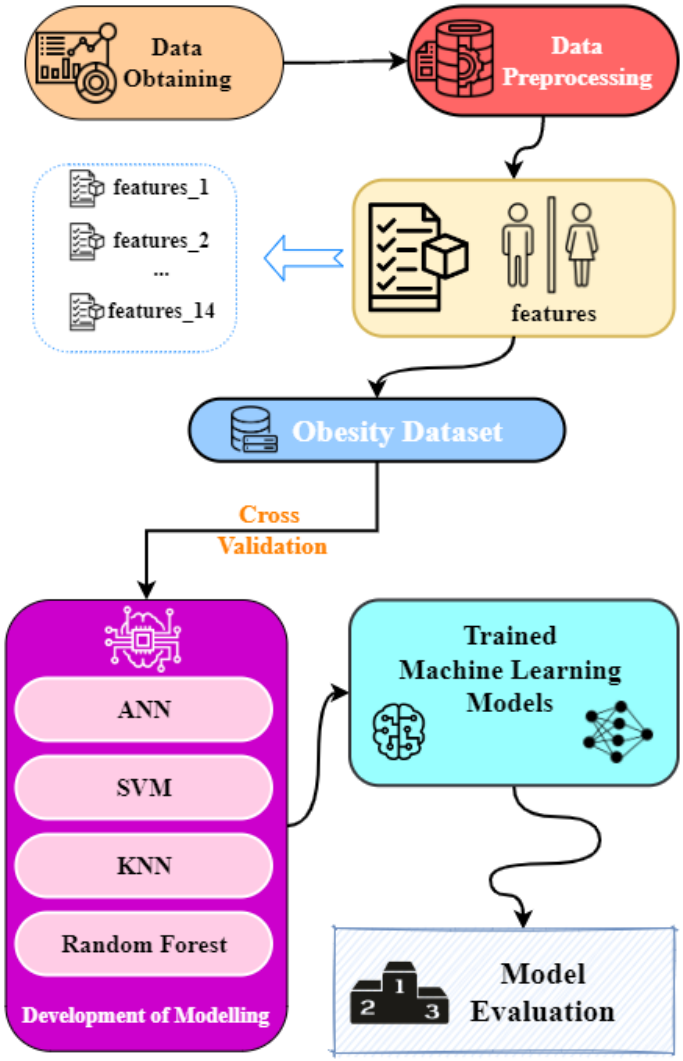

Figure 1. *Flow chart of the study*

Obesity Dataset

To create the Obesity Dataset, first of all, the variables affecting obesity were determined by examining literature. The generated dataset has 14 variables required to determine obesity. The Obesity Dataset was obtained through internet by a questionnaire applied to a total of 1610 people living in Türkiye. The data distributions of the features in the obesity dataset are given in Table 1.

Table 1. *Features and class distribution in the obesity dataset*

Attributes	**Features**	**Values**
Sex	1. Male	712
	2. Female	898
Age	Values in integers	
Height	Values in integers (cm)	
Overweight/Obese Families	1. Yes	266
	2. No	1344
Consumption of Fast Food	1. Yes	436
	2. No	1174
Frequency of Consuming Vegetables	1. Rarely	400
	2. Sometimes	708
	3. Always	502
Number of Main Meals Daily	1. 1-2	444
	2. 3	928
	3. 3+	238
Food Intake Between Meals	1. Rarely	346
	2. Sometimes	564
	3. Usually	417
	4. Always	283
Smoking	1. Yes	492
	2. No	118
Liquid Intake Daily	1. Amount smaller than one liter	456
	2. Within the range of 1 to 2 liters	523
	3. In excess of 2 liters	631
Calculation Of Calorie Intake	1. Yes	286
	2. No	1324
Physical Exercise	1. No physical activity	206
	2. In the range of 1-2 days	290
	3. In the range of 3-4 days	370
	4. In the range of 5-6 days	358
	5. 6+ days	386
Schedule Dedicated to Technology	1. Between 0 and 2 hours	382
	2. Between 3 and 5 hours	826
	3. Exceeding five hours	402
Type of Transportation Used	1. Automobile	660
	2. Motorbike	94
	3. Bike	116
	4. Public transportation	602
	5. Walking	138
Class	1. Underweight	73
	2. Normal	658
	3. Overweight	592
	4. Obesity	287

A visualized form of how data is dispersed within the Obesity dataset is described in Figure 2. As seen in Figure 2, the obesity dataset consists of a total of 1610 individuals. Among these, 898 are female and 712 are male. The youngest participant in the dataset is 18 years old, and the oldest participant is 54 years old.

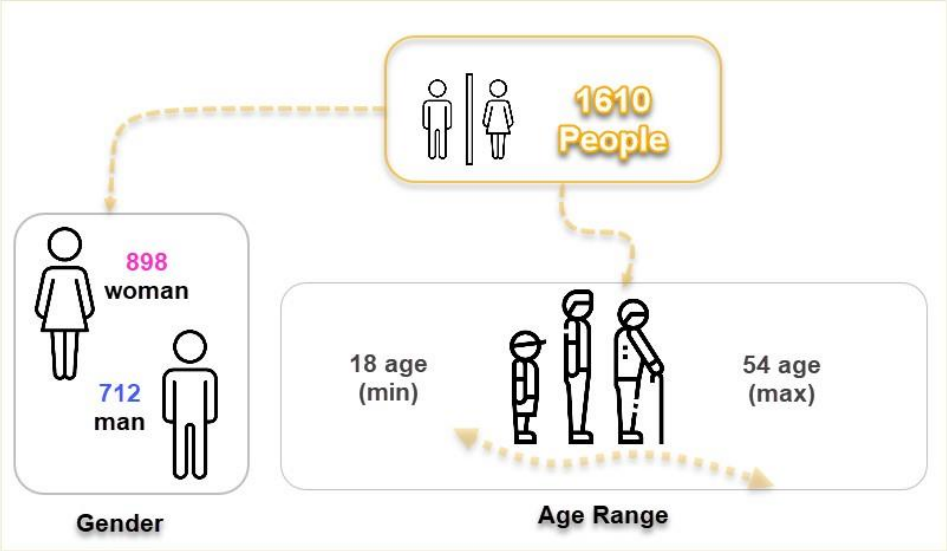

Figure 2. *Information about the study group that created the obesity dataset*

Confusion Matrix and Performance Metrics

A confusion matrix is a tabular representation implemented for evaluating the accuracy of classification in artificial intelligence methods. The table contains four distinct values, and based on these values, the performance indicators of the artificial intelligence model can be processed. Table 2 illustrates a two-class confusion matrix with its corresponding definitions.

Table 2. *Two-class confusion matrix*

Evaluation Criteria	Definition
True positive (**TP**)	The number of specimens that are predicted as well as actually classified as positive.
False positive (**FP**)	The number of specimens that are predicted as positive but actually fall under the negative category.
True negative (**TN**)	The number of specimens that are classified as negative as well as predicted as negative.
False negative (**FN**)	The number of specimens that are predicted as negative but actually belong to the positive category.

Artificial intelligence models can be evaluated using a variety of metrics to assess their performance [46, 47]. In this study, commonly used metrics such as Precision (P), Recall (R), F-measure (F), and Accuracy (AC) were utilized to evaluate the performance of artificial intelligence models. The computation of these metrics for a two-class confusion matrix is as follows; **Accuracy (AC):** refers to

the total number of correctly classified records by a classifier. It is measured as the percentage of correctly classified test sets based on the model, defining how accurate the classifier is [48].

$$\text{Accuracy (\%)} = \frac{\text{TP} + \text{TN}}{\text{TP} + \text{FP} + \text{FN} + \text{TN}} \times 100 \quad (1)$$

Precision (P): The proportion of true positive samples to all samples that are classified as positive [48, 49].

$$\text{Sensitivity (\%)} = \frac{\text{TP}}{\text{TP} + \text{FP}} \times 100 \quad (2)$$

Recall (R): As a measure of accurate identification of positive samples, it refers to the true positive rate [48, 50].

$$\text{Recall (\%)} = \frac{\text{TP}}{\text{TP} + \text{FN}} \times 100 \quad (3)$$

F1-Score (F): F-measure is calculated by combining precision and recall metrics to evaluate the model's performance [46].

$$\text{F1} - \text{Score} = \frac{2 \times \text{TP}}{2 \times \text{TP} + \text{FP} + \text{FN}} \times 100 \quad (4)$$

A four-class confusion matrix was utilized in this study due to the presence of four classes in the dataset. Table 3 depicts the definitions and values of the four-class confusion matrix.

Table 3. *Obesity data confusion matrix*

(4 x 4) Multi-Class		**Predicted Class**			
		Underweight	Normal	Overweight	Obesity
Actual Class	Underweight	**T1**	F_{12}	F_{13}	F_{14}
	Normal	F_{21}	**T2**	F_{23}	F_{24}
	Overweight	F_{31}	F_{32}	**T_3**	F_{34}
	Obesity	F_{41}	F_{42}	F_{43}	**T_4**

Table 4 illustrates the computation of TP, FP, TN, and FN values utilizing the data from a four-class confusion matrix.

Table 4. *Calculating TP, FP, TN, and FN values through a confusion matrix with four classes*

CLASS	TP	TN	FP	FN
C1	$TP_1 = T_1$	$TN_1 = T_2 + T_3 + T_4 + F_{23} + F_{24} + F_{32} + F_{34} + F_{42} + F_{43}$	$FP_1 = F_{21} + F_{31} + F_{41}$	$FN_1 = F_{12} + F_{13} + F_{14}$
C2	$TP_2 = T_2$	$TN_2 = T_1 + T_3 + T_4 + F_{13} + F_{14} + F_{31} + F_{41} + F_{34} + F_{43}$	$FP_2 = F_{12} + F_{32} + F_{42}$	$FN_2 = F_{21} + F_{23} + F_{24}$
C3	$TP_3 = T_3$	$TN_3 = T_1 + T_2 + T_4 + F_{12} + F_{14} + F_{21} + F_{24} + F_{41} + F_{42}$	$FP_3 = F_{13} + F_{23} + F_{43}$	$FN_3 = F_{31} + F_{32} + F_{34}$
C4	$TP_4 = T_4$	$TN_4 = T_1 + T_2 + T_3 + F_{12} + F_{13} + F_{21} + F_{23} + F_{31} + F_{32}$	$FP_4 = F_{14} + F_{24} + F_{34}$	$FN_4 = F_{41} + F_{42} + F_{43}$

Cross Validation

One of the popular techniques for adjusting model parameters involves sampling data to detect errors in the actual and predicted outcomes. Additionally, the cross-validation approach is utilized to enhance classification reliability. This method randomly divides the dataset into equal clusters based on a specified number, as illustrated in Figure 3. One cluster is designated as the test set while the rest are used for training, and this process is repeated for each cluster, with the test set changing at each iteration. Cross-validation is comparable to the repeated random subsampling method, except that the partitions are created such that there is no overlap between the two test sets [51]. For this research, a cross-validation value of 10 was established, which led to the partitioning of the dataset into 10 distinct portions. The training and testing procedures were executed ten times, with nine portions designated for training and one for testing in each iteration. To obtain the overall performance metrics, the results were averaged arithmetically.

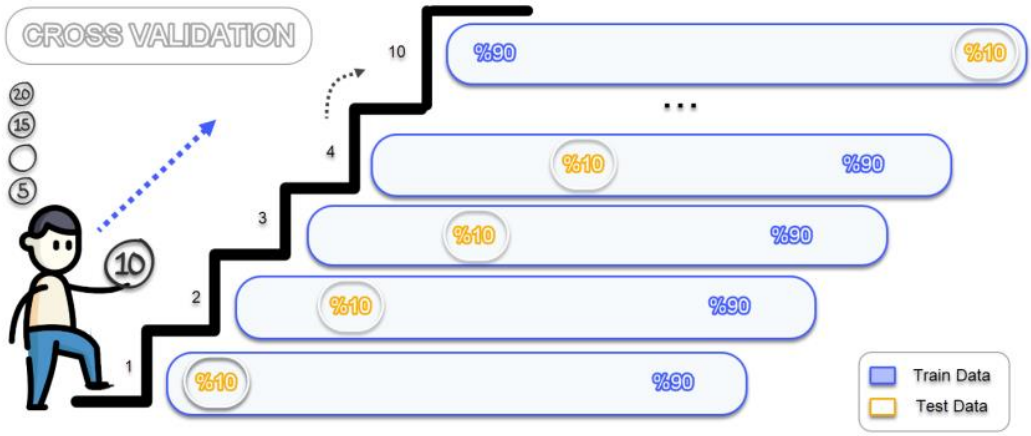

Figure 3. *Cross validation scheme used in the study*

Artificial Intelligence Models

Four distinct artificial intelligence techniques were utilized in this study, and a description of each approach is provided in the subsequent sections.

Artificial neural networks (ANN)

Artificial neural networks (AI), in which basic functions such as the ability to generate new data from data collected by the brain by learning, remembering, and generalizing by imitating the learning path of the human brain, are performed by computer software [52]. The human brain is a sophisticated system with the capacity to store and process information to solve problems. Neurons are the fundamental building blocks of this intricate structure. In recent times, one of the benefits of artificial intelligence (AI) applications is their ability to improve the accuracy and ease of using models for complex natural systems with large inputs. From the past to the present, ANN has been used in many fields and

applications [53]. Artificial Neural Networks (ANN) is a popular and effective model utilized in problem-solving and machine learning [54, 55]. ANNs are composed of simple processing units called neurons, which are extensively distributed in parallel and have the innate ability to store and retrieve relevant experimental information. An artificial neuron or processing element is the fundamental unit that constitutes the foundation of the system [56]. Artificial Neural Networks (ANNs) possess numerous characteristics that make them a highly potent and favored tool for modeling, prediction, and performance optimization of diverse systems. These features include high-speed information processing, mapping capabilities, fault tolerance, generalization, and robustness [54]. Neural networks have three primary types of layers: input, hidden, and output layers. When a neural network has multiple hidden layers, it is referred to as a multilayer neural network or deep neural network.

In Figure 4, it can be seen that each input node is linked to all nodes in the subsequent hidden layer. The neural network learns from examples through repeated connections in the subsequent steps, ultimately generating the corresponding outputs [57].

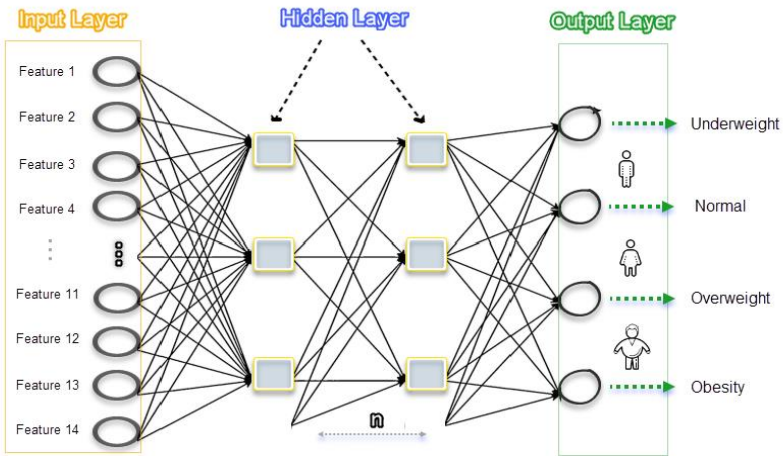

Figure 4. *The general working structure of the ANN model*

Support Vector Machine (SVM)

Support Vector Machines (SVMs) are a widely employed and highly effective machine-learning technique for data classification [56]. SVMs are supervised learning models based on statistical learning theory, which involve learning algorithms that analyze the data for classification and regression analysis. This method transforms the initial input space into a higher-dimensional feature space to enhance the classification process. With SVM, limits can be defined for both linear and nonlinear datasets. Support Vector Machines (SVM) have become widely favored due to their capability to identify optimal hyperplanes that maximize the separation between classes in the feature space [58]. The fundamental principle underlying SVM involves separating classes by drawing margins between them. As illustrated in Figure 5, these margins are calculated in a manner that maximizes the distance between the margin and the classes, thereby minimizing classification error [48, 59-61].

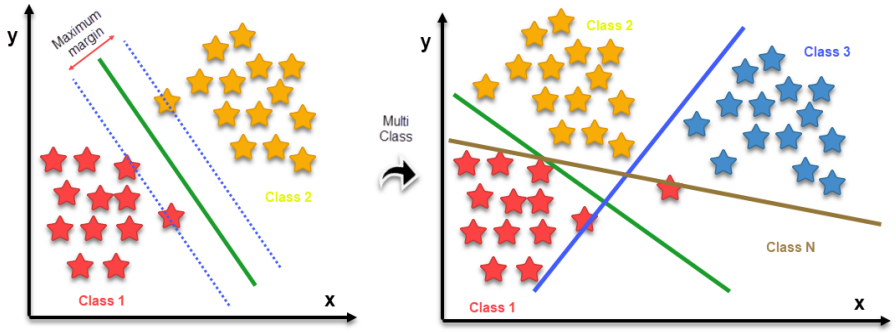

Figure 5*. The general working structure of the SVM model*

Support Vector Machines (SVM) aim to pinpoint the optimal hyperplane that minimizes classification errors while maximizing the margin, a crucial space between data points. This pursuit involves a cost parameter, which balances the desire to maximize accuracy while minimizing misclassifications [62]. Ultimately, SVM strives to delineate a decision boundary that effectively separates different classes of data, ensuring accurate classification of new, unseen data points while guarding against overfitting [63]. To achieve this, SVM employs kernel functions like linear, polynomial, or radial basis function (RBF) to transform input data into higher-dimensional spaces. Within these transformed spaces, SVM constructs a hyperplane that efficiently segregates data points into their respective classes, relying solely on a subset of training data points known as support vectors [64]. This streamlined approach enhances memory efficiency and effectiveness, especially in high-dimensional fields. One key advantage of SVM lies in its adeptness at handling high-dimensional data, rendering it suitable for applications with numerous features. Additionally, SVM boasts a solid theoretical foundation and demonstrates reduced vulnerability to overfitting compared to alternative machine learning methods. However, the performance of SVM hinges heavily on the selection of appropriate kernel functions and parameters, necessitating careful tuning to achieve optimal results [65]. SVM emerges as a versatile and robust technique widely applied across various domains such as text categorization, image recognition, and bioinformatics, owing to its ability to efficiently tackle complex classification tasks while mitigating the risk of overfitting.

K Nearest Neighbors (KNN)

K Nearest Neighbor (KNN) is a non-generalizing or sample-based learning algorithm, also referred to as a "lazy learning" algorithm, that gained popularity in statistical data analysis during the early 1970s. Unlike other algorithms, KNN does not concentrate on constructing an internal model by storing all training data samples in n-dimensional space [66-68]. KNN classifies new data points according to similarity measurements using the data. As seen in Figure 6, this algorithm calculates the classification according to the k value given as a parameter by the vote of the simple majority of its nearest neighbors and classifies accordingly. Noisy training data is also very effective, but the accuracy value varies depending on the quality of the data [68].

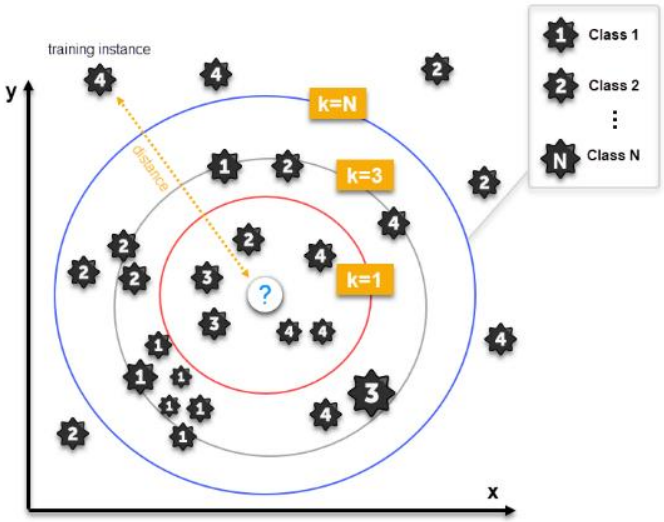

Figure 6. *The general working structure of the KNN model*

Random Forest (RF)

Random Forest is an ensemble learning approach proposed and developed by Breiman to solve classification and regression problems [69]. This algorithm creates many decision trees in general structure and combines them to get the best result [70]. The algorithm is extended by training each tree with its unique randomly generated subset of the training data, utilizing only a subset of the variables for that specific tree. Multiple classifiers are compared using ensemble return values to attain more precise results than a single classifier. To classify a sample, each tree in the forest is provided with an input vector, and a result is generated for each tree. The algorithm then branches each node using the best variable, chosen randomly at each node. The decision trees are in their largest form and are untrimmed. Data that is not utilized in training, known as out-of-bag data, can be used to provide an independent estimate of the overall accuracy of classification [56, 71, 72]. The working scheme of the Random Forest algorithm for the study is shown in Figure 7.

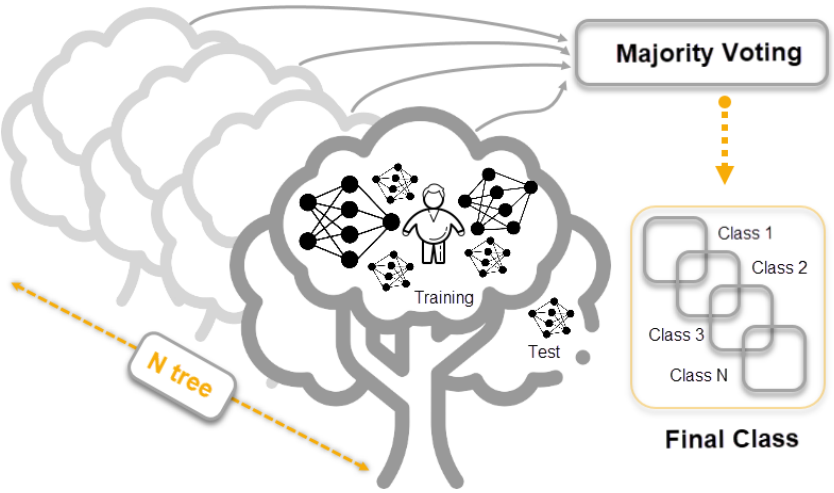

Figure 7. *Random forest general study structure*

Receiver Operating Characteristic (ROC) Curve

Evaluating the performance of artificial intelligence methods is crucial. The ROC curve is a probability curve, and the AUC-ROC curve is a commonly used metric nowadays. AUC stands for "area under the ROC curve," and it measures the extent to which the model can differentiate between classes. The ROC plot offers a means to visually represent, organize, and compare classifiers according to their performance [50, 73] (Fawcett, 2006). Spackman was one of the pioneers in using ROC charts for assessing and contrasting algorithms in machine learning [74]. The analysis of ROC curves is a common method to evaluate and compare the accuracy of classifiers over a spectrum of sensitivity and specificity values. Different parametric regression models have been suggested to model and predict ROC curves [75-77]. It is preferable to have a high AUC value in ROC curve graphs. Figure 8 provides some examples of ROC-AUC graphs. A higher AUC value indicates a better predictive ability of the machine learning model [78] (Narkhede, 2018).

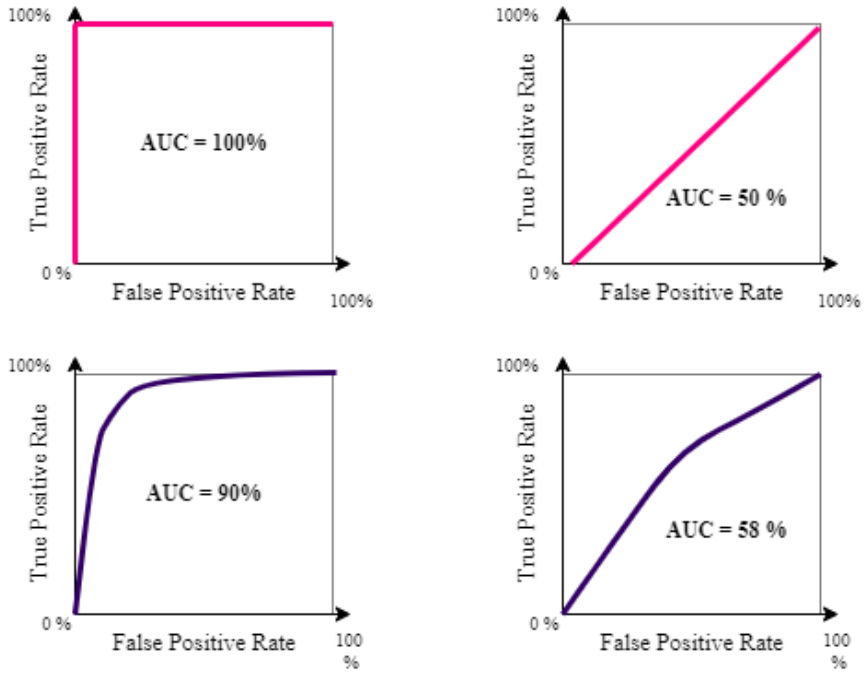

Figure 8. *ROC-AUC performance examples*

Results

This section presents experimental results obtained by training and testing artificial intelligence methods (ANN, SVM, KNN, and RF). In the subsequent section, the classification outcomes of the models employed in the investigation are outlined.

ANN Architecture-Based Classification Results

Table 5 presents the classification values obtained from the confusion matrix of the ANN model. Based on these values, the accuracy rates for the underweight, normal, overweight, and obesity categories were

calculated. The results indicate an overall classification success of 74.96%, as shown in Figure 9. However, the confusion matrix also reveals that the overweight and obesity categories were less accurately differentiated.

Table 5. *ANN confusion matrix*

ANN		**Predicted Class**			
(4 x 4)		Underweight	Normal	Overweight	Obesity
Actual Class	Underweight	**40**	28	2	3
	Normal	15	**536**	89	18
	Overweight	2	86	**445**	59
	Obesity	2	15	84	**186**

When Table 5 is examined, it is seen that 40 data in the Underweight class, 536 in the Normal class, 445 in the Overweight class, and 186 in the Obesity class are correctly classified. When TP, TN, FP, and FN data are examined, the most successful class is observed to be Underweight. It has been determined that the Normal, Overweight, and Obesity classes are highly mixed with each other. The reason is that, the training of the models is not fully realized due to the data imbalance between the classes. Classes are confused with each other since the data of the classes are very close to each other.

SVM Architecture-Based Classification Results

The classification results for the SVM model are presented in this section, with the corresponding confusion matrix given in Table 6. The accuracy rates of the underweight, normal, overweight, and obesity classes were calculated using this matrix, and it was found that the model achieved a classification success rate of 74.03%, as shown in Figure 9. However, the confusion matrix in Table 6 indicates that the SVM model had difficulty differentiating between the overweight and obesity classes.

Table 6. *SVM Confusion matrix*

SVM		**Predicted Class**			
(4 x 4)		Underweight	Normal	Overweight	Obesity
Actual Class	Underweight	**30**	37	4	2
	Normal	6	**563**	78	11
	Overweight	0	98	**426**	68
	Obesity	4	15	95	**173**

Upon analyzing Table 6, it is observed that the SVM model accurately classified 30 instances of the Underweight class, 563 instances of the Normal class, 426 instances of the Overweight class, and 173 instances of the Obesity class. A closer look at the TP, TN, FP, and FN data indicates that the Normal

class had the highest classification performance. However, due to limited data availability, the Underweight class demonstrated the lowest classification success.

KNN Architecture-Based Classification Results

Upon analyzing the classification values in Table 7, the accuracy rates of the underweight, normal, overweight, and obesity classes were computed for the KNN model. Figure 9 demonstrates a classification success of 74.03%. However, it is evident from the confusion matrix in Table 7 that the differentiation performance of the overweight and obesity classes is inadequate.

Table 7. *KNN confusion matrix*

KNN		**Predicted Class**			
(4 x 4)		Underweight	Normal	Overweight	Obesity
Actual Class	Underweight	**55**	17	1	0
	Normal	15	**551**	84	8
	Overweight	3	90	**459**	40
	Obesity	0	3	51	**233**

Upon examining Table 7, it can be observed that the number of correctly classified data is 55 in the Underweight class, 551 in the Normal class, 459 in the Overweight class, and 233 in the Obesity class for the KNN model. Analysis of the TP, TN, FP, and FN data reveals that the most successful class is Obesity. However, it is evident that the classification success of the Underweight class is the lowest due to the scarcity of data.

RF Architecture-Based Classification Results

After analyzing the classification results of the ANN model, as shown in Table 8, the accuracy rates of underweight, normal, overweight, and obesity classes were calculated. Figure 9 illustrates that the ANN model achieved the highest classification success rate of 87.82% accuracy. However, the confusion matrix in Table 8 indicates that the normal and overweight classes had low performance in terms of differentiation. Upon reviewing Table 8, it can be observed that 49 data in the Underweight class, 607 in the Normal class, 520 in the Overweight class, and 238 in the Obesity class are classified accurately. Upon analyzing the TP, TN, FP, and FN data, it can be deduced that the Normal class has the highest classification success. Due to the limited amount of data, the Underweight class has the lowest classification success.

Table 8. *RF confusion matrix*

RF		**Predicted Class**			
(4 x 4)		Underweight	Normal	Overweight	Obesity
Actual Class	Underweight	**49**	20	3	1
	Normal	2	**607**	46	3
	Overweight	0	57	**520**	15
	Obesity	0	3	46	**238**

Results of All Classification Models

The accuracy, precision, recall, and F1 Score values of each model were obtained using the confusion matrix data, and the results and graph for all models are shown in Figure 9.

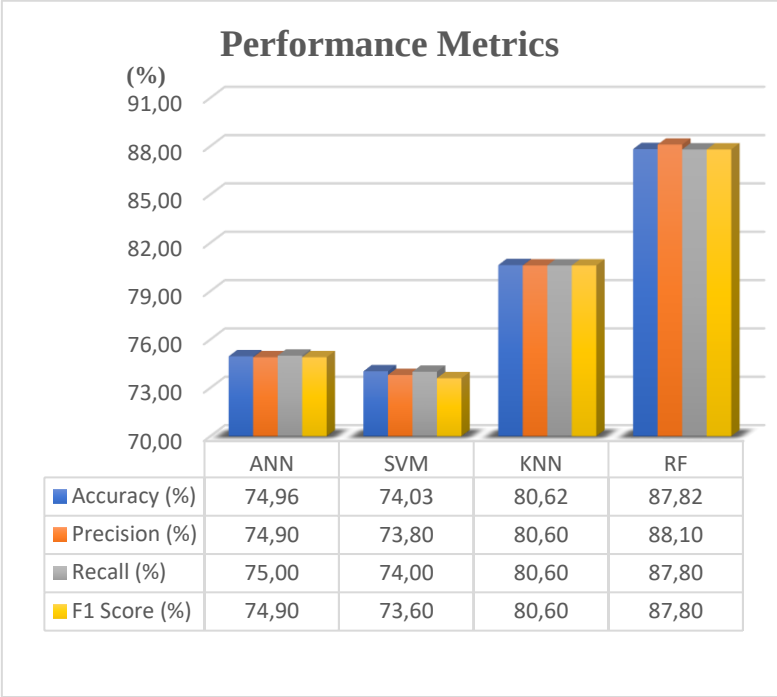

Figure 9. *Performance metrics were obtained for ANN, SVM, KNN, and RF*

Upon analyzing the outcomes presented in Figure 9, it was revealed that the RF model has the highest classification success rate (87.12%), whereas the SVM model has the lowest (74.03%). In a similar vein, the RF model exhibits the highest metric values beyond classification success, whereas the SVM model displays the lowest values. ROC curves were obtained to conduct a thorough analysis of the model's performance, and their results are shown in Figure 10 for all models.

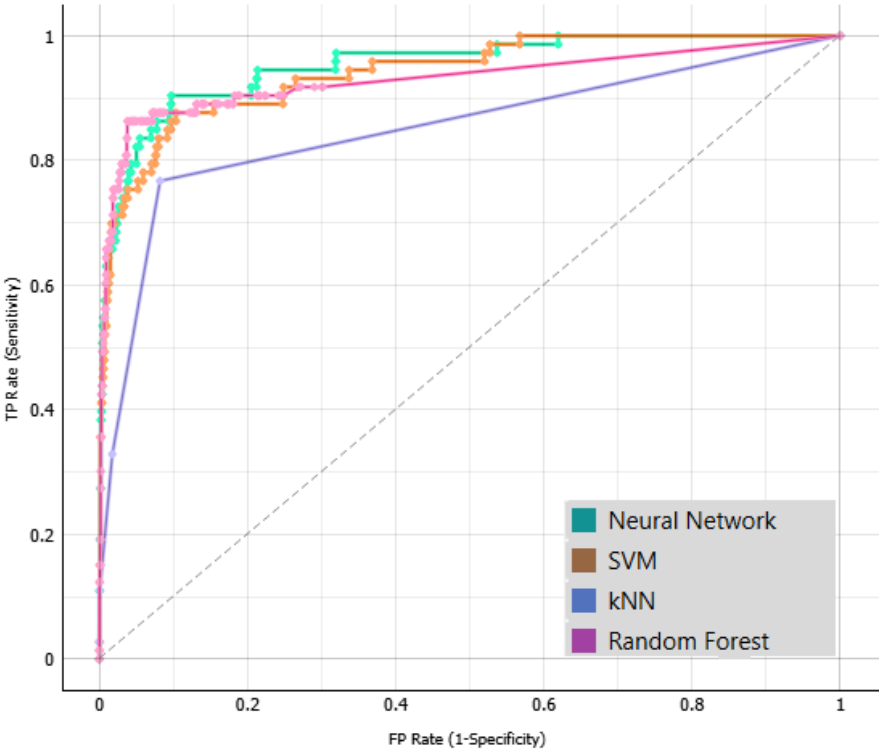

Figure 10. *ROC curves of all models*

Upon examining the ROC curves presented in Figure 10, it can be observed that the RF model achieved the most successful learning performance while the SVM model had the least successful learning performance.

Conclusions and Discussion

Obesity has recently become a rapidly increasing disease on all continents. Many diseases can occur in humans due to obesity. For this reason, it is necessary to determine the risk of obesity with regular controls and take the necessary precautions. The need for artificial intelligence methods has recently increased to accurately and quickly perform these operations. In this study, various machine learning techniques were employed to determine the obesity status of individuals using a dataset consisting of 14 features and four classes. The classification processes were conducted using ANN, SVM, KNN, and RF methods on data collected from 1610 individuals. Cross-validation was used for training and testing purposes. The RF model yielded the highest classification accuracy of 87.82%, while the SVM model had the lowest accuracy of 74.03%. The ANN model achieved a classification success of 74.96%, while the KNN model achieved a classification success of 80.62%. To achieve higher classification success, the amount of data in the dataset should be increased. In addition, equal distribution of data between classes will increase the success of classification. Classification success can be increased by using different machine learning methods. In addition, the selection of features that are effective in classification can be determined by optimization or feature selection methods, which can increase classification success and speed.

Acknowledgement -

Funding/Financial Disclosure This research received no external funding.

Ethics Committee Approval and Permissions This research was conducted with respect to participant rights and in accordance with principles of scientific integrity. Participant privacy and security were prioritized throughout the study. The ethics committee document of the research was received with decision number 2023/201 at the meeting numbered 06 of Necmettin Erbakan University Social and Human Sciences Scientific Research Ethics Committee dated 12/05/2023

Conflicts of Interest The authors declare that they have no known competing financial interests or personal relationships that could have appeared to influence the work reported in this paper.

Authors Contribution Conceptualization, Niğmet Köklü, and Süleyman Alpaslan Sulak; methodology, Niğmet Köklü, and Süleyman Alpaslan Sulak; software, Niğmet Köklü, and Süleyman Alpaslan Sulak; validation, Niğmet Köklü, and Süleyman Alpaslan Sulak; formal analysis, Niğmet Köklü; investigation, Niğmet Köklü; resources, Süleyman Alpaslan Sulak; data curation, Niğmet Köklü; writing-original draft preparation, Niğmet Köklü, and Süleyman Alpaslan Sulak; writing-review and editing, Niğmet Köklü, and Süleyman Alpaslan Sulak; visualization, Süleyman Alpaslan Sulak; supervision, Süleyman Alpaslan Sulak; All authors have read and agreed to the published version of the manuscript.

References

[1] Yetkin F. (2008). Konya il merkezinde özel hastanelere başvuran 18-60 yaş grubu kadınların obezite prevalansı and bunu etkileyen etmenler üzerine bir araştırma. Yayınlanmamış [Yüksek Lisans Tezi]. Konya. *s.* 66.

[2] Lakdawalla D & Philipson T. (2009). The growth of obesity and technological change. *Economics & Human Biology, 7*:283-293. https://doi.org/10.1016/j.ehb.2009.08.001

[3] Tan, K. C. B. (2004). Appropriate body-mass index for Asian populations and its implications for policy and intervention strategies. *The lancet*. http://dx.doi.org/10.1016/S0140-6736(03)15268-3

[4] Cervantes, R. C & Palacio, U. M. (2020). Estimation of obesity levels based on computational intelligence. *Informatics in Medicine Unlocked, 21*, 100472. https://doi.org/10.1016/j.imu.2020.100472

[5] Hill, J. O., Wyatt, H. R & Peters, J. C. (2012). Energy balance and obesity. *Circulation, 126*, 126-132. https://doi.org/10.1161/CIRCULATIONAHA.111.087213

[6] Kopelman, P. G. (2000). Obesity as a medical problem. *Nature, 404*, 635-643. https://doi.org/10.1038/35007508

[7] Deckelbaum, R. J., & Williams, C. L. (2001). Childhood obesity: the health issue. *Obesity Research. 9*, 239-243. https://doi.org/10.1038/oby.2001.125

[8] Turan, T. (2024). Optimize edilmiş denetimli öğrenme algoritmaları ile obezite analizi ve tahmini. *Mehmet Akif Ersoy Üniversitesi Fen Bilimleri Enstitüsü Dergisi*, *14*(2), 301-312. https://doi.org/10.29048/makufebed.1372323

[9] Vizmanos, B., Cascales, A. I., Rodríguez-Martín, M., Salme-rón, D., Morales, E., Aragón-Alonso, A., Garaulet, M. (2023). Lifestyle mediators of associations among siestas, obesity, and metabolic health. *Obesity, 31*(5): 1227-1239. https://doi.org/10.1002/oby.23765

[10] Ogden, C. L., Carroll, M. D., Curtin, L. R., McDowell, M. A., Tabak, C. J., & Flegal, K. M. (2006). Prevalence of overweight and obesity in the United States, 1999-2004. *Jama*, *295*(13), 1549-1555. https://doi.org/10.1001/jama.295.13.1549

[11] Ng, M., Fleming, T., Robinson, M., Thomson, B., Graetz, N., Margono, C., ... & Gakidou, E. (2014). Global, regional, and national prevalence of overweight and obesity in children and adults during 1980–2013: a systematic analysis for the Global Burden of Disease Study 2013. *The Lancet*, *384*(9945), 766-781. https://doi.org/10.1016/S0140-6736(14)60460-8

[12] Dinsa, G. D, Goryakin, Y., Fumagalli, E., & Suhrcke, M. (2012). Obesity and socioeconomic status in developing countries: a systematic review. *Obesity Reviews*, *13*, 1067-1079. https://doi.org/10.1111/j.1467-789X.2012.01017.x

[13] Stavridou, A., Kapsali, E., Panagouli, E., Thirios, A., Polychronis, K., Bacopoulou, F., Psaltopoulou, T., Tsolia, M., Sergentanis, T. N., & Tsitsika, A. (2021). Obesity in children and adolescents during COVID-19 pandemic. *Children*, *8*(2), 135. https://doi.org/10.3390/children8020135

[14] Ryan, D., Barquera, S., Barata Cavalcanti, O., & Ralston, J. (2021). The global pandemic of overweight and obesity: Addressing a twenty-First century multifactorial disease. In *Handbook of global health* (pp. 739-773). Cham: Springer International Publishing. https://doi.org/10.1007/978-3-030-45009-0_39

[15] Fock, K. M., & Khoo, J. (2013). Diet and exercise in management of obesity and overweight. *Journal of Gastroenterology and Hepatology*, *28*, 59-63. https://doi.org/10.1111/jgh.12407

[16] The GBD 2015 Obesity Collaborators. (2017). Health effects of overweight and obesity in 195 countries over 25 years. *New England Journal of Medicine*, *377*(1), 13-27. https://doi.org/10.1056/NEJMoa1614362

[17] Hainerová, I. A., & Lebl, J. (2013). Treatment options for children with monogenic forms of obesity. *Nutrition and Growth*, *106*, 105-112. https://doi.org/10.1159/000342556

[18] Reilly, J. J., Armstrong, J., Dorosty, A. R., Emmett, P. M., Ness, A., Rogers, I., Steer, C., Sherriff, A. & Avon Longitudinal Study of Parents and Children Study Team (2005). Early life risk factors for obesity in childhood: cohort study. *The BMJ*, *330*(7504), 1357. https://doi.org/10.1136/bmj.38470.670903.E0

[19] Lopez, R. P. (2007). Neighborhood risk factors for obesity. *Obesity*, *15*(8), 2111-2119. https://doi.org/10.1038/oby.2007.251

[20] Komurcu, A. & Derin, D. O. (2024). Sosyal medya kullanımının beden algısı ve yeme tutumuna etkisi. *Beslenme Bilimleri Alanında Uluslararası Araştırmalar I, 57*.

[21] Yazıcı-Gulay, M., Korkmaz, Z., Erten, Z. K., & Gürbüz, K. (2021). Çocukların fiziksel aktivite, obezite düzeylerinin incelenmesi: Kayseri ili örneği. *Genel Sağlık Bilimleri Dergisi*, *3*(3), 228-238. https://doi.org/10.51123/jgehes.2021.32

[22] Prentice, A. M., Black, A. E., Coward, W. A., & Cole, T. J. (1996). Energy expenditure in overweight and obese adults in affluent societies: an analysis of 319 doubly-labelled water measurements. *European Journal of Clinical Nutrition, 50*(2), 93-97.

[23] Finucane, M. M, Stevens, G. A., Cowan, M. J, Danaei, G., Lin, J. K., Paciorek, C. J., Singh, G. M., Gutierrez, H. R., Lu, Y., & Bahalim, A. N. (2011). National, regional, and global trends in body-mass index since 1980: systematic analysis of health examination surveys and epidemiological studies with 960 country-years and 9· 1 million participants. *The Lancet, 377*, 557-567. https://doi.org/10.1016/S0140-6736(10)62037-5

[24] Reinehr, T. (2010). Obesity and thyroid function. *Molecular and Cellular Endocrinology, 316*, 165-171. https://doi.org/10.1016/j.mce.2009.06.005

[25] Friedman, K. E, Reichmann, S. K., Costanzo, P. R & Musante, G. J. (2002). Body image partially mediates the relationship between obesity and psychological distress. *Obesity Research, 10*, 33-41. https://doi.org/10.1038/oby.2002.5

[26] Bakhshi, E., Eshraghian, M. R., Mohammad, K., Foroushani, A. R., Zeraati, H., Fotouhi, A., Siassi, F., & Seifi, B. (2008). Sociodemographic and smoking associated with obesity in adult women in Iran: results from the National Health Survey. *Journal of Public Health, 30*, 429-435. https://doi.org/10.1093/pubmed/fdn024

[27] Hills, A. P., Andersen, L. B., & Byrne, N. M. (2011). Physical activity and obesity in children. *British Journal of Sports Medicine, 45*(11), 866-870. https://doi.org/10.1136/bjsports-2011-090199

[28] Summerbell, C. D., Waters, E., Edmunds, L., Kelly, S. A., Brown, T., & Campbell, K. J. (2005). Interventions for preventing obesity in children. *Cochrane Database of Systematic Reviews*, (3). https://doi.org/10.1002/14651858.CD001871.pub2

[29] Jurić, P., Jurak, G., Morrison, S. A., Starc, G., & Sorić, M. (2023). Effectiveness of a population-scaled, school-based physical activity intervention for the prevention of childhood obesity. Obesity, 31(3), 811-822. https://doi.org/10.1002/oby.23695

[30] Strong, W. B., Malina, R. M., Blimkie, C. J., Daniels, S. R., Dishman, R. K., Gutin, B., Hergenroeder, A. C., Must, A., Nixon, P. A , Pivarnik, J M., Rowland, T., Trost, S., & Trudeau, F. (2005). Evidence based physical activity for school-age youth. *The Journal of Pediatrics, 146*(6), 732-737. https://doi.org/10.1016/j.jpeds.2005.01.055

[31] Sember, V., Jurak, G., Kovač, M., Morrison, S. A., & Starc, G. (2020). Children's physical activity, academic performance, and cognitive functioning: a systematic review and meta-analysis. *Frontiers in Public Health, 8*, 307. https://doi.org/10.3389/fpubh.2020.00307

[32] Canoy, D., & Buchan, I. (2007). Challenges in obesity epidemiology. *Obesity Reviews, 8*, 1-11. https://doi.org/10.1111/j.1467-789X.2007.00310.x

[33] Moreno, L. A., & Rodriguez, G. (2007). Dietary risk factors for development of childhood obesity. *Current Opinion in Clinical Nutrition & Metabolic Care, 10*(3), 336-341. https://doi.org/10.1097/MCO.0b013e3280a94f59

[34] Akın, E., & Şahin, M. E. (2024). Derin öğrenme ve yapay sinir ağı modelleri üzerine bir inceleme. *EMO Bilimsel Dergi, 14*(1), 27-38

[35] Maharana, A., & Nsoesie, E. O. (2018). Use of deep learning to examine the association of the built environment with prevalence of neighborhood adult obesity. *JAMA Network Open, 1*(4), 181535-181535. https://doi.org/10.1001/jamanetworkopen.2018.1535

[36] Alkhalaf, M., Yu, P., Shen, J., & Deng, C. (2022). A review of the application of machine learning in adult obesity studies. *Applied Computing and Intelligence, 2*(1), 32-48. https://doi.org/10.3934/aci.2022002

[37] Uribe, A. L. M., & Patterson, J. (2023). Are nutrition professionals ready for artificial intelligence? *Journal of Nutrition Education and Behavior*, *55*(9), 623. https://doi.org/10.1016/j.jneb.2023.07.007

[38] Atasoy, Z. B. K., Avcı, E., Beydoğan, R., Ozdemir, E., & Göktaş, P. (2024). Yapay Zeka ve Beslenme. In Göç, Ö. (Ed). *Sağlık&Bilim 2023 Yeni Nesil Teknolojiler.* Efeakademi Yayınları. https://doi.org/10.59617/efepub202367

[39] Masethe, H. D & Masethe, M. A. (2014, 22-24 October). *Prediction of heart disease using classification algorithms.* Proceedings of the world Congress on Engineering and computer Science. San Francisco, USA

[40] Tekin, N. (2023). Eğitimde yapay zekâ: türkiye kaynaklı araştırmaların eğilimleri üzerine bir içerik analizi. *Necmettin Erbakan Üniversitesi Ereğli Eğitim Fakültesi Dergisi, 5*(Özel Sayı), 387-411. https://doi.org/10.51119/ereegf.2023.49

[41] Islam, M. S., Hasan, M. M., Wang, X., Germack, H. D., & Noor-E-Alam, M. (2018). A systematic review on healthcare analytics: application and theoretical perspective of data mining. *Healthcare, 6*(2). https://doi.org/10.3390/healthcare6020054

[42] Lucas P. (2004). Bayesian analysis, pattern analysis, and data mining in health care. *Current Opinion in Critical Care, 10*, 399-403. *https://doi.org/*10.1097/01.ccx.0000141546.74590.d6

[43] Jacob, S. G & Ramani, R. G. (2012). Data mining in clinical data sets: a review. *International Journal of Applied Information Systems, 4*(6), 15-26.

[44] Milovic, B., & Milovic, M. (2012). Prediction and decision making in health care using data mining. *Kuwait Chapter of the Arabian Journal of Business and Management Review,1*(12), 126-136.

[45] Abdullah, F. S., Manan, N. S. A., Ahmad, A., Wafa, S.W., Shahril, M. R., Zulaily, N., Amin, R.M., & Ahmed, A. (2017). Data mining techniques for classification of childhood obesity among year 6 school children. In: Herawan, T., Ghazali, R., Nawi, N.M., Deris, M.M. (eds) Recent Advances on Soft Computing and Data Mining. SCDM 2016. Advances in Intelligent Systems and Computing, vol 549. Springer, Cham. DOI: https://doi.org/10.1007/978-3-319-51281-5_47

[46] Tang, T. A., Mhamdi, L., McLernon, D., Zaidi, S. A. R., & Ghogho, M. (2018). Deep recurrent neural network for intrusion detection in sdn-based networks. 2018 IEEE International Conference on Network Softwarization (NetSoft 2018)- Technical Sessions. 202-206. https://doi.org/10.1109/NETSOFT.2018.8460090

[47] Taspinar, Y. S., Cinar, I., & Koklu, M. (2021). Prediction of computer type using benchmark scores of hardware units. *Selcuk University Journal of Engineering Sciences, 20*, 11-17.

[48] Vapnik, V. N. (1999). *The Nature of Statistical Learning Theory*. Springer Science & Business media.

[49] Dwivedi, A. K. (2018). Performance evaluation of different machine learning techniques for prediction of heart disease. *Neural Computing and Applications, 29,* 685-693. https://doi.org/10.1007/s00521-016-2604-1

[50] Unal, Y., Taspinar, Y. S., Cinar, I., Kursun, R., & Koklu, M. (2022). Application of pre-trained deep convolutional neural networks for coffee beans species detection. *Food Analytical Methods, 15,* 3232-3243. https://doi.org/10.1007/s12161-022-02362-8

[51] Arlot, S., & Celisse, A. (2010). A survey of cross-validation procedures for model selection. *Statistics Surveys, 4,* 40-79. https://doi.org/10.1214/09-SS054

[52] Şeker, A., Diri, B., & Balık, H. H. (2017). Derin öğrenme yöntemleri ve uygulamaları hakkında bir inceleme. *Gazi Mühendislik Bilimleri Dergisi, 3*(3), 47-64.

[53] Keskenler, M. F., & Keskenler, E. F. (2017). Geçmişten günümüze yapay sinir ağları ve tarihçesi. *Takvim-I Vekayi, 5*(2), 8-18.

[54] Haykin, S. (2009). *Neural Networks and Learning Machines, 3/E*: Pearson Education India.

[55] Tosunoğlu, E., Yılmaz, R., Özeren, E., & Sağlam, Z. (2021). Eğitimde makine öğrenmesi: araştırmalardaki güncel eğilimler üzerine inceleme. *Ahmet Keleşoğlu Eğitim Fakültesi Dergisi, 3*(2), 178-199. https://doi.org/10.38151/akef.2021.16

[56] Ozkan, I. A., Koklu, M & Sert, I. U. (2018). Diagnosis of urinary tract infection based on artificial intelligence methods. *Computer Methods and Programs in Biomedicine, 166,* 51-59. https://doi.org/10.1016/j.cmpb.2018.10.007

[57] Kim P. (2017). *Matlab Deep Learning.* Springer.

[58] Atman Uslu, N., & Onan, A. (2023) Investigating computational ıdentity and empowerment of the students studying programming: A text mining study. *Necmettin Erbakan Üniversitesi Ereğli Eğitim Fakültesi Dergisi, 5*(1), 29-45. https://doi.org/10.51119/ereegf.2023.29

[59] Chen, W., Pourghasemi, H. R., & Naghibi, S. A. (2018). A comparative study of landslide susceptibility maps produced using support vector machine with different kernel functions and entropy data mining models in China. *Bulletin of Engineering Geology and the Environment*, *77*(2), 647-664.

[60] Mahesh, B. (2020). Machine learning algorithms-a review. *International Journal of Science and Research (IJSR). [Internet]*. 9:381-386. https://doi.org/10.21275/ART20203995

[61] Tien Bui D, Tuan, T. A., Klempe, H., Pradhan, B., & Revhaug, I. (2016). Spatial prediction models for shallow landslide hazards: a comparative assessment of the efficacy of support vector machines, artificial neural networks, kernel logistic regression, and logistic model tree. *Landslides, 13*, 361-378. https://doi.org/10.1007/s10346-015-0557-6

[62] Jakkula, V. (2006). Jakkula, V. (2006). Tutorial on support vector machine (svm). School of EECS, Washington State University, 37(2.5), 3.

[63] Patle, A., & Chouhan, D. S. (2013, 23-25 January). *SVM kernel functions for classification.* International Conference on Advances in Technology and Engineering (ICATE, 2013). Mumbai, India. https://doi.org/10.1109/ICAdTE.2013.6524743

[64] Yu, H., & Kim, S. (2012). SVM Tutorial-Classification, Regression and Ranking.In Rozenberg, G., Back, T., & Kok, J. N. (Eds), *Handbook of Natural Computing,* (pp. 479-506). Springer. https://doi.org/10.1007/s10462-018-9614-6

[65] Chauhan, V. K., Dahiya, K., & Sharma, A. (2019). Problem formulations and solvers in linear SVM: a review. *Artificial Intelligence Review*, *52*(2), 803-855. https://doi.org/10.1007/s10462-018-9614-6

[66] Aha, D. W., Kibler, D., & Albert, M. K. (1991). Instance-based learning algorithms. *Machine Learning, 6*, 37-66. https://doi.org/10.1007/BF00153759

[67] Zhang, M. L., & Zhou, Z. H., (2007). ML-KNN: A lazy learning approach to multi-label learning. *Pattern Recognition, 40*, 2038-2048. https://doi.org/10.1016/j.patcog.2006.12.019

[68] Sarker, I. H. (2021). Machine learning: Algorithms, real-world applications and research directions. *SN Computer Science*, *2*, 1-21. https://doi.org/10.1007/s42979-021-00592-x

[69] Breiman L. (2001). Random forests. *Machine Learning, 45*, 5-32. https://doi.org/10.1023/A:1010933404324

[70] Mohan, S., Thirumalai, C., & Srivastava, G. (2019). Effective heart disease prediction using hybrid machine learning techniques. *IEEE Access, 7*, 81542-81554. https://doi.org/10.1109/ACCESS.2019.2923707

[71] Archer, K. J., & Kimes, R. V. (2008). Empirical characterization of random forest variable importance measures. *Computational Statistics & Data Analysis*, 52, 2249-2260. https://doi.org/10.1016/j.csda.2007.08.015

[72] Maxwell, A. E., Warner, T. A., & Fang, F. (2018). Implementation of machine-learning classification in remote sensing: An applied review. *International Journal of Remote Sensing, 39*:2784-2817. https://doi.org/10.1080/01431161.2018.1433343

[73] Fawcett, T. (2006). An introduction to ROC analysis. *Pattern Recognition Letters*, *27*, 861-874. https://doi.org/10.1016/j.patrec.2005.10.010

[74] Spackman, K. A. (1989). Signal detection theory: Valuable tools for evaluating inductive learning. *Proceedings of the Sixth International Workshop on Machine Learning*, 160-163. https://doi.org/10.1016/B978-1-55860-036-2.50047-3

[75] Pepe, M. S. (1997). A regression modelling framework for receiver operating characteristic curves in medical diagnostic testing. *Biometrika*, *84*, 595-608. https://doi.org/10.1093/biomet/84.3.595

[76] Pepe, M. S. (2003). *The Statistical Evaluation of Medical Tests For Classification and Prediction*: Oxford University Press, USA.

[77] Luckett, D. J., Laber, E. B., El-Kamary, S.S., Fan, C., Jhaveri, R., Perou, C. M., Shebl, F. M & Kosorok, M. R. (2021). Receiver operating characteristic curves and confidence bands for support vector machines, *Biometrics*, *77*, 1422-1430. https://doi.org/10.1111/biom.13365

[78] Narkhede, S. (2018). Understanding auc-roc curve. *Towards Data Science*, *26*, 220-227.

Sinopfbd, 2024; 9(1): 240-265 **https://doi.org/10.33484/sinopfbd.1393364**

Sinop Üniversitesi Fen Bilimleri Dergisi
Sinop Uni J Nat Sci
E-ISSN: 2564-7873

https://dergipark.org.tr/tr/pub/sinopfbd

Carbon Fiber and Its Composites: Synthesis, Properties, Applications

Gamze ÖZÇAKIR

How to cite: Özçakır, G. (2024). Carbon fiber and its composites: synthesis, properties, applications. *Sinop Üniversitesi Fen Bilimleri Dergisi, 9*(1), 240-265. https://doi.org/10.33484/sinopfbd.1393364

Review

Corresponding Author
Gamze ÖZÇAKIR
gamze.ozcakir@bilecik.edu.tr

ORCID of the Author
G.Ö: 0000-0003-0357-4176

Received: 21.11.2023
Accepted: 23.05.2024

Abstract

Carbon fiber is often preferred in composite production as it is a light and strong material. Traditionally, it is produced based on Polyacrylonitrile (PAN) and Pitch. Today, biomass-based carbon fiber production has studied as an alternative to these petroleum-based initiators. Accordingly, cotton, wood, and cellulose are the most commonly used biomass types. However, environment-friendly carbon fiber does not yet possess as good tensile strength as petroleum-based ones. So, researchers added PAN during the production of bio-based carbon fiber. Carbon fiber can be produced as a composite with many materials like polymers, metals, ceramics, and cement. It has a wide range of uses. Nowadays, researchers try to improve the interface between epoxy and carbon fiber to increase the functional properties of the composite. By preparing carbon fiber-reinforced metal, it can be possible to use composite as a catalyst. Carbon fiber is used as filler in concrete production to avoid crack formation and thus, carbon fiber composites are crucial in preventing earthquake disasters. In brief, one can enable comprehensive and contemporary information about the synthesis and applications of all types of carbon fibers (PAN, Pitch, bio-based) and their composites (polymer, metal, ceramic, concrete, carbon nanotube, and graphene).

Keywords: PAN, pitch, carbon fiber, carbon fiber reinforced composite

Karbon Fiber ve Karbon Fiber Kompozitler: Sentezi, Özellikleri, Uygulama Alanları

Bilecik Seyh Edebali University, Faculty of Engineering, Department of Chemical Engineering, Bilecik, Türkiye

Öz

Karbon fiber hafif ve sağlam bir malzeme olduğundan kompozit üretiminde sıklıkla tercih edilmektedir. Geleneksel olarak Poliakrilonitril (PAN) ve Zift temelinde üretilir. Günümüzde bu petrol temelli başlatıcılara alternatif olarak biyokütle-temelli karbon fiber üretimi üzerinde çalışılmaktadır. Bu amaçla pamuk, odun ve selüloz en çok kullanılan biyokütle türleridir. Ancak çevre dostu karbon fiber henüz petrol temelli olanlar kadar iyi bir çekme mukavemetine sahip değildir. Bu nedenle, araştırmacılar biyo temelli karbon fiber üretimini PAN eşliğinde gerçekleştirmektedirler. Karbon fiber, polimerler, metaller, seramikler ve çimento gibi birçok malzemeyle kompozit olarak geliştirilebilmektedir. Geniş bir kullanım alanına sahiptir. Günümüzde araştırmacılar, kompozitin fonksiyonel özelliklerini arttırmak için epoksi ve karbon fiber arasındaki arayüzü iyileştirmeye çalışmaktadır. Karbon fiber takviyeli metal hazırlanarak kompozitin katalizör olarak kullanılması mümkün olabilir. Beton üretiminde çatlak oluşumunu önlemek amacıyla dolgu maddesi olarak karbon fiber kullanılmaktadır. Deprem felaketlerini önlemekte karbon fiber kompozitler önem taşır. Kısacası, bu çalışma ile tüm karbon fiber türleri (PAN, Zift, biyo temelli) ve kompozitlerinin

(polimer, metal, seramik, beton, karbon nanotüp ve grafen) sentezi ve uygulamaları hakkında güncel ve kapsamlı bilgi sağlanabilir.

Anahtar Kelimeler: PAN, zift, karbon fiber, karbon fiber destekli kompozitler

Introduction

Carbon fiber is defined as fiber that is at least 92% carbon by weight [1]. The most crucial feature of carbon fiber is that it is a light and strong material [2]. Because of their high strength, they are preferred in the production of composite materials [3]. Figure 1 shows the material types which can be used to make composite involving carbon fiber. The figure covered Scanning Electron Microscope (SEM) images of composite materials. As shown in Figure 1, carbon fiber is a so thin and long filament-like material. It can be used by cutting it upon request. The need for carbon fiber has been increasing since 2010. This year, 51 thousand tons of carbon fiber were produced. For 2023, this amount is expected to reach 200 thousand tons. In addition, the amount of waste carbon fiber in Europe isabout 3 thousand tons in 2020 [4].

The top 5 countries which have share in carbon fiber importation are USA, Germany, Italy, China, and United Kingdom based on 2022 data. Hence, the United States of America was the first country in ranking concerning the import of nearly 250 thousand tons of carbon fiber derivatives [5]. However, the top 5 countries for carbon fiber exportation worldwide were China, Japan, Germany, USA and France in 2022. China has a giant share of about 580 thousand tons among the other countries in the top 5 [6]. Introducing carbon fiber into the scientific literature was carried out by Thomas Edison. Edison produced carbon fiber from cotton and bamboo fibers while researching materials for use as lamp filaments. Commercialization of carbon fiber was made after the invention of the Polyacrylonitrile (PAN) process. The PAN process is an economically high carbon yield process. The PAN process is a process that still maintains its importance today. Later, a pitch-based process of carbon fiber emerged. Pitch is an inexpensive initiator which is able to be produced from petroleum, asphalt, coal tar, and polyvinyl chloride. However, the properties of pitch-based carbon fibers are not as good as PAN-based carbon fibers [3]. The wet spinning technique is generally used for PAN-based carbon fiber synthesis. However, hazardous solvents are utilized in wet spinning. Besides that, during its carbonization, toxic gaseous occurs because of nitrile groups in the PAN precursor. Because of these reasons, researchers find new precursors to obtain carbon fibers. Biomass, lignin, and cellulose are the main bio-based precursors for this approach [7]. Today, biomass-based carbon fibers have been synthesized for composites and found several applications. Huang et al. (2024) synthesized polar poplar carbon fiber and suggested that the carbon fiber can be used for the production of fire warning sensors [8]. Liu et al. (2023) improved a solvent-free method to synthesize easily down cluster-based carbon fiber aerogel. They suggested using this carbon fiber in solar steam generation [9]. Wang et al. (2022) synthesized cotton-based carbon fiber and then used it to produce a carbon fiber/metal-organic framework

composite. They used this composite as an electrode for the electro-Fenton process [10]. Carbon fiber generally is used as composites. The Matrix of the composite can be polymer, ceramic, metal, and carbon. Matrix protects the structure against high temperatures and humidity. Carbon fiber-reinforced polymer is produced for aviation and space applications. They have high strength, low weight, and fatigue behavior [11]. Today, the main research topics of carbon fiber-reinforced polymers are manufacturing heat exchangers [12] and heat pumps [13]. Besides that, recycling of waste carbon fiber reinforced polymer is a hot research topic regarding environmental concerns [14]. Carbon fiber-metal composites are used as anode material for microbial fuel cells [15], laminate production [16], hydrogen evolution [17], and benzene oxidation [18] reactions. Matrices of carbon fiber composites can be also carbon nanotubes [19] and graphene [20]. Carbon fiber is combined with ceramics to prevent crashes. Carbon fiber-reinforced ceramics have thermal stability, low density, high mechanical strength, and resistance against corrosion and oxidation. Due to these eminent properties, they can be utilized in aerospace, aviation, electronics, chemical, and medical fields [21]. To increase the tensile strength and toughness of concrete, carbon fiber reinforcement can be applied [22]. Nowadays waste carbon sources are utilized to obtain carbon fiber-reinforced concrete such as preg carbon cloth [23].

The study aimed to present the synthesis, properties, and applications of carbon fiber and its composites. Carbon fiber was investigated as PAN, Pitch, and bio-based. All composite matrices were taken into consideration which were polymer, concrete, metal, ceramic, and carbon. In literature, review articles about carbon fiber are based only on one property its mechanical characteristic [24, 25], and just one type of composite the polymer-carbon fiber [26]. This study enables us to gain comprehensive and contemporary information contributing to current review studies in literature.

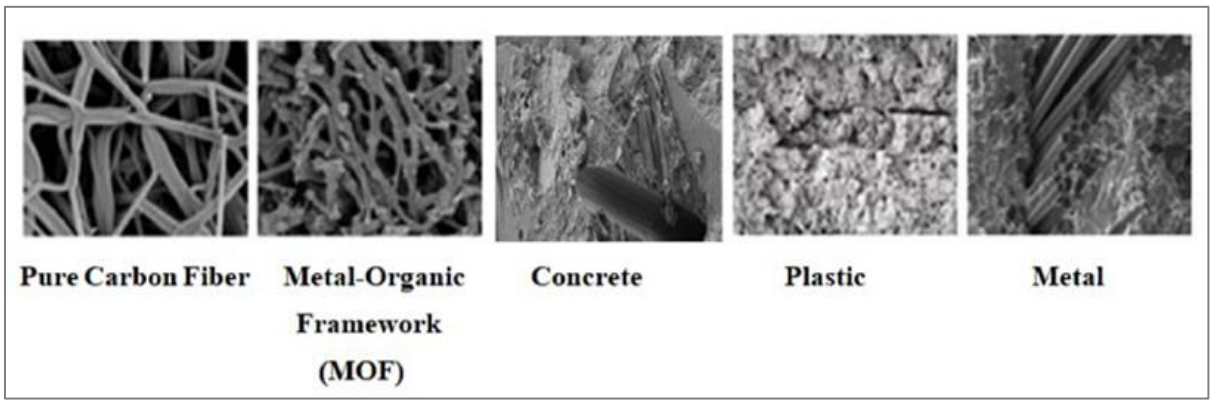

Figure 1. *Several materials for Carbon fiber composites [27-30]*

Types of Carbon Fibers

PAN based Carbon Fiber

Synthesis

PAN-based carbon fibers can quickly be synthesized. The manufacturing processes involve several steps shown in Figure 2.

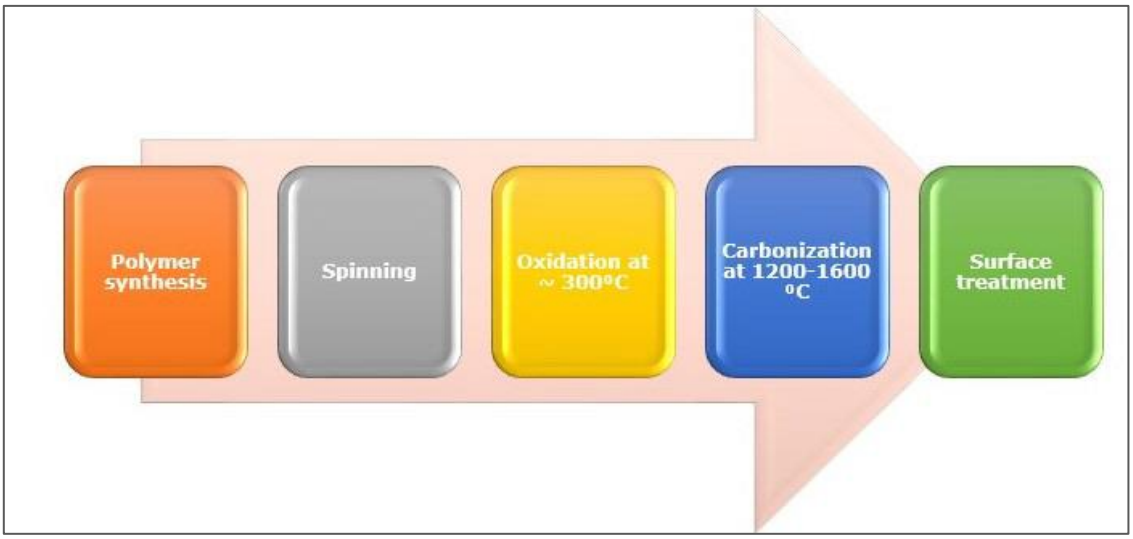

Figure 2. *PAN-based carbon fiber synthesis [31]*

The polymerization of acrylonitrile is crucial as it is highly effective in the subsequent synthesis steps of PAN-based Carbon Fiber [31]. Salts of Persulfate ($S_2O_8^{2-}$) and Iron (Fe^{3+}, Fe^{2+}) ions can be utilized as polymerization initiators [32-34]. However, since transition metals such as iron cause impurities, modifications have currently been studied [35]. Acrylonitrile (AN) can be polymerized in bulk, suspension, solution, or emulsion. Solution and suspension polymerization are the most widely used methods for the synthesis of PAN-based copolymers [31]. Solution polymerization is carried out using Dimethylacetamide (DMAc), Dimethylformamide (DMF), Dimethylsulfoxide (DMSO), or aqueous Sodium Thiocyanate solutions as solvents [36]. Since the produced copolymers have high molecular weight, diluted solutions should be used in polymerization reactions. With solution polymerization, it is possible to quickly obtain a fiber-spinning solution. However, solution polymerization has a significant disadvantage. The conversion value for obtaining PAN from acrylonitrile by this method is around 50-70%. Acrylonitrile is known to be carcinogenic. Therefore, unreacted acrylonitrile must be removed from the fiber-spinning solution. On the other hand, no by-product formed in suspension polymerization. Besides, the polymer can easily be separated by filtration and drying. The molecular weight and particle size of the polymer can be adjusted as desired and, 90% efficiency can be achieved with this method [31]. For PAN-based polymers to spin, it is necessary to work at temperatures below the melting point of the polymer. In this case, the application of molten spinning a traditional spinning method is nearly impossible. Because this method can be applied to the PAN polymer only with the addition of high amounts of solvent additives and plasticizers. So, wet spinning is preferred for spinning PAN polymer. In wet spinning, selecting a solvent in which the PAN polymer can dissolve is so crucial. For this purpose, ionic liquid, DMAc, DMF, DMSO, Zinc Chloride, and Sodium Thiocyanate solutions can be used as solvents [31]. In the wet spinning method, the polymer spinning solution is squeezed into the spin tube and it enters into the coagulation bath. The coagulation bath contains coagulants, that is, non-solvent liquids. The coagulant penetrates the extruded polymer and turns it into fiber [37]. The two

controllable variables in wet spinning are the spinning bath and the temperature and concentration of the spinning solution. At this point, generally increasing the solvent content and decreasing the bath temperature reduces diffusion. In this case, the solvent released from the polymer and the coagulant flow into the polymer decrease. The post-spinning procedure is the same for all spinning methods: washing, drawing, drying, relaxing phase, and collecting. Washing is done with water or steam. The drawing process is carried out in the environment of ethylene or glycerol in the range of 120-180 ºC. Before drying, the fibers are soaked in aqueous emulsions of esters such as polyoxyethylene derivatives. Drying and relaxation steps are crucial in removing water [31].

The oxidation is carried out at 200-300 ºC in an oxidizing atmosphere. In the oxidation stage, the density of the PAN fiber increases. Its mass composition is usually around: 70% carbon, 20% nitrogen, 10% oxygen, and a small amount of hydrogen [31]. As an alternative to oxidation in the oven, this stabilization step can be performed with plasma treatment or microwave-assisted lower energy and time [38,39]. PAN fibers stabilized in the carbonization stage are converted into carbon fibers by thermal pyrolysis in an inert atmosphere at high temperatures. The volatile components are removed. So, the carbon yield can reach around 50% by mass, depending on the PAN initiator [40]. The carbon fiber forms after carbonization and contains approximately 95% carbon and 4% nitrogen. Concerning not to damage the fiber, the heating rate is selected low. Most volatile components are removed from the structure in the range of 200-1000 ºC. The gas formed as a result of pyrolysis may contain HCN, H_2O, H_2, CO, NH_3, and CH_4 [41]. Graphite fibers form after heating above 2000 ºC [40]. Carbonization is applied to improve the adhesion of carbon fiber in the composite [42]. At surface treatment stage, fiber can be protected from high-temperature degradation. The tensile strength of carbon fiber increases [43].

Properties

The most prominent feature of PAN-based carbon fiber is its high tensile strength. Reductions in tensile strength are due to defects that occur during the synthesis process of the material. These defects occur since the PAN polymer loses about half its weight before it converts into carbon fiber. As a result of defects, various mechanical, electrical and thermal properties of carbon fiber, especially tensile strength, are affected. It is known that surface defects are more effective on tensile strength than defects that occur inside the material. Surface defects can be caused by oxidation and carbonization, as well as thermal processes used in surface treatments [2].

The thermal conductivity of PAN-based carbon fiber can be increased by using carbon nanotubes. It can be known that carbon nanotubes have high thermal conductivity. They can be grafted on PAN-based carbon fiber [44].

Application Area

Especially in the field of energy, the application areas of PAN-based Carbon Fiber are wide. It is known that successful results are obtained when integrated into carbon fibers in hydrogen storage. In addition,

researchers have obtained successful results in the use of PAN-based carbon fibers as anode material in lithium-ion batteries [45]. Besides that, PAN-based carbon fiber reinforced concrete is important for the construction industry. An environmentally friendly process can be achieved by replacing heavy and corrosive steel with carbon fiber in concrete production [46]. Table 1 displays some of the PAN-based carbon fibers in current literature.

Pitch Based Carbon Fiber

Properties

Pitch-based carbon fibers are divided into two as isotropic and anisotropic mesophase [47]. Anisotropy is a property in which the properties of the material change depending on the direction. In isotropy, the material has homogeneous properties in all directions [48]. Mesophase pitch is a liquid crystal material. It consists of various types of aromatic hydrocarbons. These hydrocarbons are stacked planarly in the structure and optical anisotropy is provided. It is known that mesophase pitch-based carbon fiber is a very light material with a tensile strength up to 4GPa, a thermal conductivity of 1000 W/mK, and a density of around 2 g/cm^3 [49]. Isotropic pitch-based carbon fibers are inexpensive but have low tensile strength (approximately 500-1000 MPa pressure) [50].

Synthesis

Carbon fiber synthesis is similarly done for both isotropic and anisotropic pitch sources. For this purpose, the synthesis procedure includes the following steps as shown in Figure 3. The raw materials of both pitch types are the same. These can be pure chemicals (aromatic compounds and polymers), petroleum, and mixtures of polyaromatic hydrocarbons, which are by-products in the production of coal. Tar initiators are pre-treated to remove impurities (coke, inorganic substances, heavy components, etc.). For this purpose, cheap and practical methods are applied in industrial production. These can be distillation, pressure use, extraction, or centrifugation [47].

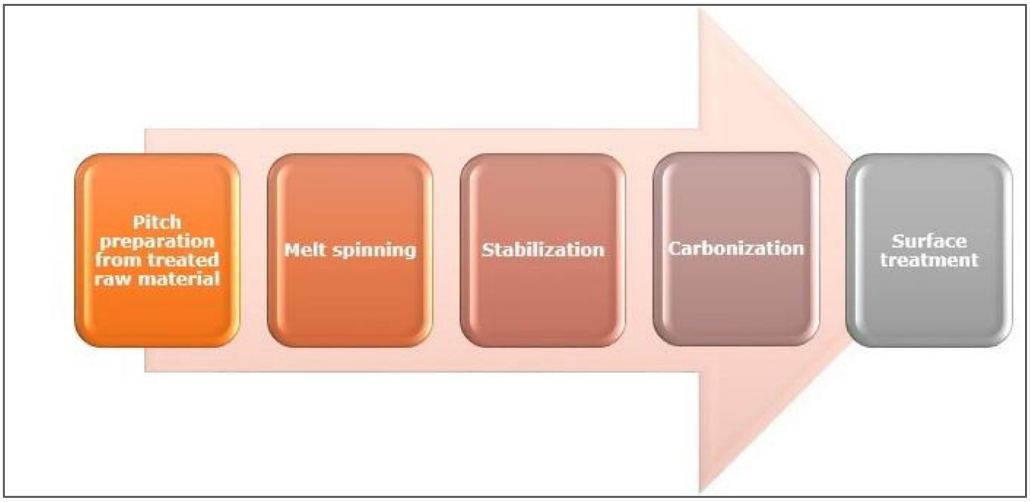

Figure 3. *Pitch-based carbon fiber synthesis [47]*

The preparation of pitch from the raw material is done under controlled conditions. Temperature, pressure, heating rate, atmosphere, and mixing speed affect pitch production [47]. The pitch is then melt-spinned and fibers are formed. For this purpose, pitch is first melted in an inert atmosphere. The melted pitch is taken from the spinning tube as fibers as a result of increased pressure [47]. The purpose of stabilization is to provide the transition of pitch fibers from thermoplastic to thermoset by oxidation. Thus, the structure and shape of the pitch fibers do not change during carbonization. The softening temperature for both pitch fibers is approximately the same (around 250 ºC). Temperature and heating rate are important in the oxidation stage. The reason is that, if the temperature is chosen lower than the softening point, there will be little change in the weight of the pitch fibers, indicating that oxidation is not taking place effectively. If the temperature is chosen too high than the softening temperature, the pitch fiber oxidizes quickly and starts to burn. On the other hand, at high heating rates, oxidation cannot be completed and the fibers stick together [47].

By carbonization, non-carbon atoms (oxygen and hydrogen) and side chains of the aromatic ring are removed. Thus, the carbon aromaticity is increased. As a result of carbonization, with increasing temperature, aromatic groups are cross-linked, condensed, and polymerized, respectively. The carbonization temperature is selected according to the characteristics of the initiating pitch. Generally, the range of 300-500 ºC is the pre-carbonization range, the main carbonization takes place in the range of 500-1400 ºC. The precise mechanical, physical, and chemical properties of carbon fiber are formed after carbonization [47].

Table 1. *PAN-based carbon fibers in current researches*

Application	Reference
Cathode material for electrochemical production H_2O_2	Xia et al. (2020) [51]
Sensor for detection of electric field in ocean	Zai et al. (2020) [52]
Separator in Li||$LiFePO_4$ battery	Deng et al. (2023) [53]
Electromagnetic wave absorption material	Li et al. (2023) [54]
Adsorbent for CO_2	Ma et al. (2022) [55]
Adsorbent for Phosphate Ions	Matsuzawa et al. (2022) [56]
Adsorbent for Acetone	Shi et al. (2022) [57]
Hydrogen Storage	Hwang et al. (2021) [58]
Catalyst for selective hydrogenation of pyrolysis Gasoline	Wu et al. (2021) [59]
Adsorbent for p-nitrophenol	Yue et al. (2021) [60]
Reinforced material for concrete	Patchen et al. (2023) [61]

Application Area

It has been proven that mesophase pitch-based carbon fiber can be used as a heat management material in composite with aluminum as a material with high thermal conductivity and low thermal expansion coefficient [62]. In another application, pitch-based carbon fiber was loaded on the carbon nanotube in the cement and increased the electrical conductivity by acting as a bridge between the nanotube particles [63]. Pitch-based carbon fiber is simultaneously used with graphite at the anode and cathode in bidirectional batteries. Thus, a lithium-ion electrolyte bidirectional battery with high local capacity and stability was produced [64]. Table 2 shows some of the PAN-based carbon fibers in current literature.

Alternative Bio-Based Carbon Fiber Resources

Lignocellulosic biomass (containing lignin and cellulose) is naturally abundant, renewable, inexpensive, and has a low environmental impact. Therefore, optimizing the carbon fiber production method from this material is important to commercialize it to replace petroleum-based carbon fiber [65].

Table 2. *Pitch-based carbon fibers in current researches*

Application	**Reference**
Cement reinforcement material to cool pavement	Wei et al. (2023) [66]
Adsorbent for iodine, methylene blue and cadmium ions	Wang et al. (2022) [67]
Adsorbent for formaldehyde	Ryu et al. (2019) [68]
Adsorbent for CO_2	Sugiyama and Hattori (2020) [69]
Adsorbent for chloroform	Yoshikawa et al. (2021) [70]
Anode material for potassium-ion batteries	Wei et al. (2021) [71]

The production of short-length carbon fiber from sustainable biomass is important because of its low environmental impact and the cheapness of its initiators compared to PAN and petroleum-based pitch. In addition, if cellulosic materials are used for this purpose, the CO_2 that plants take from the atmosphere can be stored in the form of carbon. Bamboo with high cellulosic content can be used for this purpose. The electrical conductivity of bamboo-based carbon fiber has been proven to be high [72]. There are studies using lignin-based carbon fiber in terms of environmental improvement. In one of them, the removal of methylene blue textile dye from water was studied [73]. However, the production of high-performance carbon fiber in this way is not yet possible due to the following obstacles: 1) Carbon fiber has a high ash content. 2) It does not have high strength. Mixing PAN and other polymer initiators with lignocellulosic biomass can remedy this situation. However, in this case, the process would not be environmentally friendly. Therefore, mixing lignin with other biomass may be a more effective strategy.

3) Sensitive to the spinning process [65]. Table 3 shows several materials which can be used for biomass based carbon fiber.

Table 3. *Lignin-based carbon fibers in current researches*

Biomass Type	Application	Reference
Cotton	Adsorbent for methylene blue	Chiu et al. (2012) [74]
Wood	Electrode material for supercapacitor	Jin et al. (2014) [75]
Sisal plant	Adsorbent for phosphate	Hu et al. (2018) [76]
Cotton	Electrode material for water-splitting	Hong et al. (2022) [77]
Cellulose	Adsorbent for flüoride	Zhang et al. (2019) [78]
Waste rabbit hair	Photocatalyst for methylene blue degradation	Chen et al. (2022) [79]
Cotton	Electrode for electro-Fenton degradation of Tetrabromobisphenol A	Wang et al. (2022) [10]

Carbon Fiber Composites

Properties

A composite is formed by the combination of two or more materials with different physical and chemical properties. It is possible to physically separate the materials in the composite from each other. Generally, it consists of a composite matrix and supporter. The matrix is a soft and weak material that is embedded in the support material. The support material, on the other hand, is a strong and hard material that is distributed throughout the matrix. The main purpose of composite production is to obtain a material with strong mechanical properties by combining individual components with low mechanical properties. In addition, the composite is expected to be a lightweight material [11].

The surface of carbon fiber is smooth, chemically inert, and non-polar naturally. Therefore, it is crucial to treat the carbon fiber surface to reach good interfacial adhesion between the matrix and carbon fiber and low cohesion behavior in the matrix of the composite. This can be ensured by forming chemical or physical bonds between two components of the composite such as Van der Waals attraction, hydrogen bond, and mechanical interlocking [80, 81]. For interfacial treatment of carbon fiber in the composite, three methods can be followed three methods which are wet, dry, and multi-scale. In a multi-scale approach, carbon fiber is coated with some materials. The material used at the interface of a composite is so crucial. Since the material used at the interface has a great effect on the formation and propagation of cracks and the distribution of stresses in the composite. In addition, this material affects the strength, toughness, moisture, and heat resistance of the composite. If there is poor adhesion between the fiber and the matrix, there are deficiencies in the interface material and the performance of the composite will be poor. Rare earth nanoparticles and carbon nanotubes have been the most studied interface materials

for carbon fiber composites [81]. Another choice is wet or chemical treatment. These are liquid-phase oxidation, electrochemical oxidation, and catalytic oxidation [82]. Amine groups can help to improve the surface polarity and wettability of carbon fiber. Correspondingly, amino groups connect to carboxylic groups to reach good adhesion between carbon fiber and epoxy, after oxidation treatment with acids [80]. The last route is dry or gaseous treatments such as plasma surface modification [81].
The matrices of carbon fiber composites can be very diverse. These are 1) thermoset (cyanate ester, epoxy, phenolic, polyester, polyimide, and vinyl ester) or thermoplastic (acrylonitrile butadiene styrene, polyamide, polycarbonate, polyethersulfone, polyethylene, polypropylene, and so on) polymers, 2) carbon (C-C composites), 3) metals such as nickel, 4) ceramics, 5) cement can be used [83].

Synthesis and Application Area

Discovered in 1960, this type of composite is used in automotive, civil, mechanical engineering, aerospace, shipbuilding, and wind turbine applications. Since carbon fiber is a durable and light material, it is preferred as a polymer composite material. In addition, the cost is low compared to other fibers used for filling purposes. It is preferred since it improves the thermal, mechanical, and electrical properties of the polymer [83]. Today, research on carbon fiber-polymer composites is mostly aimed at strengthening the physicochemical interaction between these two materials. This interaction is mostly made possible by Van der Walls and hydrogen bonds. The researchers aimed to improve the properties of the composite by reaching bonding energy that exceeds the cohesion forces of the polymer and carbon fiber. In addition, increasing the amount of carbon fiber in the composite can lead to brittleness in the composite [83]. Often used with thermoset matrix, especially epoxy, and carbon fiber. Furfuryl and phenolic resins form other types of thermoset matrix. Today, thermoplastic matrices (polyethersulfone (PES), polyphenyl sulfide (PPS), polyetherimide (PEI), and polyimide (PI)) have also been used. The properties of thermoplastics are that they have high ductility, withstand high temperatures, and can be produced in a shorter time [83]. The production of Carbon Fiber-Polymer composites can be in traditional ways such as extrusion, compression molding, injection molding, resin transfer molding, and vacuum transfer molding [83]. There are many types of research in the current literature about carbon fiber-polymer composites. Tam et al. (2023) investigated the effect of moisture on carbon fiber-epoxy composite interface via computational ways [84]. Chauhan et al. (2023) assessed the effect of chemical surface functionality on carbon fiber regarding its thermal conductivity effect in carbon fiber-epoxy composites [85]. Darıcık et al. (2023) used carbon nanotubes to develop the electroconductivity of carbon fiber-epoxy composites [86]. Figure 4 shows the general structure of carbon fiber-polymer composites.

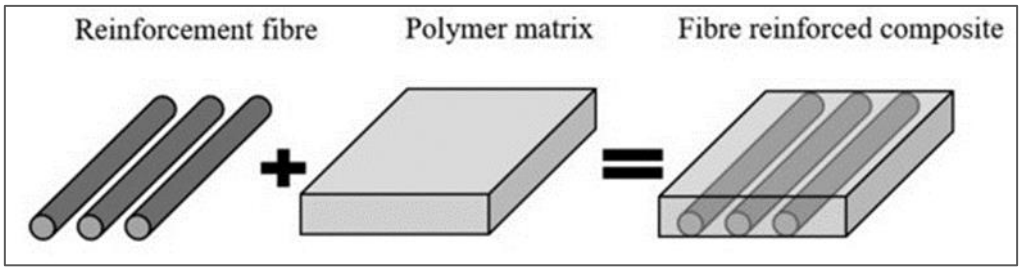

Figure 4. *General scheme for carbon fiber reinforced polymer composites [87]*

Carbon Fiber-Carbon

Various methods can be used for their synthesis. These are vacuum filtration, pressure filtration, dry synthesis, and powder molding [88]. They are used as a thermal insulator by NASA in space vehicles. It can withstand up to 2800 °C in airless conditions. It can also be used as a thermal insulator in vacuum electric furnaces. In addition to this application area, carbon fiber-carbon composites can be used for gas adsorption and separation and as cathode material in batteries. Its density is low and its porosity is high (70-90%). The disadvantages are that their mechanical properties are low and they have the potential to undergo oxidation. For this purpose, in recent years, researchers have tried coating with pyrolytic carbon, ceramics, aerogel, and nanostructures. Among these, coating with aerogels has come to the fore and is under development [88]. There are many kinds of research in literature about carbon fiber-carbon composites. Wang et al. (2023) synthesized the composite to use as a thermal insulator for electromagnetic heating furnaces. They utilized the vacuum filtration method to synthesize the composite [89]. Ding et al. (2023) developed the composite by growing carbon nanotubes on carbon fibers. They used the composite as an additive to cement. They aimed to increase the mechanical and electrical performance of the material. Besides that, this material had the property of sensing crack formation [90]. Wu et al. (2022) also investigated carbon fiber-carbon nanotube composite. They used polydopamine between interlayers of these materials. In this way, they achieved higher mechanical stability and homogenous distribution of carbon nanotubes on the surface of carbon fiber [91].

Carbon Fiber-Metal

Various metallic matrices can be composited with carbon fiber. Studies with Aluminum (Al), Titanium (Ti), Magnesium (Mg), Copper (Cu), Nickel (Ni), Tin (Sn), and Zinc (Zn) matrices are available in the literature [92-98]. To composite the carbon fiber and the metallic matrix, the surface of the carbon fiber is first treated. This process is important to strengthen the bond between the carbon fiber and the matrix. Surface treatment can be carried out by oxidative or non-oxidative means. Composite synthesis can proceed using three routes: the solid or liquid state process and the precipitation process [30]. Today, carbon fiber-metal composites can be used in the automobiles, aerospace, and petrochemical industries where metal and metal alloys are used. These materials are strong composites, have high mechanical resistance, can be easily produced, have advanced thermal and electrical properties, and have a low

friction coefficient. Researchers continue their studies to make the carbon fiber distribution in the composite more regular. In addition, mathematical modeling techniques such as fuzzy logic and neural networks can be used to examine the mechanical properties of the composite [30].

Carbon Fiber-Ceramic

Silicon carbide (SiC) composite reinforced with carbon fiber is a material developed especially for use in aerospace applications and incorporates the properties of high-temperature resistance, fracture toughness, abrasion, and thermal shock resistance. It is therefore a composite being investigated for use in rocket engines. The properties that the researchers are trying to develop for this composite are to increase the oxidation and mechanical strength of the material at ultra-high temperatures (above 3000 °C) [99]. Apart from SiC, ZrC, ZrB_2–ZrC –SiC, ZrB_2–SiC, SiC–TaC ceramics can be used as a matrix [100-103]. Currently, chemical vapor infiltration/deposition is considered as the best method for composite synthesis [99].

Carbon Fiber-Concrete

Concrete is a composite material used in building applications. Concrete contains cement, pebbly sand, water, and some additives [104]. Various types of concrete are used in large quantities throughout the world. For this reason, researchers are currently conducting research on improving the engineering properties of concrete. Developing concrete with especially high strength, toughness, and durability is the main goal of researchers. For this purpose, the prominent ones among the new types of concrete developed by researchers in literature are high-performance concrete and high-performance fiber-reinforced concrete. High-performance concrete has superior mechanical properties and durability compared to conventional concrete. In addition, high-performance concrete can be produced by mixing various mineral-containing materials to further improve its mechanical, physical, and durability properties. These materials are silica fume, ground blast furnace, and fly ash. It is possible to obtain concrete except for cement. The use of these materials in the production of high-performance concrete has several advantages. These are as follows: 1) Additional materials increase the fullness of the cement mixture due to their small size, 2) Additional materials increase the final compressive strength of the concrete, and 3) Additional materials increase the durability of the concrete. On the other hand, these additional materials have advantages as well as disadvantages. They increase the brittleness of concrete, so cracks occur over time. The formation of cracks reduces the water resistance of the cement. And as a result, the interior of the cement is exposed to moisture, bromine, and acid sulfates [105]. Different factors such as shrinkage, overloading, and adverse environmental conditions due to thermal factors may also be effective in the formation of cracks in concrete, and it is not possible to escape from the crack formation. Over time, the cracks expand in size and increase in number. Cracks can be large (over 200 microns wide) or small. Due to large cracks, water and other impurities such as sulfate, chloride ions can penetrate the concrete. In addition, microcracks, which are considered insignificant in

conventional concrete, actually disrupt the structural integrity. Microcracks have an opening between 0.1-0.3 mm. In general, researchers recommend that the maximum surface crack opening should not exceed 2 mm. Various strategies have been developed to prevent crack formation. The first of these is the manual repair of cracks. In this traditional method, cracks are filled. In this way, the penetration of corrosive substances into the concrete is prevented and the tensile strength is restored. Another strategy is to modify the concrete composition. To this end, researchers intervene during the concrete production phase to reduce the cost of repairing cracks. Fibers are additives used for this purpose. Self-healing concrete is another way of preventing crack formation [106]. Fibers can also be used for self-healing of concrete. Healing agents can be added to the concrete mix by encapsulation, vascular, or immobilization methods. In encapsulation, the capsules withstand the mechanical stress in the concrete and release their healing agents into the cracks in the concrete [107]. The crack width can be controlled by the use of fibers in concrete. In this way, the durability and tensile strength of concrete can be increased. Fibers frequently used in cement-based concrete are as follows: steel, glass, polypropylene (PP), polyvinyl alcohol (PVA), and carbon [105]. It is known that the fiber type used affects the concrete properties. Accordingly, since steel fibers have higher strength compared to PVA and PP fibers, they can reduce shrinkage in concrete and have higher resistance to cracking [108]. Glass fiber has higher chemical resistance and is lighter than steel fiber. In addition, glass fiber has a higher resistance to water and gas permeability than steel fiber [109]. Besides, it is known that steel fiber is susceptible to thermal expansion and corrosion problems [110]. The coefficient of elasticity of carbon and steel fiber reinforced concrete has proven to be higher than that of glass fiber reinforced concrete. In addition, it has been seen from previous studies that the compressive strength of carbon fiber-reinforced concrete is higher than that of glass and steel-reinforced concrete. In addition, studies have shown that the durability of carbon fiber-reinforced concrete is higher than that of steel fiber-reinforced concrete [109]. It is possible to use carbon fiber-reinforced concrete composites in columns, floors, and beams in structural applications. An example of a carbon fiber concrete composite is presented in Figure 5. Carbon fiber is not directly composited with concrete, usually, polymer additives are also used [111-113]. There are various studies on carbon fiber-reinforced concrete composites in the literature. In this review, a literature analysis was conducted in terms of the importance of the effects of these composites on the crack resistance of concrete. Liu et al. (2019) stated that the addition of polymer to carbon fiber-reinforced concrete has positive effects on the static strength of the composite. To reach this conclusion, they tested mixtures containing polymer: cement in different ratios by mass. The best results were obtained with the composite with a polymer: cement ratio of 8% by mass. In this case, they found the tensile strength for bending and splitting to be 36% and 61%, respectively. The compressive strength remains low in this case. They also observed with Scanning Electron Microscopy (SEM) images that the polymer emulsion acts as a bond between the matrix and the fiber interface. In this way, the resistance of the composite to crack formation has been increased [114]. Liu et al. (2020) investigated the effect of polymer: cement

mass ratio (0-12%) on mechanical properties at different deformation rates (45-150 s^{-1}) in carbon fiber reinforced polymer concrete. Accordingly, at the same deformation rate, with the increase of polymer content, the compressive strength first increased and then decreased. When they plotted the stress versus deformation, they found that only micro-cracks formed at low stress. The reason for this is that the elastic modulus of concrete and polymer film is approximately the same. Therefore, the polymer additive did not affect the cement behavior. However, when the peak point was exceeded, it was observed that the cracks widened. The reason for this is that the researchers showed an increase in the toughness of the composite as a result of the increase in the bond strength of the polymer and the resistance of the carbon fiber against cracking. The researchers found that 8% by mass polymer: cement ratio was optimal when considering compressive strength, toughness, and deformation [115]. Wang et al. (2021) commercially purchased PAN-based carbon fiber (tensile strength: 3530 MPa, density: 1.78 g/mL). Then they put the carbon fiber into the cement mixture in different proportions by volume. The formed sludge was molded in the presence of polycarboxylic acid and beams were produced. As a result of the impact resistance tests, the tensile and compressive strengths of the beam against time were recorded at the endurance speed of 3 m/s. Accordingly, with the increase in the carbon fiber volume in concrete, the time to reach the surface, that is, the propagation of the crack, did not change much and remained around 0.6 ms. However, with the increase in the fiber amount, the vertical displacement increased and reached 0.45 mm. This is desirable because the ductility of the beam increases with increasing vertical displacement [116]. Huang et al. (2022) wrapped the carbon fiber-reinforced polymer in fiber-reinforced concrete and examined the splitting behavior by impact test. Crack propagation in unwrapped concrete continued throughout compression. In the case of wrapping with carbon fiber composite, cracks were found during compression, but the crack width and number were less. They also investigated the effects of deformation rate and wrapping ratio on crack formation. Accordingly, at low deformation rates, the main crack was formed narrower in the carbon fiber-wrapped concrete than in the unsupported concrete, and as expected, a decrease in the main crack width was observed with the increase in the jacket ratio. As a result, they observed that the resistance to separation of concrete with carbon fiber reinforced polymer increased. However, at high deformation rates, fragmentation of the concrete was observed and the location of the main crack became undetectable. In addition, the increase in the carbon fiber ratio at high speeds greatly increased the deformation [117]. Farooq and Banthia (2022) investigated the effect of PVA, glass, steel, and carbon fiber additives on polymer cement. Besides the different fibers, the effect of the curing condition of the composite (room temperature or an oven at 80 ºC) and the resin ratio (15 or 18) were also investigated. They stated that keeping the resin ratio low is economically important. They kept the fiber amounts constant at 2% by volume in all composites. Among these fibers, the highest compression strength was obtained with the carbon fiber reinforced composite containing 18% resin (74%). They observed that the effect of composite curing at thermal or room temperature was negligible [118].

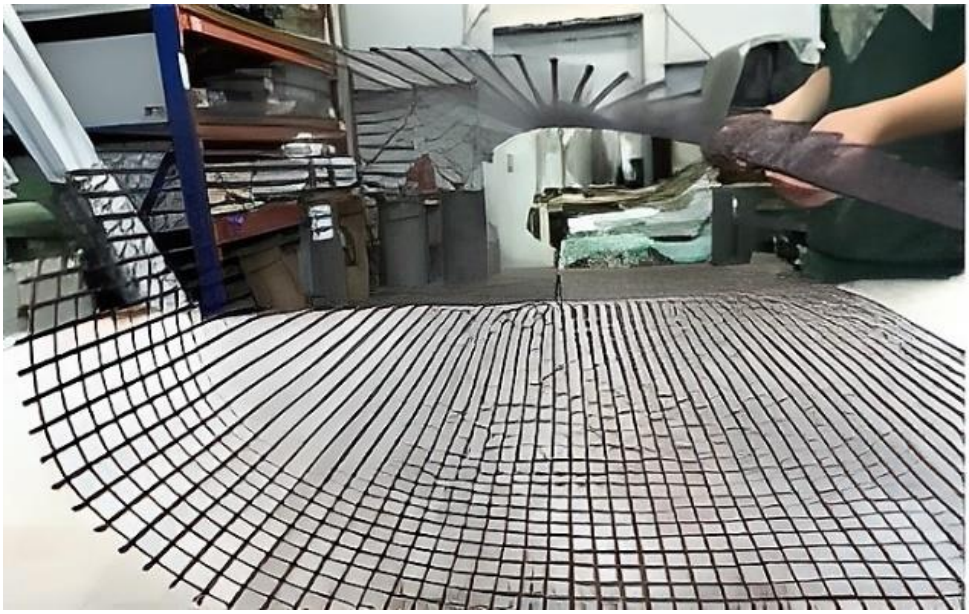

Figure 5. *Carbon fiber fabric-concrete composite [119]*

It is known that there is no escape from the formation of cracks in reinforced concrete structures. Thermal factors and overloading are among the factors that cause crack formation in concrete structures. Tensile strength of concrete, steel, glass, polymer and carbon fibers are the materials preferred during the production phase of concrete or for later reinforcement. Among these, carbon fiber reinforced concrete stands out due to its high compressive strength and elasticity coefficient. In addition, compared to the widely used steel fiber, its corrosion resistance, light weight and ability to be produced from biomass-based sources make carbon fiber a good alternative. When the literature is examined, it has been seen that polymer-added carbon fiber-concrete composites come to the forefront in terms of reducing the crack width and number of concrete as a result of strength tests. As seen in literature, researchers are trying to reduce the amount of polymer additives used in carbon fiber-concrete composites and to synthesize carbon fiber from lignin-derived biomass, which is a more environmentally friendly procedure. In addition, studies are continuing to improve the mechanical properties of the composite at high deformation rates.

Conclusions

This study aims to display the features, synthesis, and applications of carbon fibers and their composites. Besides general information, one can reach current literature about carbon fibers. The most important property of carbon fiber is that it is a light and strong material. Because of their high strength, they are utilized in the production of composite materials. Carbon fiber can be the matrix for polymer, concrete, metal, and ceramic composites. Among them, carbon fiber-reinforced polymer is the hottest study topic of today. Nowadays, researchers try to develop properties of these composites to improve the interface between the materials. This improvement aims to increase carbon fiber surface energy. Increasing surface energy means good adhesion of carbon fiber to the matrix. It can be expected that carbon fiber

has higher surface energy than matrix [120]. Carbon fiber can be based on biomass (lignin, cellulose), PAN, and Pitch. In general, carbon fiber synthesis covers five steps: precursor preparation, spinning, oxidation, carbonization, and surface treatment. Researchers heavily have studied PAN-based carbon fiber. However, the PAN-based synthesis procedure has a risk because of the emission of toxic gaseous. So, waste carbon sources such as used clothes have been alternative fiber materials. PAN, Pitch, and lignin-based carbon fibers have been mostly synthesized for use in electrochemical applications, adsorption, and concrete production. Among the other fibers which are glass and steel, carbon fibers are especially important materials for construction applications to prevent concrete deformation. However, it can not be used directly without any addition of polymer in the production of concrete.

Acknowledgement *-*

Funding/Financial Disclosure The study was not supported by any institution or organization.

Ethics Committee Approval and Permissions The study does not require ethics committee approval or any special permission.

Conflicts of Interest There is no conflict of interest.

Authors Contribution The author read and approved the final manuscript.

References

[1] Huang, X. (2009). Fabrication and properties of carbon fibers. *Materials*, *2*, 2369–403. https://doi.org/10.3390/ma2042369

[2] Jang, D., Lee, M. E., Choi, J., Cho, S. Y., & Lee, S. (2022). Strategies for the production of PAN-Based carbon fibers with high tensile strength. *Carbon*, *186*, 644–77. https://doi.org/10.1016/j.carbon.2021.10.061

[3] Chand, S. (2000). Review Carbon fibers for composites. *Journal of Materials Science*, *35*, 1303-13. https://doi.org/10.1023/A:1004780301489

[4] de Souza Abreu, F., Ribeiro, C.C., da Silva Pinto, J.D., Nsumbu, T.M., & Buono, V.T.L. (2020). Influence of adding discontinuous and dispersed carbon fiber waste on concrete performance. *Journal of Cleaner Production*, *273*, 122920.https://doi.org/10.1016/j.jclepro.2020.122920

[5] Trademap page forworldwide imported carbon fiber derivatives amount in 2022. (2023, November 21).https://www.trademap.org/Country_SelProduct.aspx?nvpm=1%7c%7c%7c%7c%7c6815%7c%7c%7c4%7c1%7c1%7c1%7c1%7c%7c2%7c1%7c1%7c1

[6] Trademap page for worldwide exported carbon fiber derivatives amount in 2022. (2023, November 21).https://www.trademap.org/Country_SelProduct.aspx?nvpm=1%7c%7c%7c%7c%7c6815%7c%7c%7c4%7c1%7c1%7c2%7c1%7c%7c2%7c1%7c1%7c1

[7] Ogale, A. A., Zhang, M., & Jin, J. (2016). Recent advances in carbon fibers derived from biobased precursors. *Journal of Applied Polymer Science*, *133*(45). https://doi.org/10.1002/app.43794

[8] Huang, C., Su, Y., Gong, H., Jiang, Y., Chen, B., Xie, Z., Zhou, J., & Li, Y. (2024). Biomass-derived multifunctional nanoscale carbon fibers toward fire warning sensors, supercapacitors and moist-

electric generators. *International Journal of Biological Macromolecules, 256,* 127878. https://doi.org/10.1016/j.ijbiomac.2023.127878

[9] Liu, X., Hou, G., Zhao, J., Zhao, W., Xu, Q., Zheng, X., Liu, Z., & Lai, Y. (2023). Self-interlocked down Biomass-based carbon fiber aerogel for highly efficient and stable solar steam generation. *Chemical Engineering Journal*, *465*, 142826. https://doi.org/10.1016/j.cej.2023.142826

[10] Wang, Y., Li, S., Hou, C., Jing, L., Ren, R., Ma, L., Wang, X., & Wang, J. (2022). Biomass-based carbon fiber/MOFs composite electrode for electro-Fenton degradation of TBBPA. *Separation and Purification Technology*, *282*, 12005. https://doi.org/10.1016/j.seppur.2021.120059

[11] Karataş, M. A., & Gökkaya, H. (2018). A review on machinability of carbon fiber reinforced polymer (CFRP) and glass fiber reinforced polymer (GFRP) composite materials. *Defence Technology*, *14*(4), 318-326. https://doi.org/10.1016/j.dt.2018.02.001

[12] Zheng, X., Kim, B. R., Hong, S. J., Lee, J. G., & Park, C. W. (2024). Heat transfer analysis of carbon fiber-reinforced corrugated polymer plate heat exchangers. *Applied Thermal Engineering*, *244*, 122684. https://doi.org/10.1016/j.applthermaleng.2024.122684

[13] Abbas, S., & Park, C. W. (2024). Machine learning based frost thickness prediction of carbon fiber-reinforced polymer composite fin for potential heat pump application. *International Communications in Heat and Mass Transfer*, *153*, 107333. https://doi.org/10.1016/j.icheatmasstransfer.2024.107333

[14] Heidarian, P., Mokhtari, F., Naebe, M., Henderson, L. C., & Varley, R. J. (2024). Reclamation and reformatting of waste carbon fibers: A paradigm shift towards sustainable waste management. *Resources, Conservation and Recycling*, *203*, 107465. https://doi.org/10.1016/j.resconrec.2024.107465

[15] Sayed, E. T., Olabi, A. G., Mouselly, M., Alawadhi, H., & Abdelkareem, M. A. (2024). Zinc-based metal organic framework on carbon fiber brush as a novel anode of yeast-based microbial fuel cell. *International Journal of Hydrogen Energy*, *52*, 856-864. https://doi.org/10.1016/j.ijhydene.2023.06.016

[16] Guo, Z. X., Shi, H. L., Ma, S. G., Cui, J. J., Chai, G. B., & Li, Y. C. (2024). An analysis of tensile and compressive properties of carbon fiber high-entropy alloy composite laminates. *Mechanics of Composite Materials*, *59*(6), 1147-1156. https://doi.org/10.1007/s11029-023-10162-2

[17] Saravanan, L., Anand, P., Fu, Y. P., Ma, Y. R., & Yeh, W. C. (2024). Enhancing the hydrogen evolution performance of tungsten diphosphide on carbon fiber through ruthenium modification. *ACS Applied Materials & Interfaces*, *16*(10), 12407-12416. https://doi.org/10.1021/acsami.3c17114

[18] Tavasolikejani, S., Hosseini, S. M., Ghiaci, M., Vangijzegem, T., & Laurent, S. (2024). Copper nanoparticles embedded into nitrogen-doped carbon fiber felt as recyclable catalyst for benzene oxidation under mild conditions. *Molecular Catalysis*, *553*, 113736. https://doi.org/10.1016/j.mcat.2023.113736

[19] Li, M., Xing, F., Li, T., Wang, S., Gu, Y., Zhang, W., Wang, Y., & Li, Q. (2023). Multiscale interfacial enhancement of surface grown carbon nanotubes carbon fiber composites. *Polymer Composites*, *44*(5), 2766-2777. https://doi.org/10.1002/pc.27278

[20] Li, N., Cheng, S., Wang, B., Zong, L., Bao, Q., Wu, G., Hu, F., Wang, J., Liu, C., & Jian, X. (2023). Chemical grafting of graphene onto carbon fiber to produce composites with improved interfacial

properties via sizing process: a step closer to industrial production. *Composites Science and Technology*, *231*, 109822. https://doi.org/10.1016/j.compscitech.2022.109822

[21] Zhu, T., & Wang, Z. (2023). Research and application prospect of short carbon fiber reinforced ceramic composites. *Journal of the European Ceramic Society*, *43*(15), 6699-6717. https://doi.org/10.1016/j.jeurceramsoc.2023.07.007

[22] Zhao, F., Shi, Z., Li, Q., Yu, S., & Liu, M. (2024). A comprehensive performance evaluation and optimization of steel/carbon fiber-reinforced eco-efficient concrete (FREC) utilizing multi-mechanical indicators. *Journal of Cleaner Production*, *441*, 140993. https://doi.org/10.1016/j.jclepro.2024.140993

[23] Zhou, Z., Zhao, B., Lone, U. A., & Fan, Y. (2024). Experimental study on mechanical properties of shredded prepreg carbon cloth waste fiber reinforced concrete. *Journal of Cleaner Production*, *436*, 140456. https://doi.org/10.1016/j.jclepro.2023.140456

[24] Tanaka, F., Ishikawa, T., & Tane, M. (2024). A comprehensive review of the elastic constants of carbon fibers: implications for design and manufacturing of high-performance composite materials. *Advanced Composite Materials*, *33*(2), 269-289. https://doi.org/10.1080/09243046.2023.2245210

[25] Song, X., Yu, M., Niu, H., Li, Y., Chen, C., Zhou, C., Liu, L., & Wu, G. (2024). Poly (methyl dihydroxybenzoate) modified waterborne polyurethane sizing coatings with chemical and hydrogen-bonded complex cross-linking structures for improving the surface wettability and mechanical properties of carbon fiber. *Progress in Organic Coatings*, *187*, 108112. https://doi.org/10.1016/j.porgcoat.2023.108112

[26] Ismail, K. B. M., Kumar, M. A., Mahalingam, S., Raj, B., & Kim, J. (2024). Carbon fiber-reinforced polymers for energy storage applications. *Journal of Energy Storage*, *84*, 110931. https://doi.org/10.1016/j.est.2024.110931

[27] Chen, J., Zheng, J., Wang, F., Huang, Q., Ji, G. (2021). Carbon fibers embedded with FeIII-MOF-5-derived composites for enhanced microwave absorption. *Carbon*, *74*, 509-517. https://doi.org/10.1016/j.carbon.2020.12.077

[28] Šahmenko, G., Krasnikovs, A., Lukašenoks, A., & Eiduks, M. (2015). Ultra high performance concrete reinforced with short steel and carbon fibers. *Envıronment Technologıes Resources*, *1*, 193-199. https://doi.org/10.17770/etr2015vol1.196

[29] Adeniran, O., Cong, W., & Aremu, A. (2022). Material design factors in the additive manufacturing of Carbon Fiber Reinforced Plastic Composites: A state-of-the-art review. *Advances in Industrial and Manufacturing Engineering*, *5*, 100100.https://doi.org/10.1016/j.aime.2022.100100

[30] Shirvanimoghaddam, K., Hamim, S.U., Akbari, M.K., Fakhrhoseini, S.M., Khayyam, H., Pakseresht, A.H., & Naebe, M. (2017). Carbon fiber reinforced metal matrix composites: Fabrication processes and properties. *Composites Part A: Applied Science and Manufacturing*, *92*, 70-96. https://doi.org/10.1016/j.compositesa.2016.10.032

[31] Frank, E., Ingildeev, D., & Buchmeiser, M. R. (2017). *High-performance PAN-based carbon fibers and their performance requirements*. In Gajanan Bhat (Ed), Structure and Properties of High-Performance Fibers, (pp. 7–30). https://doi.org/10.1016/B978-0-08-100550-7.00002-4

[32] Park, S. W., Yang, S. S., & Park, S. H. (1999). The kinetics of radical copolymerization of acrylonitrile and methylacrylate with tricaprylylmethylammonium chloride as a phase-transfer

catalyst. *Journal of Polymer Science Part A: Polymer Chemistry*, *37*(17), 3504-3512. https://doi.org/10.1002/(SICI)1099-0518(19990901)37:17<3504::AID-POLA8>3.0.CO;2-L

[33] Parts, A. G. (1959). Polymerization kinetics of acrylonitrile. *Journal of Polymer Science*, *37*(131), 131-145. https://doi.org/10.1002/pol.1959.1203713109

[34] Fordham, J. W. L., & Williams, H. L. (1951). The persulfate-iron (II) initiator system for free radical polymerizations1. *Journal of the American Chemical Society*, *73*(10), 4855-4859. https://doi.org/10.1021/ja01154a114

[35] Yan, J., Pan, X., Schmitt, M., Wang, Z., Bockstaller, M. R., & Matyjaszewski, K. (2016). Enhancing initiation efficiency in metal-free surface-initiated atom transfer radical polymerization (SI-ATRP). *ACS Macro Letters*, *5*(6), 661-665.https://doi.org/10.1021/acsmacrolett.6b00295

[36] Hao, J., An, F., Lu, C., & Liu, Y. (2019). Solvent effects on radical copolymerization of acrylonitrile and methyl acrylate: solvent polarity and solvent-monomer interaction. *Journal of Macromolecular Science, Part A*, *56*(11), 1012-1021. https://doi.org/10.1080/10601325.2019.1642767

[37] Gao, T., Yan, G., Yang, X., Yan, Q., Tian, Y., & Song, J. (2022). Wet spinning of fiber-shaped flexible Zn-ion batteries toward wearable energy storage. *Journal of Energy Chemistry*, *71*, 192–200. https://doi.org/10.1016/j.jechem.2022.02.040

[38] Hamideh Mortazavi, S., Pilehvar, S., Ghoranneviss, M., Hosseinnejad, M. T., Zargham, S., Mirarefi, A. A., & Mirarefi, A. Y. (2013). Plasma oxidation and stabilization of electrospun polyacrylonitrile nanofiber for carbon nanofiber formation. *Applied Physics A*, *113*, 703-712. https://doi.org/10.1007/s00339-013-7707-2

[39] Zhang, C., Liu, J., Guo, S., Xiao, S., Shen, Z., & Xu, L. (2018). Comparison of microwave and conventional heating methods for oxidative stabilization of polyacrylonitrile fibers at different holding time and heating rate. *Ceramics International*, *44*(12), 14377-14385. https://doi.org/10.1016/j.ceramint.2018.05.047

[40] Shokrani Havigh, R., & Mahmoudi Chenari, H. (2022). A comprehensive study on the effect of carbonization temperature on the physical and chemical properties of carbon fibers. *Scientific Reports*, *12*(1), 10704. https://doi.org/10.1038/s41598-022-15085-x

[41] Ma, Q. S., Gao, A. J., Tong, Y. J., & Zhang, Z. G. (2016). The densification mechanism of polyacrylonitrile carbon fibers during carbonization. *New carbon materials*, *31*(5), 550-554. https://doi.org/10.1016/S1872-5805(16)60031-8

[42] Lee, J. C., Lee, B. H., Kim, B. G., Park, M. J., Lee, D. Y., Kuk, I. H., Chung, H., Kang, H. S., Lee, H. S., & Ahn, D. H. (1997). The effect of carbonization temperature of PAN fiber on the properties of activated carbon fiber composites. *Carbon*, *35*(10-11), 1479-1484. https://doi.org/10.1016/S0008-6223(97)00098-5

[43] Athulya Wickramasingha, Y., Dharmasiri, B., Randall, J.D., Yin, Y., Andersson, G.G., & Nepal, D. (2022). Surface modification of carbon fiber as a protective strategy against thermal degradation. *Composites Part A Applied Science and Manuf*acturing, *153*, 106740. https://doi.org/10.1016/j.compositesa.2021.106740

[44] Naito, K., Yang, J.M., Xu, Y., & Kagawa, Y. (2010). Enhancing the thermal conductivity of polyacrylonitrile- and pitch-based carbon fibers by grafting carbon nanotubes on them. *Carbon*, *48*(6), 1849–57. https://doi.org/10.1016/j.carbon.2010.01.031

[45] Yusof, N., & Ismail, A.F. (2012). Post spinning and pyrolysis processes of polyacrylonitrile (PAN)-based carbon fiber and activated carbon fiber: A review. *Journal of Analytical and Applied Pyrolysis*, *93*, 1–13.https://doi.org/10.1016/j.jaap.2011.10.001

[46] Böhm, R., Thieme, M., Wohlfahrt, D., Wolz, D.S., Richter, B., & Jäger, H. (2018). Reinforcement systems for carbon concrete composites based on low-cost carbon fibers. *Fibers*, *6*(3), 56. https://doi.org/10.3390/fib6030056

[47] Liu, J., Chen, X., Liang, D., & Xie, Q. (2020). Development of pitch-based carbon fibers: a review. *Energy Sources, Part A: Recovery, Utilization, and Environmental Effects*, *12*(12), 3059. https://doi.org/10.1080/15567036.2020.1806952

[48] Iowa State University Center for Nondestructive Evaluation. (2024, April 5). Anisotropy and isotropy. https://www.nde-ed.org/Physics/Materials/Structure/anisotropy.xhtml#:~:text=When%20the%20properties%20of%20a,is%20said%20to%20be%20isotropic

[49] Ko, S., Choi, J. E., Lee, C. W., & Jeon, Y. P. (2020). Preparation of petroleum-based mesophase pitch toward cost-competitive high-performance carbon fibers. *Carbon Letters*, *30*(1), 35–44. https://doi.org/10.1007/s42823-019-00067-3

[50] Kim, B. J., Kotegawa, T., Eom, Y., An, J., Hong, I. P., Kato, O., & Yoon, S. H. (2016). Enhancing the tensile strength of isotropic pitch-based carbon fibers by improving the stabilization and carbonization properties of precursor pitch. *Carbon*, *99*, 649-657. https://doi.org/10.1016/j.carbon.2015.12.082

[51] Xia, G., Wang, H., Zhan, J., Yin, X., Wu, X., Yu, G., & Wu, M. (2020). Evaluation of the stability of polyacrylonitrile-based carbon fiber electrode for hydrogen peroxide production and phenol mineralization during electro-peroxone process. *Chemical Engineering Journal*, *396*, 125291. https://doi.org/10.1016/j.cej.2020.125291

[52] Zai, X., Liu, A., Tian, Y., Chai, F., & Fu, Y. (2020). Oxidation modification of polyacrylonitrile-based carbon fiber and ıts electro-chemical performance as marine electrode for electric field test. *Journal of Ocean University of China*, *19*, 361-368. https://doi.org/10.1007/s11802-020-4178-x

[53] Deng, N., Peng, Z., Tian, X., Li, Y., Yan, J., Liu, Y., & Kang, W. (2023). Yttrium trifluoride doped polyacrylonitrile based carbon nanofibers as separator coating layer for high performance lithium-metal batteries. *Journal of Colloid and Interface Science*, *634*, 949-962. https://doi.org/10.1016/j.jcis.2022.12.081

[54] Li, C., Qian, X., Hao, M., Wang, X., Zhu, S., Guo, M., & Zhang, Y. (2023). Outstanding electromagnetic wave absorption performance of polyacrylonitrile-based ultrahigh modulus carbon fibers decorated with CoZn-bimetallic ZIFs. *Journal of Alloys and Compounds*, *950*, 169912. https://doi.org/10.1016/j.jallcom.2023.169912

[55] Ma, C., Lu, T., Demir, M., Yu, Q., Hu, X., Jiang, W., & Wang, L. (2022). Polyacrylonitrile-derived N-doped nanoporous carbon fibers for CO2 adsorption. *ACS Applied Nano Materials*, *5(9)*, 13473-13481. https://doi.org/10.1021/acsanm.2c03126

[56] Matsuzawa, F., Amano, Y., & Machida, M. (2022). Phosphate ion adsorption characteristics of PAN-based activated carbon prepared by zinc chloride activation. *International Journal of*

Environmental Science and Technology, *19*, 8159-8168. https://doi.org/10.1007/s13762-021-03695-3

[57] Shi, R., Chen, H., Liu, B., Zhou, C., Pi, W., Zeng, Z., & Li, L. (2022). Porous carbon fibers from low-temperature sodium amide activation for acetone adsorption. *Materials Chemistry and Physics*, *286*, 126186. https://doi.org/10.1016/j.matchemphys.2022.126186

[58] Hwang, S. H., Kim, Y. K., Seo, H. J., Jeong, S. M., Kim, J., & Lim, S. K. (2021). The enhanced hydrogen storage capacity of carbon fibers: the effect of hollow porous structure and surface modification. *Nanomaterials*, *11*(7), 1830. https://doi.org/10.3390/nano11071830

[59] Wu, J., Li, T., Meng, G., Xiang, Y., Hai, J., & Wang, B. (2021). Carbon nanofiber supported Ni–ZnO catalyst for efficient and selective hydrogenation of pyrolysis gasoline. *Catalysis Science & Technology*, *11*(12), 4216-4225. https://doi.org/10.1039/D1CY00548K

[60] Yue, Y., Wang, Y., Qu, C., & Xu, X. (2021). Modification of polyacrylonitrile-based activated carbon fibers and their p-nitrophenol adsorption and degradation properties. *Journal of Environmental Chemical Engineering*, *9*(4), 105390. https://doi.org/10.1016/j.jece.2021.105390

[61] Patchen, A., Young, S., Goodbred, L., Puplampu, S., Chawla, V., & Penumadu, D. (2023). Lower carbon footprint concrete using recycled carbon fiber for targeted strength and insulation. *Materials*, *16*(15), 5451. https://doi.org/10.3390/ma16155451

[62] Zhu, C., Su, Y., Wang, X., Sun, H., Ouyang, Q., & Zhang, D. (2021). Process optimization, microstructure characterization and thermal properties of mesophase pitch-based carbon fiber reinforced aluminum matrix composites fabricated by vacuum hot pressing. *Composites Part B: Engineering*, *215*, 108746. https://doi.org/10.1016/j.compositesb.2021.108746

[63] Park, H. M., Kim, G. M., Lee, S. Y., Jeon, H., Kim, S. Y., & Kim, M. (2018). Electrical resistivity reduction with pitch-based carbon fiber into multi-walled carbon nanotube (MWCNT)-embedded cement composites. *Construction and Building Materials*, *165*, 484–93. https://doi.org/10.1016/j.conbuildmat.2017.12.205

[64] Gan, Q., & Fu, Y. (2023). Emerging dual carbon fiber batteries. *Electrochimica Acta*, *439*, 141597.https://doi.org/10.1016/j.electacta.2022.141597.

[65] Wu, Y., Gao, X., Nguyen, T.T., Wu, J., Guo, M., & Liu, W. (2022). Green and low-cost natural lignocellulosic biomass-based carbon fibers—processing, properties, and applications in sports equipment: A review. *Polymers*, *14*, 2591. https://doi.org/10.3390/polym14132591

[66] Wei, J., Gao, D., Wang, Y., Miao, Z., & Zhou, Y. (2023). Enhancing thermal conductivity of cement-based composites by optimizing pores and adding pitch-based carbon fibers for pavement cooling. *Energy and Buildings*, *296*, 113388. https://doi.org/10.1016/j.enbuild.2023.113388

[67] Wang, Z., Xu, Z., Guan, Y., Zhu, H., Yuan, G., Dong, Z., & Cong, Y. (2022). Preparation of pitch-based activated carbon fibers with high specific surface area and excellent adsorption properties. *Research on Chemical Intermediates*, *48*(4), 1733-1746. https://doi.org/10.1007/s11164-022-04679-9

[68] Ryu, D. Y., Shimohara, T., Nakabayashi, K., Miyawaki, J., Park, J. I., & Yoon, S. H. (2019). Urea/nitric acid co-impregnated pitch-based activated carbon fiber for the effective removal of formaldehyde. *Journal of Industrial and Engineering Chemistry*, *80*, 98-105. https://doi.org/10.1016/j.jiec.2019.07.036

[69] Sugiyama, H., & Hattori, Y. (2020). Selective and enhanced CO_2 adsorption on fluorinated activated carbon fibers. *Chemical Physics Letters*, *758*, 137909. https://doi.org/10.1016/j.cplett.2020.137909

[70] Yoshikawa, Y., Teshima, K., Futamura, R., Tanaka, H., Iiyama, T., & Kaneko, K. (2021). Structural adsorption mechanism of chloroform in narrow micropores of pitch-based activated carbon fibres. *Carbon*, *171*, 681-688. https://doi.org/10.1016/j.carbon.2020.08.020

[71] Wei, W., Wang, F., Yang, J., Zou, J., Li, J., & Shi, K. A. (2021). A superior potassium-ıon anode material from pitch-based activated carbon fibers with hierarchical pore structure prepared by metal catalytic activation. *ACS Applied Materials & Interfaces*, *13*(5), 6557-6565. https://doi.org/10.1021/acsami.0c22184

[72] Gelfond, J., Meng, T., Li, S., Li, T., & Hu, L. (2023). Highly electrically conductive biomass-derived carbon fibers for permanent carbon sequestration. *Sustainable Materials and Technologies*, *35*, e00573.https://doi.org/10.1016/j.susmat.2023.e00573

[73] Chen, J., Ghosh, T., Ayranci, C., & Tang, T. (2022). Bio-cleaned lignin-based carbon fiber and its application in adsorptive water treatment. *Journal of Applied Polymer Science*, *139*(18), 52054. https://doi.org/10.1002/app.52054

[74] Chiu, K. L., & Ng, D.H. (2012). Synthesis and characterization of cotton-made activated carbon fiber and its adsorption of methylene blue in water treatment. *Biomass and Bioenergy*, *46*, 102-110. https://doi.org/10.1016/j.biombioe.2012.09.023

[75] Jin, Z., Yan, X., Yu, Y., & Zhao, G. (2014). Sustainable activated carbon fibers from liquefied wood with controllable porosity for high-performance supercapacitors. *Journal of Materials Chemistry A*, *2*(30), 11706-11715. https://doi.org/10.1039/C4TA01413H

[76] Hu, F., Wang, M., Peng, X., Qiu, F., Zhang, T., Dai, H., & Cao, Z. (2018). High-efficient adsorption of phosphates from water by hierarchical CuAl/biomass carbon fiber layered double hydroxide. *Colloids and Surfaces A: Physicochemical and Engineering Aspects*, *555*, 314-323. https://doi.org/10.1016/j.colsurfa.2018.07.010

[77] Hong, S., Song, N., Sun, J., Chen, G., Dong, H., & Li, C. (2022). Nitrogen-doped biomass carbon fibers with surface encapsulated Co nanoparticles for electrocatalytic overall water-splitting. *Chemical Communications*, *58*(11), 1772-1775.https://doi.org/10.1039/D1CC06906C

[78] Zhang, T., Zhao, B., Chen, Q., Peng, X., Yang, D., & Qiu, F. (2019). Layered double hydroxide functionalized biomass carbon fiber for highly efficient and recyclable fluoride adsorption. *Applied Biological Chemistry*, *62*, 1-7. https://doi.org/10.1186/s13765-019-0410-z

[79] Chen, Y., Wang, C., Chen, J., Wang, S., Ju, J., & Kang, W. (2022). Preparing biomass carbon fiber derived from waste rabbit hair as a carrier of TiO_2 for photocatalytic degradation of methylene blue. *Polymers*, *14*(8), 1593.https://doi.org/10.3390/polym14081593

[80] Peng, Q., Li, Y., He, X., Lv, H., Hu, P., Shang, Y., Wang, C., Wang, R., Sritharan, T., & Du, S. (2013). Interfacial enhancement of carbon fiber composites by poly (amido amine) functionalization. *Composites Science and Technology*, *74*, 37-42. https://doi.org/10.1016/j.compscitech.2012.10.005

[81] Sharma, M., Gao, S., Mäder, E., Sharma, H., Wei, L. Y., & Bijwe, J. (2014). Carbon fiber surfaces and composite interphases. *Composites Science and Technology*, *102*, 35-50. https://doi.org/10.1016/j.compscitech.2014.07.005

[82] Li, N., Liu, G., Wang, Z., Liang, J., & Zhang, X. (2014). Effect of surface treatment on surface characteristics of carbon fibers and interfacial bonding of epoxy resin composites. *Fibers and Polymers*, *15*, 2395-2403. https://doi.org/10.1007/s12221-014-2395-x

[83] Park, S.J. (2018). *Carbon Fibers*. Springer Singapore. https://doi.org/10.1007/978-981-13-0538-2

[84] Tam, L. H., Minkeng, M.A.N., Lau, D., Mansour, W., & Wu, C. (2023). Molecular interfacial shearing creep behavior of carbon fiber/epoxy matrix interface under moisture condition. *Engineering Fracture Mechanics*, *282*, 109177. https://doi.org/10.1016/j.engfracmech.2023.109177

[85] Chauhan, A., Agnihotri, P. K., & Basu, S. (2023). Molecular dynamic study on modulating the interfacial thermal conductivity of carbon fiber/epoxy interfaces. *Computational Materials Science*, *217*, 111914. https://doi.org/10.1016/j.commatsci.2022.111914

[86] Darıcık, F., Topcu, A., Aydın, K., & Çelik, S. (2023). Carbon nanotube (CNT) modified carbon fiber/epoxy composite plates for the PEM fuel cell bipolar plate application. *International Journal of Hydrogen Energy*, *48*(3), 1090-1106. https://doi.org/10.1016/j.ijhydene.2022.09.297

[87] Hesseler, S., Stapleton, S. E., Appel, L., Schöfer, S., & Manin, B. (2021). *Modeling of reinforcement fibers and textiles*. In Nicholus Tayari Akankwasa, (Ed), Advances in Modeling and Simulation in Textile Engineering, (pp. 267-299). https://doi.org/10.1016/B978-0-12-822977-4.00010-8

[88] Yang, D., Dong, S., Hong, C., & Zhang, X. (2022). Preparation, modification, and coating for carbon-bonded carbon fiber composites: A review. *Ceramics International*, *48*(11), 14935-14958. https://doi.org/10.1016/j.ceramint.2022.03.055

[89] Wang, Y., Jiang, T., Shi, S., Xiang, L., Tang, B., Qi, Z., & Yu, J. (2023). Lightweight chopped carbon fiber/carbon composites with low thermal conductivity fabricated by vacuum filtration method. *Fullerenes, Nanotubes and Carbon Nanostructures*, *31*(7), 605-612. https://doi.org/10.1080/1536383X.2023.2194638

[90] Ding, S., Wang, X., Qiu, L., Ni, Y. Q., Dong, X., Cui, Y., & Ou, J. (2023). Self-sensing cementitious composites with hierarchical carbon fiber-carbon nanotube composite fillers for crack development monitoring of a maglev girder. *Small*, *19*(9), 2206258. https://doi.org/10.1002/smll.202206258

[91] Wu, D., Hao, Z., Sheng, Y., Zhao, Q., Dong, Q., Han, Y., & Wang, M. (2022). Construction of an orderly carbon fiber/carbon nanotubes hybrid composites by a mild, effective, and green method for highly ınterface reinforcement. *Advanced Materials Interfaces*, *9*(34), 2201360. https://doi.org/10.1002/admi.202201360

[92] Lv, Z., Sha, J., Lin, G., Wang, J., Guo, Y., & Dong, S. (2023). Mechanical and thermal expansion behavior of hybrid aluminum matrix composites reinforced with SiC particles and short carbon fibers. *Journal of Alloys and Compounds*, *947*, 169550. https://doi.org/10.1016/j.jallcom.2023.169550

[93] Zhou, Y., Zhang, P., & Ning, F. (2023). Joining of carbon fiber reinforced polymer/titanium stacks using directed energy deposition additive manufacturing. *Composite Structures*, *310*, 116775. https://doi.org/10.1016/j.compstruct.2023.116775

[94] Yang, L., Shi, X., Tian, X., Xue, Y., Wang, J., & Qi, L. (2022). Influence of pH value on the microstructure and corrosion behavior of carbon fiber reinforced magnesium matrix composites. *Journal of Materials Research and Technology*, *17*, 412-424. https://doi.org/10.1016/j.jmrt.2022.01.031

[95] Tong, Y., Wang, L., Wang, B., Hu, Y., Cai, Z., Ren, J., & Li, S. (2023). Microstructure and mechanical behavior of carbon fiber reinforced carbon, silicon carbide, and copper alloy hybrid composite fabricated by Cu-Si alloy melt infiltration. *Advanced Composites and Hybrid Materials*, *6*(1), 25. https://doi.org/10.1007/s42114-022-00612-1

[96] Xiao, J., Wang, Y., Liu, J., Yang, Y., Zhang, Y., & Luo, X. (2023). Hierarchical Ni/Ni4Mo nanosheets array on carbon fiber as a bifunctional electrocatalyst for urea-oxidation-assisted water splitting. *International Journal of Hydrogen Energy*, *51*, 982-992. https://doi.org/10.1016/j.ijhydene.2023.07.131

[97] Belgibayeva, A., Rakhatkyzy, M., Rakhmetova, A., Kalimuldina, G., Nurpeissova, A., & Bakenov, Z. (2023). Synthesis of free-standing tin phosphide/phosphate carbon composite nanofibers as anodes for lithium-ıon batteries with ımproved low-temperature performance. *Small*, *19*, 2304062. https://doi.org/10.1002/smll.202304062

[98] Hao, X., Nie, H., Ye, Z., Luo, Y., Zheng, L., & Liang, W. (2019). Mechanical properties of a novel fiber metal laminate based on a carbon fiber reinforced Zn-Al alloy composite. *Materials Science and Engineering: A*, *740*, 218-225.https://doi.org/10.1016/j.msea.2018.10.050

[99] Tang S., & Hu C. (2017). Design, preparation and properties of carbon fiber reinforced ultra-high temperature ceramic composites for aerospace applications: A review. *Journal of Materials Science and Technology*, *33*(2), 117–30.https://doi.org/10.1016/j.jmst.2016.08.004

[100] Tong, Y., Hu, Y., Liang, X., Zhang, Z., Li, Y., Chen, Z., & Hua, M. (2020). Carbon fiber reinforced ZrC based ultra-high temperature ceramic matrix composite subjected to laser ablation: Ablation resistance, microstructure and damage mechanism. *Ceramics International*, *46*(10), 14408-14415. https://doi.org/10.1016/j.ceramint.2020.02.236

[101] Kubota, Y., Arai, Y., Yano, M., Inoue, R., Goto, K., & Kogo, Y. (2019). Oxidation and recession of plain weave carbon fiber reinforced ZrB2-SiC-ZrC in oxygen–hydrogen torch environment. *Journal of the European Ceramic Society*, *39*(9), 2812-2823. https://doi.org/10.1016/j.jeurceramsoc.2019.03.010

[102] Liu, Y., Cheng, Y., Ma, D., Hu, N., Han, W., Liu, D., & Wang, A. (2022). Continuous carbon fiber reinforced ZrB_2-SiC composites fabricated by direct ink writing combined with low-temperature hot-pressing. *Journal of the European Ceramic Society*, *42*(9), 3699-3707. https://doi.org/10.1016/j.jeurceramsoc.2022.03.045

[103] Vinci, A., Zoli, L., Sciti, D., Watts, J., Hilmas, G. E., & Fahrenholtz, W. G. (2019). Mechanical behaviour of carbon fibre reinforced TaC/SiC and ZrC/SiC composites up to 2100°C. *Journal of the European Ceramic Society*, *39*(4), 780-787. https://doi.org/10.1016/j.jeurceramsoc.2018.11.017

[104] Çelik, A. İ., Özkılıç, Y. O., Zeybek, Ö., Özdöner, N., & Tayeh, B. A. (2022). Performance assessment of fiber-reinforced concrete produced with waste lathe fibers. *Sustainability*, *14*(19), 11817. https://doi.org/10.3390/su141911817

[105] Afroughsabet, V., Biolzi, L., & Ozbakkaloglu, T. (2016). High-performance fiber-reinforced concrete: a review. *Journal of Materials Science*, *51*, 6517-6551. https://doi.org/10.1007/s10853-016-9917-4

[106] Zhutovsky, S., & Nayman, S. (2022). Modeling of crack-healing by hydration products of residual cement in concrete. *Construction and Building Materials*, *18*, 340. https://doi.org/10.1016/j.conbuildmat.2022.127682

[107] Manvith Kumar Reddy, C., Ramesh, B., & Macrin, D. (2020). Effect of crystalline admixtures, polymers and fibers on self healing concrete - a review. *Materials Today: Proceedings*, *33*, 763–70. https://doi.org/10.1016/j.matpr.2020.06.122

[108] Wang, L., He, T., Zhou, Y., Tang, S., Tan, J., & Liu, Z. (2021). The influence of fiber type and length on the cracking resistance, durability and pore structure of face slab concrete. *Construction and Building Materials*, *282*, 122706. https://doi.org/10.1016/j.conbuildmat.2021.122706

[109] Raza, S. S., Qureshi, L. A., Ali, B., Raza, A., & Khan, M. M. (2021). Effect of different fibers (steel fibers, glass fibers, and carbon fibers) on mechanical properties of reactive powder concrete. *Structural Concrete*, *22*(1), 334–46.https://doi.org/10.1002/suco.201900439

[110] Ahmad, J., González-Lezcano, R. A., Majdi, A., Ben Kahla, N., Deifalla, A. F., & El-Shorbagy, M. A. (2022). Glass fibers reinforced concrete: overview on mechanical, durability and microstructure analysis. *Materials*, *15*(15), 5111.https://doi.org/10.3390/ma15155111

[111] Li, W., Tang, S., Huang, X., Liu, W., Yang, X., & Shi, T. (2022). Carbon fiber-reinforced polymer mesh fabric as shear reinforcement in reinforced concrete beams. *Journal of Building Engineering*, *53*, 104433.https://doi.org/10.1016/j.jobe.2022.104433

[112] Yu, F., Wang, S., Fang, Y., Zhang, N., Wang, Y., & Nuermaimaiti, M. (2023). Seismic behavior of interior polyvinyl chloride–carbon fiber-reinforced polymer-confined concrete column–ring beam joints. *Archives of Civil and Mechanical Engineering*, *23*(1), 1–19. https://doi.org/10.1007/s43452-022-00586-3

[113] Jeon, E. B., Ahn, S. K., Lee, I. G., Koh, H. I., Park, J., & Kim, H. S. (2015). Investigation of mechanical/dynamic properties of carbon fiber reinforced polymer concrete for low noise railway slab. *Composite Structures*, *134*, 27–35.https://doi.org/10.1016/j.compstruct.2015.08.082

[114] Liu, G. J., Bai, E. L., Xu, J. Y., & Yang, N. (2019). Mechanical properties of carbon fiber-reinforced polymer concrete with different polymer–cement ratios. *Materials*, *12*(21), 3530. https://doi.org/10.3390/ma12213530

[115] Liu, G. J., Bai, E. L., Xu, J. Y., Yang, N., & Wang, T. J. (2020). Dynamic compressive mechanical properties of carbon fiber-reinforced polymer concrete with different polymer-cement ratios at high strain rates. *Construction and Building Materials*, *261*, 119995. https://doi.org/10.1016/j.conbuildmat.2020.119995

[116] Wang, Z., Ma, G., Ma, Z., & Zhang, Y. (2021). Flexural behavior of carbon fiber-reinforced concrete beams under impact loading. *Cement and Concrete Composites*, *118*, 103910. https://doi.org/10.1016/j.cemconcomp.2020.103910

[117] Huang, L., Su, L., Xie, J., Lu, Z., Li, P., & Hu, R. (2022). Dynamic splitting behaviour of ultra-high-performance concrete confined with carbon-fibre-reinforced polymer. *Composite Structures, 284*, 115155.https://doi.org/10.1016/j.compstruct.2021.115155

[118] Farooq, M., & Banthia, N. (2022). Strain-hardening fiber reinforced polymer concrete with a low carbon footprint. *Construction and Building Materials, 314*, 125705. https://doi.org/10.1016/j.conbuildmat.2021.125705

[119] Batarlar, B., & Saatci, S. (2022). Numerical investigation on the behavior of reinforced concrete slabs strengthened with carbon fiber textile reinforcement under impact loads. *Structures, 41*, 1164–77. https://doi.org/10.1016/j.istruc.2022.05.057

[120] Pu, H., Hou, Y. L., Chen, J. Z., & Zhao, D. L. (2024). Graphene with different groups on the interfacial properties of carbon fiber/epoxy composites. *Polymer, 290*, 126512. https://doi.org/10.1016/j.polymer.2023.126512